

Pertanika Journal of

**SCIENCE &
TECHNOLOGY**

JST

VOL. 27 (1) JAN. 2019



PERTANIKA
JOURNALS

A scientific journal published by Universiti Putra Malaysia Press

Journal of Science & Technology

About the Journal

Overview

Pertanika Journal of Science & Technology (JST) is the official journal of Universiti Putra Malaysia published by UPM Press. It is an open-access online scientific journal which is free of charge. It publishes the scientific outputs. It neither accepts nor commissions third party content.

Recognized internationally as the leading peer-reviewed interdisciplinary journal devoted to the publication of original papers, it serves as a forum for practical approaches to improving quality in issues pertaining to science and engineering and its related fields.

JST is a **quarterly** (January, April, July and October) periodical that considers for publication original articles as per its scope. The journal publishes in **English** and it is open to authors around the world regardless of the nationality.

The Journal is available world-wide.

Aims and scope

Pertanika Journal of Science and Technology aims to provide a forum for high quality research related to science and engineering research. Areas relevant to the scope of the journal include: bioinformatics, bioscience, biotechnology and bio-molecular sciences, chemistry, computer science, ecology, engineering, engineering design, environmental control and management, mathematics and statistics, medicine and health sciences, nanotechnology, physics, safety and emergency management, and related fields of study.

History

Pertanika was founded in 1978. A decision was made in 1992 to streamline Pertanika into three journals as Journal of Tropical Agricultural Science, Journal of Science & Technology, and Journal of Social Sciences & Humanities to meet the need for specialised journals in areas of study aligned with the interdisciplinary strengths of the university.

After almost 25 years, as an interdisciplinary Journal of Science & Technology, the revamped journal now focuses on research in science and engineering and its related fields.

Goal of *Pertanika*

Our goal is to bring the highest quality research to the widest possible audience.

Quality

We aim for excellence, sustained by a responsible and professional approach to journal publishing. Submissions are guaranteed to receive a decision within 14 weeks. The elapsed time from submission to publication for the articles averages 5-6 months.

Abstracting and indexing of *Pertanika*

Pertanika is almost 40 years old; this accumulated knowledge has resulted in Pertanika JST being abstracted and indexed in SCOPUS (Elsevier), Thomson (ISI) Web of Knowledge [BIOSIS & CAB Abstracts], EBSCO & EBSCOhost, DOAJ, ERA, Cabell's Directories, Google Scholar, MyAIS, ISC & Rubriq (Journal Guide).

Future vision

We are continuously improving access to our journal archives, content, and research services. We have the drive to realise exciting new horizons that will benefit not only the academic community, but society itself.

Citing journal articles

The abbreviation for *Pertanika Journal of Science & Technology* is *Pertanika J. Sci. Technol.*

Publication policy

Pertanika policy prohibits an author from submitting the same manuscript for concurrent consideration by two or more publications. It prohibits as well publication of any manuscript that has already been published either in whole or substantial part elsewhere. It also does not permit publication of manuscript that has been published in full in Proceedings.

Code of Ethics

The *Pertanika* Journals and Universiti Putra Malaysia takes seriously the responsibility of all of its journal publications to reflect the highest in publication ethics. Thus all journals and journal editors are expected to abide by the Journal's codes of ethics. Refer to *Pertanika's Code of Ethics* for full details, or visit the Journal's web link at http://www.pertanika.upm.edu.my/code_of_ethics.php

International Standard Serial Number (ISSN)

An ISSN is an 8-digit code used to identify periodicals such as journals of all kinds and on all media—print and electronic. All *Pertanika* journals have ISSN as well as an e-ISSN.

Journal of Science & Technology: ISSN 0128-7680 (*Print*); ISSN 2231-8526 (*Online*).

Lag time

A decision on acceptance or rejection of a manuscript is reached in 3 to 4 months (average 14 weeks). The elapsed time from submission to publication for the articles averages 5-6 months.

Authorship

Authors are not permitted to add or remove any names from the authorship provided at the time of initial submission without the consent of the Journal's Chief Executive Editor.

Manuscript preparation

Refer to *Pertanika's INSTRUCTIONS TO AUTHORS* at the back of this journal.

Most scientific papers are prepared according to a format called IMRAD. The term represents the first letters of the words Introduction, **M**aterials and **M**ethods, **R**esults, **A**nd, **D**iscussion. IMRAD is simply a more 'defined' version of the "IBC" [Introduction, Body, Conclusion] format used for all academic writing. IMRAD indicates a pattern or format rather than a complete list of headings or components of research papers; the missing parts of a paper are: *Title, Authors, Keywords, Abstract, Conclusions, and References*. Additionally, some papers include Acknowledgments and Appendices.

The *Introduction* explains the scope and objective of the study in the light of current knowledge on the subject; the *Materials and Methods* describes how the study was conducted; the *Results* section reports what was found in the study; and the *Discussion* section explains meaning and significance of the results and provides suggestions for future directions of research. The manuscript must be prepared according to the Journal's **INSTRUCTIONS TO AUTHORS**.

Editorial process

Authors are notified with an acknowledgement containing a *Manuscript ID* on receipt of a manuscript, and upon the editorial decision regarding publication.

Pertanika follows a **double-blind peer-review** process. Manuscripts deemed suitable for publication are usually sent to reviewers. Authors are encouraged to suggest names of at least three potential reviewers at the time of submission of their manuscript to *Pertanika*, but the editors will make the final choice. The editors are not, however, bound by these suggestions.

Notification of the editorial decision is usually provided within ten to fourteen weeks from the receipt of manuscript. Publication of solicited manuscripts is not guaranteed. In most cases, manuscripts are accepted conditionally, pending an author's revision of the material.

As articles are double-blind reviewed, material that might identify authorship of the paper should be placed only on page 2 as described in the first-4 page format in *Pertanika's INSTRUCTIONS TO AUTHORS* given at the back of this journal.

The Journal's peer-review

In the peer-review process, three referees independently evaluate the scientific quality of the submitted manuscripts.

Peer reviewers are experts chosen by journal editors to provide written assessment of the **strengths** and **weaknesses** of written research, with the aim of improving the reporting of research and identifying the most appropriate and highest quality material for the journal.

Operating and review process

What happens to a manuscript once it is submitted to *Pertanika*? Typically, there are seven steps to the editorial review process:

1. The Journal's chief executive editor and the editorial board examine the paper to determine whether it is appropriate for the journal and should be reviewed. If not appropriate, the manuscript is rejected outright and the author is informed.
2. The chief executive editor sends the article-identifying information having been removed, to three reviewers. Typically, one of these is from the Journal's editorial board. Others are specialists in the subject matter represented by the article. The chief executive editor asks them to complete the review in three weeks.

Comments to authors are about the appropriateness and adequacy of the theoretical or conceptual framework, literature review, method, results and discussion, and conclusions. Reviewers often include suggestions for strengthening of the manuscript. Comments to the editor are in the nature of the significance of the work and its potential contribution to the literature.

3. The chief executive editor, in consultation with the editor-in-chief, examines the reviews and decides whether to reject the manuscript, invite the author(s) to revise and resubmit the manuscript, or seek additional reviews. Final acceptance or rejection rests with the Editor-in-Chief, who reserves the right to refuse any material for publication. In rare instances, the manuscript is accepted with almost no revision. Almost without exception, reviewers' comments (to the author) are forwarded to the author. If a revision is indicated, the editor provides guidelines for attending to the reviewers' suggestions and perhaps additional advice about revising the manuscript.
4. The authors decide whether and how to address the reviewers' comments and criticisms and the editor's concerns. The authors return a revised version of the paper to the chief executive editor along with specific information describing how they have answered the concerns of the reviewers and the editor, usually in a tabular form. The author(s) may also submit a rebuttal if there is a need especially when the author disagrees with certain comments provided by reviewer(s).
5. The chief executive editor sends the revised paper out for re-review. Typically, at least one of the original reviewers will be asked to examine the article.

6. When the reviewers have completed their work, the chief executive editor in consultation with the editorial board and the editor-in-chief examine their comments and decide whether the paper is ready to be published, needs another round of revisions, or should be rejected.
7. If the decision is to accept, an acceptance letter is sent to all the author(s), the paper is sent to the Press. The article should appear in print in approximately three months.

The Publisher ensures that the paper adheres to the correct style (in-text citations, the reference list, and tables are typical areas of concern, clarity, and grammar). The authors are asked to respond to any minor queries by the Publisher. Following these corrections, page proofs are mailed to the corresponding authors for their final approval. At this point, **only essential changes are accepted**. Finally, the article appears in the pages of the Journal and is posted on-line.



Pertanika Journal of
**SCIENCE
& TECHNOLOGY**

Vol. 27 (1) Jan. 2019



A scientific journal published by Universiti Putra Malaysia Press



EDITOR-IN-CHIEF

Mohd Adzir Mahdi

Physics, Optical Communications

CHIEF EXECUTIVE EDITOR

Abu Bakar Salleh

Biotechnology and Biomolecular Science

UNIVERSITY PUBLICATIONS COMMITTEE

Zulkifli Idrus, Chair

EDITORIAL STAFF

Journal Officers:

Kanagamalar Silvarajoo, *ScholarOne*

Teo Syin-Ying, *ScholarOne*

Ummi Fairuz Hanapi, *ScholarOne*

Editorial Assistants:

Florence Jiyom

Rahimah Razali

Zulinaardawati Kamarudin

COPY EDITORS

Crescentia Morais

Doreen Dillah

Pooja Terasha Stanslas

PRODUCTION STAFF

Pre-press Officers:

Nur Farrah Dila Ismail

Wong Lih Jiu

WEBMASTER

Mohd Nazri Othman

PUBLICITY & PRESS RELEASE

Magdalene Pokar (*ResearchSEA*)

Florence Jiyom

EDITORIAL OFFICE

JOURNAL DIVISION

Office of the Deputy Vice Chancellor (R&I)

1st Floor, IDEA Tower II

UPM-MTDC Technology Centre

Universiti Putra Malaysia

43400 Serdang, Selangor Malaysia.

Gen Enq.: +603 8947 1622 | 1616

E-mail: executive_editor.pertanika@upm.my

URL: www.journals-jd.upm.edu.my

PUBLISHER

UPM Press

Universiti Putra Malaysia

43400 UPM, Serdang, Selangor, Malaysia.

Tel: +603 8946 8855, 8946 8854

Fax: +603 8941 6172

E-mail: penerbit@putra.upm.edu.my

URL: <http://penerbit.upm.edu.my>

EDITORIAL BOARD

2018-2020

Adem Kilicman

Mathematical Sciences
Universiti Putra Malaysia, Malaysia.

Ali A. Moosavi-Movahedi

Biophysical Chemistry
University of Tehran, Tehran, Iran.

Amu Therwath

Oncology, Molecular Biology,
Université Paris, France.

Angelina Chin

Mathematics, Group Theory and
Generalisations, Ring Theory,
University of Malaya, Malaysia.

Bassim H. Hameed

Chemical Engineering: Reaction
Engineering, Environmental Catalysis
& Adsorption,
Universiti Sains Malaysia, Malaysia.

Biswa Mohan Biswal

Medical, Clinical Oncology,
Radiotherapy
Universiti Sains Malaysia, Malaysia.

Christopher G. Jesudason

Mathematical Chemistry, Molecular
Dynamics Simulations, Thermodynamics
and General Physical Theory,
University of Malaya, Malaysia.

Hari M. Srivastava

Mathematics and Statistics,
University of Victoria, Canada.

Ivan D. Rukhlenko

Nonlinear Optics, Silicon Photonics,
Plasmonics and Nanotechnology
Monash University, Australia.

Kaniraj R. Shenbaga

Geotechnical Engineering,
India.

Kanury Rao

Senior Scientist & Head, Immunology
Group, International Center for Genetic
Engineering and Biotechnology,
Immunology, Infectious Disease Biology
and System Biology
International Centre for Genetic
Engineering & Biotechnology, New
Delhi, India.

Ki-Hyung Kim

Computer and Wireless Sensor
Networks
AJOU University, Korea.

Kunnawee Kanitpong

Transportation Engineering-Road
Traffic Safety, Highway Materials and
Construction
Asian Institute of Technology, Thailand.

Megat Mohd Hamdan

Megat Ahmad
Mechanical and Manufacturing
Engineering
Universiti Pertahanan Nasional
Malaysia, Malaysia.

Mirnalini Kandiah

Public Health Nutrition, Nutritional
Epidemiology
UCSI University, Malaysia.

Mohamed Othman

Communication Technology and
Network, Scientific Computing
Universiti Putra Malaysia, Malaysia

Mohd. Ali Hassan

Bioprocess Engineering, Environmental
Biotechnology
Universiti Putra Malaysia, Malaysia.

Mohd Sapuan Salit

Concurrent Engineering and Composite
Materials
Universiti Putra Malaysia, Malaysia.

Narongrit Sombatsompop

Engineering & Technology: Materials
and Polymer Research
King Mongkut's University of
Technology Thonburi (KMUTT),
Thailand.

Prakash C. Sinha

Physical Oceanography, Mathematical
Modelling, Fluid Mechanics, Numerical
Techniques
Universiti Malaysia Terengganu,
Malaysia.

Rajinder Singh

Biotechnology, Biomolecular Sciences,
Molecular Markers/ Genetic Mapping
Malaysia Palm Oil Board, Kajang,
Malaysia.

Renuganth Varatharajoo

Engineering, Space System
Universiti Putra Malaysia, Malaysia.

Riyanto T. Bambang

Electrical Engineering, Control,
Intelligent Systems & Robotics
Bandung Institute of Technology,
Indonesia.

Roslani Abd-Shukur

Physics & Materials Physics,
Superconducting Materials
Universiti Kebangsaan Malaysia,
Malaysia.

Sabira Khatun

Engineering, Computer Systems
& Software Engineering, Applied
Mathematics
Universiti Malaysia Pahang, Malaysia.

Shiv Dutt Gupta

Director, IHMR, Health Management,
Public Health, Epidemiology, Chronic
and Non-communicable Diseases
Indian Institute of Health Management
Research, India.

Suan-Choo Cheah

Biotechnology, Plant Molecular Biology
Asiatic Centre for Genome Technology
(ACGT), Kuala Lumpur, Malaysia.

Wagar Asrar

Engineering, Computational Fluid
Dynamics, Experimental Aerodynamics
International Islamic University,
Malaysia.

Wing Keong Ng

Aquaculture, Aquatic Animal Nutrition,
Aqua Feed Technology
Universiti Sains Malaysia, Malaysia.

Yudi Samudya

Chemical Engineering, Advanced
Process Engineering
Curtin University of Technology,
Malaysia.

INTERNATIONAL ADVISORY BOARD

2018-2021

Adarsh Sandhu

Editorial Consultant for Nature
Nanotechnology and Contributing
Writer for Nature Photonics, Physics,
Magneto-resistive Semiconducting
Magnetic Field Sensors, Nano-
Bio-Magnetism, Magnetic Particle
Colloids, Point of Care Diagnostics,
Medical Physics, Scanning Hall Probe
Microscopy, Synthesis and Application
of Graphene
Electronics-Inspired Interdisciplinary
Research Institute (EIIRIS), Toyohashi
University of Technology, Japan.

Graham Megson

Computer Science
The University of Westminster, U.K.

Kuan-Chong Ting

Agricultural and Biological Engineering
University of Illinois at Urbana-
Champaign, USA.

Malin Premaratne

Advanced Computing and Simulation
Monash University, Australia.

Mohammed Ismail Elnaggar

Electrical Engineering
Ohio State University, USA.

Peter J. Heggs

Chemical Engineering
University of Leeds, U.K.

Ravi Prakash

Vice Chancellor, JUIT, Mechanical
Engineering, Machine Design,
Biomedical and Materials Science
Jaypee University of Information
Technology, Indian.

Said S.E.H. Elnashaie

Environmental and Sustainable
Engineering
Penn. State University at Harrisburg,
USA.

Suhash Chandra Dutta Roy

Electrical Engineering
Indian Institute of Technology (IIT)
Delhi, India.

Vijay Arora

Quantum and Nano-Engineering
Processes
Wilkes University, USA.

Yi Li

Chemistry, Photochemical Studies,
Organic Compounds, Chemical
Engineering
Chinese Academy of Sciences, Beijing,
China.

ABSTRACTING AND INDEXING OF PERTANIKA JOURNALS

Pertanika is almost 40 years old; this accumulated knowledge has resulted in the journals being abstracted and indexed in SCOPUS (Elsevier), Clarivate Analytics [formerly known as Thomson (ISI)] Web of Science™ Core Collection- Emerging Sources Citation Index (ESCI), Web of Knowledge [BIOSIS & CAB Abstracts], EBSCO and EBSCOhost, DOAJ, ERA, Google Scholar, TIB, MyCite, Islamic World Science Citation Center (ISC), ASEAN Citation Index (ACI), Cabell's Directories & Journal Guide.



The publisher of *Pertanika* will not be responsible for the statements made by the authors in any articles published in the journal. Under no circumstances will the publisher of this publication be liable for any loss or damage caused by your reliance on the advice, opinion or information obtained either explicitly or implied through the contents of this publication.

All rights of reproduction are reserved in respect of all papers, articles, illustrations, etc., published in *Pertanika*. *Pertanika* provides free access to the full text of research articles for anyone, web-wide. It does not charge either its authors or author-institution for refereeing/publishing outgoing articles or user-institution for accessing incoming articles.

No material published in *Pertanika* may be reproduced or stored on microfilm or in electronic, optical or magnetic form without the written authorization of the Publisher.

Copyright © 2018 Universiti Putra Malaysia Press. All Rights Reserved.



Pertanika Journal of Science & Technology
Vol. 27 (1) Jan. 2019

Contents

Foreword	i
<i>Abu Bakar Salleh</i>	
Information, Computer and Communication Technologies	
<i>Review Article</i>	1
A Review: Customers Online Security on Usage of Banking Technologies in Smartphones and Computers	
<i>Natarajan Sundaram, Cherian Thomas and Loganathan Agilandeeswari</i>	
Non-Binary Serial Turbo LDPC Codes Combined with High Order Constellations	33
<i>Latifa Mostari and Abdelmalik Taleb-Ahmed</i>	
Ma-Ease: An Android-Based Technology for Corn Production and Management	49
<i>Sales Gamponia Aribé Jr., Jhon Michael H. Turtosa, Jul Maico B. Yamba and Alvin B. Jamisola</i>	
Market Matching Online to Recommend MSME Export Products Destination by Using Fuzzy Control	69
<i>Bambang Nurdewanto, Elta Sonalitha, Ratih Salnan and Nadia Rosmalita Sari</i>	
Supervised Clustering based on a Multi-objective Genetic Algorithm	81
<i>Vipa Thananant and Surapong Auwatanamongkol</i>	
Adaptive Genetic Algorithm for Feature Weighting in Multi-Criteria Recommender Systems	123
<i>Gursimarpreet Kaur and Saroj Ratnoo</i>	
Customizable Smart Food Cabinet and Refrigerator	143
<i>Chandra Manuel, Janitra Avila, Lukas Budiman, Rico Wijaya and Rinda Hedwig</i>	
SQL-Injection Vulnerabilities Resolving using Valid Security Tool in Cloud	159
<i>Niharika Singh and Ashutosh Kumar Singh</i>	

SPAS: An Authentication Scheme to Prevent Unauthorized Access of Information from Smart Card <i>Ajay Kumar Sahu and Ashish Kumar</i>	175
-----------------------------------------------------------------------------------------------------------------------------------------	-----

Engineering Sciences

Improvement in the Mechanical Strength of Compacted Urea Fertilizer Tablets through Die Wall Lubrication <i>Intan Soraya Shamsudin, Mohd Shamsul Anuar, Yus Aniza Yusof, Ahmad Husni Mohd. Hanif and Suraya Mohd Tahir</i>	193
-------------------------------------------------------------------------------------------------------------------------------------------------------------------------------------------------------------------------------	-----

Two-dimensional Modeling of Water Distribution under Capillary Wick Irrigation System <i>Rowshon Md Kamal, Hadi Hamaaziz Muhammed, Mohammad Abdul Mojid, Ruediger Anlauf and Mohd Amin Mohd Soom</i>	205
---------------------------------------------------------------------------------------------------------------------------------------------------------------------------------------------------------	-----

Reliability based Redundancy Assessment of a Cogeneration Plant <i>Meseret Nasir, Wan Mansor Wan Muhamad and Raja Aziz Raja Maarof</i>	225
-------------------------------------------------------------------------------------------------------------------------------------------	-----

Utilization of Normal and Treated Cement Kiln Dust as Cement Replacement Materials in Concrete <i>Yaser Gamil, Ismail Bakar and Lee Yee Loon</i>	247
-----------------------------------------------------------------------------------------------------------------------------------------------------	-----

Design of Self-tuning Fuzzy PID Controllers for Position Tracking Control of Autonomous Agricultural Tractor <i>Witcha Upaphai, Pracha Bunyawanchakul and Manusak Janthong</i>	263
-----------------------------------------------------------------------------------------------------------------------------------------------------------------------------------	-----

Applied Sciences and Technologies

Review Article

A Review: Methodologies Review of Magnetic Water Treatment as Green Approach of Water Pipeline System <i>Athirah Othman, Johan Sohaili and Nur Sumaiyyah Supian</i>	281
------------------------------------------------------------------------------------------------------------------------------------------------------------------------	-----

Kenaf Fibre and Its Bio-Based Composites: A Conspectus <i>Adole Michael Adole, Jamaludin Mohamad Yatim, Suhaimi Abubakar Ramli, Athirah Othman and Norazura Azzmi Mizal</i>	297
--------------------------------------------------------------------------------------------------------------------------------------------------------------------------------	-----

The Physicochemical Properties of Cocoa Butter Equivalent Produced from Lipase- Catalyzed Palm Oil and Hydrogenated Palm Oil via Physical Fractionation <i>Siti Maslina Mohamad Alwi and Lai Oi Ming</i>	331
-------------------------------------------------------------------------------------------------------------------------------------------------------------------------------------------------------------	-----

Extraction of Subtractive Features of Prismatic Parts from STEP File for CAD/CAM Integration <i>Sattanathan Sivakumar, Venkadasamy Dhanalakshmi and Ravichandran Vishnuvardha</i>	343
--------------------------------------------------------------------------------------------------------------------------------------------------------------------------------------	-----

Medical and Health Sciences

Review Article

A Review of the Thermal Effects During Pregnancy by using Ultrasound:
Doppler Mode 357

*Umi Nadrah Amran, Farah Wahida Ahmad Zaiki and
Sulaiman Md Dom*

Simultaneous Estimation by RP-HPLC Method for the 371
Immunosuppressant Drug Combination: Mycophenolate Mofetil,
Tacrolimus with Prednisolone

Pardeep Kr. Sharma, Vijay Mishra, Surajpal Verma and Amit Bhatia

Effects of Various Drying Methods on the Vitamin C level of Papaya 387
Locally Grown in Brunei Darussalam

Nur Amirah Hair Mustapa and Siti Rohaiza Ahmad

Earth Sciences

Experimental Study of Hydraulic Jumps in an Inclined Rectangular Flume 397

Dillip K. Ghose, Priya Mandal and Sandeep Samantaray

Flow Measurement in Huma Tail distributary of Hirakud Command Area, 409
India using Chiu's Equation

Ashutosh Rath, Sandeep Samantaray and Prakash Chandra Swain

Environmental Sciences

Modelling of Pilot-Scale Anaerobic Food Wastes Composting 421
Process with Dry Leaves or Cow Manure

*Wei Jie Lim, Nyuk Ling Chin, Yus Aniza Yusof, Azmi Yahya and
Tuan Poy Tee*

Response of Cadmium Accumulation in Rice (*Oryza sativa* L. cv. SPR1) 443
Grown with Different Organic Soil Amendments

Chitsanuphong Pratum

Material Sciences

Review Article

Titanium and Titanium Based Alloys as Metallic Biomaterials in Medical 459
Applications – Spine Implant Case Study

Nur Azida Che Lah and Muhamad Hellmy Hussin

Physico-Mechanical Properties and Formaldehyde Emission of 473
Rubberwood Particleboard Made With UF Resin Admixed With
Ammonium and Aluminium-Based Hardeners

Abd Ghani Aizat, Bawon Paiman, Seng Hua Lee and Ashaari Zaidon

Chemical Sciences

Preparation and Swelling Study of CMC Hydrogel as Potential Superabsorbent 489

Nur Fitrah Che Nan, Norhazlin Zainuddin and Mansor Ahmad

Engineering Sciences

Review Article 499

A Review of the Mechanism and Role of Wax Inhibitors in the Wax Deposition and Precipitation

Lim Zhen Hao, Hikmat Said Al-Salim and Norida Ridzuan

Mathematical Sciences

Performance of SVM with Multiple Kernel Learning for Classification Tasks of Imbalanced Datasets 527

Sana Saeed and Hong Choon Ong

Foreword

Welcome to the First Issue of 2019 for the Journal of Science and Technology (JST)!

JST is an open-access journal for studies in Science and Technology published by Universiti Putra Malaysia Press. It is independently owned and managed by the university and run on a non-profit basis for the benefit of the world-wide science community.

This issue contains 30 articles; 5 are review articles and the rest are regular articles. The authors of these articles come from different countries namely Algeria, Bangladesh, Brunei, France, Germany, India, Indonesia, Malaysia, Pakistan, Philippines and Thailand. Malaysia alone contributed 14 articles.

Articles submitted in this issue cover various scopes of Science and Technology including applied sciences and technologies, chemical sciences, earth sciences, engineering sciences, environmental sciences, information, computer and communication technologies, material sciences, mathematical sciences, and medical and health sciences.

Selected from the scope of information, computer and communication technologies is an article entitled “Ma-Ease: An Android-based Technology for Corn Production and Management” by fellow researches from Philippines (*Sales Gamponia Aribé Jr., Jhon Michael H. Turtosa, Jul Maico B. Yamba and Alvin B. Jamisola*). The study focused on development of a mobile application for corn farmers needs through the cooperation of the City Agriculture Office (CAO) of Malaybalay City, Bukidnon, Philippines. The researchers emphasized on dissemination of proper information, management and techniques for a good harvest of corns through this mobile application namely Ma-Ease Application. The results showed that farmers were satisfied with the mobile application and thus the software product was formally accepted and recommended for use and deployment by the Department of Agriculture. Details of the article are available on page 49.

Selected from the scope of engineering science is an article entitled “Utilization of Normal and Treated Cement Kiln Dust as Cement Replacement Materials in Concrete” by *Yaser Gamil, Ismail Bakar and Lee Yee Loon*, fellow researchers from Faculty of Civil and Environmental Engineering, University Tun Hussein Onn Malaysia, Malaysia. The study aimed to modify Cement Kiln Dust (CKD), a by-product generated throughout the production of Ordinary Portland Cement (OPC), and investigate the difference

between the normal CKD and modified CKD. The study also emphasized that treating CKD by removing excessive and unwanted materials can improve its chemical and physical properties and the results showed that that modified CKD had better properties compared to normal CKD. Details of the article is available on page 247.

Selected from the scope of medical and health sciences is an article entitled “Effects of Various Drying Methods on the Vitamin C Level of Papaya Locally Grown in Brunei Darussalam” by *Nur Amirah Hair Mustapa* and *Siti Rohaiza Ahmad*, fellow researchers from PAPRSB Institute of Health Sciences, Universiti Brunei Darussalam, Brunei Darussalam. The study investigated the level of vitamin C in dried papaya subjected to four different drying methods including sun drying (SD), oven drying (OD), freeze-drying (FD) and deep freezing (DF). The researchers found out that the FD method resulted in the highest vitamin C levels compared to other three drying methods, hence serving as the best industrial application with good vitamin C retention in papaya. Details of the article is available on page 387.

We anticipate that you will find the evidence presented in this issue to be intriguing, thought-provoking and useful in reaching new milestones in your own research. Please recommend the journal to your colleagues and students to make this endeavour meaningful.

All the papers published in this edition underwent Pertanika’s stringent peer-review process involving a minimum of two reviewers comprising internal as well as external referees. This was to ensure that the quality of the papers justified the high ranking of the journal, which is renowned as a heavily-cited journal not only by authors and researchers in Malaysia but by those in other countries around the world as well.

We would also like to express our gratitude to all the contributors, namely the authors, reviewers and editors, who have made this issue possible.

JST is currently accepting manuscripts for upcoming issues based on original qualitative or quantitative research that opens new areas of inquiry and investigation.

Chief Executive Editor

Prof. Dato’ Dr. Abu Bakar Salleh
executive_editor.pertanika@upm.my

Review Article

A Review: Customers Online Security on Usage of Banking Technologies in Smartphones and Computers

Natarajan Sundaram^{1*}, Cherian Thomas¹ and Loganathan Agilandeswari²

¹*Department of Commerce, School of Social Sciences and Languages,
Vellore Institute of Technology, Vellore 632 014, Tamil Nadu, India*

²*Department of Digital Communication, School of Information Technology and Engineering,
Vellore Institute of Technology, Vellore 632 014, Tamil Nadu, India*

ABSTRACT

The internet brought a diffusion of technology in the banking arena. Two of the personal devices which aid this phenomenon are the computer (website) and smartphone (web application). Nowadays, banking is done vividly through the internet that causes both computer and smartphone prone to security risks. This review paper aims to highlight the earlier research deliberations, suggested solutions and the factors related to security issues in electronic banking devices in the past six years. Narrative literature review method was used by reviewing 130 papers from selected database journals. The paper discusses the articles between the years 2012 and 2018. It points and poses unanswered questions, which serve as the scope for further research. Neither a computer nor a smartphone has an upper hand when it comes to security. Security of banking technology does not depend on these devices. Rather the onus rests on the users, service providers and banks. The emerging electronic commerce and mobile commerce industry are not considered in this paper. This paper endeavours to provide a better scope for researchers in future to answer unrequited questions on the role of devices in banking technology security. All the past literature has focused on the peoples' attitude towards security threats in online banking.

This study challenges to think further, about the influence of security threats to online banking devices.

Keywords: Internet banking, mobile banking, privacy, review, risk, security, trust

ARTICLE INFO

Article history:

Received: 14 April 2018

Accepted: 12 September 2018

Published: 24 January 2019

E-mail addresses:

nsundaram@vit.ac.in (Natarajan Sundaram)

cherian28@gmail.com (Cherian Thomas)

agila.l@vit.ac.in (Loganathan Agilandeswari)

* Corresponding author

INTRODUCTION

The birth of banking technology took place with the arrival of plastic cards and Automated Teller Machines (ATM) in the 1960s'. Later, in 1983, when the internet came into existence, there was a sudden disruption of technology in the banking industry. Banks that were housed in brick and mortar structures started reaching the doorsteps of customers through the internet. Two major devices that made the banking technology disruption to reach the hands of the people were smartphones (web application) and computers (website). Similarly, disruptions also evolved these devices, which eventually led to cost effective and efficient technology to progress faster. In spite of technology disruptions that were being heralded as a positive sign for all such benefits that it had brought, it also had its own set of challenges and issues in the form of security. Figures 1 and 2 are given below to show how the internet (computer) and mobile banking (smartphone) architecture differs from each other and also about the probable online banking cyber attacks.

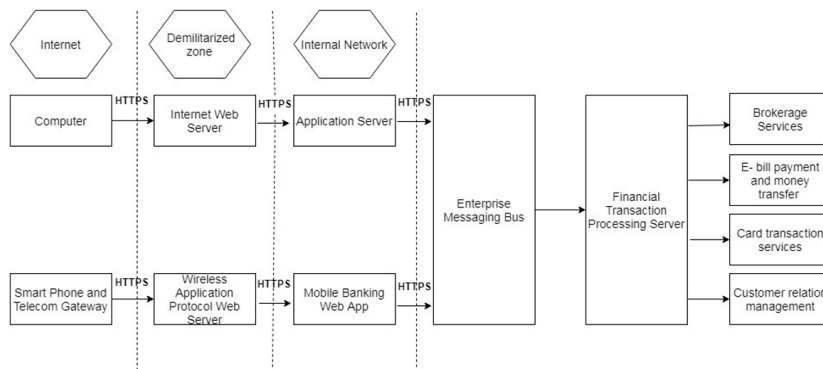


Figure 1. Architectural outlay of internet and mobile banking (Zhang & Morana, 2012)

According to the Cybersecurity Ventures Annual Cybercrime Report, 2017, the depths of security attacks were explicitly stated. The report predicted a loss of about \$6 trillion of the online banking customers by 2021 exclusively due to cyber crimes. One in six customers was said to be prone to cyber attacks, according to a research by MarkMonitor in 2014. DDoS (distributed denial-of-service) attacks, ransomware, and an increase in zero-day exploits are counted as the major factors that lay behind cyber crimes, while phishing still ruled as the major weapon of new entrant cyber attackers. The banking technology has been exposed to a large security risk due to increase in internet users world-wide, emergence of the Internet of Things (IoT) and big data, increase in wearable and wireless devices, newly written software codes, flourishing digital contents and booming sensor technology. Although biometrics have replaced the password, transition to this new technology have set to touch \$1 trillion. The occurrences in the frequency of ransomware attacks are set to reduce from 40 seconds per business firm in 2016 to 14 seconds per business firm in 2019.

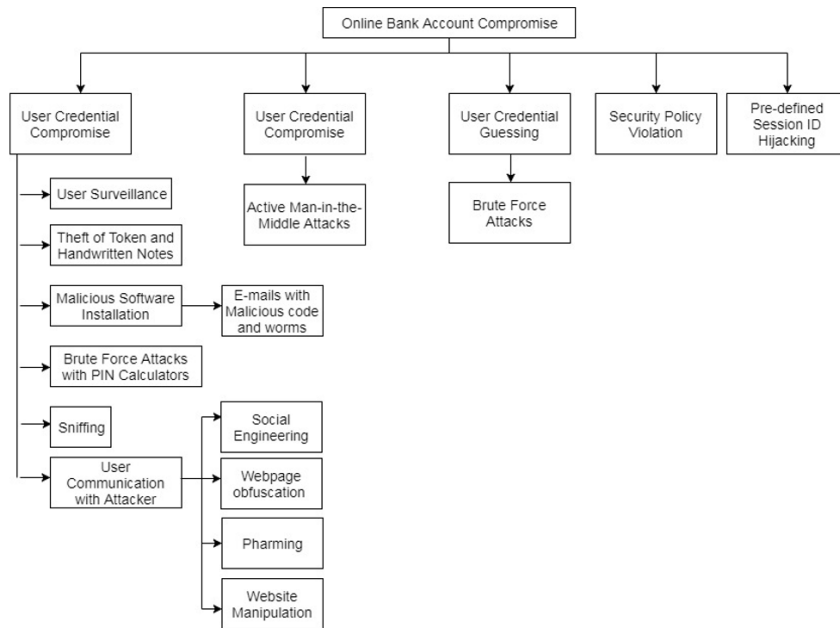


Figure 2. A bird's eye view of probable cyber attacks in the internet and mobile banking (Zhang & Morana, 2012)

By 2021, a dearth of about 3.5 million employees in cybersecurity profession is estimated. Firms are expected to spend around \$10 billion to train their employees on cybersecurity awareness. In particular, banks which are the store-house of money are extensively prone to cyber threats. Bloomberg Businessweek posits that banks globally were set to lose \$700 billion annually due to cyber threats. These factors have made the studies towards banking technology security to be highly relevant at present and in days to come. At present, the security vulnerability scales are slightly tilted towards mobile based applications than a website. According to Verizon's Data Breach Investigation Report, 2016, it was found that web applications were easy to break into using SQL (Structured Query Language) injection or malware which can go undetected. This is due to the existence of millions of legitimate users and proxy servers. However, this review paper has taken both the website (computer) and the web application (smartphones) aspects into account.

As presumed, not all the cyber crimes are motivated by monetary gains. Cyber crimes have evolved to include those crimes that are done in order to quench revenge either by an individual or a group that upholds an ideology. On the contrary, Verizon's Data Breach Investigation Report, 2016 pointed that 89% of cyber threats in 2015 were due to monetary gains and data leakage than other causes. Another dangerous trend observed is that attackers

have evolved from humans to computer bots which are trained to break security. The Financial Industry Cybersecurity Report of Security Scorecard, 2016 stated that financial industry faces the highest vulnerability compared to other industries in terms of network security and other subsequent factors.

The aim of this review paper is to transcribe the security issues of banking technology in the literary works of past six years, into one single literary piece to make a note as to where the current research stands. The discussions carried in this paper regarding banking technology security are viewed both from the customers and industry point of view. In the following sections, the paper is organized as a research methodology that discusses the approach on which the paper is built upon, followed by the review of past relevant literature. The paper finally concludes and outlines the scope and offers few areas that promote further research.

RESEARCH METHODOLOGY

The review paper was conceptualized to provide a comprehensive view of the present security landscape of banking technology. An extensive search was conducted in eight databases of publishers viz. Elsevier, Emerald, IEEE (Institute of Electrical and Electronics Engineers), Inderscience, Sage, Springer, Taylor and Francis, and Wiley. The keyword used for the search was ‘security issues on the internet or mobile banking’. A total of 130 articles were reviewed between the time period of 2012 and 2018. The year 2012 was crucial for this study since internet banking fraud cases shot from mere 94 in 2011 to 1,003 in 2012, which is an increase of 967%. The losses due to this were pegged at 3 million Euros (Febelfin, 2013).

REVIEW OF LITERATURE

The core part of the paper is presented in this section. For the reviewing convenience, the process was started by analyzing the online banking¹. It was split into two: internet banking² and mobile banking³. These were done in order to study the macro and micro security concerns. Under each form of banking, the review was branched out to deliberations, solutions and impacts that occurred in the past six years.

Online Banking Security- Deliberations, Solutions and Impact

Deliberations. Trust, security and privacy were not only technical issues but they were attitudinal problems as well. This is because banking technologies were termed as

¹ Online Banking is a generic term. It is used to denote any bank transaction done with the help of internet. It is regardless of any device or platform that is used.

² Internet Banking is a term used to denote any banking transaction that is done through a website

³ Mobile Banking is a term that is used to carry out banking transactions through a web application. The facilities offered will differ with internet banking.

'customer-centric' thus, it must include human element as well (Akram et al., 2018; Ayo et al., 2016). Attitudes like optimism, pioneering, low level of discomfort and risk perception were needed to use any technology (Boon-itt, 2015). A difference of opinion existed amongst people of different age group on trust. Millennials trusted a virtual environment like online banking whereas the older adults trust a physical bank than a virtual one (Alhabash et al., 2015). Structural assurances were the antidote to make older adults trust online banking. It was needed at the pre-adoption stage of online banking (Montazemi & Qahri-Saremi, 2015). On the gender front, a study in Portugal established that women used e-banking more than men since their risk perception was less. The female population consisted of students, unemployed and retirees. Majority of the respondents were not post graduates and had a meagre income of around 1,250 Euros (Fonseca, 2014). Further, it was found that customers did not opt for internet banking due to the lack of trust on banks' operations, whereas mobile banking was avoided due to the inherent security risk perception (Mishra & Singh, 2015). This shows that the nature of banking technology security is not only technological and attitudinal, but it is organizational as well. With regard to privacy, people felt secure while using their own device for bank transaction than a public kiosk. The absence of customer support while using a public kiosk resulted in increasing privacy anxiety (Blut et al., 2016).

Bank customers in Poland who used online banking had the trust that their banks were able to protect them from cyber intrusions (Szopiński, 2016). Finnish bank customers were less concerned about risk in the internet or mobile banking due to trust (Laukkanen, 2016). Non-users had low levels of trust in online banking. Such non-users needed actions and evidence from banks regarding privacy protection, security level and implemented fraud mechanisms, in order to become users (Riffai et al., 2012). Non-users were also found to be lesser users of the internet for any general purpose. There was a positive relationship between hours spent on the banking device and the familiarity with security issues. Hence, awareness programs had to be crafted based on the level of device usage (Jeske & Schaik, 2017). Whether it was users or non- users, it was crucial to have successful online banking transactions each time a customer had logged in. As the number of successful transactions increased, there was a decrease in security concerns. Further, in case of unsuccessful online banking transactions, a transparent and sincere dealing was expected from the part of banks, in order to build customer confidence (Ong et al., 2017).

Bank's negligence towards security issues would negatively affect customers' trust (Mason and Bohm, 2018). Both the banking sector and the police department were treating cyber frauds as mere cases though the scale of such events were alarmingly rising (Koong et al., 2017). Banks were responsible for the cyber threats that were happening and thus the study placed the thrust on an internal reconstruction and clear service standards (Andaleeb et al., 2016). Customer's trust was based on the positive relationship between

their prior experiences and awareness about fraud prevention measures of banks. It was important to notice especially when a cyber fraud occurred due to a third party breach. Age was a moderating variable in that relationship, whereas income had no role (Hoffmann & Birnbrich, 2012). Banks needed cautious customers who could reduce cyber frauds and increase security (Jansen & Schaik, 2017). Students in an educational institution had general and not contextual awareness on identity theft. A general notion that hackers targeted only the rich was a myth that surrounded them. Lack of time or negligence were the causes of students being unprepared to face identity theft threats (Seda, 2014). Banks were giving general awareness to its customers regarding cybersecurity measures, but there was a need to provide context-specific awareness (Ivaturi & Janczewskib, 2013). A reality check on bank customers' awareness about phishing was conducted. The post-test result revealed that there was an improvement in identification of phishing threats. The awful part was that respondents were not willing to incur software cost to avoid phishing threats (Arachchilage et al., 2016). In addition, age, income, education, hours spent on the internet and the technical background were found in not aiding users' ability to identify phishing websites. It was solely the user awareness programmes that alleviated security issues (Purkait et al., 2014). On the part of bank employees, they had uniform awareness on potential risk involved in online banking transactions. This demonstrated that the bank employees were well equipped to support customers in case of any cyber fraud (Murari and Tater, 2014). In another study in Australia, a comparison between bank employees and selected field employees showed that bank employees were 20 percent more aware of information security than other category of employees (Pattinson et al., 2017).

On the legal end, cyber fraud victims were denied justice by courts due to the complexity involved in collecting online banking transaction evidences from banks. The courts must act diligent while dealing with bank fraud victims and should not rely on banking evidence alone (Mason, 2013). Internet of Things was visionary and helpful aspects for humankind, but it had neglected privacy, individual choice, equality and trust. Such negligence was set to cause drastic impediments if not nipped in the bud. Though regulatory measures were in place to build online banking customers trust, there was a total silence where the Internet of Things (IoT) and online banking merged (Dutton, 2014).

In a world ridden with social media craze, it is necessary to make sure that users do not leak their personal identity on the net. The present system followed by all the banks is to create awareness, but the article of Büchi et al. (2017) pointed at the fallacy such awareness programs had, in the light of ever-changing technology. Even legal rights bestowed upon citizens were deemed useless in such a scenario. Therefore, the paper called for constant skill upgrade of users, data breach notifications, erasure, portability and sealing of private information appended with a certification. Such a holistic approach was viewed to bring more security and relevance for customer rights.

Solutions. The banking industry does accept the fact that single-factor authentication was a failure. In order to overcome this limitation, it was opined to have username and password validation, biometric authentication and embedding device with cryptography code. This opinion put a question on the ubiquity of online banking services (Blauw & Solms, 2014). An effective authentication would mean that the word 'liveness' is redefined. It requires systems to secure authentication details encrypted in a server. The systems must be able to use Artificial Intelligence to check whether the user is real, alive and are under control of the transaction (Wojewidka, 2017). The usage of decision support system was recommended, named Banksealer, to alert banks cybersecurity analysts regarding sporadic spending that were found in a customers bank account, thereby proactively preventing security flaws at the entry level itself. The software prepared real-time spending profile of each customer's bank account in order to keep a tab on any cyber flaws (Carminati et al., 2015).

An enhanced online security performance depended on the maximum disclosures of firms and the existing government regulations (Li, 2015). The top management needed to proactively treat security breaches. Rather, they were merely funding security resources only based on imposed government regulatory norms (Chaturvedi et al., 2014). A compulsory, stringent and transparent policy was needed in order to check cyber crimes. For example, the United States Securities and Exchange Commission (SEC) demands firms to file cyber crime-related issues that occurred each year in the annual report of the company (Clark & Harrell, 2013). Various vulnerability points are spotted in e-banking transaction, hence the data must be made secure. Or else, it will lead to legal, financial and reputational risks for banks. Basias et al. (2013) opined about the introduction of SOA (Service Oriented Architecture) in online banking to counter security threats. Such a framework, maintained by a third party was set to increase security manifold and leave the security threats to the hands of the experts.

Green banking activists were challenged since ATM (Automated Teller Machine) bank transaction bills did have an impact on customer relationship and it was a natural structural assurance agent. Discontinuation of paper bills was seen to bring back customers distrust on banks online banking environment (McNeish, 2015). Such an assurance is impossible in the internet or mobile banking arena. Banks are entering into cloud computing nowadays. Although it is a public storage arena, certain security measures like multi-factor biometric technology and protection gateway are needed. Once the security is in place, banks could speed up transactions, add new features and will be able to get more cloud storage space. This would bring in ease of use and security to customers (Nagaraju & Parthiban, 2015). A survey was conducted among potential online banking users to study their preference over retina scanning, fingerprint scanning and facial recognition technologies. They preferred and trusted fingerprint scanning due to the familiarity they had (Tassabehji & Kamala,

2012). It shows that bringing revolutionary security methods was not enough and instead they have to create familiarity in order to be widely used.

Impacts. Online banking trust has an influence on customers satisfaction and utility perception (Lie'bana-Cabanillas et al., 2013). But, there is an increase in ease of use diminished security (Maditinos et al., 2013). Therefore, ease of use has a negative influence on customer satisfaction. (Sikdar et al., 2015). Ease of use is a part of the solution to enhance Information and Communication Technologies. But there is a price to pay for this solution in the form of loss of security.

Banks need to start seeing banking technology from a customers' attitude perspective. (Akram et al., 2018; Ayo et al., 2016). Customers must have positive attitude towards online banking (Boon-itt, 2015). Following is the brief summary of themes on the above literature, given in Table 1.

Table 1

Brief summary about online banking reviews

<i>Deliberations</i>
<i>Trust</i>
i. Millennials trust a virtual bank more than a physical bank (Alhabash et al., 2015). In order to bring more customers, structural assurance must be given at the pre- adoption stage (Montazemi & Qahri-Saremi, 2015). Non-users need actions and evidence from banks regarding privacy protection, security level and implemented fraud mechanisms, in order to become users (Riffai et al., 2012).
ii. Customers trust banks to protect them from cyber attacks (Szopiński, 2016). Finnish bank customers are an example for this (Laukkanen, 2016). But, Bank's negligence towards security issues would negatively affect customers trust (Mason & Bohm, 2018). Therefore, customers do not opt for internet banking due to the lack of trust on banks operations (Mishra & Singh, 2015).
iii. The more the number of successful transactions, the lesser will be the security concerns of bank customers (Ong et al., 2017).
<i>Risk perception</i>
i. Women used e-banking more than men since their risk perception was less. (Fonseca, 2014).
ii. People felt secure while using their own device for bank transaction than a public kiosk (Blut et al., 2016)

Table 1 (Continue)

<i>Security</i>
<p>i. There is a positive relationship between hours spent on the banking device and the familiarity with security issues (Jeske & Schaik, 2017). Customers trust are based on the positive relationship between customers prior experiences and awareness about banks fraud prevention measures (Hoffmann & Birnbrich, 2012)</p> <p>ii. Both the banking sector and the police department are treating cyber frauds as mere cases (Koong et al., 2017). Banks were responsible for the cyber threats (Andaleeb et al., 2016).</p> <p>iii. Lack of time or negligence are the causes of students being unprepared to face identity theft threats (Seda, 2014). But, banks need cautious customers who could reduce cyber frauds and increase security (Jansen & Schaik, 2017)</p>
<i>Awareness</i>
<p>i. Banks must stop giving general awareness and start giving context-specific awareness to its customers (Ivaturi & Janczewskib, 2013).</p> <p>ii. Bank employees are uniformly aware about cyber security among themselves (Murari & Tater, 2014). Bank employees are 20% more aware about online banking safety than the other employees (Pattinson et al., 2017).</p>
<i>Regulations</i>
<p>i. Courts must act with diligence and should not only rely on banks evidence (Mason, 2013).</p> <p>ii. Internet of Things lacks regulations and therefore it is risky (Dutton, 2014).</p> <p>iii. Legal rights are useless unless proper measures are in place (Büchi et al., 2016).</p>
<i>Solutions</i>
<i>Security</i>
<p>i. Single-factor authentication is a failure (Blauw & Solms, 2014). Artificial Intelligence must be used for authenticating the transaction (Wojewidka, 2017).</p> <p>ii. Spending pattern of each customer helps banks keep track of its' customers' money (Carminati et al., 2015).</p> <p>iii. SOA (Service Oriented Architecture) maintained by a third party will increase security and bring expertise (Basias et al., 2013).</p> <p>iv. People opt for security technology based on previous experience (Tassabehji & Kamala, 2012).</p>
<i>Regulations</i>
<p>i. Companies that follow maximum disclosures of government regulations are found to be more concerned about security issues (Li, 2015). Such a disclosure must be made not out of regulatory compulsion (Chaturvedi et al., 2014). Regulatory bodies need to promote maximum disclosure norms (Clark & Harrell, 2013).</p>

Table 1 (Continue)

<i>Innovation</i>
i. Paper bills are needed as evidence for banking transactions (McNeish, 2015). Secured cloud computing is an answer to ensure that bank transaction evidences are not tampered (Nagaraju & Parthiban, 2015).
<i>Impacts</i>
<i>Trust</i>
i. Online banking trust has an influence on customers satisfaction and utility perception (Lie'bana-Cabanillas et al., 2013). But, ease of use has a negative influence on customer satisfaction (Sikdar et al., 2015).

Following are the potentially open problems that were discussed in the previous studies:

- i. Americans had issues on trust than Malaysians, due to the absence of collective culture (Yuen et al., 2015).
- ii. It is a challenge for banks to create security in developing countries (Susanto et al., 2013).

Internet Banking Security- Deliberations, Solutions and Impact

Deliberations. A look at the traditional banking would show that face-to-face bank transactions used to occur and customers could reach out to a bank employee. In the present online banking context, there was a vacuum in terms of such an interaction. Customers were seeking guarantee in this aspect, if anything goes wrong in the online world (Harrison et al., 2014). Humans were wired to act this way (Upadhyay & Jahanyan, 2016). Bank customers were divided into innovation lovers and laggards. Hence, banks had to offer different benefits to each group. Innovation lovers wanted technology usefulness, whereas laggards wanted technology simplicity (Yousafzai & Yani-de-Soriano, 2012). With changing technology, even bank regulations had changed. This kept bank customers in the dark in the internet banking space. Bashir and Madhavaiah (2014) called for transparency from banks to update customers with recent regulations. Additionally, bank customers that engaged in internet banking were bound for losses in terms of security, money and time (in case of becoming a victim of cyber fraud). These losses were bound to affect intention to use internet banking. In order to prevent it, banks could introduce money back guarantee policies or insure each bank transaction (Martins et al., 2014).

Solutions. Proactive measures from banks were needed in order to build trust. These measures were giving free security software and agreement to indemnify customers from any cyber threats (at banks' convenience and discretion). Awareness programs must be conducted by banks Information Technology officers (Chandio et al., 2013). These awareness programs must be interactive and extensive in nature (Bauer et al., 2017).

Non-users of internet banking were supposed to undergo a trial session of using internet banking. Bank employees would aid such sessions for inviting possible risk concerns and to give a firsthand experience to bank customers on how things work. It was advisable for bank employees to be available over the telephone in order to provide assurance and take proactive security measures during the time of emergency (Patsiotis et al., 2012)

Banks needed to engage in conversation with customers about security factors in internet banking. Such measures would build trust. They could provide firewalls, sophisticated encryption tools and intrusion detection systems, in order to prove that the bank is trustworthy with the money of their customers (Juwaheer et al., 2012; Tarhini et al., 2016). Preparation of risk profiling to authenticate user's web browser during each login would help banks to keep each customers bank accounts in check. Such an exercise would also improve the risk perception of customers (Butler & Butler, 2015).

Impacts. Risk existed in internet banking (Shanmugam et al., 2015). It was due to ample exposure of networks to the outside virtual world (Kesharwani & Tripathy, 2012). There was laxness on the part of banks on validating each transaction. It was suggested to add codes to each transaction in order to resolve any issues pertaining to any failed transaction (Mohammadi, 2015). There were two types of risks at play viz., internal and external risks. Internal risks were lower technical knowledge and lesser ease of use. External risks were failed transactions and internet frauds. When internal risks led to a deficiency in the usage of internet banking, external risks heightened perceived risk attitude of bank customers. Each of these risks needed to be treated separately by banks (Roy et al., 2017). Trust influenced perceived risk more than perceived ease of use. Banks were advised to keep bank customers informed about the movement of their money in the bank account, irrespective of whether it was a charge levied or payments/ receivables made (Bashir & Madhavaiah, 2015). Similarly, unless perceived risk was not taken care of, it was going to hinder convenience (Clemente-Ricolfe, 2017). Perceived risk must be replaced with perceived security in order to raise trust in internet banking (Damghanian et al., 2016). Risk and security were two things that banks were grappling with the terms of internet banking adoption. Young bank customers trusted internet banking more than the older ones due to sound technical background and risk awareness (Giovanis et al., 2012). For certain categories of people like the postponers, opponents and rejectors, for whom the risk perception was negative, had ended up causing rebellion in the form of negative word of mouth. This led to adverse social influence in the society (Mzoughi & M'Sallem, 2013).

Customers wanted web privacy. Web privacy had influence over adopting internet banking, which was moderated by the attitude to use. Only when a bank customer was able to do a transaction with ease and had an assurance on web privacy, he or she will venture to use internet banking (Rawashdeh, 2015). Not only web privacy, but the security and error-free records were also detrimental in producing customer satisfaction (Raza et al.,

2015). There was a need for increased perceived security in bank customers so that initial trust could be built. This further led to the adoption of internet banking. The challenge for banks was in creating sufficient security in developing countries. Such a challenge could be met only by government support in the form of law and funding. It was also found that government support can directly produce initial trust, but cannot compel internet banking usage (Susanto et al., 2013).

Electronic service quality has enhanced both electronic satisfaction and electronic loyalty. Electronic trust was found to be playing a moderating role in this process (Butt & Aftab, 2013, p.6). The effect of service quality on trust was much higher than the effect that trust could have on customer satisfaction (Kundu & Datta, 2015). The electronic trust had the potential to influence perceived usefulness and behavioural intention of bank customers (Mansour, 2016). Cognitive evaluation theory was borrowed to explain the role of motivation in the adoption of internet banking in developing countries. The citizens of such countries were found to undertake internet banking transactions only if they had intrinsic motivation. However, the working of intrinsic motivation was found to be moderated by trust (Akhlaq & Ahmed, 2013).

Issues of trust existed for both users and potential users. There was a cultural nuance with regard to trust issues that divided people. In a study which was conducted on trust issues taking into account the power distance and individualism, Americans had trust issues than Malaysians (Yuen et al., 2015). Trust could enhance performance expectancy and effort expectancy. This was because bank customers felt that using internet banking was something worthwhile investing in. The paper discussed as to how trust was born. Trust in a physical bank was the first step towards using the technology that this same bank provided (Chaouali et al., 2016). It was hard to create initial trust, especially for internet-only banks. Such banks needed to have service level agreements with their customers and needed to prove that each policy was simplified and matched with the banking industry standards (Kaabachi et al., 2017). Trust had a significant influence on the adoption of internet banking (Sharma et al., 2015). The elements of trust were benevolence, competence and integrity from the bankers side, which motivated bank customers to use internet banking (Yiga & Cha, 2014). Once bank customers switched to continued usage, benevolence could be replaced with shared values, since benevolence became subjective for the continued user (Yu et al., 2015).

Following is the brief summary on the above points, given in Table 2.

Table 2

Brief summary about internet banking reviews

<i>Deliberations</i>
<i>Trust</i>
<ul style="list-style-type: none"> i. Internet banking has altered a personal interaction. This creates trust vacuum (Harrison et al., 2014). ii. Money back guarantee policies or insuring each bank transaction helps to preserve the trust of customers on banks (Martins et al., 2014).
<i>Security</i>
<ul style="list-style-type: none"> i. Bank customers are of two types, innovation lovers want technology usefulness and laggards want technology simplicity. Hence, security technology must promote both want technology usefulness and technology simplicity (Yousafzai & Yani-de-Soriano, 2012).
<i>Regulations</i>
<ul style="list-style-type: none"> i. Banks must update customers with latest regulatory changes (Bashir & Madhavaiah, 2014).
<i>Solutions</i>
<i>Trust</i>
<ul style="list-style-type: none"> i. In order to build trust, banks can provide security software for less cost and indemnity agreement (Chandio et al., 2013; Juwaheer et al., 2012; Tarhini et al., 2016). In addition, interactive and extensive awareness programs must be conducted (Bauer et al., 2017). ii. Bank employees need to aid non-users at each juncture during the initial stages of internet banking usage (Patsiotis et al., 2012).
<i>Risk perception</i>
<ul style="list-style-type: none"> i. Preparation of risk profiling to authenticate user's web browser during each login would help improve the risk perception of customers (Butler and Butler, 2015).
<i>Impacts</i>
<i>Security</i>
<ul style="list-style-type: none"> i. Security was compromised since networks were exposed to the outside virtual world (Kesharwani & Tripathy, 2012). Hence, each transaction must be coded and validated in order to aid faster problem resolution (Mohammadi, 2015). ii. Internal security risks create aversion for internet banking and external risks create negative risk perception for bank customers. Each of these risks needed to be treated separately by banks (Roy et al., 2017). iii. Error free transactions led to customer satisfaction (Raza et al., 2015). Electronic service quality enhanced both electronic satisfaction and electronic loyalty (Butt & Aftab, 2013). The effect of service quality on trust was much higher than the effect that trust could have on customer satisfaction (Kundu & Datta, 2015).

Table 2 (Continue)

<i>Trust</i>
i. Bank customers will use internet banking if trust and ease of use exists (Rawashdeh, 2015).
ii. Trust influenced perceived risk more than perceived ease of use (Bashir & Madhavaiah, 2015).
iii. Trust can increase performance expectancy and effort expectancy (Chaouali et al., 2016).
iv. Trust can influence perceived usefulness and behavioural intention of bank customers (Mansour, 2016).
v. Intrinsic motivation to use internet banking is triggered by trust (Akhlaq & Ahmed, 2013).
vi. Young bank customers trusted internet banking more than the older (Giovanis et al., 2012).
vii. Initial trust must be formed through service level agreements between the bank and the customers ((Kaabachi et al., 2017). It can be also formed through benevolence, competence and integrity from the bank (Yiga & Cha, 2014). Once bank customers switched to continued usage, benevolence could be replaced with shared values (Yu et al., 2015).
<i>Risk</i>
i. Lack of attention to perceived risk would aggravate inconvenience (Clemente-Ricolfe, 2017). Perceived risk must be replaced with perceived security in order to raise trust in internet banking (Damghanian et al., 2016).
<i>Risk perception</i>
i. For certain categories of people like the postponers, opponents and rejectors, for whom the risk perception was negative, had ended up causing rebellion in the form of negative word of mouth. This led to adverse social influence in the society (Mzoughi & M'Sallem, 2013).

Following are the potentially open problems that were discussed in the previous studies:

Americans had issues on trust than Malaysians, due to the absence of collective culture (Yuen et al., 2015).

It is a challenge for banks to create security in developing countries (Susanto et al., 2013).

Mobile Banking Security -Deliberations, Solutions and Impact

Deliberations. There was no communication from the bank towards its customers on legal procedures in case of cyber frauds. In such cases, it was better if the banks could help the customers on legally carrying out the claim procedure (Purwanegara et al., 2014). The law was also not clear in punishing the guilty. In most of the cases, it was the bank which got accused. Ashta (2017) suggested for a case-by-case analysis. In cases where customers were negligent, they could be held guilty, whereas in cases where it was found that the network was insecure, the bank, service provider and the mobile operator could be held liable. Failure in the creation of awareness about safety measures was legally pointed as the guilt of banks. Mobile money economy needed laws that are both risk sensitive as well as transaction sensitive (Wonglimpiyarat, 2014).

Mobile banking users were of the opinion that it was not the banking institution that they feared, but rather it was the technology (Makanyeza, 2017). It was a norm that banks used marketing media to allay the fears caused by various risks involved in mobile banking. The banks were urged to boost up the value addition that a user would get instead of stressing on the risks that were inherent in a mobile banking environment (Glavee-Geo et al., 2017). Employing different marketing strategy as per the risk profile of users was an option that could be looked into. For frequent users, marketing of mobile banking could cancel psychological risk whereas, for infrequent users, marketing of mobile banking could cancel both financial and psychological risk (Chen, 2013). A brand name which offered trust was considered to be vital while offering mobile banking services (Tobbin, 2012). Mobile banking could not follow penetration pricing strategy which the mobile operators followed rather it had to follow skimming strategy, in order to meet security cost. To sum up, offering low-cost service and putting customers at risk with low-security level was not advisable for banks (Tran & Corner, 2016). Mobile phones were three times susceptible to phishing attacks than a desktop computer. The difference in the functioning of the system is the reason for such vulnerability (Goel & Jain, 2017). Scan and pay model lessened mobile payment process time, but such a benefit had been overshadowed by concerns about its security. It was observed that innovation had clearly let down users in this regard, without the backing of a robust security system (Taylor, 2016).

Solutions. A slew of solutions to increase mobile banking security were suggested based on the utility as follows. The smartphones ever-growing storage space was an indirect potential threat for stealing critical data that was stored in these phones (Das & Khan, 2016). Fingerprint biometric technology could be used in smartphones, using which online transactions could be undertaken. The fingerprint so collected by the banks would be encrypted for authentication. This could prevent security breach and misuse (Belkhede et al., 2012). Selfie was a new trend among millennials. In this context, asking facial recognition for bank transaction authentication is a near future possibility (Cook, 2017). Payments must be tokenized through identification numbers. This was in order to increase users privacy. None of the users information were revealed as it was eclipsed by the token which was issued. Organizations needed to register with the Token Service Providers (TSPs) to authenticate each token received (Yu et al., 2017). A model was developed by Bojjagani and Sastry (2017) for both smart and feature phones. It avoided storage of any critical bank transaction data. A 160 bytes sized encrypted message encoder known as P-224 could send the authentication details securely.

Non-repudiation of transactions must be focused rather than focusing on authentication and integrity of data that was transferred. Encryption of data was still alien in mobile payments and therefore a model known as Mobile Payment Consortia System (MPCS) using Public Key Interface (PKI) was suggested (Britto et al., 2012).

Impacts. Trust was a significant factor which reflected the mobile banking application's security character, the integrity of the information technology team and the awareness programs that banks organize (Chandio et al., 2013). Trust influenced customer loyalty towards mobile phone operators as well. It is because users conducted sensitive transactions like mobile banking over the mobile phone operator's network (de Reuver et al., 2015). Trust decided the pathway of each individual's attitude towards mobile banking (Kumar et al., 2017). Non-users lacked initial trust because third parties existed apart from banks (Xin et al., 2015). They needed structural assurances as well as familiarity (Zhou, 2012). Web applications were a means for banks to know customers more closely and also to negate trust deficiency (Berraies et al., 2017). The mere usage of web application technology was not going to help; rather there was a cycle that bank customers needed to go through when it comes in gaining initial trust. The cycle started with the influence of task-technology fit on performance expectancy, and then influence initial trust, which was an antecedent in adopting mobile banking (Oliveira et al., 2014). New users needed privacy controls and regulatory aspects in place before adopting mobile banking (Duane et al., 2014). The mediating effect of trust grew stronger when self-learning happened in customers, which influenced customers intention to use mobile banking (Shaw, 2014). Trust was a product of good service quality and was moderated by security. It had a positive significance over customer satisfaction. However, mobile banking interface had no role to play in building trust (Arcand et al., 2017). But, system quality did influence trust (Chemingui & Lallouna, 2013). With regard to the unbanked, responsible agents must be employed who can transfer money through mobile banking and thereby increase trust (Tobbin, 2012). It was trust and self-efficacy of the user that led to adopting mobile banking (Shankar & Datta, 2018).

Perceived risk and trust were used by Alalwan et al. (2016) as independent variables. A negative risk perception was a deterrent towards the adoption of mobile banking. This was attributed to the nature of mobile banking which was heterogeneous, uncertain and intangible. There was growing negative risk perception about information content and the nature of mobile banking (Sreejesh et al., 2016). All the customers would not have the same level of risk perception and it might get changed depending on the skills that each customer had (Ozturk et al., 2017). Perceived risk and perceived control had a significant influence on the adoption of mobile banking for users in urban cities. But, it was only perceived control which was predominant for users in metropolitan cities (Gupta et al., 2017). Perceived risk was divided into performance risk and privacy risk. Both such risks have negatively affected the usage of mobile payments (Khalilzadeh et al., 2017). Even in such rising risk environment, any user with a positive attitude was bound to adopt mobile banking (Garrett et al., 2014). Such a positive attitude was because of low perceived risk (Mohammadi, 2015). With regard to how non-users perceived risk, they even feared a

simple security feature like a PIN (Personal Identification Number), due to fear of theft (Sohail & Al-Jabrib, 2014).

A breach in privacy and confidentiality were found to discourage mobile banking adoption (Vaithilingam et al., 2013). If customers had a prior online shopping experience, privacy concerns about mobile payments were set to come down (Su et al., 2018). During a survey conducted among the young respondents, it was found that they were not affected monetarily or security wise. It was the fear of social rejection and the system performance failure that caused inhibition in adopting mobile banking (Yadav et al., 2015). In another study, among generation Y, it was found that security had a negative relationship with hedonic motivation to use mobile banking (Boonsiritomachai & Pitchayadejanant, 2017). Full-time employees were more worried about the risk factors when compared to students, who were only bothered about performance efficiency (Bhatiasevi, 2016). Although trust was focused on being the sole ingredient for adopting mobile banking, another study pointed at the need to add both trust and perceived risk (Slade et al., 2015). On the continuation of usage of mobile payment, aversion to risk still existed in the minds of the consumers (Cao et al., 2018). But such a risk apprehension was not about the mobile payment provider but rather it was about technology security (Thakur, 2014). Though smartphones were able to provide hedonic benefits and utility, when it came to payments, privacy and psychological risks would fail mobile payments adoption (Cocosila & Trabelsi, 2016). Smartphone users did not follow efficient smartphone security practices as per a survey conducted among students (Jones & Chin, 2015). The challenge of facing hackers lied in the fact that it was difficult to identify legitimate users. In developing world, where mobile phone Subscriber Identification Module (SIM) were shared or having ownership to more than one individual, there were all possible chances of losing money and privacy, within the customers known circle (Kizzaa, 2013). This made customer redressal for banks harder. However, on the brighter side, technology advancement was a positive sign that risks could come down and adoption rate of mobile banking would considerably pickup thereafter (Mullan et al., 2017). Social influence did reduce perceived risk in potential users of mobile banking. Such a finding was found in collective cultures that existed in China and India (Yang et al., 2012).

A survey in the United Kingdom (UK) revealed that customers were pitted against risk and trust in mobile payments (Slade et al., 2015). Mobile payments offered by banks were considered to be trustworthy than retail mobile payment providers or mobile operators (Tran & Corner, 2016). Banks were trusted since their work code stressed on the obligation to maintain secrecy about the bank customers account details. Such a trust was going to compensate the risks that customers faced. On another front, customers did acknowledge the benefits of small payments made in tolls or for using public transport. Such benefits were going to counterbalance the risks that customers face (Hampshire, 2017). Customers could savour such benefits only when they became a user and experienced such benefits

firsthand. Therefore, risks were prevalent and were hard to stop, but banks could focus on giving risk assurance, benefits and trust (Shaikh and Karjaluo, 2015). With regard to experiencing benefits, customers must be able to feel that promised benefits were delivered. If there was a bad experience, it needed to be rectified by undertaking feedback from the customer (Nel & Boshoff, 2017). Risk had more prominence in the continued usage stage whereas trust carried prominence in the pre-adoption stage (Zhou, 2013). Although the study found that trust completely did not go out of a continued usage stage, it had an indirect effect on intention to continue to use mobile payments. In the continued usage space, the importance of confirmation was stressed. Confirmation from the bank about each transaction boosted trust, customer satisfaction and perceived usefulness. It allayed privacy concerns (Susanto et al., 2016). Moreover, confirmation received from government agencies would be comparatively more convincing and satisfying for mobile banking users (Upadhyay & Chattopadhyay, 2015). Publicizing the mobile banking security measures undertaken by the bank in their website could lead to wider transparency and increased trust (Malaquias & Hwang, 2016).

Following is the brief summary on the above points, given in Table 3.

Table 3

Brief summary about mobile banking reviews

<i>Deliberations</i>
<i>Regulations</i>
<ul style="list-style-type: none"> i. Banks need to help customers in claiming losses in case of cyber frauds (Purwanegara et al., 2014). ii. Courts must not deal with bank transactions based on the precedents; rather it must be on a case-by-case basis (Ashta, 2017). Hence, Mobile banking needed laws that are both risk sensitive as well as transaction sensitive (Wonglimpiyarat, 2014).
<i>Risk perception</i>
<ul style="list-style-type: none"> i. Mobile banking users feared technology (Makanyeza, 2017). ii. Mobile banking advertisement must focus on benefits rather than risks (Glavee-Geo et al., 2017). Marketing strategy must be different between frequent and infrequent users (Chen, 2013). A brand name which offers trust was considered to be vital while offering mobile banking services (Tobbin, 2012).
<i>Security</i>
<ul style="list-style-type: none"> i. In the name of offering services at a lower cost, security must not be compromised (Tran & Corner, 2016). In that aspect, scan and pay model was a failure (Taylor, 2016). ii. Mobile phones were three times susceptible to phishing attacks than a desktop computer due to the varying system architectures (Goel & Jain, 2017).

Table 3 (Continue)

<i>Solutions</i>
<i>Security</i>
<ul style="list-style-type: none"> i. Fingerprint biometric technology should be encrypted and authenticated for safer use (Belkhede et al., 2012). ii. Selfie usage in smartphones would aid facial recognition for bank transaction authentication (Cook, 2017). iii. Tokenization of Payments using identification numbers will help keep bank transactions hidden from intruders (Yu et al., 2017). iv. Banking security technology must shift from authentication to non-repudiation of bank transactions (Britto et al., 2012).
<i>Impacts</i>
<i>Trust</i>
<ul style="list-style-type: none"> i. Trust depends on mobile banking application's security character, the information technology teams integrity and the awareness programs that banks organize (Chandio et al., 2013). Trust is also based upon mobile phone operators (de Reuver et al., 2015). ii. Initial trust starts with task-technology fit on performance expectancy (Oliveira et al., 2014). It must be supplemented with self-learning (Shaw, 2014). Trust and self-efficacy leads to mobile banking adoption (Shankar & Datta, 2018). iii. Trust is created out of good service quality (Arcand et al., 2017). iv. Trust and perceived risk must go hand in hand (Slade et al., 2015). v. Mobile payments offered by banks were considered to be trustworthy than retail mobile payment providers or mobile operators (Tran & Corner, 2016). vi. Confirmation from the bank about each transaction boosted trust, customer satisfaction and perceived usefulness (Susanto et al., 2016). Moreover, confirmation received from government agencies would be comparatively more convincing and satisfying for mobile banking users (Upadhyay & Chattopadhyay, 2015).
<i>Risk perception</i>
<ul style="list-style-type: none"> i. Non-users dread using mobile banking due to the existence of third parties (Xin et al., 2015). They even feared a simple security feature like a PIN (Personal Identification Number) (Sohail & Al-Jabrib, 2013). They need structural assurances and familiarity to overcome this aversion (Zhou, 2012). They need the help of agents, in some cases (Tobbin, 2012). ii. A negative risk perception was a deterrent towards the adoption of mobile banking (Alalwan et al., 2016). It was due to the information content and the nature of mobile banking (Sreejesh et al., 2016). But, a customer with positive attitude would overcome negative perception (Garrett et al., 2014).

Table 3 (Continue)

Risk perception

iii. Risk perception changes depending on the skills that each customer had (Ozturk et al., 2017). Perceived risk and perceived control influenced the adoption of mobile banking for urban city users. It was only perceived control for metropolitan city users (Gupta et al., 2017).

iv. Frequent users were still averse to risk (Cao et al., 2018).

v. Risk removed the hedonic motivation out of mobile banking (Cocosila & Trabelsi, 2016).

vi. Social influence reduced perceived risk in potential users of mobile banking (Yang et al., 2012).

Security

i. Privacy and confidentiality breach discouraged mobile banking adoption (Vaithilingam et al., 2013). If customers had a prior online shopping experience, privacy concerns about mobile payments were set to come down (Su et al., 2018).

ii. Security had a negative relationship with hedonic motivation to use mobile banking (Boonsiritomachai & Pitchayadejanant, 2017).

iii. Apart from security, the fear of social rejection and the system performance failure causes aversion to mobile banking (Yadav et al., 2015).

iv. Full-time employees were more worried about security than students (Bhatiasevi, 2015).

v. Publicizing the mobile banking security measures undertaken by the bank in the website could lead to wider transparency and increased trust (Malaquias & Hwang, 2016).

Following are the potentially open problems that were discussed in the previous studies:

A smartphones' ever-growing storage space was an indirect potential threat for stealing critical data that was stored in these phones (Das & Khan, 2016) Smartphone users were poor at security practices (Jones & Chin, 2015).

Frequent changes in Subscriber Identification Module (SIM) makes it hard for banks to authenticate its customers (Kizzaa, 2013).

CONCLUSION, SCOPE AND LIMITATIONS OF THE STUDY

The intensity of trust wavered between the computer (website) and smartphone (web application). There were studies still undertaken to prove the credibility of each device. Previous studies also revolved around the familiarity and the age of respondents who handled online banking for quite a long time. It was not able to set a benchmark stating the optimum level of years needed to call someone an established online banking user.

However, each of these devices was found to possess security characteristics of their own. Both the computer and the smartphone had external cyber threats, the cost involved in overcoming security issues, adequate awareness, owning up the security of the devices. Bank customers were never ready to take up the blame. Mobile phone users were more vulnerable than desktop users since the level of security that a desktop user would take to secure the device was seen to be much higher. Moreover, ignorance of a mobile phone's operational function was another reason (Kiljan et al., 2018; Zhang et al., 2017).

Protection agencies and banks were called to avoid victimization of online banking users. It also challenged the training and awareness methodology effectiveness which needed upgrading and loopholes to be plugged up. There was a missing link that awareness programs had. Such programs were deemed to be information dispensing platforms rather than hands-on training venues. "Did security upgrades kill ubiquity?" was a relevant question that was pointed out.

The core anxiety that existed both for non-users and users was assurance. This was echoed in several papers. A focus on how structural assurances could be provided and its effect on increasing electronic trust could be looked into. The role of how structural assurances and physical banks support played a major part in reducing security apprehensions could not be denied. If online banking and mobile banking were tools that banks used to reach the doorsteps of customers, the same enthusiasm from banks never existed when it came to the security of these devices while undertaking banking transactions. With regard to the web application, bank customers apprehension existed on the accounts that were vulnerable in the hands of third party service providers.

With regard to smartphones or computers, it was better to employ facial recognition security system while banking. Such a technology was emerging and ubiquitous. It promised far superior security when compared to other biometric systems, since it took the control from humans and placed it on machines in order to maintain integrity in authentication (Xiao & Yang, 2010). Studies could focus on the acceptability of such a technology among users for long-term usage.

As time passes by, the debate as to whether the bank or the customer was responsible for the cybersecurity issues have not yet reached a consensus. Ease of usage was considered hindrance for the adoption of online banking. Such a notion had been questioned now, on the premise of lack of security in online banking. Taking TAM (Technology Acceptance Model) as the base, many researchers argued regarding the relevance of trust. There was still a confusion on what trust influenced and did not.

As this paper analyzed past trends, it was observed that adoption of mobile banking was the prime arena in which security was discussed. It did not matter what device was used, but rather it was the open network that was common to both computer and smartphones that led to security issues. Neither of the devices scored higher with regard to the degree

of risk, rather, the risk was found to be prevalent. Each solution discussed was unique, however, challenges existed when it came to implementation due to time and cost that was involved. As technology became redundant, so did the solutions. Hence, a sustainable solution that would keep bank customers safe continued as a quest for researchers in the years to come. However, customers believed that regardless of the smartphone or the desktop, they trusted that bank offered devices to be safer than user-owned devices (McGill & Thompson, 2017). Figure 3 is given below as a snapshot to the differences between internet and mobile banking.

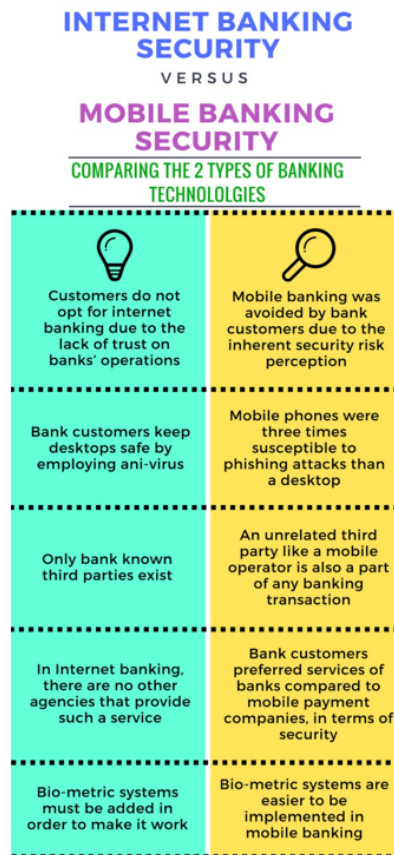


Figure 3. Differences in technology security of internet and mobile banking

This paper had focused on the banking cyber security aspects of computer and mobile phone devices since both the devices were the centre of attention when it came to Information and Communication Technology (ICT) studies. The computer was the basic device out of which other devices have evolved over time and smartphones are devices that have reached the masses extensively. The study had followed the traditional method of evaluating, analyzing and synthesizing the past six years literature works of various

authors. This paper dealt with factors that were both conceptual as well as technical aspect of security issues. An effort had been made to balance both, but it was done by keeping the conceptual aspect as the base for all the technical solutions discussed. At various junctures, the paper had also taken into account the security issues and challenges that the device produces, wherein the banking element would seem missing. Solutions discussed were not an end for security issues. Deliberations that were mentioned focused on the prevalent thoughts about bank technology security doing rounds in various circles. Impacts inferred noted on the pattern of behaviour that both humans and technology showed under various circumstances.

An aligning area was the emerging electronic commerce and mobile commerce industry which had a connection with mobile payment aspect. This paper had not ventured into those aspects.

REFERENCES

- Akhlaq, A., & Ahmed, E. (2013). The effect of motivation on trust in the acceptance of internet banking in a low income country. *International Journal of Bank Marketing*, 31(2), 115-125.
- Akram, R. N., Chen, H. H., Lopez, J., Sauveron, D., & Yang, L. T. (2018). Security, privacy and trust of user-centric solutions. *Future Generation Computer Systems*, 80, 417-420.
- Alalwan, A. A., Dwivedi, Y. K., & Rana, N. P. (2017). Factors influencing adoption of mobile banking by Jordanian bank customers: Extending UTAUT2 with trust. *International Journal of Information Management*, 37(3), 99-110.
- Alhabash, S., Jiang, M., Brooks, B., Rifon, N. J., LaRose, R., & Cotten, S. R., (2015). *Online banking for the ages: Generational differences in institutional and system trust*. Bradford, UK: Emerald Group Publishing Limited.
- Andaleeb, S. S., Rashid, M., & Rahman, Q. A. (2016). A model of customer-centric banking practices for corporate clients in Bangladesh. *International Journal of Bank Marketing*, 34(4), 458-475.
- Arachchilage, N. A. G., Love, S., & Beznosov, K. (2016). Phishing threat avoidance behaviour: An empirical investigation. *Computers in Human Behavior*, 60, 185-197.
- Arcand, M., PromTep, S., Brun, I., & Rajaobelina, L. (2017). Mobile banking service quality and customer relationships. *International Journal of Bank Marketing*, 35(7), 1068-1089.
- Ashta, A. (2017). Evolution of mobile banking regulations: a case study on legislator's behavior. *Strategic Change*, 26(1), 3-20.
- Ayo, C. K., Oni, A. A., Adewoye, O. J., & Eweoya, I. O. (2016). E-banking users' behaviour: E-service quality, attitude, and customer satisfaction. *International Journal of Bank Marketing*, 34(3), 347-367.
- Bashir, I., & Madhavaiah, C. (2014). Determinants of young consumers' intention to use Internet banking services in India. *Vision*, 18(3), 153-163.

- Bashir, I., & Madhavaiah, C. (2015). Consumer attitude and behavioural intention towards Internet banking adoption in India. *Journal of Indian Business Research*, 7(1), 67-102.
- Basias, N., Themistocleous, M., & Morabito, V. (2013). SOA adoption in e-banking. *Journal of Enterprise Information Management*, 26(6), 719-739.
- Bauer, S., Bernroider, E. W., & Chudzikowski, K. (2017). Prevention is better than cure! Designing information security awareness programs to overcome users' non-compliance with information security policies in banks. *Computers and Security*, 68, 145-159.
- Belkhebe, M., Gulhane, V., & Bajaj, P. (2012). Biometric mechanism for enhanced security of online transaction on Android system: A design approach. In *Proceedings of 14th International Conference on Advanced Communication Technology (ICACT)* (pp. 1193-1197). Pyeong Chang, Korea (South).
- Berraies, S., Ben Yahia, K., & Hannachi, M. (2017). Identifying the effects of perceived values of mobile banking applications on customers: Comparative study between baby boomers, generation X and generation Y. *International Journal of Bank Marketing*, 35(6), 1018-1038.
- Bhatiasevi, V. (2016). An extended UTAUT model to explain the adoption of mobile banking. *Information Development*, 32(4), 799-814.
- Blauw, F., & Solms, S. V., (2014). Streamlined approach to online banking authentication in South Africa and Europe. In *Proceedings of IST-Africa 2014 Conference* (pp. 1-10). Dublin, Ireland.
- Blut, M., Wang, C., & Schaefer, K. (2016). Factors influencing the acceptance of self-service technologies: A meta-analysis. *Journal of Service Research*, 19(4), 396-416.
- Bojjagani, S., & Sastry, V. N. (2017). A secure end-to-end SMS-based mobile banking protocol. *International Journal of Communication Systems*, 30(15), 1-19.
- Boon-itt, S. (2015). Managing self-service technology service quality to enhance e-satisfaction. *International Journal of Quality and Service Sciences*, 7(4), 373-391.
- Boonsiritomachai, W., & Pitchayadejanant, K. (2017). Determinants affecting mobile banking adoption by generation Y based on the Unified Theory of Acceptance and Use of Technology Model modified by the Technology Acceptance Model concept. *Kasetsart Journal of Social Sciences*, 30, 1-10.
- Britto, S., Kumar, R., & Rabara, S. A. (2012). An end-to-end secure mobile payment system using public key infrastructure system. *Journal of Algorithms and Computational Technology*, 6(3), 395-409.
- Büchi, M., Just, N., & Latzer, M. (2017). Caring is not enough: The importance of Internet skills for online privacy protection. *Information, Communication and Society*, 20(8), 1261-1278.
- Butler, M., & Butler, R. (2015). Investigating the possibility to use differentiated authentication based on risk profiling to secure online banking. *Information and Computer Security*, 23(4), 421-434.
- Butt, M. M., & Aftab, M. (2013). Incorporating attitude towards Halal banking in an integrated service quality, satisfaction, trust and loyalty model in online Islamic banking context. *International Journal of Bank Marketing*, 31(1), 6-23.
- Cao, X., Yu, L., Liu, Z., Gong, M., & Adeel, L. (2018). Understanding mobile payment users' continuance intention: A trust transfer perspective. *Internet Research*, 28(2), 456-476.

- Carminati, M., Caron, R., Maggi, F., Epifani, I., & Zanero, S. (2015). BankSealer: A decision support system for online banking fraud analysis and investigation. *Computers and Security*, 53, 175-186.
- Chandio, F. H., Irani, Z., Abbasi, M. S., & Nizamani, H. A. (2013). Acceptance of online banking information systems: an empirical case in a developing economy. *Behaviour and Information Technology*, 32(7), 668-680.
- Chaouali, W., Yahia, I. B., & Souiden, N. (2016). The interplay of counter-conformity motivation, social influence, and trust in customers' intention to adopt Internet banking services: The case of an emerging country. *Journal of Retailing and Consumer Services*, 28, 209-218.
- Chaturvedi, M., Narain Singh, A., Prasad Gupta, M., & Bhattacharya, J. (2014). Analyses of issues of information security in Indian context. *Transforming Government: People, Process and Policy*, 8(3), 374-397.
- Chemingui, H., & Lallouna, H. B. (2013). Resistance, motivations, trust and intention to use mobile financial services. *International Journal of Bank Marketing*, 31(7), 574-592.
- Chen, C. (2013). Perceived risk, usage frequency of mobile banking services. *Managing Service Quality: An International Journal*, 23(5), 410-436.
- Clark, M., & Harrell, C. E. (2013). Unlike chess, everyone must continue playing after a cyber-attack. *Journal of Investment Compliance*, 14(4), 5-12.
- Clemente-Ricolfe, J. S. (2017). Consumer perceptions of online banking in Spain using netnography: A positioning story. *International Journal of Bank Marketing*, 35(6), 966-982.
- Cocosila, M., & Trabelsi, H. (2016). An integrated value-risk investigation of contactless mobile payments adoption. *Electronic Commerce Research and Applications*, 20, 159-170.
- Cook, S. (2017). Selfie banking: is it a reality? *Biometric Technology Today*, 3, 9-11.
- Damghanian, H., Zarei, A., & Kojuri, M. A. S. (2016). Impact of perceived security on trust, perceived risk, and acceptance of online banking in Iran. *Journal of Internet Commerce*, 15(3), 214-238.
- Das, A., & Khan, H. U. (2016). Security behaviors of smartphone users. *Information and Computer Security*, 24(1), 116-134.
- de Reuver, M., Nikou, S., & Bouwman, H. (2015). The interplay of costs, trust and loyalty in a service industry in transition: The moderating effect of smartphone adoption. *Telematics and Informatics*, 32(4), 694-700.
- Duane, A., O'Reilly, P., & Andreev, P. (2014). Realising M-Payments: modelling consumers' willingness to M-pay using smart phones. *Behaviour and Information Technology*, 33(4), 318-334.
- Dutton, W. H. (2014). Putting things to work: Social and policy challenges for the internet of things. *Info*, 16(3), 1-21.
- Fonseca, J. R. (2014). E-banking Culture: A comparison of EU 27 countries and Portuguese case in the EU 27 retail banking context. *Journal of Retailing and Consumer Services*, 21(5), 708-716.
- Febelfin. (2013). *Safe internet banking? Here is some useful advice!* Retrieved March 25, 2018, from <https://www.safeinternetbanking.be/en/safe-internet-banking-here-some-useful-advice>.

- Garrett, J. L., Rodermund, R., Anderson, N., Berkowitz, S., & Robb, C. A. (2014). Adoption of mobile payment technology by consumers. *Family and Consumer Sciences Research Journal*, 42(4), 358-368.
- Giovanis, A. N., Binioris, S., & Polychronopoulos, G. (2012). An extension of TAM model with IDT and security/privacy risk in the adoption of internet banking services in Greece. *EuroMed Journal of Business*, 7(1), 24-53.
- Glavee-Geo, R., Shaikh, A. A., & Karjaluoto, H. (2017). Mobile banking services adoption in Pakistan: Are there gender differences?. *International Journal of Bank Marketing*, 35(7), 1090-1114.
- Goel, D., & Jain, A. K. (2017). Mobile phishing attacks and defence mechanisms: state of art and open research challenges. *Computers and Security*, 73, 519-544.
- Gupta, S., Yun, H., Xu, H., & Kim, H. W. (2017). An exploratory study on mobile banking adoption in Indian metropolitan and urban areas: a scenario-based experiment. *Information Technology for Development*, 23(1), 127-152.
- Hampshire, C. (2017). A mixed methods empirical exploration of UK consumer perceptions of trust, risk and usefulness of mobile payments. *International Journal of Bank Marketing*, 35(3), 354-369.
- Harrison, T. S., Onyia, O. P., & Tagg, S. K. (2014). Towards a universal model of internet banking adoption: Initial conceptualization. *International Journal of Bank Marketing*, 32(7), 647-687.
- Hoffmann, A. O., & Birnbrich, C. (2012). The impact of fraud prevention on bank-customer relationships: An empirical investigation in retail banking. *International Journal of Bank Marketing*, 30(5), 390-407.
- Ivaturi, K., & Janczewski, L. (2013). Social engineering preparedness of online banks: An Asia-Pacific perspective. *Journal of Global Information Technology Management*, 16(4), 21-46.
- Jansen, J., & Schaik, P. V. (2017). Comparing three models to explain precautionary online behavioural intentions. *Information and Computer Security*, 25(2), 165-180.
- Jeske, D., & Schaik P. V. (2017). Familiarity with Internet threats: Beyond awareness. *Computers and Security*, 66, 129-141.
- Jones, B. H., & Chin, A. G. (2015). On the efficacy of smartphone security: A critical analysis of modifications in business students' practices over time. *International Journal of Information Management*, 35(5), 561-571.
- Juwaheer, T. D., Pudaruth, S., & Ramdin, P. (2012). Factors influencing the adoption of internet banking: A case study of commercial banks in Mauritius. *World Journal of Science, Technology and Sustainable Development*, 9(3), 204-234.
- Kaabachi, S., Mrad, S. B., & Petrescu, M. (2017). Consumer initial trust toward internet-only banks in France. *International Journal of Bank Marketing*, 35(6), 903-924.
- Kesharwani, A., & Tripathy, T. (2012). Dimensionality of perceived risk and its impact on Internet banking adoption: An empirical investigation. *Services Marketing Quarterly*, 33(2), 177-193.
- Khalilzadeh, J., Ozturk, A. B., & Bilgihan, A. (2017). Security-related factors in extended UTAUT model for NFC based mobile payment in the restaurant industry. *Computers in Human Behavior*, 70, 460-474.
- Kiljan, S., Vranken, H., & Eekelen, M. V. (2018). Evaluation of transaction authentication methods for online banking. *Future Generation Computer Systems*, 80, 430-447.

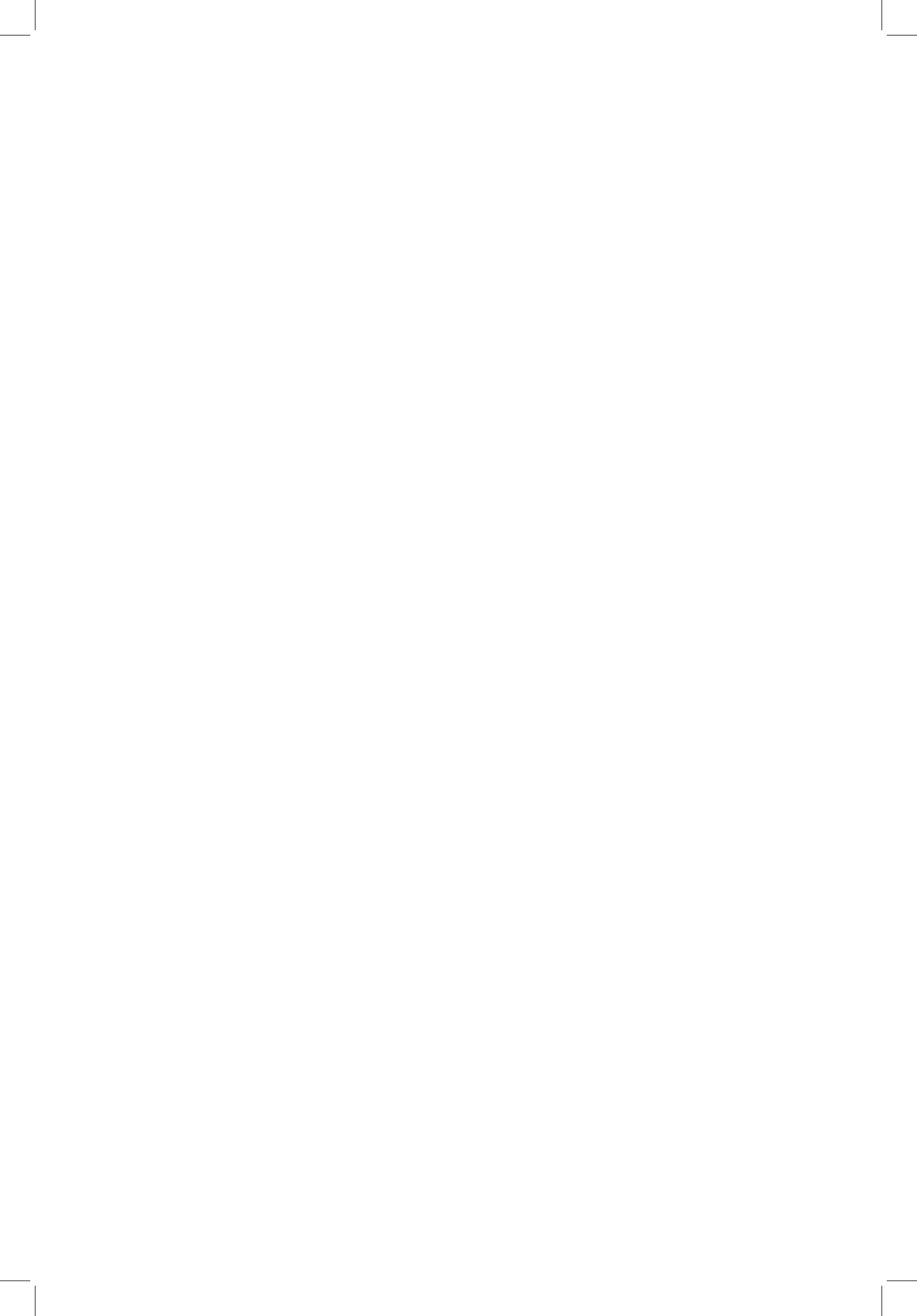
- Kizza, J. M. (2013). Mobile money technology and the fast disappearing African digital divide. *African Journal of Science, Technology, Innovation and Development*, 5(5), 373-378.
- Koong, K. S., Liu, L. C., Qin, H., & Ying, T. (2017). Occurrences of online fraud complaints: 2002 through 2015. *International Journal of Accounting and Information Management*, 25(4), 484-504.
- Kumar, V., Kumar, U., & Shareef, M. A. (2017). Mobile banking: A tradeoff between mobile technology and service for consumer behavioural intentions. *Transnational Corporations Review*, 9(4), 319-330.
- Kundu, S., & Datta, S. K. (2015). Impact of trust on the relationship of e-service quality and customer satisfaction. *EuroMed Journal of Business*, 10(1), 21-46.
- Laukkanen, T. (2016). Consumer adoption versus rejection decisions in seemingly similar service innovations: The case of the Internet and mobile banking. *Journal of Business Research*, 69(7), 2432-2439.
- Li, D. C. (2015). Online Security Performances and Information Security Disclosures. *Journal of Computer Information Systems*, 55(2), 20-28.
- Liébana-Cabanillas, F., Munoz-Leiva, F., & Rejón-Guardia, F. (2013). The determinants of satisfaction with e-banking. *Industrial Management and Data Systems*, 113(5), 750-767.
- Maditinos, D., Chatzoudes, D., & Sarigiannidis, L. (2013). An examination of the critical factors affecting consumer acceptance of online banking: A focus on the dimensions of risk. *Journal of Systems and Information Technology*, 15(1), 97-116.
- Makanyeza, C. (2017). Determinants of consumers' intention to adopt mobile banking services in Zimbabwe. *International Journal of Bank Marketing*, 35(6), 997-1017.
- Malaquias, F. F., & Hwang, Y. (2016). Trust in mobile banking under conditions of information asymmetry: Empirical evidence from Brazil. *Information Development*, 32(5), 1600-1612.
- Mansour, K. B. (2016). An analysis of business' acceptance of internet banking: An integration of e-trust to the TAM. *Journal of Business and Industrial Marketing*, 31(8), 982-994.
- MarkMonitor. (2014). *MarkMonitor Press Release*. Retrieved March 18, 2018, from <https://www.markmonitor.de/brand-protection-domain-management-resources/press-releases/release/latest-research-finds-one-in-six-online-bargain-hunters-duped-by-sites-selling-counterfeit-goods>.
- Martins, C., Oliveira, T., & Popovič, A. (2014). Understanding the Internet banking adoption: A unified theory of acceptance and use of technology and perceived risk application. *International Journal of Information Management*, 34(1), 1-13.
- Mason, S. (2013). Electronic banking and how courts approach the evidence. *Computer Law and Security Review*, 29(2), 144-151.
- Mason, S., & Bohm, N. (2018). Banking and fraud. *Computer Law and Security Review*, 33, 237-241.
- McGill, T., & Thompson, N. (2017). Old risks, new challenges: exploring differences in security between home computer and mobile device use. *Behaviour and Information Technology*, 36(11), 1111-1124.
- McNeish, J. (2015). Consumer trust and distrust: Retaining paper bills in online banking. *International Journal of Bank Marketing*, 33(1), 5-22.

- Mishra, V., & Singh, V. (2015). Selection of appropriate electronic banking channel alternative: Critical analysis using analytical hierarchy process. *International Journal of Bank Marketing*, 33(3), 223-242.
- Mohammadi, H. (2015). A study of mobile banking usage in Iran. *International Journal of Bank Marketing*, 33(6), 733-759.
- Montazemi, A. R., & Qahri-Saremi, H. (2015). Factors affecting adoption of online banking: A meta-analytic structural equation modeling study. *Information and Management*, 52(2), 210-226.
- Mullan, J., Bradley, L., & Loane, S. (2017). Bank adoption of mobile banking: stakeholder perspective. *International Journal of Bank Marketing*, 35(7), 1154-1174.
- Murari, K., & Tater, B. (2014). Employee's attitude towards adoption of IT-based banking services: A case of Indian private sector banks. *Competitiveness Review*, 24(2), 107-118.
- Mzoughi, N., & M'Sallem, W. (2013). Predictors of internet banking adoption: Profiling Tunisian postponers, opponents and rejectors. *International Journal of Bank Marketing*, 31(5), 388-408.
- Nagaraju, S., & Parthiban, L. (2015). Trusted framework for online banking in public cloud using multi-factor authentication and privacy protection gateway. *Journal of Cloud Computing*, 4(1), 1-23.
- Nel, J., & Boshoff, C. (2017). Development of application-based mobile-service trust and online trust transfer: An elaboration likelihood model perspective. *Behaviour and Information Technology*, 36(8), 809-826.
- Oliveira, T., Faria, M., Thomas, M. A., & Popovič, A. (2014). Extending the understanding of mobile banking adoption: When UTAUT meets TTF and ITM. *International Journal of Information Management*, 34(5), 689-703.
- Ong, K. S., Nguyen, B., Faridah, S., & Alwi, S. (2017). Consumer-based virtual brand personality (CBVBP), customer satisfaction and brand loyalty in the online banking industry. *International Journal of Bank Marketing*, 35(3), 370-390.
- Ozturk, A. B., Bilgihan, A., Salehi-Esfahani, S., & Hua, N. (2017). Understanding the mobile payment technology acceptance based on valence theory: A case of restaurant transactions. *International Journal of Contemporary Hospitality Management*, 29(8), 2027-2049.
- Patsiotis, A. G., Hughes, T., & Webber, D. J. (2012). Adopters and non-adopters of internet banking: A segmentation study. *International Journal of Bank Marketing*, 30(1), 20-42.
- Pattinson, M., Butavicius, M., Parsons, K., McCormac, A., & Calic, D. (2017). Managing information security awareness at an Australian bank: A comparative study. *Information and Computer Security*, 25(2), 181-189.
- Purkait, S., Kumar De, S., & Suar, D. (2014). An empirical investigation of the factors that influence Internet user's ability to correctly identify a phishing website. *Information Management and Computer Security*, 22(3), 194-234.
- Purwanegara, M., Apriningsih, A., & Andika, F. (2014). Snapshot on Indonesia regulation in mobile internet banking users attitudes. *Procedia-Social and Behavioral Sciences*, 115, 147-155.
- Rawashdeh, A. (2015). Factors affecting adoption of internet banking in Jordan: Chartered accountant's perspective. *International Journal of Bank Marketing*, 33(4), 510-529.

- Raza, S. A., Jawaid, S. T., & Hassan, A. (2015). Internet banking and customer satisfaction in Pakistan. *Qualitative Research in Financial Markets*, 7(1), 24-36.
- Riffai, M. M. M. A., Grant, K., & Edgar, D. (2012). Big TAM in Oman: Exploring the promise of on-line banking, its adoption by customers and the challenges of banking in Oman. *International journal of information management*, 32(3), 239-250.
- Roy, S. K., Balaji, M. S., Kesharwani, A., & Sekhon, H. (2017). Predicting Internet banking adoption in India: A perceived risk perspective. *Journal of Strategic Marketing*, 25(5-6), 418-438.
- Seda, L. (2014). Identity theft and university students: do they know, do they care? *Journal of Financial Crime*, 21(4), 461-483.
- Shaikh, A. A., & Karjaluoto, H. (2015). Mobile banking adoption: A literature review. *Telematics and Informatics*, 32(1), 129-142.
- Shankar, A., & Datta, B. (2018). Factors affecting mobile payment adoption intention: An Indian perspective. *Global Business Review*, 19(3S), 1-18.
- Shanmugam, M., Wang, Y. Y., Bugshan, H., & Hajli, N. (2015). Understanding customer perceptions of internet banking: the case of the UK. *Journal of Enterprise Information Management*, 28(5), 622-636.
- Sharma, S. K., Govindaluri, S. M., & Al Balushi, S. M. (2015). Predicting determinants of Internet banking adoption: A two-staged regression-neural network approach. *Management Research Review*, 38(7), 750-766.
- Shaw, N. (2014). The mediating influence of trust in the adoption of the mobile wallet. *Journal of Retailing and Consumer Services*, 21(4), 449-459.
- Sikdar, P., Kumar, A., & Makkad, M. (2015). Online banking adoption: A factor validation and satisfaction causation study in the context of Indian banking customers. *International Journal of Bank Marketing*, 33(6), 760-785.
- Slade, E. L., Dwivedi, Y. K., Piercy, N. C., & Williams, M. D. (2015). Modeling consumers' adoption intentions of remote mobile payments in the United Kingdom: extending UTAUT with innovativeness, risk, and trust. *Psychology and Marketing*, 32(8), 860-873.
- Sohail, M. S., & Al-Jabri, I. M. (2014). Attitudes towards mobile banking: are there any differences between users and non-users? *Behaviour and information technology*, 33(4), 335-344.
- Sreejesh, S., Anusree, M. R., & Mitra, A. (2016). Effect of information content and form on customers' attitude and transaction intention in mobile banking moderating role of perceived privacy concern. *International Journal of Bank Marketing*, 34(7), 1092-1113.
- Su, P., Wang, L., & Yan, J. (2018). How users' Internet experience affects the adoption of mobile payment: A mediation model. *Technology Analysis and Strategic Management*, 30(2), 186-197.
- Susanto, A., Chang, Y., & Ha, Y. (2016). Determinants of continuance intention to use the smartphone banking services: An extension to the expectation-confirmation model. *Industrial Management and Data Systems*, 116(3), 508-525.

- Susanto, A., Lee, H., Zo, H., & Ciganek, A. P. (2013). User acceptance of Internet banking in Indonesia: Initial trust formation. *Information Development*, 29(4), 309-322.
- Szopiński, T. S. (2016). Factors affecting the adoption of online banking in Poland. *Journal of Business Research*, 69(11), 4763-4768.
- Tarhini, A., El-Masri, M., Ali, M., & Serrano, A. (2016). Extending the UTAUT model to understand the customers' acceptance and use of internet banking in Lebanon: A structural equation modeling approach. *Information Technology and People*, 29(4), 830-849.
- Tassabehji, R., & Kamala, M. A. (2012). Evaluating biometrics for online banking: The case for usability. *International Journal of Information Management*, 32(5), 489-494.
- Taylor, E. (2016). Mobile payment technologies in retail: a review of potential benefits and risks. *International Journal of Retail and Distribution Management*, 44(2), 159-177.
- Thakur, R. (2014). What keeps mobile banking customers loyal? *International Journal of Bank Marketing*, 32(7), 628-646.
- Tobbin, P. (2012). Towards a model of adoption in mobile banking by the unbanked: A qualitative study. *Info*, 14(5), 74-88s.
- Tran, H. T. T., & Corner, J. (2016). The impact of communication channels on mobile banking adoption. *International Journal of Bank Marketing*, 34(1), 78-109.
- Upadhyay, P., & Chattopadhyay, M. (2015). Examining mobile based payment services adoption issues: A new approach using hierarchical clustering and self-organizing maps. *Journal of Enterprise Information Management*, 28(4), 490-507.
- Upadhyay, P., & Jahanyan, S. (2016). Analyzing user perspective on the factors affecting use intention of mobile based transfer payment. *Internet Research*, 26(1), 38-56.
- Vaithilingam, S., Nair, M., & Guru, B. K. (2013). Do trust and security matter for the development of M-banking? Evidence from a developing country. *Journal of Asia-Pacific Business*, 14(1), 4-24.
- Wojewidka J. (2017). Why the mobile biometrics surge demands true liveness. *Biometric Technology Today*, 10, 8-11.
- Wonglimpiyarat, J. (2014). Competition and challenges of mobile banking: A systematic review of major bank models in the Thai banking industry. *The Journal of High Technology Management Research*, 25(2), 123-131.
- Xiao, Q., & Yang, X. D. (2010). Facial recognition in uncontrolled conditions for information security. *EURASIP Journal on Advances in Signal Processing*, 1, 1-9.
- Xin, H., Techatassanasoontorn, A. A., & Tan, F. B. (2015). Antecedents of consumer trust in mobile payment adoption. *Journal of Computer Information Systems*, 55(4), 1-10.
- Yadav, R., Chauhan, V., & Pathak, G. S. (2015). Intention to adopt internet banking in an emerging economy: A perspective of Indian youth. *International Journal of Bank Marketing*, 33(4), 530-544.

- Yang, S., Lu, Y., Gupta, S., Cao, Y., & Zhang, R. (2012). Mobile payment services adoption across time: An empirical study of the effects of behavioral beliefs, social influences, and personal traits. *Computers in Human Behavior*, 28(1), 129-142.
- Yiga, C., & Cha, K. J. (2016). Toward understanding the importance of trust in influencing Internet banking adoption in Uganda. *Information Development*, 32(3), 622-636.
- Yousafzai, S., & Yani-de-Soriano, M. (2012). Understanding customer-specific factors underpinning internet banking adoption. *International Journal of Bank Marketing*, 30(1), 60-81.
- Yu, P. L., Balaji, M. S., & Khong, K. W. (2015). Building trust in internet banking: a trustworthiness perspective. *Industrial Management and Data Systems*, 115(2), 235-252.
- Yu, X., Kywe, S. M., & Li, Y. (2017). Security Issues of In-Store Mobile Payment. In *Handbook of Blockchain, Digital Finance, and Inclusion*, 2, 115-144.
- Yuen, Y. Y., Yeow, P. H., & Lim, N. (2015). Internet banking acceptance in the United States and Malaysia: a cross-cultural examination. *Marketing Intelligence and Planning*, 33(3), 292-308.
- Zhang, W., & Morana, M. (2012, April 15). *Architectural Design Patterns for SSO (Single Sign On) Design and Use Cases for Financial Web Applications*. Retrieved April 7, 2018, from https://www.slideshare.net/marco_morana/presentation-sso-designsecurity
- Zhang, X. J., Li, Z., & Deng, H. (2017). Information security behaviors of smartphone users in China: An empirical analysis. *The Electronic Library*, 35(6), 1177-1190.
- Zhou, T. (2012). Understanding users' initial trust in mobile banking: An elaboration likelihood perspective. *Computers in Human Behavior*, 28(4), 1518-1525.
- Zhou, T. (2013). An empirical examination of continuance intention of mobile payment services. *Decision Support Systems*, 54(2), 1085-1091.



Non-Binary Serial Turbo LDPC Codes Combined with High Order Constellations

Latifa Mostari^{1*} and Abdelmalik Taleb-Ahmed²

¹Department of Electronics, Faculty of Technology, Hassiba Benbouali University of Chlef, Chlef 02000, Algeria

²IEMN UMR CNRS 8520, Polytechnic University of Hauts-de-France, Valenciennes 59313, France

ABSTRACT

Given the increasing number of applications requiring high data transmission, this is the reason for the use of high order constellations such as Quadrature Amplitude Modulation (QAM). However, communication systems using QAM require a high signal to noise ratio. To overcome this disadvantage, it is interesting to combine high error correction codes such as Low-Density Parity-Check (LDPC) codes with QAM. Although the LDPC codes are good codes for a system using QAM, concatenation of these codes with iterative decoding is still attractive to construct more powerful codes. In this context, we propose the non-binary serial turbo LDPC code. It is obtained by a serial combination of two identical regular non-binary LDPC codes, separated by an interleaver introducing the diversity. Regular codes were used to avoid the complexity of irregular codes despite that they have better performance than the regular code. Simulation results show that the performance of non-binary serial turbo LDPC code, with 16-QAM, 64-QAM and 256-QAM constellations using Gray mapping under Gaussian and Rayleigh channels, are higher than that of non-binary LDPC codes.

Keywords: Iterative decoding, Low-Density Parity-Check codes, non-binary, serial concatenation, turbo-code

ARTICLE INFO

Article history:

Received: 02 November 2017

Accepted: 19 June 2018

Published: 24 January 2019

E-mail addresses:

lmostari@univ-chlef.dz (Latifa Mostari)

Abdelmalik.Taleb-Ahmed@univ-valenciennes.fr (Abdelmalik Taleb-Ahmed)

* Corresponding author

INTRODUCTION

With the Internet democratization, mobile, user requirements become increasingly large and diverse. Faced with such requirements, digital communications are an essential solution now. One solution among others, is to increase the spectral efficiency while guaranteeing an unchanged transmission quality.

In 1948, Shannon (1948) proved that there was a limit spectral efficiency that we could not overcome if we wanted a transmission without errors. Shannon was able to give a limit without giving the code to correct errors. In order to realize the coding solution, intensive research efforts have been made worldwide. The key is to realize a code to get closer to the Shannon limit, and also to achieve a good trade-off performance/complexity. Until the 80s, the code that achieved the Shannon limit with reasonable complexity was not yet introduced. Two large error correcting code families were imposed: the block codes which were subdivided into several types and convolution codes (Elias, 1955).

It can be shown that the performance of a binary code can be improved with the increasing of the block length, but a large block length increases the complexity (Beermann et al., 2013 & Moision, 2013). One way to resolve this problem is to use concatenated codes. The code concatenation is the combination, in parallel, in serial or hybrid, two or more error correcting codes, convolutional or block, of small to moderate lengths.

Berrou (1993) showed that the performance of concatenated codes could be improved with an iterative decoding. This new scheme of code, called turbo-code can achieve the Shannon limit. Turbo-codes may block turbo-codes or convolutional turbo-codes (Berrou et al., 1993 & Pyndiah, 1998) depending on the type of concatenated codes. Thus, depending on the type of concatenation, parallel or serial, we can have parallel or series turbo codes.

After the power of iterative decoding, which was highlighted by the invention of turbo codes. The binary LDPC, which had been neglected because of their complexity, for many years since they were introduced by Gallager in 1962 (Gallager, 1962 & Gallager, 1963), had been rediscovered by Mackay (MacKay et al., 1995) in 1995 Spielman and others (Sipser et al., 1996) in 1996. LDPC codes are linear block codes based on low-density parity-check matrices, that is to say that the number of non-zero elements of the matrix is much less than the number of 0.

A significant contribution was introduced by Luby and others in 1997 (Luby et al., 1979) which introduced and set the irregular LDPC codes. These later have the main characteristic to perform better than regular code. LDPC codes can be regular or irregular according to the regular or irregular distribution of non-zero elements in the matrix. An LDPC code is called regular if the number of non-zeros elements in each columns and/or in each row of the matrix H , is constant. But if the number of non-zeros in each row or column are not constant the code is called an irregular LDPC code.

In 2002 Davey and Mackey (2002) studied the non-binary LDPC codes. LDPC codes can be binary or non-binary codes according to the non-zeros elements in the parity check matrix. If the non-zeros elements in matrix H , are binary (or non-binary), LDPC codes are binary (or non-binary). Non-binary LDPC codes are designed in high order Galois Fields $GF(q)$ where q is the cardinality of the Galois field. The non-binary LDPC codes perform better than their binary equivalents when the coded block is low to moderate length, or when the modulation used has a high order stats. However, the advantages of using non-binary

LDPC codes involve a significant increase in decoding complexity. More the Galois Field order is higher the complexity becomes important. For a Galois Field $GF(q)$, the complexity is of order $O(q^2)$. Similarly, the memory required for storing messages is of order $O(q)$.

LDPC codes are represented by their parity check matrix, and by a graphical representation, called the Tanner graph corresponds to the parity check matrix. The Tanner graph is a bipartite graph composed of two types of nodes: variable nodes representing the symbols of the coded block and the check nodes represent parity check equations. These two types of nodes are connected by branches according to the non-zero elements of the matrix H . The number of variable and check nodes corresponds, respectively, to the number of matrix columns and rows.

The Tanner graph is used as a transmission medium by the decoder. At first all variable nodes are initialized. After, each check node receives messages arriving from the variable nodes that are connected by her branches, then calculates and sends the resulting message that is related to all messages except the input message that the resulting message will be sent. Then, these same operations are performed by the variable nodes.

In Davey and McKay (2002), the authors proposed the first practical iterative decoding algorithm for non-binary LDPC codes. This algorithm, called Sum-Product Algorithm (SPA), is an optimal iterative decoding with computational complexity. Several algorithms have been proposed to reduce the complexity of the non-binary SPA (Barnault et al., 2003; Wymeersch et al., 2004; Spagnol et al., 2009), each one with a particular performance/complexity trade-off, such as: FFT-SPA (Fast Fourier Transform), Min-Sum Algorithm, Extended Min-Sum algorithm (Declercq et al., 2007; Voicila et al., 2010) and the Min-Max Algorithm (Savi, 2008), the Simplified Min-Sum Algorithm (Wang et al., 2013).

Many applications have adopted LDPC codes as industry standards, such as WLANs (IEEE 802.11n), WiMAX (IEEE 802.16e), WiFi, DVB-S2, 10 GBase-T Ethernet (IEEE 802.3an) and the ITU-T standard for networking over power lines, phone lines, and coaxial cable (G.hn/G.9960) (Chandrasetty et al., 2011)

An increasing number of applications requires high-speed transmission without increasing the bandwidth of the transmission channel, i.e. high spectral efficiency transmissions, while guaranteeing an unchanged transmission quality. This is the reason for the use of a system combining a high-order constellation with high errors correcting code. For this system, the QAM, is highly recommended as a high order constellation.

LDPC codes are selected as candidate for 5th generation wireless communications (5G) (Tahir et al., 2017). It is essential to develop a new error correction coding technique for 5G and Satellite communication systems.

Although non-binary LDPC codes are good error-correcting codes for a system using a higher order constellation, QAM, concatenation of these codes with iterative decoding is still attractive to a construct powerful errors correcting codes (Mostari et al., 2018; AlMuaini et al., 2013; Hung et al., 2011; Kumar et al., 2013) with reasonable complexity (Mostari et al., 2018).

The original LDPC codes concatenated in parallel PCGCs (Parallel Concatenated Gallager Codes), were introduced in (Behairy et al., 2000) as a class of concatenated codes in which two LDPC codes are irregular binary LDPC codes having different parameters interact in parallel without interleavers. The interleaver runs as a permutation, it changes the weight distribution of the code. It is therefore useful in increasing the minimum distance of the code. In Behairy et al. (2014) and Wang et al. (2012) a serial concatenation of binary irregular LDPC codes, is also introduced.

The authors (Behairy et al., 2000) showed how the different components LDPC codes with different parameters affected the overall performance in a Gaussian channel. Although they had limited their description of PCGC to a code rate equals to 1/3 by combining two LDPC codes of code rate equals to 1/2, they predicted that the conclusions are easily extended to the case where three or more codes are used as presented in (Behairy et al., 2014). Also, the authors (Behairy et al., 2000) showed that the interleaver was not necessary when the LDPC code was concatenated with another. To study the interleaving effect between component LDPC codes, a PCGC has been modified to use an interleaver as presented in (Belgheit et al., 2012) for irregular codes. However, the irregular LDPC codes have an error floor and a higher coding complexity than regular codes, although they are more efficient than regular code.

In this work, we studied the concatenation of two identical regular non-binary LDPC codes arranged in serial, using an interleaver between two LDPC codes that composed it, and we performed the decoding operation iteratively between the component codes. In our simulation, we used a high order constellation using Gray mapping under Gaussian and Rayleigh channels.

The rest of the paper is organized as follows. Section 2 introduces the non-binary LDPC encoding. Gray-QAM mapping and demapping is studied in section 3. FFT-SPA algorithm that used in our simulation is introduced in section 4. In sections 5 and 6, the parallel turbo LDPC encoding and decoding are investigated, respectively. Finally, the simulation results and concluding remarks are given in section 7 and 8, respectively.

MATERIALS AND METHODS

Non-Binary LDPC Encoding

Non-binary LDPC codes are defined by their parity check matrix $(M \times N)$ - H , where the non-zero elements in this matrix belong to the Galois Field $GF(2^p)$ ($p > 1$). The symbols of information block, of size $(N-M)$, belong to $GF(2^p)$. An encoder output can be expressed as a sequence of symbols in $GF(2^p)$.

The encoding is doing by several methods. In this work, one used the known encoding method by LU decomposition of H , this encoding type is systematic. It means that the codeword $C = [C_1 C_2 \dots C_N]$, is as follows:

$$C = [C_R C_I]$$

Where $C = [C_I C_2 \dots C_{N-M}]$ is the information block of size $(N-M)$ and $C_R = [C_1 C_2 \dots C_{N-M}]$ is the redundancy block of size M . Therefore, the code rate is given by $R=(N-M)/N$.

At the encoder output, each non-binary codeword $C = [C_1 C_2 \dots C_N]$ is converted to binary block $U = [u_1 C_2 \dots u_{p \times N}]$. Then, binary codeword generated, is mapped by 2^{2m} -QAM-Gary mapping, where m is an integer.

Gray-Qam Mapping and Demapping

2^{2m} -QAM transmit, at each time 2^{2m} binary symbols. Each set of $2m$ binary symbols is associated to a symbol $c = a + jb$, where a and $b \in \{\pm 1, \pm 3, \pm 5, \dots, 2m \pm 1\}$. After passing through the transmission channel, the observation relating to the symbol c is represented by the symbols $c' = a' + jb'$. The transmitted symbols are better follow a Gray mapping, it allows to affirm that there is usually only one erroneous symbol.

The simplest diagram of a digital transmission system as part of the association of an LDPC code and a 2^{2m} -QAM, is given in the Figure 1.

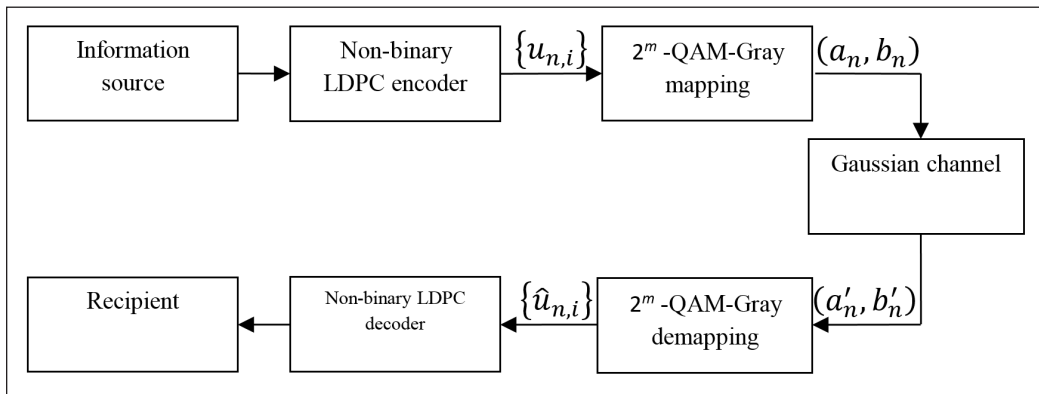


Figure 1. Diagram of a digital transmission system

At the reception, 2^{2m} -QAM-Gray demapping treat each symbols c' representative of the symbols c to extract $2m$ samples $\{\check{u}_{n,i}\}$, $i \in \{1, \dots, 2m\}$ each representative of a binary symbol $u_{n,i}$. The sample $\check{u}_{n,i}$, the soft output demapping, is obtained using two relationships, LLR($u_{n,i}$) (Log-Likelihood Ratio) (Mostari et al., 2017) or APP($u_{n,i}$) (A Posteriori Probability). In this work, one used APP computation:

For a Gaussian transmission channel, with the noise variance σ^2 , the m relations in phase eventually lead to the following expressions (Barnault et al., 2003):

$$APP(u_{n,i} = 0) = \frac{\sum_{j=1}^{2^{m-1}} \exp\left\{-\frac{1}{2\sigma^2}(a'_n - a_{i,j}^0)^2\right\}}{\sum_{j=1}^{2^{m-1}} \exp\left\{-\frac{1}{2\sigma^2}(a'_n - a_{i,j}^0)^2\right\} + \sum_{j=1}^{2^{m-1}} \exp\left\{-\frac{1}{2\sigma^2}(a'_n - a_{i,j}^1)^2\right\}}, \quad i \in \{1, \dots, m\}$$

$$APP(u_{n,i} = 1) = 1 - APP(u_{n,i} = 0), i \in \{1, \dots, m\}$$

Where $a_{i,j}^k$ are possible values of the symbol a_n when the symbol $u_{n,i}$ to be transmitted has the value k ($k = 0$ or 1).

Similarly, for a Gaussian channel, the p relations in the quadrature path eventually lead to the following expressions (Moon, 2005):

$$APP(u_{n,i} = 0) = \frac{\sum_{j=1}^{2^{m-1}} \exp\left\{-\frac{1}{2\sigma^2}(b'_n - b_{i,j}^0)^2\right\}}{\sum_{j=1}^{2^{m-1}} \exp\left\{-\frac{1}{2\sigma^2}(b'_n - b_{i,j}^0)^2\right\} + \sum_{j=1}^{2^{m-1}} \exp\left\{-\frac{1}{2\sigma^2}(b'_n - b_{i,j}^1)^2\right\}}, i \in \{m + 1, \dots, 2m\}$$

$$APP(u_{n,i} = 1) = 1 - APP(u_{n,i} = 0), i \in \{m + 1, \dots, 2m\}$$

Where $b_{i,j}^k$ are possible values of the symbol b_n when the symbol $u_{n,i}$ to be transmitted has the value k ($k = 0$ or 1).

Since non-binary LDPC decoding uses the soft output demapping of non-binary symbols, each p sample $\check{u}_{n,i}$ is used to obtain the soft output demapping of a non-binary symbol a , $a \in GF(2^p)$. Therefore, we obtain a bloc F of N components from a block of length pN . Each components in F is a vector of length 2^p :

$$F_i = \begin{pmatrix} APP(0) \\ APP(1) \\ \vdots \\ APP(2^p - 1) \end{pmatrix}, i \in \{1, \dots, N\} \quad \text{with } APP(a) = \prod_{i=1}^p APP(u_i)$$

Non-Binary LDPC Decoding: FFT-SPA

FFT-SPA (Wang et al., 2013) initializes each variable node v_n in the Tanner graph by the 2^p possible APPs of non-binary symbols. Messages $a_{m,n}$, $m \in \{1, \dots, M\}$, and $n \in \{1, \dots, N\}$ in variable nodes are given by:

$$a_{m,n} = F_n$$

After, each check node c_m in the Tanner graph receives messages $a_{m,n}$ arriving from variable nodes that are connected by their branches, then calculates and sends the resulting message that is related to all messages except the input message that the resulting message will be sent:

$$\beta_{m,n}(h_{ij} \otimes a) = FFT^{-1} \left(\prod_{n' \in N_m/n} FFT \left(\alpha_{m,n'}(h_{ij} \otimes a) \right) \right)$$

Where N_m is the set of check nodes with $h_{ij} \neq 0$ (h_{ij} , $i \in \{1, \dots, M\}$ and $j \in \{1, \dots, N\}$ represent elements of H).

Then, each variable node v_n receives messages $\beta_{m,n}$ arriving from check nodes that are connected by their branches, then calculates and sends the resulting message that is related to all messages except the input message that the resulting message will be sent:

$$\alpha_{m,n}(a) = \delta_{m,n} \gamma_n(a) \prod_{m' \in M_n/m} \beta_{m',n}(a)$$

Where M_n is the set of variable nodes with $h_{ij} \neq 0$.

Then, a posteriori information associated to each variable node is calculated before taking a decision.

$$\tilde{\gamma}_n(a) = \delta_n \gamma_n(a) \prod_{m' \in M_n} \beta_{m',n}(a)$$

The decision is given by

$$Z_n = \underset{a}{\operatorname{argmax}}(\tilde{\gamma}_n(a))$$

Finally, after a number of iterations or in case the syndrome is zero, the algorithm stops.

Serial Turbo LDPC Coding

The serial turbo encoder is built using a serial concatenation of two systematic component encoders separated by an interleaver noted π . In this work, each component encoder is non-binary regular LDPC encoder.

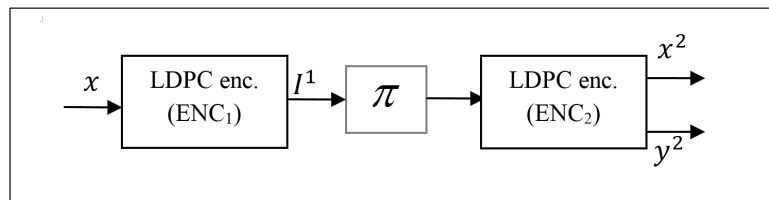


Figure 2. Serial turbo LDPC encoder

Figure 2 represents the block diagram of a rate R_{SC} serial turbo LDPC encoder (Berrou, 2007), where R_{SC} is given by:

$$R_{sc} = R_1 R_2$$

where R_1 is the code rate of the first component encoder ENC_1 and R_2 is the code rate of the second component encoder ENC_2 .

The first component encoder ENC_1 encodes the information block x of size $N-M$, $= [x_1 x_2 \dots x_{N-M}]$, using a parity check matrix H_1 of size $(L-N) \times (N-M)$, and generates the coded information block of size N :

$$I^1 = [y^1 x^1] = [y_1^1 y_2^1 \dots y_M^1 x_1^1 x_2^1 \dots x_{N-M}^1]$$

where x_1 is a systematic block $x^1 = x$, and y^1 is a parity block.

The second encoder ENC_2 uses the interleaved block $I_{interleaved}^1$, of size N , using a parity check matrix H_2 of size $(L-N) \times N$, and generates the coded information block of size L :

$$I^2 = [y^2 x^2] = [y_1^2 y_2^2 \dots y_{L-N}^2 x_1^2 x_2^2 \dots x_N^2]$$

where x^2 is an interleaved systematic block $x^2 = x_{interleaved}^1 = x_{interleaved}$, and y^2 is a parity block. Thus, the turbo LDPC encoder encodes the information block x of size $N-M$, $[x_1 x_2 \dots x_{N-M}]$, and generates the coded information block of size L :

$$[y^2 x^2] = [y_1^2 y_2^2 \dots y_{L-N}^2 x_1^2 x_2^2 \dots x_N^2]$$

Serial Turbo LDPC Decoding

A serial turbo-decoder (Berrou, 2007) presented at Figure 3, consists of two decoders DEC_1 and DEC_2 associated respectively to the codes ENC_1 and ENC_2 disposed in serial, of an interleaver and a deinterleaver noted π^{-1} .

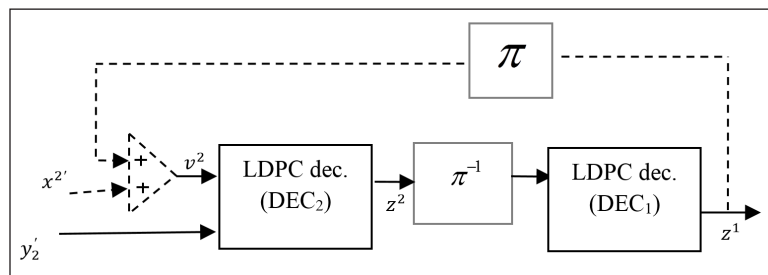


Figure 3. Serial turbo LDPC decoder

Each component LDPC decoder is decoded by using soft-input soft-output decoding algorithm, as described in section 4, using the “FFT-Sum-Product Algorithm”.

In the proposed non-binary turbo LDPC decoder, each non-binary turbo LDPC code contains two non-binary LDPC decoders decoded iteratively. Therefore, each turbo iteration, $iter_{turbo}$ of the non-binary turbo LDPC code contains multiple LDPC iterations $iter_{ldpc}$.

The turbo LDPC decoder receives the soft observations $x^{2'}$ and $y^{2'}$ and estimates the message transmitted. where $x^{2'}$ denotes the received block corresponding to the interleaved systematic information block, while $y^{2'}$ denotes the received blocks corresponding to the parity block of the second decoders.

In the first iteration $iter_{turbo}$, the first decoder DEC_2 generates the soft information block $z^2 = [z_1^2 z_2^2 \dots z_N^2]$, after a fixed number of iterations $iter_{ldpc}$, using the following received block:

$$[y^{2'} x^{2'}] = [y_1^{2'} y_2^{2'} \dots y_{L-N}^{2'} x_1^{2'} x_2^{2'} \dots x_N^{2'}]$$

The second decoder DEC_1 generates the soft information block $Z^1 = [z_1^1 z_2^1 \dots z_N^1]$, after a fixed number of iterations $iter_{ldpc}$, using, $z_{deinterleaved}^2$, the deinterleaved block of the information generated by the first decoder DEC_2 ,

For next iterations $iter_{turbo}$, the first decoder DEC_2 uses, $z_{interleaved}^1$, the interleaved block of the block generated by the second decoder DEC_1 to do the decoding. The turbo LDPC decoder input becomes:

$$[y^{2'} v^2] = [y_1^{2'} y_2^{2'} \dots y_{L-N}^{2'} v_1 v_2 \dots v_N]$$

$$\text{Where } v^2 = x^{2'} + z_{interleaved}^1$$

Decoding stops at the end of a fixed number of iteration, and the final decision comes from DEC_1 . One iteration corresponds to one pass from DEC_2 to DEC_1 .

RESULTS AND DISCUSSION

Simulations

In this section, we discuss the performance of non-binary serial turbo LDPC codes and non-binary LDPC codes constructed on GF(4), with the same block length and code rate, combined with high order constellations (16-QAM, 64-QAM and 256-QAM) using Gray mapping, over Gaussian and Rayleigh channels. Simulation results are given in terms of Bit Error Rate (BER) versus E_b/N_0 , where E_b is the energy per information and N_0 is the spectral density noise, using Matlab.

The non-binary LDPC code is made by a parity check matrix with the parameters ($w_c = 4, M = 1024, N = 1536$) decoded by FFT-SPA, and the serial turbo LDPC code is composed of two regular non-binary LDPC codes decoded by FFT-SPA: the inner-code is a rate 1/2 non-binary LDPC code with the parameters ($w_c = 2, M = 512, N = 1536$), and the outer-LDPC code is a rate 2/3 non-binary LDPC code with the parameters $w_c = 4, M = 1024, N = 1536$). The number of iterations in turbo LDPC code is set to 2 using 2 iterations in each component non-binary LDPC code, ($iter_{turbo} = 2, iter_{ldpc} = 2$), and the maximum number of a single LDPC code is set to 2, $iter_{ldpc} = 2$.

Simulation results in Figures 4,5 and 6 show that the proposed code outperforms the single LDPC codes. In order to investigate the performance of serial turbo LDPC code in a Rayleigh channel, performance comparison is conducted on a Rayleigh channel, with 16-QAM, 64-QAM and 256-QAM, respectively in Figures 7, 8 and 9.

The simulation results presented in all figures show that turbo LDPC code outperforms LDPC code. Turbo LDPC code needs less number of iterations to achieve the same performance of single LDPC code. As seen in Figures 7, 8 and 9, the coding gain between a single LDPC code and a serial turbo LDPC code increases in a Rayleigh channel. This increase is due to the interleaver in the serial turbo LDPC code. It means that the interleaver has a good effect in fading channels.

As mentioned before, achieving high spectral efficiency using high order constellations with high quality is the key requirement of future wireless systems and mobile

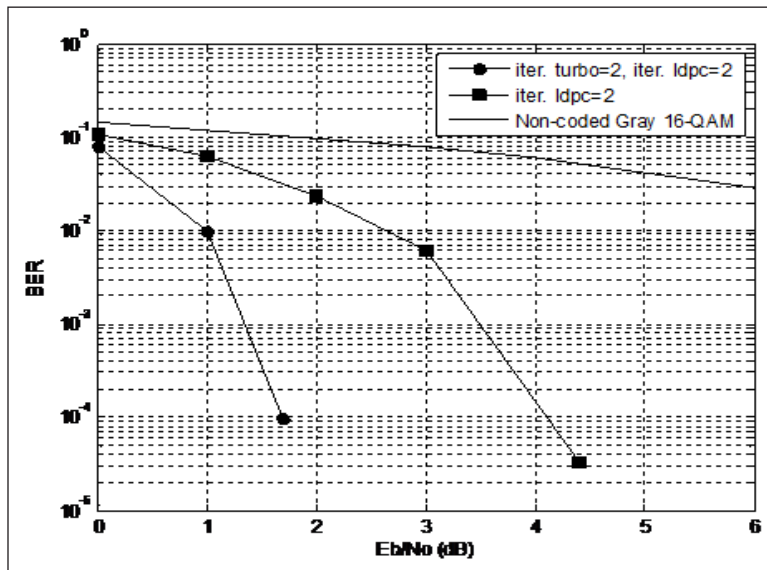


Figure 4. Performance comparison of a rate 1/3 non-binary turbo LDPC code with a rate 1/3 non-binary LDPC code associated with 16-QAM constellation under Gaussian channel

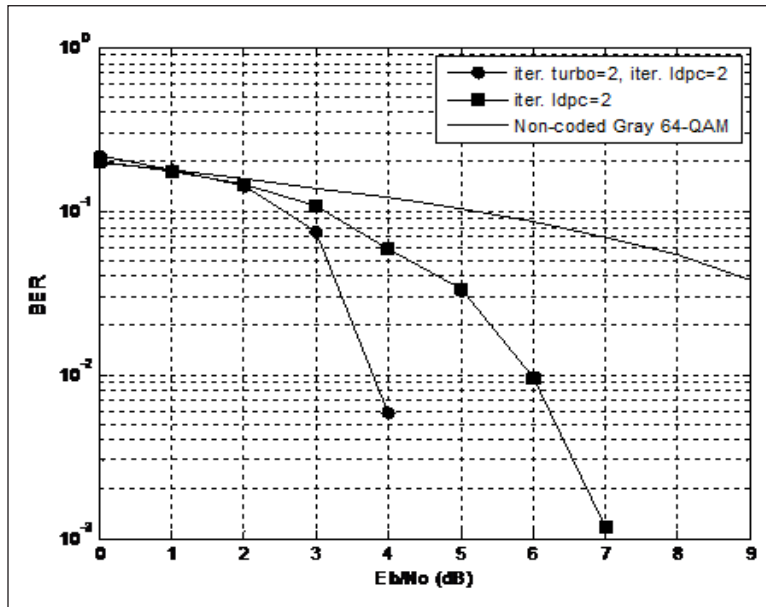


Figure 5. Performance comparison of a rate 1/3 non-binary turbo LDPC code with a rate 1/3 non-binary LDPC code associated with 64-QAM constellation under Gaussian channel

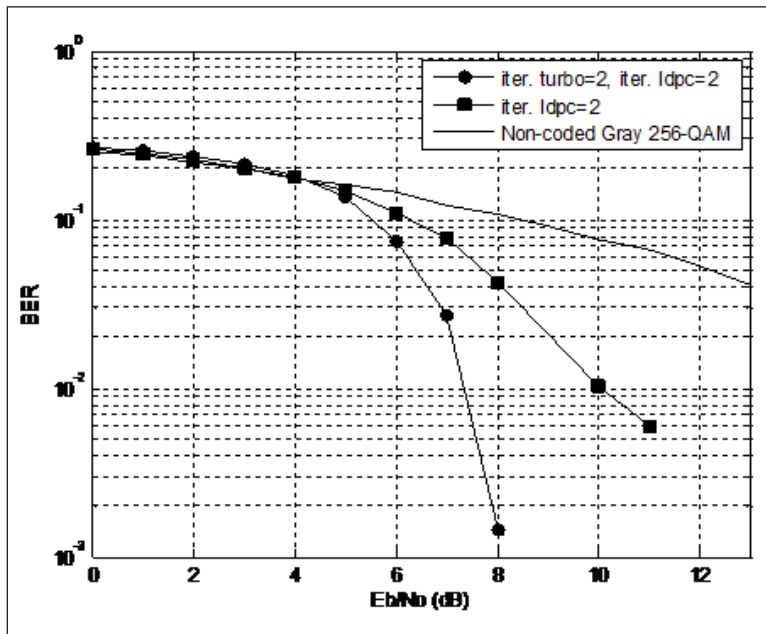


Figure 6. Performance comparison of a rate 1/3 non-binary turbo LDPC code with a rate 1/3 non-binary LDPC code associated with 256-QAM constellation under Gaussian channel

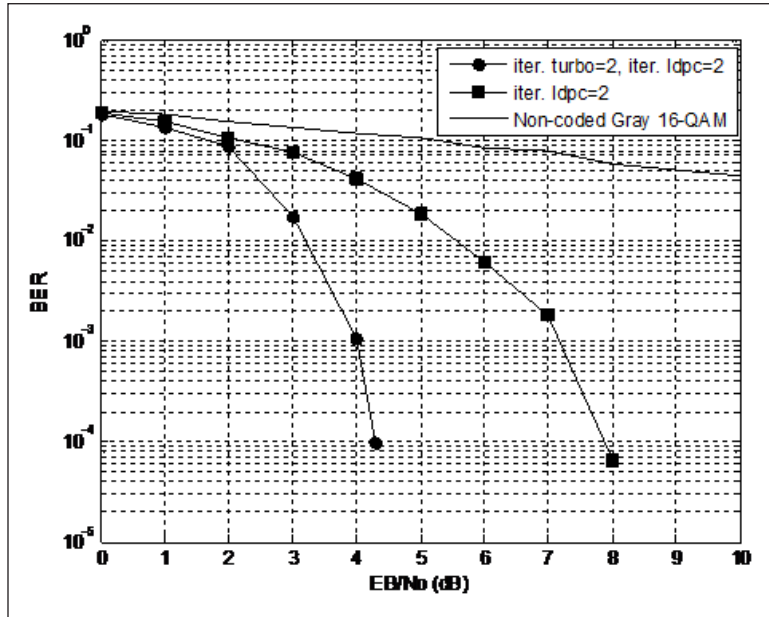


Figure 7. Performance comparison of a rate 1/3 non-binary turbo LDPC code with a rate 1/3 non-binary LDPC code associated with 16-QAM constellation under Rayleigh channel

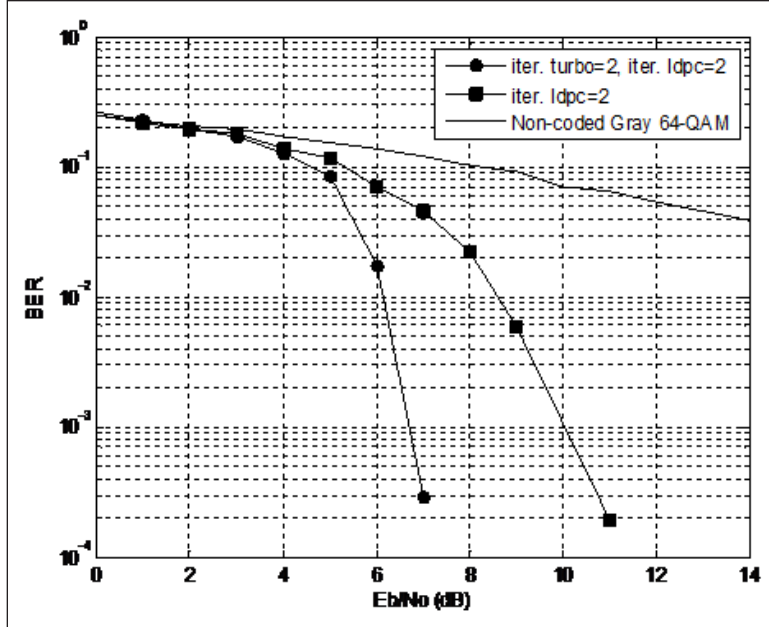


Figure 8. Performance comparison of a rate 1/3 non-binary turbo LDPC code with a rate 1/3 non-binary LDPC code associated with 64-QAM constellation under Rayleigh channel

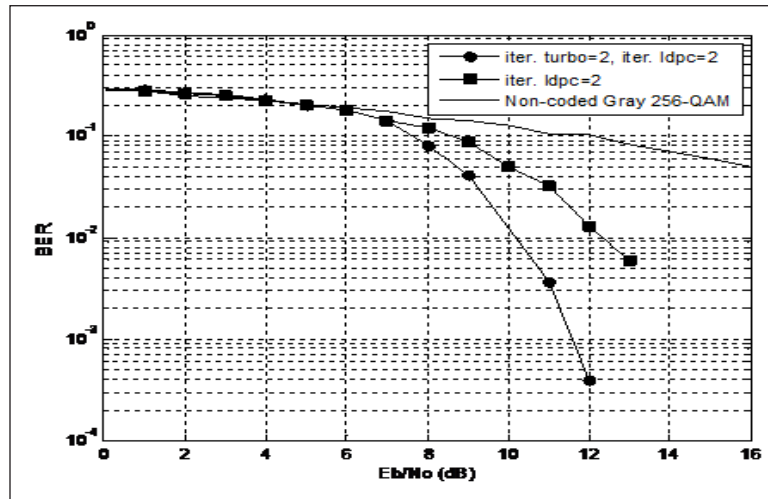


Figure 9. Performance comparison of a rate 1/3 non-binary turbo LDPC code with a rate 1/3 non-binary LDPC code associated with 256-QAM constellation under Rayleigh channel

communications. Thus, the transmission with high spectral efficiency needs a high performance error correcting code such as LDPC codes. Simulation results show that the performance of the proposed code, with higher order constellations (16-QAM, 64-QAM and 256-QAM) using Gray mapping, under Gaussian and Rayleigh channels has higher performance than a single non-binary LDPC code with the same block length. Also, we show that the interleaver in the proposed code has a positive effect on the performance. Therefore, the proposed code is a good error correcting code for high spectral efficiency system.

CONCLUSION

In this work, we proposed a non-binary turbo LDPC code. It is an error correcting code scheme based on the serial concatenation of non-binary LDPC. Simulation results show that the performance of non-binary turbo LDPC code, with high order constellation using Gray mapping under Gaussian and Rayleigh channels, is higher than the performance of a rate 1/3 non-binary LDPC code.

REFERENCES

- AlMuaini, S. A., Al-Dweik, A., & Al-Qutayri, M. (2013). BER performance of turbo product LDPC codes with non-sequential decoding. In *2013 6th Joint IFIP on Wireless and Mobile Networking Conference (WMNC)* (pp. 1-6). Dubai, United Arab Emirates.
- Barnault, L., & Declercq, D. (2003). Fast decoding algorithm for LDPC over GF(2/sup q). In *Proceedings of Information Theory Workshop* (pp. 70-73). Paris, France.

- Beermann, M., Monró, E., Schmalen, L., & Vary, P. (2013, October). High speed decoding of non-binary irregular LDPC codes using GPUs. In *2013 IEEE Workshop on Signal Processing Systems (SiPS)* (pp. 36-41). Taipei City, Taiwan.
- Behairy, H. M., & Benaissa, M. (2013). Multiple parallel concatenated gallager codes: Code design and decoding techniques. *IETE Journal of Research*, *59*(6), 659-664.
- Behairy, H., & Chang, S. C. (2000). Parallel Concatenated Gallager Codes. *Electronics Letters*, *36*(24), 2025-2026.
- Belgheit, B., Boukelif, A., Lakhder, A. M., & Kamline, M. (2012). Parallel concatenated Gallager codes matrix and the effect of interleaver. *International Journal of Electronics*, *99*(9), 1281-1289.
- Berrou, C. (2007). *Codes et Turbo-Codes*. Paris: Springer.
- Berrou, C., Glavieux, A., & Thitimajshima, P. (1993). Near Shannon limit error-correcting coding and decoding: Turbo-codes. 1. In *Proceedings of ICC '93 - IEEE International Conference on Communications* (Vol. 2, pp. 1064-1070). Geneva, Switzerland.
- Chandrasetty, V. A., & Aziz, S. M. (2011). FPGA implementation of a LDPC decoder using a reduced complexity message passing algorithm. *Journal of Networks*, *6*(1), 36-45.
- Davey, M., & MacKay, D. (2002). Low-Density Parity Check Codes over $GF(q)$. *IEEE Communications Letters*, *2*(6), 165–167.
- Declercq, D., & Fossorier, M. (2007). Decoding Algorithms for Non binary LDPC Codes over $GF(q)$. *IEEE Transactions on Communications*, *55*(4), 633-643.
- Elias, P. (1955). Coding for noisy channels. *IRE Convention Record*, *3*(4), 37-46.
- Gallager, R. G. (1962). Low-Density Parity-Check Codes. *IEEE Transaction Information Theory*, *8*(1), 21–28.
- Gallager, R. G. (1963). *Low-density parity-check codes*. Cambridge: MIT Press.
- Hung, J. H., Shyu, J. S., & Chen, S. G. (2011, May). A New High-Performance and Low-Complexity Turbo-LDPC Code. In *2011 International Conference on Multimedia and Signal Processing (CMSP)* (Vol. 1, pp. 68-72). Guilin, Guangxi, China.
- Kumar, R. P., & Kshetrimayum, R. S. (2013, February). An Efficient Methodology for Parallel Concatenation of LDPC codes with reduced complexity and decoding delay. In *2013 National Conference on Communications (NCC)* (pp. 1-5). New Delhi, India.
- Luby, M. G., Mitzenmacher, M., Shokrollahi, M. A., Spielman, D. A., & Stemann, V. (1997, May). Practical loss-resilient codes. In *Proceedings of the twenty-ninth annual ACM symposium on Theory of computing* (pp. 150-159). Texas, USA.
- MacKay, D. J., & Neal, R. M. (1995, December). Good codes based on very sparse matrices. In *IMA International Conference on Cryptography and Coding* (pp. 100-111). Cirencester, UK.
- Moon, T. K. (2005). *Error Correction Coding Mathematical Methods and Algorithms*. New Jersey: John Wiley & Sons, Inc.

- Moision, B. (2013). Decoding complexity and performance of short-block LDPC codes over $GF(q)$. *Interplanetary Network Progress Report*, 194, 1-16.
- Mostari, L., Taleb-Ahmed, A., & Bounoua, A. (2018). High performance LDPC codes for high spectral efficiency transmission. *Internetworking Indonesia Journal*, 10(1), 09-15.
- Mostari, L., & Taleb-Ahmed, A. (in press). High performance short-block binary regular LDPC codes. *Alexandria Engineering Journal*.
- Mostari, L., & Taleb-Ahmed, A. (2017). Simplified log likelihood ratio for binary LDPC codes. *Journal of Engineering Science and Technology Review*, 07(1), 37-40.
- Pyndiah, R. (1998). Near Optimum Decoding of Product Codes: Block Turbo-Codes. *IEEE Transactions on Communications*, 46(8), 1003-1010.
- Savin, V. (2008, July). Min-Max decoding for non binary LDPC codes. In *IEEE International Symposium on Information Theory (ISIT 2008)* (pp. 960-964). Toronto, ON, Canada.
- Shannon, C. E. (1948). A mathematical theory of communication. *Bell System Technical Journal*, 27(3), 379-423.
- Sipser, M., & Spielman, D. A. (1996). Expander Codes. *IRE Transaction on Information Theory*, 42(6), 1710-1722.
- Spagnol, C., Popovici, E., & Marnane, W. (2009). Hardware implementation of $GF(2^m)$ LDPC decoders. *IEEE Transactions Circuits Systems I: Regular Papers*, 56(12), 2609-2620.
- Tahir, B., Schwarz, S., & Rupp, M. (2017, May). BER comparison between Convolutional, Turbo, LDPC, and Polar codes. In *2017 24th International Conference on Telecommunications (ICT)* (pp. 1-7). Limassol, Cyprus.
- Voicila, A., Declercq, D., Verdier, F., Fossorier, M., & Urard, P. (2010). Low-complexity decoding for non-binary LDPC codes in high order fields. *IEEE Transactions on Communications*, 58(5), 1365-1375.
- Wang, C., Chen, X., Li, Z., & Yang, S. (2013). A Simplified min-sum decoding algorithm for non-binary LDPC codes. *IEEE Transactions on Communications*, 61(1), 24-32.
- Wymeersch, H., Steendam, H., & Moeneclaey, M. (2004, June). Log-domain decoding of LDPC codes over $GF(q)$. In *2004 IEEE International Conference on Communications (Vol. 2, pp. 772-776)*. Paris, France.
- Wang, Z., & Zhang, M. (2012, April). A serial concatenated scheme for LDPC code to achieve better error correction performance. In *2012 2nd International Conference on Consumer Electronics, Communications and Networks (CECNet)* (pp. 1587-1589). Yichang, China.



Ma-Ease: An Android-Based Technology for Corn Production and Management

Sales Gamponia Aribe Jr.^{1*}, Jhon Michael H. Turtosa², Jul Maico B. Yamba³ and Alvin B. Jamisola⁴

¹Department of Information Technology, Bukidnon State University, Fortich Street, Malaybalay City, 8700 Philippines

²Zone 2, Barangay 1, Heights, Malaybalay City, 8700 Philippines

³Crossing Sta. Clara, Naga, Zamboanga Sibugay, 7004 Philippines

⁴Purok 3, Laguitas, Malaybalay City, 8700 Philippines

ABSTRACT

Corn production is second to rice as the most important agricultural product in the country. Thus, proper information, management, and technology dissemination in corn farming are greatly needed for a good harvest. The study aims to develop a mobile application to comprehensively address the needs of corn farmers thru dissemination of proper information, management, and techniques through the cooperation of the City Agriculture Office (CAO) of Malaybalay City, Bukidnon, Philippines. It is anchored on the Unified Theory of Acceptance and the Use of Technology (UTAUT) Model, where there are core and direct determinants of user reception and usage behavior, as well as moderating factors on user's acceptance on mobile services and applications especially in the area of agriculture. The researchers use the method of "Modified Waterfall Model" or MWF Model as the process model for the development of Ma-Ease Application. The sequential structure of this approach ensures that all requirements are achieved before moving onto the next step and no important steps are left out in the development process. A presentation was conducted

with the CAO Malaybalay officials and local corn farmers to introduce our technological solutions in the corn production like local and up-to-date weather updates, proper nutrient inputs and corn farming activities, efficient cost management, and control of corn pests and diseases. Effectivity tests were done during their actual interaction and engagement with the finished product and finding shows that the Ma-Ease mobile app

ARTICLE INFO

Article history:

Received: 02 March 2018

Accepted: 30 August 2018

Published: 24 January 2019

E-mail addresses:

sg.aribe@buku.edu.ph (Sales Gamponia Aribe Jr.)

jhonturtosa@gmail.com (Jhon Michael H. Turtosa)

jamz7690@gmail.com (Jul Maico B. Yamba)

therealvinjamisola@gmail.com (Alvin B. Jamisola)

* Corresponding author

has a grand mean of 4.175 for its acceptability and satisfaction rate which covers the area of functionality, reliability, usability, maintainability, efficiency and user interface. Thus, the software product was formally accepted and recommended for use and deployment by the Department of Agriculture (DA).

Keywords: Corn farming mobile application, corn farming software solution, corn management, corn production, ICT in agriculture, ICT in corn farming, technofarm, technology in corn farming

INTRODUCTION

Over the years, corn farming has been a significant source of income and food among Filipinos. Corn still remains as the most popular agricultural commodity produced by farmers within the province as a majority of the agricultural lands in the province of Bukidnon is devoted to corn especially in Malaybalay City. In fact, according to the Department of Agriculture, corn is the second most important crop in the country and about 14 million Filipinos prefer white corn staple and corn accounts for about 50% of livestock mixed feeds. Furthermore, according to Philippine Statistic Authority in “Rice and Corn Situation and Outlook Report, April 2018” (Philippine Statistics Authority, 2018) which is shown in Figure 1, the corn output of the Philippines from January to March 2018 was 2.48 million metric tons which was 4.66% higher than the 2.37 million metric tons recorded in the year 2017. The harvest area has expanded from 695.74 thousand hectares to 722.46 thousand hectares or equivalent to 3.85% increase. The yield per share has also increased from 3.40 metric tons to 3.43 metric tons, an increase by 0.79%. Table 1 also shows that the increments in these corn outputs were noted in Cagayan Valley with 2.61%,

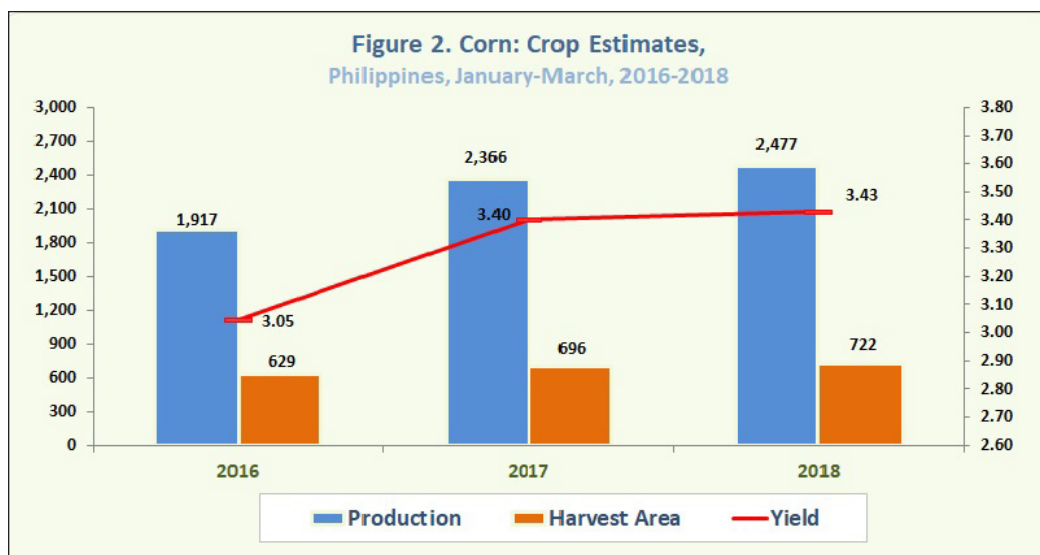


Figure 1. Corn: Crop estimates, Philippines, January-March, 2016-2018

Table 1
 Corn: Crop estimates by region, Philippines, January-March, 2016-2018

Item	January-March										% Point Contrib'n	
	2016		2017		2018		2018/2017		2107/2016			Percent share
	(1)	(2)	(3)	(4)	(5)	(6)	(7)	(8)	(9)	(10)		
PRODUCTION (MT)												
PHILIPPINES	1,916,945	2,366,294	2,476,573	110,280	4.66	449,349	23.44	100.00	4.66			
CAR	68,719	73,185	64,900	(8,285)	(11.32)	4,466	6.50	2.62	(0.35)			
Ilocos	315,992	380,415	385,287	4,872	1.28	64,423	20.39	15.56	0.21			
Cagayan Valley	579,901	559,869	621,714	61,846	11.05	(20,033)	(3.45)	25.10	2.61			
Central Luzon	111,607	112,240	124,654	12,414	11.06	633	0.57	5.03	0.52			
CALABARZON	20,987	20,499	23,851	3,352	16.35	(488)	(2.33)	0.96	0.14			
MIMAROPA	52,216	48,447	57,109	8,662	17.88	(3,769)	(7.22)	2.31	0.37			
Bicol	55,225	63,114	63,847	733	1.16	7,889	14.29	2.58	0.03			
Western Visayas	69,932	89,704	84,984	(4,720)	(5.26)	19,772	28.27	3.43	(0.20)			
Central Visayas	17,757	21,090	22,151	1,061	5.03	3,333	18.77	0.89	0.04			
Eastern Visayas	12,503	11,649	10,528	(1,121)	(9.62)	(854)	(6.83)	0.43	(0.05)			
Zamboanga Peninsula	42,114	40,275	57,359	17,084	42.42	(1,839)	(4.37)	2.32	0.72			
Northern Mindanao	249,121	316,675	317,762	1,087	0.34	67,554	27.12	12.83	0.05			
Davao Region	42,125	53,305	55,941	2,636	4.95	11,180	26.54	2.26	0.11			
SOCCSKSARGEN	204,637	255,622	264,931	9,309	3.64	50,985	24.91	10.70	0.39			
Caraga	1,518	1,079	2,144	1,065	98.70	(439)	(28.91)	0.09	0.05			
ARMM	72,591	319,126	319,411	285	0.09	246,535	339.62	12.90	0.01			

Zamboanga Peninsula with 0.72%, Central Luzon with 0.52%, Soccsksargen with 0.39%, Mimaropa with 0.37% and even Northern Mindanao Region with 0.05% where the City of Malaybalay belongs.

As being one of the important agricultural products in the country, the need for proper information, management, and technology dissemination in corn farming is an important tool. The researchers came up with an idea to develop a mobile application which is the Ma-Ease: An Android-Based Technology for Corn Production and Management. The aim of the researchers is to help the Department of Agriculture to disseminate information. Thus, implementation of effective production is just one of the few of the challenges corn farmers are facing. With the use of the information from the Department of Agriculture, the researchers were motivated to develop a mobile application that would help the farmers in disseminating information, awareness, knowledge, and technology in corn farming. Mobile phones offer many advantages: voice communications affordability, instant and convenient service delivery and wide ownership.

Figure 2 illustrates the conceptual view of the development of Ma-Ease: An Android-Based Technology for Corn Production and Management for corn farmers in Malaybalay City, using an Input-Process-Output (IPO) Model. This pattern is a widely approach model for conceptualizing a systems analysis and software engineering in order to identify the flow of data (input), the steps of the transformation of data (output) and the effect of transformation process (output).

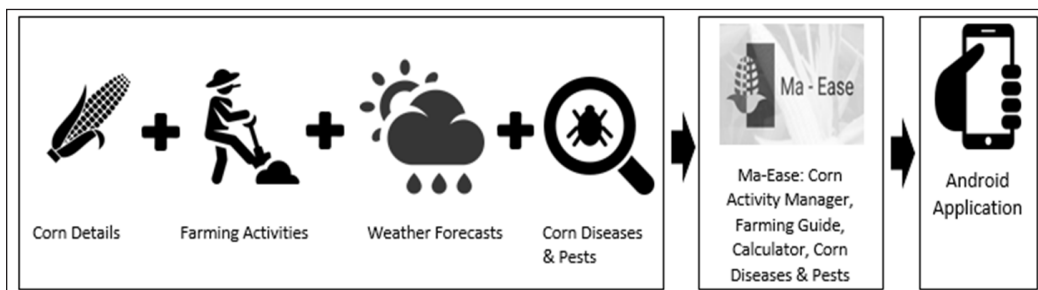


Figure 2. Conceptual framework of Ma-Ease mobile application

With the development of the mobile application, the application requires an input containing corn details which includes farm name, location, soil type, seed type, date of planting, farming activities, local-based weather forecasts, and corn diseases and pests. The application will then compute basic calculation activities for corn farmers like calculate a number of seed bags and fertilizer sacks to acquire in the field as well as the recommended inputs for the plant. The application will also give important information and solution to most common problems in the field like pests and weeds. By selecting from the list of pests and weeds in the database, the mobile application will prompt solutions.

By implementing the mobile application, the mobility of accessing important information in corn farming will be achieved, making corn farmers well informed about the corn production and for easy and accurate nutrient inputs. Moreover, using the application will help corn farmers to have a quality harvest.

Different studies have been conducted related to growth and productivity of the corn but offer limited services. In a study entitled “ICT in Agriculture”, Pehu et al. (2011) only mentioned about accurate soil analyses and improved farming practices which were needed because productivity gains were highest in healthy soils. This statement was also claimed by Lee (2014), a corn specialist at The University of Georgia, who studied only on the nutrients to the corn plant. Song (2006) also cited country-specific technology dissemination strategies which proved to be successful in catering to the needs of the farmers. Some examples of these strategies include effective dissemination method in Indonesia through technology showcase or technofarm demonstration; introduction of new varieties in Malaysia through farm demonstrations, short courses, and hands-on training; participatory approaches in technology promotion and dissemination in the Philippines; and many others. A study by delos Santos et al. (2013) also mentioned about agricultural extension agents who derived their climate-related information primarily from the national meteorological agency called Philippine Atmospheric, Geophysical and Astronomical Services Administration (PAGASA) while farmers relied only on television and radio for their advanced weather information. In fact, these extension agents were not the main source of climate-related information for farmers. Drought at any stage of crop development affects production, but the maximum damage is inflicted when it occurs around flowering (Nguyen & Blum, 2004).

Some dedicated mobile apps for agriculture exists but only offers partial features and functionalities. According to World Bank, in environments where information is scarce, leveraging existing resources will be crucial for success. First, the m-ARD (Mobile Applications for Agricultural and Rural Development) apps, for example, were developed to make publicly available accurate, granular data such as weather forecasts with integrated flood and drought information at the village or community levels. These services could increase incomes and create further opportunities for people in rural and underserved places in developing countries throughout the ecosystem for m-ARD apps (Qiang et al., 2011). Second, eWarning was created through PlanteInfo, a Danish initiative supporting decision-making in national plant production. eWarning provided farmers with real-time weather information sourced by the AgriMeteorological Information System and Danish Meteorological Institute where farmers requested information through SMS (Short Message Service) in two forms: push-type and pull-type messages. The same software was also created by Yakima software firm, customizing a weather website for specific locations to provide weather alerts to farmers in the United States. These warnings included frost alerts,

the speed of the wind with recommendations for spraying pesticide and other information on disease outbursts. Eventually, the service offered climatic information in Spanish, making it easier for native Spanish speakers to make interpretations and decisions (Lester, 2010). Third, Nutrient Manager for Rice (NMRice) Mobile was a mobile application available for farmers in agricultural countries like China, Indonesia, Nigeria and the Philippines. As Global Media Arts or GMA News Network (2011) cited, since the launch of the application, it already received a total of more than 6,000 calls from the farmers. The disadvantage of the application was that it did not offer offline support. Further, NMRice Mobile was designed only for rice farmers, which has different characteristics and environment needed for corn. Lastly, was the Farmers' Text Center (FTC), an SMS based service for answering agriculture-related queries. Philippine eExtension Service was an addition to Techno Gabay, a national extension system that provides farmers with access to best practices to improve agricultural approaches and boost agricultural productivity.

While existing studies about corn production have been clearly established, they have not been addressed holistically and comprehensively to improve farming methods and practices suggested by the Department of Agriculture. The same is true for the existing mobile applications that do not offer vast and up-to-date information and issue from agriculture professionals. Compared to the Ma-Ease Mobile application, information, and management needed in corn production are already provided. Farmers need not wait for the experts since the information provided by the app is from the Department of Agriculture. It also provides accurate and reliable weather information, a 7-day weather forecast on the different regions in the Philippines thru Philippine Atmospheric, Geophysical and Astronomical Services Administration.

The present study will help corn farmers experience the full benefits of mobile phones by the development of a mobile application with important key features that help. Likewise, the study is anchored on Unified Theory of Acceptance and Use of Technology or UTAUT (Ghazizadeh, 2012) which combined the traditional mobile technology acceptance, like Technology Acceptance Model (TAM), Theory of Reasoned Action (TRA) and Theory of Planned Behaviour (TPB) and introduces new model of user acceptance in a unified view. In the UTAUT model, four core determinants of usage and intention (social influence, effort expectancy, performance expectancy, and facilitating conditions) and four moderating variables (voluntariness of use, age, experience, and gender) acting as the key relationships were considered. The aim of formulating this theory is to provide a deeper understanding of individual and organizational acceptance of IT and mobile services and applications to researchers and managers. Figure 3 shows the connection of the core determinants as well as the moderating factor related to user behavior. The Ma-Ease application is the knowledge-based application for mobile phones which provides crop advisors, Department of Agriculture workers, and corn farmers a comprehensive guideline for their corn fields

wherever they are in the City of Malaybalay. This application can also minimize effort and time to access information at the Department of Agriculture since the information is already implemented in an android based application. With the Ma-Ease application, the corn farmers are no longer required to exert time to go to the Department of Agriculture for further explanation on how to do corn production except for soil analysis and other critical agricultural matters.

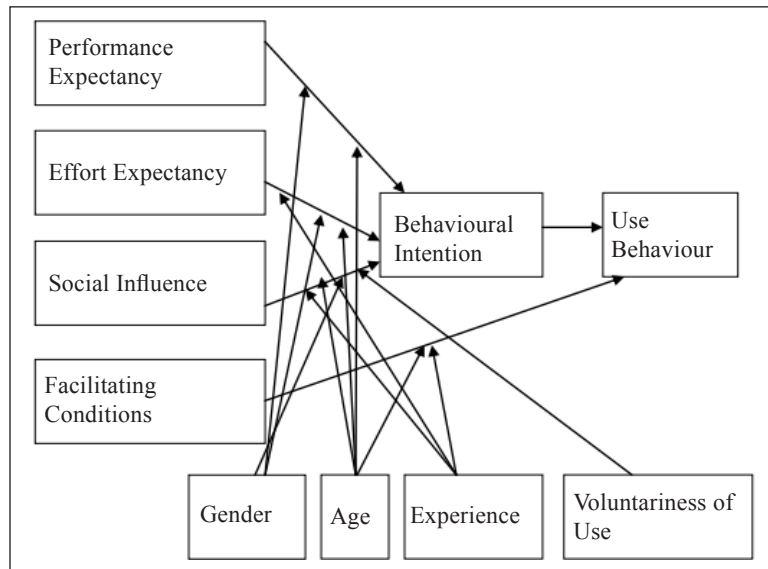


Figure 3. Unified Theory of Acceptance and Use of Technology Model (UTAUT)

METHOD

The researchers used the method of “Modified Waterfall Model” or MWF Model as the process model for the development of Ma-Ease Application. The sequential structure of this approach ensures that all requirements were achieved before moving onto the next step and no important steps were left out in the development process. Developed by Winston W. Royce on 1970, this model served as a response to the apparent problems with the “pure” waterfall model and used iteration through certain phases in the methodology to guarantee the quality of the output generated in each phase and performed improvement or necessary checking to correct or improve further the framework as a whole. The researchers used a judgment sampling method by selecting a sample based on who attended the Stakeholder’s Forum on Corn Farming App last May 22, 2017, where 20 local farmers graced the invitation. These farmers resided and farmed in Barangay Laguitas, Dalwangan, Patpat, and Kalasungay in the City of Malaybalay, Province of Bukidnon, Philippines who were truly representative of the entire population of local farmers in the city per consultation with the agriculturists and officials.

Looking at the Modified Waterfall model graphic in Figure 4, the development team coordinated with the business and technical entities to define both functional and non-functional requirements of the Ma-Ease App. This was an iterative process to define, classify, and arrange all requirements according to priority prior to starting the General Systems Design (GSD) phase. The General Design phase was the first interpretation of these requirements into systems conceptual designs. During the GSD phase, the requirements gathered from the corn farmers and employees of Department of Agriculture were validated and finalized. Through the GSD and Architectural Review Board 2 or ARB 2 (composed of the development team and thesis adviser) processes, the technical team established and confirmed a mutual understanding and agreement of all the requirements as well as the solutions design and architectural approaches. Changes in requirements beyond the GSD established a change in scope typically invoking the change in the control process. Hence, all requirements were finalized before the Detailed Systems Design (DSD) phase began. The development team designed and architected the solution as outlined in the DSD. Problems and issues during this phase were encountered which required the team to undergo ARB 3. The testing phase is inclusive of the following: unit testing, module testing, systems integration testing, user acceptance testing, and performance testing. The User Acceptance Testing which was done on May 22, 2017, was the necessary checkpoint to proceed to the deployment phase. Thus, the MWF model provides an orderly arrangement of development steps with some flexible repetitive stages to streamline the adequacy of documentation and design reviews. The Modified Waterfall method is perhaps the preferred method of choice for technology-intrinsic software development initiatives.

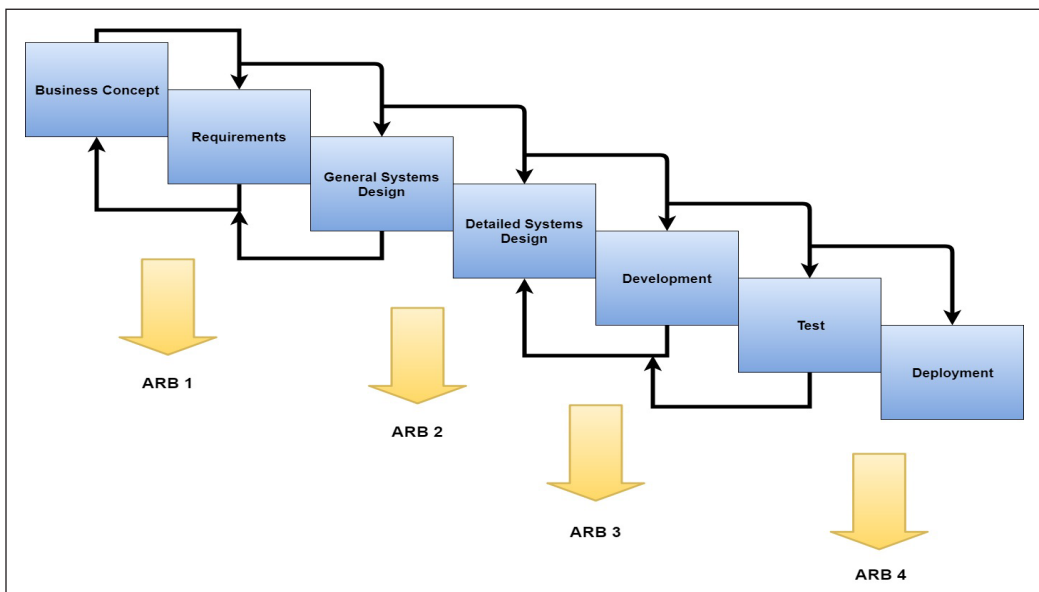


Figure 4. Modified Waterfall Model (MWF)

Requirements Gathering and Analysis of Corn Farming Related Data

Data gathering was done through surveying and interviewing local farmers in Malaybalay City. Agriculturists, thesis adviser, and officials of the Department of Agriculture were the consultants in the formulation of questions in the survey form. The partner agency initiated to call for a Stakeholder’s Forum on Corn Farming App last May 22, 2017, and 20 local farmers from Barangay Laguitas, Dalwangan, Patpat, and Kalasungay responded positively to the invitation. This survey form was distributed to the invitees and the researchers conducted a follow-up interview for further information. The researchers used judgment sampling as a common nonprobability method for sampling. The researcher selected the sample based on judgment since the attendees of the forum were the truly representative of the entire population of local farmers. After requirements gathering, the data was analyzed and interpreted and the possibility of incorporating the requirements of the mobile application to be developed was also studied. Finally, a requirement description document was generated which guided the next phase of the model.

Design of Ma-Ease Application

After compiling and analyzing a list of all needed requirements by the researchers, the design phase commenced as shown in Figure 5. Based on the user requirements provided by the local farmers and employees of the Department of Agriculture and the detailed analysis of a new mobile app conducted by the analyst, the new system was designed and developed by the developer/programmer. The tester performed feature testing for the mobile app to assess its functionality. If failed, an in-development process would be repeated,

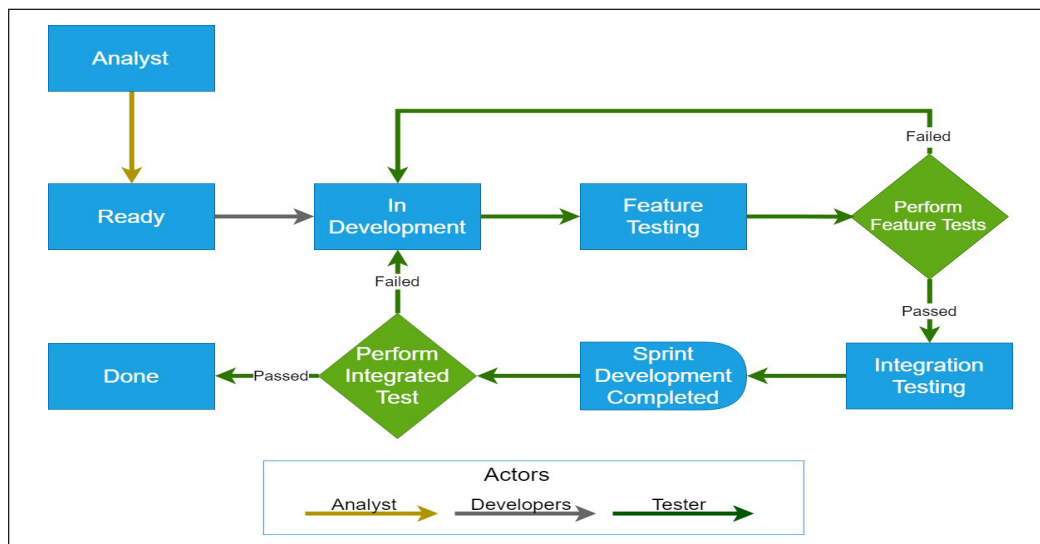


Figure 5. Design and Development Process

otherwise, integration testing and sprint development would be conducted and completed. When integration testing did not perform well, iteration went back to the in-development process in order to make necessary corrections, otherwise, Ma-Ease App was done.

Development of Ma-Ease Application

In this phase, the application design needs to be implemented to make a workable system. This phase included the specification of software and hardware requirements of the application. In order to develop Ma-Ease mobile application, the system minimum requirements were as follows:

- Microsoft® Windows® 7/8/10 (32- or 64-bit)
- 3 GB RAM minimum, 8 GB RAM (Random Access Memory) recommended; plus 1 GB for the Android Emulator.
- Minimum of 2 GB disk space (500 MB for IDE + 1.5 GB for Android SDK or Software Development Kit and emulator system image)
- 1280 x 800 minimum screen resolution.

This phase also required the coding of design into computer language using Android Studio Framework which is a Java-Based Language for mobile devices. The researchers converted the program specifications into computer instructions which they referred to as a program. The application design was referred to and changed according to the development needs when the application lacked in its functionalities. At the end of the development phase, a working prototype with the necessary functions was now operational.

Testing and Deployment of Ma-Ease Application to Local Farmers and Employees of Department of Agriculture-Malaybalay City

Before the researchers actually implement the system into operation, a test run of the system was done to remove all the bugs, if any. It is a significant phase of an effective system. After modifying the whole programs of the system, a functional test plan was developed by the researchers and testers ran the program on a given set of test data using administrator privileges – the Department of Agriculture representatives or local farmers. After testing, the application was ready to go live, which is known as the implementation phase. This was done initially by presenting our proposed mobile application to the Office of the Department of Agriculture – Malaybalay City together with the corn farmers, and finally, it was formally accepted by the DA Officials last May 22, 2017, as part of its Deployment Phase 1 as shown in Figure 6. This phase allowed the attendees to install the app on their phone via Android Application Package or APK. Phase 2 of its deployment was the integration of the app in the Google Play Store so that the app will be made available to all other corn farmers. Phase 3 involved information dissemination in partnership with Department of Agriculture – City of Malaybalay thru seminars and forums where more farmers would be invited to assess the acceptability rate of the mobile application.



Figure 6. Presentation and acceptance of Ma-Ease Project to the local corn farmers and Department of Agriculture Employees/Officials on May 22, 2017

RESULTS AND DISCUSSION

The research produced an offline Android-based application that will serve as a tool for the corn farmers in Malaybalay City, Bukidnon to improve their agricultural methods and boost agricultural productivity. Results were gathered by the researchers through thorough testing and evaluation made with the Office of Malaybalay City Agriculture and corn farmers in Malaybalay City as part of the Modified Waterfall Model.

Analysis

Table 2 shows the number of respondents who provided their satisfaction ratings and user experience with the mobile application using various criteria. On functionality, 50% of the respondents found the app very satisfactory. On reliability testing, 8 respondents agreed that the application is satisfactory. On usability and maintainability criteria, 9 or 45% of the respondents rated Ma-Ease as satisfactory. On efficiency testing, more than 50% say they are satisfied. Their user experience on the layout and design says 60% are VERY satisfied with the application program. Interestingly and unexpectedly, 2 of the respondents were not satisfied with the application in terms of reliability and usability which brought the attention of the researchers to improve the system in the specified area.

Table 3 shows the grand satisfaction ratings of the respondents using different criteria while engaging with the completed mobile application. Results reveal that the user finds the user interface VERY satisfactory with a mean of 4.6, while they were satisfied with the application in terms of functionality, reliability, usability, maintainability, and efficiency. With a grand mean of 4.175, the corn farmers and officials of the Department of Agriculture were satisfied with the software which means that they are willing to try this new technology in corn farming.

Table 2

Summary of respondents' response of its satisfaction rating with Ma-Ease mobile application on its functional and non-functional requirements

Ma-Ease Mobile Application Evaluation	Very Satisfied	Satisfied	Neutral	Un-satisfied	Very Unsatisfied
Functionality	10	7	3	0	0
Reliability	6	8	1	5	0
Usability	5	9	4	2	0
Maintainability	8	9	3	0	0
Efficiency	7	11	2	0	0
User Interface	12	8	0	0	0

Table 3

Summary of qualitative description on user's response based on their satisfaction ratings with Ma-Ease mobile application

Ma-Ease Mobile Application Evaluation	5	4	3	2	1	Average	Qualitative Description
Functionality	10	7	3	0	0	4.35	Satisfied
Reliability	6	8	1	5	0	3.75	Satisfied
Usability	5	9	4	2	0	3.85	Satisfied
Maintainability	8	9	3	0	0	4.25	Satisfied
Efficiency	7	11	2	0	0	4.25	Satisfied
User Interface	12	8	0	0	0	4.6	VERY Satisfied
GRAND MEAN						4.175	SATISFIED

This research was able to develop the Ma-Ease application in order to provide a software tool for the corn farmers in Malaybalay City which offers accessibility to practices and technology in farming's method of production. Thus, it provides workers and farmers with comprehensive site-specific farming guidelines for their corn fields.

Figure 7 shows the level 1 detailed view of activities when the farmer is engaged with the mobile application with PAGASA as the source of weather updates.

The following figures describe the use-case diagram. Figure 8 is the general use-case diagram with the end user interacting with the major processes of the application. Figure 9 shows the use-case diagram when the farmer interacts with the corn activity manager. This enables the user to add the following details: date of planting, seed type, and soil type. Figure 10 displays the different information guide related to pests, farming activities, weather, and farming history. Figure 11 illustrates how to add and calculate wages of the laborer using two methods: price per kilo and percent per kilo. Figure 12 shows how to add and view farming expense. Viewing of expenses maybe shown by total or individual. Figure 13 shows how the app notifies the user of the farming activities which includes pest termination, harvesting, and soil fertilization.

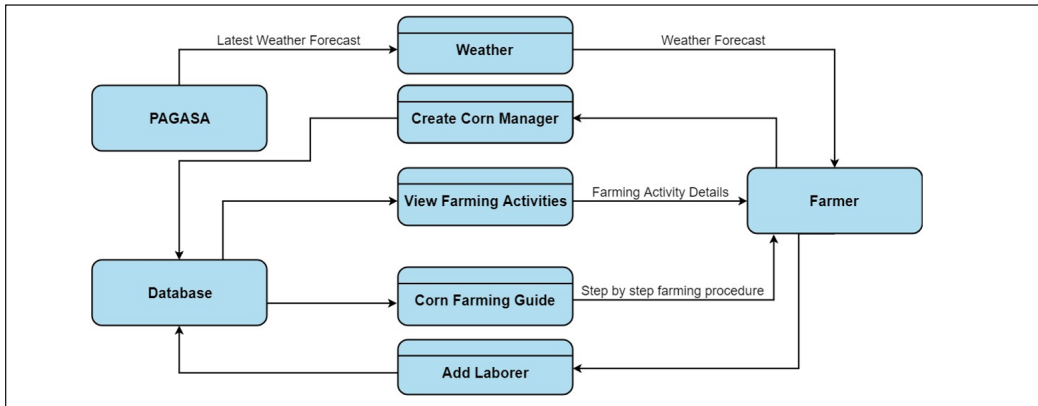


Figure 7. Detailed view of farmer's interaction of the mobile application

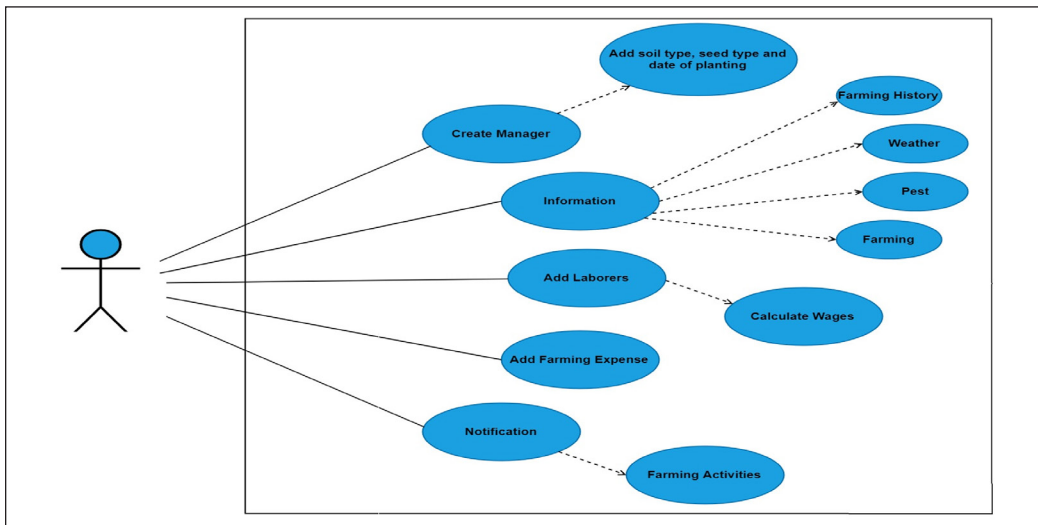


Figure 8. General use-case diagram of Ma-Ease Processes

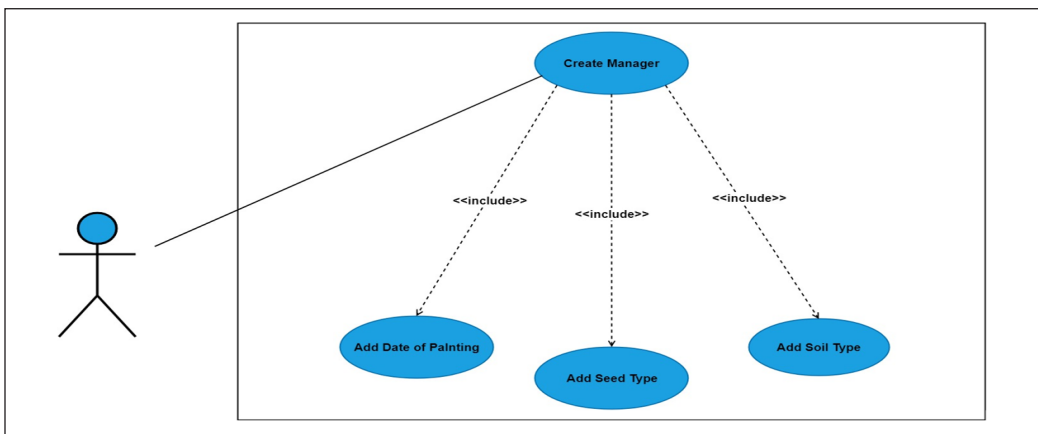


Figure 9. Use-Case diagram for creating corn activity manager

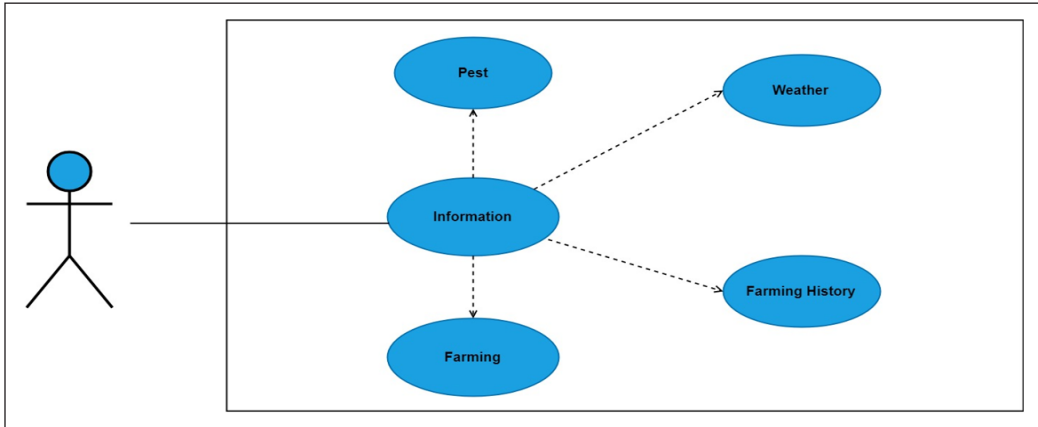


Figure 10. Use-case diagram for viewing of different information guide

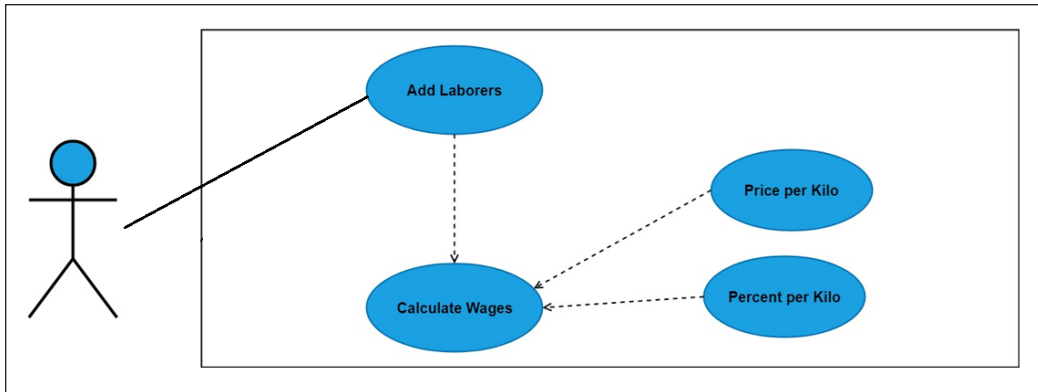


Figure 11. Use-case diagram for adding and calculating of laborer's wages

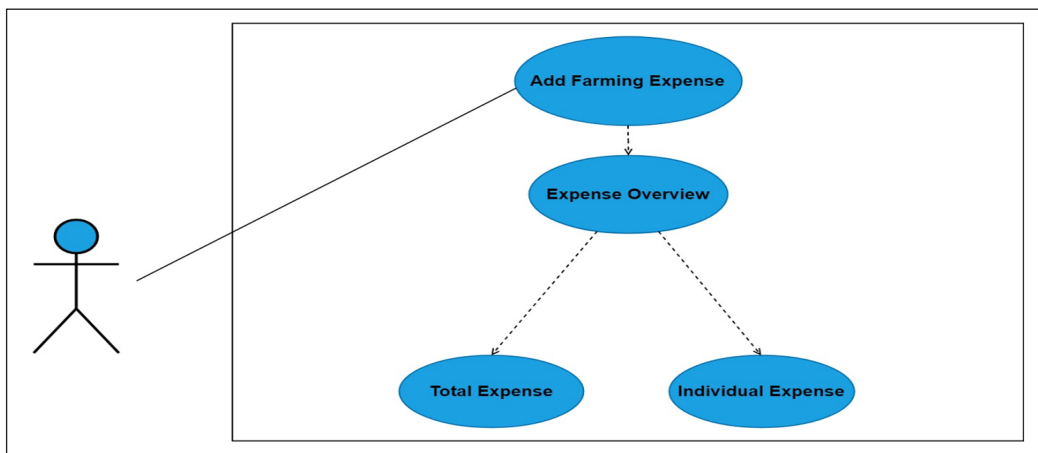


Figure 12. Use-case diagram for adding of farming expense

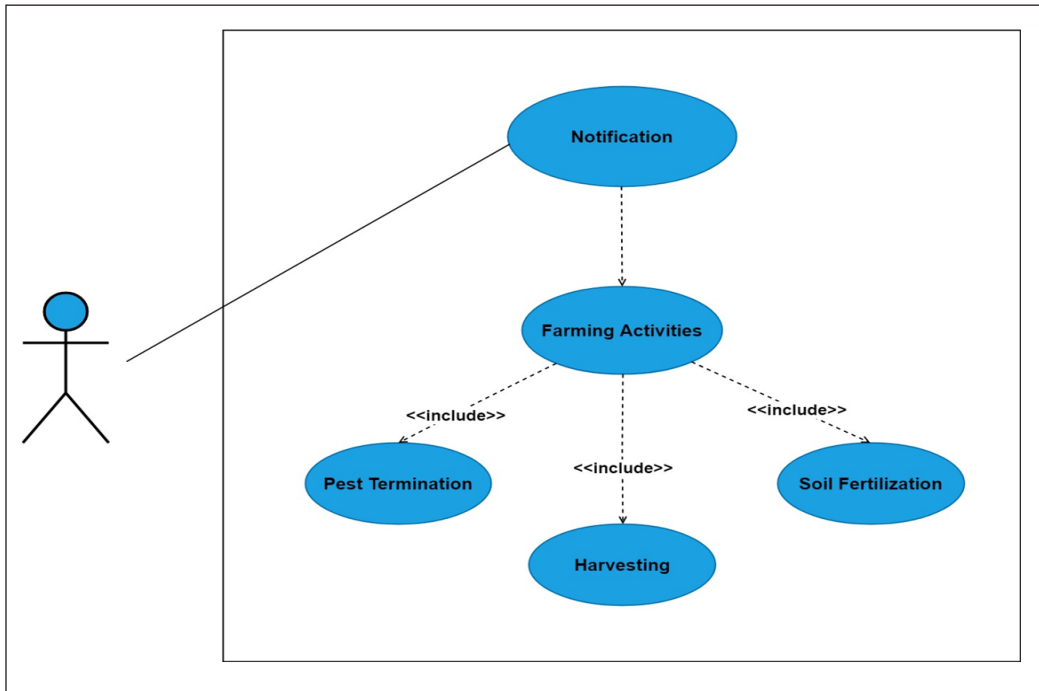


Figure 13. Use-case diagram for notification of farming activities

The following figures also shows the user interface of Ma-Ease Mobile App. Figure 14 shows a splash screen when the user opens the application on their mobile devices. Figure 15 shows the home page when the user accesses the main page of the Ma-Ease



Figure 14. Screenshot of Ma-Ease splash screen



Figure 15. Ma-Ease Home page

application which displays various menu options for corn farming such as Weather, Corn Activity Manager, Calculator, Farming Guide, and Corn Diseases and Pest Control. Figure 16 shows sample interface when the user chooses to select weather forecast option in order to check current climate condition of his/her current location. Figure 17 displays table of contents of farming guide which is translated in Filipino language so that farmer can better understand the contents. Figure 18 shows the actual contents when the user selects Topic 2 “Pagpili ng nababagay na barayti at mahusay na kalidad ng mga binhi” which in English means “Selection of suitable varieties and good quality seeds”. Figure 19 also lists all types of corn diseases and Figure 20 describes in details the sample disease termed “Downy Mildew” using its scientific name, information, symptoms and recommended solutions.



Figure 16. Guide on how to use the Weather Forecast

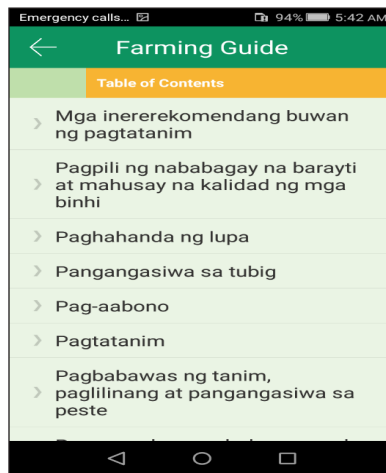


Figure 17. Farming guide table of contents

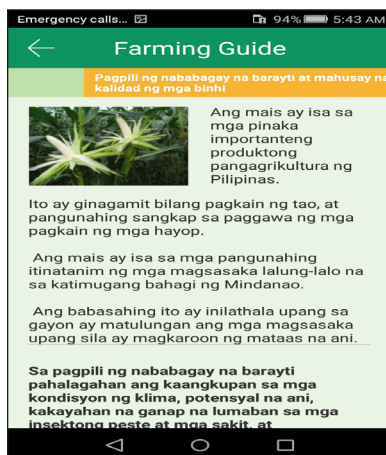


Figure 18. Farming Guide contents

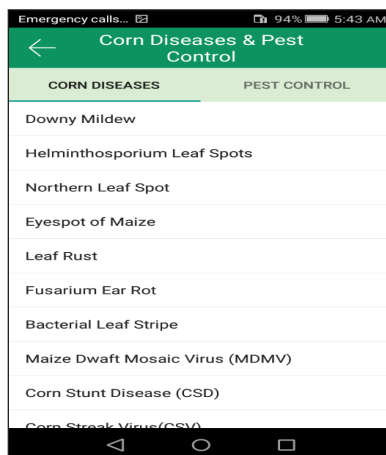


Figure 19. List of corn diseases

All of these information are provided by the Department of Agriculture. While Figure 21 lists all types of corn pests, Figure 22 also mentions “Asian Corn Borer” in specifics the scientific name, local name, damages, and the recommended solutions prescribed by DA. Figure 23 calculates number of hybrid and non-hybrid corn seed and fertilizer which requires an input data of total land area in hectares (ha). Figure 24 is a corn activity manager form which allows the user to create farm details per location. Figure 25 is a sample output when a farm details is created. It displays summary of farm using farm name and location. Lastly, Figure 26 shows additional activities once a farm is created. It includes manager, farming expense and harvest. The app provides access to best practices and latest approach to improve agricultural practices and optimize corn production.



Figure 20. Sample corn disease with the scientific name, information, symptoms, and recommended solutions

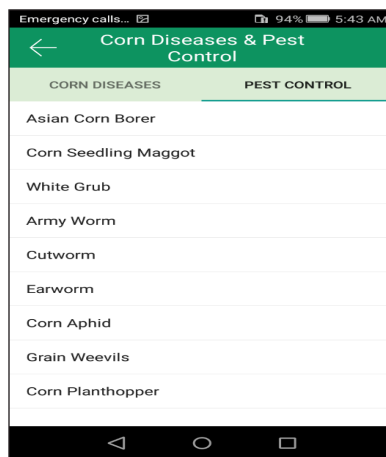


Figure 21. List of corn pests



Figure 22. Sample corn pest with the scientific name, local name, damages and recommended solutions

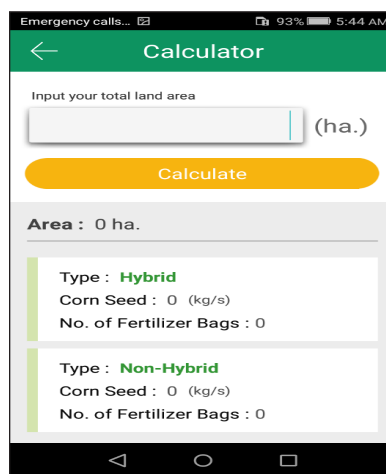


Figure 23. Corn seed and fertilizer calculator

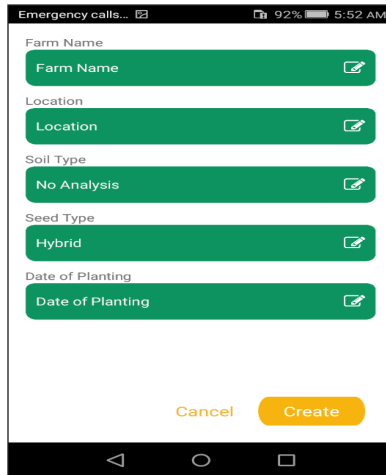


Figure 24. Corn activity manager form to create a farm

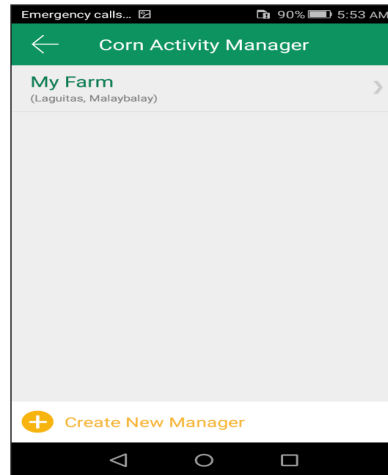


Figure 25. Creating a farm with the name and location

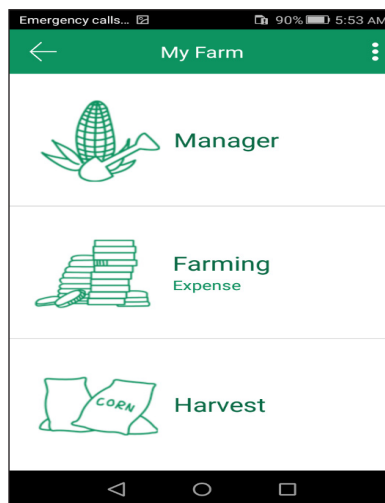


Figure 26. List of farming activities

CONCLUSION

After conducting series of tests, results show a grand mean of 4.175 which means corn farmers are satisfied with the Ma-Ease mobile app in terms of functionality, reliability, usability, maintainability, efficiency, and user interface. Furthermore, these findings show that the application was able to deliver its function to provide comprehensive information and farming guide to corn farmers, access to electronic weather information sourced by the PAGASA and other top issues and concerns confronting cities' corn growers in order to optimize farm productivity. Thus, the software product was formally accepted and recommended for use and deployment by the Department of Agriculture.

Recommendations

This study has a number of limitations which are recommended for future studies. First, the mobile application should also be available on other platforms like iOS and web. Although Android has various users especially in low socio-economic countries like the Philippines, there are already farmers which use non-android phones and own their personal computers at home.

Secondly and lastly, the mobile application should provide data about soil analysis. The current feature of the mobile application only suggests the general recommendation of fertilizer for every land. It is recommended that the future application should provide specific recommendations for the specified type of soil through the help of the Department of Agriculture in coordination with these offices: Bureau of Soils and Water Management and Fertilizer and Pesticide Authority.

REFERENCES

- de los Santos, W. L., Lansigan, F. P., & Hansen, J. (2007). Linking corn production, climate information and farm-level decision-making: a case study in Isabela, Philippines. In M. V. K. Sivakumar & J. Hansen (Eds.), *Climate Prediction and Agriculture* (pp. 157-164). Berlin: Springer.
- Food and Fertilizer Technology Center. (2006). *Effective Methods of Disseminating New Technology Considering the Viewpoint of Farmers*. Retrieved March 2, 2018, from http://www.ffc.agnet.org/library.php?func=view&id=20110720155616&type_id=1.
- Ghazizadeh, S. (2012). *Acceptance Theory on Mobile Services and Applications*. University of Applied Sciences, Finland. Retrieved October 05, 2017, from http://www.theus.fi/bistream/handle/10024/44638/Thesis_Final.pdf
- GMA News Online. (2011, January 25). World's First Mobile App for Rice Production Unveiled. *GMA News Online*. Retrieved July 2, 2016, from <http://www.gmanetwork.com/news/scitech/content/211446/worlds-first-mobile-app-for-rice-production-unveiled/story/>.
- Lee, D. (2014). *A Good to Corn Production in Georgia 2014*. The University of Georgia, Georgia. Retrieved October 05, 2017, from <http://grains.caes.uga.edu/>
- Lester, D. (2010, March 4). Sensors, Software Send Ag Alerts to Farmer Phones. *Seattle Times*. Retrieved July 2, 2016, from http://seattletimes.nsource.com/html/localnews/2011254603_apwafarmtechnology.html.
- Nguyen, H. T., & Blum, A. (Eds.). (2004). *Physiology and biotechnology integration for plant breeding*. New York: CRC Press.
- Pehu, E., Belden, C., Majumdar, S., & Jantunen, T. (2011). Increasing Crop, Livestock and Fishery Productivity through ICT. In *ICT in Agriculture: Connecting Smallholders to Knowledge, Networks, and Institutions* (pp. 85–112). Washington, D. C.: World Bank.

Sales Gamponia Aribe Jr., Jhon Michael H. Turtosa, Jul Maico B. Yamba and Alvin B. Jamisola

Philippine Statistics Authority. (2018, April). *Rice and Corn Situation and Outlook*. Retrieved July 2, 2016, from <https://psa.gov.ph/content/rice-and-corn-situation-and-outlook-reports>.

Qiang, C. Z., Kuek, S. C., Dymond, A., & Esselaar, S. (2011). *Mobile Applications for Agriculture and Rural Development*. Washington D. C.: World Bank.

Market Matching Online to Recommend MSME Export Products Destination by Using Fuzzy Control

Nurdewanto Bambang^{1*}, Sonalitha Elta¹, Ratih Salnan² and Nadia Rosmalita Sari³

¹Department of Information System, Faculty of Information Technology, University of Merdeka Malang, Malang, Indonesia

²Faculty of Engineering, Universitas Brawijaya, Malang, Jawa Timur 65145, Indonesia

³Faculty of Computer Science, Universitas Brawijaya, Malang, Jawa Timur 65145, Indonesia

ABSTRACT

MSME is a business group of society that does not have an integrated system like a large industry which makes it difficult to access information toward the location of foreign markets. This study develops Market Matching application to determine the location of foreign marketing and the type of products that must be exported to reduce the number of losses due to the congestion of turnover of goods to make it profitable for MSME. Stages to develop this market matching system are the identification and analysis of ongoing export marketing activities in MSME, designing marketing system that fits the analysis, establishing market matching system, and system implementation. This study proposes fuzzy control to determine the number of export and export market destination. Market matching application obtained recommendation of export destination based on the types of product and level of importer need. This study obtained the system's accuracy in 100% range.

Keywords: Economy, fuzzy control, market matching, Micro Small Medium Enterprises (MSME)

INTRODUCTION

When the economic crisis occurs in the world, it will automatically worsen economic condition in Indonesia. The crisis condition hits the world in the period of 1997 to 1998. This caused the Indonesian economy getting worse and worse, but only the sector of MSME (Micro Small Medium Enterprises) were able to remain strong (Suci, 2017). Based on data from Statistic's

ARTICLE INFO

Article history:

Received: 10 November 2017

Accepted: 28 August 2018

Published: 24 January 2019

E-mail addresses:

nurdewa@unmer.ac.id (Nurdewanto Bambang)

elta.sonalitha@unmer.ac.id (Sonalitha Elta)

salnanratih@gmail.com (Ratih Salnan)

nadiaroosmalitasari@gmail.com (Nadia Rosmalita Sari)

* Corresponding author

Center Indonesia, after the crisis, the number of MSME in Indonesia was not reduced, even increased until 2012. In that year the number of MSME reached the percentage of 99.99%, and the remaining 0.01% was a large-scale business. MSME is a productive business to be developed to support macro and micro economic development in Indonesia and affects other sectors, for example banking services sector.

Currently, MSME export products have constraints in slow product turnover in importer countries because the product stock is not sold out soon in those countries and sometimes it reaches the expiration limit. This is because there is no information about the development of market location and MSME competition with the same product. The lack of information on the amount of demand and supply of products in each country greatly affects the turnover of goods. For example, there are five industries with the same type of product delivering to Australia where the demand for the product is small. Without proper information the five industries only export products regardless of the availability of products in the country. Therefore, the number of products in Australia exceeds the number of request. This resulted in the accumulation of products, so the industry losses due to the lack of sales. Products with fast turnover are goods sold out in a relatively quick time. Determination of the right export market based on the criteria needed is one of the efforts made by business actors in order to increase profits and reduce losses due to the risk of delayed turnover of the products.

Considerations of the purpose of the goods export are the criteria to be taken into account. Criteria considered include: (1) financial limitations of MSME in producing commodities; (2) the difficulty in knowing the needs of the export market, (3) the difficulty of knowing the fast or slow turnover of goods in the market.

MSME become the target of this study object, because MSME is a business group of society that does not have an integrated system like a large industry. MSME are difficult to conduct surveys and market analysis by themselves, due to limited capital and human resources in the field of information technology. This study proposes fuzzy control to determine the right target market at MSME in the world. Fuzzy control method is used to overcome the determination of a market that is influenced by the subjectivity of marketing actors. Determination of this market cannot be separated from the subjectivity and experience of MSME export marketing actors. Some target markets for the same product will elicit a complex calculation to consider which markets and countries in which the product will be distributed.

Sari et al. (2017) stated that fuzzy had reasoning ability that was similar to human reasoning ability. This is because the fuzzy system has the ability to provide responses based on inaccurate, qualitative, and ambiguous information. Therefore, in this study, output would be used as consideration in deciding the export destination of goods.

Recent Studies

Some previous researchers have successfully executed market matching by using a variety of approaches. Ackermann, et al. (2009) executed market matching with a stable matching approach introduced by Gale and Shapley. Stable matching can be computed in polynomial time, but many real-life markets lack a central authority to match agents. In those markets, match behaviors are formed by actions of dynamics. The results show that coordination is necessary in two-sided markets, as well as these markets do not stabilize quickly.

Che and Tercieux (2013) studied efficient and stable mechanisms in many-to-one matching markets when the number of agents was large and individuals' preferences were drawn randomly from a class of distributions allowing for both common value and idiosyncratic components. They proposed a new mechanism that was asymptotically efficient, asymptotically stable and asymptotically incentive compatible. The result of this study is the proposed mechanism is able to link matching markets efficiently and stable.

This research is a development of previous research (Nurdewanto, Amrullah, & Sonalitha, 2017). In the previous research, the application was developed in the form of a simple market matching application. The application was developed only limited to search market (importer) based on data base worldwide. This application is used by MSME to search for market destination with input category "goods" and "continent". The application produces the output of the name of the importer in accordance with the category and the continent.

Based on that background and previous research, to be more effective and efficient, an approach is needed by using artificial intelligence for market matching globally (many to many). The proposed approach is fuzzy control. This application is able to know the location of importer according to product type and capacity of product that can be imported. Fuzzy can provide the best option for MSMEs to determine the location of the importer based on the capacity of the appropriate product to be imported.

Fuzzy Controls

This study used fuzzy control to determine the location of foreign marketing and the types of product that must be exported. In fuzzy method, every consequence of the IF-THEN rules should be modeled with a fuzzy set with the same membership function (Sari & Mahmudy, 2017). As a result, the inference output of each rule is given explicitly. Fuzzy control has several stages, namely fuzzification, fuzzy inference engine, and defuzzification (Sari et al., 2017) shown in Figure 1.

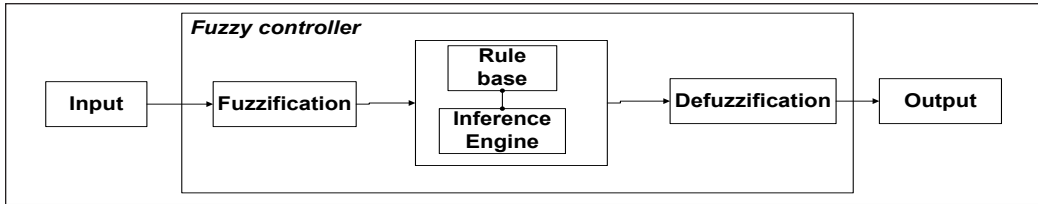


Figure 1. Fuzzy Control's Diagram

Note: Adapted from Sari et al., 2016 and Farzilah et al., 2017)

Fuzzification. The input and output variables in fuzzy control were divided into one or more fuzzy sets (Noor & Kamal, 2017). In this process, the parameters used to determine the market were efficiently represented as input variables. The input variables used in this study were Stock, Capacity, and Competitive, while the output variable in this process was in the form of Export (the amount of goods). The fuzzy set is a unity representing a particular state in a fuzzy variable. In this process used fuzzy set of three linguistic variables which were LOW, MEDIUM, and HIGH. The formation of this fuzzy set was customized based on expert opinion. The function for determining membership value is illustrated by Triangular Fuzzy Number shown in Figures 2, 3 and 4 (Sameer & Bakar, 2017). Membership function in each set is formulated in Eq. (1) - Eq. (10), where μ is the degree of membership and x is the object set (Sameer & Bakar, 2017).

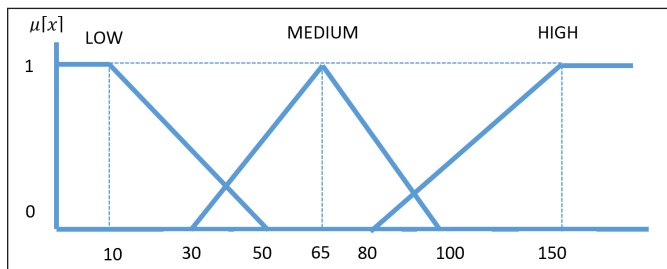


Figure 2. An example of Triangular Fuzzy Number Variable Input "Stock"

$$\mu_{StockLOW}[x] = \begin{cases} 1, & x \leq 10 \\ \frac{50 - x}{50 - 10}, & 10 < x < 50 \\ 0, & x \geq 50 \end{cases} \quad (1)$$

$$\mu_{StockMEDIUM}[x] = \begin{cases} 0, & x \leq 30 \text{ or } x \geq 100 \\ \frac{x - 30}{65 - 30}, & 10 < x \leq 65 \\ \frac{100 - x}{100 - 65}, & 65 < x < 100 \end{cases} \quad (2)$$

$$\mu_{StockHIGH}[x] = \begin{cases} 0, & x \leq 80 \\ \frac{x - 80}{150 - 80}, & 80 \leq x \leq 150 \\ 1, & x \geq 150 \end{cases} \quad (3)$$

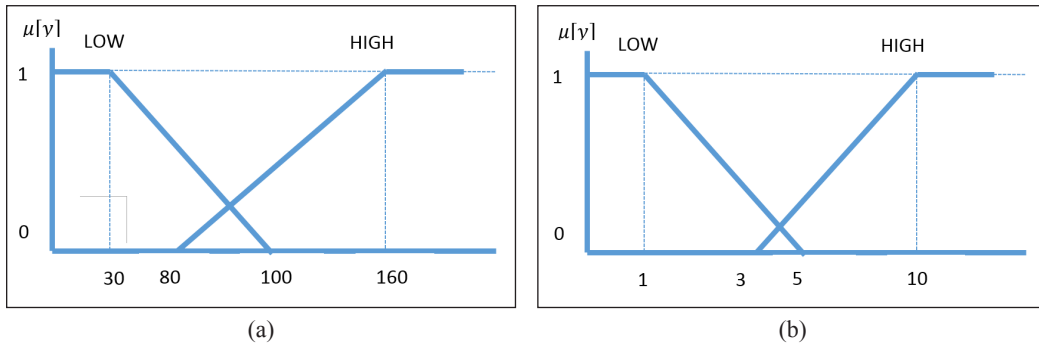


Figure 3. An example of Triangular Fuzzy Number Variable Input: (a) “Capacity”; and (b) “Competitive”

$$\mu_{Low\ Capacity}[y] = \begin{cases} 1, & y \leq 30 \\ \frac{100 - y}{100 - 30}, & 30 < y < 100 \\ 0, & y \geq 100 \end{cases} \quad (4)$$

$$\mu_{High\ Capacity}[y] = \begin{cases} 0, & y \leq 80 \\ \frac{y - 80}{160 - 80}, & 80 < y < 160 \\ 1, & y \geq 160 \end{cases} \quad (5)$$

$$\mu_{Low\ Competitive}[z] = \begin{cases} 1, & z \leq 1 \\ \frac{5 - z}{5 - 1}, & 1 < z < 5 \\ 0, & z \geq 5 \end{cases} \quad (6)$$

$$\mu_{High\ Competitive}[z] = \begin{cases} 0, & z \leq 3 \\ \frac{z - 3}{10 - 3}, & 3 < z < 10 \\ 1, & z \geq 10 \end{cases} \quad (7)$$

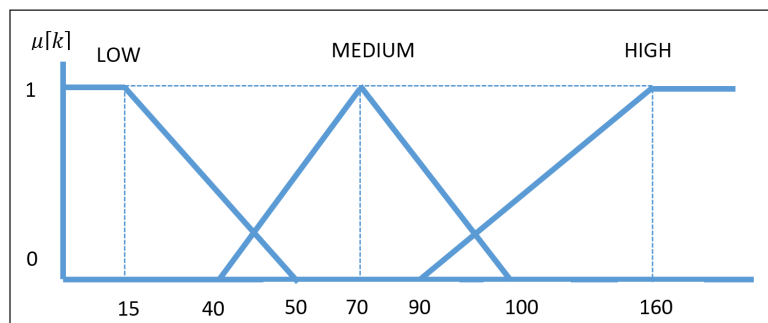


Figure 4. An example of Triangular Fuzzy Number Variable Input “Export”

$$\mu_{Low Export}[k] = \begin{cases} 1, & k \leq 15 \\ \frac{50 - k}{50 - 15}, & 15 < k < 50 \\ 0, & k \geq 50 \end{cases} \quad (8)$$

$$\mu_{Medium Export}[k] = \begin{cases} 0, & k \leq 40 \text{ atau } k \geq 100 \\ \frac{k - 40}{70 - 40}, & 40 < k \leq 70 \\ \frac{100 - k}{100 - 70}, & 70 < k < 100 \end{cases} \quad (9)$$

$$\mu_{High Export}[k] = \begin{cases} 0, & k \leq 90 \\ \frac{k - 90}{160 - 90}, & 90 < k < 160 \\ 1, & k \geq 160 \end{cases} \quad (10)$$

Fuzzy Inference Engine. The results of the fuzzy membership value calculation process were then inferenced against fuzzy rules. In fuzzy control, the implication function used is Min. There are three input variables (t) that need to be implemented against fuzzy rules. The calculation of the number of rules is by multiplying the number of fuzzy set (two linguistic variables) by the number of input variable. In this stage the number of rules used 13 rules obtained from all input combinations. The fuzzy rules used in this study are shown in Table 1.

Table 1
The formation of Fuzzy Rules

Fuzzy Rules
[R1] IF stock LOW AND capacity LOW AND competitive LOW THEN export LOW
[R2] IF stock LOW AND capacity LOW AND competitive HIGH THEN export LOW
[R3] IF stock LOW AND capacity HIGH AND competitive LOW THEN en export HIGH
[R4] IF stock LOW AND capacity HIGH AND competitive HIGH THEN export MEDIUM
[R5] IF stock MEDIUM AND capacity LOW AND competitive LOW THEN export LOW
[R6] IF stock MEDIUM and capacity LOW AND competitive HIGH THEN export LOW
[R7] IF stock MEDIUM AND capacity HIGH AND competitive LOW THEN export HIGH
[R8] IF stock MEDIUM AND capacity HIGH AND competitive HIGH THEN export MEDIUM
[R9] IF stock HIGH AND capacity LOW AND competitive LOW THEN export MEDIUM
[R10] IF stock HIGH AND capacity LOW AND competitive HIGH THEN export LOW
[R11] IF stock HIGH AND capacity HIGH AND competitive LOW THEN export HIGH
[R12] IF stock HIGH AND capacity HIGH AND competitive HIGH THEN export LOW

Defuzzification

To get the output value (crisp) is by converting the input into a number on the fuzzy set domain or by defuzzification (Sari et al., 2016). Having obtained the value of α_i , then will be the process of calculating the value of each consequence each rule z_i in accordance

with the membership function used. The defuzzification method in fuzzy control is Center Average Defuzzifier which is formulated in Eq. (11).

$$Z = \sum_{i=1}^n \alpha_i z_i \frac{\sum_{i=1}^n \alpha_i z_i}{\sum_{i=1}^n \alpha_i}$$

Where, in above Z is the result of defuzzification, whereas α_i is the membership value antecedent, and z_i is the inference result of each rule.

RESULT AND DISCUSSION

The Dataset

MSME become the target of this study object, because MSME is a business group of society that does not have an integrated system like a large industry. MSME are difficult to conduct surveys and market analysis by themselves, due to limited capital and human resources in the field of information technology.

The case study used is the right selection of importers with the right amount, so that the exports made by MSME are efficient. This study used importer or buyer data which consisted of Buyer, Address, City, Nation, Region, Contact (Telephone, fax, Email), and Product. The data obtained from the Department of Industry and Trade of East Java Province in 2010. This study used sample data of four data. Company data is shown in Table 2. The data would be processed and be input data.

Table 2
MSME data in some regions

No	Buyer Name	Product
1	BOS LIMITED	Furniture
2	CENTURY CO., LTD.	Furniture
3	BOS LIMITED	Watches
4	Advertising Co., Ltd.	Watches

Experiment. This section presents case study related to matching market. There is a problem and a solution. The solution is a proposed approach in this study that is using fuzzy control method with the provisions that have been described in Section Fuzzy Control. The problem is that there is a buyer who imports the furniture product that is BOS LIMITED (BL).

BL \rightarrow Stock = 12, capacity = 200, competitive = 2

Fuzzification. The membership function at fuzzification stage of the “Stock” input variable is shown in Table 3. While the fuzzification membership function in the input variables “Capacity” and “Competitive” are shown in Table 4 and Table 5.

Table 3
Fuzzification process in “Stock”

EMPLOYEE “BL”		
PARAMETER	MIN	MAX
LOW	10	50
MEDIUM	30	100
HIGH	80	150

Table 4
Fuzzification process in “Capacity”

EMPLOYEE “BL”		
PARAMETER	MIN	MAX
LOW	30	100
HIGH	80	160

Table 5
Fuzzification process in “Competitive”

EMPLOYEE “BL”		
PARAMETER	MIN	MAX
LOW	1	5
HIGH	3	10

Based on calculations using Eq. (1) - Eq. (7) obtained the membership VALUE on each input variable as follows.

$$\begin{aligned} \mu_{StockLow}[15] &= 0.95 & \mu_{CapacityLow}[100] &= 0 & \mu_{CapacityLow}[5] &= 0.75 \\ \mu_{StockMedium}[15] &= 0 & \mu_{CapacityHigh}[100] &= 1 & \mu_{CapacityHigh}[5] &= 0 \\ \mu_{StockHigh}[15] &= 0 & & & & \end{aligned}$$

Fuzzy Inference Engine. Based on the formation of membership function at fuzzification stage, can be done next process that is fuzzy inference engine. In this stage the process of calculating the function of the implication by applying fuzzy rules that have been established previously. The results of the implication value calculation are shown in Table 6.

[R1] IF stock LOW AND capacity LOW AND competitive LOW THEN Export MEDIUM formula

$$\begin{aligned} \alpha\text{-predicate}_1 &= \mu\text{StockLow} \cap \mu\text{CapacityLow} \cap \mu\text{CompetitiveLow} \\ &= \min(\mu\text{StockLow}(12), \mu\text{CapacityLow}(200), \mu\text{CompetitiveLow}(2)) \\ &= \min(0.95; 0; 0.75) \\ &= 0 \\ 0 &= \frac{50 - z_1}{50 - 15} \Rightarrow z_1 = 50 \end{aligned}$$

Table 6
The results of implication value calculation

Fuzzy Rules	$\alpha\text{-predicate}_n$	Implication Value Z_n	$\alpha\text{-predicate}_n \cdot Z_n$
[R1]	0	50	0
[R2]	0	50	0
[R3]	0.75	142.5	106.875
[R4]	0	40	0
[R5]	0	50	0
[R6]	0	50	0
[R7]	0	90	0
[R8]	0	40	0
[R9]	0	40	0
[R10]	0	50	0
[R11]	0	90	0
[R12]	0	50	0
Σ	0.75		106.875

Defuzzification. Having obtained the value of α predicate and implication value (Z_n), then it will be done the process of calculating the defuzzification value by using Eq. (11). Based on the results of defuzzification calculation obtained the final value or crisp value of 143. The value is the number of goods from a company to be ready for export.

$$z = \frac{\sum_{n=1}^{12} \alpha\text{-predicate}_n \times z_n}{\sum_{n=1}^{12} \alpha\text{-predicate}_n} = \frac{106.875}{0.75} = 142.5 = 143$$

Based on the results of manual calculations by using fuzzy control, it can be seen that on the BOS LIMITED buyer there are 143 items amount (Figure 5). The results are in accordance to the data base on the system developed. Therefore, the result of manual calculations with the system is accurate. The accuracy generated between manual calculations and output system in this study is 100%.

No.	Buyer Name	Produk	Ekspor
1	BOS LIMITED	Furniture	143
2	CENTURY CO., LTD. -	Furniture	107
3	BOS LIMITED	Watches	126
4	Advertising Co., Ltd.	Watches	83

Figure 5. Display of Importer Result “Export” (Amount of goods). BL Buyer produces 143 outputs (capacity of goods)

CONCLUSION

Fuzzy control method used in this study can be implemented to determine the number of export and export destination in a company. This study obtained the system’s accuracy in 100% range. This study is still in progress, so the data used in this study is sample data. In this study, fuzzy rule determination is done manually based on expert opinion. If the fuzzy rules are determined manually, it will be more experimental. There is a probability that the determination is less fit. Therefore, the implementation of genetic algorithm in subsequent study is needed to optimize fuzzy rules. The optimization of fuzzy rules aims to improve the accuracy of the system better. Genetic Algorithm has been widely used to solve problems related to optimization such as study that has been done by (Wijyaningrum & Mahmudy, 2016).

ACKNOWLEDGEMENT

We are thankful to God who has given us the power, good sense and confidence to complete this research analysis successfully, and I am grateful to my research supervisor and to the Faculty of Information Technology University of Merdeka Malang and Ministry of Research, Technology, and Higher Education valuable suggestions and guidance. I also would like to express my gratitude to the editor and to others who have made suggestions and given help with comments and feedbacks in improving this paper.

REFERENCES

- Ackermann, H., Goldberg, P. W., Mirrokni, V. S., Röglin, H., & Vöcking, B. (2009). Uncoordinated two-sided matching markets. *ACM SIGecom Exchanges*, 8(1), 8-15.
- Che, Y. K., & Tercieux, O. (2013). Efficiency and stability in large matching markets. *American Economic Assosiation*, 2013, 1–56.

- Farzilah, N., Mailah, Y. H., Amran, M., & Radzi, M. (2017). DC-link Capacitor Voltage Regulation with Effort-reduction Fuzzy Logic Control for Three-level Inverter-based Shunt Active Power Filter. *Pertanika Journal of Science and Technology*, 25(S), 11–20.
- Noor, I. M. M., & Kamal, M. (2017). Control of Wastewater Treatment by using the Integration MATLAB and LabVIEW. *Pertanika Journal of Science and Technology*, 25(S), 77–84.
- Nurdewanto, B., Amrullah, F., & Sonalitha, E. (2017). Aplikasi Market Matching Untuk Pencarian Tujuan Export Produk UMKM [Market Matching Application For Searching Purpose Of Export Of UMKM Products]. In *Seminar Nasional Sistem Informatika (SENASIF)* (Vol. 1, pp. 874–879). Universitas Merdeka Malang, Indonesia.
- Sameer, F., & Bakar, M. R. A. (2017). Modified Kohonen Network Algorithm for Selection of the Initial Centres of Gustafson-Kessel Algorithm in Credit Scoring. *Pertanika Journal of Science and Technology*, 25(1), 77–90.
- Sari, N. R., & Mahmudy, W. F. (2017). *Fuzzy inference system Tsukamoto untuk menentukan kelayakan calon pegawai* [FIS Tsukamoto for Determine Eligibility of Prospective Employees] (pp. 245–252). Presented at the Seminar Nasional Sistem Informasi Indonesia (SESINDO 2015), Institut Teknologi Sepuluh Nopember (ITS): Open Access Journal of Information Systems (OAJIS).
- Sari, N. R., Mahmudy, W. F., & Wibawa, A. P. (2016). Backpropagation on Neural Network Method For Inflation Rate Forecasting in Indonesia. *International Journal of Advances in Soft Computing and its Applications*, 8(3), 70–87.
- Sari, N. R., Mahmudy, W. F., & Wibawa, A. P. (2017). The Effectiveness of Hybrid Backpropagation Neural Network Model and TSK Fuzzy Inference System for Inflation Forecasting. *Journal of Telecommunication, Electronic and Computer Engineering (JTEC)*, 9(2), 111–117.
- Suci, Y. R. (2017). Perkembangan UMKM (Usaha Mikro Kecil dan Menengah) di Indonesia [UMKM Development in Indonesia]. *Jurnal Ilmiah Cano Ekonomos*, 6(1), 51–58.
- Wijayaningrum, V. N., & Mahmudy, W. F. (2016). Optimization of Ship's Route Scheduling Using Genetic Algorithm. *Indonesian Journal of Electrical Engineering and Computer Science*, 2(1), 180–186.



Supervised Clustering based on a Multi-objective Genetic Algorithm

Vipa Thananant* and Surapong Auwatanamongkol

*School of Applied Statistics, National Institute of Development Administration,
Bangkok 10240, Thailand*

ABSTRACT

Supervised clustering organizes data instances into clusters on the basis of similarities between the data instances as well as class labels for the data instances. Supervised clustering seeks to meet multiple objectives, such as compactness of clusters, homogeneity of data in clusters with respect to their class labels, and separateness of clusters. With these objectives in mind, a new supervised clustering algorithm based on a multi-objective crowding genetic algorithm, named SC-MOGA, is proposed in this paper. The algorithm searches for the optimal clustering solution that simultaneously achieves the three objectives mentioned above. The SC-MOGA performs very well on a small dataset, but for a large dataset it may not be able to converge to an optimal solution or can take a very long running time to converge to a solution. Hence, a data sampling method based on the Bisecting K-Means algorithm is also introduced, to find representatives for supervised clustering. This method groups the data instances of a dataset into small clusters, each containing data instances with the same class label. Data representatives are then randomly selected from each cluster. The experimental results show that SC-MOGA with the proposed data sampling method is very effective. It outperforms three previously proposed supervised clustering algorithms, namely SRIDHCR, LK-Means and SCEC, in terms of four cluster validity indexes. The experimental results show that the proposed data sampling method

not only helps to reduce the number of data instances to be clustered by the SC-MOGA, but also enhances the quality of the data clustering results.

Keywords: Crowding genetic algorithm, data sampling, multi-objective optimization, Pareto optimal solutions, supervised clustering

ARTICLE INFO

Article history:

Received: 4 January 2018

Accepted: 27 September 2018

Published: 24 January 2019

E-mail addresses:

vipa@cpc.ac.th (Vipa Thananant)

surapong@as.nida.ac.th (Surapong Auwatanamongkol)

* Corresponding author

INTRODUCTION

Nowadays, very large amounts of data are generated and collected from diverse sources. There is a growing need to obtain useful information or patterns from data that have been collected. One of the essential tools for extracting such information or patterns is data clustering (Kaufman & Rousseeuw, 1990). Traditional (unsupervised) clustering tries to group data instances into clusters such that intra distances (distances between data instances in the same clusters) are minimal, while inter distances (distances between data instances from different clusters) are maximal (Jain & Dubes, 1988). Unsupervised clustering does not rely on predefined classes or class-labelled training examples like supervised clustering to group data instances into cluster. It is not necessarily guaranteed to group data objects with the same class together. Besides these two objectives, supervised clustering incorporates the third objective, which of minimal impurity level, which requires all data instances in each cluster to have the same class label. Some of the existing supervised clustering algorithms may consider different objectives – for example, SRIDHCR (Eick et al., 2004) considers only the impurity level and the number of clusters.

Supervised clustering is useful for various applications. In general, supervised clustering can be used for creating background knowledge for a dataset, dataset compression and editing (Eick et al., 2004), regional learning and evaluating distance functions in distance function learning (Eick et al., 2006). Finley and Joachims (2005) presented an SVM algorithm for training a clustering algorithm that optimized a variety of clustering performance measures. The algorithm had been used for noun-phrase and news article clustering. Eick et al. (2006) introduced a supervised clustering approach, SCAH algorithm, for region discovery. Haider et al. (2007) presented a supervised clustering algorithm for Streaming Data and applied it for email batch detection to filter spams. Maji (2010) proposed a novel supervised attribute clustering algorithm to find groups of co-regulated genes with respect to their gene expressions. Grbovic et al. (2013) studied supervised clustering, MM-PL algorithm, for the context of label ranking data. This algorithm can be used to divide the section of target marketing. Peralta et al. (2013) proposed LK-Means, an algorithm for supervised clustering based on a variant of K-Means which incorporated information about class labels. It had been shown that it could be used to generate a codebook for a visual recognition task.

Supervised Clustering problems can be viewed as optimization problems with multi objectives such as minimizing intra cluster distances, maximizing inter cluster distances and minimizing cluster impurity with respect to the class labels of data instances in clusters. To solve multi-objective optimization problems, evolutionary algorithms has become very popular due to their effectiveness to find the optimal solutions (Deb, 2001). An evolutionary algorithm based on a genetic algorithm had been proposed to solve supervised clustering problems. The algorithm, namely SCEC, combines multiple objective values of supervised

clustering into single objective value using a weighed sum of the multiple objective values. It has been shown to outperform some supervised clustering algorithms such as LK-means and SRIDHCR algorithm, using four evaluation metrics (Adjusted Mutual Information (AMI) (Vinh et al., 2009), Adjusted Variation of Information (AVI) (Vinh et al., 2009), Adjusted Rand Index (ARI) (Hubert & Arabie, 1985) and Mirkin distance (MD) (Mirkin & Chernyj, 1970). These evaluation metrics are based on the contingency table shown in Table 1. Based on the results of the four evaluation metrics, they are still far from desirable values. SCEC also considers only two objectives for optimization, i.e. intra cluster distance (compactness) and cluster impurity. Moreover, the weighed sum scheme for combining multi objectives requires proper setting of the weight values which can be difficult for three or more objectives. It had been shown that the scheme cannot find the non-dominated or Pareto-optimal solutions if the Pareto-optimal front was non-convex (Deb, 2001).

Table 1
The contingency table

Y/Z	Z ₁	Z ₂	...	Z _B	Total
Y ₁	u ₁₁	u ₁₂	...	u _{1B}	r ₁
Y ₂	u ₂₁	u ₂₂	...	u _{2B}	r ₂
⋮	⋮	⋮	⋮	⋮	⋮
Y _A	u _{A1}	u _{A2}	...	u _{AB}	r _A
Total	c ₁	c ₂		c _B	N

Convergence and diversity are the two conflicting goals of evolutionary algorithm. On one hand, if the algorithm focuses more on the convergence to reach the optimal solutions, diversity of chromosomes in the population must be low so the search of the algorithm can be more focus on very good solutions in the population. This may lead to premature convergence to suboptimal solutions. On the other hand, if the algorithm focuses on diversity which allows the algorithm to search more broadly on potential solutions, the convergence becomes slow. A genetic algorithm faces the problem of trying to achieve the two conflicting goals at the same time. De Jong (1975) proposed crowding as a technique to improve population diversity in a genetic algorithm while maintaining the good convergence. The main concept of crowding is to replace a parent chromosome with its most similar offspring if it is fitter than the parent chromosome. With this replacement strategy, multiple subpopulations are formed which allow the search to continue in each population concurrently. This helps diversify the search to many parts of the search space and enhance the chance to find the optimal solutions. At the end, the crowding genetic

algorithm converges to multiple solutions, so it is suitable for multi-modal optimization problems.

In this paper, we propose a new supervised clustering algorithm based on a multi-objective crowding genetic algorithm. Unlike the SCEC, it considers three objective functions to optimize, i.e. intra cluster distances (compactness of clusters), inter cluster distances (separateness of clusters) and impurity levels of clusters. A Pareto ranking scheme is employed to rank chromosomes in the population based on the three objective functions. The ranks of the chromosomes are used in the parent replacement process of the crowding. The crowding can enhance the diversity of the search and so the chance of finding the optimal solutions. For a large dataset, the search space for the genetic algorithm can be very large which can prohibit the algorithm to converge to the optimal solutions. Therefore, a data sampling method based on clustering sampling approach is proposed to create a small set of data representatives for supervised clustering. A clustering algorithm based on bisecting K-means is used to group the data instances in the given dataset into clusters, each with data instances of the same class label. The data instances are then sampled from each cluster to form a representative dataset for clustering by the proposed algorithm. The results of experiments reveal that the proposed algorithm can find better clustering solutions than SCEC, SRIDHCR and LK-Means in terms of the four aforementioned evaluation metrics. The experimental results also show that the proposed sampling technique is effective to create a good representative dataset for the given dataset. The sampling technique not only helps reduce the running time of the proposed algorithm, but also helps the algorithm to converge better to the optimal solutions since it can reduce the size of search space for the genetic algorithm.

Supervised Clustering

Some existing supervised clustering algorithms are briefly presented in this section.

SRIDHCR

The objective of SRIDHCR is to minimize the following fitness function ($f(X)$):

$$f(X) = I(X) + \alpha * P(K) \quad [1]$$

where X is a clustering solution containing K clusters, $I(X)$ is the average impurity level of the clusters (the average percentage of minority data instances in a cluster whose class labels are different from that of the majority), α is the weight (between 0 and 2) imposed on the penalty value $P(K)$ where $P(K)=0$ when K is less than the number of actual classes (A) in the given dataset and $P(K) = \sqrt{\frac{K-A}{N}}$ when $K \geq$ the number of actual classes, and N is the number of data instances.

For each run of SRIDHCR, a number of initial cluster representatives are selected randomly from the data instances. The remaining data instances are then assigned to their

closest representatives to form clusters. For each iteration, a new candidate set of cluster representatives is created by adding one data instance that is not a representative and removing one data instance that is. The current set of cluster representatives, S , is replaced with the best candidate set X for which $f(X)$ is better than $f(S)$. The iteration stops when no improvement of the fitness function value is achieved. This search process is tried for several runs and the best solution among all runs is reported. SRIDHCR also varies the value of K to determine its optimal value.

SCEC

SCEC (Eick et al., 2004) adopts the same objective function $f(X)$ as SRIDHCR. SCEC searches for the optimal set of cluster representatives by following an evolutionary computing approach. SCEC first randomly creates a population of solutions or chromosomes. Each of these specifies a set of representatives of clusters. SCEC selects two chromosomes randomly from the population, and the chromosome with the better fitness value is chosen to become one of the parent chromosomes for the reproduction of offspring. Three genetic operators are used to create a new offspring chromosome for the next generation. These are crossover, mutation and copy operators. For the crossover, two parent chromosomes are recombined to create two offspring chromosomes. The mutation operator selects one data representative randomly and replaces it with a randomly selected non-representative one. The copy operator simply copies the parent chromosomes to the new population. Finally, to build a cluster, data instances are assigned to their nearest representatives. The evolutionary process is performed repeatedly until the population converges.

Labelled K-Means (LK-Means)

The LK-Means algorithm (Peralta et al., 2013) is similar to the traditional unsupervised K-Means algorithm, but class labels of the data instances are considered in the evaluation of the LK-Means fitness function. The fitness function of LK-Means is based on two criteria: (1) a discriminative score based on class labels; and (2) a generative score based on a traditional metric for unsupervised clustering. We assume a dataset X with N training instances (x_i, y_i) , where $x_i \in \mathbb{R}^d$, $y_i \in [1, \dots, L]$, $i \in [1 \dots N]$ and X is partitioned into K clusters. LK-Means replaces the traditional K-Means fitness function by the following Equation 2:

$$F(a_k^l, \partial_{nk}^l) = \sum_{n=1}^N \left[\beta \sum_{k=1}^K \sum_{l=1}^L \partial_{nk}^l \|x_n - a_k^l\|^2 \omega_k^l + (1 - \beta) \sum_{k=1}^K \partial_{nk} \|x_n - a_k\|^2 \right] \quad [2]$$

where β and $1 - \beta$ are the weights for the supervised and unsupervised clustering scores, respectively. The value of β is between 0 and 1. a_k^l is the supervised mean of the data instances in cluster C_k with label l . ∂_{nk}^l is the supervised indicator that assigns instance x_n to the mean a_k^l . ω_k^l is a prior factor for data instances with label l inside cluster C_k . ∂_{nk}

is the unsupervised indicator for data instance x_n and cluster C_k . ∂_{nk} is the unsupervised mean for cluster C_k .

The LK-Means algorithm can be described as follows:

1. Initialize K initial means of clusters randomly.
2. Associate each data instance with the means of the clusters and compute the initial value of ∂_{nk}^l (using Equation 4 below)
3. Compute the supervised means a_k^l (using Equation 3) and then ω_k^l (using Equation 8)
4. Compute the unsupervised means a_k (using Equation 7)
5. Compute the supervised indicator ∂_{nk}^l (using Equation 5)
6. Compute the fitness function F (using Equation 2)
7. Repeat steps 3 to 6 until the value of the fitness function F converges (or the change of the fitness function value is below a given threshold).

To compute a_k^l use the following equation:

$$a_k^l = \frac{\beta \sum_{n=1}^N \partial_{nk}^l x_n + (1-\beta) \sum_{n=1}^N \partial_{nk} (x_n - \tilde{a}_k + \tilde{\omega}_k^l \tilde{a}_k^l)}{\beta \sum_{n=1}^N \partial_{nk}^l + (1-\beta) \tilde{\omega}_k^l \sum_{n=1}^N \partial_{nk}} \quad [3]$$

where \tilde{a}_k , $\tilde{\omega}_k^l$ and \tilde{a}_k^l are the previous iteration values of a_k , ω_k^l and a_k^l . ∂_{nk}^l , ∂_{nk} , \tilde{a}_k , $\tilde{\omega}_k^l$ and \tilde{a}_k^l need to be initialized before computing a_k^l in Equation 3

The initial value of ∂_{nk}^l can be computed from:

$$\partial_{nk}^l = \frac{\theta_{nk}^l + \sigma}{1 + L * K * \sigma} \quad [4]$$

$$\text{where } \theta_{nk}^l = \begin{cases} 1 & \text{if } x_n \in C_k \wedge y_n = l \\ 0 & \text{otherwise} \end{cases}$$

θ_{nk}^l is equal to one when the data instance x_n is in cluster C_k and has the class label of l . Otherwise it is equal to zero. A constant $\sigma = 0.001$ is the compensate value of the label uncertainty.

After initialization, ∂_{nk}^l can be evaluated from:

$$\partial_{nk}^l = \begin{cases} 1 & \text{if } k = \operatorname{argmin}_j [\beta \|\partial_{nj}^l x_n - a_j^l\|^2 \omega_j^l + (1-\beta) \|\partial_{nj} x_n - a_j\|^2] \\ 0 & \text{otherwise} \end{cases} \quad [5]$$

where ∂_{nk} can be computed using the following equation:

$$\partial_{nk} = \begin{cases} 1 & \text{if } x_n \in C_k \\ 0 & \text{otherwise} \end{cases} \quad [6]$$

a_k can be computed using the following equation:

$$a_k = \sum_{l=1}^L \omega_k^l a_k^l \quad [7]$$

ω_k^l using the following equation:

$$\omega_k^l = \frac{\sum_{n=1}^N \partial_{nk}^l}{\sum_{n=1}^N \partial_{nk}} \quad [8]$$

ω_k^l is between 0 and 1. When ω_k^l is equal to 1, all data instances in cluster k have only label l . On the other hand, when ω_k^l is equal to 0, no data instance in cluster k has label l .

Proposed Algorithm

SC-MOGA

The proposed algorithm searches for clustering solutions that minimize two objective functions, namely the impurity level (f_1) and the sum squared error (SSE) or compactness (f_2), and maximize the third objective function, namely the inter cluster distance or separateness (f_3), as follows:

$$f_1 = \sum_{i=1}^K \text{the percentage of minority data instances in the } i^{\text{th}} \text{ cluster}$$

$$f_2 = \sum_{j=1}^N (\text{Euclidean distance}(x_j, \text{the center of the cluster containing } x_j))^2$$

$$f_3 = \frac{2}{K(K-1)} \sum_{s=1}^{K-1} \sum_{t=s+1}^K \text{Euclidean distance}(\text{the center of cluster } s, \text{the center of cluster } t)$$

where N is the number of data instances to be clustered and K is the number of clusters. SC-MOGA represents clustering solutions or chromosomes by integer encoding (Hruschka et al., 2009). Each gene in the chromosome is an integer between 1 and K . It represents

Algorithm SC-MOGA

1. $n = 1$
 2. Initialize the chromosome population of size N randomly
 - while** $n \leq$ the number of generations **do**
 3. The chromosomes in the current population are randomly paired
 4. Evaluate the three fitness function values of each chromosome and rank all chromosomes based on Pareto dominances
 - for** each pair of chromosomes **do**
 5. Recombine the two chromosomes, parent1 and parent2, to create two offspring, child1 and child2
 6. Mutate child1 and child2 with a predefined mutation probability
 7. Rank child1 and child2 against the current population
 - if** $\text{distance}(\text{parent1}, \text{child1}) + \text{distance}(\text{parent2}, \text{child2}) < \text{distance}(\text{parent1}, \text{child2}) + \text{distance}(\text{parent2}, \text{child1})$ **then**
 - q1 = either parent1 or child1 whichever has better ranking
 - q2 = either parent2 or child2 whichever has better ranking
 - else**
 - q1 = either parent1 or child2 whichever has better ranking
 - q2 = either parent2 or child1 whichever has better ranking
 - end if**
 8. Place q1 and q2 in the new population
 - end for**
 9. Replace the current population with the new population
 10. $n = n + 1$
-

the identity of the cluster to which the corresponding data instance is assigned (Figure 1). The length of the chromosome is therefore equal to the number of data instances.

With this encoding scheme, the shape of each cluster defined by a chromosome can be globular or non-globular one. However, one distinct clustering can have several chromosome representations. For instance, the chromosomes [1,1,1,1,2,2,2,2,3,3], [1,1,1,1,3,3,3,3,2,2] and [2,2,2,2,1,1,1,1,3,3] represent the same clustering solution: the clustering contains three clusters, the first cluster with the first four data instances, the second with the next four data instances and the third with the last two data instances. Finding clustering solutions that optimize the three objective functions therefore becomes a multi-modal multi-objective optimization problem, since the same optimal clustering can be represented by multiple solutions in the search space. A multi-objective crowding genetic algorithm method is chosen as the search method for SC-MOGA, since it can converge to multiple solutions simultaneously. The SC-MOGA algorithm is summarized below:

The solution with the best ranking in the final population becomes the clustering solution. When there is a tie on ranking, the orders of the solutions are considered to break the tie.

In Steps 4 and 7: Ranking a chromosome is performed against the current population, based on how many chromosomes there are in the population that are dominated by the chromosome (Fonseca & Fleming, 1993). Suppose a chromosome A has three fitness values f_{1A} , f_{2A} , f_{3A} and a chromosome B has three fitness values f_{1B} , f_{2B} , f_{3B} . The goal is to minimize the two fitness values f_1 , f_2 and maximize the fitness value f_3 , then chromosome A dominates chromosome B when $f_{1A} \leq f_{1B}$ and $f_{2A} \leq f_{2B}$ and $f_{3A} \geq f_{3B}$.

In Step 5: Uniform crossover (Syswerda, 1989) is applied with a crossover probability = 0.5. The uniform crossover is used instead of one point or two point crossover since it is not sensitive to the order of data instances of the chromosome encoding.

In Step 6: Mutation is performed with a given mutation probability on each gene in a chromosome. It assigns each gene a new random value between 1 and K.

In Step 7 and 8: distance (i_1, i_2) is the distance between two chromosomes i_1 and i_2 . It is measured in terms of Hamming distance (Hamming, 1950). Based on the crowding method (De Jong, 1975), a parent chromosome will be replaced by its closest (most similar) child if the child is fitter than its parent (has higher Pareto ranking than its parent). Either the parent chromosome or its closest child with better ranking than the parent chromosome is kept temporarily in the new population.

In step 9 and 10: the new population replaces the current population and the algorithm proceeds to the next generation.

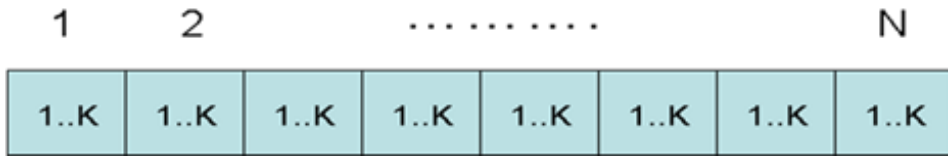


Figure 1. Chromosome Encoding for SC-MOGA

SC-MOGA with Data Sampling

For very large datasets, the search space for SC-MOGA also becomes very large, so it may not be able to converge to the optimal solution or can take a significant amount of running time before it converges. To overcome the problem, a stratified random sampling (Cadima et al., 2005) is performed on the given dataset to get a small representative dataset for SC-MOGA. The sampling is based on segmenting the dataset into compact clusters. Each cluster contains data with the same class label, the clusters represent strata and so a number of data instances are randomly sampled from each strata. To segment the dataset as mentioned above, a Bisecting K-means approach is adopted. The stratified random sampling procedure is summarized below:

procedure STRATIFIED_RANDOM_SAMPLING

1. Split the given dataset into two clusters using the K-Means algorithm ($K = 2$) and insert the two clusters into an empty list of candidate clusters for Bisecting
2. **repeat**
 Remove the cluster with the highest impurity level (represented by the percentage of minority data instances whose class labels are different from that of the majority) from the list and split the cluster into two using the K-Means algorithm. Then insert the clusters back into the list. When there is a tie on impurity, remove the cluster with the highest SSE
until all clusters in the list contain no impurity (zero impurity level)
3. Proportionally allocate n_h data samples to each cluster or stratum in the list of m clusters, as follows

$$n_h = S * \left(\frac{N_h SE_h}{\sum_{i=1}^m N_i SE_i} \right)$$

where n_h represents the sample size allocated to each stratum h , N_i represents the size of stratum i , SE_i represents the sum squared error of each stratum i as follows

$$SE_i = \sum_{j=1}^{N_i} (\text{Euclidean distance}(x_j, \text{stratum_center}(i)))^2$$

x_j represents the j^{th} data instance of stratum i and $\text{stratum_center}(i)$ represents the center of stratum i , S represents the expected sample size calculated from (Krejcie & Morgan, 1970)

$$S = \frac{\chi^2 NF(1 - F)}{(d^2 (N - 1)) + (\chi^2 F(1 - F))}$$

where χ^2 is the designated chi-square value, N is the size of the population, F is the population fraction, and d is the precision degree. Each stratum is allocated at least one data sample ($n_i \geq 1$). Hence the total sample size is:

$$\text{Sample Size} = \sum_{k=1}^m n_k$$

4. For each stratum i , randomly sample n_i data instances from the stratum. All samples now form a representative dataset for the SC-MOGA.

end procedure

After performing SC-MOGA on the representative dataset, representatives of each stratum may be grouped into different clusters. Since each stratum represents a compact group of data instances with the same class label, all data in each stratum should be assigned to the same SC-MOGA cluster. The winner-take-all strategy is adopted in this case, so that all data instances in a stratum are assigned to the same cluster, the one that has the highest number of representatives of the stratum. If there is more than one such cluster, one can be chosen randomly among them.

EXPERIMENTS AND RESULTS

Two experiments were conducted to evaluate the performances of the proposed algorithms. A notebook with 2.5 GHz Core i5 processor and 4GB of RAM was used to run all the test cases in the experiments.

The First Experiment

The first experiment is intended to evaluate the performance of SC-MOGA and SC-MOGA with data sampling against some existing algorithms, namely LK-Means and SRIDHCR. Because of the difficulties we encountered when implementing the two algorithms, the experimental results for LK-Means and SRIDHCR on eight datasets in Peralta et al. (2013) were used for the comparison. The eight datasets, taken from the UCI Machine Learning Repository (Lichman, 2013), are Iris, Statlog ('Heart'), Glass Identification ('Glass'), Pima Indians Diabetes ('Diabetes'), Statlog ('Vehicle Silhouettes'), Image Segmentation, Ionosphere and Connectionist Bench (Sonar, Mines vs. Rocks) ('Sonar'). Before performing the clustering, the variable values in the datasets were normalized using a max-min normalization scheme. The details of the dataset are shown in Table 2.

Table 2

Details of the eight UCI Machine Learning Repository Datasets

Dataset Name	# objects	# variables	# classes
Iris	150	4	3
Heart	270	13	2
Glass	214	9	6
Diabetes	768	8	2
Vehicle Silhouettes	846	18	4
Image Segmentation	2310	19	7
Ionosphere	351	34	2
Sonar	208	60	2

To measure the performance of the SC-MOGA, we applied ten-fold cross validation. For each fold, the genetic algorithm was tried for five runs. The five solutions, one from each run, were ranked, and the one with the highest Pareto ranking among them was selected as the optimal solution for the fold. Finally, the averages of the four metrics of the ten folds for the optimal solutions were computed. We followed the experiments of Peralta et al. (2013) that selected five values for the number of clusters (K) ranging from the lower bound value, which is the actual number of classes, to the upper bound value of $\lceil \sqrt{\text{number of data instances (or sample size)}/2} \rceil$ with equal intervals. Several trials of the experiment were conducted with varying parameter values. The best performance of the algorithm in terms of cluster validity indexes were achieved with the following setting of the parameter values:

Size of population = $N \log K$

Crossover Operations = Uniform crossover with probability of 0.5

Mutation probability = 0.01

Number of generations per run = 500 (except that for Vehicle Silhouettes the number was 1,000 and for Image Segmentation it was 10,000)

Table 3

Sampling parameter values used by SC-MOGA with data sampling on the first eight datasets

Dataset	Number of Data Objects (N)	χ^2 chi-square	Population Fraction (F)	Precision Degree (d)	Expected Sample Size (S)	Number of Strata (m)	Actual sample size $\sum_{k=1}^m n_k$
Iris	150	3.841	0.5	0.05	109	14	109
Heart	270	3.841	0.5	0.05	159	191	260
Glass	214	3.841	0.5	0.05	138	22	138
Diabetes	768	3.841	0.5	0.05	257	529	605
Vehicle Silhouettes	846	3.841	0.5	0.05	265	749	818
Image Segmentation	2310	3.841	0.5	0.05	330	1105	1191
Ionosphere	351	3.841	0.5	0.05	184	240	335
Sonar	208	3.841	0.5	0.05	136	8	136

Table 3 shows all the sampling parameter values used in the experiments for SC-MOGA with data sampling. The four cluster validity indexes were used for the performance comparison. The validity index results for the eight datasets are shown in Tables 4 to 7 (the first eight datasets in each of these tables). The results of SCEC and the rest of datasets in the tables come from the second experiment and will be explained later. One-sided paired t-tests were performed to compare the performances of SC-MOGA, SC-MOGA with data sampling, LK-Means and SRIDHCR. To do the t-test between two algorithms for

each index, we computed the differences between the indexes achieved by the two algorithms for the eight datasets and for all Ks (number of clusters). The results of the tests are shown in Tables 8 and 9. The results in Table 8 show that SC-MOGA achieved better performances than SRIDHCR and LK-Means, with a confidence of more than 95% for all four indexes, but its performance was not better than SC-MOGA with data sampling. The results in Table 9 show that SC-MOGA with data sampling achieved a better performance than SRIDHCR, LK-Means and SC-MOGA with a confidence level of more than 95% for all four indexes.

Table 4

Adjusted Mutual Information (AMI) results on 23 datasets

Dataset	Number of clusters					
Iris	K=3	K=5	K=7	K=9	K=11	Mean
SRIDHCR	0.196	0.260	0.204	0.236	0.241	0.227
LK-Means	0.655	0.538	0.497	0.451	0.387	0.506
SCEC	0.912	0.691	0.589	0.543	0.483	0.644
SC-MOGA	0.912	0.740	0.611	0.548	0.503	0.663
SC-MOGA with data sampling	1	1	0.950	0.908	0.908	0.953
Heart	K=2	K=5	K=8	K=11	K=14	Mean
SRIDHCR	0.011	0.082	0.078	0.104	0.097	0.074
LK-Means	0.293	0.212	0.137	0.134	0.104	0.176
SCEC	0.417	0.247	0.185	0.192	0.171	0.242
SC-MOGA	0.658	0.441	0.331	0.295	0.259	0.397
SC-MOGA with data sampling	0.719	0.441	0.350	0.295	0.272	0.415
Glass	K=6	K=7	K=8	K=9	K=10	Mean
SRIDHCR	0.093	0.132	0.138	0.092	0.106	0.112
LK-Means	0.148	0.159	0.156	0.132	0.149	0.149
SCEC	0.478	0.492	0.457	0.437	0.432	0.459
SC-MOGA	0.532	0.577	0.516	0.482	0.467	0.515
SC-MOGA with data sampling	0.759	0.718	0.743	0.715	0.715	0.730
Diabetes	K=2	K=7	K=12	K=17	K=22	Mean
SRIDHCR	0.113	0.049	0.044	0.043	0.041	0.058
LK-Means	0.086	0.068	0.047	0.040	0.043	0.057
SCEC	0.194	0.089	0.095	0.080	0.081	0.108
SC-MOGA	0.375	0.269	0.198	0.160	0.129	0.226
SC-MOGA with data sampling	0.430	0.280	0.234	0.188	0.141	0.255

Table 4 (Continue)

Dataset	Number of clusters					
Vehicle Silhouettes	K=4	K=8	K=12	K=16	K=20	Mean
SRIDHCR	0.076	0.107	0.132	0.141	0.116	0.114
LK-Means	0.112	0.129	0.128	0.118	0.117	0.121
SCEC	0.270	0.325	0.297	0.268	0.207	0.273
SC-MOGA	0.492	0.417	0.345	0.369	0.335	0.392
SC-MOGA with data sampling	0.522	0.429	0.393	0.380	0.346	0.414
Image Segmentation	K=7	K=14	K=21	K=28	K=35	Mean
SRIDHCR	0.446	0.522	0.469	0.428	0.392	0.451
LK-Means	0.548	0.551	0.492	0.439	0.411	0.488
SCEC	0.755	0.655	0.600	0.540	0.465	0.603
SC-MOGA	0.625	0.601	0.565	0.521	0.465	0.555
SC-MOGA with data sampling	0.750	0.653	0.592	0.556	0.486	0.607
Ionosphere	K=2	K=5	K=8	K=11	K=14	Mean
SRIDHCR	0.053	0.112	0.069	0.082	0.075	0.078
LK-Means	0.174	0.177	0.125	0.156	0.108	0.148
SCEC	0.371	0.304	0.299	0.281	0.248	0.301
SC-MOGA	0.390	0.375	0.301	0.273	0.236	0.315
SC-MOGA with data sampling	0.511	0.417	0.361	0.313	0.284	0.377
Sonar	K=2	K=4	K=6	K=8	K=10	Mean
SRIDHCR	0.012	0.001	0.050	0.019	0.020	0.020
LK-Means	0.094	0.036	0.017	0.039	0.058	0.049
SCEC	0.225	0.198	0.180	0.192	0.191	0.197
SC-MOGA	0.474	0.484	0.414	0.349	0.311	0.406
SC-MOGA with data sampling	1	0.961	0.859	0.961	0.961	0.948
BS	K=3	K=7	K=11	K=15	K=19	Mean
SRIDHCR	N/A	N/A	N/A	N/A	N/A	N/A
LK-Means	N/A	N/A	N/A	N/A	N/A	N/A
SCEC	0.508	0.301	0.256	0.246	0.227	0.308
SC-MOGA	0.608	0.342	0.275	0.238	0.214	0.335
SC-MOGA with data sampling	0.613	0.364	0.292	0.257	0.235	0.352

Table 4 (Continue)

Dataset	Number of clusters					Mean
	K=2	K=7	K=12	K=17	K=22	
BTSC	K=2	K=7	K=12	K=17	K=22	Mean
SRIDHCR	N/A	N/A	N/A	N/A	N/A	N/A
LK-Means	N/A	N/A	N/A	N/A	N/A	N/A
SCEC	0.094	0.094	0.038	0.045	0.038	0.062
SC-MOGA	0.147	0.169	0.143	0.098	0.038	0.119
SC-MOGA with data sampling	0.292	0.334	0.280	0.233	0.225	0.273
CMSC	K=2	K=6	K=10	K=14	K=18	Mean
SRIDHCR	N/A	N/A	N/A	N/A	N/A	N/A
LK-Means	N/A	N/A	N/A	N/A	N/A	N/A
SCEC	0.005	0.009	0.031	0.037	0.050	0.026
SC-MOGA	0.035	0.032	0.036	0.035	0.036	0.035
SC-MOGA with data sampling	0.473	0.311	0.268	0.254	0.198	0.301
CMC	K=3	K=9	K=15	K=21	K=27	Mean
SRIDHCR	N/A	N/A	N/A	N/A	N/A	N/A
LK-Means	N/A	N/A	N/A	N/A	N/A	N/A
SCEC	0.054	0.057	0.049	0.044	0.043	0.049
SC-MOGA	0.228	0.092	0.074	0.009	0.007	0.082
SC-MOGA with data sampling	0.650	0.801	0.566	0.401	0.396	0.563
HS	K=2	K=5	K=8	K=11	K=14	Mean
SRIDHCR	N/A	N/A	N/A	N/A	N/A	N/A
LK-Means	N/A	N/A	N/A	N/A	N/A	N/A
SCEC	0.099	0.059	0.062	0.055	0.051	0.065
SC-MOGA	0.118	0.285	0.237	0.244	0.222	0.221
SC-MOGA with data sampling	0.152	0.355	0.373	0.329	0.320	0.306
LD	K=2	K=5	K=8	K=11	K=14	Mean
SRIDHCR	N/A	N/A	N/A	N/A	N/A	N/A
LK-Means	N/A	N/A	N/A	N/A	N/A	N/A
SCEC	0.048	0.074	0.065	0.076	0.081	0.069
SC-MOGA	0.255	0.451	0.338	0.285	0.257	0.317
SC-MOGA with data sampling	0.351	0.496	0.597	0.637	0.530	0.522

Table 4 (Continue)

Dataset	Number of clusters					Mean
	K=2	K=6	K=10	K=14	K=18	
MP	K=2	K=6	K=10	K=14	K=18	Mean
SRIDHCR	N/A	N/A	N/A	N/A	N/A	N/A
LK-Means	N/A	N/A	N/A	N/A	N/A	N/A
SCEC	0.310	0.301	0.274	0.233	0.247	0.273
SC-MOGA	0.497	0.390	0.294	0.253	0.205	0.328
SC-MOGA with data sampling	0.616	0.431	0.369	0.341	0.296	0.411
Musk	K=2	K=6	K=10	K=14	K=18	Mean
SRIDHCR	N/A	N/A	N/A	N/A	N/A	N/A
LK-Means	N/A	N/A	N/A	N/A	N/A	N/A
SCEC	0.148	0.120	0.117	0.143	0.117	0.129
SC-MOGA	0.255	0.312	0.303	0.257	0.200	0.265
SC-MOGA with data sampling	0.889	0.790	0.981	0.881	0.915	0.891
Seeds	K=3	K=5	K=7	K=9	K=11	Mean
SRIDHCR	N/A	N/A	N/A	N/A	N/A	N/A
LK-Means	N/A	N/A	N/A	N/A	N/A	N/A
SCEC	0.777	0.669	0.669	0.541	0.480	0.627
SC-MOGA	0.828	0.697	0.591	0.539	0.471	0.625
SC-MOGA with data sampling	1	1	0.767	0.675	0.644	0.817
SPECTF	K=2	K=5	K=8	K=11	K=14	Mean
SRIDHCR	N/A	N/A	N/A	N/A	N/A	N/A
LK-Means	N/A	N/A	N/A	N/A	N/A	N/A
SCEC	0.050	0.092	0.086	0.085	0.098	0.082
SC-MOGA	0.061	0.101	0.260	0.230	0.205	0.171
SC-MOGA with data sampling	1	1	1	1	1	1
SPF	K=7	K=14	K=21	K=28	K=35	Mean
SRIDHCR	N/A	N/A	N/A	N/A	N/A	N/A
LK-Means	N/A	N/A	N/A	N/A	N/A	N/A
SCEC	0.385	0.394	0.299	0.277	0.275	0.326
SC-MOGA	0.227	0.150	0.064	0.006	0.007	0.091
SC-MOGA with data sampling	0.574	0.707	0.694	0.599	0.607	0.636

Table 4 (Continue)

Dataset	Number of clusters					Mean
	K=3	K=5	K=7	K=9	K=11	
TAE	K=3	K=5	K=7	K=9	K=11	Mean
SRIDHCR	N/A	N/A	N/A	N/A	N/A	N/A
LK-Means	N/A	N/A	N/A	N/A	N/A	N/A
SCEC	0.141	0.122	0.114	0.134	0.116	0.125
SC-MOGA	0.432	0.465	0.369	0.461	0.411	0.428
SC-MOGA with data sampling	0.649	0.638	0.534	0.566	0.503	0.578
Vertebral	K=3	K=6	K=9	K=12	K=15	Mean
SRIDHCR	N/A	N/A	N/A	N/A	N/A	N/A
LK-Means	N/A	N/A	N/A	N/A	N/A	N/A
SCEC	0.548	0.548	0.338	0.321	0.281	0.407
SC-MOGA	0.557	0.548	0.431	0.420	0.326	0.456
SC-MOGA with data sampling	0.667	0.666	0.578	0.618	0.652	0.636
Wilt	K=2	K=5	K=8	K=11	K=14	Mean
SRIDHCR	N/A	N/A	N/A	N/A	N/A	N/A
LK-Means	N/A	N/A	N/A	N/A	N/A	N/A
SCEC	0.019	0.021	0.024	0.026	0.010	0.020
SC-MOGA	0.027	0.049	0.055	0.059	0.040	0.046
SC-MOGA with data sampling	0.879	0.800	1	0.853	0.793	0.865
Wine	K=3	K=5	K=7	K=9	K=11	Mean
SRIDHCR	N/A	N/A	N/A	N/A	N/A	N/A
LK-Means	N/A	N/A	N/A	N/A	N/A	N/A
SCEC	0.925	0.693	0.629	0.528	0.461	0.647
SC-MOGA	0.972	0.713	0.604	0.528	0.471	0.658
SC-MOGA with data sampling	1	0.902	0.939	0.748	0.738	0.865

Table 5

Adjusted Rand Index (ARI) results on 23 datasets

Dataset	Number of clusters					
Iris	K=3	K=5	K=7	K=9	K=11	Mean
SRIDHCR	0.190	0.259	0.196	0.221	0.233	0.220
LK-Means	0.644	0.568	0.552	0.527	0.457	0.550
SCEC	0.922	0.740	0.627	0.571	0.471	0.666
SC-MOGA	0.922	0.792	0.656	0.532	0.504	0.681
SC-MOGA with data sampling	1	1	0.980	0.961	0.961	0.980
Heart	K=2	K=5	K=8	K=11	K=14	Mean
SRIDHCR	0.019	0.110	0.099	0.111	0.099	0.088
LK-Means	0.315	0.257	0.164	0.155	0.119	0.202
SCEC	0.525	0.368	0.193	0.227	0.164	0.295
SC-MOGA	0.763	0.436	0.254	0.211	0.150	0.363
SC-MOGA with data sampling	0.816	0.439	0.306	0.212	0.184	0.391
Glass	K=6	K=7	K=8	K=9	K=10	Mean
SRIDHCR	0.074	0.092	0.104	0.079	0.091	0.088
LK-Means	0.168	0.134	0.143	0.119	0.137	0.140
SCEC	0.413	0.392	0.419	0.355	0.364	0.389
SC-MOGA	0.424	0.460	0.395	0.388	0.336	0.401
SC-MOGA with data sampling	0.786	0.776	0.754	0.732	0.666	0.743
Diabetes	K=2	K=7	K=12	K=17	K=22	Mean
SRIDHCR	0.182	0.059	0.068	0.048	0.041	0.080
LK-Means	0.150	0.089	0.060	0.043	0.045	0.077
SCEC	0.292	0.115	0.116	0.058	0.057	0.128
SC-MOGA	0.370	0.269	0.140	0.083	0.069	0.186
SC-MOGA with data sampling	0.508	0.284	0.146	0.094	0.062	0.219
Vehicle Silhouettes	K=4	K=8	K=12	K=16	K=20	Mean
SRIDHCR	0.051	0.082	0.109	0.110	0.088	0.088
LK-Means	0.082	0.103	0.108	0.098	0.100	0.098
SCEC	0.260	0.295	0.243	0.216	0.185	0.240
SC-MOGA	0.465	0.378	0.269	0.273	0.219	0.321
SC-MOGA with data sampling	0.506	0.385	0.318	0.264	0.222	0.339

Table 5 (Continue)

Dataset	Number of clusters					
Image Segmentation	K=7	K=14	K=21	K=28	K=35	Mean
SRIDHCR	0.446	0.483	0.410	0.326	0.278	0.389
LK-Means	0.447	0.502	0.444	0.388	0.357	0.428
SCEC	0.716	0.621	0.585	0.521	0.442	0.577
SC-MOGA	0.532	0.517	0.480	0.457	0.397	0.477
SC-MOGA with data sampling	0.692	0.589	0.502	0.496	0.409	0.538
Ionosphere	K=2	K=5	K=8	K=11	K=14	Mean
SRIDHCR	0.115	0.163	0.112	0.120	0.080	0.118
LK-Means	0.196	0.199	0.130	0.189	0.124	0.168
SCEC	0.447	0.426	0.408	0.366	0.247	0.379
SC-MOGA	0.387	0.390	0.301	0.279	0.248	0.321
SC-MOGA with data sampling	0.630	0.499	0.364	0.292	0.264	0.410
Sonar	K=2	K=4	K=6	K=8	K=10	Mean
SRIDHCR	0.042	0.001	0.048	0.018	0.025	0.027
LK-Means	0.103	0.044	0.034	0.052	0.059	0.058
SCEC	0.297	0.278	0.222	0.202	0.174	0.235
SC-MOGA	0.575	0.556	0.417	0.305	0.242	0.419
SC-MOGA with data sampling	1	0.990	0.941	0.990	0.990	0.982
BS	K=3	K=7	K=11	K=15	K=19	Mean
SRIDHCR	N/A	N/A	N/A	N/A	N/A	N/A
LK-Means	N/A	N/A	N/A	N/A	N/A	N/A
SCEC	0.594	0.278	0.192	0.156	0.124	0.269
SC-MOGA	0.649	0.273	0.186	0.127	0.100	0.267
SC-MOGA with data sampling	0.649	0.305	0.192	0.157	0.128	0.286
BTSC	K=2	K=7	K=12	K=17	K=22	Mean
SRIDHCR	N/A	N/A	N/A	N/A	N/A	N/A
LK-Means	N/A	N/A	N/A	N/A	N/A	N/A
SCEC	0.227	0.227	0.027	0.038	0.032	0.110
SC-MOGA	0.066	0.116	0.076	0.032	0.013	0.061
SC-MOGA with data sampling	0.470	0.508	0.493	0.474	0.492	0.487

Table 5 (Continue)

Dataset	Number of clusters					Mean
	K=2	K=6	K=10	K=14	K=18	
CMSC						
SRIDHCR	N/A	N/A	N/A	N/A	N/A	N/A
LK-Means	N/A	N/A	N/A	N/A	N/A	N/A
SCEC	0.005	0.005	0.007	0.014	0.017	0.010
SC-MOGA	0.086	0.092	0.069	0.014	0.017	0.056
SC-MOGA with data sampling	0.679	0.509	0.476	0.462	0.432	0.512
CMC						
SRIDHCR	N/A	N/A	N/A	N/A	N/A	N/A
LK-Means	N/A	N/A	N/A	N/A	N/A	N/A
SCEC	0.055	0.043	0.033	0.025	0.021	0.035
SC-MOGA	0.225	0.078	0.053	0.005	0.004	0.073
SC-MOGA with data sampling	0.619	0.904	0.658	0.396	0.416	0.599
HS						
SRIDHCR	N/A	N/A	N/A	N/A	N/A	N/A
LK-Means	N/A	N/A	N/A	N/A	N/A	N/A
SCEC	0.229	0.106	0.088	0.056	0.037	0.103
SC-MOGA	0.083	0.245	0.161	0.136	0.113	0.148
SC-MOGA with data sampling	0.292	0.565	0.616	0.538	0.591	0.520
LD						
SRIDHCR	N/A	N/A	N/A	N/A	N/A	N/A
LK-Means	N/A	N/A	N/A	N/A	N/A	N/A
SCEC	0.085	0.092	0.078	0.060	0.074	0.078
SC-MOGA	0.331	0.474	0.273	0.194	0.153	0.285
SC-MOGA with data sampling	0.379	0.713	0.818	0.853	0.744	0.701
MP						
SRIDHCR	N/A	N/A	N/A	N/A	N/A	N/A
LK-Means	N/A	N/A	N/A	N/A	N/A	N/A
SCEC	0.249	0.377	0.191	0.138	0.141	0.219
SC-MOGA	0.514	0.349	0.199	0.144	0.102	0.262
SC-MOGA with data sampling	0.648	0.622	0.508	0.505	0.433	0.543

Table 5 (Continue)

Dataset	Number of clusters					
Musk	K=2	K=6	K=10	K=14	K=18	Mean
SRIDHCR	N/A	N/A	N/A	N/A	N/A	N/A
LK-Means	N/A	N/A	N/A	N/A	N/A	N/A
SCEC	0.182	0.094	0.092	0.111	0.092	0.114
SC-MOGA	0.278	0.306	0.218	0.147	0.100	0.210
SC-MOGA with data sampling	0.934	0.923	0.996	0.967	0.977	0.959
Seeds	K=3	K=5	K=7	K=9	K=11	Mean
SRIDHCR	N/A	N/A	N/A	N/A	N/A	N/A
LK-Means	N/A	N/A	N/A	N/A	N/A	N/A
SCEC	0.824	0.772	0.772	0.632	0.480	0.696
SC-MOGA	0.846	0.744	0.572	0.529	0.383	0.615
SC-MOGA with data sampling	1	1	0.834	0.722	0.710	0.853
SPECTF	K=2	K=5	K=8	K=11	K=14	Mean
SRIDHCR	N/A	N/A	N/A	N/A	N/A	N/A
LK-Means	N/A	N/A	N/A	N/A	N/A	N/A
SCEC	0.141	0.077	0.053	0.044	0.043	0.072
SC-MOGA	0.143	0.102	0.170	0.143	0.109	0.133
SC-MOGA with data sampling	1	1	1	1	1	1
SPF	K=7	K=14	K=21	K=28	K=35	Mean
SRIDHCR	N/A	N/A	N/A	N/A	N/A	N/A
LK-Means	N/A	N/A	N/A	N/A	N/A	N/A
SCEC	0.301	0.304	0.268	0.201	0.178	0.250
SC-MOGA	0.223	0.120	0.041	0.003	0.003	0.078
SC-MOGA with data sampling	0.533	0.702	0.710	0.594	0.600	0.628
TAE	K=3	K=5	K=7	K=9	K=11	Mean
SRIDHCR	N/A	N/A	N/A	N/A	N/A	N/A
LK-Means	N/A	N/A	N/A	N/A	N/A	N/A
SCEC	0.147	0.150	0.121	0.124	0.105	0.129
SC-MOGA	0.437	0.486	0.299	0.455	0.369	0.409
SC-MOGA with data sampling	0.650	0.610	0.399	0.619	0.523	0.560

Table 5 (Continue)

Dataset	Number of clusters					Mean
	K=3	K=6	K=9	K=12	K=15	
Vertebral	K=3	K=6	K=9	K=12	K=15	Mean
SRIDHCR	N/A	N/A	N/A	N/A	N/A	N/A
LK-Means	N/A	N/A	N/A	N/A	N/A	N/A
SCEC	0.646	0.646	0.316	0.313	0.236	0.431
SC-MOGA	0.447	0.535	0.360	0.327	0.219	0.378
SC-MOGA with data sampling	0.730	0.661	0.453	0.649	0.666	0.632
Wilt	K=2	K=5	K=8	K=11	K=14	Mean
SRIDHCR	N/A	N/A	N/A	N/A	N/A	N/A
LK-Means	N/A	N/A	N/A	N/A	N/A	N/A
SCEC	0.002	0.005	0.002	0.001	0.001	0.002
SC-MOGA	0.018	0.010	0.009	0.007	0.006	0.010
SC-MOGA with data sampling	0.956	0.926	1	0.941	0.911	0.947
Wine	K=3	K=5	K=7	K=9	K=11	Mean
SRIDHCR	N/A	N/A	N/A	N/A	N/A	N/A
LK-Means	N/A	N/A	N/A	N/A	N/A	N/A
SCEC	0.947	0.732	0.659	0.509	0.381	0.646
SC-MOGA	0.982	0.744	0.630	0.499	0.421	0.655
SC-MOGA with data sampling	1	0.944	0.971	0.797	0.831	0.909

Table 6

Adjusted Variation of Information (AVI) results on 23 datasets

Dataset	Number of clusters					Mean
	K=3	K=5	K=7	K=9	K=11	
Iris	K=3	K=5	K=7	K=9	K=11	Mean
SRIDHCR	0.224	0.286	0.221	0.261	0.280	0.254
LK-Means	0.715	0.613	0.591	0.560	0.485	0.593
SCEC	0.913	0.799	0.727	0.698	0.646	0.757
SC-MOGA	0.913	0.850	0.750	0.708	0.669	0.778
SC-MOGA with data sampling	1	1	0.975	0.952	0.952	0.976

Table 6 (Continue)

Dataset	Number of clusters					
Heart	K=2	K=5	K=8	K=11	K=14	Mean
SRIDHCR	0.011	0.112	0.115	0.163	0.159	0.112
LK-Means	0.300	0.271	0.188	0.201	0.164	0.225
SCEC	0.420	0.319	0.273	0.289	0.267	0.314
SC-MOGA	0.660	0.612	0.498	0.456	0.411	0.527
SC-MOGA with data sampling	0.720	0.612	0.518	0.456	0.428	0.547
Glass	K=6	K=7	K=8	K=9	K=10	Mean
SRIDHCR	0.100	0.149	0.150	0.109	0.128	0.127
LK-Means	0.216	0.183	0.187	0.154	0.179	0.184
SCEC	0.487	0.499	0.486	0.497	0.508	0.495
SC-MOGA	0.550	0.615	0.580	0.550	0.546	0.568
SC-MOGA with data sampling	0.823	0.808	0.781	0.779	0.733	0.785
Diabetes	K=2	K=7	K=12	K=17	K=22	Mean
SRIDHCR	0.117	0.071	0.068	0.068	0.068	0.078
LK-Means	0.105	0.092	0.069	0.065	0.069	0.080
SCEC	0.194	0.131	0.146	0.130	0.132	0.147
SC-MOGA	0.388	0.398	0.313	0.260	0.213	0.314
SC-MOGA with data sampling	0.444	0.413	0.370	0.307	0.233	0.353
Vehicle Silhouettes	K=4	K=8	K=12	K=16	K=20	Mean
SRIDHCR	0.076	0.107	0.132	0.141	0.116	0.114
LK-Means	0.121	0.149	0.164	0.157	0.163	0.151
SCEC	0.276	0.383	0.378	0.350	0.291	0.336
SC-MOGA	0.500	0.493	0.441	0.491	0.458	0.477
SC-MOGA with data sampling	0.529	0.512	0.502	0.506	0.473	0.504
Image Segmentation	K=7	K=14	K=21	K=28	K=35	Mean
SRIDHCR	0.561	0.583	0.568	0.544	0.513	0.554
LK-Means	0.570	0.615	0.580	0.549	0.531	0.569
SCEC	0.758	0.740	0.730	0.720	0.704	0.730
SC-MOGA	0.640	0.619	0.585	0.556	0.501	0.580
SC-MOGA with data sampling	0.778	0.746	0.735	0.724	0.671	0.731

Table 6 (Continue)

Dataset	Number of clusters					Mean
	K=2	K=5	K=8	K=11	K=14	
Ionosphere	K=2	K=5	K=8	K=11	K=14	Mean
SRIDHCR	0.059	0.132	0.084	0.106	0.106	0.097
LK-Means	0.182	0.225	0.173	0.212	0.160	0.190
SCEC	0.418	0.400	0.420	0.409	0.381	0.406
SC-MOGA	0.402	0.523	0.453	0.429	0.389	0.439
SC-MOGA with data sampling	0.520	0.554	0.531	0.477	0.441	0.505
Sonar	K=2	K=4	K=6	K=8	K=10	Mean
SRIDHCR	0.012	0.001	0.065	0.028	0.033	0.028
LK-Means	0.099	0.048	0.026	0.056	0.075	0.061
SCEC	0.225	0.256	0.255	0.281	0.285	0.260
SC-MOGA	0.478	0.626	0.586	0.518	0.475	0.537
SC-MOGA with data sampling	1	0.980	0.924	0.980	0.980	0.973
BS	K=3	K=7	K=11	K=15	K=19	Mean
SRIDHCR	N/A	N/A	N/A	N/A	N/A	N/A
LK-Means	N/A	N/A	N/A	N/A	N/A	N/A
SCEC	0.540	0.406	0.368	0.365	0.343	0.404
SC-MOGA	0.646	0.464	0.396	0.356	0.327	0.438
SC-MOGA with data sampling	0.650	0.486	0.420	0.379	0.356	0.458
BTSC	K=2	K=7	K=12	K=17	K=22	Mean
SRIDHCR	N/A	N/A	N/A	N/A	N/A	N/A
LK-Means	N/A	N/A	N/A	N/A	N/A	N/A
SCEC	0.101	0.101	0.060	0.073	0.064	0.080
SC-MOGA	0.150	0.261	0.232	0.164	0.064	0.174
SC-MOGA with data sampling	0.299	0.464	0.401	0.344	0.335	0.369
CMSC	K=2	K=6	K=10	K=14	K=18	Mean
SRIDHCR	N/A	N/A	N/A	N/A	N/A	N/A
LK-Means	N/A	N/A	N/A	N/A	N/A	N/A
SCEC	0.007	0.015	0.055	0.068	0.090	0.047
SC-MOGA	0.044	0.052	0.062	0.064	0.065	0.057
SC-MOGA with data sampling	0.546	0.457	0.405	0.392	0.314	0.423

Table 6 (Continue)

Dataset	Number of clusters					Mean
	K=3	K=9	K=15	K=21	K=27	
CMC	K=3	K=9	K=15	K=21	K=27	Mean
SRIDHCR	N/A	N/A	N/A	N/A	N/A	N/A
LK-Means	N/A	N/A	N/A	N/A	N/A	N/A
SCEC	0.055	0.076	0.070	0.065	0.065	0.066
SC-MOGA	0.232	0.126	0.107	0.013	0.011	0.098
SC-MOGA with data sampling	0.432	0.875	0.696	0.546	0.532	0.616
HS	K=2	K=5	K=8	K=11	K=14	Mean
SRIDHCR	N/A	N/A	N/A	N/A	N/A	N/A
LK-Means	N/A	N/A	N/A	N/A	N/A	N/A
SCEC	0.110	0.080	0.092	0.086	0.083	0.090
SC-MOGA	0.127	0.417	0.363	0.392	0.363	0.332
SC-MOGA with data sampling	0.157	0.473	0.512	0.466	0.458	0.413
LD	K=2	K=5	K=8	K=11	K=14	Mean
SRIDHCR	N/A	N/A	N/A	N/A	N/A	N/A
LK-Means	N/A	N/A	N/A	N/A	N/A	N/A
SCEC	0.053	0.101	0.096	0.118	0.128	0.099
SC-MOGA	0.257	0.618	0.506	0.442	0.408	0.446
SC-MOGA with data sampling	0.353	0.664	0.717	0.753	0.669	0.631
MP	K=2	K=6	K=10	K=14	K=18	Mean
SRIDHCR	N/A	N/A	N/A	N/A	N/A	N/A
LK-Means	N/A	N/A	N/A	N/A	N/A	N/A
SCEC	0.342	0.398	0.422	0.367	0.396	0.385
SC-MOGA	0.511	0.562	0.453	0.401	0.331	0.452
SC-MOGA with data sampling	0.625	0.572	0.514	0.487	0.434	0.526
Musk	K=2	K=6	K=10	K=14	K=18	Mean
SRIDHCR	N/A	N/A	N/A	N/A	N/A	N/A
LK-Means	N/A	N/A	N/A	N/A	N/A	N/A
SCEC	0.149	0.184	0.180	0.224	0.180	0.183
SC-MOGA	0.256	0.438	0.466	0.407	0.324	0.378
SC-MOGA with data sampling	0.892	0.882	0.990	0.937	0.955	0.931

Table 6 (Continue)

Dataset	Number of clusters					
	K=3	K=5	K=7	K=9	K=11	Mean
Seeds						
SRIDHCR	N/A	N/A	N/A	N/A	N/A	N/A
LK-Means	N/A	N/A	N/A	N/A	N/A	N/A
SCEC	0.777	0.754	0.754	0.681	0.631	0.719
SC-MOGA	0.830	0.808	0.743	0.700	0.640	0.744
SC-MOGA with data sampling	1	1	0.868	0.806	0.783	0.891
SPECTF	K=2	K=5	K=8	K=11	K=14	Mean
SRIDHCR	N/A	N/A	N/A	N/A	N/A	N/A
LK-Means	N/A	N/A	N/A	N/A	N/A	N/A
SCEC	0.074	0.136	0.133	0.137	0.164	0.129
SC-MOGA	0.079	0.143	0.412	0.374	0.341	0.270
SC-MOGA with data sampling	1	1	1	1	1	1
SPF	K=7	K=14	K=21	K=28	K=35	Mean
SRIDHCR	N/A	N/A	N/A	N/A	N/A	N/A
LK-Means	N/A	N/A	N/A	N/A	N/A	N/A
SCEC	0.398	0.407	0.385	0.348	0.366	0.381
SC-MOGA	0.244	0.184	0.083	0.009	0.009	0.106
SC-MOGA with data sampling	0.664	0.765	0.776	0.709	0.719	0.727
TAE	K=3	K=5	K=7	K=9	K=11	Mean
SRIDHCR	N/A	N/A	N/A	N/A	N/A	N/A
LK-Means	N/A	N/A	N/A	N/A	N/A	N/A
SCEC	0.145	0.140	0.140	0.178	0.158	0.152
SC-MOGA	0.444	0.538	0.446	0.604	0.558	0.518
SC-MOGA with data sampling	0.655	0.638	0.555	0.696	0.649	0.639
Vertebral	K=3	K=6	K=9	K=12	K=15	Mean
SRIDHCR	N/A	N/A	N/A	N/A	N/A	N/A
LK-Means	N/A	N/A	N/A	N/A	N/A	N/A
SCEC	0.549	0.549	0.441	0.430	0.392	0.472
SC-MOGA	0.564	0.676	0.576	0.584	0.466	0.573
SC-MOGA with data sampling	0.779	0.724	0.618	0.764	0.789	0.735

Table 6 (Continue)

Dataset	Number of clusters					
Wilt	K=2	K=5	K=8	K=11	K=14	Mean
SRIDHCR	N/A	N/A	N/A	N/A	N/A	N/A
LK-Means	N/A	N/A	N/A	N/A	N/A	N/A
SCEC	0.019	0.021	0.010	0.010	0.040	0.020
SC-MOGA	0.027	0.049	0.055	0.022	0.041	0.039
SC-MOGA with data sampling	0.908	0.870	1	0.921	0.850	0.910
Wine	K=3	K=5	K=7	K=9	K=11	Mean
SRIDHCR	N/A	N/A	N/A	N/A	N/A	N/A
LK-Means	N/A	N/A	N/A	N/A	N/A	N/A
SCEC	0.927	0.809	0.772	0.691	0.631	0.766
SC-MOGA	0.973	0.823	0.753	0.688	0.641	0.776
SC-MOGA with data sampling	1	0.949	0.968	0.856	0.849	0.924

Table 7

Mirkin distance (MD) results on 23 datasets

Dataset	Number of clusters					
Iris	K=3	K=5	K=7	K=9	K=11	Mean
SRIDHCR	0.393	0.349	0.352	0.333	0.328	0.351
LK-Means	0.158	0.158	0.148	0.147	0.158	0.154
SCEC	0.034	0.107	0.148	0.165	0.198	0.130
SC-MOGA	0.034	0.086	0.136	0.178	0.187	0.124
SC-MOGA with data sampling	0	0	0.008	0.017	0.017	0.008
Heart	K=2	K=5	K=8	K=11	K=14	Mean
SRIDHCR	0.491	0.450	0.451	0.445	0.450	0.457
LK-Means	0.347	0.361	0.402	0.403	0.419	0.386
SCEC	0.237	0.317	0.406	0.389	0.421	0.354
SC-MOGA	0.118	0.283	0.375	0.397	0.428	0.320
SC-MOGA with data sampling	0.092	0.281	0.349	0.397	0.411	0.306

Table 7 (Continue)

Dataset	Number of clusters					
	K=6	K=7	K=8	K=9	K=10	Mean
Glass						
SRIDHCR	0.325	0.302	0.309	0.298	0.286	0.304
LK-Means	0.324	0.314	0.317	0.291	0.267	0.303
SCEC	0.230	0.245	0.213	0.219	0.208	0.223
SC-MOGA	0.211	0.195	0.207	0.206	0.215	0.207
SC-MOGA with data sampling	0.088	0.095	0.099	0.112	0.134	0.106
Diabetes	K=2	K=7	K=12	K=17	K=22	Mean
SRIDHCR	0.406	0.493	0.493	0.506	0.512	0.482
LK-Means	0.419	0.471	0.492	0.504	0.503	0.478
SCEC	0.351	0.467	0.470	0.507	0.509	0.461
SC-MOGA	0.315	0.386	0.461	0.494	0.502	0.432
SC-MOGA with data sampling	0.246	0.378	0.458	0.488	0.507	0.415
Vehicle Silhouettes	K=4	K=8	K=12	K=16	K=20	Mean
SRIDHCR	0.391	0.319	0.281	0.264	0.262	0.303
LK-Means	0.381	0.287	0.261	0.258	0.246	0.287
SCEC	0.289	0.229	0.225	0.228	0.235	0.241
SC-MOGA	0.207	0.201	0.215	0.205	0.216	0.209
SC-MOGA with data sampling	0.189	0.194	0.201	0.208	0.215	0.201
Image Segmentation	K=7	K=14	K=21	K=28	K=35	Mean
SRIDHCR	0.149	0.111	0.112	0.120	0.124	0.123
LK-Means	0.154	0.104	0.107	0.109	0.111	0.117
SCEC	0.070	0.077	0.081	0.086	0.091	0.081
SC-MOGA	0.123	0.126	0.134	0.137	0.143	0.133
SC-MOGA with data sampling	0.082	0.081	0.099	0.097	0.106	0.093
Ionosphere	K=2	K=5	K=8	K=11	K=14	Mean
SRIDHCR	0.429	0.420	0.450	0.445	0.474	0.444
LK-Means	0.398	0.403	0.440	0.411	0.444	0.419
SCEC	0.269	0.294	0.302	0.329	0.396	0.318
SC-MOGA	0.306	0.293	0.356	0.442	0.464	0.372
SC-MOGA with data sampling	0.185	0.257	0.332	0.372	0.387	0.307

Table 7 (Continue)

Dataset	Number of clusters					
Sonar	K=2	K=4	K=6	K=8	K=10	Mean
SRIDHCR	0.479	0.506	0.474	0.503	0.480	0.488
LK-Means	0.455	0.460	0.458	0.444	0.440	0.451
SCEC	0.351	0.361	0.389	0.399	0.413	0.383
SC-MOGA	0.212	0.222	0.292	0.347	0.378	0.290
SC-MOGA with data sampling	0	0.005	0.029	0.005	0.005	0.009
BS	K=3	K=7	K=11	K=15	K=19	Mean
SRIDHCR	N/A	N/A	N/A	N/A	N/A	N/A
LK-Means	N/A	N/A	N/A	N/A	N/A	N/A
SCEC	0.196	0.326	0.359	0.372	0.385	0.328
SC-MOGA	0.170	0.328	0.362	0.384	0.394	0.328
SC-MOGA with data sampling	0.169	0.316	0.359	0.372	0.383	0.320
BTSC	K=2	K=7	K=12	K=17	K=22	Mean
SRIDHCR	N/A	N/A	N/A	N/A	N/A	N/A
LK-Means	N/A	N/A	N/A	N/A	N/A	N/A
SCEC	0.343	0.343	0.586	0.581	0.596	0.490
SC-MOGA	0.501	0.523	0.561	0.598	0.614	0.559
SC-MOGA with data sampling	0.242	0.258	0.267	0.280	0.270	0.263
CMSC	K=2	K=6	K=10	K=14	K=18	Mean
SRIDHCR	N/A	N/A	N/A	N/A	N/A	N/A
LK-Means	N/A	N/A	N/A	N/A	N/A	N/A
SCEC	0.501	0.718	0.735	0.772	0.778	0.701
SC-MOGA	0.388	0.632	0.740	0.794	0.805	0.672
SC-MOGA with data sampling	0.102	0.194	0.215	0.224	0.244	0.196
CMC	K=3	K=9	K=15	K=21	K=27	Mean
SRIDHCR	N/A	N/A	N/A	N/A	N/A	N/A
LK-Means	N/A	N/A	N/A	N/A	N/A	N/A
SCEC	0.439	0.375	0.361	0.360	0.358	0.379
SC-MOGA	0.361	0.353	0.354	0.365	0.363	0.359
SC-MOGA with data sampling	0.189	0.043	0.144	0.237	0.232	0.169

Table 7 (Continue)

Dataset	Number of clusters					Mean
	K=2	K=5	K=8	K=11	K=14	
HS	K=2	K=5	K=8	K=11	K=14	Mean
SRIDHCR	N/A	N/A	N/A	N/A	N/A	N/A
LK-Means	N/A	N/A	N/A	N/A	N/A	N/A
SCEC	0.350	0.476	0.509	0.544	0.565	0.489
SC-MOGA	0.499	0.424	0.480	0.507	0.523	0.487
SC-MOGA with data sampling	0.332	0.225	0.199	0.243	0.213	0.242
LD	K=2	K=5	K=8	K=11	K=14	Mean
SRIDHCR	N/A	N/A	N/A	N/A	N/A	N/A
LK-Means	N/A	N/A	N/A	N/A	N/A	N/A
SCEC	0.455	0.459	0.468	0.478	0.471	0.466
SC-MOGA	0.335	0.266	0.369	0.410	0.431	0.362
SC-MOGA with data sampling	0.310	0.144	0.091	0.073	0.129	0.149
MP	K=2	K=6	K=10	K=14	K=18	Mean
SRIDHCR	N/A	N/A	N/A	N/A	N/A	N/A
LK-Means	N/A	N/A	N/A	N/A	N/A	N/A
SCEC	0.376	0.311	0.404	0.430	0.429	0.390
SC-MOGA	0.243	0.325	0.400	0.427	0.448	0.369
SC-MOGA with data sampling	0.176	0.189	0.246	0.247	0.283	0.228
Musk	K=2	K=6	K=10	K=14	K=18	Mean
SRIDHCR	N/A	N/A	N/A	N/A	N/A	N/A
LK-Means	N/A	N/A	N/A	N/A	N/A	N/A
SCEC	0.409	0.458	0.459	0.450	0.459	0.447
SC-MOGA	0.361	0.350	0.395	0.432	0.456	0.399
SC-MOGA with data sampling	0.033	0.038	0.002	0.016	0.011	0.020
Seeds	K=3	K=5	K=7	K=9	K=11	Mean
SRIDHCR	N/A	N/A	N/A	N/A	N/A	N/A
LK-Means	N/A	N/A	N/A	N/A	N/A	N/A
SCEC	0.078	0.096	0.096	0.146	0.197	0.123
SC-MOGA	0.068	0.105	0.165	0.180	0.226	0.149
SC-MOGA with data sampling	0	0	0.069	0.112	0.117	0.060

Table 7 (Continue)

Dataset	Number of clusters					Mean
	K=2	K=5	K=8	K=11	K=14	
SPECTF	K=2	K=5	K=8	K=11	K=14	Mean
SRIDHCR	N/A	N/A	N/A	N/A	N/A	N/A
LK-Means	N/A	N/A	N/A	N/A	N/A	N/A
SCEC	0.305	0.537	0.558	0.591	0.611	0.520
SC-MOGA	0.448	0.592	0.512	0.536	0.566	0.531
SC-MOGA with data sampling	0	0	0	0	0	0
SPF	K=7	K=14	K=21	K=28	K=35	Mean
SRIDHCR	N/A	N/A	N/A	N/A	N/A	N/A
LK-Means	N/A	N/A	N/A	N/A	N/A	N/A
SCEC	0.226	0.225	0.190	0.209	0.203	0.211
SC-MOGA	0.235	0.230	0.238	0.241	0.241	0.237
SC-MOGA with data sampling	0.188	0.093	0.088	0.118	0.117	0.121
TAE	K=3	K=5	K=7	K=9	K=11	Mean
SRIDHCR	N/A	N/A	N/A	N/A	N/A	N/A
LK-Means	N/A	N/A	N/A	N/A	N/A	N/A
SCEC	0.386	0.352	0.353	0.324	0.326	0.348
SC-MOGA	0.257	0.211	0.287	0.206	0.231	0.238
SC-MOGA with data sampling	0.156	0.175	0.282	0.152	0.183	0.190
Vertebral	K=3	K=6	K=9	K=12	K=15	Mean
SRIDHCR	N/A	N/A	N/A	N/A	N/A	N/A
LK-Means	N/A	N/A	N/A	N/A	N/A	N/A
SCEC	0.165	0.165	0.283	0.283	0.308	0.241
SC-MOGA	0.261	0.198	0.260	0.269	0.309	0.259
SC-MOGA with data sampling	0.134	0.165	0.255	0.151	0.144	0.170
Wilt	K=2	K=5	K=8	K=11	K=14	Mean
SRIDHCR	N/A	N/A	N/A	N/A	N/A	N/A
LK-Means	N/A	N/A	N/A	N/A	N/A	N/A
SCEC	0.498	0.682	0.803	0.828	0.836	0.729
SC-MOGA	0.436	0.757	0.835	0.871	0.830	0.746
SC-MOGA with data sampling	0.003	0.005	0	0.004	0.006	0.004

Table 7 (Continue)

Dataset	Number of clusters					Mean
	K=3	K=5	K=7	K=9	K=11	
Wine	K=3	K=5	K=7	K=9	K=11	Mean
SRIDHCR	N/A	N/A	N/A	N/A	N/A	N/A
LK-Means	N/A	N/A	N/A	N/A	N/A	N/A
SCEC	0.024	0.111	0.137	0.190	0.231	0.139
SC-MOGA	0.008	0.106	0.148	0.193	0.171	0.125
SC-MOGA with data sampling	0	0.025	0.013	0.085	0.071	0.039

Table 8

Confidence levels of paired *t*-test between SC-MOGA and the other three algorithms based on the eight datasets and different numbers of clusters

	SRIDHCR	LK-Means	SC-MOGA with data sampling
Based on AMI, SC-MOGA performs better than	100%	100%	0%
Based on ARI, SC-MOGA performs better than	100%	100%	0%
Based on AVI, SC-MOGA performs better than	100%	100%	0%
Based on MD, SC-MOGA performs better than	100%	100%	0%

Table 9

Confidence levels of paired *t*-test between SC-MOGA with data sampling and the other three algorithms based on the eight datasets and different numbers of clusters

	SRIDHCR	LK-Means	SC-MOGA
Based on AMI, SC-MOGA with data sampling performs better than	100%	100%	100%
Based on ARI, SC-MOGA with data sampling performs better than	100%	100%	100%
Based on AVI, SC-MOGA with data sampling performs better than	100%	100%	100%
Based on MD, SC-MOGA with data sampling performs better than	100%	100%	100%

The Second Experiment

The second experiment is intended to compare the performances of SC-MOGA and SC-MOGA with data sampling against SCEC, which is also based on a genetic algorithm. The testing datasets comprise the eight datasets used in the first experiment and another fifteen datasets. These fifteen datasets are also from the UCI Machine Learning Repository (Lichman, 2013). They are Balance Scale ('BS'), Blood Transfusion Service Center ('BTSC'), Climate Model Simulation Crashes ('CMSC'), Contraceptive Method Choice ('CMC'), Haberman's Survival ('HS'), Liver Disorders ('LD'), MONK's Problems ('MP'), Musk (Version 1) ('Musk'), Seeds, SPECTF Heart ('SPECTF'), Steel Plates Faults ('SPF'), Teaching Assistant Evaluation ('TAE'), Vertebral, Wilt and Wine. All datasets were preprocessed by max-min normalization. The details of the fifteen datasets are shown in Table 10. The setups for the second experiment were the same as those for the first experiment.

Table 11 shows all the sampling parameter values used in the experiments for SC-MOGA with data sampling. We implemented SCEC and ran it based on the experiment setups in Eick, Zeidat and Zhao (2004): size of population is 400, Crossover rate increases from 0 to 0.95, Mutation rate decreases from 0.95 to 0, Number of generations is 1,500, Copy rate is 0.05. The value of the parameter α in equation 1 was chosen from the 11 values between 0 and 2.0 with a step of 0.2, which yielded the best performance. The four cluster validity indexes were used to compare the performance. The four validity index results for the 23 datasets are shown in Tables 4 to 7. One-sided paired t-tests were carried out to compare the performances of SC-MOGA, SC-MOGA with data sampling and SCEC. To carry out the t-test between two algorithms for each index, we computed the differences between the indexes achieved by the two algorithms for the 23 datasets and for all K_s (number of clusters). The results of the tests are shown in Tables 12 and 13. The results in Table 12 show that SC-MOGA achieved better performances than SCEC with a confidence level of more than 95% for all four indexes, but did not perform better than SC-MOGA with data sampling. The results in Table 13 show that SC-MOGA with data sampling achieved a better performance than SCEC and SC-MOGA with confidence levels of more than 95% for all four indexes.

It can be concluded from the t-test results for the two experiments that the proposed SC-MOGA and SC-MOGA with data sampling methods achieved better performances than the other three algorithms in existence. It can also be seen from the results that SC-MOGA with data sampling achieved better performances than SC-MOGA. For the sake of brevity, the plots of AMI against running time in seconds on the eight datasets for SCEC, SC-MOGA and SC-MOGA with data sampling are shown in Figures 2 to 9. The plots for the other datasets exhibit similar results. It can be seen from the figures that although SCEC can converge quickly, it experienced premature convergences to local optima, while

SC-MOGA and SC-MOGA with data sampling took more time but were able to converge to better solutions. It can also be seen that SC-MOGA with data sampling took less time than SC-MOGA to converge, and that it converged to better solutions. This shows that the proposed sampling method is very effective for sampling good representatives of the given dataset, reducing the size of search space and allowing the genetic algorithm to converge to better solutions.

For a very large dataset, the search space for the proposed genetic algorithm can be huge, therefore, SC-MOGA or SC-MOGA with data sampling may take quite a large number generations to converge to solutions. Some future work could be done to further improve the performance of the proposed algorithm. For example, to help the algorithm converge more quickly it is possible to incorporate specialized genetic operators which perform some local search for offspring with fitness values better than their parent chromosomes. This would accelerate the search to converge more quickly toward the potential optimal solution. Some other evolutionary algorithms such as particle swarm

Table 10

Details of the fifteen UCI Machine Learning Repository Datasets

Dataset Name	# objects	# variables	# classes
BS	625	4	3
BTSC	748	4	2
CMSC	540	18	2
CMC	1473	9	3
HS	306	3	2
LD	345	6	2
MP	432	6	2
Musk	476	166	2
Seeds	210	7	3
SPECTF	267	44	2
SPF	1941	27	7
TAE	151	5	3
Vertebral	310	6	3
Wilt	4339	5	2
Wine	178	13	3

Table 11
Sampling parameter values used by SC-MOGA with data sampling on the additional 15 datasets

Dataset	Number of Data Objects (N)	χ^2 chi-square	Population Fraction (F)	Precision Degree (d)	Expected Sample Size (S)	Number of Strata (m)	Actual Sample size $\sum_{k=1}^m n_k$
BS	625	3.841	0.5	0.05	239	322	431
BTSC	748	3.841	0.5	0.05	255	368	495
CMSC	540	3.841	0.5	0.05	225	183	289
CMC	1473	3.841	0.5	0.05	305	43	306
HS	306	3.841	0.5	0.05	171	144	216
LD	345	3.841	0.5	0.05	183	109	212
MP	432	3.841	0.5	0.05	204	150	211
Musk	476	3.841	0.5	0.05	213	10	213
Seeds	210	3.841	0.5	0.05	136	14	136
SPECTF	267	3.841	0.5	0.05	158	16	158
SPF	1941	3.841	0.5	0.05	321	38	321
TAE	151	3.841	0.5	0.05	109	41	109
Vertebral	310	3.841	0.5	0.05	172	14	172
Wilt	4339	3.841	0.5	0.05	353	12	353
Wine	178	3.841	0.5	0.05	122	12	122

intelligence have proven to be very effective for solving large dimensional optimization problems, so it is possible to use these algorithms for searching clustering solutions instead of the genetic algorithm.

Table 12

Confidence levels of paired *t*-test based on the four indexes between SC-MOGA and the other two algorithms based on the 23 datasets and different numbers of clusters

	SCEC	SC-MOGA with data sampling
Based on AMI, SC-MOGA performs better than	100%	0%
Based on ARI, SC-MOGA performs better than	99%	0%
Based on AVI, SC-MOGA performs better than	100%	0%
Based on MD, SC-MOGA performs better than	98%	0%

Table 13

Confidence levels of paired *t*-test based on the four indexes between the SC-MOGA with data sampling and the other two algorithms, based on the 23 datasets and different numbers of clusters.

	SCEC	SC-MOGA
Based on AMI, SC-MOGA with data sampling performs better than	100%	100%
Based on ARI, SC-MOGA with data sampling performs better than	100%	100%
Based on AVI, SC-MOGA with data sampling performs better than	100%	100%
Based on MD, SC-MOGA with data sampling performs better than	100%	100%

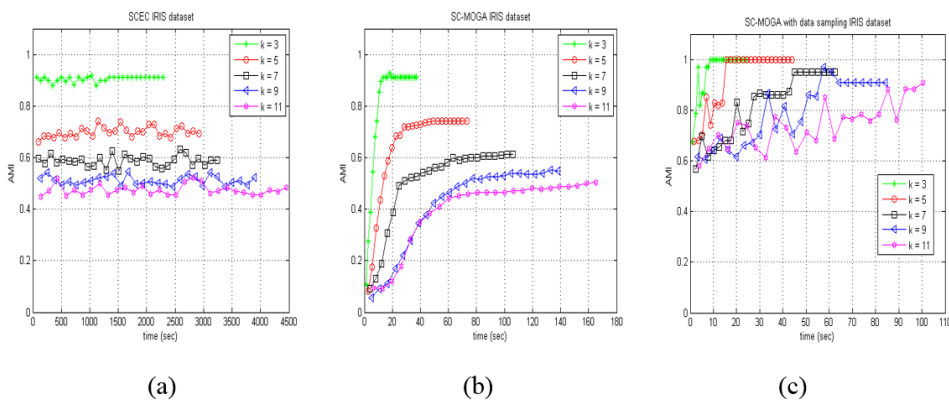


Figure 2. (a), (b), (c) Plots of AMI against running time in seconds on Iris for SCEC, SC-MOGA and SC-MOGA with data sampling, respectively

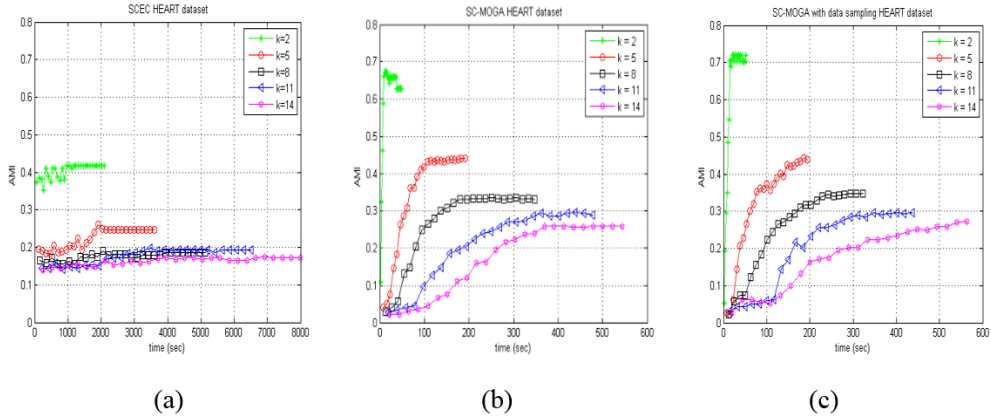


Figure 3. (a), (b), (c) Plots of AMI against running time in seconds on Heart for SCEC, SC-MOGA and SC-MOGA with data sampling, respectively

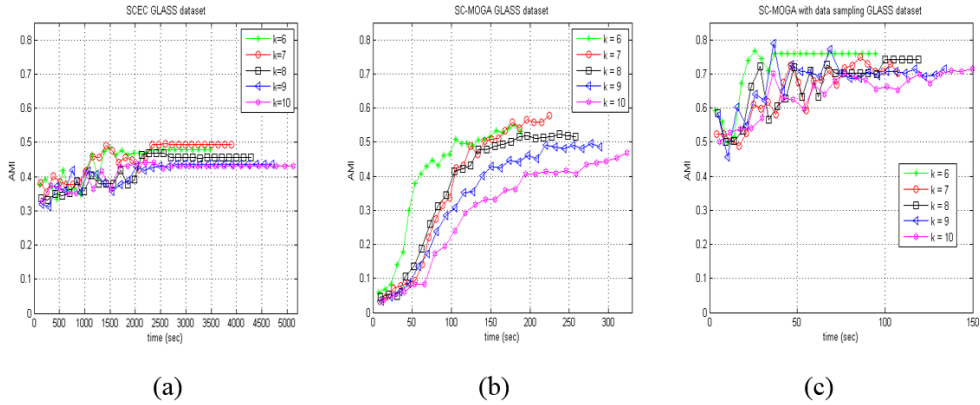


Figure 4. (a), (b), (c) Plots of AMI against running time in seconds on Glass for SCEC, SC-MOGA and SC-MOGA with data sampling, respectively

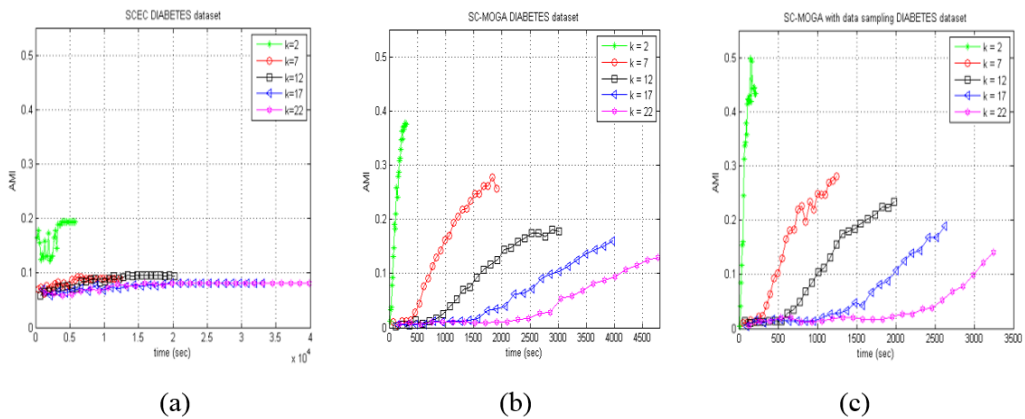


Figure 5. (a), (b), (c) Plots of AMI against running time in seconds on Diabetes for SCEC, SC-MOGA and SC-MOGA with data sampling, respectively

Supervised Clustering based on a Multi-objective Genetic Algorithm

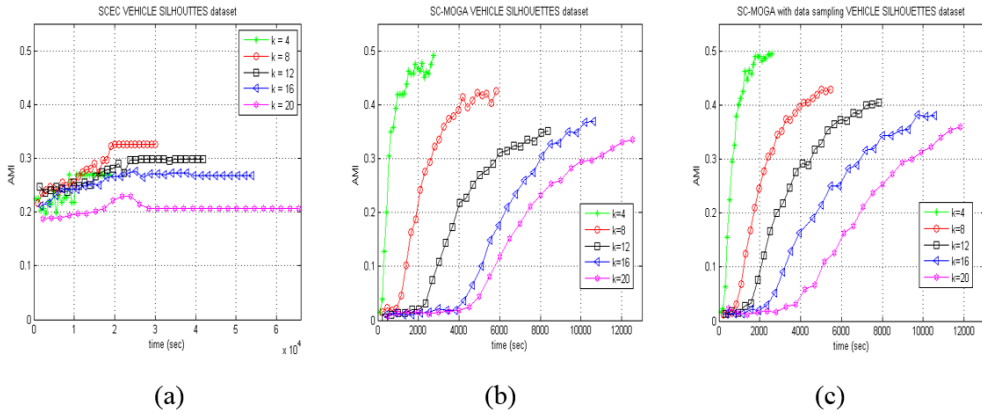


Figure 6. (a), (b), (c) Plots of AMI against running time in seconds on Vehicle Silhouettes for SCEC, SC-MOGA and SC-MOGA with data sampling, respectively

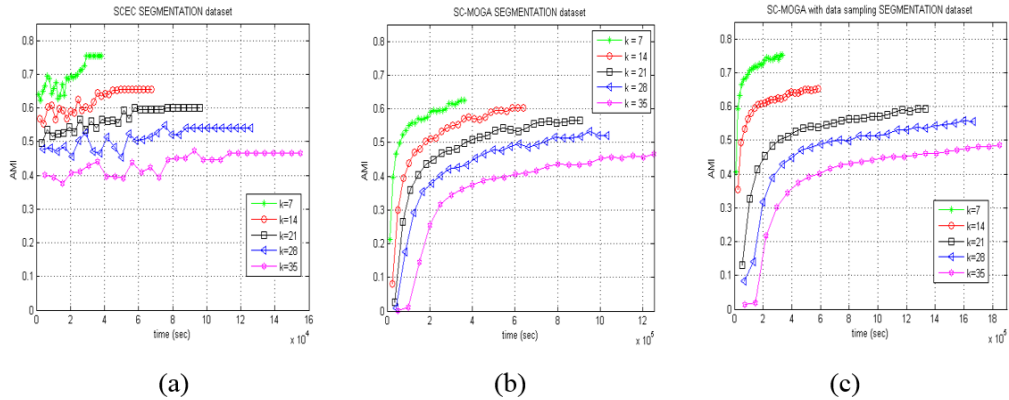


Figure 7. (a), (b), (c) Plots of AMI against running time in seconds on Segmentation for SCEC, SC-MOGA and SC-MOGA with data sampling, respectively

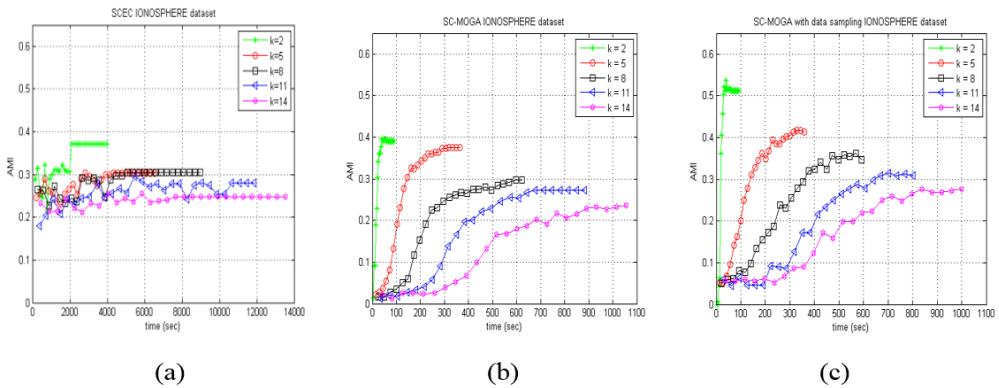


Figure 8. (a), (b), (c) Plots of AMI against running time in seconds on Ionosphere for SCEC, SC-MOGA and SC-MOGA with data sampling, respectively

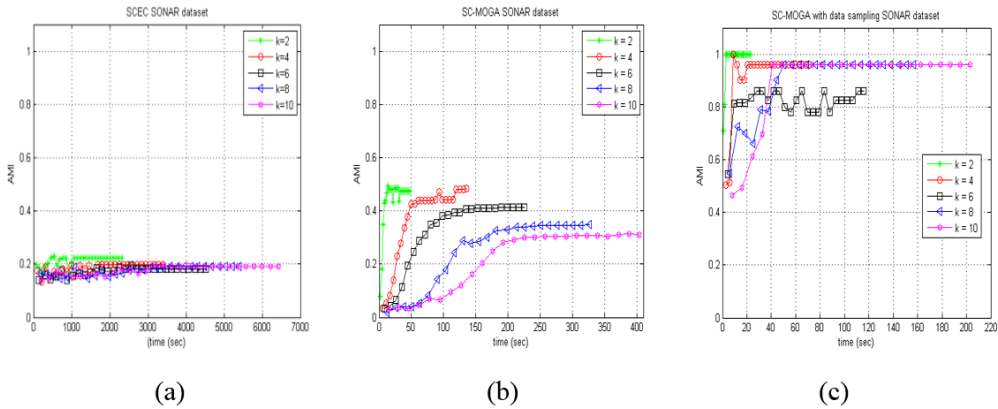


Figure 9. (a), (b), (c) Plots of AMI against running time on Sonar for SCEC, SC-MOGA and SC-MOGA with data sampling, respectively

Convergence of the Three Objective Functions

Figures 10 and 11 show the convergence of the normalized values (using a max-min normalization scheme) of the three objective functions, impurity level, SSE and inter cluster distance, on the Iris dataset for SC-MOGA and SC-MOGA with data sampling. The convergence of the normalized values of the three objective functions on the other testing datasets exhibit quite the same patterns so they are not included in this paper. The convergence plots of AMI for SC-MOGA and SC-MOGA with data sampling are also shown in figure 10(a) and figure 11(a) for comparison with those of the three objective functions. It can be seen from the figures 10(a) and 11(a) - 10(f) and 11(f) that when the number of generations of the genetic algorithms increases, the SSE and the impurity level decreases while the inter cluster distance (as well as the AMI) increases until they all converge. The results show that the proposed algorithms can simultaneously optimize the three objective functions leading to a good clustering solution as measured by the AMI value. It can also be seen that as the number of clusters, K , increases, it takes more number of generations for the genetic algorithms to converge to an optimal solution. This is due the fact that the search space for the genetic algorithms becomes more complex as the value of K increases.

Supervised Clustering based on a Multi-objective Genetic Algorithm

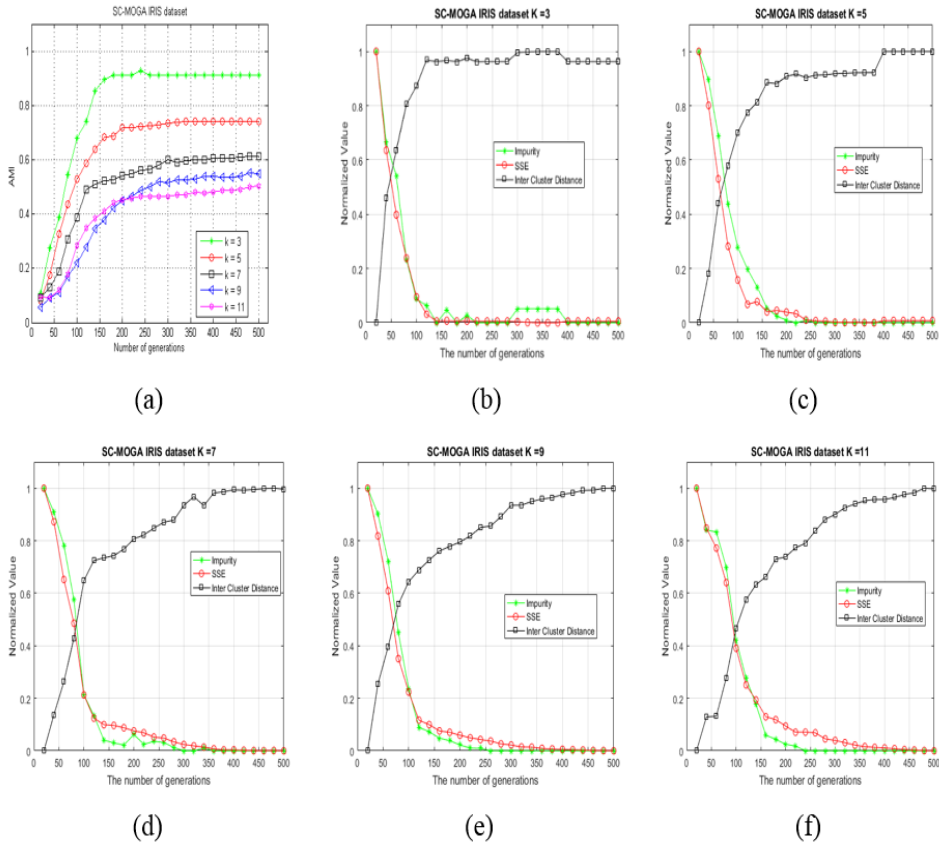


Figure 10. (a) Plots of AMI on Iris within 500 generations for SC-MOGA when $K = 3, 5, 7, 9$ and 11 . (b) – (f) Plots of normalized values of impurity, SSE and inter cluster distance within 500 generations for SC-MOGA when $K = 3, 5, 7, 9$ and 11 , respectively.

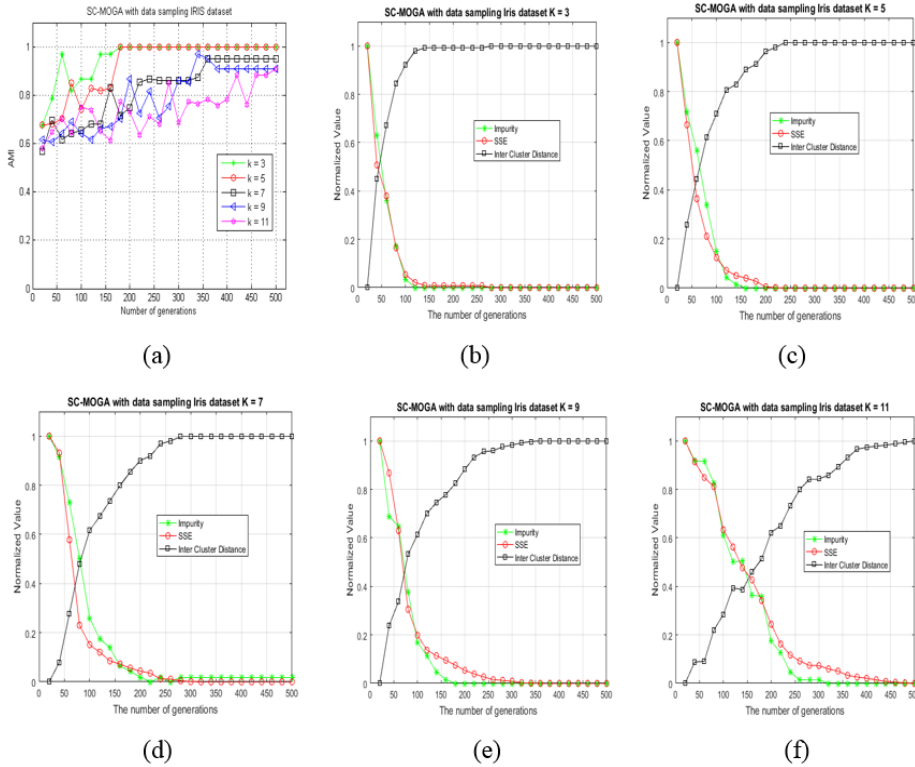


Figure 11. (a) Plots of AMI on Iris within 500 generations for SC-MOGA with data sampling when $K = 3, 5, 7, 9$ and 11 . (b) – (f) Plots of normalized values of impurity, SSE and inter cluster distance within 500 generations for SC-MOGA with data sampling when $K = 3, 5, 7, 9$ and 11 , respectively.

CONCLUSION

A novel supervised clustering algorithm based on a multi-objective genetic algorithm, namely SC-MOGA, is proposed in this paper. The SC-MOGA incorporates three objectives for supervised clustering. The first objective is to minimize the sum squared errors (compactness) of the clusters, the second objective is to minimize the level of impurity of the data in the clusters and the third objective is to maximize the inter cluster distance (separateness). The SC-MOGA applies the crowding genetic algorithm to search for the clustering solutions in a multimodal solution space. For large datasets, a data sampling method using the Bisecting K-Means approach is also proposed to sample the representatives of the dataset for clustering. The experimental results show that the SC-MOGA and SC-MOGA with data sampling are very effective for supervised clustering. They outperform some existing algorithms, i.e. LK-Means, SRIDHCR and SCEC. The experiment results also show that the proposed data sampling method not only helps reduce the sample size for SC-MOGA but also helps SC-MOGA to converge to better clustering solutions.

REFERENCES

- Cadima, E. L., Caramelo, A. M., Afonso-Dias, M., Conte de Barros, P., Tandstad, M. O., & de Leiva Moreno, J. I. (2005). *Sampling methods applied to fisheries science: a manual* (FAO Fisheries Technical Paper No. 434). Retrieved September 3, 2016, from <http://www.fao.org/docrep/009/a0198e/A0198E00.htm>
- De Jong, K. A. (1975). *An analysis of the behaviour of a class of genetic adaptive systems* (PhD thesis). Department of Computer and Communication Sciences, University of Michigan, MI.
- Deb, K. (2001). *Multi-Objective Optimization Using Evolutionary Algorithms*. New York, NY: John Wiley & Sons, Inc.
- Eick, C. F., Rouhana, A., Bagherjeiran, A., & Vilalta, R. (2006). Using clustering to learn distance functions for supervised similarity assessment. *Engineering Applications of Artificial Intelligence*, 19(4), 395–401.
- Eick, C. F., Vaezian, B., Jiang, D., & Wang, J. (2006). Discovery of interesting regions in spatial data sets using supervised clustering. In *Proceedings of the 10th European Conference on Principles and Practice of Knowledge Discovery in Databases* (pp. 127–138). Berlin, Germany.
- Eick, C. F., Zeidat, N., & Vilalta, R. (2004). Using representative-based clustering for nearest neighbor dataset editing. In *Proceedings of the 4th IEEE International Conference on Data Mining* (pp. 375–378). DC, USA.
- Eick, C. F., Zeidat, N., & Zhao, Z. (2004). Supervised clustering – algorithms and benefits. In *Proceedings of the 16th IEEE International Conference on Tools with Artificial Intelligence* (pp.774-776). DC, USA.
- Finley, T., & Joachims, T. (2005). Supervised clustering with support vector machines. In *Proceedings of the 22nd International Conference on Machine Learning* (pp.17–224). NY, USA.
- Fonseca, C. M., & Fleming, P. J. (1993). Genetic algorithms for multiobjective optimization: Formulation, discussion and generalization. In *Proceedings of the 5th International Conference on Genetic Algorithms* (pp. 416-423). CA, USA.
- Grbovic, M., Djuric, N., Guo, S., & Vucetic, S. (2013). Supervised clustering of label ranking data using label preference information. *Journal Machine Learning*, 93(2–3), 191–225.
- Haider, P., Brefeld, U., & Scheffer, T. (2007). Supervised clustering of streaming data for email batch detection. In *Proceedings of the 24th International Conference on Machine Learning* (pp. 345–352). OR, USA.
- Hamming, R. W. (1950). Error detecting and error correcting codes. *Bell System Technical Journal*, 29(2), 147–160. doi: 10.1002/j.1538-7305.1950.tb00463.x
- Hruschka, E. R., Campello, R. J. G. B., Freitas, A. A., & de Carvalho, A. C. P. L. F. (2009). A survey of evolutionary algorithms for clustering. *IEEE Transactions on Systems, Man, and Cybernetics, Part C: Applications and Reviews*, 39(2), 133–155. doi: 10.1109/TSMCC.2008.2007252
- Hubert, L., & Arabie, P. (1985). Comparing partitions. *Journal of Classifications*, 2(1), 193–218. doi: 10.1007/BF01908075
- Jain, A. K., & Dubes, R. C. (1988). *Algorithms for clustering data*. Upper Saddle River, NJ: Prentice-Hall, Inc.
- Kaufman, L., & Rousseeuw, P. J. (1990). *Finding groups in data: An introduction to cluster analysis*. Hoboken: John Wiley & Sons. doi: 10.1002/9780470316801

- Krejcie, R. V., & Morgan, D. W. (1970). Determining sample size for research activities. *Educational and Psychological Measurement*, 30(3), 607–610.
- Lichman, M. (2013). *UCI Machine Learning Repository*. Retrieved September 3, 2016, from <http://archive.ics.uci.edu/ml>
- Maji, P. (2010). Mutual information-based supervised attribute clustering for microarray sample classification. *IEEE Transactions on Knowledge and Data Engineering*, 24(1), 127–140. doi:10.1109/TKDE.2010.210
- Mirkin, B. G., & Chernyj, L. B. (1970). Measurement of the distance between distinct partitions of a finite set of objects. *Automation and Remote Control*, 5, 786–792.
- Peralta, B., Espinace, P., & Soto, A. (2013). Enhancing K-Means using class labels. *Journal Intelligent Data Analysis*, 17(6), 1023–1039.
- Syswerda, G. (1989). Uniform crossover in genetic algorithms. In *Proceedings of the 3rd International Conference on Genetic Algorithms* (pp. 2-9). CA, USA.
- Vinh, N. X., Epps, J., & Bailey, J. (2009). Information theoretic measures for clusterings comparison: Is a correction for chance necessary? In *Proceedings of the 26th Annual International Conference on Machine Learning* (pp. 1073-1080). Quebec, Canada.

Adaptive Genetic Algorithm for Feature Weighting in Multi-Criteria Recommender Systems

Gursimarpreet Kaur^{1*} and Saroj Ratnoo²

¹Space Applications Centre, Indian Space Research Organization,
Ahmedabad 380015, India

²Department of Computer Science and Engineering,
Guru Jambheshwar University of Science and Technology, Hisar 125001, India

ABSTRACT

Recommender Systems (RS) have proven to be a successful personalization technique in this era of ever increasing information overload. Among many available recommendation techniques, Collaborative Filtering (CF) is the most popularly used. However, most of the CF applications use single ratings for recommending items and the use of multi-criteria ratings in the recommendation process is still under-explored. This paper proposes multi-criteria RS based on Adaptive Genetic Algorithm (AGA). The AGA design, which updates the crossover and mutation rates dynamically, is employed to model the users' preferences for multi-criteria ratings on different attributes of items. The AGA optimizes a user's preferences for different attributes in the form of a weight vector. Thus, the AGA finds an individual optimal weight vector in relation to each user. The weight vector is used to recommend items to the respective user. The experiments are conducted on Yahoo movies, a well known multi-criteria rating dataset. The experimental results confirm that the AGA based multi-criteria RS outperforms the traditional single criteria based Collaborative Filtering RS and the simple GA based multi-criteria RS.

Keywords: Collaborative filtering, Genetic Algorithms, multi-criteria, Recommender Systems

ARTICLE INFO

Article history:

Received: 18 January 2018

Accepted: 12 September 2018

Published: 24 January 2019

E-mail addresses:

gursimarpreet8029@gmail.com (Gursimarpreet Kaur)

ratnoo.saroj@gmail.com (Saroj Ratnoo)

* Corresponding author

INTRODUCTION

The exponential growth of information on the internet has led to the problem of information overload. Although, it has become convenient for users to access a wide range of information, at the same time

it is all the more possible now to get astray while searching for some specific information of interest on the internet. More often, the users have to pass through many links before reaching the information that they need. In this scenario, Recommender Systems (RS) have emerged as an important tool to provide users only the selective choices. Recommender Systems are personalized information filtering techniques that suggest only a limited number of items that are most likely to be of interest or to be suitable to one's needs (Ricci, Rokach, Shapira, & Kantor, 2011). RS have been widely implemented in the application domains like recommending music, movies, online courses, learning material, books and video. These are categorized into five basic classes i.e. content-based, Collaborative Filtering (CF) based, demography-based, knowledge-based and community-based (Adomavicius & Tuzhilin, 2005). Though, each technique has its own pros and cons; the CF technique is the most popular one among all of these. One of the major limitations of the existing RS is that these are based on overall rating value as the sole criterion for evaluating users' preferences. Users might express their opinion based on different features or attributes of an item, so even if two users agree on global ratings, they may have completely diverse preferences on different features of that item (Sanchez-Vilas, Ismoilov, Lousame, Sanchez, & Lama, 2011). A user may prefer a movie because of its story-line whereas another user may like the movie due to acting or extraordinary visual effects. Both of these users rate the particular movie high, but for different reasons. Hence, in such cases, it is inappropriate to find similarities between such users only on the basis of overall rating as the single criteria. Nothing is more annoying than getting recommendations for the items in which a user is least interested. By using multi-criteria ratings, we can gather information about the specific preferences of users based on the different attributes of items to be recommended and avail the opportunity to generate more accurate recommendations (Adomavicius & Kwon, 2007; Wang & Geng, 2008; Adomavicius, Manouselis, & Kwon, 2011; Zarrinkalam & Kahani, 2012).

A Genetic Algorithm (GA) is a stochastic search technique based on the mechanism of natural selection and genetic evolution to solve complex optimization problems. Genetic Algorithms (GAs) have been widely and effectively used in the field of recommender systems (Fong, Ho, & Hang, 2008; Bobadilla, Ortega, Hernando, & Alcalá, 2011; Sohrabi, Mahmoudian, & Raeesi, 2011). Since a user gives different importance or priority to each feature in multi-criteria RS, GAs have been mainly used for optimizing weights given by users to different features of an item (Fong, Ho, & Hang, 2008; Hwang & Hwang, 2010; Salehi, Pourzaferani, & Razavi, 2013; Parveen, Kant, Dwivedi, & Jaiswal, 2015). Although all these authors have reported the effectiveness of their research as compared to the traditional recommender systems, all these works use a static set of the parameters that are fixed at the beginning of a GA run. Setting appropriate values for crossover and mutation rates, the two GA main operators, is of significant importance for the success

of a GA. Optimal values of these operators are problem specific and most often these are determined by hit and trial method. A GA with such a parameter setting may get stuck in local convergence and does not guarantee optimal results. To alleviate this problem, an Adaptive Genetic Algorithm (AGA) can be used. In AGA, parameter values for GA operators get updated dynamically according to the fitness values of the solutions at that particular generation (Srinivas & Patnaik, 1994). Since an AGA is capable of maintaining a better balance between exploration and exploitation, it avoids premature convergence which is essential for finding global optimal solutions.

This paper proposes a multi-criteria recommender system that uses an adaptive GA to optimize weights for the four criteria (acting, direction, story and visuals) given in the Yahoo movies dataset. The Adaptive GA successfully models an individual user's preferences given to different criteria in terms of weights to reason out why the particular user prefers some movies over the others. The main contribution of this paper is the design and application of an adaptive GA for optimizing weights for a Collaborative Filtering based multi-criteria RS for the movie recommendation. The experiments reveal that the recommendations made by the proposed AGA based multi-criteria recommender system are more accurate than the recommendations made by a traditional single criterion based recommendation technique. Moreover, as the proposed AGA sets the probability of crossover and mutation dynamically depending on the state of the GA population (converging or diverging); it achieves a significant performance improvement as compared to the simple GA based RS.

The rest of the paper is organized as follows: After the introduction in section I, section II presents the essential background and related work on multi-criteria RS. It reviews the status of research in applying GA and AGA to model users' preferences. Section III proposes the adaptive GA design. Section IV illustrates the overall design of RS using AGA with the help of a block diagram. The experimental design and results are described in section V. Section VI concludes the paper and points to future research directions.

BACKGROUND DETAILS AND RELATED WORK

Recommender Systems

Recommender systems suggest interesting items in the cases where the range of choices exceeds a user's ability to view them to reach a proper decision. This narrowing down of items aids in improving browsing and consumption experience of customers and thus increases customer loyalty and sales provided that recommendations made are correct according to the tastes and interests of diverse users. Most of the popular RS are based on Collaborative Filtering (CF) technique for making recommendations. A Collaborative Filter based RS presumes that the users who have similar preferences in past are likely to have same preferences in future too. Recommender Systems (RS) use some form of user feedback which is generally in the form of item ratings. At present, most of the RS use

only the overall rating values of items for gaining access to users' opinions. RS based on a single criterion as overall ratings consider two users similar if they have similar overall ratings. However, an agreement between two users on overall rating does not necessarily mean that these users have similar preferences for the various aspects of the item. A RS will be more effective if it not only finds what people like but also captures the essence why they like it, i.e., it should recognize preferences not just patterns. Hence, the focus of research has recently shifted from single criteria RS (SCRS) based on overall ratings to multi-criteria RS (MCRS) that account for preferences of users for different attributes of items to make more valuable recommendations (Adomavicius & Kwon, 2007; Teng & Lee, 2007; Hassan & Hamada, 2016, 2017).

Multi-criteria Recommender Systems (MCRS)

A Multi-criteria RS (MCRS) is relatively a new technique that takes into account user's ratings on many attributes in addition to the overall ratings. In MCRS, the overall rating is predicted quite differently as compared to that of single criterion based recommendation techniques. The overall rating is resolved based on a number of ratings given to the attributes of items. Hence, MCRS need to capture the degree or the weight of users' preferences for different facets of items of their interest. The main objective of MCRS is to model a user's preferences from the values of multi-criteria ratings assigned by that user to the various items' attributes. This amounts to searching for a vector of optimal weights for reflecting an individual user's preferences over multiple criteria which is an optimization problem. (Adomavicius & Kwon, 2007; Manouselis & Costopoulou, 2007; Lakiotaki, Tsafarakis, & Matsatsinis, 2008; Adomavicius, Manouselis, & Kwon, 2011; Hassan & Hamada, 2016). The foremost contribution in developing MCRS came from (Adomavicius & Kwon, 2007). The authors analyzed the MCRS framework on Yahoo movie dataset and their results confirmed the superiority of MCRS over SCRS with respect to error rates, precision, recall and f-measure etc. Since their inception, MCRS have proved their merit in several application domains (Li, Wang & Geng, 2008; Adomavicius, Manouselis & Kwon, 2011; Sanchez-Vilas, Ismoilov, Lousame, Sanchez, & Lama, 2011; Sohrabi, Mahmoudian & Raesi, 2011; Jannach, Karakaya & Gedikli, 2012; Rodriguez, Posse & Zhang, 2012; Salehi, Pourzaferani, & Razavi, 2013; Parveen, Kant, Dwivedi, & Jaiswal, 2015). Overall, there is still a scope to further explore MCRS techniques for making the recommendation process more accurate and effective.

Genetic Algorithms in MCRS

A GA follows meta-heuristic technique motivated by the principle of natural genetics and evolution. GAs have been consistently used to solve difficult optimization and search problems. For the operation of a GA, an initial population of solutions is created

randomly in which each solution is a finite length string known as a chromosome. At every evolutionary step, the fitness function is applied to compute the fitness of each individual solution. A fitness function is an application dependent predefined quality criterion. A fitness proportionate selection is carried out to create a new population by probabilistically taking fittest individuals from the previous population. These solutions then reproduce to form new individuals on the application of genetic operators, i.e., crossover and mutation. This whole process is repeated until a stopping criterion is reached (Goldberg, 1989; Michalewicz, 1996).

Counting on GAs' promising history in the domain of optimization, researchers have used GAs to search for an optimal weight vector for a user's preferences in case of MCRS. Fong, Ho & Hang, (2008) proposed a novel MCRS method by taking the input data from both *Movielens* and *IMDB* movies datasets. A total of 37 features were taken from both datasets in order to prevent any bias from one set of data. Then the weights of these criteria were optimized using a GA. Hwang & Hwang, (2010) proposed a framework for integrating CF technique with GA, wherein GA was used for criteria weighting. Some more GA based MCRS proposals were suggested in (Jannach, Karakaya & Gedikli, 2012; Rodriguez, Posse & Zhang, 2012; Geng, Li, Jiao, Gong, Cai & Wu, 2015). Recently, Parveen, Kant, Dwivedi and Jaiswal (2015) treated the problem of n-MCRS as n single criteria problems. They solved these individual problems and then the overall rating was taken as the aggregation of these ratings. A GA was used to optimize priorities of users on these criteria. In addition, some multi-objective pareto-efficient approaches have also been promulgated in the domain of MCRS (Ribeiro, Lacerda, Veloso & Ziviani, 2012; Ribeiro, Ziviani, Moura, Hata, Lacerda, & Veloso, 2014).

This is an established fact that setting of GA parameters (most importantly crossover probability (p_c) and mutation probability (p_m)) is one of the common factors that contribute to the success or failure of a GA to search for the globally optimal solution. Most of the GA implementations for optimizing users' preferences over different attributes set the parameters by hit and trial method and used a static parameter setting. In these implementations, the parameters are usually tuned experimentally by trying many combinations of values of probability of crossover (p_c), probability of mutation (p_m), and population size and then their effect is analyzed on the final solution. The combination of parameters that appears best somehow is fixed prior to running GA and the parameter setting remains the same for the whole GA process. Crossover and mutation probabilities mainly control the extent of exploitation and exploration during the lifetime of a GA. A GA is successful in realizing its full potential only if it is able to achieve an appropriate balance between exploitation and exploration. An *ad hoc* static parameter setting directs the evolution towards local convergence. Adaptive GAs, instead of relying on constant values of crossover and mutation rates fixed at the beginning of GA, are able to determine these parameters adaptively by

using the information contained in the state of the current GA population. AGAs can achieve a better balance in exploitation and exploration by changing the crossover and mutation probabilities dynamically to match the diverging or converging status of the GA population at hand and hence, these can maintain diversity in addition to preserving the convergence capacity (Pellerin, Pigeon, & Delisle, 2004; Srinivas & Patnaik, 1994).

We have come across only one attempt of using adaptive genetic algorithms for improving prediction accuracy of multi-criteria recommender systems by (Hassan and Hamada 2017). The proposed approach integrates a SlopeOne algorithm (SoA) with adaptive GA to determine the level of significance in improving the prediction accuracy of AGA based MCRS as compared to single rating based SoA. In this paper, we have taken up the task of applying an adaptive GA framework to arrive at better optimal weights for users' preferences that are subsequently input to a collaborative filtering based RS for making more accurate recommendations.

THE PROPOSED AGA DESIGN

The multi-criteria RS proposed in this paper is based on Adaptive Genetic Algorithm to improve the accuracy of recommendations. We have implemented two versions of AGA to find out the optimal weights of four feature ratings, i.e., Acting, Direction, Story and Visuals given in Yahoo movies dataset. In the first version, the crossover and mutation probabilities are updated from one generation to the next. The change in probabilities depends on the state of the GA population. These probabilities, once updated for a generation remains same for all the individuals in the GA population at that generation. In the second version of AGA within each generation, crossover and mutation probabilities vary from individual to individual chromosome in the GA population depending on their fitness. This section illustrates the design of the AGA in detail.

Chromosome Encoding and Population Initialization

Since the aim of AGA is to find the optimal weights of ratings of four features (Acting, Direction, Story and Visuals of Yahoo movies dataset), each of these features is treated as a gene and together these four features form a chromosome. Each gene in this string represents an explicit attribute weight and it can take any value between 0 and 1. Value of a gene suggests the amount of preference a user has for the particular feature. A value near 0 is treated as dislike, 0.5 is average liking and a value near 1 indicates that the user likes this particular feature of the movie. Hence, chromosomes are real-encoded as they can take any real value between 0 and 1. The value of each gene is further normalized by dividing it by the sum of the overall initial chromosome weight vector as shown in the second row of Figure 1. This way the sum of all weights is always 1. The population is initialized randomly the same way as the individual chromosome.

	Acting	Direction	Story	Visuals
Weights	W1	W2	W3	W4
Initial random weights	0.8	0.4	0.3	0.2
Normalized weights $= \frac{w_i}{\sum_{i=1}^n w_i} = 1.7$	0.470	0.235	0.176	0.117

Figure 1. Chromosome encoding

Fitness Function

Fitness function is also known as objective function or evaluation function as it evaluates the goodness or worth of each individual solution in the population of a GA. Fitness is evaluated at each generation right from the initialization of population. Selection of fitness function is very crucial in the functioning of a Genetic Algorithm. Convergence to an optimal solution is dependent on the type of fitness function selected. Our AGA based multi-criteria RS uses fitness function which minimizes the difference between overall ratings and the aggregate of individual ratings of different criteria's, as given in equation 1.

$$fitness\ function := \sum_{i=1}^N \left| r_{overall} - \frac{w_1 r_1 + w_2 r_2 + \dots + w_k r_k}{w_1 + w_2 + \dots + w_k} \right| \quad (1)$$

Where w_1, w_2, \dots, w_k are the weights assigned by AGA and r_1, r_2, \dots, r_k are the ratings given by a user to the k criteria. The overall score given by a user to a movie is represented by ' $r_{overall}$ ' and N denotes the number of items (or say movies) rated by that particular user (Parveen, Kant, Dwivedi, & Jaiswal, 2015).

Selection

Selection is an operator which allows better fit individuals to get selected for the successive generations. Selection has no relation to the type of problem or fitness function and thus it is an independent portion of a GA. This RS uses roulette wheel selection which is also known as fitness proportionate selection. In this, a probability of selection is assigned to each individual by dividing its fitness by total fitness of the population which results in a normalized value between 0 and 1. By this technique, highly fit chromosomes have more chances of survival to the successive generations as compared to the weaker ones that keep getting eliminated as a GA progresses.

Adaptive Crossover and Mutation

Crossover or recombination operator takes two better fit parent solutions and produces offspring which are likely to have high fitness as compared to the parents. Many types of crossover operators can be found in the literature, for example, single point, double point, uniform and heuristic etc. Our AGA based RS uses adaptive heuristic crossover which is a good option for real coded GAs. It helps to maintain diversity as it not only repositions genetic material but also introduces new one. Expression for the heuristic crossover for two parents Q and P , out of which Q is better fit parent, is given below.

$$Offspring1 = r(Q - p) + Q \quad (2)$$

$$Offspring2 = r(Q) + (1 - r)P \quad (3)$$

In equations 2 and 3, r is a random number between 0 and 1. A larger value of r makes the crossover more exploratory.

The crossover and mutation probabilities are dynamically updated as given in (Srinivas & Patnaik, 1994). Crossover probability, p_c for the two versions of adaptive GA is calculated adaptively by using equations 4 and 5.

Crossover probability for the first version which is to be updated from generation to generation but remains fixed for all the individuals in the GA population.

$$p_c = \begin{cases} \frac{k_1}{f_{max} - f_{avg}} & \text{for } f_{max} > f_{avg} \\ k_1 & \text{otherwise} \end{cases} \quad (4)$$

Crossover probability for the second version that is to be updated for every individual separately in the GA population.

$$p_c = \begin{cases} \frac{k_1 \times (f_{max} - f_{best_par})}{f_{max} - f_{avg}} & \text{for } f_{max} > f_{avg} \text{ and } f_{best_par} > f_{avg} \\ k_1 & \text{otherwise} \end{cases} \quad (5)$$

The values f_{max} , f_{avg} , f_{best_par} respectively represent the maximum fitness, average fitness of the generation and fitness value of the better fit parent out of the two parents to be crossed.

Mutation is a genetic operator which alters one or more gene values, resulting in a different chromosome. Purpose of applying mutation operator is to recover the lost genetic material and thus introduce some amount of diversity in the population. There are many types of mutation operators and we have applied an adaptive random mutation, i.e., some genes are randomly changed by a value between 0 and 1. The way mutation probabilities are computed dynamically for the two respective AGAs are given in the equations 6 and 7.

Mutation probability for the first version which is to be updated from generation to generation but remains fixed for all the individuals in the GA population.

$$p_m = \begin{cases} \frac{k_2}{f_{max} - f_{avg}} & \text{for } f_{max} > f_{avg} \\ k_2 & \text{otherwise} \end{cases} \quad (6)$$

Mutation probability for the second version that is to be updated for individuals in the GA population.

$$p_m = \begin{cases} \frac{k_2 \times (f_{max} - f_{ind})}{f_{max} - f_{avg}} & \text{for } f_{max} > f_{avg} \text{ and } f_{ind} > f_{avg} \\ k_2 & \text{otherwise} \end{cases} \quad (7)$$

The value f_{ind} in equation 7 is the fitness of the individual to be mutated.

When f_{max} is closer to f_{avg} then the status of GA is closer to convergence and hence the value of mutation and crossover probabilities increase to avoid local convergence. Further, if the f_{max} is very close to f_{ind} or f_{best_par} , the crossover and mutation probabilities acquire low values, i.e., the better individuals with fitness near to maximum fitness do not require to be crossed or mutated with high probabilities and vice-versa. This preserves individual with fitness closer to the max fitness into the successive generation and disrupts the individuals with low fitness by applying crossover and mutation with higher probabilities. The crossover and mutation probabilities become literally zero when $f_{max} = f_{best_par}$ and $f_{max} = f_{ind}$ respectively. The probabilities become k_1 and k_2 when $f_{best_par} = f_{avg}$ and $f_{ind} = f_{avg}$ respectively. The individuals with average fitness are also disrupted with high probabilities. The values for k_1 and k_2 are kept to be 1.0 and 0.5. The high values of k_1 and k_2 are there to produce chaotic conditions when GA is about to converge to take it out of local convergence.

Stopping Criteria

All the above steps of a GA are repeated until the stopping criterion is reached. For our GA, stopping criteria is stall generation limit. In this approach, GA keeps on going until there is no change in the best fitness value over some predefined number of generations. On reaching this criterion, individual with best fitness value is returned, which is a weight vector corresponding to the four criteria's.

AGA BASED MULTI-CRITERIA RECOMMENDER SYSTEM ARCHITECTURE

In this section, we discuss the proposed RS which is based on AGA. In this RS, YAHOO movie dataset is used which has individual ratings for different criteria and an overall criterion for each movie. Here, we describe how to incorporate these multi-criteria ratings

into the CF approach. The overall rating is not an independent rating and it is some aggregation function f , of different criteria ratings.

$$r_{overall} = f(r_1, r_2 \dots r_k)$$

Where $r_{overall}$ is the overall rating of a movie and $r_1, r_2 \dots r_k$ are the individual ratings for the k criteria; the value of k is 4 in this case (i.e. for Acting, Direction, Story and Visuals). The aggregation function models a user's preferences and to figure out the aggregation function f , some technique is required, which in our case is AGA. We have used AGA to optimize weights of these four criteria as different users place different priorities on these movie attributes. The block diagram for the overall architecture for the proposed recommender system is shown in Figure 2.

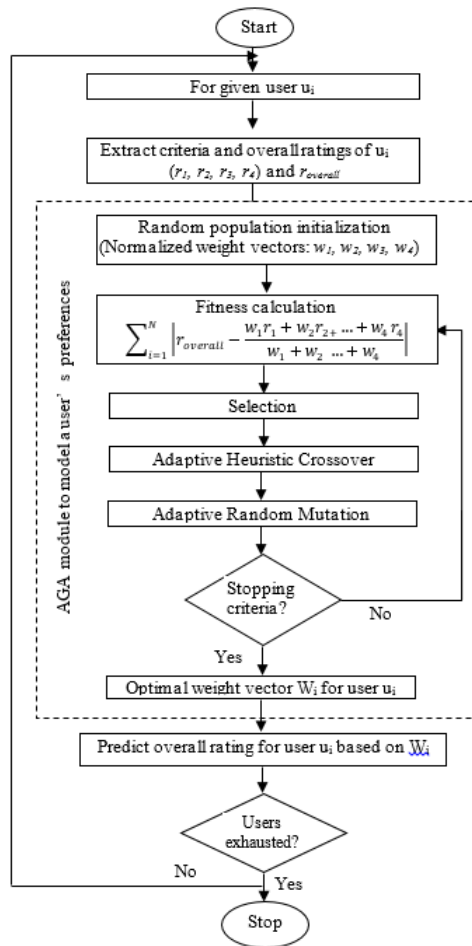


Figure 2. The architecture of AGA based multi-criteria recommender system

EXPERIMENTAL DESIGN AND RESULTS

There are two objectives of this experimental evaluation- i) to compare the performance of a single criterion traditional Item-based Collaborative Filtering RS with a GA based multi-criteria RS. ii) To compare the performance of the AGA against the simple GA in the domain of multi-criteria RS. All the genetic algorithms used for the experimentation in this paper have been implemented on Windows 7 platform using R studio. We have used 'recommenderlab' R package for making collaborative filtering based recommendations. To evaluate the performance of the proposed system, a fraction of randomly selected ratings given by a user have been used for building the model and the rest of the ratings have been used for the test purpose.

The Dataset

We have taken data on Yahoo Movies from Jannach, Karakaya and Gedikli (2012) in ready to use form who extracted it from the website (<http://movies.yahoo.com>). In this dataset, each movie has 5 ratings, i.e., 4 criteria ratings (acting, direction, story and visual effects) and 1 overall rating. The dataset contains 976 movies from 6078 users. Each rating has a value in the range 1 to 5. We have considered ratings by the users who have rated more than 10 movies and those movies which have been rated at least by 10 users. This way the rating data comes from overall 50 users.

Recommendation Algorithms

To compare and evaluate the proposed RS, we have used 5 variations of algorithms i) Traditional Item-based Collaborative Filtering (TICF) which finds out similarity between the items rated by different users, based on the similarity it chooses a neighbor set for the current user and then it presents recommendation. ii) Genetic algorithm based CF (GA_CF), which applies a GA to find out optimal weights for the criteria and then based on these weights, it calculates the overall ratings for making recommendations. iii) Mean_CF algorithm which simply takes the mean of the ratings for the four criteria as the overall rating. iv) Adapt_CF which uses an adaptive version of the GA for optimizing weights. This algorithm computes the probabilities of crossover and mutation (p_c and p_m) for every new generation adaptively, however the probabilities remain constant over a generation. v) Adaptive_CF which computes the probabilities of GA operators (P_c and P_m) for each individual separately as defined in section 4. This adaptive version of GA automatically adjusts these probabilities according to the fitness of the individuals participating in the reproduction process of the GA.

Evaluation Metrics

We have used four metrics to compare the performance of these 5 algorithms, i.e. Mean Absolute Error (MAE), Precision, Recall and F1 measure. The performance metrics are defined below.

$$MAE = \frac{1}{N} \sum_{i=1}^N |r_{overall} - r'_{overall}|$$

$$precision = \frac{\text{correctly recommended movies}}{\text{total movies recommended}}$$

$$recall = \frac{\text{correctly recommended movies}}{\text{total no of relevant items}}$$

$$F1 = \frac{2 * precision * recall}{precision + recall}$$

Where N is the number of movies rated by the i^{th} user, $r_{overall}$ is overall rating predicted by the RS under consideration and $r'_{overall}$ is the actual overall rating given by the user to that movie.

Determining the Parameters for the Simple GA

As described earlier, the parameter setting is very important in the performance of a GA, especially the values of p_c and p_m influence the success of a GA to reach the optimal solution. We have attempted to find out an optimal parameter setting for our simple GA implementations by trying different combinations of these two values. From our experiments, we found out that GA gives maximum fitness value for the precision, recall and F-measure at $p_m=0.01$ and $p_c=0.7-0.8$ which can be observed from the line charts shown in Figure 3-5. According to these observations, we have chosen the crossover and mutation probabilities for GA_CF algorithm (simple GA) only whereas these probabilities are dynamically adjusted for the latter two versions of the AGA based recommendation algorithms (Adapt_CF and Adaptive_CF) as described in sub-section 3.4. Each chromosome in the GA population represents the weights given to four criteria by an individual user. The population size has been tuned experimentally and a population size of 50 chromosomes was found to be sufficient. The experimental parameters are summarized in Table 1.

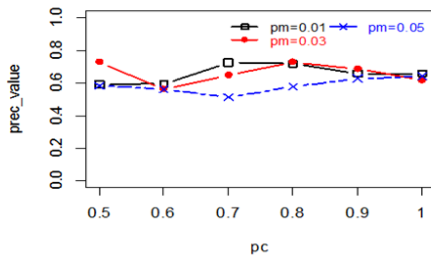


Figure 3. Precision values for different crossover and mutation rates

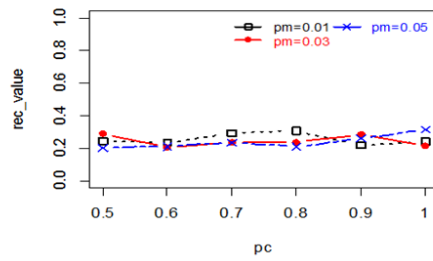


Figure 4. Recall values for different crossover and mutation rates

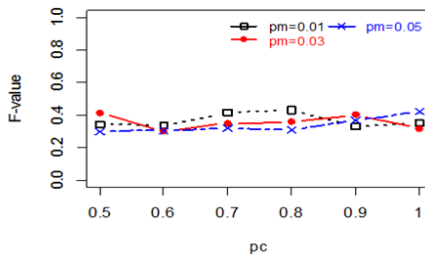


Figure 5

F-values for different crossover and mutation rates

Table 1

Parameter setting for GA

Parameter	Value
Chromosome Length	number of criteria ratings =4 (acting, direction, story and visuals in case of Yahoo movie data set)
Population Size	50
Crossover probability for simple GA, p_c (GA_CF)	0.75
Crossover probability, p_c (Adapt_CF and Adaptive CF)	Dynamical adjusted (described in section 3.4)
Mutation probability, p_m (GA_CF)	0.01
Mutation probability, p_m (Adapt_CF and Adaptive CF)	Dynamically adjusted (described in section 3.4)
Stopping Criteria	Stall generations

RESULTS AND DISCUSSION

Experiments were conducted on Yahoo movie dataset on 50 users using Item-based Collaborative Filtering method. We had evaluated the performance on four evaluation metrics, i.e., MAE, precision, Recall and F-measure for all the 5 algorithms used in this

research. Each experiment was repeated 20 times and then average values of the evaluation metrics were recorded. The results are presented in the Table 2. For graphic illustration, these results are also portrayed in the form of bar charts given in Figures 6-9.

Table 2

Evaluation metrics

Algorithm	Error rates	Precision	Recall	F-measure
TICF	2.70645	0.4596	0.11143	0.17938
Mean_CF	1.133275	0.2968	0.17351	0.21902
GA_CF	1.01702	0.5904	0.24200	0.34289
Adapt_CF	0.697769	0.7586	0.22299	0.34467
Adaptive_CF	0.458239	0.8358	0.31325	0.45706

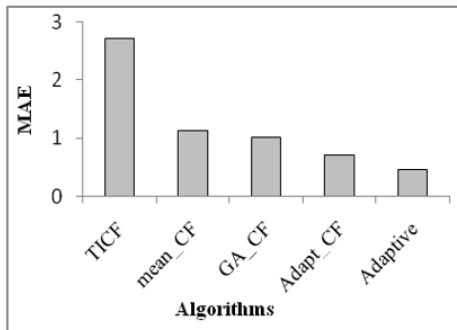


Figure 6. Comparison of error values

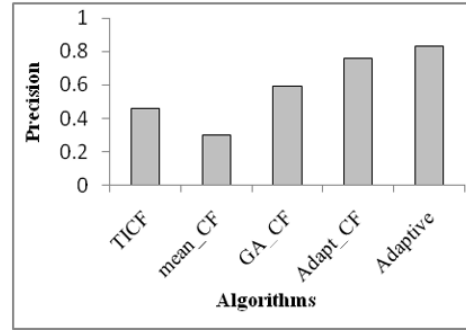


Figure 7. Comparison of precision values

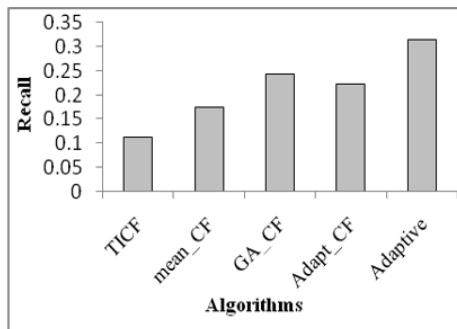


Figure 8. Comparison of recall values

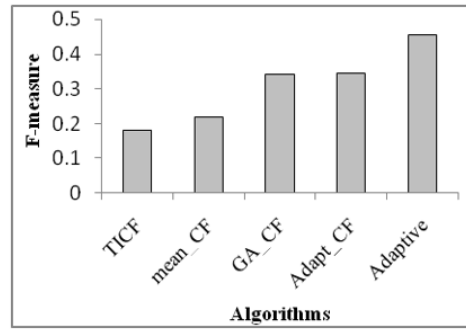


Figure 9. Comparison of F-measure values

On the whole, the results happen to support our claim that the GA based multi-criteria RS should give better performance than the single criteria traditional TICF and adaptive GA based multi-criteria RS must be a better choice than the simple GA based multi-criteria RS for optimizing weights for multiple criteria ratings.

To further validate if the proposed AGA-based multi-criteria RS is statistically significantly better than the other algorithms, we have applied the Wilcoxon signed rank test on error rates obtained by the 5 algorithms at a significance level of 5 percent ($\alpha=0.05$). The error rates were recorded over 20 samples (Table 4 in Appendix I). The results of Wilcoxon signed rank test (p-values) are presented in Table 3.

Table 3

The results of Wilcoxon Signed Rank test on error rates

	TICF	GA_CF	Mean_CF	Adapt_CF	Adaptive_CF
TICF	-	-	-	-	-
GA_CF	0.000195	-	-	-	-
Mean_CF	0.000381	0.647000	-	-	-
Adapt_CF	0.000195	0.165000	0.029000	-	-
Adptive_CF	0.001953	0.001209	0.000580	0.01208	-

The null hypothesis that there is no difference between the performances of the two pairs of algorithms is rejected if the p-value at the cross-section of these algorithms in the table is less than the significance level ($\alpha=0.05$). The results of Wilcoxon Signed Rank test authenticate the following:

The performance of each multi-criteria based algorithm is significantly better than the traditional item-based collaborative filtering based recommender system. Hence, multi-criteria ratings should be taken into account for recommending items.

The performance of the Adapt_CF is significantly better than the simple Mean_CF. Hence, taking mean of multi-criteria ratings is not a good choice for making recommendations.

The performance of Adaptive_CF is significantly better than all the other algorithms. Hence, it can be asserted that the adaptive GA, which adjusts the crossover and mutation rates for every individual separately in the GA population, is a better choice for optimizing the weights for the multi-criteria user ratings.

CONCLUSION

In this paper, we have proposed a novel Adaptive Genetic Algorithm (AGA) approach for the optimization of feature weights of the multi-criteria ratings. Subsequently, these weights are used in recommending movies using item-based CF. The experimental results show that additional information gathered from the various criteria's is useful in enhancing the performance of a RS. The experimental results confirm that the proposed AGA based RS outperforms the traditional item based collaborative filtering and the simple GA based

RS. In future, parallel and hybrid GAs can be applied for optimizing weights of the multi-criteria ratings for the recommendation process.

REFERENCES

- Adomavicius, G., & Tuzhilin, A. (2005). Toward the next generation of recommender systems: a survey of the state-of-the-art and possible extensions. *IEEE Transactions on Knowledge and Data Engineering*, 17(6), 734–749.
- Adomavicius, G., & Kwon, Y. (2007). New recommendation techniques for multi-criteria rating. *IEEE Intelligent Systems*, 22(3), 48-55.
- Adomavicius, G., & Kwon, Y. (2007). Multi-criteria Recommender Systems. In F. Ricci, L. Rokach & B. Shapira (Eds.), *Recommender systems handbook* (pp. 847-880). MA: Springer.
- Adomavicius, G., Manouselis, N., & Kwon, Y. (2011). Multi-Criteria Recommender Systems. In F. Ricci, L. Rokach, B. Shapira, & P. B. Kantor (Eds.), *Recommender Systems Handbook* (pp. 769–803). MA: Springer.
- Bobadilla, J., Ortega, F., Hernando, A., & Alcalá, J. (2011). Improving collaborative filtering recommender system results and performance using genetic algorithms. *Knowledge-Based Systems*, 24(8), 1310–1316.
- Burke, R. (2002). Hybrid Recommender Systems: Survey and Experiments. *Journal of Convergence Information Technology*, 12(4), 331–370.
- Fong, S., Ho, Y., & Hang, Y. (2008, September). Using Genetic Algorithm for Hybrid Modes of Collaborative Filtering in Online Recommenders. In *8th International Conference on Hybrid Intelligent Systems (HIS)* (pp. 174–179). Barcelona, Spain.
- Fuchs, M., & Zanker, M. (2012). Multi-criteria Ratings for Recommender Systems: An Empirical Analysis in the Tourism Domain. In C. Huemer & P. Lops (Eds.), *E-Commerce and Web Technologies* (Vol. 123, pp. 100–111). Heidelberg: Springer.
- Geng, B., Li, L., Jiao, L., Gong, M., Cai, Q., & Wu, Y. (2015). NNIA-RS: A multi-objective optimization based recommender system. *Physica A: Statistical Mechanics and its Applications*, 424, 383–397.
- Goldberg, D. E. (1989). *Genetic Algorithms in search, optimization and machine learning*. Boston: Addison-Wesley Longman Publishing Co., Inc.
- Hassan, M., & Hamada, M. (2016, January). Recommending learning peers for collaborative learning through social network sites. In *7th International Conference on Intelligent Systems, Modeling and Simulations (ISMS)* (pp. 60-63). Bangkok, Thailand.
- Hassan, M., & Hamada, M. (2017, September). Improving prediction accuracy of multi-criteria recommender systems using adaptive genetic algorithms. In *Proceedings of Intelligent Systems Conference* (pp. 326-330). London, UK.
- Hwang, C., & Hwang, C. (2010). Genetic algorithms for feature weighting in multi-criteria recommender systems. *Journal of Convergence Information Technology*, 5(8), 126–136.
- Jannach, D., Karakaya, Z., & Gedikli, F. (2012, June). Accuracy improvements for multi-criteria recommender systems. In *Proceedings of the 13th ACM Conference on Electronic Commerce: ACM* (pp. 674–689). New York, NY, USA.

- Lakiotaki, K., Tsafarakis, S., & Matsatsinis, N. (2008, October). UTA-rec: a recommender system based on multiple criteria analysis. In *Proceedings of the 2008 ACM Conference on Recommender Systems: ACM* (pp. 219–226). New York, NY, USA.
- Li, Q., Wang, C., & Geng, G. (2008, April). Improving personalized services in mobile commerce by a novel multicriteria rating approach. In *Proceedings of the 17th International Conference on World Wide Web: ACM* (pp. 1235–1236). New York, NY, USA.
- Manouselis, N., & Costopoulou, C. (2007). Analysis and classification of multi-criteria recommender systems. *World Wide Web*, 10(4), 415–441.
- Michalewicz, Z. (1996). *Genetic Algorithms + Data Structures = Evolution Programs*. Heidelberg: Springer.
- Parveen, R., Kant, V., Dwivedi, P., & Jaiswal, A. K. (2015, December). Enhancing recommendation quality of a multi criterion recommender system using genetic algorithm. In *International Conference on Mining Intelligence and Knowledge Exploration* (pp. 526–535). Hyderabad, India.
- Pellerin, E., Pigeon, L., & Delisle, S. (2004, April). Self-adaptive parameters in genetic algorithms. In *Proceedings of Data Mining and Knowledge Discovery: Theory, Tools and Technology* (Vol. 5433, pp. 53–64). Orlando, USA.
- Ribeiro, M. T., Lacerda, A., Veloso, A., & Ziviani, N. (2012, September). Pareto-efficient Hybridization for Multi-objective Recommender Systems. In *Proceedings of the 6th ACM Conference on Recommender Systems: ACM* (pp. 19–26). New York, NY, USA.
- Ribeiro, M. T., Ziviani, N., Moura, E. S. D., Hata, I., Lacerda, A., & Veloso, A. (2014). Multiobjective Pareto-Efficient Approaches for Recommender Systems. *ACM Transactions on Intelligent System and Technology*, 5(4), 53:1–53:20.
- Ricci, F., Rokach, L., Shapira, B., & Kantor, P. B. (Eds.). (2011). *Recommender Systems Handbook*. MA: Springer.
- Rodriguez, M., Posse, C., & Zhang, E. (2012, September). Multiple Objective Optimization in Recommender Systems. In *Proceedings of the 6th ACM Conference on Recommender Systems: ACM* (pp. 11–18). New York, NY, USA.
- Salehi, M., Pourzaferani, M., & Razavi, S. A. (2013). Hybrid attribute-based recommender system for learning material using genetic algorithm and a multidimensional information model. *Egyptian Informatics Journal*, 14(1), 67–78.
- Sanchez-Vilas, F., Ismoilov, J., Lousame, F. P., Sanchez, E., & Lama, M. (2011, August). Applying Multicriteria Algorithms to Restaurant Recommendation. In *Proceedings of the 2011 IEEE/WIC/ACM International Conferences on Web Intelligence and Intelligent Agent Technology: IEEE Computer Society* (Vol. 01, pp. 87–91). Washington, DC, USA.
- Sohrabi, B., Mahmoudian, P., & Raeesi, I. (2011). A framework for improving e-commerce websites usability using a hybrid genetic algorithm and neural network system. *Neural Computing and Applications*, 21(5), 1017–1029.

- Srinivas, M., & Patnaik, L. M. (1994). Adaptive probabilities of crossover and mutation in genetic algorithms. *IEEE Transactions on Systems, Man, and Cybernetics*, 24(4), 656–667.
- Teng, W. G., & Lee, H. H. (2007). Collaborative recommendation with multi-criteria ratings. *Journal of Computers*, 17(4), 69-78.
- Zarrinkalam, F., & Kahani, M. (2012, October). A multi-criteria hybrid citation recommendation system based on linked data. In *2012 2nd International eConference on Computer and Knowledge Engineering: ICCKE* (pp. 283–288). Ferdowsi University of Mashhad, Mashhad, Iran.

APPENDIX

Table 4

Error values of the twenty samples on the five algorithms

	TICF	Mean_CF	GA_CF	Adapt_CF	Adaptive_CF
Sample1	2.252210	0.30358791	0.9441119	0.8656271	0.4191331
Sample2	2.080407	2.311775	0.6546858	1.638706	0.8639765
Sample 3	2.454835	0.034196329	1.400590	1.009136	0.039842894
Sample 4	1.840278	1.125000	0.3163882	0.9796618	0.5076028
Sample 5	3.025597	1.596193	2.204970	0.16569957	0.9105495
Sample 6	3.274992	1.469172	0.9571358	0.4018334	0.25714517
Sample 7	2.264099	1.404465	0.6124009	1.028368	0.18682236
Sample 8	1.852795	0.7500	0.4429009	0.978819	0.2759654
Sample 9	4.562475	1.584251	0.24309682	0.20558747	0.4631856
Sample 10	3.451920	1.490113	1.776992	0.5789364	0.6911059
Sample11	1.826062	1.00000	0.4000063	0.22063870	0.27242824
Sample12	1.031181	0.7482874	0.7577126	0.6602477	0.7451005
Sample13	4.009927	1.667480	1.318044	0.7366487	0.5083829
Sample14	2.770606	1.609785	0.5218467	0.7403089	0.5770359
Sample15	1.133881	0.125000	1.685471	0.4490401	0.061920783
Sample16	2.539588	0.3132505	1.215395	0.5467240	0.6818667
Sample17	3.522435	1.615295	2.667531	0.4646946	0.3153118
Sample18	3.164317	0.50000	0.8873312	0.8245014	0.7348388
Sample19	3.996181	0.6969514	0.7485456	0.72782	0.3554881
Sample20	3.075476	2.320742	0.5853438	0.7324	0.2970926
Average	2.70645	1.133275	1.01702	0.697769	0.458239



Customizable Smart Food Cabinet and Refrigerator

Chandra Manuel, Janitra Avila, Lukas Budiman, Rico Wijaya and Rinda Hedwig*

Computer Engineering Department, Faculty of Engineering, Bina Nusantara University, 9 K.H. Syahdan, Jakarta 11480, Indonesia

ABSTRACT

This smart appliances project is intended to create home appliances which are able to interconnect one another and share data to provide a convenient and comfortable environment to users. For this project, we successfully developed a smart food cabinet with the abilities to perform several things such as giving information about the items stored within the smart food cabinet to its users via a mobile application. By using the information, the users contact the store to order the items needed. The food cabinet takes the data from the smart cabinet about the items and combines them to its own data to give information about recipe selection according to the availability of the items in both smart food cabinet and refrigerator. The system is built based on Arduino and Raspberry Pi, and the results show that the recipes displayed in the LCD are according to the availability of the items. The information can be accessed via an Android-based application in a smartphone.

Keywords: Data sharing, smart appliances, smart cabinet, smart home, smart refrigerator

INTRODUCTION

In 2016, the Computer Engineering Department of Bina Nusantara University and Research Interest Group of Photonics and Computer Systems were assigned to develop a smart home appliances project. Two or more of the appliances should be able to interconnect

to one another for data sharing and give valuable information to users which finally can support the users to live healthier, more comfortable, and feel secure with his/her home environment, especially for disability or elderly (Skubic et al., 2009). Figure 1 shows the research roadmap for this research, and the first project has already been accomplished by developing a smart refrigerator which has the ability to inform

ARTICLE INFO

Article history:

Received: 28 February 2018

Accepted: 10 July 2018

Published: 24 January 2019

E-mail addresses:

chandra.maknuel@yahoo.com (Chandra Manuel)

janitraavila@gmail.com (Janitra Avila)

me@lukasnetwork.com (Lukas Budiman)

rico.wijaya@binus.edu (Rico Wijaya)

rinda@binus.edu (Rinda Hedwig)

* Corresponding author

its items stored therein, to order items needed via mobile application, and to display some recipes according to available items (Pratama et al., 2018). Therefore, we carry on the project by developing a smart food cabinet with similar abilities, but it can take data from the smart refrigerator to combine the data and to give better recipes selection to the users according to the availability of the items in both stored appliances.

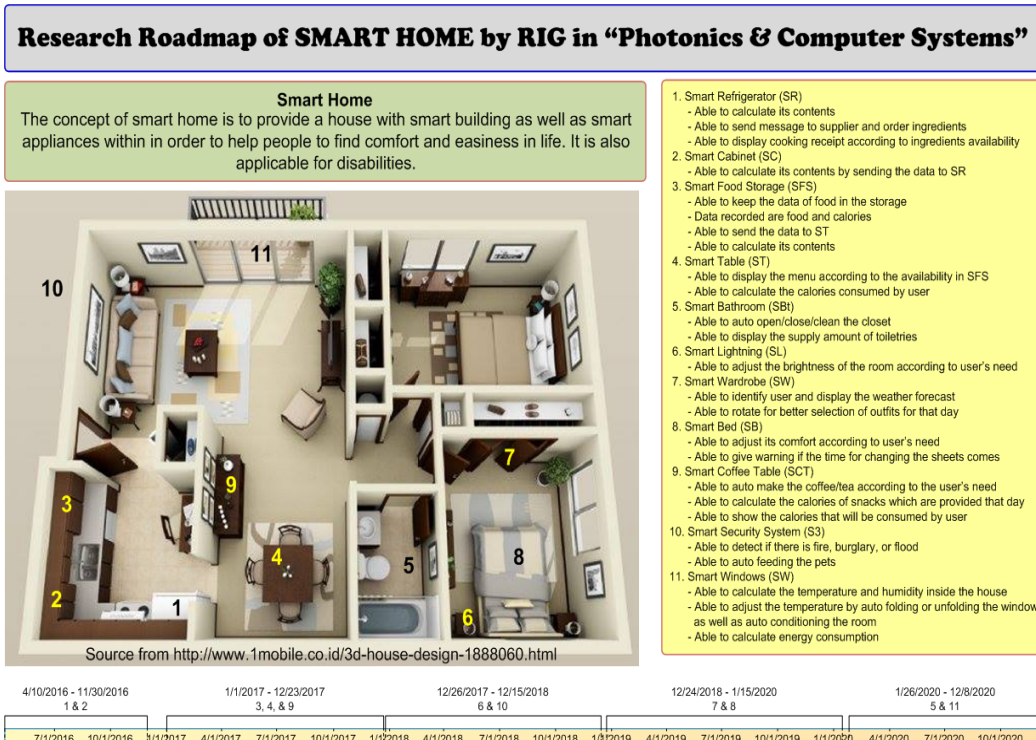


Figure 1. Research roadmap of “Smart Home”

The concept of smart cabinet we study, is basically for smart medicine cabinet (Wan, 1999; McLaughlin, 1973; Balasingam, 2011; Lanka, 2008; Jiang & Xu, 2014; Rejoyce et al., 2016; Calabretto et al., 2001) in which one of them was built with online system through the Internet (Wan, 2003), and some were equipped with antenna arrays which were used for real-time inventory monitoring (Boryssenko & Boryssenko, 2011). The other model of smart cabinet was for storing food in the kitchen by using camera for monitoring the inside of the cabinet (Logan, 2006). Besides the cabinet, a smart tray with a tag system was also developed in order to help user in arranging items inside the cabinet (Vaselloff, 2006; Handfield, 2006). The smart kitchen cabinet which had been developed, had its limitation in which the RFID connection inside the cabinet was not all stable and the accuracy of the load cell needed further improvement for better sensitivity (Amutha et al., 2012).

The smart food cabinet we develop in this paper is based on the previous experiment by Higgins et al. (2014 & 2017) but with several modifications. One of its modification is that it can take data of items stored within the smart refrigerator and combine the data, and display cooking recipes according to the items stored in both the smart food cabinet and the refrigerator. Moreover, the information about items' availability can be accessed via a smartphone by the user or the user and by having the information, the user can order the items from the stores through the mobile application. However, the information about calories and expired date have not been included in this design. In the next project, we plan to develop a smart table which is equipped with the information about calories which can be transferred to the smart table from the smart food cabinet.

The main purpose of this research is to build smart modules that can be customized according to user's needs and installed in the current refrigerator or then the users' food cabinet. Therefore, in the first design, the user determines the items stored both in the food cabinet and the refrigerator as needed. The smart modules can be customized easily and placed in the food cabinet and the refrigerator so that function of the refrigerator is better than the regular ones.

METHODS

Experimental Setup

The diagram block of the system is drawn in Figure 2. The system used load cell (Muller et al., 2010) as the weight sensor to determine the weight of each items. The items stored in the cabinet were sugar, potatoes, onions, salt, pepper, turmeric, cooking oil, and flour while the items stored in the refrigerator were eggs, carton milk, carrots, and tomatoes. The sensors used in the refrigerator were ultrasonic (Sigfusson et al., 2004) sensors, and switches which were placed in the compartment according to its items stored. Actually, the module could be customized according to the user's needs. The number of compartments or shelves installed or used as the saver could be added or reduced from the specific design and the purposes also could be changed according to users. The specification in this research is the minimum requirements.

In this paper, we focus more on the smart food cabinet since the smart refrigerator is discussed in different paper. As seen in Figure 2, the loadcell data is sent and processed in Arduino and the result is sent directly to Raspberry Pi to be combined with the data from the smart refrigerator. The combined data is processed into information about the availability and the weight measured for each item. The information can be seen via both Android based smart phone and LCD. The users can order the items from the stores by sending short messages (SMS) or WhatsApp (WA) application. Instead of information of the available items, the smart food cabinet shows the recipes according to the combined available items from both smart refrigerator can be accessed only from LCD temporarily.

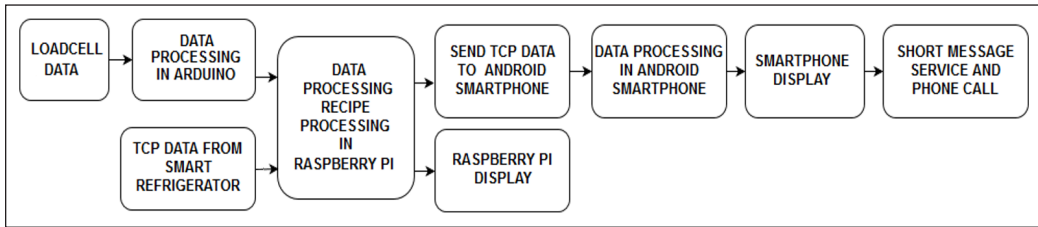


Figure 2. Diagram block of the system

The topology used in this experiment is not using public internet protocol (IP) as we can see in Figure 3. The interconnection is among a smart refrigerator, a smart food cabinet, and an Android based smartphone while the local interconnection is between a smart refrigerator and a smart food cabinet. Inside the Wi-Fi router, there is also a VPN interconnection to the internet server which functions as an alternate connection between the one with and without public IP. The smartphone receives and transmits the data from the server as an intermediate.

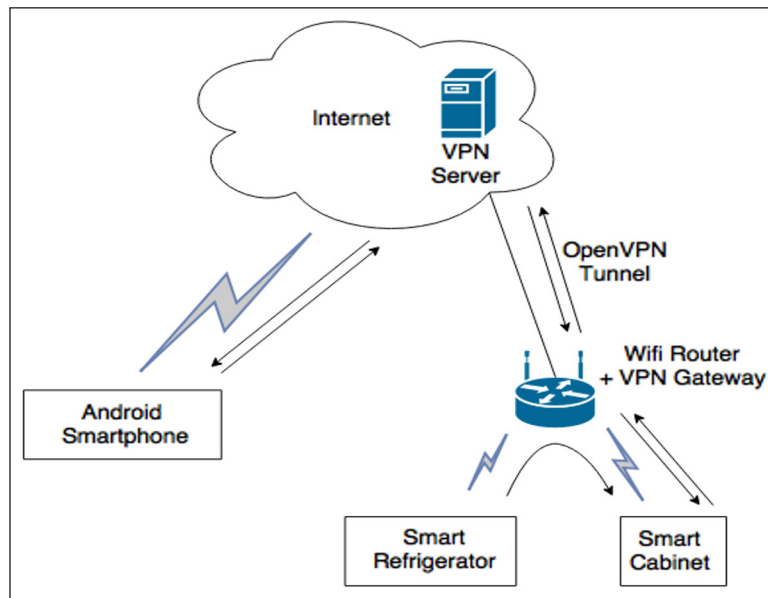


Figure 3. The topology that is used without public IP accessed

Figure 4 shows the flowchart of the whole system. In the beginning, the program initializes all necessary variables then it continues by running three threads; the transmission control protocol (TCP) thread, the serial communication, and the recipe database. The program finishes whenever an exit button is pressed.

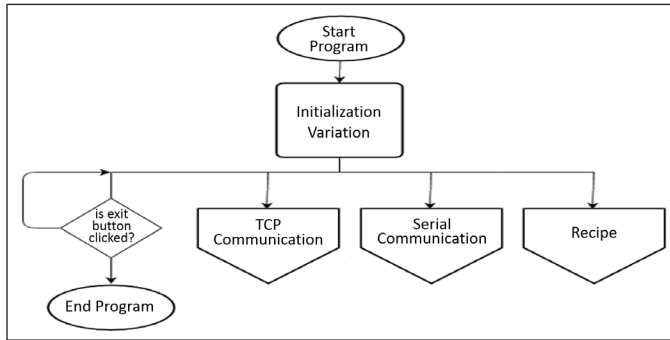


Figure 4. Main flowchart diagram

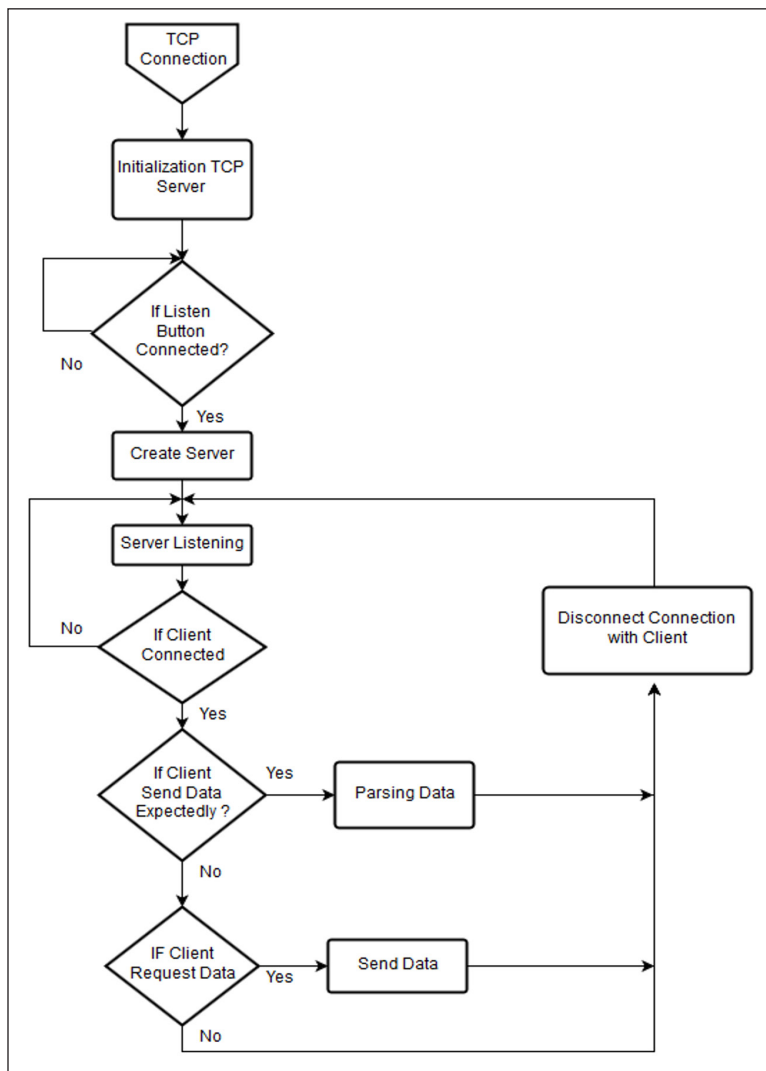


Figure 5. TCP communication flowchart

It can be seen in Figure 5 that TCP communication thread is initializing the listen push button and when it is pushed, it creates a server and waits until all clients send the data. If the data are on the right format, they are transferred to the variables otherwise they are removed. The information of the items' availability is sent to the clients whenever there is a request. This process is a looping process and it always checks the client from time to time.

In serial communication thread, shown in Figure 6, the first step is deleting all data in the internal serial port of Raspberry Pi then this action is followed by checking the refresh port button until it is pushed to refresh the serial port inside the combo box. The crucial

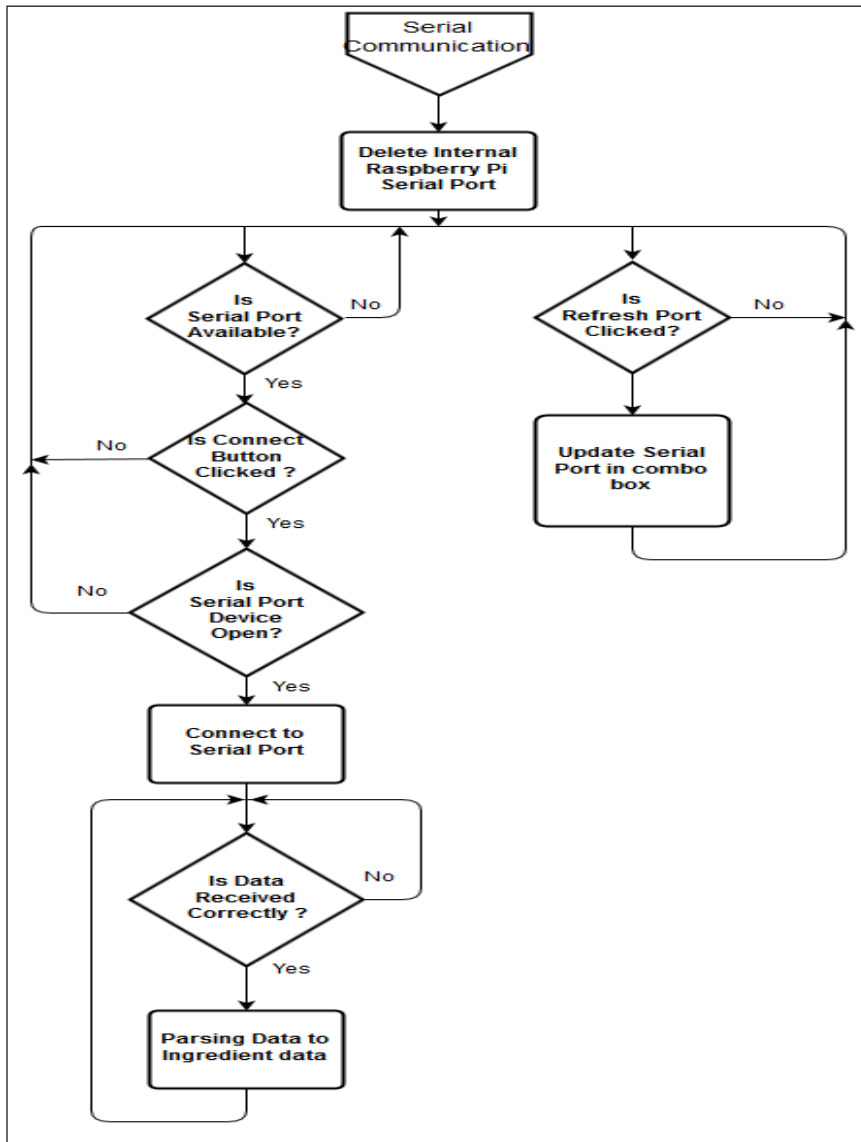


Figure 6. Serial communication flowchart

process is checking the format of the data which later on is compared with the acceptable format. These data are used for providing the correct recipes according to the availability of the items in both smart refrigerator and smart food cabinet.

The detailed flowchart of how recipes can be selected and displayed in the LCD according to the available items in both smart refrigerator and food cabinet can be seen in Figure 7. In this thread, the program initializes variables used in recipe database and separates them in the form of table which can be accessed via graphic user interface (GUI). The selection includes “save”, “add”, and “refresh”. Each selection does the process according to its name where “save” for saving the recipe in the database, “add” for adding the recipe in the table and after ‘add’, it should be followed with “save” for saving it in the database. “Refresh” is for refreshing the display. The additional “edit” and “delete” selections are also used for editing and deleting the recipes.

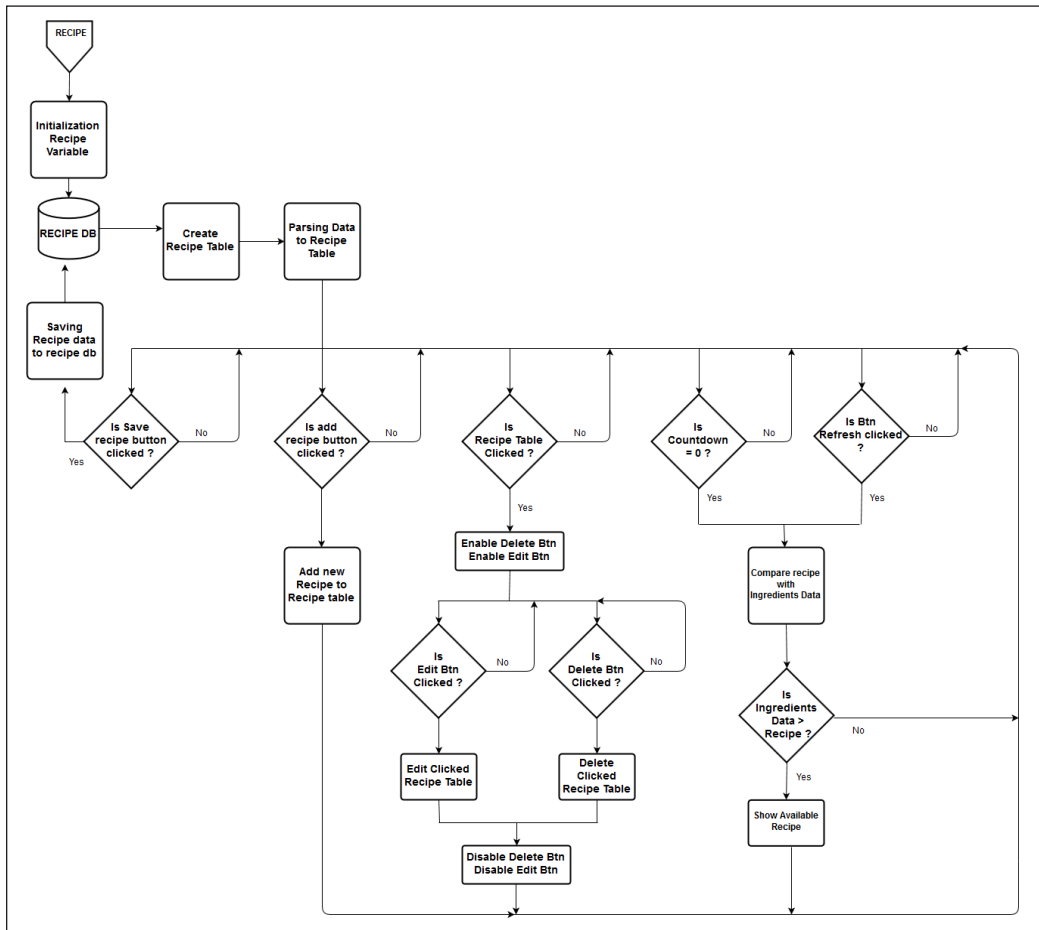


Figure 7. Flowchart of database of recipe

Figure 8 shows the flowchart of Android application for the smart food cabinet. This flowchart shows that initialization of the program is by refreshing all variables. Android sends the request to IP to detect both local network and the Internet. The data sent via IP is displayed in the smartphone and LCD as shown in e Figure 9. Users can see the items availability both in the smart refrigerator and food cabinet from the smartphone and can select the media for sending messages to the desired store for ordering the items. Users can use SMS, WA, or direct call via phone the store for ordering the items. While in LCD, users can see the recipe selection and items availability at the same time. However, the process of ordering items should be via a smartphone and should not be from the LCD. It can be seen in Figure 9, the first column shows the selected recipes according to the availability of the items. The recipe is seen in the second and third column while the last one shows the availability of the items.

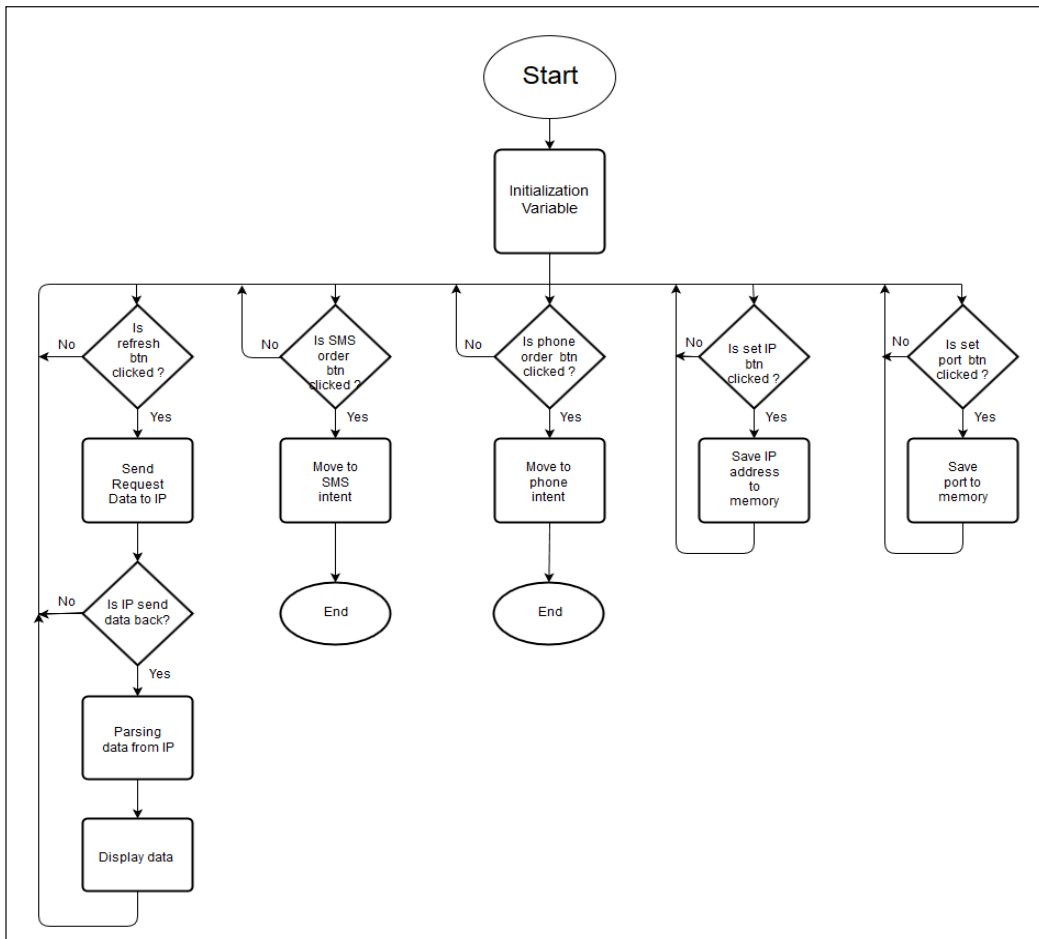


Figure 8. Flowchart of Android application in the smartphone



Figure 9. LCD displayed the recipe according to the availability items either in smart refrigerator or smart food cabinet

Figure 10 shows three different menus in the Android applications; (a) the availability of the items, and (b) the selection for order either with SMS or phone call even by WA. The whole system can be seen in Figure 11 and this system is registered for a simple patent.

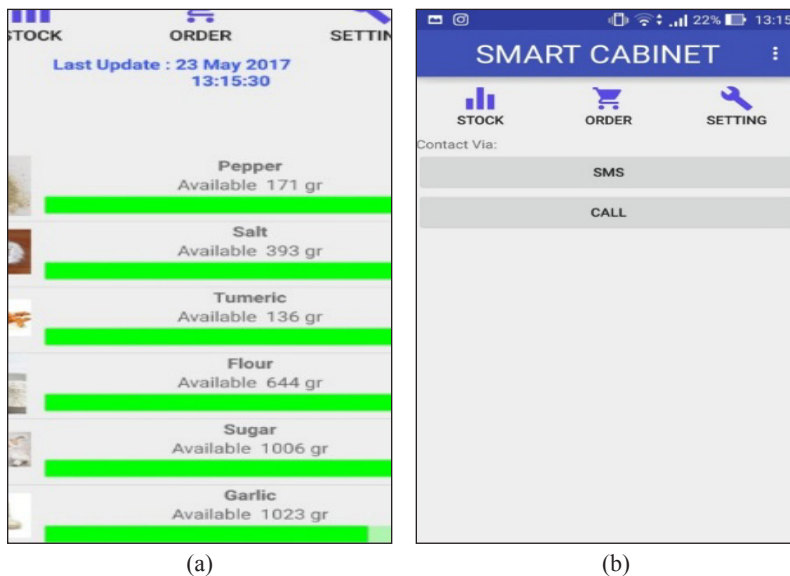


Figure 10. Android application displayed in the smartphone: (a) availability of items, and (b) selection for order

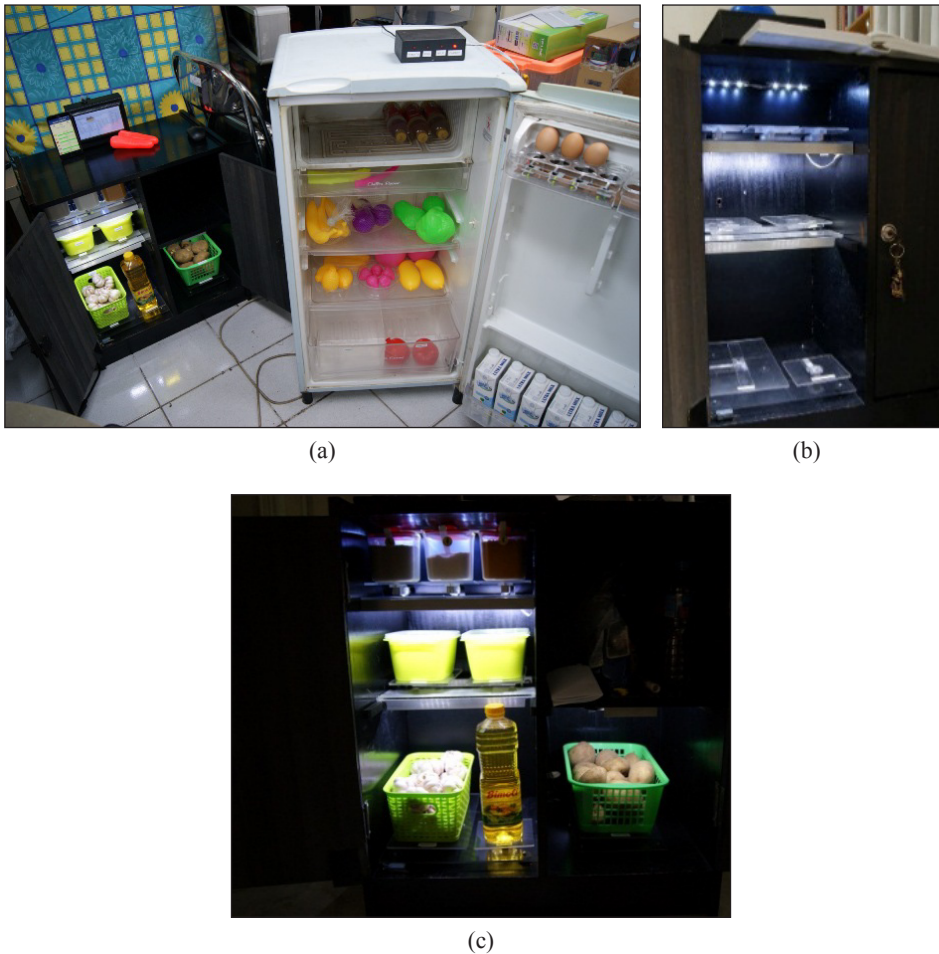
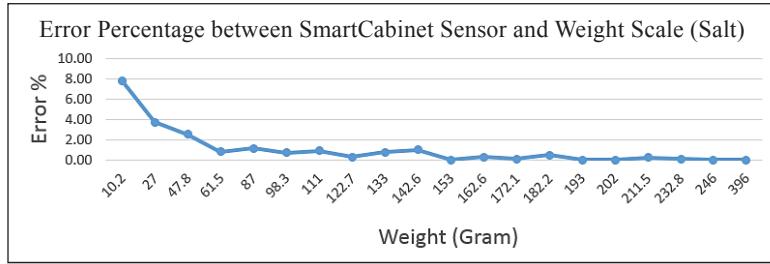


Figure 11. (a) The smart food cabinet and smart refrigerator, (b) smart food cabinet and its loadcell, and (c) smart food cabinet with its compartments on the loadcell

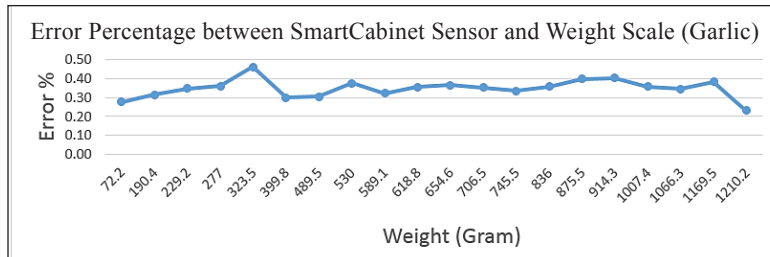
RESULTS AND DISCUSSION

After designing the system, we tested the accuracy of information given by loadcell and compared to the accuracy measured by using a calibrated digital weight (JCS-3A; resolution 0.1 gram; capacity 3 kg). The information was tested for its accuracy when it was displayed both in the LCD and the smartphone. The last one, we measured its accuracy of the recipes displayed according to the availability of the items.

On the first experiment when we compared the accuracy reading from the loadcell and from the digital weight, we found out there were several error readings which was not significant, as low as 7.84% to 0.28% as shown in Figure 12. The error depended on the sensitivity of the loadcell, especially when we used two kinds of loadcell. To measure salt, pepper, and turmeric, we used 1 kg loadcell since users normally did not keep a large number



(a)

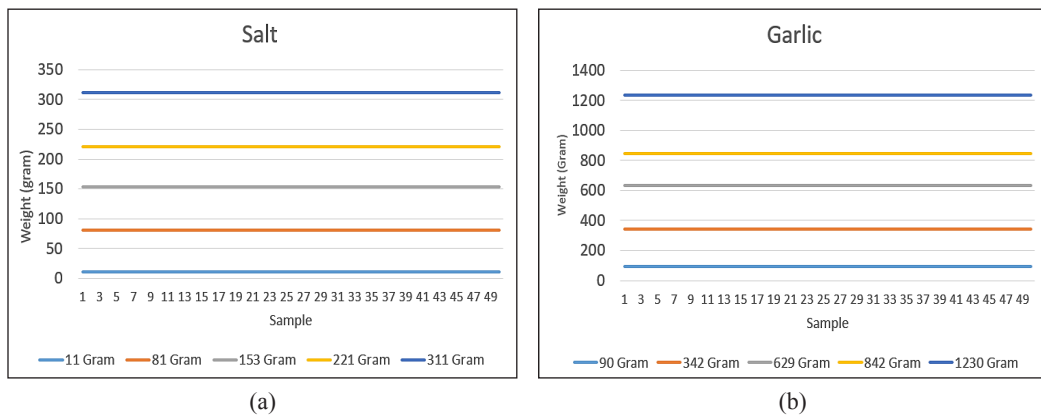


(b)

Figure 12. Error reading for: (a) loadcell with capacity of 1kg and (b) loadcell with capacity of 5 kg

of these ingredients. On the other hand, we used loadcell of 5 kg since users tended to save big sum of sugar, potatoes, onions, cooking oil, and flour. The sensitivity of readings was determined by the type of loadcell. Nevertheless, the consistency of measurement results is good as it is shown in Figure 13. In this paper, we only provide the measurement results of salt and garlic as representative data since the rest of measurement is almost similar.

From the measurement results, we sent the data directly to both a smartphone and an LCD and we measured the time respond of data transfer. Figure 14 shows the results of this measurement where the average response time is 237 ms or as similar as real time measurement.



(a)

(b)

Figure 13. Reproducibility testing of weight reading by loadcell for: (a) salt, and (b) garlic

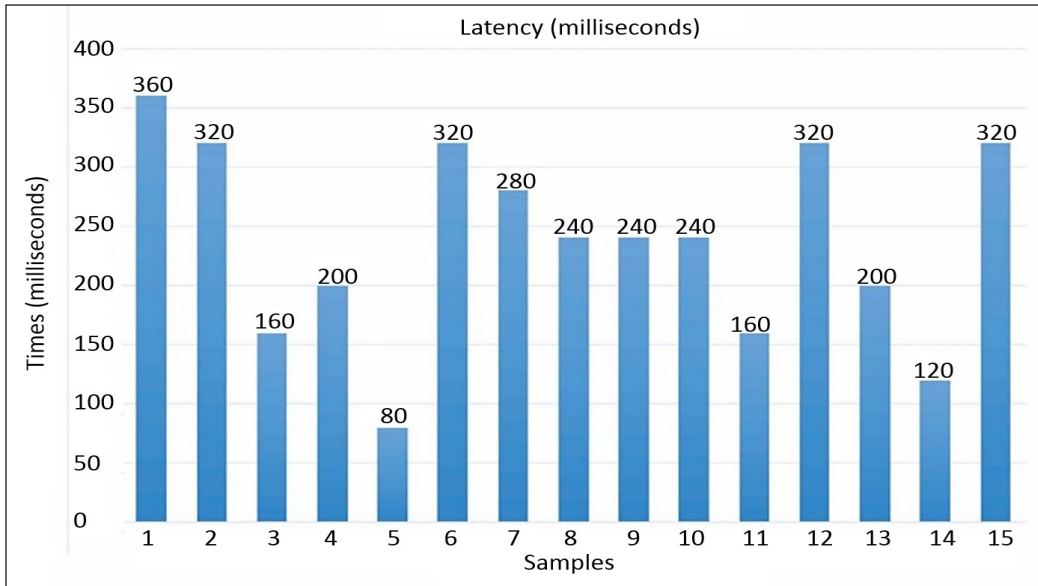


Figure 14. The latency of data transmission

Figure 15 shows some examples of recipe displayed according to the availability of the items. The items seen next to the LCD means that they are not in the sensor that is why they are read as ‘not available’ and the smartphone shows the availability of the items. In Figure 15(a) the recipes selection are garlic, prime ribs and oven-roasted asparagus where both of these recipes do not need eggs, milk, and cooking oil. Figure 15(b) shows the recipe selection of fried egg, omelet with milk, fried calamari, plain stir-fried kangkong leaves, curry tikka masala sauce, scones, potato soup, fluffy pancakes, garlic prime ribs, sweet potatoes casserole, mashed potatoes, oven-roasted asparagus, and French toast that did not need carrots as ingredients.

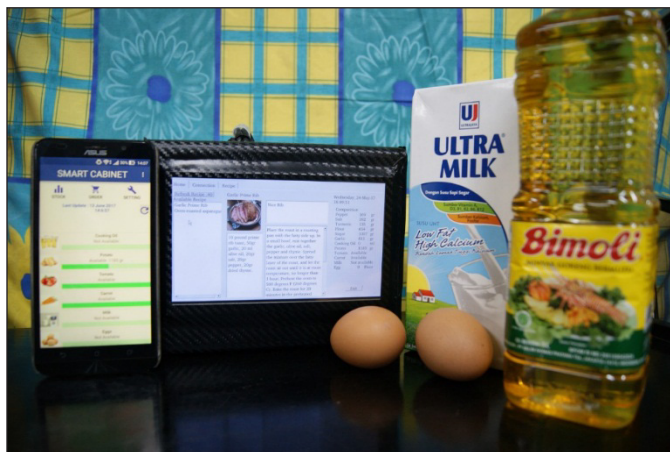


Figure 15(a). The recipe selection when eggs, milk, and cooking oil were not available



Figure 15(b). The recipe selection when and carrots were not available

As for the price comparison, the whole smart modules in both refrigerator and food cabinet consumed less than US\$ 300 while in the commercial smart refrigerator ranged from US\$ 3500 to US\$ 5800 (NBCNEWS.com, 2013; Eadicicco, 2016; The Australian, 2018). The ability was almost similar but is not widely affordable for people in the development country like Indonesia.

CONCLUSION

Designing and building a smart food cabinet system that can receive data from smart refrigerator in this work has been successfully done. The data read from each sensor are successfully transmitted to the embedded system based on Arduino and Raspberry Pi in a real-time transmission. The information of the availability of items both in smart food cabinet and smart refrigerator can be accessed from either LCD or smartphone which also lead the selection of desired recipe according to the availability of items.

The smart module in this project can be customized by the user by using the current cabinet and refrigerator s/he has without any necessity to buy the new ones. In the future, the system will be combined with a smart table for calories information to make the users have additional benefit from this project. Moreover, the price of each smart modules are less than US\$300 and it is a lot cheaper than the one available in the market.

ACKNOWLEDGEMENT

This work was partially supported by Research Grant from Ministry of Research Technology and Higher Education of Republic of Indonesia under contract number 0422/K3/KM/2017 on May 24, 2017 between KOPERTIS III and Bina Nusantara University.

REFERENCES

- Amutha, K. P., Sethukkarasi, C., & Pitchiah, R. (2012). Smart Kitchen Cabinet for Aware Home. In *SMART 2012, The First International Conference on Smart Systems, Devices and Technologies* (pp. 9-14). Stuttgart, Germany.
- Balasingam, A. V. (2011, August 4). *Patent No. US 20110187549 A1*. USA.
- Boryszenko, A., & Boryszenko, E. (2011). Antenna array design for HF RFID smart cabinet. In *IEEE International Conference on Microwaves, Communications, Antennas and Electronic Systems (COMCAS 2011)* (pp. 1-3). Tel Aviv, Israel.
- Calabretto, J.P., Warren, J. Darzanos, K., & Fry, B. (2001). Enhancing Communication between Patients and Community Pharmacists with an Internet Medicine Cabinet. In L. S. J. Smith (Ed.), *HIC 2001: Ninth National Health Informatics Conference* (pp. 188-194). Brunswick East: Health Informatics Society of Australia.
- Eadicicco, L. (2016, May 4). Behold Samsung's New \$5,800 Smart Refrigerator. *TIME*. Retrieved April 30, 2018, from <http://time.com/4318290/samsungs-smart-refrigerator-family-hub/>
- Handfield, M. L. (2006, July 25). *Patent No. US 7080755 B2*. USA.
- Higgins, K. T. (2014, August 14). *Patent No. US 20140229343 A1*. USA.
- Higgins, K. T. (2017, July 20). *Patent No. US 20170205274 A1*. USA.
- Jiang, Q., & Xu, J. (2014). Design of Smart Medicine Cabinet Based on STM32F107 and Network. *Applied Mechanics and Materials*, 719-720, 567-572.
- Lanka, P. G. (2008, November 20). *Patent No. US 20080283542 A1*. USA.
- Logan, J. (2006, October 26). *Patent No. US 20060237427 A1*. USA.
- McLaughlin, J. (1973, Oct 2). *Patent No. US 3762601 A*. USA.
- Muller, I., de Brito, R. M., Pereira, C. E., & Brusamarello, V. (2010). Load cells in force sensing analysis -- theory and a novel application. *IEEE Instrumentation and Measurement Magazine*, 13(1), 15-19.
- NBCNEWS.com. (2013, April 1). LG Smart Fridge Spots Spoiled Food, Order Groceries. *NBCNEWS.com*. Retrieved April 30, 2018, from http://www.nbcnews.com/id/50364798/ns/technology_and_science-tech_and_gadgets/t/lg-smart-fridge-spots-spoiled-food-orders-groceries/
- Pratama, T. L., Akbar, I. R., Hartanto, W., & Hedwig, R. (2018). Smart Refrigerator that Guides User to Provide Recipe in Accordance to Items Availability. *Internetworking Indonesia Journal*, 10(1), 23-28.
- Rejoyce, G., Oni, O., Oshin, O., Idachaba, F., & Nkordeh, N. (2016, July). Development and Implementation of a Smart Medical Cabinet using RFID Technology in Developing Countries. In *World Congress on Engineering* (pp. 1-4). London, U.K.
- Sigfusson, H., Ziegler, G. R., & Coupland, J. N. (2004). Ultrasonic monitoring of food freezing. *Journal of Food Engineering*, 62(3), 263-269.
- Skubic, M., Alexander, G., Popescu, M., Rantz, M., & Keller, J. (2009). A smart home application to eldercare: Current status and lessons learned. *Technology and Health Care*, 17(3), 183-201.

The Australian. (2018, January 16). *Samsung's smart fridge keeps track of your food stocks*. Retrieved April 30, 2018, from <https://www.theaustralian.com.au/life/personal-technology/samsungs-smart-fridge-keeps-track-of-your-food-stocks/news-story/ecd0463d9578dc5a1eabac4813067541>

Vaseloff, D. V. (2006, November 7). *Patent No. US 7132926 B2*. USA.

Wan, D. (1999). Magic Medicine Cabinet: A Situated Portal for Consumer Healthcare. In H. W. Gellersen (Ed.), *Handheld and Ubiquitous Computing* (Vol. 1707, pp. 352-355). Heidelberg: Springer-Verlag.

Wan, D. G. (2003, March 25). *Patent No. US 6539281 B2*. USA.



SQL-Injection Vulnerabilities Resolving using *Valid* Security Tool in Cloud

Niharika Singh^{1*} and Ashutosh Kumar Singh²

¹Department of Computer Engineering, National Institute of Technology Kurukshetra, Haryana, 136118 India

²Department of Computer Applications, National Institute of Technology Kurukshetra, Haryana, 136118 India

ABSTRACT

The cloud is storing a huge amount of the data, including personal and confidential details. It involves the third party over the internet and proposes many unreliable strings which can be proven as loopholes. Thus, securing the data in the cloud tends to be a major point of concern. SQL Injection Attacks (SQLIAs) are being acknowledged as one of the foremost web applications security threats. It initiates a vulnerable query to destroy the connected server systems and help attackers with unauthorized access to the databases resulting in identity theft and security violations. The paper proposes a hybrid solution whose information utility is higher than the solutions that are being proposed earlier. As the methodology is concerned over static, dynamic and runtime detection and prevention mechanism. It also classifies the malicious queries and inspires the system to be well prepared for the secure working environment by implementing a demonstration design. Through the experimental implementation, the query associativity makes success probability of 0.775 using the associativity formula that in fraction, results in a durable comparative solution proposed till date.

Keywords: Cloud security, malicious nodes, SQL injection attack

INTRODUCTION

During the last decade, cloud computing and big data have appeared as two emerging technologies. These technologies have become one of the fieriest topics of recent times in the IT industry that made large steps in a relatively very short period of time. The methodology groundwork of cloud computing includes virtualizations and Service Oriented Architecture (SOA) of hardware and software. One mainstream of

ARTICLE INFO

Article history:

Received: 30 September 2017

Accepted: 28 August 2018

Published: 24 January 2019

E-mail addresses:

niharika.academics@gmail.com (Niharika Singh)

ashutosh@nitkkr.ac.in (Ashutosh Kumar Singh)

* Corresponding author

resource sharing promotes various cloud assistances (such as software cloud, application cloud, infrastructure cloud, business cloud, storage cloud). These offer various services for different domains (Casassa-Mont, et al., 2015). Involving the third party over the internet proposes many unreliable strings as loopholes (Swanson & Stinson, 2015). The cloud is storing a huge amount of data including personal and confidential details. Thus, securing the data in the cloud tends to be a major concern. On applying and detecting suitable methods for providing the privacy check to the insecure uncertainties itself is a major challenge of the cloud computing (Plischkea et al., 2013).

Web servers which provide customer services are usually connected to highly-sensitive information contained backend databases. Sometimes, these backend databases are vulnerable to the harmful attacks, such as SQL Injection Attacks (SQLIAs). SQLIA are one of the foremost security threats to web services and applications (Eyal, Birman, & van Renesse, 2015). It initiates a vulnerable query to destroy the connected server systems and gives attackers unauthorized access to databases. It provides right to delete, modify and retrieve valuable and confidential information stored in databases. This results in identity theft and security violations (Dharam & Shiva, 2013). SQLIAs come in the picture when the data provided by the external users are directly included in SQL query but are not properly validated. According to a study, it was stated that 75% of the cyber-attacks are outperformed at the application layer. Also, over the audited websites where 97% of them are clearly targeted (Eyal et al., 2015; Narayanan et al., 2011; Plischkea et al., 2013). Thus, for the SQLIAs an inadequate input validation has been identified as one of the major causes within a web application. For the first level of defense against SQLIAs, these input validations can serve satisfactorily, but it may not be much defence against injecting SQL queries attack techniques.

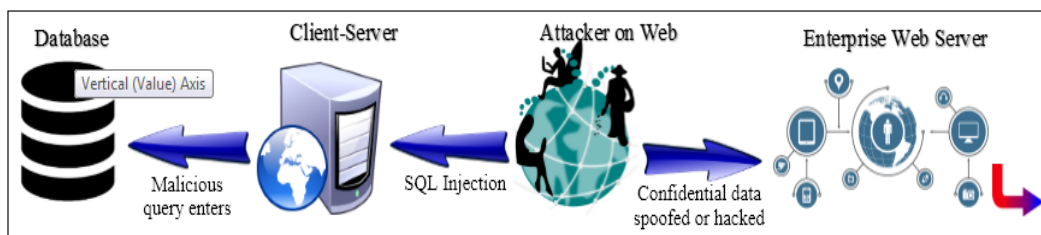


Figure 1. Representation of how attacker initiates SQL Injection Attack

A variety of tools are introduced as a solution for SQLIAs keyword based filtering, machine learning and decision trees. These solutions for the firewalls and Intrusion Detection Systems (IDSs) are ineffective against SQLIAs because some ports are open in firewalls for the regular web traffic at the application level that are used to perform SQLIAs. Thus, if attackers get breakthrough (Kiani et al., 2008) as shown in Figure 1 and find loopholes to attack, it will result in damaging the firewall and IDS.

The paper considers the SQL injection attack, which is its own kind of code injection attack. Though, the SQLIA is very common, there must be some privacy measures to protect our databases from SQL Injection Attacks. Day by day, our databases are getting modular, so is the Injection attacks, but proportionally. Thus, SQLIA is a considerable concern in the real world. Hence, research on this problem bears significant practical importance. In concern, we have developed the detection and prevention method that tries to achieve the high Information Utility Rate (IUR) using the query associativity and tautology logics. Where, 'A tautology is a statement that is always *True* regardless of the truth values of the individual statements'. This is considered as the base idea for the proposed approach and is processed with "query associativity". The methodology is dogged over static, dynamic and runtime detection and prevention mechanism. This also filters out the malicious queries and inspires the system to be well prepared for the secure working environment (Ping et al., 2016; Halfond & Orso, 2005; Narayanan et al., 2011).

Related Work

Today, for web applications SQL injection attacks are counted among the top-most threats. These attacks are launched through the specially crafted user inputs over web applications which uses low-level string operations in order to construct SQL queries. A research study can be outperformed on the basis of the work previously done in the subsequent manner.

A model-based tool AMNESIA was proposed by Halfond and colleague (2005) to detect illegal queries (before the execution on the database). This includes detection on both static as well as dynamic injected query attacks. In the static part, to automatically build a model of legitimate queries the technique uses program analysis. On the other hand, dynamic part runtime monitoring is used to inspect the dynamically generated queries (Narayanan et al., 2011; Halfond & Orso, 2005). Bandhakavi, Bisht, Madhusudan, & Venkatakrisnan (2007) introduced another model CANDID that detects SQL injection to dynamically mine programmer-intended query structure on any input and compare it against the structure of actual query issued. The approach is based upon inferring intended queries considering symbolic query computed on a program run. A new detecting method was proposed based on single character to detect parsing and black list based attacks which are experimentally defined by using both attacks and normal samples (Sonoda, Matsuda, Koizumi, & Hirasawa, 2011) in different types of SQLIAs that are extensively reviewed till date. It analyzes various recently developed defensive mechanisms also shows how each technique might help in preventing and detecting all SQLIA types. It introduces PSIAQOP (Preventing SQL Injection Attacks based on Query Optimization Process) depending on heuristic rules to prevent all SQLIAs types (Al-Khashab, Al-Anzi, & Salman, 2011). In order to overcome the weakness a detection method is proposed that uses machine learning and probabilistic study. It gives the formula to calculate parameter of the zeta distribution.

The model proposes an SQL injection attack detection methodology using the proposed formula (Oosawa & Matsuda, 2014).

Some other well-known interrelated web application vulnerabilities of SQL attacks are Cross-Site Scripting (XSS) and Cross-Site Request Forgery (CSRF). By getting inspired to detect such vulnerable queries a method was proposed which detects and recognize SQL injection that are based on defined and identified criteria. The model is able to generate report regarding the vulnerability level and decrement in possibility of SQL injection attack onto the web application (Buja et al., 2014). To detect dynamic injected queries a new approach was suggested that detect and prevents SQL injection attacks on checking whether user inputs cause changes in query intended results. Attacker if uses space, single quotes or double dashes in input the proposed method detects and tokenizes the query and a query with injection separately. When tokens are formed, it stores onto an array representing every token as an element of an array. Two arrays are resulted from both queries (original and injected) then the length is compared to detect if it is injected or not. Further the access is granted or denied on the basis of comparison (Ntagwabira & Kang, 2010). Ping et al., (2016) proposed a method of preventing SQL injection attacks by ISR (Instruction Set Randomization), and built a prototype system based on this strategy. The prototype system randomizes the SQL keywords in the application, because the SQL statement injected by the attacker is not randomized, so the SQL injection can be easily detected. Also, the experimental results show that this system has a good effect on preventing SQL injection and low running cost. Similarly, Yassin et al. (2017) proposed the detection solution for Software as a Service (SaaS) providers. To achieve SQL query/HTTP request mapping, they planned an event-correlation based on the similarity between literals in SQL queries and parameters in HTTP requests. Many researchers worked in the field, but still an appropriate satisfactory solution was not found which could be announced as best to defeat the SQL injection attacks including (Yassin et al., 2017; Uwagbole et al., 2017). Hence, the comparison summary of work done in SQLIA solution techniques is shown in Table 1.

Problem Statement

The main objective of the research is connected to Table-1 where, we focus to get better information utility rate. It is said that ‘the higher the Information Utility Rate, the higher will be the Privacy’ but, this decreases the data accessibility. This limitation of higher IUR leads to examine models to get a “balance between Data accessibility, Data Privacy and Data Utility”. Hence, our objective is based upon getting a Moderate/High information utility than the other research solutions. Thus, the results lead to achieve an IUR percentage range that would lie between 80-90% that is considered to be a balanced range in all technical aspects. In association, we proposed a hybrid solution working to get high information utility than the other research solutions. The solution works over Prevention and Detection

Table 1
Summarized View of State-of-art work done in SQLIA solution techniques

<i>Information utility</i>	<i>Privacy access</i>	<i>Approach</i>	<i>Advantage</i>	<i>Disadvantage</i>	<i>Complexity</i>
High	Pattern matching based privacy using authenticated data structures	Policy-oriented over low privacy strength	Reduction in communication overhead providing ease during the implementation and computations.	Lacks in diversity.	Low
Low	Prevention through parsing and triggering queries for privacy policy with defined data accessibility level	Query optimization over strong privacy strengths	Providing a record-level SQLIAs protection to prevent eves-dropping across multiple data environment.	Comparison results are less satisfactory.	High
Moderate	Filtered and linkable data privacy with specific data accessibility	Linkable policy with limited information access using Heuristic rules and output filtering	Provides required malicious and benign URLs for three phases of testing, validating, and training. Addresses issues of policy anomalies mechanisms, also reduces overhead computation.	Vulnerable to unauthorized access as only detection method is introduced	High

to improve firewall security. The other researchers encountered various solutions to get approximate results for a secure SQLIA free environment. Early experiments have a success score range of 50-70% (Plischkea et al., 2013; Eyal et al., 2015; Narayanan et al., 2011). The proposed logics were categorized into as either detection method or prevention methods but the combinations were hardly proposed. Hence, to achieve 100% success rate solution for SQLIA security is quite difficult. A few researchers have tried to achieve a satisfying success rate, but is not much convincing due to the quality attributes (Dharam et al., 2013). Hence, a model is required that would result with 80-90% success rate range of security bar. Also, a solution that would come up with all proximities and could be analyzed in proposed methodology. Thus, we strictly compare the work with Casassa-Mont et al., (2015) and Ntagwabira & Kang (2010) improving the loopholes using tautology logics. Therefore, the experimental results are reasonable enough to validate all those claims that are suggested through the proposed work.

Proposed Solution

Client-Side Attacking Shot. The introduced approach is a three-tier (Client-Logic Access- Data Server) runtime detection and prevention methodology. It deals with process organization, accessibility and exchange of queries. It ensures that the Data-Server tier would not execute any vulnerable code that affects the hosted operating systems and devices partially or completely. The technique works over the database server side being associated with a distributed cloud environment. It provides a security controlling system ensuring secure execution of all the requested queries without any database hacking or fabrication.

Procedure

Receive_Query Unveil_Message
(*T: Tier level number*)

Begin

Update *access_table* row T to increase *input_count*;

End

Procedure

Finish_Query (T: Tier level number)

Begin

Update *access_table* row T to increase *consumed_count*;

End

Procedure Upon_Idle

Begin

Report to *controller_server* non-zero difference for previously unreported *access_table* rows;

End

This algorithm for tier-architecture detects the completion of the query exchange process at n-tier level. As the queries $Q = \{q_1, q_2, q_3 \dots q_s\}$ $Q = \{q_1, q_2, q_3 \dots q_s\}$ go through a tier architecture representation for $T = \{t_1, t_2, t_3 \dots t_n\}$. For the proposed scenario, it works over up to $n=3$ levels. The architecture is dependent upon the three-tier architecture system which is divided as follows:

First tier (client tier) - This tier consists of applications that are accessed through a centralized system. Here, it is concerned over web browsers, servers or standalone application running on different machines that processes queries to request and response through the central server. If there are S servers that share a communication through Q queries, the ratio of detecting a breakthrough would be directly proportional to R number of activities where $R = \{r_1, r_2, r_3 \dots r_t\}$. Now, on the whole the query associativity would be:

$$Q_i = \sum_{i=1}^t (r_1 + r_2 + r_3 \dots r_t) \quad (1)$$

Here, the R outperforms s number of queries. Thus,

$$Q_i = (q_1, q_2, q_3 \dots q_s)_1 + (q_1, q_2, q_3 \dots q_s)_2 + \dots + (q_1, q_2, q_3 \dots q_s)_t \quad (2)$$

$$Q_i = t(q_1, q_2, q_3 \dots q_s) \quad (3)$$

$$Q_i = tQ \quad (4)$$

$$\text{For which if we have } i = 1, Q \cong t \quad (5)$$

The queries when are processed through distributed servers produce results into HTML web pages. The web pages are uniquely identified with their corresponding *url*. To find the associative probability it is further divided by 100 for the overall evaluation.

Second tier (logic access tier) – The layer concerns over the server codes that may include platform or software applications. These codes process and set up communicational behavior among local and remote system servers outperforming over network languages. Thus, the layer is responsible for the following measures: authentication, authorization, caching, exception management, validation. These measures effectively logs and audit the progressive Q queries.

Third tier (data server tier) – This layer embraces all the database objects that might be used by applications (such as schemas, views, tables and stored procedures). It considers database services over distinct servers. Data server tier stores SQL server object definitions of available instant-level objects stored in database. The layer tools can be listed as: Application Developer, Database Administrator, Independent Software Vendor, IT Administrator, etc. supporting the operations: *Extract, Deploy, Register, Unregister, Upgrade* that helps in *Export_Import* of the request–response queries.

The 3-Tier architecture provides a support to the “Valid security” scheme which helps reducing SQL vulnerability rate in websites over the client side.

Security Policy Framework. Malicious SQLIA can be introduced into vulnerable applications using different input mechanisms. To get rid of such exasperating threats to the database-driven applications “Valid Security” can be introduced. During the process, a conditional query statement is fixed over the firewall on the client side it results to be always *True*. It bounds the parameters to some defined SQL structure, thereafter, for the attacker it is not possible to inject additional SQL code.

It is a runtime monitoring and prevention strategy which is more complex than defensive coding schemes. For the tautology logic encapsulation Proxy Server is introduced between SQL Server and Web Server. Attacker attacks using the SQL query with randomized value to proxy server, received by the client. Then, it is accessed through “Valid security” that stores an activity-access table over the proxy server to de-randomize the query. Further, it sends the satisfactorily secure and filtered query to the server for the processing then downloads HTML page or the website content, see Figure 2.

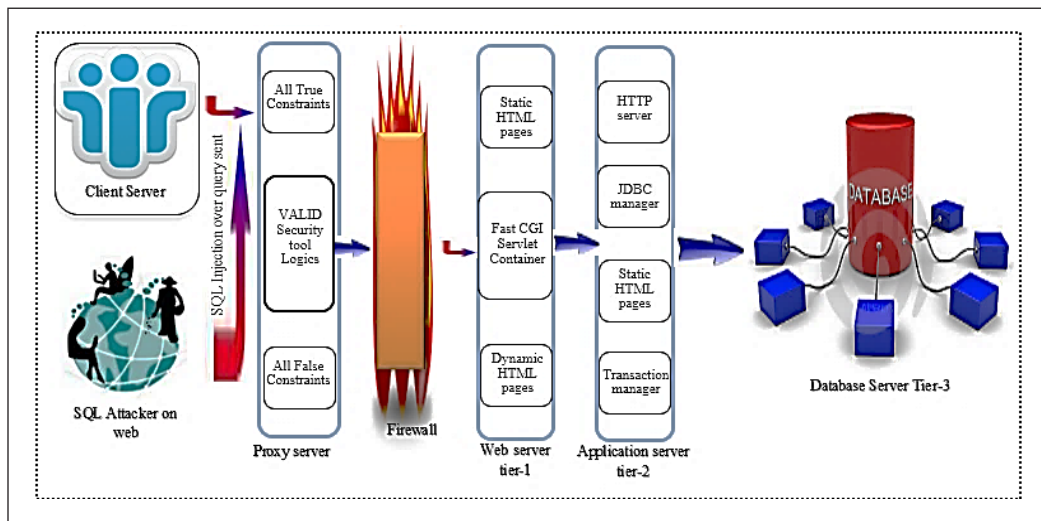


Figure 2. Working of proposed Valid Security Tool SQLIA solution

Take an example of spoofed SQL query that contains WHERE clause in it to consider the query processing as a tautology on the attacker’s end or universally. The two clause elimination procedures, say V_1 and V_2 which are recommended to be *Valid* and *Unsatisfiable* respectively, encounters with a vulnerable SQL query Q . Influentially both the procedures are equally effective. In conjunction, when Q processes through the proxy server, it passes through either V_1 or through V_2 that in results of give any false for V_1 and any single true for V_2 it would filter out the query and remove the vulnerability attached using some parameterized queries. There it is followed as *Valid* constraints are updated on the basis of the proposed machine learning whereas *Unsatisfiability* constraints are manually updated. On passing through it pairs up as if:

$$V_1(Q) \text{ and } V_2(Q) \supseteq V_3(Q) \quad (6)$$

For which we have queries to pass through the filter if V_3 is the all formula clause \forall , i.e.

$$V_1(Q) \subset V_2(Q) \subseteq \forall V_3(Q) \quad V_1(Q) \subset V_2(Q) \subseteq \forall V_3(Q) \quad (7)$$

But, here V_2 would be equally effective only if it satisfies twice over the V_1 reordering in concern to the propositional logic:

$$\neg\neg Q \equiv Q \quad (8)$$

Where, Q is the SQL query represented in propositional logic. Thus, on the basis it is easy to remove the vulnerable or malicious queries on the runtime that neutralizes SQL injection attacks. Here the dynamic part of it inspects dynamically generated queries and checks them using some predefined rules. For the mapping concern of the inputs and vulnerabilities machine learning methodology is introduced to generalize the dynamic generation of the queries. The system learns the query activities with the help of cookies C that get attached to the browser and stores activity in the Activity-Access table A (with i number of entries) put away over proxy server. For which it would be satisfiable:

$$C \in A_i \quad (9)$$

When it learns from the frequent access it starts filtering the dynamically injected queries as well and extracts the user inputs.

Progressive Algorithm

To understand the detailed concept of the solution, a step-to-step process is explained. To implement the methodology, one needs to go through the main process that initially calls to setup a PROXY_SERVER then after validation CLOUD_SERVER_HANDSHAKE is configured. It proceeds to install VALID_SECURITY_TOOL (proposed method installation over proxy). It includes an ACTIVITY_ACCESS_TABLE putting in place to record all true and all false activities for corresponding queries in Algorithm 1.

Algorithm-1: Query Access and Denial System for SQL injection attack.

Begin

Initialize $Q = \{q_1, q_2, q_3, \dots, q_s\}$

Install and Process VALID_SECURITY_TOOL()

Create ACTIVITY_ACCESS_TABLE()

Initialize matrix $arr[i][j]$ and Set $arr[0:i-1][0:j-1]$;

Apply STORE_CONSTRAINT (where, $i = \text{MANUALLY_STORE_CONSTRAINT}()$ and $j = \text{MACHINE_LEARNING_CONSTRAINT}()$)

If TRUE $\rightarrow Q_s(i,j)$ Const=1

```

Else FALSE  $\rightarrow$   $Q_s(i,j)$  Const=0.
Call query  $Q_s()$  and Break STORE_CONSTRAINT to generate INPUT_QUEUE(Q)
Match INPUT_QUEUE( $\leftrightarrow$ )STORE_CONSTRAINT()
If (Match= all TRUE), then (ACCESS_QUERY  $\rightarrow$ ALLOW)
Else if (Match= all FALSE), then
    Repeat for TRUE and Match= all TRUE;
    Set Access query  $\rightarrow$ ALLOW;
    Else (Access query  $\rightarrow$ DENY)
Store access results  $\rightarrow$ ACTIVITY_ACCESS_TABLE()
Report PROXY_SERVER() ABOUT UPDATE
Call THREE_TIER()
Process through CLIENT_TIER() and Calculate QUERY_ASSOCIATIVITY
Access  $P_i$  through LOGIC_ACCESS_TIER;
Store content over DATA_SERVER_TIER
Finish Query  $\rightarrow Q_s()$  and Set  $S=s+1$ 
Repeat for  $Q$ ;
End

```

RESULTS AND ANALYSIS

Implementation Environment

The proposed architecture demands a powerful and effective justification environment for which a technical platform has been performed. Performance section is divided into two phases depicting as setup phase and experimental phase giving a description over hardware and software components.

System Setup

Initiating over a supercomputer sometimes is a difficult task, but here an archetype is to be designed for execution of queries and transactions for carrying up over inter and intra-cloud. Thus, Table 2 shows system configuration scenario instigating technical attributes like RAM, OS, Hard-disk, etc. required for the implementation of the proposed algorithm.

Experimental Setup

To set up the cloud, there is a need to arrange a client-server picture. It can be configured as master-slave server maintenance using open source platform. In concern to our proposed scheme justification we are using a latest configured machine which may satisfy the data owner, needs for preserving the sensitiveness following the *Valid* Security Tool whose configuration is defined in Table 3. For the further proceeding and understanding Table 4 is designed with the detailed description for experimental technical configurations, including the cluster server worked over different ports.

Table 2
Technical details of implementation environment

Setup phase	Technical attributes	Configuration
<i>System setup (minimum requirements)</i>	RAM Capacity	8 GB
	Processor	Intel(R) Core(TM) i7 CPU Q 740 @ 1.73GHz 1.73GHz Turbo up to 1.93 GHz
	Operating system	Windows 7 ultimate
	Hard-disk	1 TB
	Graphic card (if required)	NVIDIA GeForce GT 425M-2GB

Table 3
Experimental technical configuration details of implementation setup phase

Setup phase	Technical attributes	Configuration
<i>Experimental Setup</i>	Query size	30
	Valid Constraints (dynamic)	15 initially
	Unsatisfiable Constraints (static)	15 initially
	Target number of Nodes	3
	Database	MySQL
	Platform	Open Jave Development Kit JVM
	Infrastructure	Open Source Server-Oriented

Table 4
Server oriented details

Setup phase	Source	Server type	Configuration
<i>Validation Setup</i>	Server-1 (Client)	Master Server	WAMP SERVER, Open Source Platform
		Apache Server	80 PORT
		MySQL Server	3306 PORT
		Proxy Server	8080 PORT
	Server-2 (Attacker)	Master Server	WAMP SERVER, Open Source Platform
		Apache Server	8081 and 8180 PORT
		MySQL Server	3309 PORT
	Server-3 (Cloud Node-1)	Slave Server	XAMPP SERVER-1, Open Source
		Apache Server	9090 and 443 PORT
	Server-4 (Cloud Node-2)	MySQL Server	3307 PORT
		Language	Python
		Slave Server	XAMPP SERVER-2, Open Source
Apache Server		8080 and 8181 PORT	
		MySQL Server	3308 PORT
		Language	Python

Evaluation Scenario

Here, in this section our scheme is analyzed on the basis of the experimental computation and performance. We are evaluating some thorough perceptible results to justify the formulation with examples. We first assess the computation and communication overhead, and further give the details about the data spoofing through SQLIAs.

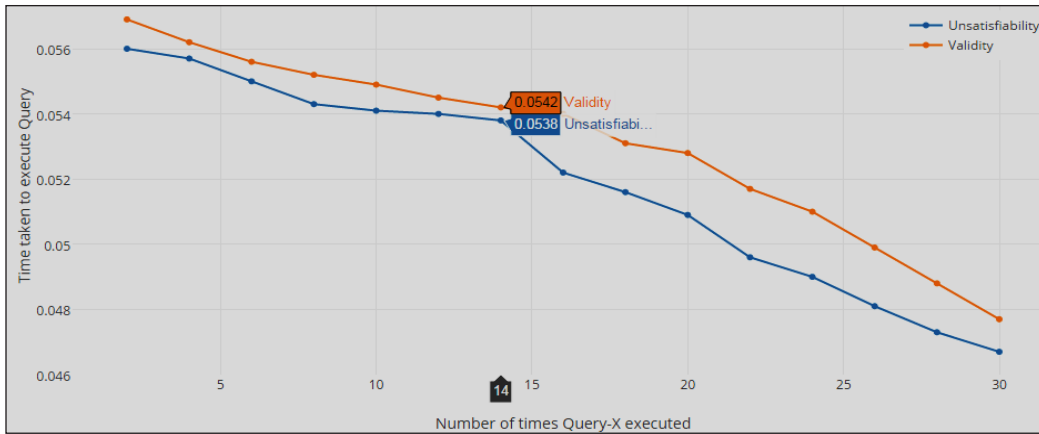


Figure 3. Minimum value calculated when *i* no Valid and Unsatisfiable query runs over

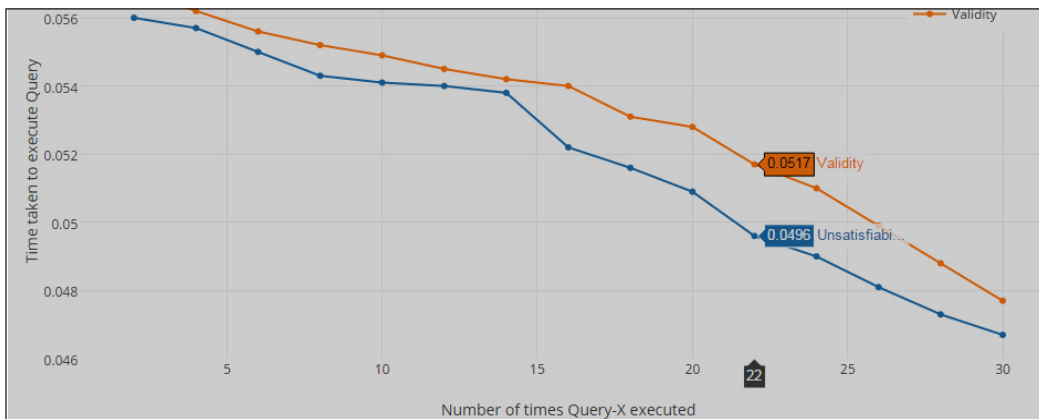


Figure 4. Maximum value calculated when *i* no. of Valid and Unsatisfiable query runs over

For the performance validation of the *Valid Security* tool set of thirty queries has been analyzed that includes original and injected queries. Taking two queries initially, i.e. $n=2$, including WHERE clause results in Figure 3 and Figure 4 that shows *Validity* and *Unsatisfiability* values. The Figures 3 and 4 show the minimum and maximum time

gaps, respectively, taken when run for about thirty (30) times, respectively. The lines are contracted somewhere with small gaps, but in some cases, it is wide which is all due to the learning process installed over ACCESS_ACTIVITY_TABLE.

On processing $n=30$ the results are shown in Figure 5. It depicts that it makes viable negotiated inferences during the time stamping, when these queries are analyzed in a queue. Minimum difference evaluated is measured to have 0.00003 seconds. In fraction, it is a very small difference when is outperformed on a single machine to get the utility. Calculating the query associativity makes success probability of 0.775 (from Equation 1-5) using the associativity formula. Here, we find the Information Utility Rate (IUR) in terms of probability and resulted in 0.775. This indicates the percentage of proposed approach in comparison to other proposed models to get 80-90% success rate range of security bar. This IUR rate is comparatively higher than references considered in related work. Also, to our competitive models i.e. Casassa-Mont et al., (2015) and Ntagwabira and Kang (2010). Where, Casassa-Mont and colleagues in 2015 attained 0.74 IUR and Ntagwabira and Kang (2010) achieved 0.65. We have considered one classic and one latest model for comparison. Figures 5 and 6 are comparative analysis in comparison to model proposed by Casassa et al., (2015), and Ntagwabira and Kang (2010). The work presented in these models are implemented in same platform. Thus, experimental results provide average negotiation comparison and query cycle satisfiability and un-satisfiability rate, see figure 5 and 6. In Figure 6, contracting lines are representing the smallest average by considering four different queries in each model. It has a very small difference of negotiation. A complete cycle includes the static and dynamic variability and the process that leads to filtration after the detection of injected SQL queries. Thus, this experimental setup justifies its work by producing a balance in-between.

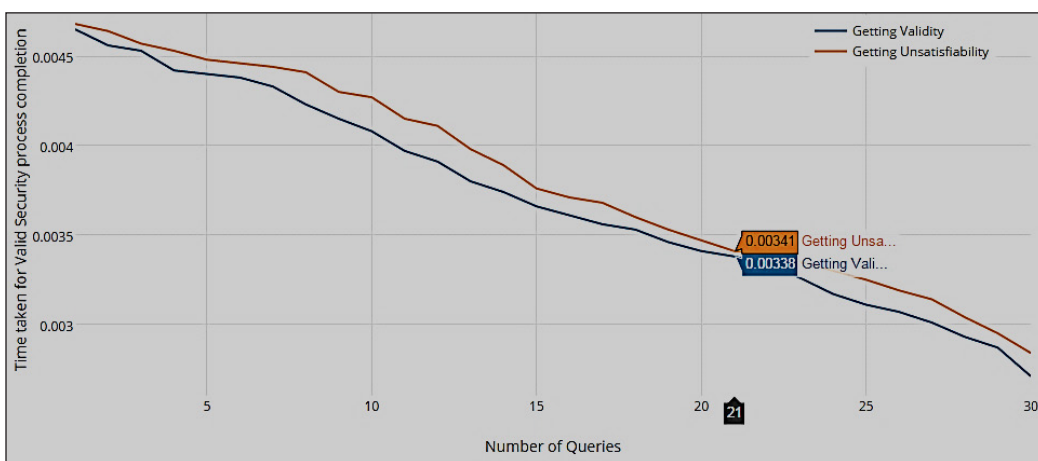


Figure 5. Representation of time taken to complete the cycle by $n=30$ queries

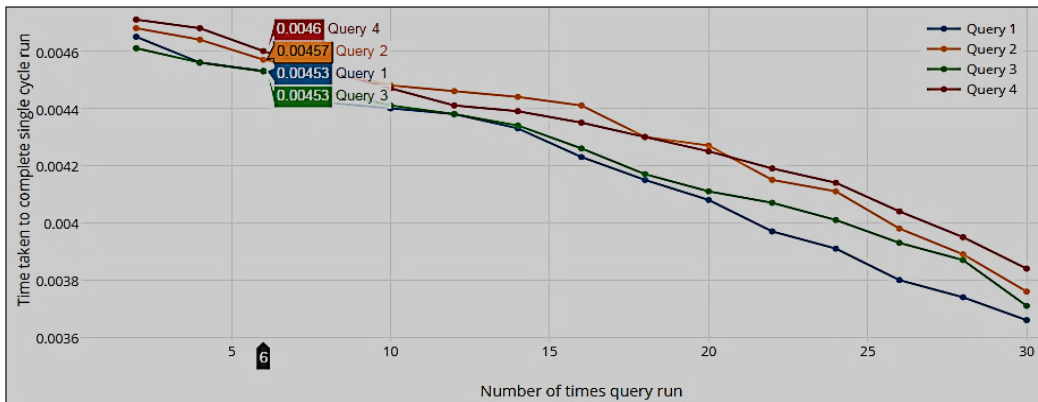


Figure 6. Average negotiation comparison for 4 random queries

CONCLUSION

SQLIAs inadequate input validation has been identified as one of the major causes within a web application. According to a study, it was stated that 75% of cyber-attacks are outperformed at the application layer and over the audited websites where 97% of them are clearly targeted. In the paper, the computation experimental performance of the proposed *Valid* Security tool solution results to justify the formulation with 70-80% success in securing the dataset from ‘SQL injections’ injected by attacker belongs to outside the cloud. We focus to get better information utility rate to get a Moderate/High information utility than the other research solutions. The solution works over Prevention and Detection to improve firewall security. Also, the results lead to achieve an IUR percentage range that would lie between 80-90% that is considered to be a balanced range in all technical aspects.

REFERENCES

- Al-Khashab, E., Al-Anzi, F. S., & Salman, A. A. (2011, April). PSIAQOP: preventing SQL injection attacks based on query optimization process. In *Proceedings of the Second Kuwait Conference on e-Services and e-Systems* (p. 10). Kuwait City, Kuwait. doi:10.1145/2107556.2107566
- Bandhakavi, S., Bisht, P., Madhusudan, P., & Venkatakrishnan, V. N. (2007, October). CANDID: preventing sql injection attacks using dynamic candidate evaluations. In *Proceedings of the 14th ACM conference on Computer and communications security* (pp. 12-24). Alexandria, Virginia, USA. doi:10.1145/1315245.1315249
- Buja, G., Jalil, K. B. A., Ali, F. B. H. M., & Rahman, T. F. A. (2014, April). Detection model for SQL injection attack: An approach for preventing a web application from the SQL injection attack. In *2014 IEEE Symposium on Computer Applications and Industrial Electronics (ISCAIE)* (pp. 60-64). Penang, Malaysia.
- Casassa-Mont, M., Matteucci, I., Petrocchi, M., & Sbodio, M. L. (2015). Towards safer information sharing in the cloud. *International Journal of Information Security*, 14(4), 319-334. doi:10.1007/s10207-014-0258-5

- Dharam, R., & Shiva, S. G. (2013, April). Runtime monitors to detect and prevent union query based SQL injection attacks. In *2013 Tenth International Conference on Information Technology: New Generations (ITNG)* (pp. 357-362). Las Vegas, NV, USA. doi:10.1109/ITNG.2013.57
- Eyal, I., Birman, K., & van Renesse, R. (2015, June). Cache serializability: Reducing inconsistency in edge transactions. In *2015 IEEE 35th International Conference on Distributed Computing Systems (ICDCS)* (pp. 686-695). Columbus, OH, USA. doi:10.1109/ICDCS.2015.75
- Halfond, W. G., & Orso, A. (2005, May). Combining static analysis and runtime monitoring to counter SQL-injection attacks. In *ACM SIGSOFT software engineering notes* (Vol. 30, No. 4, pp. 1-7). St. Louis, Missouri. doi:10.1145/1083246.1083250
- Kiani, M., Clark, A., & Mohay, G. (2008, March). Evaluation of anomaly based character distribution models in the detection of SQL injection attacks. In *Third International Conference on Availability, Reliability and Security (ARES 08)* (pp. 47-55). Barcelona, Spain. doi:10.1109/ARES.2008.123
- Ntagwabira, L., & Kang, S. L. (2010, July). Use of Query Tokenization to detect and prevent SQL Injection Attacks. In *2010 3rd IEEE International Conference on Computer Science and Information Technology (ICCSIT)* (Vol. 2, pp. 438-440). Chengdu, China. doi:10.1109/ICCSIT.2010.5565202
- Narayanan, S. N., Pais, A. R., & Mohandas, R. (2011, August). Detection and prevention of sql injection attacks using semantic equivalence. In *5th International Conference on Information Processing (ICIP 2011)* (pp. 103-112). Bangalore, India.
- Oosawa, T., & Matsuda, T. (2014, October). SQL injection attack detection method using the approximation function of zeta distribution. In *2014 IEEE International Conference on Systems, Man and Cybernetics (SMC)* (pp. 819-824). San Diego, CA, USA. doi:10.1109/SMC.2014.6974012
- Ping, C., Jinshuang, W., Lin, P., & Han, Y. (2016, October). Research and implementation of SQL injection prevention method based on ISR. In *2016 2nd IEEE International Conference on Computer and Communications (ICCC)* (pp. 1153-1156). Chengdu, China. doi:10.1109/CompComm.2016.7924885
- Privacy Technical Assistance Center. (2013). *Data De-identification: An Overview of Basic Terms*. Retrieved November 15, 2016, from https://studentprivacy.ed.gov/sites/default/files/resource_document/file/data_deidentification_terms_0.pdf
- Plischke, E., Borgonovo, E., & Smith, C. L. (2013). Global sensitivity measures from given data. *European Journal of Operational Research*, 226(3), 536-550. doi:10.1016/j.ejor.2012.11.047
- Swanson, C. M., & Stinson, D. R. (2015). Extended results on privacy against coalitions of users in user-private information retrieval protocols. *Cryptography and Communications*, 7(4), 415-437. doi:10.1007/s12095-015-0125-x
- Soria-Comas, J., Domingo-Ferrer, J., Sánchez, D., & Martínez, S. (2014). Enhancing data utility in differential privacy via microaggregation-based k-anonymity. *The VLDB Journal—The International Journal on Very Large Data Bases*, 23(5), 771-794. doi:10.1007/s00778-014-0351-4
- Sonoda, M., Matsuda, T., Koizumi, D., & Hirasawa, S. (2011, November). On automatic detection of SQL injection attacks by the feature extraction of the single character. In *Proceedings of the 4th international conference on Security of information and networks* (pp. 81-86). Sydney, Australia. doi:10.1145/2070425.2070440

- Uwagbole, S. O., Buchanan, W. J., & Fan, L. (2017, May). Applied machine learning predictive analytics to SQL injection attack detection and prevention. In *2017 IFIP/IEEE Symposium on Integrated Network and Service Management (IM)* (pp. 1087-1090). Lisbon, Portugal. doi:10.23919/INM.2017.7987433
- Yassin, M., Ould-Slimane, H., Talhi, C., & Boucheneb, H. (2017, June). SQLIIDaaS: A SQL injection intrusion detection framework as a service for SaaS providers. In *2017 IEEE 4th International Conference on Cyber Security and Cloud Computing (CSCloud)* (pp. 163-170). New York, USA. doi:10.1109/CSCloud.2017.27

SPAS: An Authentication Scheme to Prevent Unauthorized Access of Information from Smart Card

Ajay Kumar Sahu^{1*} and Ashish Kumar²

¹*Department of Computer Science and Engineering,
Raj Kumar Goel Institute of Technology and Management, Ghaziabad 201004,
Uttar Pradesh, India*

²*Department of Computer Science and Engineering, ITS, Greater Noida 201306,
Uttar Pradesh, India*

ABSTRACT

Nowadays internet has become indispensable part of one's life. Therefore, security and privacy are of critical concern to retain user's confidence in network services and applications. Several password verification based schemes/protocols have been used for authentication over insecure channel to protect resources from unauthorized access in networked environment. However, the schemes were not fault tolerant. Also, the feasibility for implementation in some of the applications was questionable. Therefore, we have devised a scheme SPAS (Secure and Provable Authentication Scheme) to overcome the issues prevalent in existing schemes. The objective was to keep the computational and communication cost low. The analysis of the presented scheme SPAS over existing schemes corroborates its effectiveness in tackling various attacks and uniqueness. Further, the performance analysis of the presented scheme is also given to strengthen the proposal.

Keywords: Hash function, identity; security, information retrieval, key agreement, mutual authentication, password, smart card

ARTICLE INFO

Article history:

Received: 18 April 2018

Accepted: 12 September 2018

Published: 24 January 2019

E-mail addresses:

ajay4989@gmail.com (Ajay Kumar Sahu)

ashishese29@gmail.com (Ashish Kumar)

* Corresponding author

INTRODUCTION

Growing usage and applications of technology in all possible domains of human lives is posing a challenge. It has become hard to authenticate the user. Many online frauds are reported in the literature accounted for significant financial loss.

Consequently, the need arises to authenticate the genuine users over an insecure channel like Internet. The most commonly used technique is password based authentication protocol (ElGamal, 1985; Kocher et al., 1999; Lamport, 1981; Tang et al., 2002). The password based techniques are prone to various attacks due to human cognitive capability of designing and remembering complex passwords. Using a smart card, having various advantages like portability, low cost and availability. By using the smart card we can practically and efficiently implement these password based authentication protocols easily (Chang & Wu, 1991; Chien et al., 2002; Hwang & Li, 2000; Ku & Chen, 2004; Messerges et al., 2002; Yang & Shieh, 1999) easily. Several protocols considering static identity have been proposed in the literature (Karuppiah & Saravanan, 2014; Karuppiah & Saravanan, 2015; Kumar et al., 2011; Song, 2010; Wang et al., 2014). Static identity based protocols are easier targets for the attackers. Recently, researchers have designed schemes (Chang & Chang, 2009; Chang et al., 2013; Das et al., 2004; Khan et al., 2014; Li et al., 2014; Wen & Li, 2011; Wang et al., 2009) based on dynamic identity to manage the static identity problem. However, the schemes suffers with high storage and computation cost. In some cases they were shown to be unsafe. Kumari et al. (2014), stated that Chang et al. (2013) protocol was susceptible to various attacks like impersonation, password guessing and anonymity violation. Later suggested an enhanced protocol (“An improved remote user authentication scheme with key agreement”) to overcome existing security and identity concerns. However, analysis of the protocol proposed by Kumari et al. (2014) revealed that it violated on certain aspects i.e. chip/smart card loss and user anonymity and compromised the offered safety against various attacks. In this protocol attacker may leak the privacy and can steal server’s secret key as well as password of the authenticate user, which may impact the entire system. Therefore, we have designed and proposed an efficient, Secure and Provable Authentication Scheme (SPAS), to overcome the observed security weaknesses.

The remaining section in this paper is structured in a systematic way as follows: Notations, System design and Capabilities of adversary are shown in as part 2; we proposed SPAS (Secure and Provable Authentication Scheme) in part 3; Security analysis of suggested scheme is illustrated in part 4; Performance evaluation is shown in part 5 and lastly, conclusion of our scheme is discussed.

NOTATIONS, SYSTEM DESIGN AND CAPABILITIES OF ADVERSARY

In this section, initially basic notations are described then demonstrate system design and capabilities of adversary being used in the scheme.

Notations and Description

The following symbols/notations are preferred in this paper as described in Table 1.

Table 1

Symbols/Notations

Symbol	Description
u_i	Remote user
s_i	System server
sc_i	Smart Card
id_i	User's identity
$c_i d_i$	User's variable identity
$p_w d_i$	User's password
α	Random number chosen from user
$mp_w d_i$	Encrypted/modified password
β_i	Random number chosen by Server for user
x_1, x_2	Server's private key and Server's secret number
$h(.)$	Hash operation
\parallel	Concatenation process
\oplus	XOR operation
t_1	User's current timestamp
t_2	Server's current timestamp
Δt	maximum transmission delay time
γ	Random Number Chosen by smart card
n	Number of times user registers in case of smart card lost
Z	Adversary /Attacker

System Design

Our scheme includes five fundamental stages as described in section 3. Initially, user's information is fed to the terminal and forwarded to the server for registration. Thereafter, server delivers the chip card to remote user along-with security parameters. The registration phase is required only once in our scheme unless and otherwise required re-registration in unavoidable conditions. For accessing resources, permission is given by the server once the credentials are verified in Login stage. The communication takes place only after both, the server and user validates each other. The login and authentication process is usually done several times. In the scheme, a two factor authentication process is used to ensure that chip card owner can be allowed the accessing of the server. Password update and chip card loss re-registration stages are the very useful approaches to overcome the security issues in our proposed scheme.

Capabilities of the Adversary

According to various researches (Chang & Chang, 2005; Wang et al., 2014) of two-factor authentication, the adversary Z has the following capabilities:

In the open communication channel, the adversary Z having full control as it can intercept, remove, update or again send the eavesdropped messages over open communication media.

Adversary Z can get the password of an authenticate user by an infected card reader or obtain the smart card parameters but both cannot be achieved simultaneously.

Adversary Z can also obtain the servers secret key in the case of forwarding secrecy.

THE PROPOSED AUTHENTICATION SCHEME: SPAS

The working of proposed SPAS (Secure and Provable Authentication Scheme) is shown in Figure 1. It consists of five stages namely: 1. Registration stage, 2. Login stage, 3. Verification stage, 4. Password update stage and 5. Re - registration stage. The SPAS is a simple, adequate and most secure based on variable identity authentication scheme to prevent those attacks that exist in the scheme (Kumari et al., 2014). To reduce storage cost, computing complexity as well as to maintain its high performance along with certified security, we need OR, Ex-OR, and elementary hash operations in our scheme.

Within registration stage, the smart card contains data which is dependant on the information produces through user and several credentials inserted through server. In the login/verification phase, both the user and server authenticate each other and after successful mutual authentication, a session key is established before communication between them as various schemes (Kumari & Khan, 2013; Tu et al., 2015; Lu et al., 2015). The initial validity is checked by the smart card then sends user's information towards server for more verification. If the authentication of the server or user fails, this is recommended that the login stage is denied.

User's Registration Stage

In the beginning of this phase u_i registers/re-registers with s_i whenever want some services from it. Assume x_1 and x_2 are private keys and a secret number of the s_i . Suppose n specifies how many times a user registers by authentication server s_i . In mishap-penning cases like chip card loss, theft or snatched, the chip card can revoke through applying the value of n and value of n is saved in a database of user's history on s_i . The authentication server stores these secret key x_1 and number x_2 securely. The entire registration phase having a number of computation steps as follows:

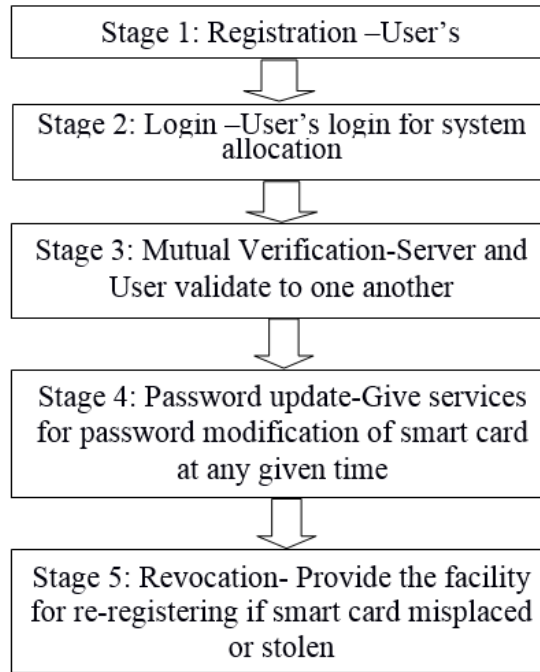


Figure 1. Methodology Used

- User u_i select id_i , $p_w d_i$ and an arbitrary number α .
- Compute $mp_w d_i = h(\alpha \| p_w d_i)$ then transfers $\{id_i, mp_w d_i\}$ towards s_i .
- The registration credentials of user are verified by the server. If selected identity is matched with another in the database, s_i warns u_i to select another id_i .
- Set $n = 0$ by s_i for unique u_i , moreover, specify $n = 1$ by s_i for re-registering user's into the server. Increment n each time of re-registration then id_i will be stored in the database.
- After getting $\{id_i, mp_w d_i\}$, server selects a random number β_i , which is different for each user.
- Server computes $A_i = h(id_u \| \beta_i \| mp_w d_i)$, where $id_u = (id_i \| n)$, $B_i = h(h(id_i) \| x_1) \oplus mp_w d_i$, $C_i = \beta_i \oplus h(h(id_i) \| x_1) \oplus mp_w d_i$ and $D_i = \beta_i \oplus h(x_2 \| x_1)$.
- Stores $\{C_i, A_i, D_i, h(\cdot)\}$ into chip card and deliver $\{chip\ card, B_i\}$ to u_i .
- u_i computes $E_i = h(id_i \| p_w d_i) \oplus \alpha$, $F_i = B_i \oplus \alpha$ and stores $\{E_i, F_i\}$ into chip card.

User's Login Stage

For obtaining services from s_i , a user must login into the server. For this, it must insert its personal chip card into device then insert own id_i as well as pwd_i , further:

- Compute $\alpha = E_i \oplus h(id_i \| p_w d_i)$, $mp_w d_i = h(\alpha \| p_w d_i)$, $h(h(id_i) \| x_i) = F_i \oplus mp_w d_i \oplus \alpha$, $\beta_i = C_i \oplus h(h(id_i) \| x_i) \oplus mp_w d_i$.
- Smart card checks $A_i ? = h(id_i \| \beta_i \| mp_w d_i)$ i.e it is correct or not.
- If not correct, chip card drops this session. If correct, computes $h(x_2 \| x_i) = \beta_i \oplus D_i$, $B_i = F_i \oplus \alpha$.
- Smart card acquires current time-stamp t_1 , computes $c_i d_i = h(id_i) \oplus h(B_i \| \beta_i \| t_1)$, $B_i' = B_i \oplus h(\beta_i \| t_1)$, $G_i = B_i \oplus mp_w d_i$.
- Select arbitrary no. γ , compute $H_i = h(h(id_i) \| \gamma)$, $I_i = G_i \oplus H_i$, $J_i = h(B_i \| \beta_i \| H_i \| t_1)$, $K_i = \beta_i \oplus (h(x_2 \| x_i) \| t_1)$.
- Transmits $\{c_i d_i, B_i', J_i, K_i, t_1, I_i\}$ to server via public channel.

Verification Stage

After getting login request message $\{c_i d_i, B_i', J_i, K_i, t_1, I_i\}$ from u_i , the server authenticates the user and after proper mutual authentication, session key will be established as follows:

- Server set current time instant t_2 , verify t_1 is authentic or not, means $t_2 - t_1 \leq \Delta t$.
- If t_1 is not correct, server denies all the login request and drop this session.
- For obtaining the value of n in database, determine $id_u = (id_i \| n)$.
- If timestamp t_1 is valid, server compute $\beta_i = K_i \oplus (h(x_2 \| x_i) \| t_1)$, $B_i = B_i' \oplus h(\beta_i \| t_1)$, $h(id_i) = c_i d_i \oplus h(B_i \| \beta_i \| t_1)$, $G_i^* = h(h(id_i) \| x_i)$, $H_i^* = G_i^* \oplus I_i$.
- Verify equation $J_i ? = h(B_i \| \beta_i \| H_i^* \| t_1)$ holds or not.
- If true, server acquires current timestamp t_3 , compute $a = h(G_i^* \| \beta_i \| t_3)$, transmits $\{a, t_3\}$ towards the user.
- After getting $\{a, t_3\}$ from the server, smart card verifies validity of t_3 .
- If timestamp t_3 is true, check the equation $a ? = h(G_i \| \beta_i \| t_3)$ holds or not. If correct, both u_i and s_i mutual validate to one another otherwise, will be aborted by the server.
- Server and user agreed upon a common session key. Compute session key for the user is $s_k = h(G_i \| \beta_i \| t_1 \| t_3 \| h(x_2 \| x_i) \| H_i)$ and server $s_k^* = h(G_i^* \| \beta_i \| t_1 \| t_3 \| h(x_2 \| x_i) \| H_i^*)$.

Password Update Stage

Considering security parameters, if any user desires to modify its own password $p_w d_i$ with new password $p_w d_{new}$ in the system, user inserts its own chip card into a device of chip card reader then input its own id_i and $p_w d_i$. The following computation has been performed by the smart card without the involvement of remote server S .

- Smart card computes $\alpha = E_i \oplus h(id_i \| p_w d_i)$, $mp_w d_i = h(\alpha \| p_w d_i)$, $h(h(id_i) \| x_i) = F_i \oplus mp_w d_i \oplus \alpha$, $\beta_i = C_i \oplus h(h(id_i) \| x_i) \oplus mp_w d_i$.
- Verify equation $A_i ? = h(id_i \| \beta_i \| mp_w d_i)$ is correct or not.
- If true, a user is permitted to modify his pwd_i otherwise session is aborted.

- Smart card computes $mp_w d_i^{new} = h(\alpha \| p_w d_i^{new})$, $E_i^{new} = h(id_i \| p_w d_i^{new}) \oplus \alpha$, $F_i^{new} = F_i \oplus mp_w d_i \oplus mp_w d_i^{new}$, $C_i^{new} = C_i \oplus mp_w d_i \oplus mp_w d_i^{new}$, $A_i^{new} = h(id_u \| \beta_i \| mp_w d_i^{new})$.
- Replaces old $\{E_i, A_i, F_i, C_i\}$ with $\{E_i^{new}, A_i^{new}, F_i^{new}, C_i^{new}\}$.
- Hence, modified password has changed successfully and session is terminated.

Revocation Stage of Lost Smart Card

When any user misplaces smart card then it forwards an application towards server for its revocation. At that moment server asks some credentials from the user to check the authenticity, like *Adhaar number, Mobile OTP, Birth date, a card number of identity proof, Voter identity, Name of mother's maiden* or any other user's known value. Subsequently after checking the validity of the revocation request generating by user server updates existing value of n for re-registering the chip card. In each time of misplaced or lost smart card case, n is incremented by 1. Then after, user re-registers with the server without updating its own identity. For the revocation/re-registration of a card, it is expected from a customer that does not avail any earlier values like earlier password, an arbitrary number otherwise by availing same values which are already stored within misplaced or stolen smart card anybody may masquerade as a server's legitimate user.

SECURITY ANALYSIS OF PROPOSED SCHEME

Here we have analyzed SPAS scheme and shown that this scheme is robust and secure against various attacks:

Provide User's Un-traceability and Anonymity

In the scheme, it is hard to track privacy/identity and the claim is corroborated by the analysis of the scheme.

- When attacker Z receives $\{E_z, F_z, C_z, A_z, D_z\}$ parameters from smart card then calculate $\alpha_z = E_z \oplus h(id_z \| p_w d_z)$, $mp_w d_z = h(\alpha_z \| p_w d_z)$, $h(h(id_z)) \| x_1 = F_z \oplus mp_w d_z \oplus \alpha_z$, $\beta_z = h(h(id_z) \| x_1) \oplus C_z \oplus mp_w d_z$, $h(x_2 \| x_1) = \beta_z \oplus D_z$. Hence, attacker can achieve the parameter value of $h(x_2 \| x_1)$.
- Any login message as $\{c, d_i, B_i', J_i, K_i, t_i, I_i\}$ intercepted by attacker can calculate these parameters like $\beta_i = K_i \oplus (h(x_2 \| x_1) \| t_i)$, $B_i = B_i' \oplus h(\beta_i \| t_i)$, $h(id_i) = c, d_i \oplus h(B_i \| \beta_i \| t_i)$. As a result, an attacker can obtain the $h(id_i)$ in place of original id of any legal end user. Hence, confirm that the scheme maintain user's un-traceability and anonymity.

Resist Off-line Password Assumption Attack

In such type of violation, attacker may guess password by applying user's smart card in offline manner. Here, attacker may arrange smart card of any user from either stolen/misplaced, then compute the following:

- An attacker can obtain the value of α_i from above section then compute $E_i \oplus \alpha_i = h(id_i \| p_w d_i)$.
- From $h(id_i \| p_w d_i)$, the attacker cannot obtain the original password without knowing id_i of the user.

Prevent Chip Card Loss/Misplaced Attack

Suppose adversary get hold of the chip card of legal user and rival succeeds in obtaining entire information, in such case the scheme will show that Z cannot get favourable information. From the above two sections, anyone can recognize values of $\{h(id_i), B_i, \beta_i, \alpha_i\}$ from attacks but not $\{id_i, p_w d_i\}$, so $G_i = h(h(id_i) \| x_1)$ cannot be computed and x_1 (secret key) cannot be known. Further, the value of parameter of $I_i = G_i \oplus H_i$ cannot be computed without G_i . Suppose at any time the server receives the message $\{c, d_i, B_i', J_i^{**}, K_i, t_i, I_i^{**}\}$ from attacker, but the server will not accept this login request as $J_i^{**} \neq J_i^*$ for different G_i . Hence, our scheme can prevent the chip card loss/misplaced attack.

Prevent User Mask and Server Pose Violation

Any attacker Z needs the correct login request $\{c, d_i, B_i', J_i, K_i, t_i, I_i\}$ if willing to mask an authenticate customer for the server. As described in previous section, no attacker can satisfy the authentication equation of $J_i^{**} = J_i^*$ successfully without G_i^* . Hence, the suggested scheme avoids user mask violation. Assume that, any adversary computes the valid value of $a = h(G_i^* \| \beta_i \| t_3)$, then masquerading attack is possible in server but attacker cannot obtain correct value of a as confidential key x_1 or G_i cannot be achieved. Hence, suggested scheme prevents server posed violations.

Prevent Forward Secrecy

This is used as very helpful tool for providing secure information to users. Here, with the help of following parameters $\{h(id_i \| x_1), \beta_i, h(x_2 \| x_1), h(h(id_i) \| \gamma)\}$, session key is obtained by adversary as: $s_k = h(h(id_i \| x_1) \| \beta_i \| t_1 \| t_3 \| h(x_2 \| x_1) \| h(h(id_i) \| \gamma))$ that means it is necessary for attacker to know the parameter value of $h(h(id_i) \| \gamma)$. In our scheme, if an attacker can obtain $\{h(id_i \| x_1), \beta_i, h(x_2 \| x_1), h(id_i)\}$, but cannot obtain the number γ anyhow, since it is computed arbitrary in each session. Hence, early session keys cannot be achieved by adversary accurately.

Prevent Replay Violation

To prevent replay attack, we use the concept of current timestamps in scheme. When server receives the request of login message as in the form $\{c, d_i, B_i', J_i, K_i, t_i, I_i\}$, the validity of timestamp t_i is checked by server immediately. Likely, the response message is received by user as $\{a, t_3\}$ from server, then verify authenticity of t_3 firstly. If time instant was not

appropriate, login request messages will be denied by both user and server. So, the suggested scheme prevents replay violation.

Resist Conspirator Attack

In view of the suggested idea, user transfers modified password in place of plain text. A random number α is used by the user for protecting password against conspirator's attack and compute the value of modified password as $mp_w d_i = h(\alpha \| p_w d_i)$. Here, attacker doesn't know the value of $\{\alpha, p_w d_i\}$ both, and cannot guess both of them simultaneously in polynomial time. Hence, in the scheme, there is no opportunity for prediction of possible password and check its prediction is correct. So, the scheme prevents from insider attack.

Maintain Mutual Verification

The suggested idea describe that validity of legal user verified through server by checking the validity of the equation $J_i = h(B_i \| \beta_i \| H_i^* \| t_1)$? In the same way, the user check the authenticity of the server by verifying the equation $a? = h(G_i \| \beta_i \| t_3)$. In this manner to provide proper and secure communication both server and user validate to each other. Hence, suggested scheme must maintain mutual verification.

Provide Session Key Establishment

Here, session key $s_k = h(G_i \| \beta_i \| t_1 \| t_3 \| h(x_2 \| x_1) \| H_i)$ is computed by user and the session key $s_k^* = h(G_i^* \| \beta_i \| t_1 \| t_3 \| h(x_2 \| x_1) \| H_i^*)$ is computed by server in the last of each session. Hence, both of user and server can exchange their information securely and user will access the desired services from server safely because this scheme also provides forward secrecy, that is why our scheme must provide reasonable along with safe session key.

PERFORMANCE ANALYSIS

Here we measure and evaluate various performance parameters of the proposed SPAS scheme i.e. the storage capacity, communication cost, computational cost and security parameters under various known attacks in contrast to other schemes (Kumari et al., 2014; Kaul & Awasthi, 2016; Chaudhary et al., 2015; Jung et al., 2016). Suppose time complexity of hash function is t_h moreover time complexity of XOR function is t_{\oplus} . In our scheme, we made some assumptions on parameters like random numbers, secret numbers, identity, password, and time-stamps i.e. 128-bits. The efficiency comparisons regarding various schemes are described in Table 2. Aforementioned table analyzes and computes storage cost, communication cost along with computational complexity cost over various schemes with our proposed scheme and sum-up in the last.

Table 2

Efficiency Comparison related with Memory requirements (in bits), Transmission cost (in bits) and Computational complexity cost (in bits)

Protocols	Proposed Scheme	Kumari et al. (2014)	Kaul and Awasthi (2016)	Chaudhary et al. (2015)	Jung et al. (2016)
Memory Space in smart card (bits)	$6 * 128 = 768$ bits	$6 * 128 = 768$ bits	$5 * 128 = 640$ bits	$7 * 128 = 896$ bits	$4 * 128 = 512$ bits
Transmission Cost (bits)	$8 * 128 = 1024$ bits	$7 * 128 = 896$ bits	$6 * 128 = 768$ bits	$8 * 128 = 1024$ bits	$9 * 128 = 1152$ bits
Computational Complexity Cost					
Registration Phase (User Side)	$2t_h + 2t_\oplus$	$1t_h + 2t_\oplus$	$2t_h + 2t_\oplus$	$1t_h + 2t_\oplus$	$1t_h$
Registration Phase (Server Side)	$6t_h + 4t_\oplus$	$4t_h + 3t_\oplus$	$4t_h + 5t_\oplus$	$3t_h + 3t_\oplus$	$3t_h + 1t_\oplus$
Login Phase	$12t_h + 11t_\oplus$	$8t_h + 10t_\oplus$	$8t_h + 12t_\oplus$	$8t_h + 9t_\oplus$	$4t_h + 3t_\oplus$
Authentication Phase	$8t_h + 4t_\oplus$	$6t_h + 3t_\oplus$	$6t_h + 9t_\oplus$	$6t_h + 4t_\oplus$	$7t_h + 4t_\oplus$
Password Change Phase	$9t_h + 10t_\oplus$	$6t_h + 7t_\oplus$	$10t_h + 12t_\oplus$	$6t_h + 7t_\oplus$	$7t_h + 3t_\oplus$
Sum of Computational Cost	$37t_h + 31t_\oplus$	$25t_h + 25t_\oplus$	$30t_h + 40t_\oplus$	$24t_h + 25t_\oplus$	$22t_h + 11t_\oplus$

The storage cost is defined as a number of parameters stored in the smart card. Parameters like $\{A_i, C_i, D_i, E_i, F_i, \text{hash}\}$ are saved in smart card’s memory in the scheme. Hence, cost of memory space/storage is $6 * 128 = 768$ bits. Figure 2 shows the comparison graph of storage space estimation cost (in bits) of presented scheme SPAS along with various other relevant schemes.

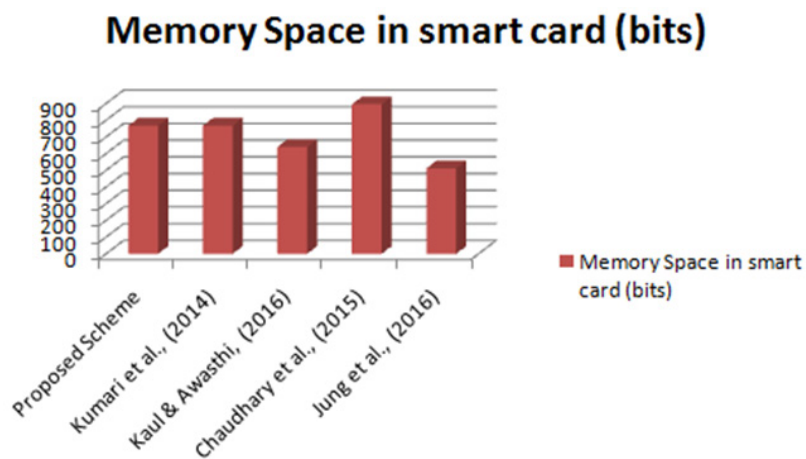


Figure 2. Storage cost comparison

- The total number of bits used in transmitting in login and authentication stage for whole messages are termed as transmission or communication cost.
- The scheme uses 6 parameters in login phase as $\{c_i, d_i, \beta_i, J_i, K_i, t_i, I_i\}$ which requires $6 \times 128 = 768$ bits and for mutual authentication the number of parameters are $\{a, t_3\}$, requiring $2 \times 128 = 256$ bits. Hence, overhead for communication becomes $= 6 \times 128 + 2 \times 128 = 1024$ bits. Figure 3 shows the comparison graph of communication cost estimation (in bits) of our scheme along with various other relevant schemes.
- At user end, SPAS uses two hash functions along with two XOR function during registration phase. Therefore $2t_{h(\cdot)} + 2t_{\oplus}$ is the computational complexity. Correspondingly, the server uses six hash function along with four XOR function during the registration phase, therefore, computational complexity is $6t_{h(\cdot)} + 4t_{\oplus}$ at server end.
- During login stage, the scheme needs twelve hash functions along with eleven XOR functions to produce login request. Hence, $12t_{h(\cdot)} + 11t_{\oplus}$ is the computational cost for login message.

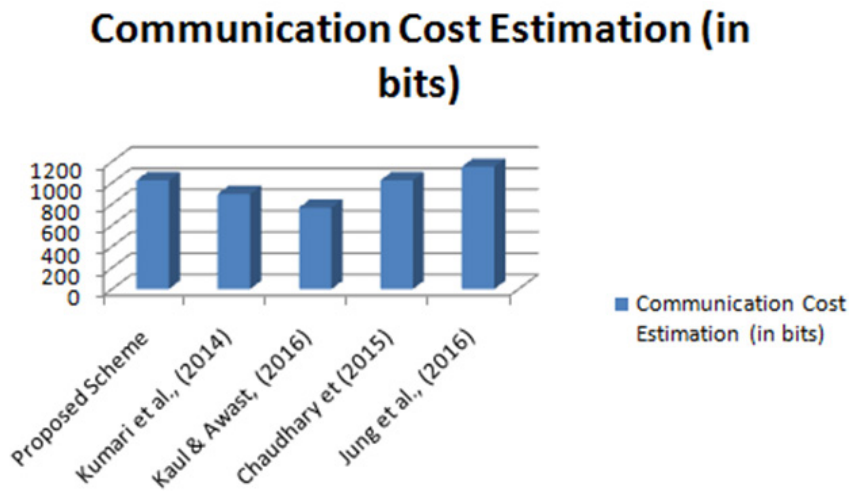


Figure 3. Communication Cost Comparison

- During mutual verification phase, a user needs one hash function, as well as server, needs seven hash along with four XOR functions. Hence, total computational cost for verification/authentication requires $8t_{h(\cdot)} + 4t_{\oplus}$ operations.
- Figure 4 shows the comparison graph of computational complexity estimation cost in (bits) of scheme versus other relevant schemes. In the suggested scheme, computational complexity cost in (bits) is slightly higher than other's scheme (Kumari et al., 2014; Chaudhary et al., 2015; Jung et al., 2016) which is not

baseless as this increased computational cost prevents it from different attacks possible in the network.

- After analysis, we found that schemes as Kaul and Awasthi, (2016); Chaudhary et al. (2015) and Jung et al.(2016) also suffer various attacks like server pose violation, conspirator violation, user impersonation attack, off-line password attack.
- Since the scheme uses low memory (bits) and having low computational cost (bits), and communication cost (bits) as well as secure against various attacks, therefore, we concluded that suggested idea/scheme performed most excellent from others so that we can implement it more practically than others over insecure networks.
- We demonstrated the security analysis of various protocols in Table 3 and achievements/goals in Table 4. Here, Figure 5 shows graph of security characteristics comparison and Figure 6 presents the graph of goal/achievements comparison.

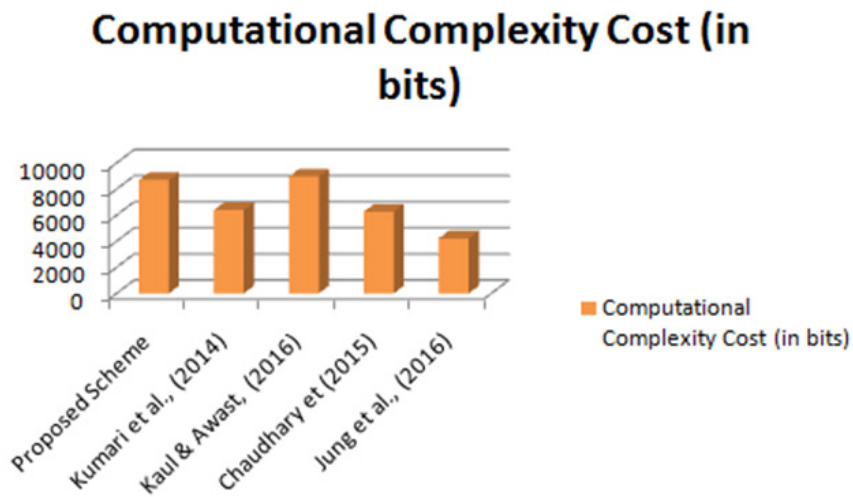


Figure 4. Computational Cost Comparison

Table 3

Security characteristics of our suggested scheme along with various other relevant schemes

S. No.	Security Characteristics	Proposed Scheme	Kumari et al. (2014)	Kaul and Awasthi, (2016)	Chaudhary et al. (2015)	Jung et al. (2016)
1	Conspirator Attack	No	Yes	No	No	No
2	Chip Card Loss attack	No	Yes	No	No	Yes

Table 3 (Continue)

S. No.	Security Characteristics	Proposed Scheme	Kumari et al. (2014)	Kaul and Awasthi (2016)	Chaudhary et al. (2015)	Jung et al. (2016)
3	User mask violation/attack	No	No	No	Yes	No
4	Server mask violation/attack	No	No	No	Yes	Yes
5	On-line password assumption violation	No	No	No	No	Yes
6	Off-line password assumption violation	No	Yes	No	No	Yes
7	Replay violation	No	Yes	No	No	No
8	Denial of service violation	No	No	No	No	Yes
9	Man in middle attack	No	Yes	No	Yes	Yes
10	Lifted verifier violation	No	Yes	Yes	No	No

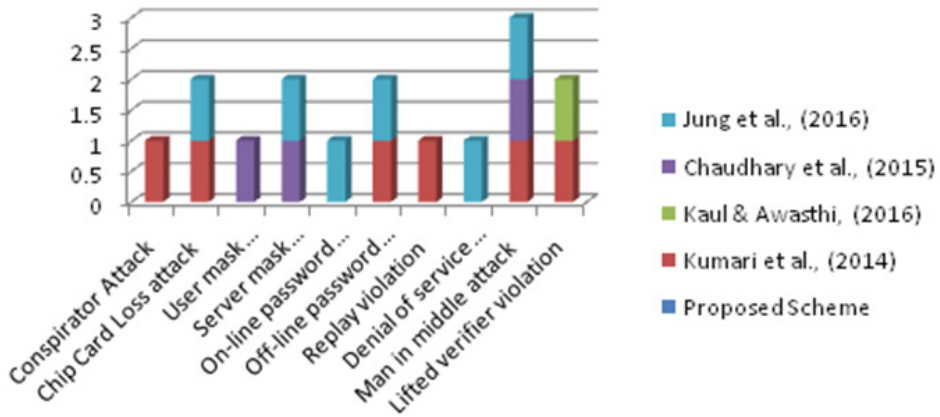


Figure 5. Security Characteristics Comparison Graph

Table 4

Goal/Achievements Comparison

S. No.	Protocols	Proposed Scheme	Kumari et al. (2014)	Kaul and Awasthi (2016)	Chaudhary et al. (2015)	Jung et al. (2016)
1	User's anonymity and un-traceability	Yes	No	No	Yes	No
2	Support forward secrecy	Yes	No	No	Yes	Yes
3	Maintain Mutual Verification	Yes	No	No	Yes	Yes
4	Compromise secret key	No	Yes	No	No	No
5	Compromise session key	No	Yes	No	No	No
6	Single registration	Yes	Yes	Yes	Yes	Yes
7	Freely change password	Yes	Yes	Yes	Yes	Yes
8	No need of verification table	Yes	Yes	Yes	Yes	Yes
9	Provide fast incorrect password checking facility	Yes	Yes	Yes	Yes	No
10	Scope of verification characteristics in chip card	Yes	Yes	No	No	No
11	Storage, functional as well as transmission cost must be low	Yes	Yes	No	Yes	No

We implemented the scheme in Python and the security features are tested/validate on AVISPA (Automated Validation of Internet Security Protocols and Applications) tool. AVISPA is having four tools to check the validation of security protocols.

- On-the-fly Model-Checker (OFMC)
- Constraint-Logic-based Attack Searcher (CL-AtSe)
- SAT-based Model-Checker (SATMC)
- Tree Automata based on Automatic Approximations for the Analysis of Security Protocols (TA4SP)

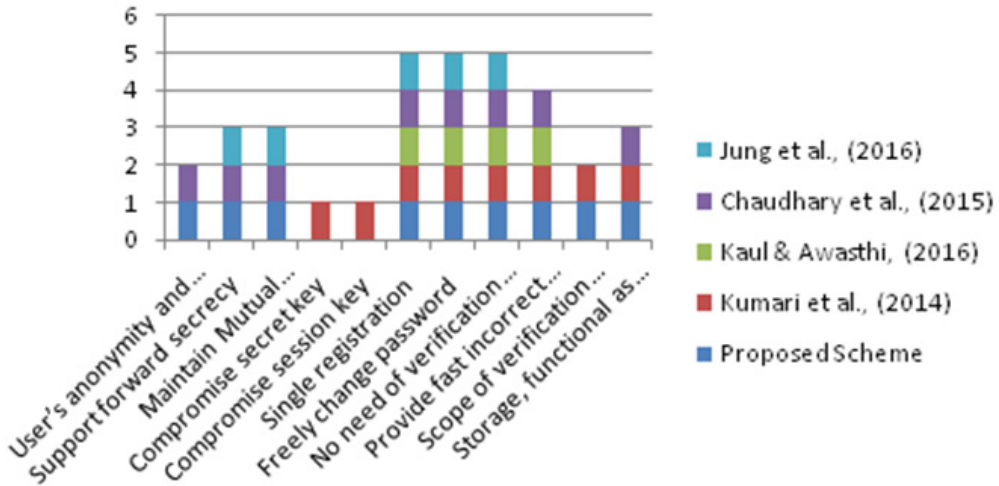


Figure 6. Goal/Achievements Comparison Graph

Figure 7 shows process flow diagram of AVISPA tool. The security analysis of the presented scheme has confirmed its performance in terms of reliability and safety because all the observations, trials, measuring operations return the same outcome on repeated testing. Moreover, the scheme is free from outside attacks, hazard, and insecurity, threat arising from loss of smart card. Analysis of the scheme shows that it is robust against all known attacks and ensures anonymity and privacy as there is no adverse effect of any types of attacks and it can withstands all such types of rigorous conditions. Moreover, its expandability characteristic is having the ability to support extra network users.

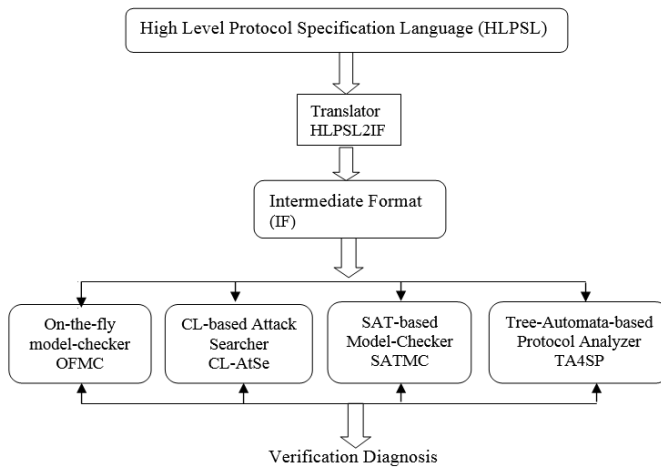


Figure 7. AVISPA TOOL

CONCLUSION

The SPAS scheme is introduced in this paper. The scheme ensures security, privacy and confidentiality of a user. It is an improvement over all the existing schemes (Chaudhary et al., 2015; Das et al., 2004; Jung et al., 2016; Kaul & Awasthi, 2016; Kumari et al., 2014). During investigation we found that earlier works were not secure enough for practical applications because all security parameters can be easily obtained by the challenger and are vulnerable to chip card loss violation as well as user un-traceability violation attack. Moreover, an adversary can get server's secret key, as well as password of the entire registered user's and also the session key for server, which may lead to destroying the whole system. During performance analysis of the scheme it is found that it incurs some extra bits of memory, and increased computational and communication cost but it helps to prevent smart card loss and user anonymity violation attack. The analysis of the scheme has confirmed its feasibility and performance in practical approach. The proposed scheme may be used in such applications which providing privacy protection with low-computation-ability devices. Thus, our idea is practically more acceptable to operate secure remote access over the public environment as well as may be simply integrated into various types of services such as academics, banking, and business applications. After performance and efficiency comparison, we demonstrate that suggested idea is safer as well as relevant to practical approach.

REFERENCES

- Chang, C. C., & Wu, T. C. (1991). Remote password authentication with smart cards. *IEEE Proceedings-E Computers and Digital Techniques*, 138(3), 165-168. doi:10.1049/ip-e.1991.0022
- Chang, Y. F., & Chang, C. C. (2005). Authentication schemes with no verification Table. *Applied Mathematics and Computation*, 167, 820-832. doi:10.1016/j.amc.2004.06.118
- Chang, Y. F., & Chang, H. C. (2009). Security of dynamic ID-based remote user authentication scheme. In *Fifth International Joint Conference on INC, IMS and IDC* (pp. 2108-2110). Seoul, South Korea. doi: 10.1109/NCM.2009.101
- Chang, Y. F., Tai, W. L., & Chang, H. C. (2013). Untraceable dynamic-identity-based remote user authentication scheme with verifiable password update. *International Journal of Communication Systems*, 27(11), 3430-3440. doi:10.1002/dac.2552
- Chaudhary, S. A., Farash, M. S., Naqvi, H., Kumari, S., & Khan, M. K. (2015). An enhanced privacy preserving remote user authentication scheme with provable security. *Security and Communication Networks*, 8, 3782-3795. doi:10.1002/sec.1299
- Chien, H. Y., Jan, J. K., & Tseng, Y. M. (2002). An efficient and practical solution to remote authentication: smart card. *Computers and Security*, 21(4), 372-375. doi:10.1016/S0167-4048(02)00415-7

- Das, M. L., Saxena, A., & Gulati, V. P. (2004). A Dynamic ID-based Remote User Authentication Scheme. *IEEE Transactions on Consumer Electronics*, 50(2), 629-631. doi:10.1109/TCE.2004.1309441
- ElGamal, T. (1985). A public key cryptosystem and a signature scheme based on discrete logarithms. *IEEE Transactions on Information Theory*, 31(4), 469-472. doi:0018-9448/85/0700-0469
- Hwang, M. S., & Li, L. H. (2000). A new remote user authentication scheme using smart cards. *IEEE Transactions on Consumer Electronics*, 46(1), 28-30. doi:10.1109/30.826377
- Jung, J., Lee, D., Kim, J., Lee, Y., Kang, D., & Won, D. (2016). Cryptanalysis and improvement of efficient password-based user authentication scheme using hash function. In *Proceedings of the 10th International Conference on Ubiquitous Information Management and Communication* (pp. 23). New York, NY, USA. doi:10.1145/2857546.2857570
- Karuppiah, M., & Saravanan, R. (2014). A secure remote user mutual authentication scheme using smart cards. *Journal of Information Security and Applications*, 19(4), 1-13. doi:10.1016/j.jisa.2014.09.006
- Karuppiah, M., & Saravanan, R. (2015). Cryptanalysis and an improvement of new remote mutual authentication scheme using Smart Cards. *Journal of Discrete Mathematical Sciences and Cryptography*, 18(5), 623-649. doi:10.1080/09720529.2015.1013693
- Kaul, S. D., & Awasthi, A. K. (2016). Security enhancement of an improved remote user authentication scheme with key agreement. *Wireless Personal Communications*, 89(2), 621-637. doi:10.1007/s11277-016-3297-6
- Khan, M. K., Kumari, S., Wang, X. M., & Kumar, R. (2014, August 24-27). Security Issues of Chen et al.'s dynamic ID-based authentication scheme. In *12th International Conference on Dependable, Autonomic and Secure Computing (DASC)* (pp. 125-128). Dalian, China. doi:10.1109/DASC.2014.31
- Kocher, P., Jaffe, J., & Jun, B. (1999). Differential Power Analysis. In M. Wiener (Eds.), *Advances in Cryptology-CRYPTO'99* (pp. 388-397). Berlin, Heidelberg: Springer. doi:10.1007/3-540-48405-1_25
- Ku, W. C., & Chen, S. M. (2004). Weaknesses and improvements of an efficient password based remote user authentication scheme using smart cards. *IEEE Transactions on Consumer Electronics*, 50(1), 204-207. doi:10.1109/TCE.2004.1277863
- Kumar, M., Gupta, M. K., & Kumari, S. (2011). An improved efficient remote password authentication scheme with smart card over insecure networks. *International Journal of Network Security*, 13(3), 167-177. doi:10.1007/s00607-013-0308-2
- Kumari, S., & Khan, M. K. (2013). Cryptanalysis and improvement of a robust smart-card-based remote user password authentication scheme. *International Journal of Communication Systems*, 27(12), 3939-3955. doi:10.1002/dac.2590
- Kumari, S., Khan, M. K., & Li, X. (2014). An improved remote user authentication scheme with key agreement. *Computers and Electrical Engineering*, 40(6), 1997-2012. doi:10.1016/j.compeleceng.2014.05.007
- Lampert, L. (1981). Password authentication with insecure communication. *Communications of the ACM*, 24(11), 770-772. doi:0001-0782/81/1100-772

- Li, X., Niu, J., Liu, Y., Liao, J., & Liang, W. (2014). Robust dynamic ID-based remote user authentication scheme using smart cards. *International Journal of Ad Hoc and Ubiquitous Computing*, 17(4), 254-264. doi:10.1504/IJAHUC.2014.066423
- Lu, Y., Li, L., Peng, H., & Yang, Y. (2015). A secure and efficient mutual authentication scheme for session initiation protocol. *Peer-to-Peer Networking and Applications*, 9(2), 449-459. doi: 10.1007/s12083-015-0363-x
- Madhusudhan, R., & Mittal, R. C. (2012). Dynamic ID-based remote user password authentication schemes using smart cards: A review. *Journal of Network and Computer Applications*, 35, 1235-1248.
- Messerges, T. S., Dabbish, E. A., & Sloan, R. H. (2002). Examining smart-card security under the threat of power analysis attacks. *IEEE Transaction on Computers*, 51(5), 541-552. doi: 10.1109/TC.2002.1004593
- Song, R. (2010). Advanced smart card based password authentication protocol. *Computer Standards & Interfaces*, 32, 321-325. doi:10.1016/j.csi.2010.03.008
- Tang, Y. L., Hwang, M. S., & Lee, C. C. (2002). A simple remote user authentication scheme. *Mathematical and Computer Modelling*, 36, 103-107. doi:SO895-7177(02)00106-1
- Tu, H., Kumar, N., Chilamkurti, N., & Rho, S. (2015). An improved authentication protocol for session initiation protocol using smart card. *Peer-to-Peer Networking and Applications*, 8(5), 903-910. doi:10.1007/s12083-014-0248-4
- Wang, D., He, D., Wang, P., & Chu, C. H. (2014). Anonymous two-factor authentication in distributed systems: Certain goals are beyond attainment. *IEEE Transactions on Dependable and Secure Computing*, 12(4), 428-442. doi:10.1109/TDSC.2014.2355850
- Wang, Y. Y., Liu, J. Y., Xiao, F. X., & Dan, J. (2009). A more efficient and secure dynamic ID-based remote user authentication scheme. *Computer Communications*, 32(4), 583-585. doi:10.1016/j.comcom.2008.11.008
- Wen, F., & Li, X. (2011). An improved dynamic id-based remote user authentication with key agreement scheme. *Computers and Electrical Engineering*, 38, 381-387. doi:10.1016/j.compeleceng.2011.11.010
- Yang, W. H., & Shieh, S. P. (1999). Password authentication schemes with smart cards. *Computers and Security*, 18(8), 727-733. doi:0167-4048/99

Improvement in the Mechanical Strength of Compacted Urea Fertilizer Tablets through Die Wall Lubrication

Intan Soraya Shamsudin¹, Mohd Shamsul Anuar^{1*}, Yus Aniza Yusof¹, Ahmad Husni Mohd. Hanif² and Suraya Mohd Tahir³

¹Department of Process and Food Engineering, Faculty of Engineering, Universiti Putra Malaysia, 43400 UPM, Serdang, Selangor, Malaysia

²Department of Land Management, Faculty of Agriculture, Universiti Putra Malaysia, 43400 UPM, Serdang, Selangor, Malaysia

³Department of Mechanical and Manufacturing Engineering, Faculty of Engineering, Universiti Putra Malaysia, 43400 UPM, Serdang, Selangor, Malaysia

ABSTRACT

This research was conducted to investigate the compaction performance and mechanical strength of compacted urea fertilizer in unlubricated and lubricated die systems. The ground urea 46% N fertilizer was compacted in a 13 mm flat-face cylindrical die set in both unlubricated and lubricated die systems with vegetable fatty acids and magnesium stearate as lubricants at various compaction stresses to produce urea fertilizer tablets. In conclusion, a lubricated die system reduces the frictional effects during the production of urea fertilizer tablets and also produces a mechanically stronger urea fertilizer tablet than those produced in an unlubricated die system. In addition, the vegetable fatty acids and magnesium stearate lubricants are found to improve the compaction performance of urea fertilizer tablet as well as its mechanical strength.

Keywords: Ejection, fertilizer, lubricant, mechanical strength, uniaxial die compaction, urea

ARTICLE INFO

Article history:

Received: 09 May 2017

Accepted: 02 November 2018

Published: 24 January 2019

E-mail addresses:

soraya7787@gmail.com (Intan Soraya Shamsudin)

mshamsul@upm.edu.my (Mohd Shamsul Anuar)

yus.aniza@upm.edu.my (Yus Aniza Yusof)

husni@upm.edu.my (Ahmad Husni Mohd. Hanif)

su_mtahir@upm.edu.my (Suraya Mohd Tahir)

* Corresponding author

INTRODUCTION

The development of slow release agricultural based-fertilizer is important in order to retain the concentration of the nutrient, mainly nitrogen within the plant roots for a desired length of time (Tzika et al., 2003). Slow release fertilizer can be categorized into organic fertilizer and water-soluble inorganic fertilizer. While these types of fertilizers have been widely used as slow

release fertilizers, they possess different characteristics. The living micro presence in the organic fertilizer makes it unstable and the solubility has been limited by the low absorption of water into the fertilizer (Tzika et al., 2003). Whereas, the chemical compounds present in the water-soluble inorganic fertilizer makes it stable and the solubility is controlled by coating the fertilizer with a hydrophobic polymer (Tzika et al., 2003).

The lubrication of compact water-soluble inorganic fertilizers is one of the ways to produce slow release urea fertilizers by improving its physical appearance and integrity to form a coherent tablet. Recently, the compaction of urea into tablet form has shown promising characteristics as a controlled release vehicle for ammonium ions but large frictional effects were observed during the compaction of the urea powders into tablet form (Shamsudin, Anuar, Yusof, Mohd Hanif, & Tahir, 2014).

Urea fertilizer or scientifically known as carbamide; is a white crystalline water-soluble compound containing 46% nitrogen (N) (Watson, Stevens, Garrett, & McMurray, 1990; Jones, Koenig, Ellsworth, Brown, & Jackson, 2007). Its importance as a fertilizer has grown progressively and represents 40% of world N consumption (Watson et al., 1990). It is produced from a variety of manufacturing processes such as prilling, pan and drum granulation and fluidized bed granulation, which eventually forming small urea pellets size range from 1 to 4 mm each (Jones et al., 2007). Urea fertilizer is highly soluble in water and tends to volatile into ammonia gas (Jones et al., 2007) if it is handled improperly during broadcasting on the soil. In this research, the urea was manufactured by Petronas Fertilizer (Kedah) Sdn. Bhd., Malaysia in granular form and having 46% nitrogen, 1% biuret and 0.5% moisture by its maximum weight.

An established conventional die wall lubricant; magnesium stearate is often employed as lubricant in pharmaceutical industry due to its lubricating properties; forming a low shear strength between the die wall and the compact. Thereby, it facilitates the uniform transmission of stresses within the compact and thus, reduces the frictional effects that occurred between the die wall and the compact during the ejection process (Briscoe & Rough, 1998). Thus, the lubrication is important to prevent the wall friction from hindering the force transmissions and producing unwanted density gradients within the formed powder compact (Briscoe & Evans, 1991). Apart from that, the lubricant is able to form a hydrophobic film around the powders and thus, negatively affect the tablet crushing strength, disintegration time, friability and dissolution (Sheikh-Salem & Fell, 1981; Bolhuis, Lerk, Zijlstra, & Boer, 1975; Levy & Gumtow, 1963). Another recent research (Ariyasu, Hattori, & Otsuka, 2016) suggested some mechanisms on how the magnesium stearate delayed the tablet dissolution. The established magnesium stearate lubricant used in this current work consists of 3.8 – 5.0 % magnesium. Other new viable lubricants to be used during the compaction process are continuously researched and developed such as the work evaluating the use of sucrose fatty acids esters (Nakamura et al., 2017). In this current work, another type of lubricant, a vegetable based fatty acids lubricant or its

commercially name; TriStar 149 derived from 0.1% Lauric and Myristic, 49.1% Palmitic, 50.2 % Stearic and 0.5% Arachidic fatty acid is also evaluated and used as a comparison to the established magnesium stearate lubricant.

Therefore, it is the aim of this work to assess the lubricant performance in the compaction of urea powder into tablet form using magnesium stearate and vegetable fatty acids in reducing the frictional effects during the urea fertilizer tablet production and improving the urea fertilizer tablet mechanical integrity.

MATERIALS AND METHODS

Powder Preparation

Urea 46% N in granular form was manufactured and purchased from Petronas Fertilizer (Kedah) Sdn. Bhd., Malaysia. To obtain urea powder in laboratory, 100 g urea granules were ground for 1 minute using an electric grinder (model RT-02A grinder, Taiwan) in order to obtain urea powder with a relatively uniform mean particle size distribution as described in Table 1.

The lubricants; magnesium stearate was purchased from Acros Organic, Belgium while the vegetable fatty acids lubricant was provided by Hemo Asia Sdn Bhd, Malaysia. All the lubricants were used as received.

Physical Properties of Powders

The moisture content of the powders was obtained by using the oven method. 5 g of each powder was dried in an oven dryer (Jeio Tech, Korea) at 105 °C for 1 day. The true density of the powder was determined by using an automatic helium AccuPyc II 1340 Gas Pycnometer (Micromeritics Instrument Corp., USA). The bulk density was measured by pouring 25 g \pm 0.01 g powder into 100 ml graduated cylinder and slightly tapped twice to avoid the powder from sticking onto the wall and bottom of the cylinder. The bulk density can be calculated by dividing the mass of the powder by the volume occupied in the cylinder (Kumar & Kothari, 1999). Tapped density was obtained using GeoPyc 1360 Tap Density Analyzer (Micromeritics Instrument Corp., USA).

Formation of Urea Fertilizer Tablet

1.0 g \pm 0.01 g of the urea powder was compacted inside a 13mm evacuable pellet die (Specac, UK) set according to laboratory uniaxial die compaction method (Figure 1). The urea fertilizer tablet was formed in a room temperature between 20-25°C using a universal testing machine (model 5566, Instron, Canton MA, USA). The process involved three main consecutive stages; filling of die with the accurate powder (die filling stage), the application of stress onto the powder bed and forming a tablet (loading stage), the removal of stress

(unloading stage) and finally the produced tablet was ejected from the die (ejection stage).

In this study, various compaction stresses ranging from 37.7 MPa to 188.3 MPa were used for comparison purposes. For the assessment of the lubrication performance, the die wall, upper and lower punch surfaces were lubricated with magnesium stearate or vegetable fatty acids. Ethanol was utilized prior to each compression to remove any sticking powder on the die wall. The loading and unloading processes were conducted at a constant rate of 0.1 mm/s and 0.0167 mm/s (Mohammed et al., 2005). The applied force and displacement were recorded automatically by a compatible computer software called Bluehill (Canton MA, USA). Then, the produced urea fertilizer tablet was ejected from the die at a constant ejection rate of 0.083 mm/s. The data of the force-displacement during ejection was again recorded automatically by Bluehill software (Canton Ma, USA). The work of deformation (plastic work during loading-unloading and ejection work during ejection) during the compaction process was calculated based upon the recorded force and displacement data.

The physical testing of the urea fertilizer tablet was performed 24 hours after ejection (Krycer et al., 1982; Mollan & Celik, 1996). The physical measurements and tests performed were: weight by electronic mass balance (OHAUS, Switzerland); tablet thickness and diameter by vernier caliper (Mitutoyo, Japan).

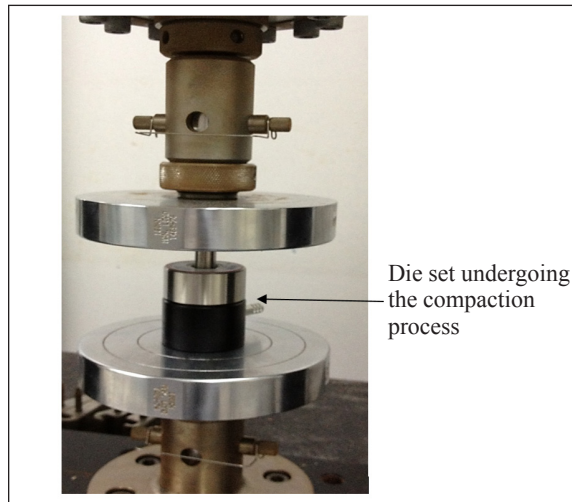


Figure 1. The laboratory uniaxial die compaction process using a universal testing machine

Strength of Urea Fertilizer Tablet

The strength of the urea fertilizer tablet was measured by applying a compressive stress, which is also known as the Indirect Tensile test or the Brazilian test. The tablet was placed between a pair of flat platens. A compressive stress was applied to the tablet at a constant

rate of 0.0116 mm/s (Mohammed et al., 2005]. In this study, only tablets that failed through diametrical fracture or split into two halves with the fracture plane running through the center of the compact, indicating ideal tensile failure (Hiestand & Smith, 1984) were accepted. The tensile strength (σ) of the compact can be calculated using the following equation (Fell & Newton, 1970):

$$\sigma = \frac{2P}{DH} \quad (1)$$

where P , D and H are the maximum force recorded before fracture during the Brazillian test, diameter and thickness of the tablet. The tensile strength of the tablet was determined in four replicates using a universal testing machine (model 5566, Instron, Canton MA, USA).

Statistical Analysis

The experimental data are presented as mean and standard error of $n=4$ replicates (mean \pm SE). Statistically analysis was performed using Minitab 16 Statistical Software. The data were analyzed by a one-way analysis of variance (ANOVA) and followed by Tukey's test for multiple comparisons. The differences were defined as significantly different at $p < 0.05$.

Theoretical Background

Work of Deformation: Plastic Deformation. The compaction process in lubricated and unlubricated dies needs an energy to deform the powder. The work or energy used to compact the urea powder in lubricated and unlubricated die to produce the urea fertilizer tablets can be calculated from the upper punch forces and displacements (Ragnarsson & Sjogren, 1983). It is used to deform the particles both elastically or plastically, interparticle friction, friction with the die wall, to create new surfaces by fragmentation and forming the interparticles bonding (Alderborn, 2007). In this work, only the plastic work is calculated from the force-displacement data obtained during the loading-unloading stage of the compaction process.

Work of Die Wall Friction. The last stage in the compaction process; ejection stage is an important stage which determines the quality of the tablets once they come out from the die. The mechanism of the ejection process which involved friction with die wall could produce work of die wall friction (Sugimori & Mori, 1989). The work of die wall friction could be calculated by integrating the area under the curve of the ejection force and displacement data obtained during the ejection process.

RESULT AND DISCUSSION

Physical Properties of the Raw Materials

Table 1
Physical properties of materials used in this work

Material properties	Urea 46 % N	Magnesium stearate	Vegetable fatty acids
Moisture content (%)	3.94	1.65	0.09
True density (kgm ⁻³)	1341	1088	985
Bulk density (kgm ⁻³)	470	250	310
Tapped density (kgm ⁻³)	783	483	474

Plastic Work

A common derived parameter to reflect particle deformation during the compaction process to form the urea fertilizer tablets is by quantifying its plastic work formation. From Figure 2, the plastic work increases as the compaction stress increases for both lubricated and unlubricated die systems. An increase in the plastic work indicates that the compaction stress has been transferred from the upper punch to the powder respectively. Apparently, urea fertilizer tablets in lubricated die produced high plastic work than those in unlubricated die at various compaction stresses, demonstrating that the lubricant facilitates the uniform transmission of compaction stress and hence, forming a strong coherent urea fertilizer tablet.

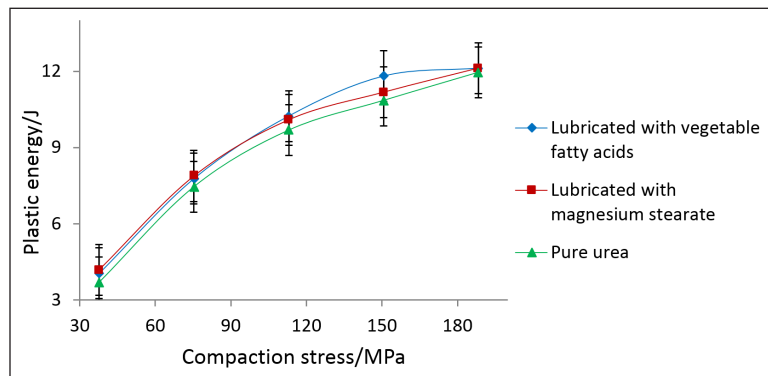


Figure 2. Plastic work of urea fertilizer tablets in lubricated and unlubricated dies (standard errors are indicated by error bars)

At low compaction stresses ranging from 37.7 MPa to 113.0 MPa, the urea fertilizer tablet in vegetable fatty acids and magnesium stearate lubricated dies showed statistically no significant different ($p > 0.05$). However, both the lubricants differ significantly with unlubricated urea tablet ($p < 0.05$). It seems that the lubricants do not show any significant difference at low compaction stresses. As the compaction stress increased, the plastic work for both lubricants increased gradually and the plastic works for the vegetable fatty acids

lubricant urea fertilizer tablets were observed to become more constant at 150.7 MPa and 188.3 MPa, in comparison to the magnesium stearate lubricant which exhibited increasing plastic work in the same region. This indicates that vegetable fatty acids lubricant urea fertilizer tablets need approximately a low compaction stress; 150.7 MPa to achieve the optimum plastic work in comparison to the magnesium stearate lubricant urea fertilizer tablets and unlubricated urea fertilizer tablets. Overall, the magnitudes of the final plastic works obtained at the highest compaction stress used in this work (at 188.3 MPa) were similar for both the lubricants and higher in comparison to the unlubricated system.

Ejection Stress and Ejection Work

A higher compaction stress generates a higher residual die wall stresses and frictional stresses at the die walls prior to ejection (Sugimori & Mori, 1989; Briscoe & Rough, 1998). During the ejection, these stresses have to be overcome (Briscoe & Rough, 1998). Unlubricated urea fertilizer tablet exhibited the highest maximum ejection stress in comparison to the urea fertilizer tablet lubricated with vegetable fatty acids and magnesium stearate. The magnesium stearate lubricant acted as a lubricant to reduce the friction between die wall and urea particles as the tablet was formed and ejected. Also, the vegetable fatty acids lubricant had same performance as the magnesium stearate where no significant differences ($p > 0.05$) were found for all the compaction stresses.

The tablet-die wall frictional effect was investigated by ejecting the urea fertilizer tablet in lubricated and unlubricated dies at various compaction stresses. The maximum ejection stress of urea fertilizer tablet in lubricated and unlubricated dies is plotted as a function of compaction stress as shown in Figure 3. As the compaction stress increased, the maximum ejection stress increased.

The ejection work against various compaction stresses was plotted in Figure 4. The ejection work is calculated from the force-displacement data obtained during the ejection of the urea fertilizer tablet from the die cavity. It gives a first-order estimation of the tablet

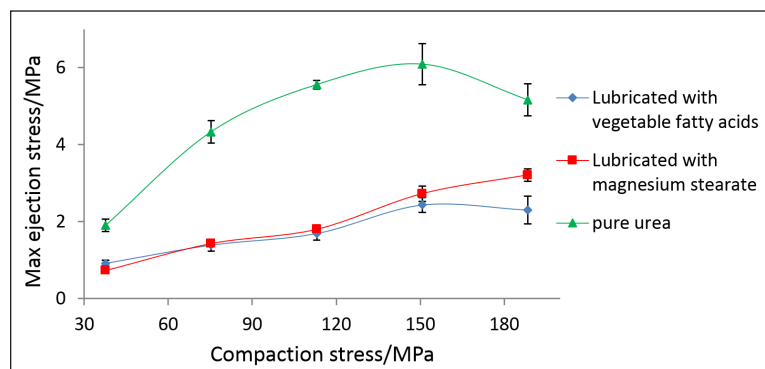


Figure 3. Maximum ejection stress of urea compact in lubricated and unlubricated dies (standard errors are indicated by error bars)

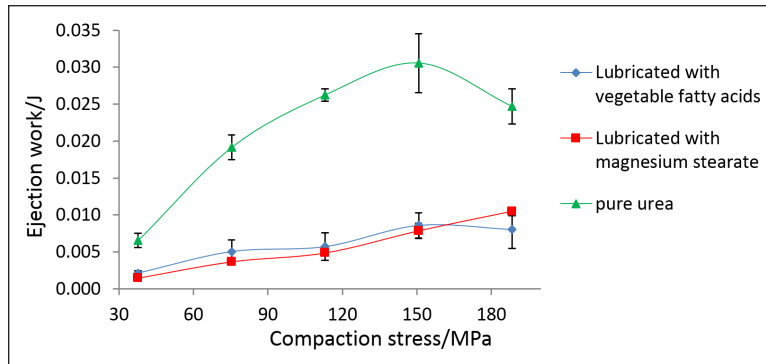


Figure 4. The ejection work of urea fertilizer tablet in lubricated and unlubricated dies (standard errors are indicated by error bars)

stored elastic energy (Anuar & Briscoe, 2009). In Figure 4, the ejection work was found to increase with increasing compaction stress in both in unlubricated and lubricated die systems. The unlubricated die systems possessed higher ejection works in comparison to the lubricated system, which could be explained by observing their maximum ejection stress in Figure 3. Hence, as a first-order approximation, the urea fertilizer tablets formed in a lubricated die system have lower stored elastic energies in comparison to the tablets formed in the unlubricated die. Both lubricated die with vegetable fatty acids and magnesium stearate showed no significant different ($p > 0.05$) for ejection work at all compaction stresses.

Mechanical Strength

Figure 5 shows the tensile strengths of urea fertilizer tablets in lubricated and unlubricated dies increase in proportion to the compaction stresses. It also can be observed that the tensile strength of the urea fertilizer tablet formed in a lubricated die shows a significant difference ($p < 0.05$) in comparison to those formed in an unlubricated die. Apart from that, the lubrication of the urea fertilizer tablet with magnesium stearate and vegetable fatty acids gives significant difference ($p < 0.05$) at all compaction stresses.

This compaction behaviour can be assumed to be due to the increase in the inter-particulate bonding due to a higher contact area between the particles during the plastic deformation (Shamsudin et al., 2010) thus, enhancing the mechanical strength of the tablet. This is supported by data shown earlier in Figure 2, where the increase in the plastic work is observed with the increase in the compaction stress. Therefore, a high tensile strength is required for crack propagation in lubricated urea fertilizer tablet due to the increase in the inter-particulate bonding within the tablet (Figure 5). Based upon the increase in the plastic deformation (Figure 2) and the resulting mechanical strength (Figure 5) obtained in

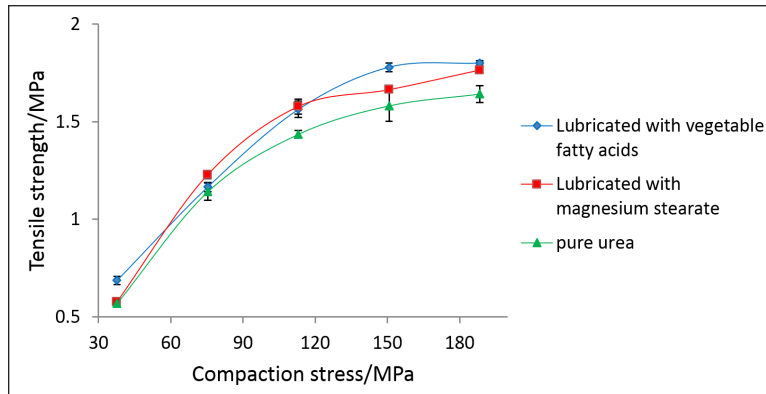


Figure 5. The tensile strength of urea compact in lubricated and unlubricated dies (standard errors are indicated by error bars)

a lubricated die system, these give further indication that the formed urea fertilizer tablets in the lubricated die system have relatively lower stored elastic energies in line with the low values of the ejection works (Figure 4).

CONCLUSION

The effect of die wall lubrication in the compaction of urea 46% N powder has been investigated experimentally using the uniaxial die compaction method. As observed, the urea powder can be characterized as having poor flow powder based upon its Carr Index and Hausner Ratio values. During the compaction, the lubricated urea tablets with vegetable fatty acids and magnesium stearate experienced high plastic deformation. The lubricants improve the ejection process by reducing the frictional effects, where the unlubricated system requires high ejection stress and ejection work compared to the lubricated systems. For the diametrical strength assessment, the lubricated die system produces urea fertilizer tablets that are relatively stronger than those produced in the unlubricated die system. Vegetable fatty acids lubricated die system produces urea fertilizer tablets exhibiting the highest mechanical strength for the range of compaction stresses utilized in this work. Unlubricated die system produces urea fertilizer tablets having low tensile strengths. It can be concluded that a lubricated die system produces mechanically stronger urea fertilizer tablets and the performances of both the vegetable fatty acids and magnesium stearate lubricants are dependent upon the compaction stress.

ACKNOWLEDGEMENT

The funding of this study was provided by Universiti Putra Malaysia Research University Grant project no 05-02-12-1921RU and Graduate Research Fellowship of Universiti Putra Malaysia.

REFERENCES

- Alderborn, G. (2013). Tablet and compaction. In M. Aulton & K. Taylor (Eds.), *Aulton's Pharmaceutics, The design and Manufacture of Medicines, Fourth edition* (pp. 505-549). Edinburgh: Elsevier.
- Anuar, M. S., & Briscoe, B. J. (2009). The elastic relaxation of starch tablets during ejection. *Powder Technology*, 195(2), 96-104.
- Ariyasu, A., Hattori, Y., & Otsuka, M. (2016). Delay effect of magnesium stearate on tablet dissolution in acidic medium. *International Journal of Pharmaceutics*, 511(2), 757-764.
- Bolhuis, G. K., Lerk, C. F., Zijlstra, H. T., & de Boer, A. H. (1975). Film formation by magnesium stearate during mixing and its effect on tableting. *Pharmaceutisch Weekblad*, 110, 317-325.
- Briscoe, B. J., & Evans, P. D. (1991). Wall friction in the compaction of agglomerated ceramic powders. *Powder Technology*, 65(1-3), 7-20.
- Briscoe, B. J., & Rough, S. L. (1998). The effects of wall friction on the ejection of pressed ceramic parts. *Powder Technology*, 99(3), 228-233.
- Fell, J. T., & Newton, J. M. (1970). Determination of the tensile strength of tablets by the diametrical compression test. *Journal of Pharmaceutical Science*, 59(5), 688-691.
- Hiestand, H. E. N., & Smith, D. P. (1984). Indices of Tableting Performance. *Powder Technology*, 38(2), 145-159.
- Jones, C., Koenig, R., Ellsworth, J., Brown, B., & Jackson, G. (2007). *Management of Urea Fertilizer to Minimize Volatilization*. Montana: Montana State University Extension Service.
- Krycer, I., Pope, D. G., & Hersey, J. A. (1982). An evaluation of the techniques employed investigate powder compaction behaviour. *International Journal of Pharmaceutics*, 12(2-3), 113-134.
- Kumar, V., & Kothari, S. H. (1999). Effect of compressional force on the crystallinity of directly compressible cellulose excipients. *International Journal of Pharmaceutics*, 177(2), 173-182.
- Levy, G., & Gumtow, R. H. (1963). Effect of certain tablet formulation factors on dissolution rate of the active ingredient III tablet lubricants. *Journal of Pharmaceutical Science*, 52(11), 1139-1144.
- Mohammed, H., Briscoe, B. J., & Pitt, K. G. (2005). The interrelationship between compaction behaviour and the mechanical strength of pure pharmaceutical tablets. *Chemical Engineering Science*, 60(14), 3941-3947.
- Mollan, M. J., & Celik, M. (1996). The effects of lubrication on the compaction and post-compaction properties of directly compressible maltodextrins. *International Journal of Pharmaceutics*, 144(1), 1-9.
- Nakamura, S., Ishii, N., Nakashima, N., Sakamoto, T., & Yuasa, H. (2017). Evaluation of sucrose fatty acid esters as lubricants in tablet manufacturing. *Chemical and Pharmaceutical Bulletin*, 65(5), 432-441.
- Ragnarsson, G., & Sjogren, J. (1983). Work of friction and network during compaction. *Journal of Pharmacy and Pharmacology*, 35(4), 201-204.
- Shamsudin, I. S., Anuar, M. S., & Tahir, S. M. (2010). Compaction of Sweet Potato (*Ipomoea Batatas* L.) and *Stevia Rebaudiana* Food Powders. *Particulate Science and Technology*, 30(2), 136-144.

- Shamsudin, I. S., Anuar, M. S., Yusof, Y. A., Mohd Hanif, A. H., & Tahir, S. M. (2014). Effect of particle size on direct compaction of urea fertilizer. *Particulate Science and Technology*, 32(6), 544-553.
- Sheikh-Salem, M., & Fell, J. T. (1981). The influence of magnesium stearate on time dependent strength changes in tablets. *Drug Development and Industrial Pharmacy*, 7(6), 669-674.
- Sugimori, K., & Mori, S. (1989). Characterization of die wall pressure to predict capping of flat- or convex-faced drug tablets of various sizes. *Powder Technology*, 58(4), 259-264.
- Tzika, M., Alexandridou, S., & Kiparissides, C. (2003). Evaluation of the morphological release characteristics of coated fertilizer granules produced in a Wurster fluidized bed. *Powder Technology*, 132(1), 16-24
- Watson, C. J., Stevens, R. J., Garrett, M. K., & McMurray, C. H. (1990). Efficiency and future potential of urea for temperate grassland. *Fertilizer Research*, 26(1-3), 341-357.



Two-dimensional Modeling of Water Distribution under Capillary Wick Irrigation System

Rowshon Md Kamal^{1*}, Hadi Hamaaziz Muhammed¹, Mohammad Abdul Mojid², Ruediger Anlauf³ and Mohd Amin Mohd Soom⁴

¹Department of Biological and Agricultural Engineering, Faculty of Engineering, Universiti Putra Malaysia, 43400 UPM, Serdang, Selangor, Malaysia

²Department of Irrigation and Water Management, Faculty of Agricultural Engineering and Technology, Bangladesh Agricultural University, Mymensingh 2202, Bangladesh

³Faculty of Agricultural Sciences and Landscape Architecture, University of Applied Sciences, Osnabrück 49009, Germany

⁴Faculty of Sustainable Agriculture, Universiti Malaysia Sabah, 88400 Kota Kinabalu, Sabah, Malaysia

ABSTRACT

Competition for limited available water for crop production is an ever-increasing issue for farmers due to increasing demand of irrigation water worldwide. Due to high energy cost in operating pressurized irrigation systems, energy-efficient low-pressure wick irrigation systems can play important roles for smallholder greenhouse crop production by ensuring higher water use efficiency than most traditional approaches. The objectives of this study were to investigate HYDRUS 2D-simulated water distribution patterns in soil and soilless growing media, and to evaluate water balance in these media under capillary wick irrigation system. To accomplish these objectives, eggplants (*Solanum melongena* L.) were grown in potted peatgro and sandy clay loam in a greenhouse experiment, water distribution was simulated by using HYDRUS 2D software package and compared with the measured values, and water uptake by the plant roots was determined for water balance calculation. The wetting pattern was found axially symmetric in both growing media (peatgro and

soil) under the wick emitters. The simulated water distribution in both growing media revealed dependency of spatial extent of the wetted zone on water application period and hydraulic properties of the media. The mean absolute error (MAE) in water content over depth varied from 0.04 to 0.10 m³ m⁻³ and

ARTICLE INFO

Article history:

Received: 04 July 2018

Accepted: 30 August 2018

Published: 24 January 2019

E-mail addresses:

rowshon@yahoo.com (Rowshon Md Kamal)

hadiazizm@gmail.com (Hadi Hamaaziz Muhammed)

ma_mojid@yahoo.com (Mohammad Abdul Mojid)

r.anlauf@hs-osnabrueck.de (Ruediger Anlauf)

mohd.amin@ums.edu.my (Mohd Amin Mohd Soom)

* Corresponding author

Current affiliation:

Hadi Hamaaziz Muhammed

Research Center, Sulaimani Polytechnic University, Sulaymaniyah 46001, KRG/Iraq

the root mean square error (RMSE) varied from 0.04 to 0.11 m³ m⁻³. Deviations between the measured and simulated water contents in the peatgro medium were larger over depth than over lateral distance. In contrast, the model criteria matched well for the sandy clay loam and provided MAE of 0.01 to 0.02 m³ m⁻³ and RMSE of 0.01 to 0.03 m³ m⁻³, indicating good agreement between the measured and simulated water contents.

Keywords: Numerical modeling, water balance, water distribution, Wick irrigation

INTRODUCTION

Global agriculture has changed dramatically over the last few decades, and the use of soilless cultures has expanded considerably (Raviv and Lieth 2007). Plant production in containers/pots is characterized as either soilless or soil-based medium; typically, the latter is found in usual practices. Currently, several crops are cultivated on different substrates such as peat, perlite, rockwool, coconut coir and scoria (Bougoul and Boulard, 2006; Naddaf et al., 2011). The soilless substrates are characterized by greater fluctuations in the key variables that affect conditions of crop growth. Compared to mineral soils, soilless media in containers, usually, have a smaller root zone, higher water holding capacity, higher percentage of available water, lower water tension and higher hydraulic conductivity (Schröder & Lieth, 2002). But, supplying too little or too much water results in decreasing plant productivity or, when extreme, can cause plant damage (Raviv and Lieth, 2007). Excessive water application can also cause runoff, causing soil erosion and nutrient loss. Consequently, growers often intend to optimize root-zone conditions for betterment of their crops by looking for new design and implementing systems that allow better control of the root-zone variables. They always look for a cost-effective water- and fertilizer-efficient irrigation system.

Three main types of irrigation system – overhead sprinklers, drippers and sub-irrigation – are commonly used to produce potted plants. The sub-irrigation system includes three irrigation methods: ebb and flow (Ebb) system, capillary mat system and capillary wick system (CWS) (Son et al., 2006). The CWS is often regarded as an efficient system for potted plants since it reduces costs of water and labor compared to conventional irrigation systems (Dole et al., 1994). It is a more efficient and environment-friendly system with minimum water and nutrient loss than other irrigation systems, and it augments water and nutrient uptakes by plants (In et al., 2003) with a resulting higher and good quality production. Additionally, being easy and cheap, the installation and operation of the method are inexpensive (Bainbridge, 2002). A few researchers have developed and tried the capillary wick irrigation system for potted plant production in greenhouses and nurseries in Japan and South Korea (Kwon et al., 1999). They reported avoiding excess water loss and obtaining uniformity in production as the important advantages of CWS. The ability of a capillary wick system in raising water was reported to be 10 to 20 cm (Lee et al., 2010;

Wesonga et al., 2014). The reported disadvantages of the system are that the wick materials become moldy causing development of biological activities in the water reservoirs over time that are likely to hamper water transport (Toth et al., 1988; Bainbridge, 2002) and build up of salt in the upper portion of the growing media when irrigation water is saline (Raviv and Lieth, 2007).

In order to design and manage a cost-effective and efficient capillary wick irrigation system, prior knowledge of the extent of wetted volume of root zone under wick emitters is essential. Furthermore, knowledge about vertical and horizontal distances to which water extends within growing media under a point source is vital in designing efficient micro-irrigation systems. Therefore, two-dimensional modeling is essential for determining the horizontal and vertical directions of water movement within soil profile (Naglic et al., 2012). Type of the wick material controls water absorption from the source/reservoir and distribution into the growing media. Although several studies (Assouline, 2002; Li et al., 2006; Shen and Hao, 2006; Huang and Han, 2011) analyzed relationships between dripper discharge and wetting pattern for drip irrigation, to our knowledge, no studies have yet investigated water distribution and wetting pattern in soils and soilless growing media under wick irrigation system because wetting pattern in growing media under wick irrigation requires accurately measured parameters using several equipment. Also, little is known about two-dimensional modeling of water movement through the root zone and root-water uptake for potted plants. In this study, we investigated two-dimensional water distribution in two growing media – sandy clay loam and peatgro – and their wetting patterns under wick irrigation system and evaluated water balance for the potted plants.

MATERIALS AND METHODS

Container Setup

The experiment was done in a non-controlled greenhouse at a cash-crop field, which is used for teaching and research under the Universiti Putra Malaysia (UPM). Two plastic containers, each of 40 cm diameter and 43 cm height, were used: one for peatgro medium and the other for field soil (sandy clay loam). Each container was located under a PVC pipe, which was connected to a bucket that served as a water source/reservoir (Figure 1). A constant water level was maintained inside the PVC pipe by controlling water entry into it by means of a float placed in the bucket. A 3-cm gravel layer was placed at the bottom of both containers and was covered with nylon net to facilitate drainage and prevent water-logging in the containers. A small hole was made at the base of each container to drain out excess water, if there is any. One container was filled with peatgro and the other with sandy clay loam, which was collected from a vegetable farm of the UPM near the experimental greenhouse. Two representative eggplants (*Solanum melongena* L.) of 8 weeks old were excavated from the vegetable farm and transplanted in the containers. When

filling with the growing media, the containers were instrumented with ECH₂O-5TE data logger–capacitance sensors (Decagon Devices, Pullman, WA, USA) in order to measure water contents of the growing media. Three ECH₂O sensors were installed horizontally in each container, 5 cm away from the trunk of the plant and at 10, 20 and 30 cm depths from the surface of the growing media. Two additional ECH₂O sensors were installed, also horizontally, at 8 and 16 cm lateral distances from the trunk of the plant and at 10 cm depth. Horizontal position of the sensors in the containers enhanced their good contact with the growing media and minimized measurement error. The ECH₂O sensors were calibrated a priori for water content measurement in the two growing media against their gravimetric water contents at different bulk densities. The gravimetric water contents of peatgro were determined by drying the material in oven at 60°C for 48 h following Cobos and Chambers (2010). Following Phogat et al. (2013b), the growing media in both containers with plants were saturated to remove air pockets and make the media settle. The plants were then irrigated manually for 10 days to enable them to adapt to the container environment. Three replicates of the growing media samples were collected in core samplers (5.2 cm diameter × 5 cm height) to determine (only) texture of the soil and bulk density of both media. Water content measurements in the containers with the ECH₂O sensors were initiated after 10 days of planting.



Figure 1. Assembling of the watering system and container planted with eggplants in the growing media (peatgro and soil): (a) view of water control at inlet and (b) wick watering system

Wick Irrigation

Irrigation was applied to the plants in the containers with wick emitter (1 cm width × 25 cm length) having a discharge rate of 0.015 L h⁻¹. The emitter was located on a half-circle of the container surface and 5 cm away from the plant trunk (Figure 1). The quantity of water application was based on evapotranspiration (ET_c) of eggplants grown in greenhouse. In

order to determine ET_c , the growing media in the containers were saturated and, afterwards, allowed to drain out excess water through the opening at the bottom for one hour. Each container with the plant was weighed with an analytical balance immediately after one hour drainage process and also 24 hours after the drainage process. The loss of weight of each container between the two measurements was ET_c , which was expressed in terms of depth over the surface of the growing media in the container. The measurement was repeated for five times during a two-week period. It should be noted that the crop was in the second stage of vegetative and growth period. The observed average ET_c was 5 mm day^{-1} . Irrigation was initiated on 1 September 2014 and terminated on 21 September 2014. Irrigation was applied continuously (24 hours a day) during the 21 days of simulation.

Theory of Numerical Modeling by HYDRUS 2D

Water movement in soil and peatgro medium under capillary wick irrigation system was simulated by employing HYDRUS 2D/3D simulation model of Šimůnek et al. (2012). This software package is capable of simulating two- and three-dimensional variably-saturated water flow, heat transport and transport of multiple solutes. It solves Richard's equation numerically by using finite element method for variably-saturated water flow and advection–dispersion equations for heat, water and solute transports. Additionally, the HYDRUS model allows users to specify water uptake by plant roots that influences spatial distribution of water and salinity of water during irrigation events. Assuming that the air phase does not play any important role in the flow process of water and also water flow due to thermal gradient is negligible, the two-dimensional governing flow equation is described by modifying Richard's equation (Celia et al., 1990) as

$$\frac{\partial \theta}{\partial t} = \frac{\partial}{\partial x_i} \left[K \left(K_{ij}^A \frac{\partial h}{\partial x_j} + K_{iz}^A \right) \right] - S(h, x, z) \quad (1)$$

where θ is volumetric water content (L^3L^{-3}), h is pressure head (L), x_i ($i = 1, 2$) is horizontal coordinate (L), z is vertical coordinate (positive upward), t is time (T), K_{ij}^A are components of a dimensionless anisotropy tensor K^A , K is unsaturated hydraulic conductivity (LT^{-1}) and $S(h, x, z)$ is a sink term that represents root-water uptake (T^{-1}).

HYDRUS 2D/3D code was used to solve Eq. (1) using finite element method on the basis of mass conservative iterative scheme. Water extraction, $S(h, x, z)$, was calculated based on Feddes' model (Feddes et al., 1978), which sets root-water uptake rates according to soil-water pressure head, h , at any point in the root zone. Feddes' model also defines the conditions in which transpiration is reduced below potential when soil cannot supply the amount of water required by crops under predominant climate conditions (Phogat et al., 2012). In addition, additive or multiplicative model can be used for implementing osmotic

head reduction in HYDRUS code; the later model was considered for simulation in this study. Based on space and time, the actual local uncompensated root-water uptake was obtained by (Feddes et al., 1978; van Genuchten, 1987; Šimůnek and Hopmans, 2009)

$$\begin{aligned}
 S(h, h\phi, x, z, t) &= \alpha(h, h\phi, x, z, t)b(x, z, t)S_p(x, z, t) \\
 &= \alpha(h, h\phi, x, z, t)b(x, z, t)L_t T_p(t)
 \end{aligned}
 \tag{2}$$

where $S(h, h\phi, x, z, t)$ is actual volume of water removed from a unit volume of soil per unit time ($L^3 L^{-3} T^{-1}$), $S_p(x, z, t)$ is potential volume of water removed from a unit volume of soil per unit time ($L^3 L^{-3} T^{-1}$), $\alpha(h, h\phi, x, z, t)$ is a prescribed dimensionless stress response function ($0 \leq \alpha \leq 1$) of soil-water pressure head (h) and osmotic pressure head ($h\phi$), $b(x, z, t)$ is a normalized root-density distribution function (L^{-3}), T_p is potential transpiration rate (LT^{-1}) and L_t is width [L] of the soil surface associated with the transpiration process. The actual transpiration rate, T_a (LT^{-1}), was then obtained by integrating Eq. (2) over the root domain Ω_R as

$$T_a(t) = T_p(t) \int_{\Omega_R} \alpha(h, h\phi, x, z, t)b(x, z, t)d\Omega
 \tag{3}$$

The soil-water retention function and unsaturated hydraulic conductivity function were described by using van Genuchten–Mualem constitutive relationships (Mualem, 1976; van Genuchten, 1980) as

$$\begin{aligned}
 \theta(h) &= \theta(r) + \frac{\theta_s - \theta_r}{[1 + (\alpha h)^n]^m} \text{ for } h < 0 \\
 \theta(h) &= \theta_s \text{ for } h \geq 0
 \end{aligned}
 \tag{4}$$

$$K(h) = K_s S_e^l \left[1 - \left(1 - S_e^{\frac{1}{m}} \right)^m \right]^2
 \tag{5}$$

where θ_r and θ_s denote residual and saturated water content, respectively ($L^3 L^{-3}$), $m = (1 - 1/n)$, K_s is saturated hydraulic conductivity ($L T^{-1}$), α is inverse of the air-entry value (L^{-1}), n is a pore-size distribution index >1 , l is a pore-connectivity parameter and S_e is effective saturation given by

$$S_e = \frac{\theta - \theta_r}{\theta_s - \theta_r}
 \tag{6}$$

The governing water-flow and solute-transport equations in the HYDRUS package are solved using Galerkin finite element method applied to a network of triangular elements. The program interface allows users to manipulate time discretization and specification of boundary conditions.

Estimation of Hydraulic Properties of the Growing Media

Running the HYDRUS code requires assigning van-Genuchten parameters (θ_r , θ_s , α , n , l and K_s) to describe soil hydraulic functions (Eqns. (4) and (5)). Direct determination of these soil hydraulic parameters in the field or laboratory is time consuming and costly. So, they were estimated (Table 1) by using ROSETTA model (Schaap et al., 2001), which is a pedo-transfer function software and uses a neural network model to predict the hydraulic parameters from soil data. Soil particle size and bulk density, determined from the soil samples of planted container, were input to the ROSETTA model. The parameter l (Eq. (5)) was taken as 0.5 since this value was estimated for many soils by Mualem (1976). The ROSETTA model cannot, however, provide hydraulic parameters of soilless substrates. So, for peatgro, following Anlauf (2014), the hydraulic parameters were estimated from the measured pF/water-retention values by nonlinear least-square fit using EXCEL solver function.

Table 1
Hydraulic parameters of peatgro and sandy clay loam (Equations 4 and 5) used in model

Growing media	Saturated water content, θ_s ($\text{m}^3 \text{m}^{-3}$)	Residual water content, θ_r ($\text{m}^3 \text{m}^{-3}$)	Inverse air-entry value, α (cm^{-1})	Pore-size distribution index, n	Saturated hydraulic conductivity, K_s (cm day^{-1})	Pore-connectivity parameter, l (-)
Peatgro	0.68	0.0	0.027	2.26	5875.2	0.5
Sandy clay loam	0.39	0.1	0.059	1.48	31.44	0.5

Root Distribution and Water Uptake Parameters

Plant-root distribution influences soil water and salinity distributions in the root domain under micro-irrigation. Because of constrained root growth in a closed system, such as in a container, its distribution for container-grown plants differs substantially from field-grown plants. Phogat et al. (2013b) reported that in a closed system, roots developed more in vertical direction than in horizontal direction. Consequently, the root distribution for eggplants in the container was described by using the model of Vrugt et al. (2001), according to which the two-dimensional root-distribution function, $b(x, z)$, is defined in HYDRUS by

$$b(x, z) = \left(1 - \frac{z}{z_m}\right) \left(1 - \frac{r}{r_m}\right) e^{-\left(\frac{P_z}{z_m}|z^*-z| + \frac{P_r}{r_m}|r^*-r|\right)} \quad (7)$$

where z is depth (L) in the soil/peatgro profile (x, z), z_m is maximum rooting depth (L) of the eggplants that was taken as the depth of container (40 cm), r is radial distance from the plant (L) and r_m is maximum rooting length in radial direction (L) that was taken equal

to the radius of the container (20 cm). In Equation (7), p_z (-), z^* (L), p_r (-) and r^* (L) are all empirical parameters. When transferring the plants to the containers, both horizontal and vertical dimensions of the roots were measured following Phogat et al. (2013b). The parameters z^* and r^* represent, two-dimensionally, the zone of maximum root-water uptake. The value of z^* was taken as 17 cm and that of r^* was taken as 6 cm (Figure 2).



Figure 2. Root distribution of a transplanted eggplant in the potted growing media

Hanson et al. (2006) considered the values of p_z and p_r for tomato plant to be unity. The root system of tomato is considered mostly similar to that of eggplant and, consequently, p_z and p_r were set equal to one except for $r > r^*$ and $z > z^*$ when they became zero (Ramos et al., 2012). The effects of water stress reduction were considered from the model of Feddes et al. (1978). The assigned model parameters are given in Table 2; the values of the parameters were adopted from tomato to be used for eggplants following Selim et al. (2013).

Table 2
Recommended parameters of Feddes et al. (1978) model for evaluating the effects of water stress reduction

Growing media	Parameters of Feddes et al. (1978) model						
	p_o (cm)	p_{opt} (cm)	p_{2H} (cm)	p_{2L} (cm)	p_3 (cm)	r_{2H} (cm day ⁻¹)	r_{2L} (cm day ⁻¹)
Peatgro	-1	-2	-25	-50	-100	0.5	0.1
Sandy clay loam	-1	-2	-800	-1500	-8000	0.5	0.1

- p_o : pressure head below which plant roots begin to extract water from the soil
- p_{opt} : pressure head below which plant roots extract water at the maximum rate
- p_{2H} : limiting pressure head below which plant roots are not able to extract water at the maximum rate at potential transpiration rate of 0.5 cm day⁻¹
- p_{2L} : limiting pressure head at potential transpiration rate of 0.1 cm day⁻¹
- p_3 : pressure head below which plant roots stop uptaking water, which is usually taken at wilting point
- r_{2H} : potential transpiration rate at which the limiting pressure head allows extracting water at the maximum rate
- r_{2L} : potential transpiration rate at which the limiting pressure head allows extracting water at the minimum rate

Multiplicative models were employed to combine the effects of water and salinity stress on root-water uptake. The threshold model of Maas (1990) was used to describe the osmotic effects with a threshold EC_e of 2.5 dS m^{-1} to correspond to EC of the nutrient solution, and the decline per unit increase (slope) in EC_e beyond the threshold value was fixed at 5% following Ünlükara et al. (2010). Note that, in HYDRUS, the simulation model requires salinity of nutrient solution as input.

Flow Domain and Simulations

HYDRUS 2D/3D was employed to simulate transient axis-symmetrical two-dimensional movement of water and solute by assuming that a two-dimensional problem approximates a three-dimensional flow process. The simulation domain was represented by a 40-cm deep and 20-cm wide half of cylindrical cross section of the growing media. A 25-cm long wick was set 5 cm away from the plant trunk in the containers. The transport domain was discretized into 3321 nodes, which corresponded to 6400 structured triangular elements as illustrated in Figure 3. The observation nodes corresponded to the locations where the five ECH_2O sensors were installed (three sensors at 10, 20 and 30 cm depth, and two sensors at 10 cm depth and at 8 and 16 cm lateral distance from the plant trunk). Simulations were done for sandy clay loam and peatgro medium over a period of 21 days without interruption.

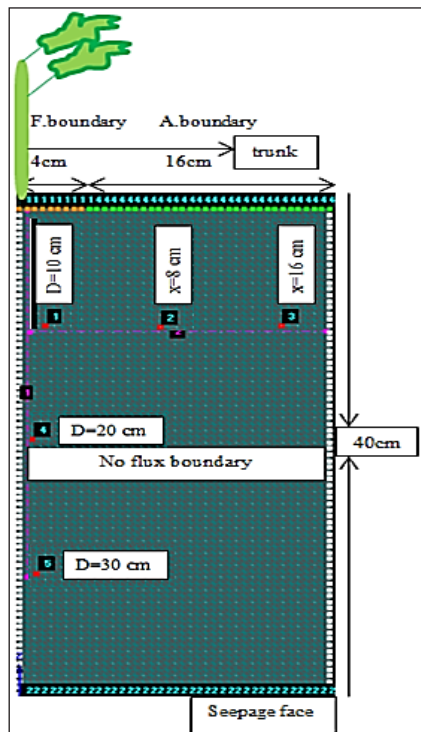


Figure 3. Axisymmetrical domain geometry of potted growing media with finite element discretization used in HYDRUS 2D simulations with observation nodes

Initial and Boundary Conditions

HYDRUS 2D/3D requires setting boundary conditions along the outer sides of the flow domain. The upper surface of the growing media was subject to atmospheric boundary condition with a constant flux of 6.96 cm day⁻¹ (0.015 L h⁻¹) imposed by the wick emitter that resulted in a two-dimensional axis-symmetrical water flow. The boundary flux of half circle was set on 4 cm since the wetted diameter of the surface was 8 cm. The atmospheric boundary conditions were represented by actual evaporation ($E_a = 0.3 \text{ cm day}^{-1}$) and actual transpiration ($T_p = 0.2 \text{ cm day}^{-1}$). The vertical sides of the flow domain were no flow boundaries except for a 2-cm seepage face at the bottom boundary. The flux was determined by dividing wick discharge (370 cm³ day⁻¹) by the area of wetted surface (50.24 cm²). The discharge of the wick (q_e , ml day⁻¹) was quantified by

$$q_e = 32.85 h_c^{-0.26} \tag{8}$$

where h_c is capillary height of water (cm) in the wick. The initial soil-water distribution was based on the ECH₂O sensor-measured values that varied from 0.22 to 0.27 m³ m⁻³ from top to the bottom of the container. The initial peatgro-water distribution varied from 0.20 to 0.30 m³ m⁻³ from top to the bottom of the container.

Statistical criteria

The performance of the model was evaluated by comparing the measured and HYDRUS-2D-simulated water-content distributions at different positions of the soil and peatgro medium at different times. The quantitative measures of uncertainty, MAE and RMSE, were estimated by

$$MAE = \frac{1}{N} \sum_{i=1}^N |M_i - S_i| \tag{9}$$

and

$$RMSE = \sqrt{\frac{1}{N} \sum_{i=1}^N (M_i - S_i)^2} \tag{10}$$

where M_i and S_i are the measured and simulated values of an output variable and N is the number of observations.

RESULTS AND DISCUSSION

Water Distribution and Wetting Pattern in the Growing Media

Tables 3–6 compare simulated water contents in the two growing media at different depths, lateral distances from the wick emitter and times with their measured water contents

within the flow domain. The distribution of water in the two growing media reflects water availability for eggplants, and plays an important role in water flow through the root zone. Two statistical indicators, MAE and RMSE, evaluated the level of agreement between the simulated and measured water contents at 10, 20 and 30 cm depths, and at 8 and 16 cm lateral distances with 10 cm depth. The measured water contents matched the simulated values well, both spatially and temporally, for the soil, but the agreement between the measured and simulated water contents was fair for the peatgro medium.

Water contents in the peatgro at all depths increased gradually with time until 15th day of simulation, and then decreased gradually during the following five days as illustrated in Figure 4. The decrease in water content with depth in the later days was attributed, mainly, to reduced wick efficiency as demonstrated by the observed lower wick discharge (330 ml day^{-1}) in the last week of simulation than that (370 ml day^{-1}) at the beginning of

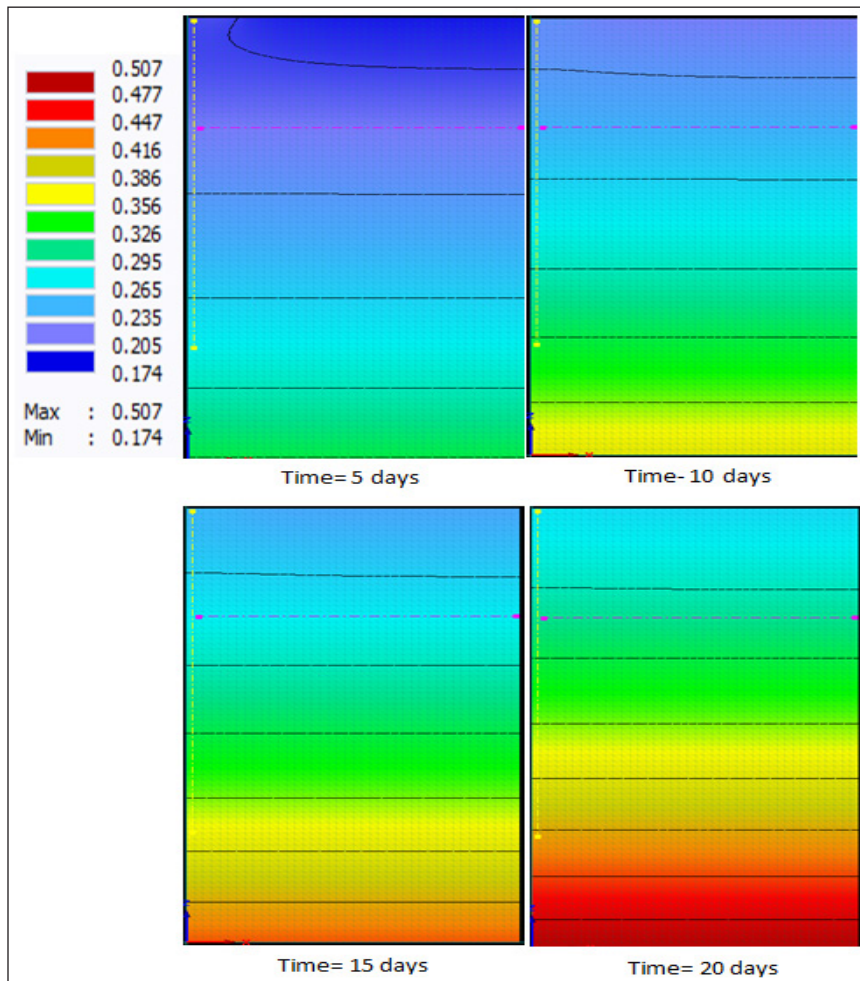


Figure 4. Distribution of simulated water content ($\text{m}^3 \text{ m}^{-3}$) in the peatgro medium

the experiment. Deeper depths exhibited larger deviations in water content due to that the lower part of the peatgro medium was in contact with the outside air through the drainage opening. Consequently, some water of the medium was lost in the form of evaporation. In contrast, the simulated water content increased with increasing depth; this trend in water content appeared to be more realistic than the trend in the observed water contents. Unlike the deviations in water content over depth, the deviations over lateral distance were more consistent (Table 4). The mean absolute error, MAE, in water contents over depth varied from 0.04 to 0.10 $\text{m}^3 \text{m}^{-3}$ and the RMSE varied from 0.04 to 0.10 $\text{m}^3 \text{m}^{-3}$, indicating considerable deviations between the measured and simulated water contents. The deviations might possibly be related to model input parameters, model structure and, to some extent, measurement errors. The accuracy of simulations also depended on the estimated hydraulic parameters used in the modeling and, hence, they should closely represent the experimental media (Phogat et al., 2012).

Table 3
Comparison of measured (M) and simulated (S) peatgro-water contents ($\text{m}^3 \text{m}^{-3}$) at different times and depths along with the mean absolute error (MAE) and root-mean square error (RMSE) of the water contents

Depth in container (cm)	Time (days)								Statistical indicators	
	5		10		15		20			
	M	S	M	S	M	S	M	S	MAE	RMSE
10	0.27	0.22	0.27	0.25	0.31	0.28	0.27	0.31	0.04	0.04
20	0.26	0.25	0.27	0.29	0.32	0.32	0.25	0.36	0.04	0.06
30	0.23	0.28	0.24	0.33	0.29	0.38	0.25	0.42	0.10	0.11

Table 4
Comparison of measured (M) and simulated (S) peatgro-water contents ($\text{m}^3 \text{m}^{-3}$) at different times and distances from the emitter along with the mean absolute error (MAE) and root-mean square error (RMSE) of the water contents

Distance from emitter (cm)	Time (days)								Statistical indicators	
	5		10		15		20			
	M	S	M	S	M	S	M	S	MAE	RMSE
8	0.20	0.21	0.21	0.24	0.22	0.27	0.24	0.30	0.04	0.04
16	0.19	0.21	0.20	0.24	0.22	0.27	0.23	0.30	0.05	0.05

Similar to peatgro, the simulated water distribution in sandy clay loam was visually compared with the measured water distribution in Figure 5 for 10, 20 and 30 cm depths, and 8 and 16 cm lateral distances from the emitter with 10 cm depth. The water contents and statistical indicators are summarized in Tables 5 and 6. The small values of MAE (0.01 to 0.02 $\text{m}^3 \text{m}^{-3}$) and RMSE (0.01 to 0.03 $\text{m}^3 \text{m}^{-3}$) for water contents at different depths

indicated good matching between the measured and simulated water contents. In case of lateral water distribution, the average MAE and RMSE, both of 0.025, also implied good performance of the model for predicting water contents. It is noted that water distribution

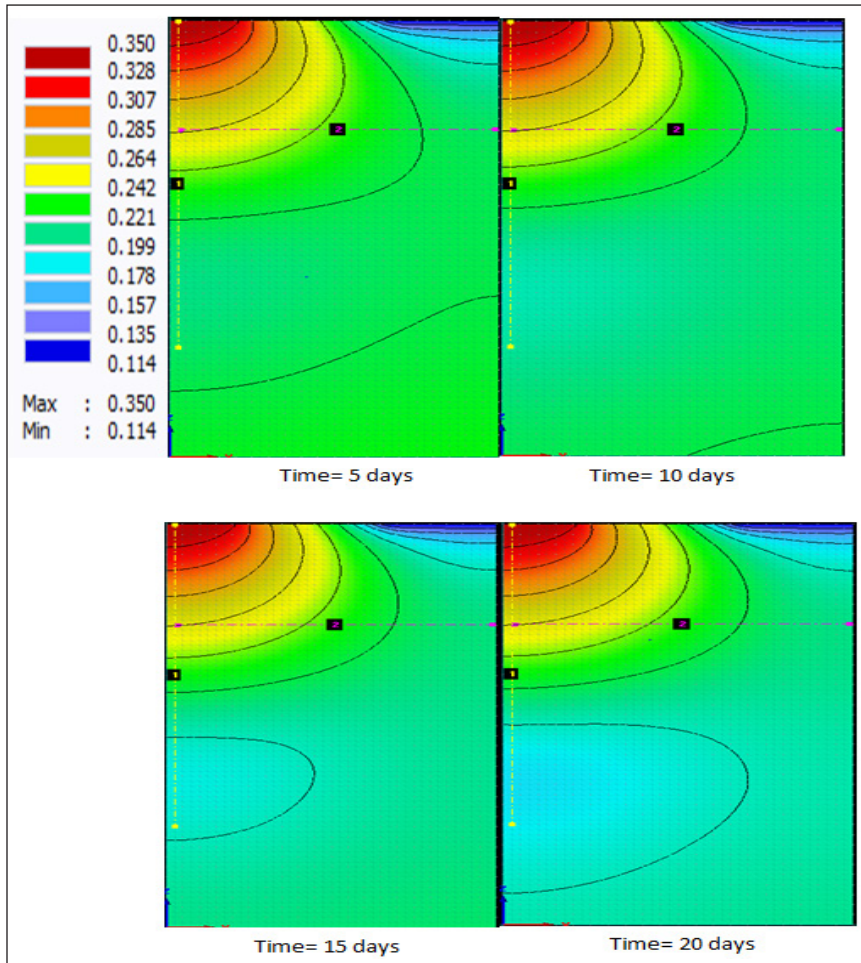


Figure 5. Distribution of simulated water content ($m^3 m^{-3}$) in sandy clay loam

Table 5
Comparison of measured (*M*) and simulated (*S*) soil-water contents ($m^3 m^{-3}$) at different times and depths along with the mean absolute error (MAE) and root-mean square error (RMSE) of the water contents

Depth in container (cm)	Time (days)								Statistical indicators	
	5		10		15		20			
	M	S	M	S	M	S	M	S	MAE	RMSE
10	0.25	0.26	0.23	0.26	0.25	0.26	0.22	0.26	0.02	0.03
20	0.24	0.23	0.21	0.23	0.20	0.22	0.21	0.22	0.02	0.02
30	0.23	0.21	0.21	0.20	0.19	0.19	0.17	0.18	0.01	0.01

Table 6

Comparison of measured (*M*) and simulated (*S*) soil water contents ($m^3 m^{-3}$) at different times and distances from the emitter along with the mean absolute error (MAE) and root-mean square error (RMSE) of the water contents

Distance from emitter (cm)	Time (days)								Statistical indicators	
	5		10		15		20			
	M	S	M	S	M	S	M	S	MAE	RMSE
8	0.22	0.20	0.20	0.17	0.17	0.14	0.14	0.12	0.03	0.03
16	0.20	0.18	0.17	0.14	0.14	0.12	0.13	0.12	0.02	0.02

over depth was different in sandy clay loam from that in the peatgro medium. Both the measured and simulated water contents in the soil decreased with increasing depth, showing that a balance between the wick discharge and crop evapotranspiration was established.

The comparison of water-content distributions in the two growing media revealed that the wetted volume and lateral movement of water were greater in peatgro than in sandy clay loam during the simulation period. Because of different hydraulic properties (residual and saturated water contents), the peatgro medium could uptake water again and redistribute it, thus increasing the wetted volume and length of lateral movement. The low discharge rate of emitter, on the other hand, allowed more water to move in the vertical direction than in the horizontal direction (Badr and Taalab, 2007). The close agreement between the measured and simulated water contents in the two growing media demonstrated that the HYDRUS 2D/3D software package can successfully predict water movement in different growing media-filled containers planted with eggplants. Phogat et al. (2012), Ramos et al. (2012) and Phogat et al. (2013a & b) also reported good performance of HYDRUS 2D/3D for predicting water movement in different soils.

Water Balance Components

The water balance is based on the law of mass conservation, based on which the change in water content (ΔS) in a given volume of a growing medium in a given period of time is equal to the difference between the amount of water added to the medium and the amount of water withdrawn from it. The water balance is thus expressed by (Phogat et al., 2013a)

$$\Delta S = I + R + ET - D \quad (11)$$

where *I* is irrigation, *R* is rainfall (not present in greenhouse experiment), *ET* is crop evapotranspiration and *D* is drainage, the dimensions of all components of Eq. (11) are in length. The simulated components of water balance over the 21-day experimental period are provided in Tables 7 and 8. The measured drainage was nil/zero during the experimental period. HYDRUS 2D/3D also simulated zero drainage during this period (Table 7). With a drip irrigation system, on the other hand, the amount of drainage could be up to 49% of

the total water balance in a planted container (Phogat et al., 2013b). So, there is a clear advantage of the capillary wick system in saving irrigation water. Also, the simulated root-water uptake (actual transpiration, T_a) was 17.5% of the applied water in the potted peatgro medium against 52.7% of the applied water in sandy clay loam, implying a lower water uptake rate in coarse texture medium than in fine texture medium. Selim et al. (2013) also observed similar results; root-water uptake rate was lower in sand than in loamy sand. As depicted in Figure 6, root-water uptake rate varied from 1.4 to 1.6 mm day⁻¹ for peatgro and 1.7 to 2.0 mm day⁻¹ for sandy clay loam. The closely matched potential root-water uptake and actual root-water uptake (Table 8) under capillary wick irrigation indicated high irrigation efficiency of the wick system. In addition, the wick irrigation system can be controlled and adjusted to the water requirement of plants. Evaporation from the peatgro medium was 65.6% of the applied water (Table 7) that was considerably large compared to evaporation from sandy clay loam (47.3%). Argo (1998) reported a surface evaporation loss of 50% of applied water from the peatgro medium. The evaporation loss depends, mainly, on the component materials of the growing media in addition to the prevailing climatic conditions. Any fiber material in the growing medium adopts the role of capillary tube, and accelerates evaporation by transporting water to the medium surface (Argo, 1998). The simulated water balance in the two growing media under slightly, but sustained, deficit irrigation demonstrated that plant roots were forced to extract whatever water was applied and stored in the root zone.

Table 7
Simulated components of water balance of the source and sink after 21 days

Components		Peatgro medium		Sandy clay loam	
		(mm)	(%)	(mm)	(%)
Sources	Irrigation	105.0	66.2	105	82.0
	Soil-water depletion	53.7	33.8	23.0	18.0
Sinks	Actual root uptake	54.7	34.4	67.5	52.7
	Evaporation	104.3	65.6	60.5	47.3
	Drainage	0	0	0	0

Table 8
Simulated components of daily water balance under capillary wick irrigation

Components	Peatgro medium	Sandy clay loam
	(mm day ⁻¹)	(mm day ⁻¹)
Potential root-water uptake	2	2
Actual root-water uptake	1.67	1.77
Evaporation	3	1.8
Drainage	0	0

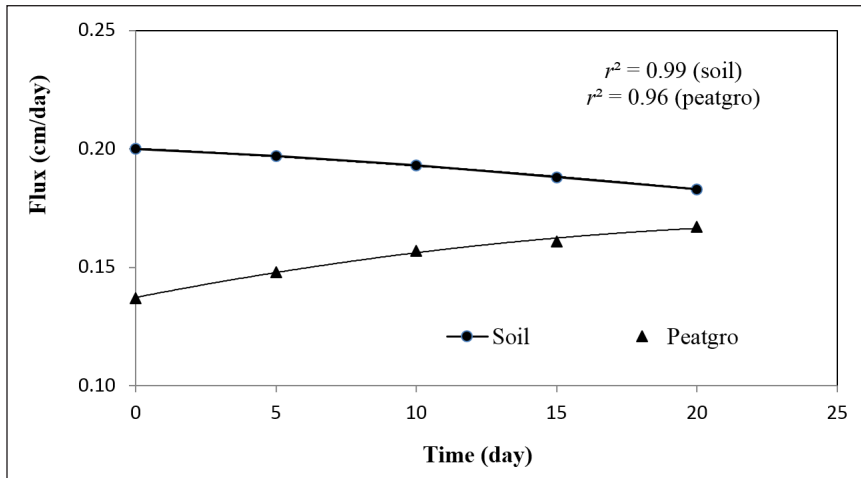


Figure 6. Simulated actual root-water uptake for sandy clay loam and peatgro medium

CONCLUSION

Water distribution pattern in the crop-growing media under wick emitters differed from traditional and modern watering methods in that the emitters' flow wetted the growing media in an axially symmetric pattern rather than in a one-dimensional pattern. This study combined HYDRUS 2D modeling with potted eggplant cultivation in two growing media and compared simulated and measured water contents as well as estimated root-water uptake under capillary wick irrigation system. Water application period and hydraulic properties of the growing media controlled spatial extent of the wetted zone in the media. Water movement below the emission point was more prominent in vertical direction than in horizontal direction. Consequently, for growing media with high infiltration capacity like peatgro, capillary wick irrigation is recommended from top of the media instead of within the media in order to retain water and fertilizer for a prolonged time. The observed and simulated zero drainage over a 21-day experimental period demonstrated no water wastage in capillary wick irrigation system with high efficiency. Water-uptake efficiency was higher in sandy clay loam (finer medium) than in peatgro medium (coarser medium). The predicted water distribution agreed well with the observed values for both growing media with relatively small MAE and RMSE; however, the model performed better for sandy clay loam than for the peatgro medium. Although, the potential and actual root-water uptakes agreed well, the later (1.77 mm day^{-1}) was higher in sandy clay loam than in the peatgro medium (1.67 mm day^{-1}). The predicted surface evaporation over 21 days accounted for 65.6% of the applied water in peatgro medium against 47.3% in sandy clay loam. More experiments and modeling study over longer time period are needed to assess maximum lateral extent of water distribution, and water and nutrient uptake by potted plants under wick irrigation system.

ACKNOWLEDGMENTS

This research was supported by a grant of Universiti Putra Malaysia (UPM). The authors gratefully acknowledge the financial support from the Putra Grant No: 9411100 of UPM. They also acknowledge the supports rendered by the staffs of the Laboratory and Technology Park UPM (TPU) for providing technical supports in conducting the experiments.

REFERENCES

- Assouline, S. (2002). The effects of micro-drip and conventional drip irrigation on water distribution and uptake. *Soil Science American Journal* 66(5), 1630-1636.
- Anlauf, R. (2014). *Using the EXCEL solver function to estimate the van Genuchten parameters from measured pF/water content values*. Retrieved July 4, 2017, from <http://www.al.hs-osnabrueck.de/anlauf.html>
- Argo, W. R. (1998). Root medium physical properties. *Horticulture Technology*, 8(4), 481-485.
- Badr, M., & Taalab, A. (2007). Effect of drip irrigation and discharge rate on water and solute dynamics in sandy soil and tomato yield. *Australian Journal of Basic Applied Science*, 1(4), 545-552.
- Bainbridge, D. A. (2002). Alternative irrigation systems for arid land restoration. *Ecological Restoration*, 20(1), 23-30.
- Bougoul, S., & Boulard, T. (2006). Water dynamics in two rockwool slab growing substrates of contrasting densities. *Scientia Horticulturae*, 107(4), 399-404.
- Cobos, D. R., & Chambers, C. (2010). *Calibrating ECH2O soil moisture sensors*. Decagon Devices, Application Note. Retrieved July 4, 2017, from <http://citeseerx.ist.psu.edu/viewdoc/download?doi=10.1.1.559.4409&rep=rep1&type=pdf>
- Celia, M. A., Bouloutas, E. T., & Zarba, R. L. (1990). A general mass-conservative numerical solution for the unsaturated flow equation. *Water Resources Research*, 26(7), 1483-1496.
- Dole, J. M., Cole, J. C., & von Broembsen, S. L. (1994). Growth of poinsettias, nutrient leaching, and water-use efficiency respond to irrigation methods. *Scientia Horticulturae*, 29(8), 858-864.
- Feddes, R. A., Kowalik, P. J., & Zaradny, H. (1978). *Simulation of field water use and crop yield*. Wageningen: Centre for Agricultural Publishing and Documentation.
- Hanson, B. R., Šimůnek, J., & Hopmans, J. W. (2006). Evaluation of urea–ammonium–nitrate fertigation with drip irrigation using numerical modeling. *Agricultural Water Management*, 86(1), 102-113.
- Huang, Z. Y., Liu, R. X., & Han, L. B. (2011). Dynamics of water movement in subsurface soil of drip irrigation lawn. *Journal of Northwest Forestry University*, 26(5), 59-65.
- So, S., Kang, H., Cho, K. H., & Lee, C. W. (2003). Production of cyclamen using capillary wick system: I. influence of wick material and root substrate composition. *Journal of Korean Flower Resources Society*, 11(2), 199-206.
- Kwon, K. M., & Broschat, T. K. (1999). Differences in bedding plant growth and nitrate loss with a controlled-release fertilizer and two irrigation systems. *Horticulture Technology*, 9(2), 206-209.

- Lee, C., So, I., Jeong, S., & Huh, M. (2010). Application of subirrigation using capillary wick system to pot production. *Journal of Agriculture and Life Science*, 44(3), 7-14.
- Mingsi, L., Shaozhong, K., & Haiyan, S. (2006). Relationships between dripper discharge and soil wetting pattern for drip irrigation. *Transactions of the Chinese Society of Agricultural Engineering (Transactions of the CSAE)*, 22(4), 32-35.
- Liu, Z., Li, P., Hu, Y., & Wang, J. (2015). Wetting patterns and water distributions in cultivation media under drip irrigation. *Computers and Electronics in Agriculture*, 112, 200-208.
- Maas, E. (1990). Crop salt tolerance. In K. K. Tanji (Ed.), *Agricultural Salinity Assessment and Management* (pp. 262–304). New York: American Society of Civil Engineering.
- Mualem, Y. (1976). A new model for predicting the hydraulic conductivity of unsaturated porous media. *Water Resources Research*, 12(3), 513-522.
- Al Naddaf, O., Livieratos, I., Stamatakis, A., Tsirogiannis, I., Gizas, G., & Savvas, D. (2011). Hydraulic characteristics of composted pig manure, perlite, and mixtures of them, and their impact on cucumber grown on bags. *Scientia horticultrae*, 129(1), 135-141.
- Naglič, B., Kechavarzi, C., & Pintar, M. (2012). Modelling of water distribution under drip irrigation systems. *Hmeljarski Bilten*, 19, 100-114.
- Phogat, V., Skewes, M. A., Mahadevan, M., & Cox, J. W. (2013a). Evaluation of soil plant system response to pulsed drip irrigation of an almond tree under sustained stress conditions. *Agricultural Water Management*, 118, 1-11.
- Phogat, V., Skewes, M., Cox, J. W., Alam, J., Grigson, G., & Šimůnek, J. (2013b). Evaluation of water movement and nitrate dynamics in a lysimeter planted with an orange tree. *Agricultural Water Management*, 127, 74-84.
- Phogat, V., Mahadevan, M., Skewes, M., & Cox, J. W. (2012). Modelling soil water and salt dynamics under pulsed and continuous surface drip irrigation of almond and implications of system design. *Irrigation Science*, 30(4), 315-333.
- Ramos, T., Šimůnek, J., Gonçalves, M., Martins, J., Prazeres, A., & Pereira, L. (2012). Two-dimensional modeling of water and nitrogen fate from sweet sorghum irrigated with fresh and blended saline waters. *Agricultural Water Management*, 111, 87-104.
- Raviv, M., & Lieth, J. H. (2007). *Soilless culture: Theory and practice*. San Diego: Elsevier.
- Schaap, M. G., Leij, F. J., & van Genuchten, M. T. (2001). Rosetta: A computer program for estimating soil hydraulic parameters with hierarchical pedotransfer functions. *Journal of Hydrology*, 251(3), 163–176.
- Schröder, F., & Lieth, J. H. (2002). Irrigation control in hydroponics. D. Savvas & H. Passam (Eds.), *Hydroponic Production of Vegetables and Ornamentals* (pp. 263-298). Athens: Embryo Publication.
- Shen, M. W., Hao, S., & Fei, L. (2006). Numerical simulation of the effect of irrigation method on soil water movement in greenhouse. *Journal of Zhejiang University*, 32(2), 186-190.
- Selim, T., Berndtsson, R., & Persson, M. (2013). Simulation of soil water and salinity distribution under surface drip irrigation. *Irrigation and Drainage*, 62(3), 352-362.

- Simunek, J., Van Genuchten, M. T., & Sejna, M. (2012). *The HYDRUS software package for simulating the two-and three-dimensional movement of water, heat, and multiple solutes in variably-saturated media* (Technical Manual Ver. 2). Retrieved July 4, 2017, from https://www.researchgate.net/profile/Jiri_Jirka_Simunek/publication/236901785_The_HYDRUS-2D_Software_Package_for_Simulating_Water_Flow_and_Solute_Transport_in_Two_Dimensional_Variably_Saturated_Media_Version_20/links/565dc02108aeafc2aac88886/The-HYDRUS-2D-Software-Package-for-Simulating-Water-Flow-and-Solute-Transport-in-Two-Dimensional-Variably-Saturated-Media-Version-20.pdf
- Šimůnek, J., & Hopmans, J. W. (2009). Modeling compensated root water and nutrient uptake. *Ecological Modelling*, 220(4), 505-521.
- Son, J., Oh, M., Lu, Y., Kim, K., & Giacomelli, G. (2006). Nutrient-flow wick culture system for potted plant production: System characteristics and plant growth. *Scientia Horticulturae*, 107(4), 392-398.
- Toth, J., Nurthen, E., & Chan, K. (1988). A simple wick method for watering potted plants which maintains a chosen moisture regime. *Animal Production Science*, 28(6), 805-808.
- Ünlükara, A., Kurunç, A., Kesmez, G. D., Yurtseven, E., & Suarez, D. L. (2010). Effects of salinity on eggplant (*solanum melongena* L.) growth and evapotranspiration. *Irrigation and Drainage*, 59(2), 203-214.
- Van Genuchten, M. T. (1980). A closed-form equation for predicting the hydraulic conductivity of unsaturated soils. *Soil Science Society of America Journal*, 44(5), 892-898.
- Van Genuchten, M. T. (1987). *A numerical model for water and solute movement in and below the root zone*. Washington D. C.: United States Department of Agriculture Agricultural Research Service US Salinity Laboratory.
- Vrugt, J., Hopmans, J., & Šimunek, J. (2001). Calibration of a two-dimensional root water uptake model. *Soil Science Society of America Journal*, 65(4), 1027-1037.
- Wesonga, J. M., Wainaina, C., Ombwara, F. K., Masinde, P. W., & Home, P. G. (2014). Wick material and media for capillary wick based irrigation system in kenya. *International Journal of Science and Research*, 3(4), 2319-7064.



Reliability based Redundancy Assessment of a Cogeneration Plant

Meseret Nasir* , Wan Mansor Wan Muhamad and Raja Aziz Raja Maarof

Mechanical Engineering Section, Universiti Kuala Lumpur, Malaysia France institute, 43650 UniKL, Bandar Baru Bangi, Selangor, Malaysia

ABSTRACT

Cogeneration systems are extensively used in Malaysia to produce power as a primary source. However, in the event of cogeneration system failure, the customer or the client are forced to use a redundancy to avoid power interruptions. There are two methods commonly used as a backup in the cogeneration systems which are Generator set and public utility. In order to choose the best redundancy for a particular cogeneration system, it is essential to evaluate the economic benefit analysis by considering several factors such as Maximum demand charge, installation cost and Discount interest. In the evaluation of economic benefit, this study identifies the number of failure and associated downtime using reliability and availability approach, and then present value method was applied. The result shows that the usage of public utility as redundancy is beneficial if the cogeneration system operates within five years period. However, if the cogeneration system operates more than five years, generator set option would be a better option to minimize the total cost. This research also addresses the effect of various factors such as installation cost, maximum demand charge, fuel cost, discount interest rate and production capacity. In general, the output of the research would be beneficial for the plant operator to select the appropriate redundancy option based on the economic advantages.

Keywords: Cogeneration, gas turbine, public utility, redundancy, reliability

ARTICLE INFO

Article history:

Received: 22 January 2018

Accepted: 28 August 2018

Published: 24 January 2019

E-mail addresses:

meseret@unikl.edu.my/meseretreshid@gmail.com (Meseret Nasir)

drwmansor@unikl.edu.my (Wan Mansor Wan Muhamad)

azizmaarof@unikl.edu.my (Raja Aziz Raja Maarof)

* Corresponding author

INTRODUCTION

Cogeneration is a system using a single source of fuel to generate electricity and waste heat (Chen et al., 2018). This waste heat is useful to generate chilled water or steam depending on the customer need(s) (Reshid et al., 2017a, 2017b). The performance of cogeneration system is

linked with availability. In the cogeneration system, high availability is the most important factor to avoid power interruption (Eti et al., 2007). In order to meet high availability, it is necessary that all equipment/subsystems of cogeneration plant remain in upstate condition for a longer duration of time. In other words, it is imperative for all subsystems to perform satisfactorily during their expected life span.

The performance of a cogeneration system relies on the availability and operating conditions of the equipment (Ramesh & Saravannan, 2011b). In a situation of a 1% reduction in availability for a macro cogeneration system, this results in unplanned shutdowns which causes about \$500,000 loss of income (Meherwan, 2002). This economic loss has been estimated to be about 30% of the total cost of electricity generated by the cogeneration plant (Gräber, 2004; Lemma & Hashim, 2013). Such a proportion of expenditure is considered higher than what is encountered in other industries. One of the main reasons for the reduction of availability is failure. Failure is an unavoidable phenomenon which can occur unexpectedly. When failure occurs, efforts are needed to maintain the system and avert the associated risk due to it. The common practice to avert the associated risks due to failure is using redundancy or back up system. Generally cogeneration system uses two common redundancy options such as Generator set and public utility. Generator set (Genset) refers to a gas turbine driven generator as a redundancy used in a cogeneration plant. On the other hand, public utility refers to a cogeneration plant that taps electricity from the national power grid to avoid power interruptions. When the cogeneration system fails, the clients who are using the system as primary source of power are forced to use redundancy. However, the associated cost using redundancy is very high.

There are four major reasons for the need of redundancy (Pham & Wang, 1996). First is scheduled equipment maintenance. During the scheduled maintenance, the equipment will cease to function, for preventive maintenance or the Overhaul. Therefore, there is a need to have redundancy to continue supplying electric power to the user. The second reason is equipment failure. In such case, the equipment or the system needs to undergo corrective maintenance. During this time, the redundancy needs to supply the required demand to the client. Third is demand variations as the cogeneration plant is highly dependent on environmental conditions. The change in the environmental condition will cause fluctuation in demand. In order to cope with such circumstance, redundancy should be integrated. Finally, redundancy is needed due to special operating conditions. This condition refers to the startup and shutdown of plants which may cause trip or unexpected failure.

The economic analysis of power generating system is more closely linked to system availability and reliability analysis. This is because production interruption is one of the major worry for plant owners (Dougan & Reilly, 1993; Lewis & Lewis, 1987; Vega et al., 1998). The downtime cost in the power plant is very expensive apart from the maintenance cost of the equipment. During the plant outage, power is purchased from other sources to

meet the demand of the utility system. Additionally, as Meherwan (2002) highlights, this can be very costly in terms of operation. Most power purchase agreements have articles which include maximum demand charge payments. This makes the power plant availability crucial for the power generation system (Meherwan, 2002). Unplanned outages may happen during peak generation seasons and usually result in significant losses. Richwine (2004) estimated that forced outages cost from 3 to 4.5 times as much as planned outages. Qiu et al. (2011) had established the failure cost model for power generating equipment in which it estimated the failure cost considering the probabilistic nature of failure. The probabilistic nature of failure was formulated using Weibull distribution. In their study, the cost of repair was only estimated, however; the failure cost should include the downtime cost which was caused by the failure.

Christiansen (2013) estimated unplanned outage events for 388 combined-cycle plants. The author collected 15-years data over 3000 units of the combined cycle power plant. The study identified the causes and durations of forced outages and unscheduled maintenance. Furthermore, reliability and availability were established for each class of plant. The costs to render the unit serviceable for each main outage were calculated, as were net revenues lost due to unplanned outages. Furthermore, Grace and Christiansen (2013) estimated the cost of unplanned outage events for combined-cycle systems. The study provided a detailed listing of events that caused forced and unscheduled maintenance outages in combined-cycle power plants, costs associated with such events and a quantified assessment of the economic impact that such outage events could have on overall maintenance costs and lost revenue.

Although several researches have been done on redundancy of power generating cogeneration plant, there still is lacking of research regarding the suitability of redundancy type to cogeneration plant. In fact, the choice of selecting the redundancy is normally left to the user. Thus, to avoid additional capital expenditure requirements, public utility is normally chosen to as redundancy, without considering the operation costs. From the experience of the cogeneration operators, the use of public utility can be expensive due to high cost of maximum demand charge that comes with, which is neglected in reviewed papers on redundancy. Thus, this paper analyses various redundancy options by considering several factors such as maximum demand charge, installation cost interest discount rate and failure frequency.

METHOD

In order to evaluate the redundancy options of the cogeneration power system, the main requirement is to develop appropriate methodology which includes reliability, availability and economic assessment. The flow chart of the methodology is presented in Figure 1.

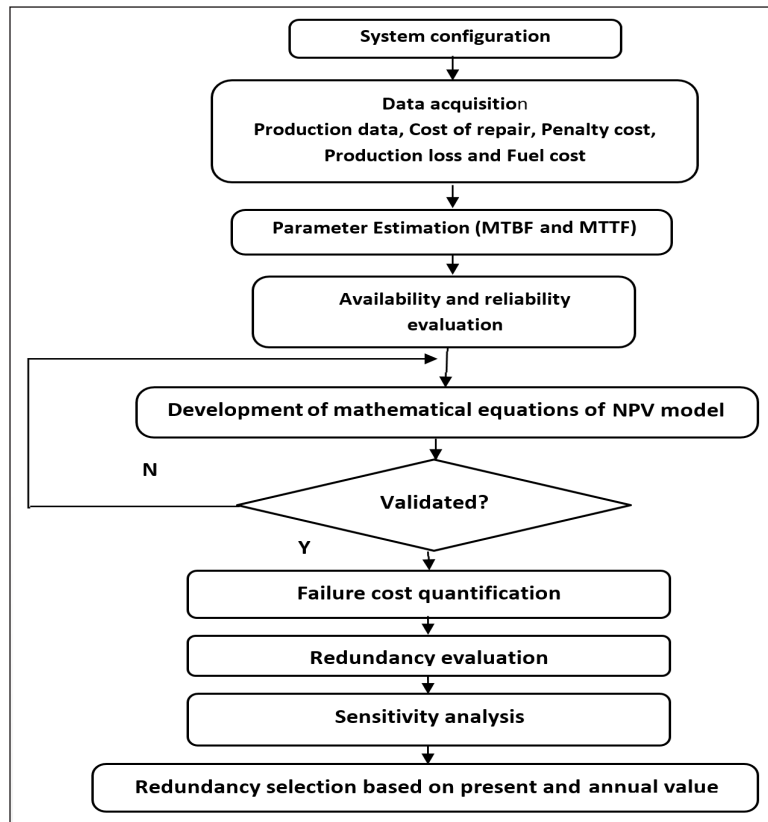


Figure 1. Methodology flow chart

Cogeneration System Configuration and Functional Block Diagram

A cogeneration system is a complex repairable system consisting of various subsystems such as gas turbine, heat recovery steam generator, steam absorption chillers, electric chillers and thermal energy storage systems which are linked in series, parallel or the combination of both (Arora & Kumar, 1997). The general network and configuration of the cogeneration system is depicted in Figure 3 Simulation block for power generation. The two main systems in the cogeneration system are gas-turbine (GT) and heat recovery steam generator (HRSG) (Shaaban et al., 2011; Soares et al., 2001). However, the configuration of cogeneration system differs depending on the consumer requirements and the site condition. Therefore, it is essential to integrate the cogeneration system with steam absorption chiller (SAC), auxiliary gas boiler (AGB), thermal energy storage (TES), and electrical chiller (EC) for the tropical region due to the need for high cooling loads. This fundamental configuration is useful to mitigate the wasted energy and increases the utilisation of the cogeneration system.

As observed in Figure 2, the gas turbine generates electric power and waste heat. The electric power goes to electric chillers and to the customer for electricity usage. The electric chiller uses electricity to produce the chilled water to supplement the high cooling load during the peak hour. This chilled water may also be reserved in the thermal storage. The waste heat generated from the gas turbine goes to heat recovery steam generator to produce steam. This steam is used for process heating in the steam absorption chillers. Finally, the chilled water will be supplied to the customer.

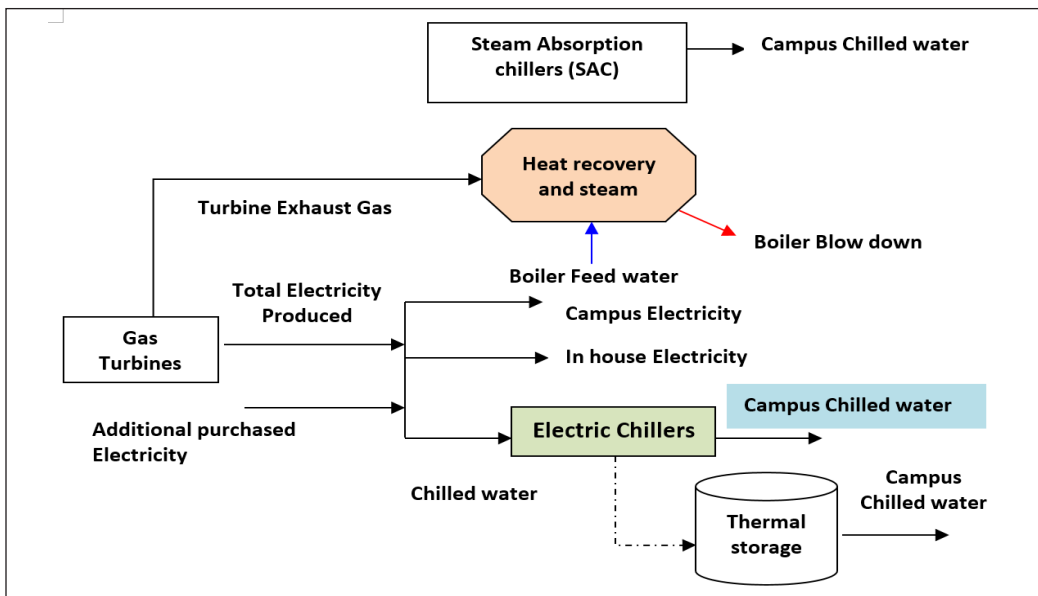


Figure 2. System configuration of cogeneration

Data Acquisition

The required data to develop the models are failure, repair and cost data. The failure and repair data are commonly used to develop the availability and reliability model. Unfortunately, the failure and repair data are scarce in many cases due to improper documentation of maintenance data (Louit et al., 2009). Therefore this study utilizes production data instead of maintenance data in the evaluation of availability and reliability. This is because production data is abundantly available. The operational hourly production data were collected from the plant historical production data and online observation to develop characterization of the cogeneration system for the period of five year. The collected data was filtered to exclude the holidays and schedule maintenance which was identified using calendar and the plant maintenance schedule. The reason is during the holiday or schedule maintenance, the system will be off or the generation capacity will be deliberately reduced. The performance data during this period does not reflect the characteristic of

the system. Thus, this substantiates justification to regard the said period as irrelevant to the analysis. Furthermore, the performance data during start up and shutdown were also excluded from the analysis; because the system performance is low at these periods but most importantly, it is not due to the equipment problem.

The system operation and maintenance cost data were also gathered from the plant and literature to evaluate the redundancy options.

Parameter Estimation

Without reliability and availability assessment, it is difficult to predict the number of failures and downtimes which is used as an input for consequences assessment. In binary system performance evaluation, the equipment is characterized into two states such as working and failed state. These two states of the system can be determined by analysis of the mean time between failure (MTBF) and the mean time to repair (MTTR). MTBF estimates how frequently the system will fail. MTBF is also a basic parameters for reliability (Wang & Sivazlian, 1997). This can be represented by;

$$MTBF = \frac{\text{Accumulated operating time}}{\text{Frequency of failure}} \quad (1)$$

MTTR gauges how quickly the system is back to service. This can be represented by;

$$MTTR = \frac{\text{Accumulated down time}}{\text{Frequency of failure}} \quad (2)$$

In this study, exponential distribution can be used to evaluate the system or equipment reliability and availability for useful period of the bathtub curve (Rausand & Høyland, 2003). The exponential distribution is a good estimation for repairable system as most of the repairable component or system lies in the useful period of the bathtub curve. The useful period of the bathtub curve uses a constant failure rate which means that it can be approximated by the average actual changing rate during the respected time duration.

Equations (3) and (4) are used to define the system or equipment reliability and availability respectively.

$$R(t) = e^{-\lambda t} \quad (3)$$

$$A(t) = \frac{\mu}{\lambda + \mu} + \frac{\mu}{\lambda + \mu} e^{-\left(\lambda + \mu\right)t} \quad (4)$$

where λ is the failure rate and μ is repair rate of the equipment. λ and μ can be defined as Equation (5) and (6) respectively.

$$\lambda = \frac{1}{MTBF} \quad (5)$$

$$\mu = \frac{1}{MTTR} \quad (6)$$

The system reliability of series and parallel system configuration which contain n equipment can be represented by Equation (7) and (8) respectively (Rausand & Høyland, 2003).

$$R_s(t) = \prod_{i=1}^n \exp[-\lambda_i t] = \exp\left(-\sum_{i=1}^n \lambda_i t\right) \quad (7)$$

$$R_s(t) = 1 - \prod_{i=1}^n [1 - \exp(-\lambda_i t)] \quad (8)$$

Similarly, the availability of the series and parallel system can be defined using Equation (9) and (10).

$$A_s(t) = A_1(t)A_2(t)\dots A_n(t) = \prod_{i=1}^n A_i(t) \quad (9)$$

$$\begin{aligned} A_s(t) &= 1 - (1 - A_1(t))(1 - A_2(t))\dots(1 - A_n(t)) \\ &= 1 - \prod_{i=1}^n [1 - A_i(t)] \end{aligned} \quad (10)$$

Using Equations (7)-(10) depending on the configuration of the system, the cumulative number of failure and down time can be found using Equation (11) and (12) respectively.

$$N(t) = \lambda \cdot t \quad (11)$$

$$D(t) = [1 - A(t)] \cdot t \quad (12)$$

where $N(t)$ is the cumulative expected number of failure, $D(t)$ is the cumulative expected down time and λ is the constant system failure rate.

Estimation of Cost of Redundancy

In this section, the associated cost of public utility and Genset were formulated mathematically. Each redundancy options depend on various factors.

Cost of using Public Utility as Redundancy

When the cogeneration system used public utility as redundancy, the operator need to consider maximum demand charge due to hookup electricity from the grid, cost of repair and opportunity loss. Thus, the total expected cost can be estimated by Equation (13)

$$\left[\begin{array}{l} \text{Total Expected} \\ \text{cost of failure} \end{array} \right] = \left[\begin{array}{l} \text{Expected} \\ \text{cost of repair} \end{array} \right] + \left[\begin{array}{l} \text{Expected cost of electricity supplied} \\ \text{by redundancy} \end{array} \right] + \left[\begin{array}{l} \text{Expected cost of} \\ \text{opportunity loss} \end{array} \right] - \left[\begin{array}{l} \text{Expected} \\ \text{fuel save} \end{array} \right] \quad (13)$$

Cost of Repair

When the system failed, corrective maintenance is applied to bring back the system into functional state. The cost of corrective maintenance (C_{cm}) can be defined as Equation (14).

$$C_{cm} = NC_r \quad (14)$$

where N is the frequency of failure per year and C_r is cost of repair per failure.

Maximum Demand Charge

Public utility supplies to a Co-generator in the incident that the Co-generator does not produce electricity due to plant failure. The Co-generator has an option of firm or non-firm supply. Non-firm standby means that public utility does not guarantee that supply can be given when the Co-generator fails. Due to its connection to public utility, maximum demand charge cost is imposed when the system fails. This cost is highly dependent on the frequency of the failure. The maximum demand charge cost per year (C_p) can be estimated using Equation (15)

$$C_p = NC_{Max}KZ \quad (15)$$

where C_{Max} is the Maximum demand charge cost per kw, K is the capacity in kw required per connection, and Z is the percentage ratio of the system hook-up of electricity from redundancy. This means only certain failures which get higher restore time will be hooked up with electricity from redundancy. The minimum waiting time to hook up electricity from redundancy system is based on the contract agreement between the cogeneration plant and the user. Thus, Z can be defined by applying Equation (16) based on the historical data of a cogeneration system.

$$Z = \frac{\text{Number of hook up redundancy due to failure}}{\text{Total failure frequency}} \quad (16)$$

Cost of Supplied Power by Public Utility

During system outage, the plant needs to purchase power from the public utility to avoid the customer damaging cost. This cost can be calculated using Equation (17)

$$C_s = D_t C_R E_R \quad (17)$$

where D_t is the total amount of time the plant would be out of service per year as a result of failure, C_R is cost of electricity rate per kw from public utility and E_R is the amount of energy supplied by the redundancy per hour.

Loss of Opportunity

Whenever the failure occurs, the system is down for repair action. This unavailability of the system will cause opportunity loss. This loss can be represented by

$$C_{Lp} = D_t CL \quad (18)$$

where C is cost per kw charged to clients and L is the possible amount of power delivered to clients during the service outage.

Fuel Save

When the system uses the public utility as redundancy in the event of failure, it is not required to supply the fuel for the cogeneration system as the system is down for maintenance action. This fuel save F_s can be estimated using Equation (15)

$$F_s = C_f D_t Y \quad (19)$$

where C_f is the cost of fuel per GJ and Y is the amount fuel required to operate cogeneration per hour.

Therefore, the annual expected cost of failure (AECF) can be obtained using equation (20)

$$AECF = NC_r + NC_{Max} KZ + D_t CL + D_t C_R E_R + C_f D_t Y \quad (20)$$

Cost of using Gen Set

If the plant uses a Gen set as redundancy, three main cost need to be considered, namely capital which is related to installation cost, cost of repaired which is related to maintenance and fuel cost which is related to operation cost. All these costs can be represented by Equation (21)

$$AECF_{GenSet} = [C_i Q] \left[\frac{A}{P}, i, m \right] + NC_r + D_i C_f L \quad (21)$$

where Q is the capacity of redundancy, C_i is the cost of installation per KW and C_f is the cost of fuel to operate the Gen set.

The annual expected cost of failure can also be represented by the net present value (PV) using Equation (22) (Sullivan et al., 2000). The present value means the monetary amount that should be deposited at a certain rate to pay outlay after n years. This means that all the annual costs are recalculated to the equivalent value of the present time.

$$PV = AEFC \left(\frac{P}{A}, i, m \right) \quad (22)$$

where $\left(\frac{P}{A}, i, m \right)$ is the present worth factor, m is number of years and i is the interest rate.

RESULTS AND DISCUSSION

Case Study

Universiti Teknologi PETRONAS (UTP) power generation cogeneration was taken as a case study. The availability and reliability of the power generation was linked to the operation of the two parallel gas turbines installed in the plant. The failure of any one of the two gas turbines would cause reduction of power being generated. If both turbines failed, no power will be generated to be supplied to the client. To avoid this occurrence, the system needs to have back up power supply. For the case of this plant, the backup is obtained from the national grid. This similar case is being practiced by other cogeneration plants (Haghifam & Manbachi, 2011; Ramesh & Saravannan, 2011a, 2011b; Shaaban et al., 2011). One of the main disadvantages of using the national grid as back up is the high cost of maximum demand charge. This, in turn, leads to high cost charged for any hook up to the national grid when turbine(s) failed. The configuration of power generation system is indicated in Figure 3. In this research, a cogeneration plant which consists of two gas turbines is taken as a case study. The turbines are connected using parallel configuration to produce electricity for the university area as shown in Figure 3. This simulation block diagram is developed using BlockSim software. When both turbines fail, the system used public utility as redundancy. To determine MTBF and MTTR, five years of historical performance data of Gas turbine were used. In order to capture the failure event and MTBF from gas turbine performance, the minimum acceptable performance of the gas turbine was determine based five years daily historical and technical data. Thus, 1497KW is considered as minimum acceptable performance for both turbines. Any performance of

gas turbine below the minimum level is considered as the gas turbine in failed state. Based on this assumption, the MTTF, MTBF, downtime, operating hours, and failure event are estimated as shown Table 1.

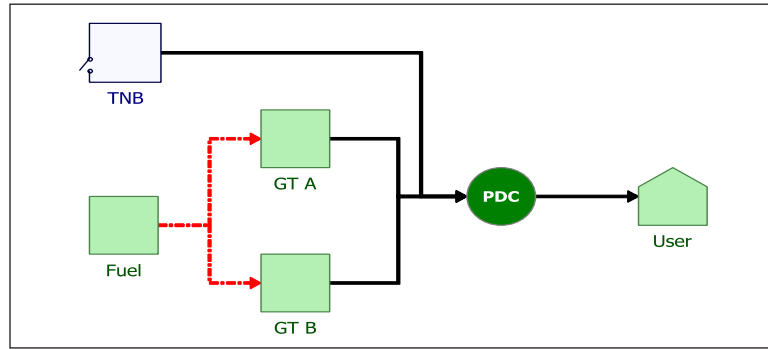


Figure 3. Simulation block for power generation

Table 1
Reliability and availability parameters

Parameters	Unit	Value
Accumulated Operating Hours	Hr	14270
Accumulated Downtime Hours	Hr	594
Failure Frequency	Number of failure	54
MTBF	Hr	264.3
MTTR	Hr	11

Estimation of Availability and Reliability

The availability and reliability analysis were performed using BlockSim software. Figure 4 illustrates the availability of power generation system. The plot reflects that the use of redundancy may enhance the performance of the system. The mean availability of the system with redundancy was about 98% while the mean availability of power generation without redundancy is about 85%. The increment of performance obviously will enhance the profitability of the system and create conducive working environment for the utility plant, even though the cost of redundancy is expensive.

Figure 5 shows the reliability of the system with and without the effect of redundancy. The reliability of the system working without redundancy is less than the system working with reliability. If the system was working without redundancy, there is a high probability that the system may experience a failure compared to the system working with redundancy.

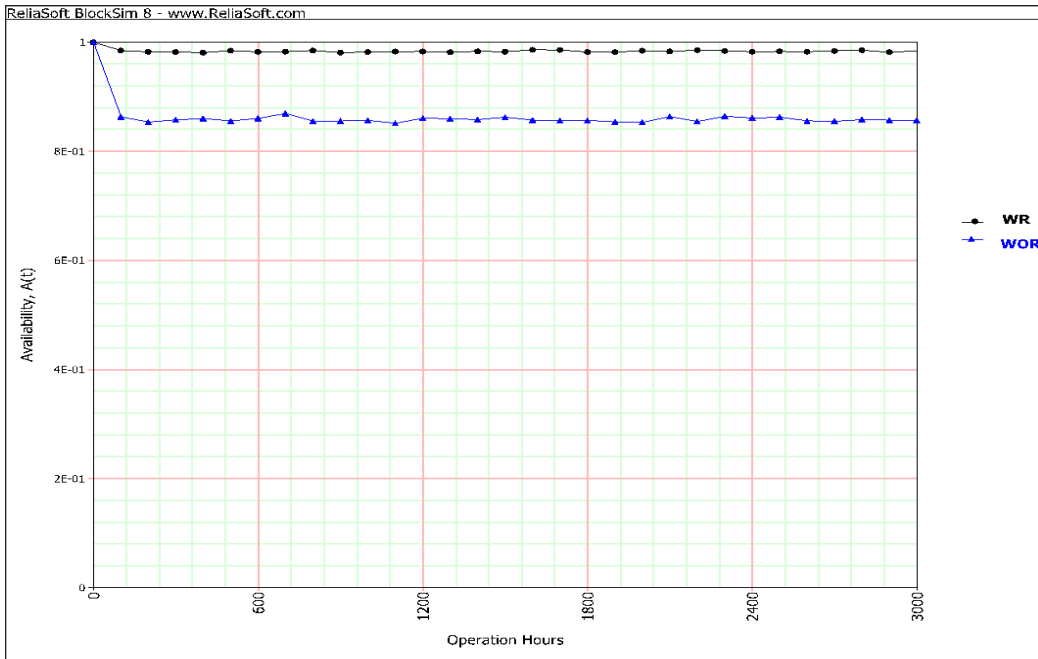


Figure 4. Binary system availability of power generation with redundancy (WR) and without redundancy (WRO)

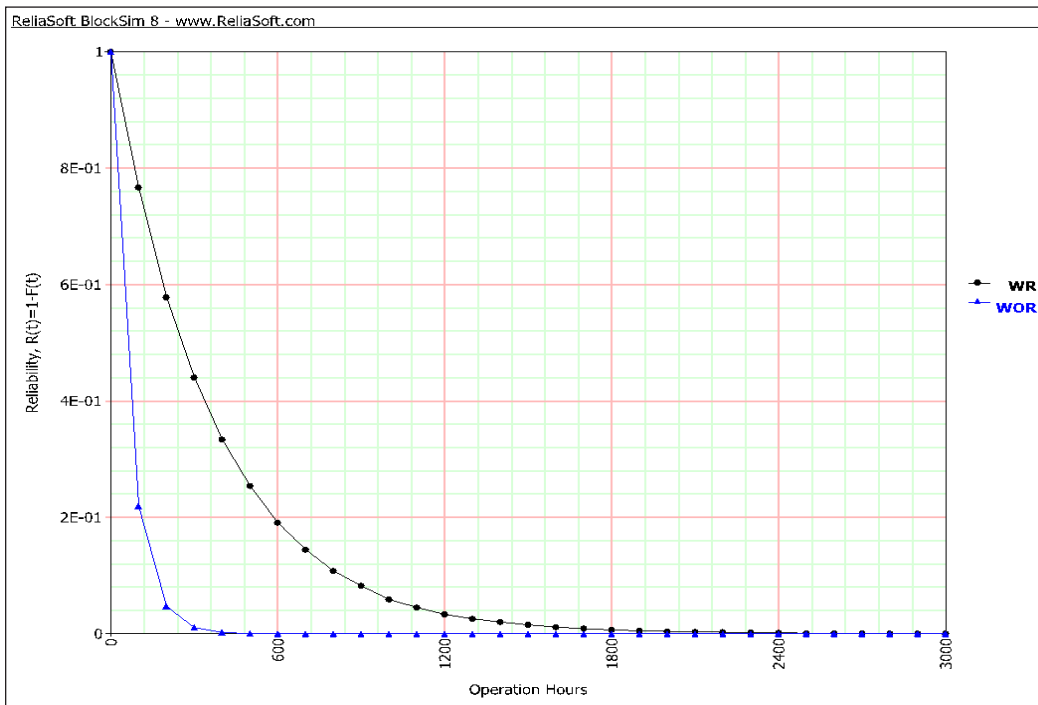


Figure 5. Binary system reliability of power generation system with redundancy (WR) and without redundancy (WRO)

Estimation of Cumulative Number of Failure and Downtimes

Figure 6 and 7 show that cumulative number of failure and downtime of power generation through time respectively. As indicated in the plots, the model predicted value was compared with actual failure frequency and downtime. The validation results show that the model prediction was closer to actual data. This validation results were further confirmed using t-test by considering five years observation data. Table 2 shows that the summary of statistical results using cumulative downtime hours. The statistical results indicate that there is no statistical difference between the predicted and actual downtime and number of failure. The P value results indicate 0.095 and 0.062 for cumulative failure and down time. This mean that statistically no significant different between the model and actual data as the significance value (p) is greater than 0.05 with 95% confidence level.

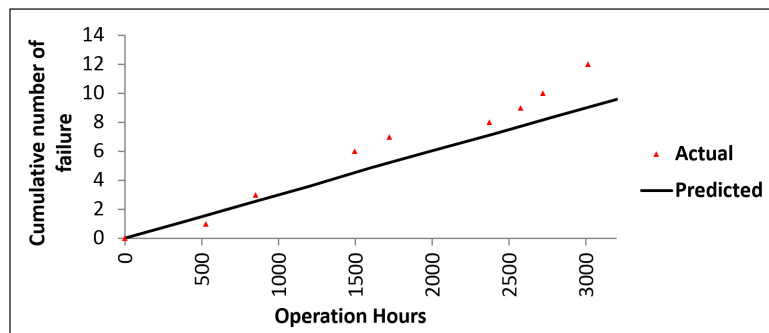


Figure 7. Cumulative downtime hours

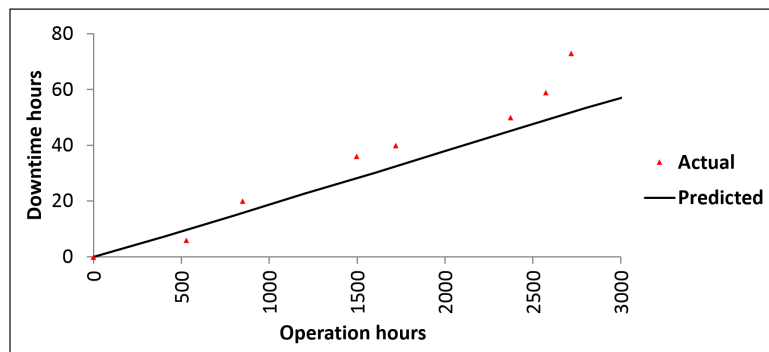


Figure 6. Cumulative number of failures

Table 2
Statistical validation with cumulative number of failures and downtime hours

Statistical Parameters	Cumulative Number of failure	Cumulative downtime hours
P value	0.095	0.062
t critical value	2.2622	2.30600

Validation and Sensitivity Analysis of Redundancy Cost

The system operation and maintenance cost data were also gathered from the plant and literature to evaluate the cost of redundancy. The sample costs data considered in this study are shown in Table 3.

Table 3
Input parameters for redundancy cost evaluation

Parameters	Unit	Values
Cost of Maximum demand	RM / KW	48.6
Cost of Electricity	RM/ KW	0.22
Cost of repair	RM/failure	100000
Cost of fuel	RM/GJ	6.066
Fuel flow	RM/GJ/Hr	49.74
Investment Cost for Gen set	RM/ KW	999
Production cost of Gen set	RM/set	0.17
Current demand of the campus	KW/day	5000
Maximum demand	KW	8400

The expected cost of failure were estimating the cost of failure caused by the actual downtime and failure frequency, and then compared with the cost calculated with the predicted failure and down time using Equation (20) and (21). The results are shown in Table 4 and 5. The estimated present value of failure cost for the actual failure and down time is -RM 7,722,356 while the present cost of failure for predicted failure and down time is RM 7,338,172. The annual value for five years using the actual down time and number of failure is RM 2,545,317 while the annual cost of failure for predicted failure and down time is RM 2,582,199. Based on the present and annual cost of failure, the deviation between the actual and predicted value is 1.43% which falls within acceptable margin. Thus, the developed failure cost model is useful to predict the impact of failure in monetary value.

Table 4
Cumulative failure cost based on actual number of failure and downtimes

Year	Expected Cost of production loss (RM)	Expected Penalty cost	Expected Cost of supplied power	Expected Cost of repair	Fuel cost saving	Total Expected cost of failure
0	0	0	0	0	0	0
1	-53,391	-1,270,353	-69,095	-777,945	18,952	-2,151,833
2	-97,884	-2,328,981	-126,674	-1,426,233	34,746	-3,945,026
3	-134,962	-3,211,171	-174,656	-1,966,473	47,907	-5,439,354
4	-165,859	-3,946,329	-214,641	-2,416,672	58,875	-6,684,628
5	-191,607	-4,558,961	-247,963	-2,791,839	68,015	-7,722,356

Note: The unit of all costs used in this study is Malaysian Ringgit (RM)

Table 5
Cumulative failure cost based on predicted number of failure and downtime

Year	Expected Cost of production loss	Expected Penalty cost	Expected Cost of supplied power	Expected Cost of repair	Fuel cost saving	Total Expected cost of failure
0	0	0	0	0	0	0
1	-73,333	-1,071,630	-56,667	-583,333	-20,115	-1,764,848
2	-128,333	-2,474,955	-99,167	-1,347,222	-35,201	-4,014,476
3	-184,988	-3,325,455	-142,946	-1,810,185	-49,215	-5,414,359
4	-228,095	-4,122,799	-175,845	-2,244,213	-61,039	-6,709,913
5	-265,229	-4,647,799	-204,539	-2,565,715	-71,224	-7,612,057

Note: The unit of all costs used in this study is Malaysian Ringgit (RM)

As can be seen in Figure 8, 58.5% of the failure cost was due to penalty cost (maximum demand charge) of failure, 35.8% was the cost incurred to restore the system, 3.2 % was contributed by the electricity used during downtime of the cogeneration systems and 2.5% was the estimated loss of power due to cogeneration system failure. It can be observed that Maximum demand charge contributes to the high cost of using public utility as a redundancy system for cogeneration plant. Public utility is a power supplied by the national electricity. Basically the use of redundancy is associated with number of failure. This means that it relates further with reliability and availability. Hence, predicting the number of failure and down time will support the development of maintenance strategy, thus reducing the frequency of occurrence for redundancy to be utilized. This also helps in reducing the cost of maximum demand charge to be borne by the client. Essentially, the reliability and availability of the power generation system is enhanced. It also minimizes the cost of failure associated with redundancy.

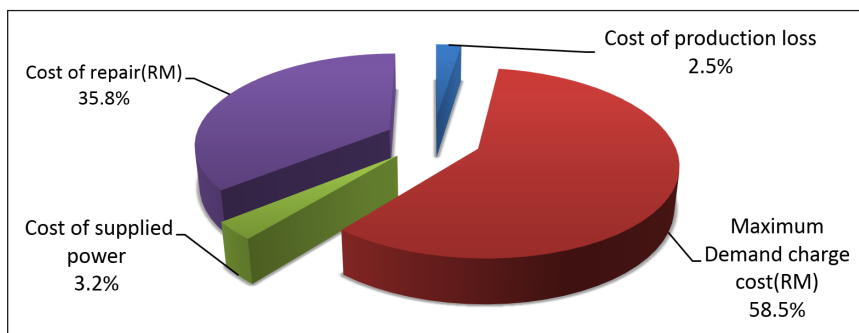


Figure 8. Contribution of failure cost

Spider Plot Analysis

The redundancy selection is affected by several factors such as Maximum demand charge, installation cost and Discount interest. These factors are not constant from place to place and through time as well. In order to analyse the effect of each parameter, the spider plot analysis was used. Figure 9 and 10 showed the effect of various parameters for both redundancy possibilities such as public utility and Gen set respectively. The intersection of each curve with the abscissa shows the decision reversal point - the percentage change from each factor's most likely value at which the PW is zero. As shown in Figure 9, the slope of Maximum demand charge and MARR steeper compare to other factors which means that the PV for public utility is more sensitive to Maximum demand charge and MARR. Similarly, Figure 10 shows the installation cost is more sensitive to Gen set compared to other factors. Thus, the cogeneration operator need to look closely on Maximum demand charge, MARR and installation cost to choose the best redundancy options.

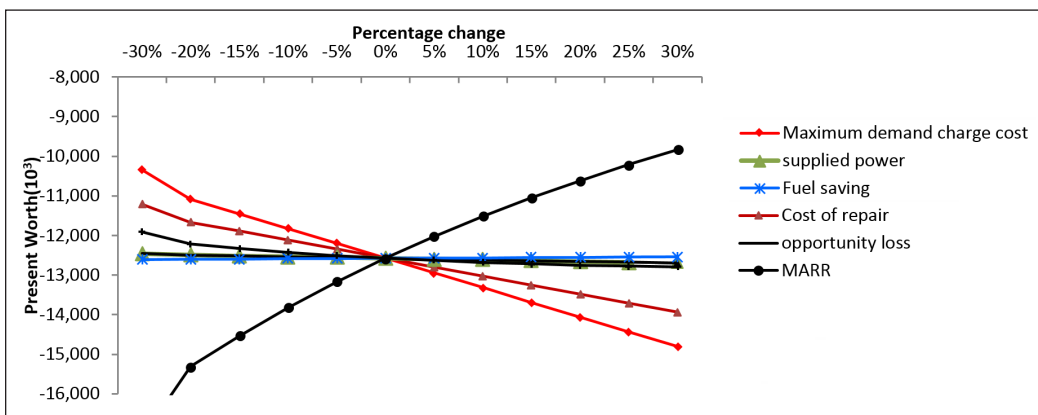


Figure 9. Sensitivity analysis for public utility

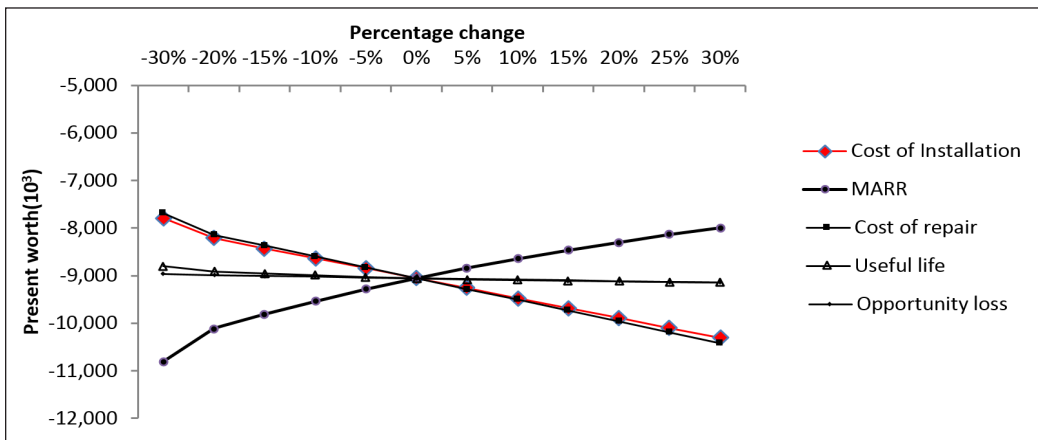


Figure 10. Sensitivity analysis for Gen set

Redundancy Evaluation of Power Generation System

Redundancy is essential for power generation to improve the performance of the system but it is very expensive to operate as it incurs maximum demand charge penalty. To avoid the redundancy totally from the system is difficult because the customer damaging cost of the utility system is substantial. However, one can minimize the effect of redundancy by selecting the suitable type. Currently, the campus electricity generation system uses public utility as redundancy, but it can alternately install Gen set as redundancy options. In order to compare these two redundancy options, Equation (22) were used to estimate the associated present of each redundancy option for a 20 years' life span. The results of present value of each redundancy are presented in Figure 11. This result shows that in the first 5 years, the present value of public utility is less than Gen set which means that it is a better option than Genset if the useful period of cogeneration is less than 5 years. However, when the useful period of cogeneration is greater than five years, Gen set would serve well as the present value is less than public utility. The present value for public utility and Genset redundancy at the end of 20 years were RM11, 948,611 and RM8,721,946 respectively. Thus, by the end of year 20, using Gen set would minimise 24% of the redundancy cost compared to Public utility.

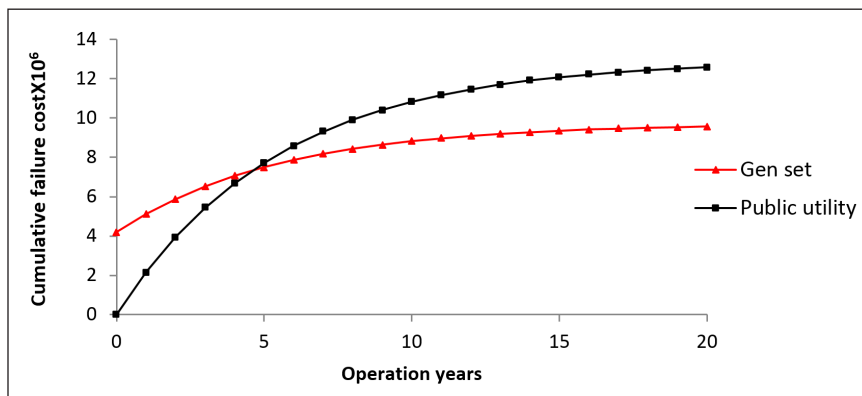


Figure 11. Comparison of Gen set and public utility based on failure cost evaluation

Effect of Installation Cost, Maximum Demand Charge and Discount Interest On Redundancy Selection

There are certain factors which can affect the failure cost of Gen set and public utility such as installation cost, capacity, maximum demand charge, and interest rate. These parameters may vary from time to time or place to place. Thus, there is a need for sensitivity analysis in order to identify the breakeven point for decision making. Regarding installation cost, the information taken from gas turbine hand book (Farmer & De Biasi, 2010) infers that Gen set installation range from approximately \$300 per kW for very large utility-scale

plants to \$1,000 per kW for small industrial cogeneration installation. However, the prices of construction can vary as a result of local labour market conditions and the geographic conditions of the site. Figure 12 shows the effect of cost of installation on annual cost for different redundancy options. The variation in installation cost affect the Gen set redundancy than public utility because the public utility redundancy is already installed and functions with the existing system. The plot result indicates that if the cost of installation was less than RM1714.73 per kW, Gen set would be preferable to public utility. However, if the cost of installation for Gen set is higher than RM1714.73, public utility would be a better option.

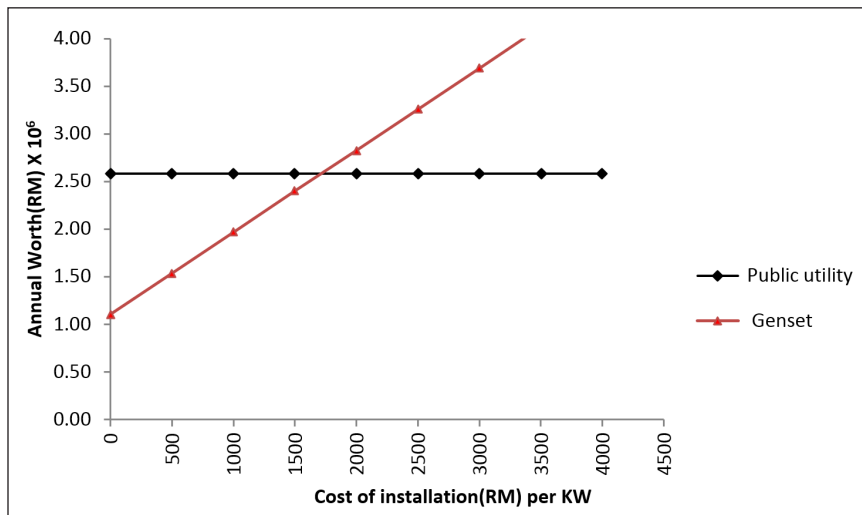


Figure 12. Effect of installation cost on redundancy evaluation

The second factor is the maximum demand charge. The maximum demand costs may vary depending on the plant’s location. In areas where electricity costs are high, for a base-load cogeneration system, its costs can account for up to 70% of the total plant consequence costs. The sensitivity was done by varying the maximum demand charge from RM0 to RM60 per kW. Figure 13 shows that the breakeven value for maximum demand charge cost is RM28.92 per kW. If the maximum demand charge is less than 28.92 kW per hour, using public utility as redundancy could be a better option. On the contrary, if the penalty cost is higher than RM28.92 per kW, Gen set could be a better option.

The installed capacity of the Gen set varies based on the demand of customer and interest of the owner to make a decision on the redundancy. So, one needs to see the effect of installed capacity by comparing with the existing installed public utility. Figure 14 shows the comparison of public utility redundancy with Gen set when the capacity is increasing. The breakeven capacity is 7.43 MW. If the plant installed the Gen set capacity at less than 7.43 MW, the public utility option should be rejected. If the plant installed more than 7.43 MW, it is better to use public utility as redundancy than Gen set.

The minimum attractive rate of return (MARR) is one of the factors that may affect the consequence of failure, which also varies through time. The effect of MARR on redundancy selection is shown in Figure 15. As it can be seen from the graph, if the MAAR is less than 35%, Gen set can be chosen as redundancy. If discount rate is greater than 35%, public utility is the better redundancy option. Spacing is different for this section.

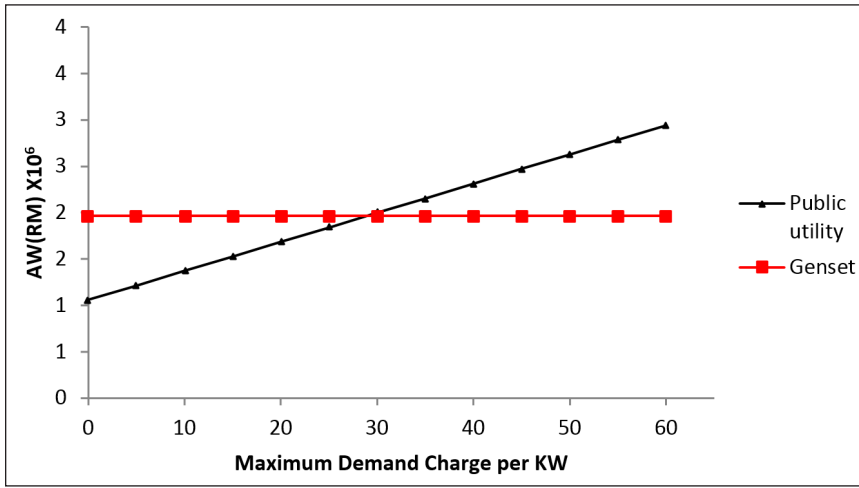


Figure 13. Effect of maximum demand charge on redundancy evaluation

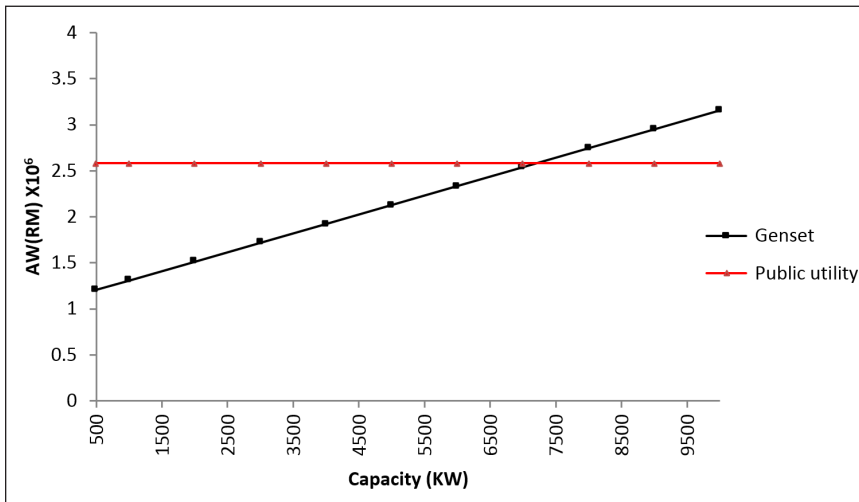


Figure 14. Effect of capacity on redundancy evaluation

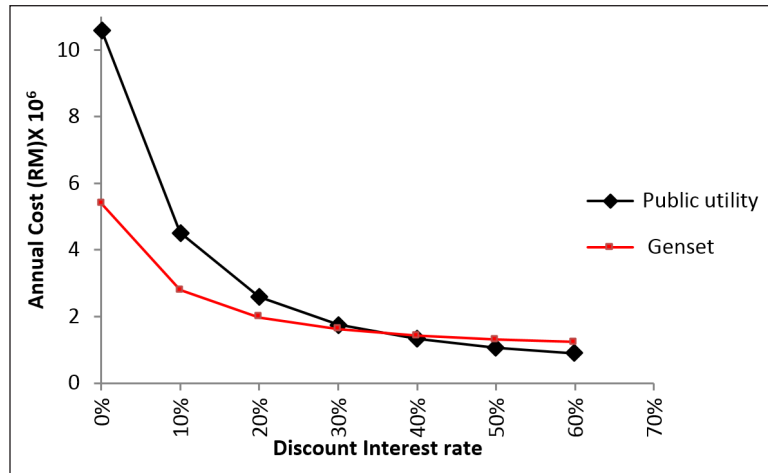


Figure 15. Effect of interest rate on redundancy evaluation

CONCLUSION

This study is very useful as it analyses various redundancy options for cogeneration system from an economic perspective. Furthermore, it developed a reliability based cost model which included reliability and availability concept to analyse the economic benefits on the selection of redundancy for cogeneration plants. This paper also examines various factors which can affect the selection of redundancy. The case study findings indicated that genset redundancy is better if the cogeneration plant operates for a period of more than five years. However, in short term cogeneration operations which accounts for less than five years, the public utility would be a better options. The sensitivity analysis also indicated Maximum demand charge, MARR and installation cost have significant effect on the selection of redundancy. In general, this study is very useful for cogeneration operators to select the best redundancy option which incurs minimum cost.

REFERENCES

- Arora, N., & Kumar, D. (1997). Availability analysis of steam and power generation systems in the thermal power plant. *Microelectronics Reliability*, 37(5), 795-799.
- Chen, H., Xu, J., Xiao, Y., Qi, Z., Xu, G., & Yang, Y. (2018). An Improved Heating System with Waste Pressure Utilization in a Combined Heat and Power Unit. *Energies*, 11(6), 1-20.
- Christiansen, T. (2013). Risk-Based Assessment of Unplanned Outage Events and Costs for Combined-Cycle Plants. *Journal of Engineering for Gas Turbines and Power*, 135, 021801-021801.
- Dougan, K. W., & Reilly, M. C. (1993). Quantitative reliability methods improve plant uptime. *Hydrocarbon Processing: (United States)*, 72(8), 131-141.

- Eti, M. C., Ogaji, S. O. T., & Probert, S. D. (2007). Integrating reliability, availability, maintainability and supportability with risk analysis for improved operation of the Afam thermal power-station. *Applied Energy*, 84(2), 202-221.
- Farmer, R., & De Biasi, B. (2010). Gas turbine world handbook. *Gas Turbine World*, Fairfield, CT.
- Gräber, U. (2004). Advanced maintenance strategies for power plant operators—introducing inter-plant life cycle management. *International Journal of Pressure Vessels and Piping*, 81(10), 861-865.
- Grace, D., & Christiansen, T. (2012, August 30). Quantifying the cost of unplanned outage events for combined-cycle plants. *Energy-Tech Magazine*. Retrieved October 10, 2017, from https://www.energy-tech.com/ram/article_b362347c-4a9d-542a-b9b4-fdd137136342.html
- Haghifam, M. R., & Manbachi, M. (2011). Reliability and availability modelling of combined heat and power (CHP) systems. *International Journal of Electrical Power & Energy Systems*, 33(3), 385-393.
- Lemma, T. A., & Hashim, F. M. (2013). IFDD: Intelligent fault detection and diagnosis-application to a cogeneration and cooling plant. *Asian Journal of Scientific Research*, 6(3), 478-487.
- Lewis, E. E., & Lewis, E. E. (1987). *Introduction to reliability engineering*. New York: Wiley.
- Louit, D. M., Pascual, R., & Jardine, A. K. (2009). A practical procedure for the selection of time-to-failure models based on the assessment of trends in maintenance data. *Reliability Engineering and System Safety*, 94(10), 1618-1628.
- Boyce, M. P. (2011). *Gas turbine engineering handbook*. Waltham: Elsevier.
- Pham, H., & Wang, H. (1996). Imperfect maintenance. *European Journal of Operational Research*, 94(3), 425-438.
- Qiu, G., Xia, C., & Zhang, H. (2011, March). Estimation of Failure Cost in Life Cycle Cost of Power Equipment. In *2011 Asia-Pacific Power and Energy Engineering Conference (APPEEC)* (pp. 1-4). Wuhan, China.
- Ramesh, V., & Saravannan, R. (2011a). Reliability assessment of a co-generation power plant in a sugar mill using fault tree analysis. *Energy Sources, Part A: Recovery, Utilization, and Environmental Effects*, 33(12), 1168-1183.
- Ramesh, V., & Saravannan, R. (2011b). Reliability Assessment of Cogeneration Power Plant in Textile Mill Using Fault Tree Analysis. *Journal of Failure Analysis and Prevention*, 11(1), 56-70.
- Rausand, M., & Høyland, A. (2003). *System reliability theory: models, statistical methods, and applications* (Vol. 396). Hoboken: John Wiley & Sons.
- Reshid, M. N., Muhamad, W. M. W., & Maarof, R. A. R. (2017a). Empirical Analysis of Chilled Water Generation for Off Peak Period of Cogeneration plant Using Neural Network. *International Journal of Applied Engineering Research*, 12(24), 14669-14676.
- Reshid, M. N., Muhamad, W. M. W., & Majid, M. A. A. (2017b). Transient Simulation of a Waste Heat Recovery from Gas Turbine Exhaust. *Journal of Applied Sciences*, 17, 22-31.
- Richwine, R. R. (2004). Casom 18: The relationship between scheduled maintenance and forced outages and its economic impact on selecting availability goals. *World Energy Council, Section 6*, 1-3.

- Shaaban, M., Azit, A. H., & Nor, K. M. (2011). Grid integration policies of gas-fired cogeneration in Peninsular Malaysia: fallacies and counterexamples. *Energy Policy*, 39(9), 5063-5075.
- Soares, J. B., Szklo, A. S., & Tolmasquim, M. T. (2001). Incentive policies for natural gas-fired cogeneration in Brazil's industrial sector—case studies: chemical plant and pulp mill. *Energy Policy*, 29(3), 205-215.
- Sullivan, W. G., Wicks, E. M., & Luxhoj, J. T. (2000). *Engineering economy* (Vol. 12). Upper Saddle River, NJ: Prentice Hall.
- Vega, F., Hill, D. K., & Collins, C. (1998, May). Plant Reliability Analysis in LNG Plants. In *Twelfth International Conference & Exhibition on Liquefied Natural Gas* (pp. 1-22). Perth, Australia.
- Wang, K. H., & Sivazlian, B. D. (1997). Life cycle cost analysis for availability system with parallel components. *Computers & Industrial Engineering*, 33(1), 129-132.

Utilization of Normal and Treated Cement Kiln Dust as Cement Replacement Materials in Concrete

Yaser Gamil*, Ismail Bakar and Lee Yee Loon

Faculty of Civil and Environmental Engineering, University Tun Hussein Onn Malaysia, 86400 UTHM, Parit Raja, Batu Pahat, Johor, Malaysia

ABSTRACT

Cement Kiln Dust (CKD) is a by-product generated throughout the production of Ordinary Portland Cement (OPC). It is normally emitted to the atmosphere or converted into liquid and subsequently drained out as effluents to landfills and wastage areas. It impacted human health and the environment negatively. However, it can be utilized in concrete as raw cement replacement materials due to its engineering properties which work as an alternative binder of OPC in addition to that it has benefits in creating economic and environmental advantages. This study aimed to modify CKD and investigate the chemical composition of normal-CKD and modified -CKD accordingly. The term modified noted that CKD has gone through a process of modification using heating process. The reactivity property of CKD was investigated using pH analysis. Then, mix proportions of different percentage of normal-CKD and modified -CKD were developed to study the addition effects on the compressive and flexural strength for different curing period. The trend of strength development over the addition of CKD was also analyzed. OPC was replaced by CKD at 0% and successively increased by 10% to 100% through binder weight (OPC). A fixed amount of water to binder (W/B) with a ratio of 0.45 was used for all hybrids. The mixes were formed into the specimen and tested for compressive strength and flexural strength at 7, 14 and 28 curing days. The medium particle size of CKD used was less than 10 μ m. The results of compressive and flexural strength showed that modified-CKD resulted in better

properties and 10% replacement showed the maximum values of compressive and flexural strength as a result considered best percentage replacement in agreement with its noteworthy results.

Keywords: Chemical compositions, CKD, compressive strength, flexural strength, reactivity

ARTICLE INFO

Article history:

Received: 03 December 2017

Accepted: 28 August 2018

Published: 24 January 2019

E-mail addresses:

yaseruthm@yahoo.com (Yaser Gamil)

bismail@uthm.edu.my (Ismail Bakar)

drlee@chemann.com (Lee Yee Loon)

* Corresponding author

INTRODUCTION

The accelerated growth of construction industries has been associated with the high demand of natural materials used in all activities which correlated with the depletion of natural resource and subsequently triggered the environmental pollution which turned out to be unsuitable for a living (Rahman et al., 2011). Cement is the main material used in the built environment. It is available in nature as limestones and then subjected production process to produce OPC in mines and factories (Khanna, 2009). It is the main material that provides bonds between concrete ingredients. It has been revealed that the worldwide production of cement in 2014 was 4.18 billion metric tons of that 83.2 million metric tons were produced in USA (Statista, 2016). These quantities reflect the huge number of by-products generated annually from the production of cement; among the several types of by-products is CKD which is produced as dust or slurry (Konsta-Gdoutos et al., 2003; Al-Harthy et al., 2003). It is the most challenge in terms of tangible hazard for the environmental health (Taubert, 2008; Khanna, 2009). In the USA, about 1,403,062 metric tons of CKD have emitted annually to the atmosphere (Daous, 2004; Taubert, 2008). In response to the global interest for the nature conservation which has increased since the 1990s, researchers have focused on the reuse of CKD encompassing its engineering properties and content of chemical compositions as well as its physical microstructures. CKD is a material that has uniform size and in the form of fine powdery (Siddique, 2008). It comes in the form of dust or slurry and its size is normally between 20 μm and 20nm (Lee et al., 2007).

Table 1 presents the chronological study from literature which focuses on the use of normal CKD in concrete and other applications but there is no study that investigates the possibility of treating and modifying the property of CKD and utilizing that as cement replacement materials.

CKD can be used in other engineering applications for example as soil stabilization agent, and cracking filler (Siddique, 2008). A study by Baghdadi (1990) has successfully utilized CKD to stabilize clay soil. The stabilized clay has shown a considerable decreasing in plasticity index and an increase in the compression strength. The maximum strength was recorded after 28 days (8.8×10^3 kPa). The study indicated that CKD has high potential to improve the maximum dry density and reduced the optimum moisture content of kaolinite clay. Therefore, it can be used in modifications of soil property. To support that, Miller, & Azad (2000) studied the influence on stabilization with CKD and it was found that adding CKD to soil had increased the UCS. Furthermore, Peethamparan et al (2008) investigated the influence of adding CKD to the physical and chemical properties of soil. It was found CKD paste gave an early indication of its suitability to be as a soil stabilization agent.

It has been demonstrated that CKD has high ability to interact with concrete's elementary materials such as OPC, water, and aggregate (Khanna, 2009). The reactivity is very important to improve the bonds among concrete ingredients. Rahman et al. (2011)

Table 1
Chronological study on the utilization of CKD in concrete

Study	Replacement Percentage	Maximum compressive strength achieved	References
The study focused on the effect of normal CKD on mortar and concrete blend	5, 10, 15, 20, 25, 30%	Compression strength was recorded to be 55,53,51,44, 42 and 41Mpa respectively after 28 days	Al-Harthy et al., 2003
Normal dust CKD was used for concrete strengthening	5 and 10%	The maximum compressive strength was recorded in 28 curing days to be 34.79 and 36.89MPa respectively	Maslehuddin et al., 2008
Normal CKD was used as partial cement replacement materials	5 –15%,	Compressive strength was approximately 51 and 42MPa respectively	Khanna, 2009
In this study the additives have less significant impact of compressive strength	10, 30 and 50%	compressive strength were 28, 25, 22 MPa respectively	Mohammad & Hilal, 2010
Silica fume was mixed with normal CKD	10%, 60% and 100 %).	18MPa ,17.4MPa	Wahab, 2013
Super plasticizer added with normal CKD in normal concrete	0% CKD, (10% and 20% CKD)	Achieved 31.33MPa ,10.86MPa and 19.71MPa	Abdulabbas, 2013
In this study, combination of normal CKD and Rice Husk Ash were incorporated and was found that, combining two of these wastes as replacement of cement led to enhanced or acceptable properties.	0%, 10%, 20%, 30%, 40% and 50%.	Compressive strengths of 29 N/mm ² and 28N/mm ² were obtained at 10% and 20% of replacement of cement respectively	Afolayan et al., 2015

indicated that the addition 34% of CKD to concrete had increased the pH to more than 10, which led to the increase of the solidification and strength of concrete.

Recent studies have further used CKD in different applications. Beltagui et al. (2018) had investigated the feasibility of incorporating different by-products and the study found that KD content possible to achieve the required strength was 90% CKD blended with 10% cement. Another study by Sharma & Goyal (2018) investigated the possibility of incorporating CKD with OPC to improve carbonation process and it was found that the finer particle size of CKD particles and presence of alkali in CKD further promoted the carbonation reaction.

It was emphasized by Taubert (2008) that CKD was a particulate mixture of partially calcined and unreacted raw feed, clinker dust and ash, enriched with alkali sulfates, halides, and other volatiles. In spite of these claims, this study introduced a new technique to modify the chemical and physical property of CKD. Hence, it is suggested in this study to modify its characteristics using specific temperature regime to remove excessive materials. Based on the past technical report developed by US army (1994), it is shown that for the

material to be reactive pH scale has to be about 12.4. Even with all the studies discussed, the application of normal and modified –CKD in concrete and its impact on the primary properties has yet to be investigated in depth. Therefore, the current study focused on the potential of unmodified and modified CKD by micronization process as cement replacement materials in concrete which emphasized the novelty of this work. The term micronization in this study is meant by the process of altering the shape, size, and removal of excessive materials of CKD by implying certain temperature regime.

MATERIALS AND METHODS

This study mainly consists of three phases. The first phases discussed on the literature analysis on the utilization of CKD in previous studies. Then, the second phases involved the preliminary inspections and preparation of study materials and the preparation of specimens. The third phase presented the characterization of specimens for both compressive and flexural strength and analysis of the results and findings conclusions. Figure 1 illustrates the flowchart and experimental setup of this research (Gamil & Bakar, 2016).

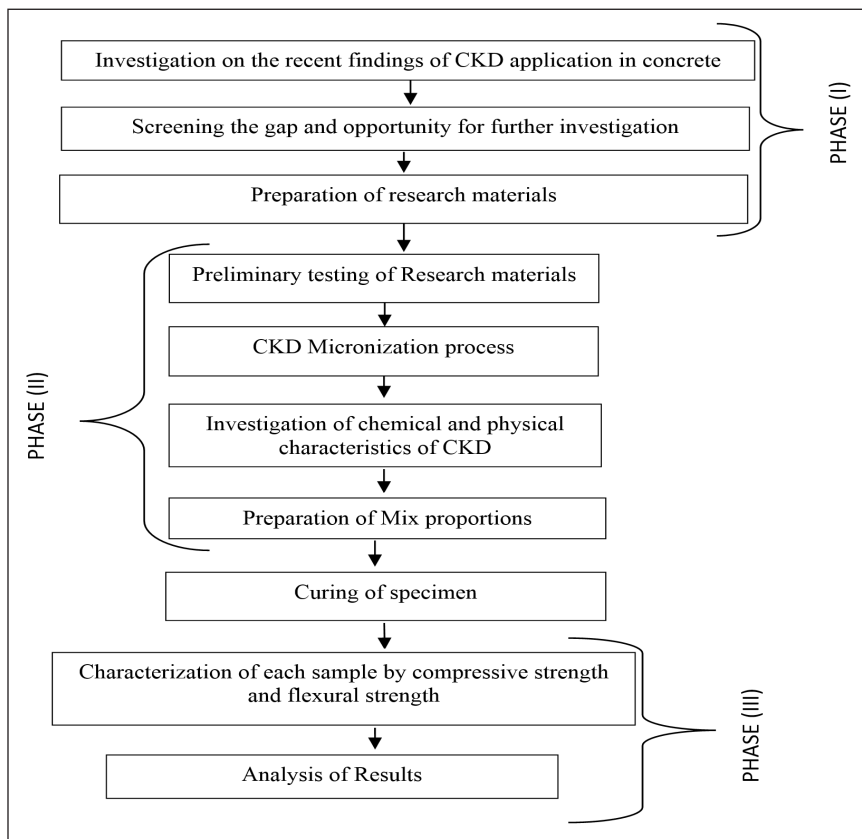


Figure 1. Flowchart of the experimental setups

OPC type 1 (ASTM, 2016) with a specific gravity of 3.04 .CKD samples were collected in bulk from cement factory located in Negeri Sembilan, Malaysia. The factory is considered as one of the main sources of cement provision in Malaysia. CKD was then crushed using crusher and then sieved to produce Nano-particles passing 10 μ m and stored at room temperature to maintain its moisture content at a constant temperature. Sand (fine aggregate) was collected from the commercial sector in Malaysia with a specific gravity of 2.63. The coarse aggregate was sieved and the particles less than 20 mm were used with a specific gravity of 2.61. The coarse aggregate was sieved as it is part of the technical requirements.

Specimen Preparation

The Specimen Preparation in the current work consists of a collection of samples, pretreatment and primary testing of raw materials. Factorial Complete Randomized Design (CRD) (10*2*1) in triplicate was used to study the effectiveness of CKD. The experimental work was designed as follow; ten (10) replacement percentage (10-100 %) was added to concrete, two (2) modified and unmodified-CKD, one (1) control (without CKD) making a total of three (3) groups. CRD is essentially a statistical concept which is used to run random factors.

Preparation of Modified -CKD

Heating is a method to achieve higher pozzolanic reactivity (Matias et al., 2014). In order to produce modified -CKD, the raw CKD was dried in a furnace. The temperature of the furnace was set at 550°C for one hour to reduce the diameter of CKD particles and remove excessive and unwanted particles which might be in the form organic materials or any other unfavorable materials. The specified temperature regime was adopted from a study by Budak et al. (2010) whereby it was proven that thermally modified dust had higher potential in improving the pozzolanic reactivity and the suggested range of temperature was between 500°C and 700°C to improve performance and the samples modified with this temperature gains higher compressive strength in comparison with other samples. In another literature by Lee et al. (2007), the treatment process for Rice Husk Ash (RHA) by interfering temperature regime was at its best to be 500°C to create amorphous biomass silica used in concrete. Another study by Gamil et al. (2018), implied modification of Palm Oil Fuel Ash (POFA) by treating using heating process for an hour under the set of temperature regime of 500°C. The process of treating CKD was adopted from the before mentioned studies.

Experimental Procedures

Twenty-one samples of concrete mixtures were blended separately for each curing day and mechanical property (compressive and flexural) with different replacement (10-100%) of CKD (normal and modified) of the amount of OPC and then the mixture sample was incubated at laboratory temperature for 28 days and then examined for compressive strength. The control sample was conducted without CKD addition. The same proportions were used to develop prisms to examine flexural strength. Table 2 shows the mix proportions and their significant factors.

Table 2
Experimental design and mix proportions with important factors

	Considered Factors			
	Symbols	Replaced percentage of OPC (%)	Water-cement ratio	Curing time (Days)
Control	M0	0	0.45	7, 14, 28
Normal-CKD	M1-M10	(10-100)	0.45	7, 14, 28
Modified-CKD	M11-M20	(10-100)	0.45	7, 14, 28

M*: Mix

The chemical compositions of CKD and OPC were determined using X-ray Fluorescence (XRF) according to the method described by ASTM (2014). In brief: XRF basically carried out according to the standard in which the sample of CKD was formed as pallet then incubated for overnight then analyzed for chemical compositions.

pH values of the mixture and control were recorded at the incubation periods to determine the acidity, alkalinity, and reactivity of the concrete based on ASTM (2001). For this purpose, pH meter was calibrated before each measurement according to the manufacturer's guidelines to produce precise results. The sample was in the form of slurry concrete and pH meter was utilized to determine each value. The method used to record pH was that in each percentage replacement the recorder was placed and recorded at different locations of the specimen. In this study only up to 50% was recorded because the main purpose was to prove the reactivity of CKD and that was demonstrated in figure 3.

The compressive strength of each concrete mixture was measured to investigate the compressive strength increment and decrement with the variations of additives percentages of CKD over different curing time. A fixed size of (100*100*100) mm for each sample was used to determine the compressive strength according to BS 1881-part 116-1989 (British Standard, 1881). The universal testing machine was used to carry out compressive strength. The loading rate of the universal testing machine was 15 MPa per minute. Flexural strength (modulus of rupture) of each concrete sample was conducted using concrete beam mold

sample with size (100*100*500) mm in the form of prisms which was prepared prior to the test. This particular mold size was chosen because the size of aggregate is less than 20 mm. Three-point loading was used to carry out the tests in accordance with ASTM (1967) and ASTM (2002) (2012).

RESULTS AND ANALYSIS

Physical and Chemical Properties of Normal -CKD and Modified -CKD

CKD is fine materials which it can naturally exist as either in dust or slurry form if it is transmitted into a liquid state. In this study, fine powder CKD was used, the color was found to be grey to black for normal- CKD. However, modified- CKD turned out to be light grey due to the removal of excessive constituents. Figure 2 shows the physical differences between both types. The color of normal-CKD changed from blackish to light brownish which showed the effect of heating on the physical properties. It is clear that the size distribution of CKD depends on many factors which include the type of stones, method of processing, and CKD collection process (Khanna, 2009). The nominal size of CKD used in this study is less than 10 μ m and Specific Gravity (SG) for both normal and modified -CKD was in the range of 2.64–2.75. It is important to study the chemical compositions of CKD for both normal and modified types.

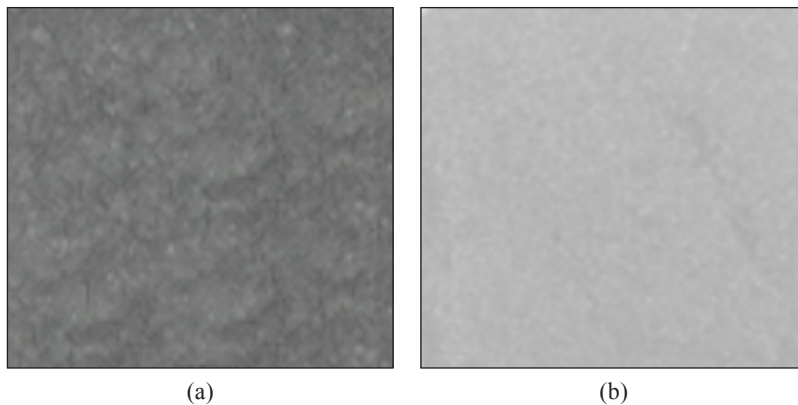


Figure 2. A) Normal-CKD; B) Modified-CKD

Table 3 shows the comparison of the chemical composition of normal-CKD, modified -CKD, and OPC. Generally, CKD exhibit noticeable alkalinity in the form of lime (CaO) which initially carries 44.05% in normal-CKD and 44.3% in modified-CKD. This, therefore increase the possibility of higher reactivity, In addition, the amount of K₂O and Na₂O in CKD is relatively higher as compared to OPC. It is also shown that CKD has slightly higher percentage of Silica which illustrates that CKD can be utilized to replace OPC in

reasonable percentage. The primary constituents of CKD are calcium carbonate and silicon dioxide which has an approximately similar percentage as OPC. It also has high alkalinity in terms of chloride and sulfate which helps to make the hybrid more reactive with other concrete materials.

Table 3
Chemical composition of OPC, normal CKD and modified-CKD

Chemical composition mass (%)	OPC	normal-CKD	Modified-CKD
Silicon dioxide (SiO ₂)	21.6	17.3	17.83
Aluminum trioxide (Al ₂ O ₃)	6.2	3.81	3.91
Ferric Oxide (Fe ₂ O ₃)	3.13	2.99	3.04
Calcium oxide (CaO)	62.7	44.05	44.3
Magnesium Oxide (MgO)	1.48	2.00	2.04
Potassium oxide (K ₂ O)	1.01	2.18	2.71
Sulfur oxide (SO ₃)	2.73	3.02	3.76
Phosphorus oxide (P ₂ O ₅)	0.21	1.22	2.05
TiO ₂	0.1	0.25	0.31

Effect of CKD Addition on pH

In this section, an investigation of the effects of adding OPC, modified-CKD, and normal-CKD to the mix and its reactivity was based on the measurement of pH values. The reason of performing pH analysis is to examine the alkalinity of CKD in order to check its reactivity with other concrete materials.

Figure 3 illustrates the value of pH scale and the amount of percentage of the components added to the mix. It is shown that, for OPC graph, pH value tends to increase with the percentage addition because OPC contains higher alkalinity and high precipitation of silica and lime, therefore, the hybrid becomes more reactive to bind the concrete ingredient. However, for CKD it is obvious that modified-CKD is more reactive than normal-CKD due to the removal of unwanted and excessive constituents.

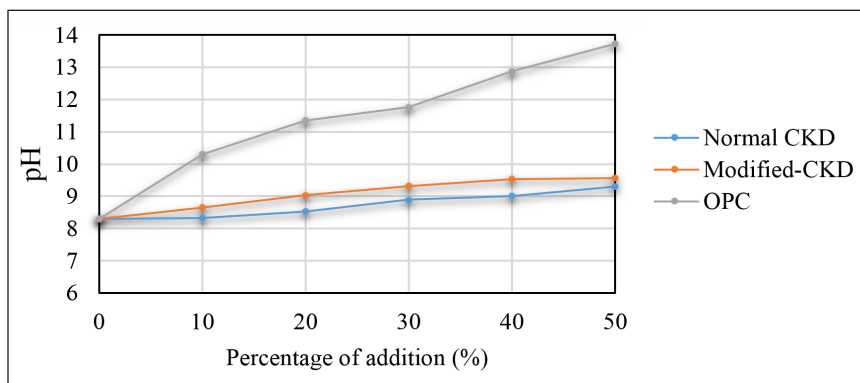


Figure 3. pH of normal CKD, modified-CKD and OPC

Compressive Strength and Flexural Strength

In this part, results of compressive and flexural strength for normal and modified -CKD for different curing period and different mix proportions are discussed.

Variations of Normal -CKD Percentages

This subsection introduces the results of using normal-CKD to replace OPC and strength developments were recorded over the curing days.

Figure 4 illustrates the compressive and flexural strength for variations percentages of normal-CKD for 7 days. From the figure, there is linear declination of compressive and flexural strength with the increment of normal-CKD. The maximum compressive and flexural strength exhibits at 10% addition which are 26.91MPa and 4.32MPa respectively. There is a considerable drop of compressive and flexural strength when the addition of 20%, however, it gradually decreases after the amount of CKD approaches 50%.

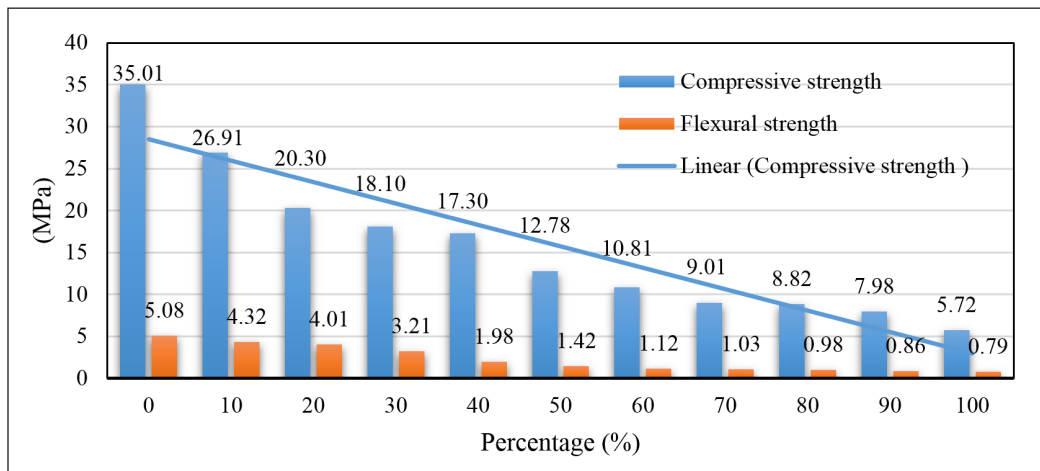


Figure 4. Variation of normal-CKD for 7 days curing

Figure 5 shows the results of compressive and flexural strength for 14 days curing. It is shown that samples with 10% replacement exhibit high compressive and flexural strength then the declination occur with the increment of CKD addition. Yet, in 14 days curing these is noticeable improvement of the strength due to late carbonation process between binder and other concrete materials.

Figure 6 illustrates the compressive strength and flexural strength and the variations percentages of normal-CKD for 28 days. For 10% the strength has considerably improved and reached 35.31MPa which is considered acceptable to be used as cement replacement material, soil stabilization and other related construction work (Siddique, 2008).

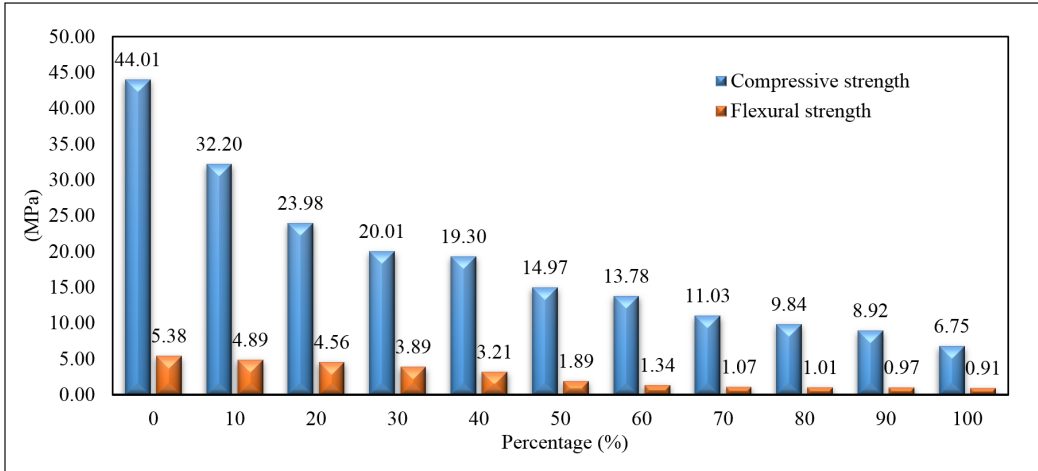


Figure 5. Variation of normal-CKD for 14 days curing

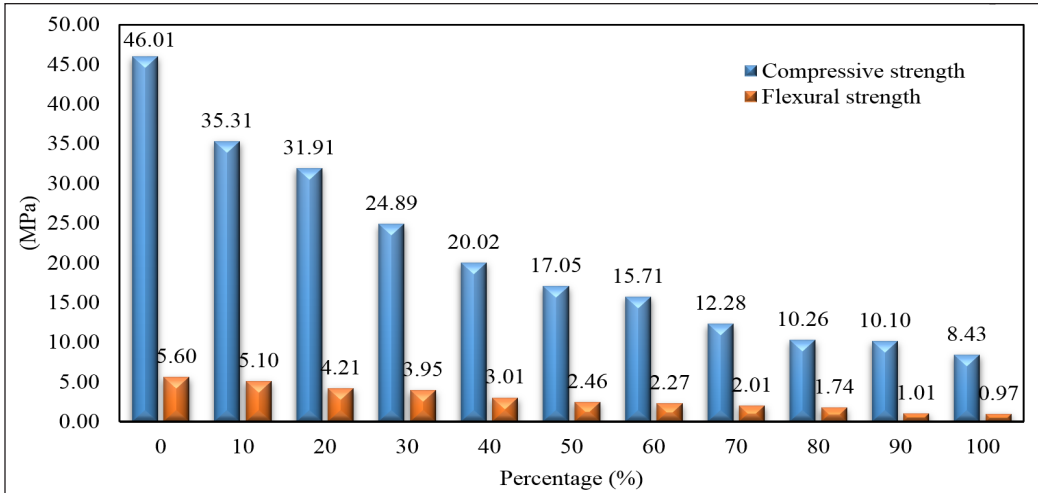


Figure 6. Variation of normal-CKD for 28 days curing

Variations of Modified -CKD Percentages

This section introduces the results of using modified-CKD with various percentages.

Figure 7 shows the compressive strength and flexural strength and the variations percentages of modified -CKD for 7 days. For 10% the strength has considerably resulted in a better outcome for compressive and flexural strength which are 35.01Mpa and 5.08Mpa respectively.

Figure 8 indicates the compressive strength and flexural strength and the variations percentages of modified -CKD for 14 days. It is shown the strength increases in comparison with normal CKD. For specimen with 10% replacement, the value increases to 44.01MPa and 5.38MPa respectively.

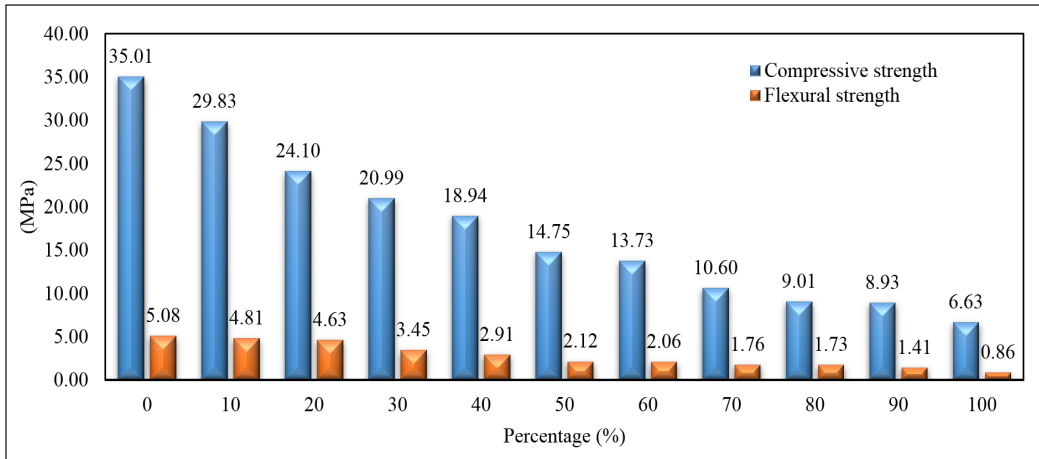


Figure 7. Variation of Modified-CKD for 7 days curing

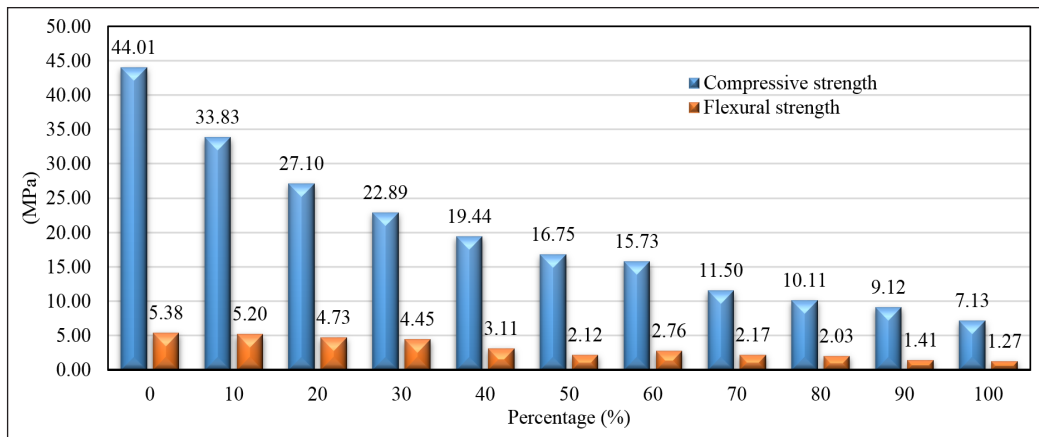


Figure 8. Variation of modified-CKD for 14 days curing

Figure 9 illustrates the compressive strength and flexural strength and the variations percentages of modified -CKD for 28 days. It is shown the strength increased in comparison with normal CKD. There is a noticeable increment of strength in comparison with unmodified -CKD. In 28 days, the peak value reached 39.11MPa which are considered crucial to prove that CKD can be used as a partial replacement material in concrete (Siddique, 2009).

Figures 10 and 11 show the compressive and flexural strength for 10% CKD addition for both modified and unmodified materials. There is an increment of both compressive and flexural strength is proportional to curing period. Therefore, it is evident that 10% is an acceptable ratio to be used. This also proves that producing high flexural and compressive strength is very essential in concrete.

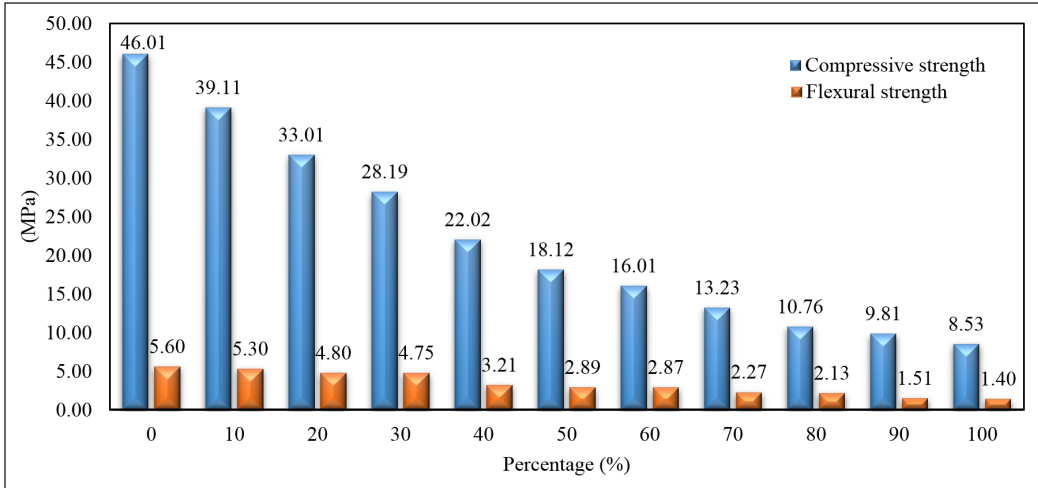


Figure 9. Variation of modified-CKD for 28 days curing

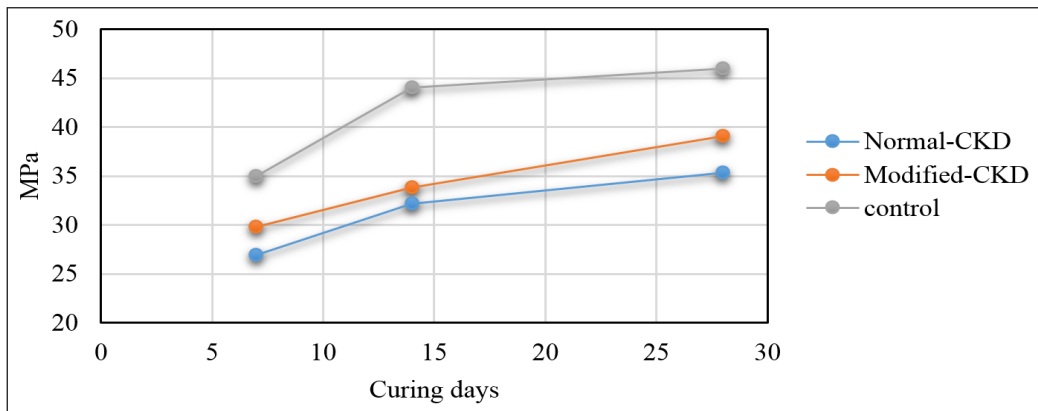


Figure 10. Compressive strength trends for 10% addition

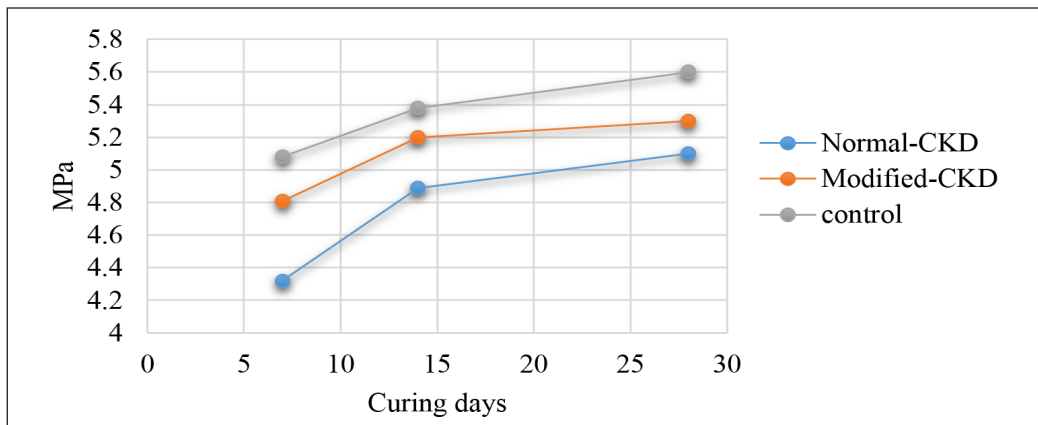


Figure 11. Flexural strength trends for 10% addition

The reason that control mix has higher flexural and compressive strength because there was no CKD added to the mix. The purpose is to filter in which percentage of addition CKD could give a best of compressive and flexural strength.

In comparison with previous findings listed in Table 1, modified-CKD in this study achieved at 10% replacement in 28 days curing a value of 39.11Mpa compressive strength which is higher comparing to a study by Maslehuiddin et al. (2008) whereby compressive strength was recorded at 10% and 28 days curing were recorded as 36.89Mpa and a study by Mohammad and Hilal (2010) achieved 28Mpa at 28 curing days. The reason beyond that, this study modified the CKD by removing excess carbon contents and this could be justified due to the different sources of raw OPC.

CONCLUSION

With vivid evident, CKD is a useful by-product materials which derived from the production of OPC. It has a very significant influence on the primary property of concrete. It displayed high reactivity due to the fact that it contains high amount of silica CaO. Therefore, it is concluded that CKD can be used as cement replacement which helps to generate income from secondary materials. It is also emphasized that treating CKD by removing excessive and unwanted materials can improve its chemical and physical properties. From the results, it was proven that 10% replacement of OPC by CKD has achieved 39.11Mpa compressive strength. This was also proven by Al-Rezaiqi et al. (2018) which found that replacing CKD more than 20% of OPC had negligible effect of concrete strength. Irrevocably, with its proven properties, there is a possibility for CKD to be used in construction works, for example, as filler in embankments and modification additive for soft soil and other construction solutions. This study also concluded, CKD can be modified by the interference of heating process to remove excessive materials and resulted in better property.

ACKNOWLEDGMENTS

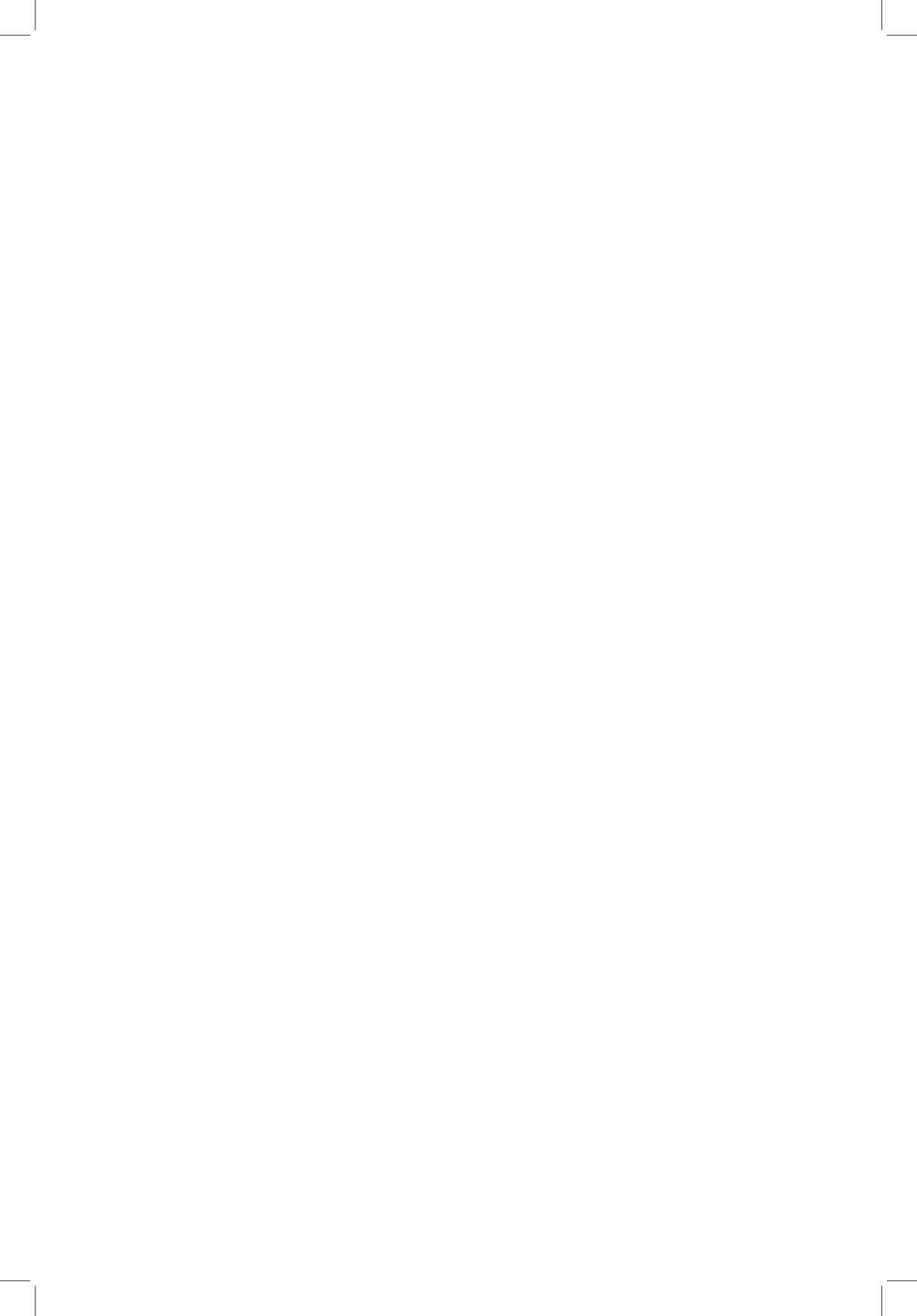
The authors would like to acknowledge the Yemen Ministry of Higher Education and University of Tun Hussein Onn Malaysia for the financial support of this research. Technical support from laboratory coordinators is highly appreciated.

REFERENCES

- Abdulabbas, Z. H. (2013). Utilization of Cement Kiln Dust in Concrete Manufacturing Zainab Hasan. *Jordan Journal of Civil Engineering*, 7(1), 111-125.
- Afolayan, J. O., Amartey, Y. D., & Oriola, F. O. P. (2015). Effects of combining rice husk ash and cement kiln dust on the compressive strength of concrete. *International Journal of Advances in Engineering and Technology*, 8(5), 739-746.

- Al-Harthy, A. S., Taha, R., & Al-Maamary, F. (2003). Effect of cement kiln dust (CKD) on the mortar and concrete mixtures. *Construction and Building Materials*, 17(5), 353-360.
- Al-Rezaieqi, J., Alnuaimi, A., & Hago, A. W. (2018). Efficiency factors of burnt clay and cement kiln dust and their effects on properties of blended concrete. *Applied Clay Science*, 157, 51-64.
- ASTM. (1967). *Standard specification for portland cement*. American Society for Testing and Materials. West Conshohocken, PA.
- ASTM. (2001). *Standard Test Method for pH of Soils*. American Society for Testing and Materials. West Conshohocken, PA.
- ASTM. (2002). *Standard Test Method for Flexural Strength of Concrete (Using Simple Beam with Third-Point Loading)*. American Society for Testing and Materials. West Conshohocken, PA.
- ASTM. (2012). *Standard Test Method for Flexural Performance of Fiber-Reinforced Concrete (Using Beam With Third-Point Loading)*. American Society for Testing and Materials. West Conshohocken, PA.
- ASTM. (2014). *X-ray Florescence (XRF), chemical composition*. American Society for Testing and Materials. West Conshohocken, PA.
- ASTM. (2016). *Standard Test Method for Compressive Strength of Cylindrical Concrete Specimens*. American Society for Testing and Materials. West Conshohocken, PA.
- Baghdadi, Z. A. (1990). Utilization of kiln dust in clay stabilization. *Journal of King Abdulaziz University*, 2, 153-163.
- Beltagui, H., Sonebi, M., Maguire, K., & Taylor, S. (2018). Feasibility of backfilling mines using cement kiln dust, fly ash, and cement blends. In *MATEC Web of Conferences* (Vol. 149, p. 01072). Les Ulis: EDP Sciences.
- British Standard. (1881). *Testing concrete - Part 116: method for determination of compressive strength of concrete cubes*. Chiswick: Gibb Limited.
- Budak, M., Akkurt, S., & Böke, H. (2010). Evaluation of heat treated clay for potential use in intervention mortars. *Applied Clay Science*, 49(4), 414-419.
- Daous, M. A. (2004). Utilization of cement kiln dust and fly ash in cement blends in Saudi Arabia. *Engineering Sciences*, 15(1), 1-12.
- Gamil, Y. M. R., & Bakar, I. H. (2016). The Development of Mathematical Prediction Model to Predict Resilient Modulus for Natural Soil Stabilized by Pofa-OPC Additive for the Use in Unpaved Road Design. In *IOP Conference Series: Materials Science and Engineering* (Vol. 136, No. 1, p. 012007). Bristol: IOP Publishing.
- Gamil, Y., Zamahri, K. A., & Bakar, I. (2018). Application of Scheffe's Theory to Develop Mathematical Prediction Model to Predict UCS for Hybrid Containing Organic Soil and POFA-OPC Additives. *Civil Engineering and Architecture*, 6(2), 54-64.
- Khanna, O. S. (2009). *Characterization and Utilization of Cement Kiln Dusts (CKDs) as Partial Replacements of Portland Cement*. (Doctoral dissertation). University of Toronto, Canada.

- Konsta-Gdoutos, M. S., & Shah, S. P. (2003). Cement Kiln Dust (CKD): Characterisation and utilisation in cement and concrete. In R. K. Dhir, M. D. Newlands, & K. A. Paine (Eds.), *Role of Cement Science in Sustainable Development - Proceedings of the International Symposium dedicated to Professor Fred Glasser, University of Aberdeen, Scotland* (pp. 59-70). Dundee, United Kingdom.
- Lee, Y. L., Koh, H. B., Wong, C. K., Suraya, H. A., Suhaizad, B. S., & Hung, Y. T. (2007). Micronised Biomass Silica and Nanoparticles Synthesis-Recent Development. *Malaysian Construction Research Journal*, 1(1), 21-29.
- Maslehuddin, M., Al-Amoudi, O. S. B., Shameem, M., Rehman, M. K., & Ibrahim, M. (2008). Usage of cement kiln dust in cement products—research review and preliminary investigations. *Construction and Building Materials*, 22(12), 2369-2375.
- Matias, G., Faria, P., & Torres, I. (2014). Lime mortars with heat treated clays and ceramic waste: A review. *Construction and Building Materials*, 73, 125-136.
- Miller, G. A., & Azad, S. (2000). Influence of soil type on stabilization with cement kiln dust. *Construction and Building Materials*, 14(2), 89-97.
- Mohammad, A. M., & Hilal, N. N. (2010). Re-using The By-product of Cement Industry (Cement Kiln Dust) To Produce The Concrete. *Anbar Journal for Engineering Sciences*, 3(2), 1-14.
- Peethamparan, S., Olek, J., & Lovell, J. (2008). Influence of chemical and physical characteristics of cement kiln dust (CKDs) on their hydration behavior and potential suitability for soil stabilization. *Cement and concrete research*, 38(6), 803-815.
- Rahman, M. K., Rehman, S., & Al-Amoudi, O. S. B. (2011). Literature review on cement kiln dust usage in soil and waste stabilization and experimental investigation. *International Journal of Research and Reviews in Applied Sciences*, 7(1), 77-87.
- Sharma, D., & Goyal, S. (2018). Accelerated carbonation curing of cement mortars containing cement kiln dust: An effective way of CO₂ sequestration and carbon footprint reduction. *Journal of Cleaner Production*, 192, 844-854.
- Siddique, R. (2008). Cement Kiln Dust. In R. Siddique (Ed.), *Waste Materials and By-Products in Concrete* (pp. 351-380). Heidelberg: Springer.
- Siddique, R. (2009). Utilization of waste materials and by-products in producing controlled low-strength materials. *Resources, conservation, and recycling*, 54(1), 1-8.
- Statista.com. (2016). *The United States and world cement production in 2010 and 2015 (in million metric tons)*. Retrieved July, 4, 2016, from <http://www.statista.com/statistics/219343/cement-production-worldwide>.
- Taubert, D. H. (2008, May). Beneficial uses of cement kiln dust. In *Cement Industry Technical Conference Record* (pp. 210-228). Miami, FL, USA.
- US Army. (1994). *Soil Stabilization for Pavements*. (Technical Manual NO. 5-822-14). Department of the Army, the Navy, and the Air Force.
- Wahab, R. K. A. (2013). Effect of adding Silica fume to the Cement Kiln Dust (CKD). *Journal of American Science*, 9(12), 274-281.



Design of Self-tuning Fuzzy PID Controllers for Position Tracking Control of Autonomous Agricultural Tractor

Witcha Upaphai¹, Pracha Bunyawanchakul^{1*} and Manusak Janthong²

¹*Department of Mechanical Engineering, Srinakharinwirot University, Ongkaruk District, Nakhonnayok province, 26120 Thailand*

²*Department of Mechanical Engineering, Rajamangala University of Technology Thanyaburi, Thanyaburi District, Pathumthani province, 12110 Thailand*

ABSTRACT

As tractors have played an important role in improving agricultural productivity, enhancing the efficiency of tractor has become of interest in recent years. In this study, a design of self-tuning fuzzy PID tracking control for a tractor is proposed. The steering control is performed on the front wheels, whereas the tractor is rear-wheel drive. Efficiency of the proposed self-tuning fuzzy PID controllers is compared to the results from the conventional PID controller testing at different trajectory scenarios under the specified accuracy of GPS and acceleration of the tractor. The experimental results show that the proposed self-tuning control exhibits better performance than the conventional PID technique in terms of the fast response of the steering wheels, and the small distance and heading angle errors.

Keywords: PID controller, self-tuning fuzzy PID controller, tractor, trajectory

INTRODUCTION

Thai agriculture needs a new approach so as to “work less but accomplish more”. A tractor is one of labor-saving devices that could help Thai farmers to achieve this

objective. The modification of a tractor into an autonomous driverless vehicle is one of innovations which researchers have been currently working on. Several studies have concentrated on the design and test of controllers used in an autonomous driverless tractors.

Huynh et al. (2012), for example, utilized the nonlinear PI and the GPS sensor

ARTICLE INFO

Article history:

Received: 5 February 2018

Accepted: 12 September 2018

Published: 24 January 2019

E-mail addresses:

gs571120036@swu.ac.th (Witcha Upaphai)

prachabu@g.swu.ac.th (Pracha Bunyawanchakul)

manusak.j@en.rmutt.ac.th (Manusak Janthong)

* Corresponding author

for trajectory control of a driverless tractor-trailer with accuracy of tracking. In a recent study on the design of an autonomous tractor by Kayacan et al. (2015), a fuzzy logic controller worked in parallel with a type-2 fuzzy neural network was applied to control the position while moving on prescribed trajectory. Ruangurai et al. (2015) adapted the PID controller to model the tracking system of the tractor, and in the same year, Moon et al. (2013) developed a path tracking model from kinematic and dynamic equations considering wheel slipping while moving by means of the PID controller.

It is obvious that controller selection is important for designers to achieve better efficiency of the navigation system of the autonomous tractor. The PID controller is one of the widely used controllers thanks to its functional simplicity. The PID controller consists of three term combination. “P” is proportional to the actual value of the error and “I” is integral controller generally used to decrease the steady state error while “D” is derivative controller which causes the output to decrease if the process variable is increasing rapidly.

Apart from being used to control the motion of the tractor, the PID controller has been widely employed by researchers to effectively control other systems. A position control scheme for a radio telescope (antenna) was presented using the PID controller designed in MATLAB Simulink environment in the presence of wind disturbance in the system model (Zaber et al., 2015). Basnayake et al. (2017) concluded that the geometric PID controller could ensure the stability of the Segway type mobile robot, constrained under no slip condition. A PID controller designed for Automatic Voltage Regulator systems was proposed using Simulink in MATLAB to compare PID with P, PI and PD controllers (Ratanaworahirunkun et al., 2013). Despite being widely used as a practical and simple controller with easy tunability, the PID controller has its own limitations with respect to the system stability control due to its linearity as the behavior of most systems is nonlinear and time varying. It cannot offer a good dynamic performance while wide range of parameters is considered.

In recent years, fuzzy logic based controllers, which have better performance in terms of its heuristic nature associated with simplicity and effectiveness for both linear and nonlinear systems, have been proposed in many studies. The fuzzy logic is used to address the vague events or situations. The significance of fuzzy logic controllers is its logical reasoning or ability to make decisions with human-like logical thinking and solving complex problems. The fuzzy logic controller consists of the three main processes. First, the process of converting classical data into membership functions (MFs) which is called the Fuzzification. Then Fuzzy Inference which is the process of combining membership functions with the control rules to derive the fuzzy output. The final process is Defuzzification which provides a real number as an output.

Recently, fuzzy logic controllers have been utilized in several studies. The design of a mobile robot to track the desired target and to avoid obstacles using the fuzzy logic

controller was presented (Handayani et al., 2017). Allou et al. (2017) proposed the design of the path tracking controller based on fuzzy logic to control the speed and the steering angle of a four-wheel drive electric vehicle to follow the desired trajectory.

To integrate the advantages of PID and fuzzy logic based controllers, both are applied together to successfully increase the efficiency of control systems. This approach is also known as the self-tuning fuzzy PID technique. Regarding its working principle, Awouda and Mergani (2017) stated that the fuzzy auto-tuning of PID controller was to find the fuzzy logic relationships between three parameters of PID with error and change of error, calculate error and change of error in cycle in the operation of control system and adjust parameter of PID (K_p , K_i , K_d) on-line according to the fuzzy logic control principle. Pan and Zhou (2017) presented an adaptive fuzzy PID controller for maintaining vehicle yaw stability in different road conditions. Heikkinen et al. (2017) utilized a self-tuning fuzzy PID controller to control an autonomous differential drive mobile robot. In their paper, Su et al. (2016) developed a dynamic model using Lagrange method to the on-ball balancing mobile robot and a fuzzy self-adjusting PID controller was proposed to control the robot's balance.

In this work, the self-tuning fuzzy PID controller is utilized for the motion of the tractor because the controller is able to tune gain value by itself according to a variety of areas where a tractor drive. An old tractor was modified into an autonomous driverless vehicle. The hydraulic system of this two-rear wheel drive tractor is electronically controlled. The steering system uses an AC Servo Motor. A GPS receiver and IMU sensor are used to locate the current position and direction of the tractor as an input of the self-tuning fuzzy PID controller which regulates speed and steer system of the tractor while moving along different prescribed trajectories. It is expected that our design will serve as a significant step towards the prototype of an autonomous tractor with inexpensive GPS guidance system and IMU sensor. In addition, the proposed control system is simple while providing satisfactory outcomes.

Theory of PID Controller

A PID controller is a feedback control system that minimizes the difference of the output and set point by adjusting three parameters: K_i , K_d and K_p . The block diagram of the PID controller is shown in Figure 1.

Figure 1 shows the block diagram of the PID controller that consists of three subblocks : proportional, integral, and derivative terms. The summation of the outputs of all term is represented by $u(t)$ which is the output of the PID controller. The error function $e(t)$ is the difference between the output and the set point. The PID model can be expressed in the following equation.

$$u(t) = K_p e(t) + K_i \int_0^t e(\tau) d\tau + K_d \frac{d}{dt} e(t) \tag{1}$$

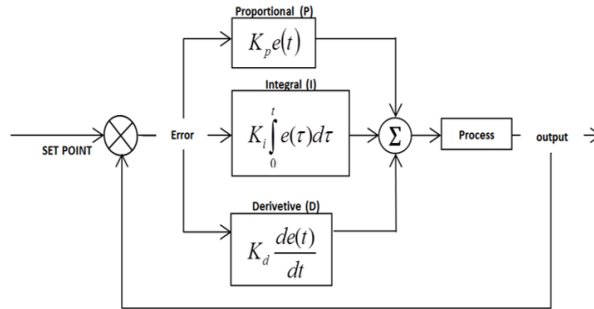


Figure 1. Block diagram of the PID controller

Theory of Self-tuning Fuzzy PID Controller

The self-tuning fuzzy PID controller employs the combination of PID and fuzzy algorithms. The Fuzzy controller is responsible for adjusting the PID gains to optimize the output. The block diagram of the self-tuning fuzzy PID controller is illustrated in Figure 2.

In Figure 2, the self-tuning fuzzy PID controller receives the inputs e and \dot{e} to perform the fuzzification that transforms numerical inputs into language variable to identify the membership function as shown in Figure 3.

In Figure 3, functions of language variable consist of NB, NM, NS, Z, PS, PM, and PB which are identified by the input e . For instance, if e is within 15° , the status will be PS, and if K_i is within -6 m, the status will be NM. The status of ตัวแปรเชิงภาษา is evaluated by the process of Fuzzy Inference based on the fuzzy conditions where the condition (IF, THEN) is used to provide the output from the corresponding input and the conditions (AND, OR) are used for multiple inputs. Membership function rule is shown in Table 1.

From Table 1, the outputs of PID gains K_p, K_i, K_d can be obtained. For example, if K_p is PS and K_i is NM, $K_p = Z, K_i = P,$ and $K_d = Z$ will be obtained. The outputs from the membership function rule is consequently processed by the defuzzification that transforms them into actual quantity used to tune the system gains. Let μ_n be the output from the fuzzification and, y_n be the degree of membership. The defuzzification can be performed using (2).

$$Y_{(K_p, K_i, K_d)} = \frac{\sum \mu_n y_n}{\sum \mu_n} \tag{2}$$

Where $Y_{(K_p, K_i, K_d)}$ is the numerical variable that vary from time to time. This outcome to tune the gains $K_p, K_i,$ and K_d of the PID controller in (1) is used.

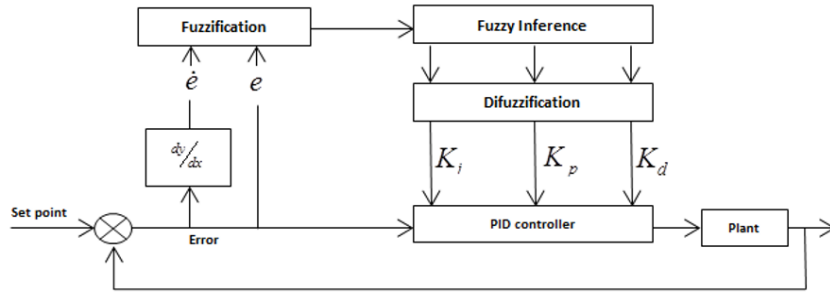


Figure 2. Self-tuning fuzzy PID controller

Table 1

Membership function rule

\dot{e}	e	NB	NM	NS	ZE	PS	PM	PB
	Kp							
	Ki							
	Kd							
NB		P	Z	N	N	N	Z	P
		N	P	P	N	P	P	N
		P	N	N	N	N	Z	P
NM		P	P	Z	Z	Z	P	P
		N	Z	P	P	P	Z	N
		P	Z	Z	N	Z	Z	P
NS		P	P	Z	N	Z	P	P
		N	N	Z	P	Z	N	N
		P	P	Z	N	Z	P	P
ZE		P	P	P	Z	P	P	P
		N	N	N	Z	N	N	N
		P	P	P	Z	P	P	P
PS		P	P	Z	N	Z	P	P
		N	N	Z	P	Z	N	N
		P	P	Z	N	Z	P	P
PM		P	P	Z	N	Z	P	P
		N	Z	P	P	P	Z	N
		P	Z	Z	N	Z	Z	P
PB		P	Z	N	N	P	Z	P
		N	P	P	P	N	P	N
		P	Z	N	N	P	Z	P

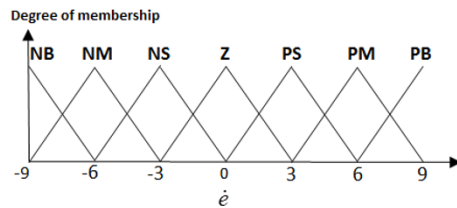
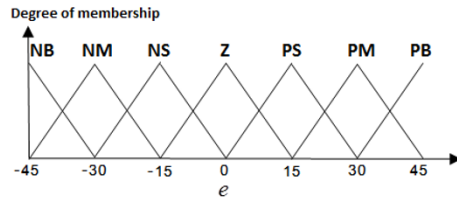


Figure 3. Fuzzification

METHODOLOGY

This work was divided into two parts including design and test steps. The first part consisted of plant and controller design for the autonomous driverless tractor. The second part of our work was to test for the efficiency of the proposed Self-tuning Fuzzy PID Controller for tracking.

Design of the Autonomous Driverless Tractor

The experimental hydraulic tractor has a maximum dimension of 110 x 180 x 130 cm. The diameters of front and rear wheels are 90 cm and 60 cm, respectively. The tractor uses a 15-horsepower gasoline engine to drive a hydraulic pump that generates pressure to be transmitted to the hydraulic motor for driving the rear wheels. The system has low maintenance costs and ease of use suitable for agricultural operation requiring high drawbar force. The directional control is operated through 1:80 ratio speed reducer gearbox to increase the motor rotating speed. The photograph of the designed tractor is given in Figure 4. The control system of the autonomous driverless tractor is created according to working diagram as shown in Figure 5.

The block diagram of the control system of the autonomous driverless tractor is shown in Figure 5. The target PC is installed on the tractor and the main PC is placed on the station. Both PCs communicate through WIFI by using Bullet M2 Point-to-Point Bridge transmission with 630 mW of output power (Horkaew, 2008). The target PC receives data from a GPS receiver through the serial port, which is used to locate the position of the tractor while moving. In this research, the Garmin GPS-72 receiver which has a radial error of no more than 5 meters in real time (Garmin Ltd., 2009) was used. The GPS works with a Pololu CHR-6dm IMU sensor, which is adapted for use with the tractor (Elecmaster, n.d.). The data is transmitted through the serial port to calculate the tractor attitude and



Figure 4. Photograph of Hydraulic Tractor

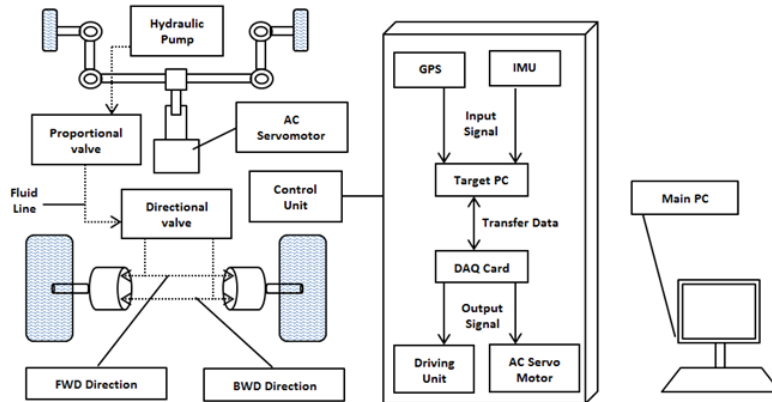


Figure 5. Working Diagram of Autonomous tractor

heading in relative to magnetic north. When the position and direction of the tractor is set, a control signal is processed and transmitted through the NI PCI-6221 data acquisition (DAQ) card which connects the equipment and sensors through the terminal block. The DAQ card reads and transmits electric signals, and these are retained in the target PC board attached to the tractor for measurement, analysis, and storage. The results are then displayed using LabVIEW software on main PC. The three signals used are: 1) Analog I/O for measuring the signals from the sensors and for generating analog signals, which are normally between -10V and +10V; 2) Digital I/O for acquiring and generating digital signals; and 3) Counter I/O for measuring the signals from the encoder or generating pulses to transmit signals to the equipment for controlling the steering system and the movement of the tractor (Chivapansri, 2013).

In addition, the steering system uses a 0.4 kW Panasonic MINAS A5II AC Servo Motor having high-precision positioning of the 1,048,576 pulses/rev (Panasonic Corporation, 2009). In this paper, the velocity mode was used to control the motor. It receives an analog input signal in the range of -10 V and +10 V for being a power source for direction control through a 1:80 ratio. A 4/3 directional control valve is used to control the forward and backward rotation of the wheels, and a proportional valve is used to control the speed of the wheels with a voltage in the range of 0-9 volts at 0-2 m/s.

Algorithm for Tractor Control

LabVIEW was used to process the data from/to the tractor. To control the motion of the vehicle, three important tasks, including identify the trajectory, formulating equations for the distance error and heading error, and designing the self-tuning fuzzy PID controller, are required. The diagram of the control algorithm is illustrated in Figure 6.

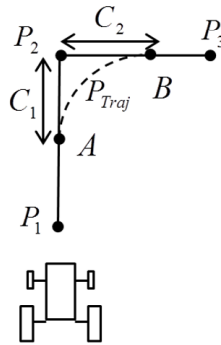


Figure 9. A curved line constructed from two straight lines

Where \mathcal{I} and T are time and the time duration between P_S and P_E , respectively. v_{\max} and P_1 is the maximum velocity (m/s) and acceleration (m/s^2) of the tractor, respectively.

Figure 9 shows the construction of a curved line from two straight lines. The first straight line is between P_1 and P_2 , and the second straight line is between P_2 and P_3 . The dash-curved line in Figure 9 starts from A (Latitude, Longitude) and ends with curve line trajectory P_{Traj} that can be calculated using the following equation. (Luca, A.D., 2015; Upaphai et al., 2017)

$$P_{Traj} = A + V_1 m_2 t + \frac{t^2}{2\Delta t} (V_2 m_3 - V_1 m_2) \tag{6}$$

Where V_1 and V_2 are the velocity for the first and second straight lines, respectively. m_{12} and m_{23} are the directional vectors, and Δt is the time difference that can be obtained from the following equations.

$$m_2 = \frac{P_2 - P_1}{\|P_2 - P_1\|} \tag{7}$$

$$m_3 = \frac{P_3 - P_2}{\|P_3 - P_2\|} \tag{8}$$

$$\Delta t = \frac{2l_1}{V_1} \tag{9}$$

Defining the Equations of Distance and Heading Errors of the Tractor. The equations used to maintain the position of the tractor consists of the distance and heading error equations. The distance error from the trajectory is given by (10). On the other hand, the heading error, which is defined as the difference of the yaw angle from the trajectory, can be formulated in (11) (Upaphai et al., 2017; Phothongkum, 2016).

$$Distance\ error = \sqrt{(x_{ref} - x_{act})^2 + (y_{ref} - y_{act})^2} \tag{10}$$

$$Heading\ error = atan2((y_{ref} - y_{act}), (x_{ref} - x_{act})) - \theta_{act} \tag{11}$$

The reference position (x_{ref}, y_{ref}) can be obtained from the defined trajectory model, whereas the actual position (x_{act}, y_{act}) and steering angle are provided by GPS and IMU. The outputs of (10) and (11) are consequently given to the self-tuning fuzzy PID controller to search for the optimal gains that result in the minimization of these error functions.

The Design of Self-tuning Fuzzy PID Controller. The Fuzzy PID controller is designed by applying LabVIEW program. The main controller consists of distance and heading control units. The block diagram of both units is illustrated in Figure 10.

The inputs for the self-tuning fuzzy PID controller in terms of the distance and heading errors and their derivative are represented by the matrices e and \dot{e} in the above figure. These error functions are then given to the Fuzzy system in LabVIEW. In the fuzzification process, the seven variables are defined : NB, NM, NS, ZE, PS, PM, and PB, and construct the membership function of distance and Heading errors as demonstrated in Figure 3. For example, if the heading error of the tractor is 30° and the distance error is 3 m, the outcomes of language variable are PM and PS. These results are processed by the Fuzzy Inference which employed the defined membership functions as reported in Table 1. The Defuzzification provides the language variable of P,N,P and $y_{(K_p, K_i, K_d)}$ as given in (2). y_{K_p} is multiplied by e to obtain the proportional term to regulate the heading and distance errors of the tractor. y_{K_i} is multiplied by the integration of e to obtain the integral term to control the steady-state error, and y_{K_d} is multiplied by \dot{e} to define the derivative term to control the overshoot in the tracking process.

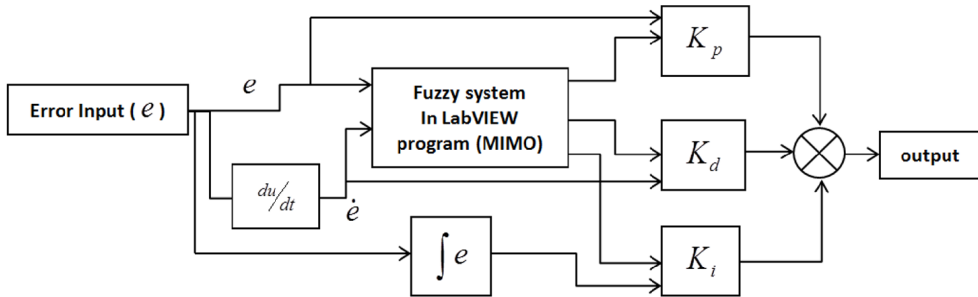


Figure 10. Block diagram of self-tuning fuzzy PID controller.

Evaluation of the Effectiveness of the Proposed Tracking System

The proposed self-tuning Fuzzy PID approach is evaluated by comparing to the conventional PID control. The results of straight-line motion and combined straight/curved lines (N-Shaped) from two techniques are assessed. To begin with, the PID controller that can take the linear input is used to manage the motion of the tractor. In this experiment, the controller gains on a trial and error basis are adjusted. After that the proposed self-tuning fuzzy PID controller is applied to take the nonlinear input in the tracking process. All results are reported in terms of the average heading and distances errors as given in (12) and (13).

$$\text{Average heading error} = \frac{\sum_{i=1}^n D}{n_d} \quad (12)$$

$$\text{Average distance error} = \frac{\sum_{i=1}^n D}{n_d} \quad (13)$$

In (12), and (13), n_h and n_d are the total number of heading error points and distance error points, respectively. $\Sigma + H$ and $\Sigma - H$ are the summations of the heading errors deviated to the right and left, respectively. ΣD is the summation of the distance errors.

The metrics in (12) and (13) are used to evaluate the comparative effectiveness of our approach with respect to the reference method. However, maintaining the same condition of the landscape and weather throughout the test is essential, since this can affect the functionality of the GPS.

RESULTS AND DISCUSSION

Experimental Results of the Straight Line Trajectory Tracking Control of the Tractor. In this experiment, the starting and ending points of the straight-line trajectory were set at (14.0371 latitude, 100.724 longitude) and (14.0372 latitude, 100.7243 longitude), respectively, as shown in Figure 11. The maximum speed was set to 1 m/s.

To compare the effectiveness of the conventional PID and self-tuning fuzzy PID controllers, the gains of the PID control loop were set to $K_p = 12$, $K_i = 0$, and $K_d = 0$. The membership function rules of the self-tuning fuzzy PID controller were set as reported in Table 1. The experimental results are shown in Figures 12 to 14.

Figure 12 compares the results of the trajectory tracking of the tractor controlled by the conventional PID controller (red dashed line), self-tuning fuzzy PID controller (blue solid line), and the prescribed straight-line trajectory (black dotted line). From this figure, it can be noticed that the self-tuning fuzzy PID control provides a faster response to the steering wheel compared to the other. Therefore, the heading angle of the tractor (blue solid line) is relatively smoother. On the other hand, the maximum errors from the prescribed trajectory

of both control systems are 2 m due to the error of GPS according to the specifications of the equipment, Garmin GPS-72, which has a radial real-time error less than 5 m.

Figure 13 compares the heading errors resulted from the conventional PID Controller (red dashed line) and self-tuning fuzzy PID controller (blue solid line). The conventional PID Control (red dashed line) provides the maximum heading errors of -18 degree and 25 degree, while the self-tuning fuzzy PID control (blue solid line) provides the maximum heading errors of -15 degree and 14 degree. The average heading errors from the conventional PID and self-tuning fuzzy PID controllers, are from -14.35 to 22.46 degree and from -11.82 to 10.66 degree, respectively. It can be clearly seen that the proposed self-tuning fuzzy PID control system has a faster response to the steering wheel, and has a smaller average heading error. Hence, the proposed automatic control system outperforms the conventional PID techniques.

Figure 14 shows the distance errors of the autonomous tractor controlled by the conventional PID controller (red dashed line) and self-tuning fuzzy PID controller (blue solid line). The distance errors from the conventional PID and self-tuning fuzzy PID controllers are 4-7m and 3-5.8m, respectively. In addition, the average distance errors from the conventional PID and self-tuning fuzzy PID controllers are 5.23 m and 4.41 m, respectively. It can be noticed that the self-tuning fuzzy PID controller gives better tracking performance compared to the results from the conventional PID. The proposed self-tuning fuzzy PID controller also provides more consistent speed as well as smaller average distance error.



Figure 11. Straight line trajectory

Design of Controllers for Autonomous Tractor

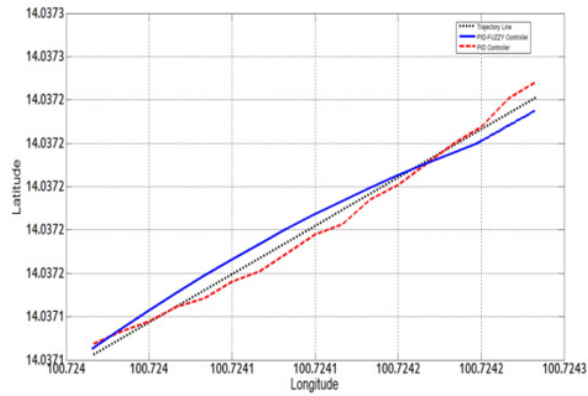


Figure 12. Experimental results of straight line trajectory tracking Control

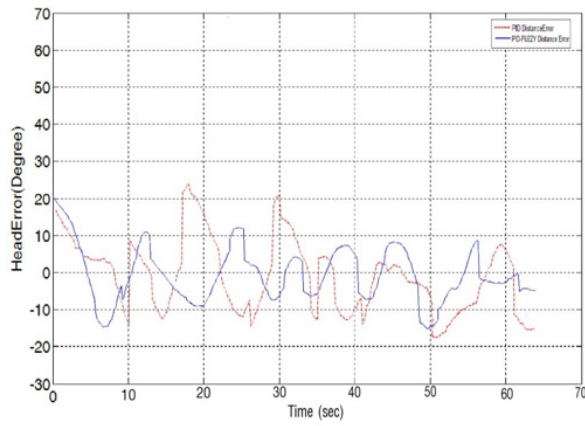


Figure 13. Heading error of the tractor

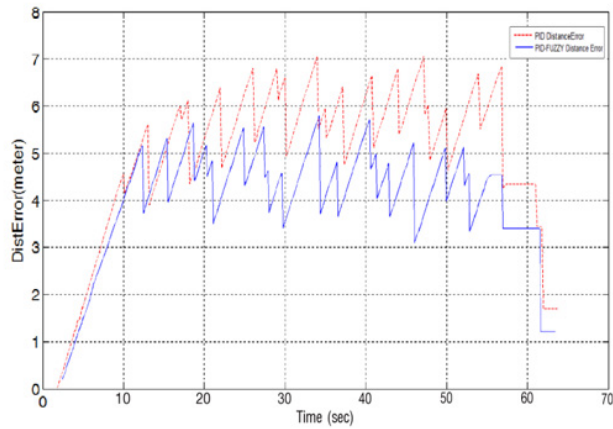


Figure 14. Distance error of the tractor



Figure 15. N-shaped trajectory

Experimental Results of The N-shaped Trajectory Tracking Control of The Tractor

The N-shaped trajectory that consists of both straight and curved lines was set with the same starting point, ending point, maximum speed, and controller gains as defined in the previous experiment. The comparisons of the results from the conventional PID and the proposed self-tuning fuzzy PID techniques are shown in Figures 16 to 18.

Figure 16 compares the results of the trajectory tracking of the tractor controlled by the conventional PID controller (red dashed line), self-tuning fuzzy PID controller (blue solid line), and the prescribed straight-line trajectory (black dotted line). From this figure, it can be noticed that the response of the conventional PID controller is so slow that it provides poor tracking performance along the first curve and the other compared the proposed automatic control technique. However, the moderate response of the acceleration of the vehicle may bring some amount of error to the system.

Figure 17 compares the heading errors resulted from the conventional PID controller (red dashed line) and self-tuning fuzzy PID controller (blue solid line). The conventional PID controller (red dashed line) provides the maximum heading errors of -48 degree and 35 degree, while the self-tuning fuzzy PID controller (blue solid line) provides the maximum heading errors of -10 degree and 20 degree. The average heading errors from the errors from the conventional PID and self-tuning fuzzy PID controllers are 4.69 m and 4.64 m, respectively. It can be noticed that the self-tuning fuzzy PID controller gives better tracking performance compared to the results from the conventional PID. The proposed self-tuning fuzzy PID controller also provides more consistent speed as well as smaller average distance error. Hence, the proposed automatic control system outperforms the conventional PID techniques.

Figure 18 shows the distance errors of the autonomous tractor controlled by the conventional PID controller (red dashed line) and self-tuning fuzzy PID controller (blue solid line). The distance errors from the conventional PID and self-tuning fuzzy PID controllers are 0.9 - 9 m and 2 - 6.8 m, respectively. In addition, the average distance errors from the conventional PID and self-tuning fuzzy PID controllers are 4.69 m and 4.64 m, respectively. It can be noticed that the self-tuning fuzzy PID controller gives better tracking performance compared to the results from the conventional PID. The proposed self-tuning fuzzy PID controller also provides more consistent speed as well as smaller average distance error.

In summary, the average values of heading and distance errors for the straight line and N-shaped cases, resulted from the conventional PID controller and the proposed self-tuning fuzzy PID approach, are reported in Table 2.

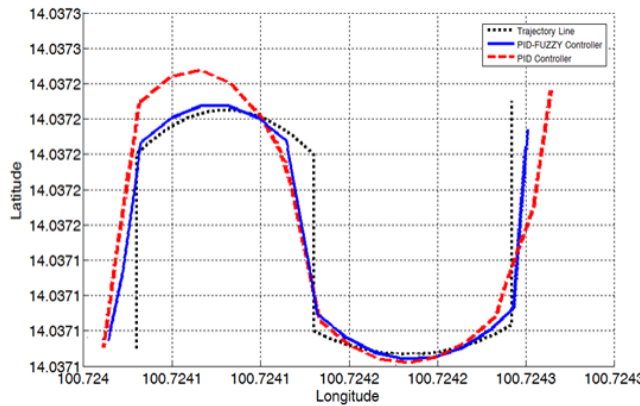


Figure 16. Experimental results of the N-shaped trajectory tracking control of the tractor

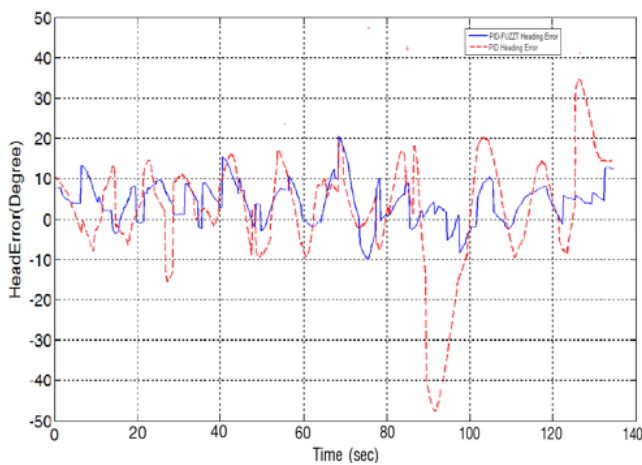


Figure 17. Heading error of the tractor

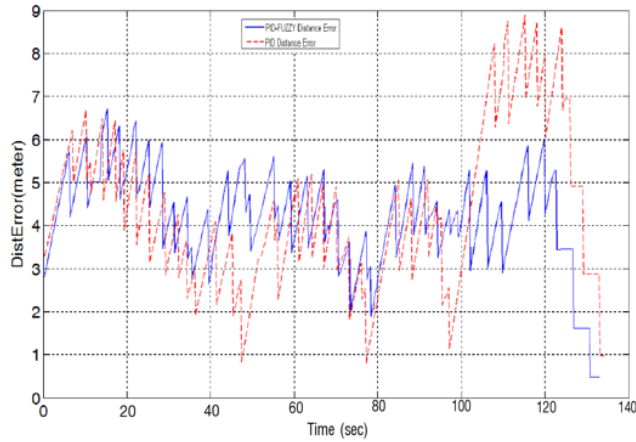


Figure 18. Distance error of the tractor

Table 2

Tracking control results of the conventional PID controller and the proposed self-tuning fuzzy PID controller

	Case of error	PID controller	Self-tuning fuzzy PID controller
	Heading error	-18 to 25 deg	-15 to 14 deg
Straight line	Distance error	4 to 7 m	3 to 5.8 m
trajectory	Ave. heading error	-14.35 to 22.46 deg	-11.82 to 10.66 deg
	Ave. distance error	5.23 m	4.91 m
	Heading error	-48 to 35 deg	-10 to 20 deg
N-Shaped	Distance error	0 to 9 m	2 to 6.8 m
trajectory	Ave. heading error	-11.73 to 8.92 deg	-3.13 to 6.27 deg
	Ave. distance error	4.69 m	4.64 m

CONCLUSIONS

This article presented a design of self-tuning fuzzy PID tracking control for a tractor. The efficiency of the proposed controller is compared to that of the conventional PID controller. From the experimental results, the proposed self-tuning fuzzy PID approach shows the high efficiency. In particular, the faster response of steering wheel from the self-tuning fuzzy PID controller leads to relatively small errors. The performance of the design is limited by the specifications of the tractor's drive system and the accuracy of the GPS used in this work. It is believed that the proposed design technique can be well applied to any high performance/precision systems to perform better tracking control.

ACKNOWLEDGMENTS

Our heartfelt appreciation goes to Department of Mechanical Engineering of Srinakharinwirot University and Rajamangala University of Technology Thanyaburi in Thailand, which provided research grant from annual income budget 2018.

REFERENCES

- Allou, S., Zennir, Y., & Belmeguenai, A. (2017). Fuzzy logic controller for autonomous vehicle path tracking. In *Proceedings of 2017 18th International Conference on Sciences and Techniques of Automatic Control and Computer Engineering (STA)* (pp. 328-333). Monastir, Tunisia.
- Awouda, A. V. A., & Mergani, M. H. (2017). Design of self- tuning PID controller using fuzzy logic for DC motor speed. *International Journal of Social Science and Technology*, 2(4), 27-33.
- Basnayake, I. D., Madhushani, T. W. U., & Maithripala, D. H. S. (2017). Intrinsic PID controller for a Segway type mobile robot. In *Proceedings of 2017 IEEE International Conference on Industrial and Information Systems (ICIIS)* (pp. 1-6). Peradeniya, Sri Lanka.
- Chivapansri, K. (2013). *Principles of data acquisition (DAQ card): basic labVIEW. LabVIEW graphical system design* (pp. 42-44). Bangkok: Se-Education Public Company Limited.
- Garmin Ltd. (2009). *GPS 72H owner's manual*. Retrieved May 4, 2015, from http://static.garmincdn.com/pumac/GPS72H_OwnersManual.pdf
- Handayani, A. S., Dewi, T., Husni, N. L., Nurmaini, S., & Yani, I. (2017). Target tracking in mobile robot under uncertain environment using fuzzy logic controller. In *Proceedings of 2017 4th International Conference on Electrical Engineering, Computer Science and Informatics (EECSI)* (pp. 1-5). Yogyakarta, Indonesia.
- Heikkinen, J., Stotckaia, A. D., & Minav, T. (2017). Self-tuning parameter fuzzy PID controller for autonomous differential drive mobile robot. In *Proceedings of 2017 XX IEEE International Conference on Soft Computing and Measurements (SCM)* (pp. 382-385). St. Petersburg, Russia.
- Horkaew, P. (2008). *423305 Computer and communication. Chapter 11 Point-to-Point Access* (pp.111-119). Retrieved May 4, 2015, from <http://personal.sut.ac.th/paramate/files/compcom/compcomm11.pdf>

- Huynh, V. T., Smith, R. N., Kwok, N. M., & Katupitiya, J. (2012). A nonlinear PI and back stepping based controller for tractor-steerable trailer influenced by slip. In *Proceedings of the 2012 IEEE International Conference on Robotics and Automation (ICRA)* (pp. 245-252). IEEE, Minneapolis, MN.
- Kayacan, E., Kayacan, E., Ramon, H., Kaynak, O., & Saeys, W. (2015). Towards agrobots: trajectory control of an autonomous tractor using type-2 fuzzy logic controllers. *IEEE/ASME Transactions on Mechatronics*, 20(1), 287– 298.
- Luca, A. D. (2015). *Trajectory planning in Cartesian space*. Retrieved May 4, 2015, from http://www.diag.uniroma1.it/~deluca/rob1_en/14_TrajectoryPlanningCartesian.pdf, access on 29/04/2016.
- Moon, H. C., Woo, H. J., Zhe, H. X., Kim, H. J., Kim, J. H., Kim, Y. J., & Kye, J.E. (2013). Auto-guidance system for tillage tractor. In *Proceedings of 2013 13th International Conference on Control, Automation and Systems (ICCAS)* (pp. 1347-1350). Kimdaejung Convention Center, Gwangju, Korea.
- Pan, S., & Zhou, H. (2017). An adaptive fuzzy PID control strategy for vehicle yaw stability. In *Proceedings of 2017 IEEE 2nd Information Technology, Networking, Electronic and Automation Control Conference (ITNEC)* (pp. 642-646). Chengdu, China.
- Panasonic Corporation. (2009). *Operating instruction (overall) AC servo motor and driver MINAS A5II/A5 series*. Retrieved May 4, 2015, from http://industrial.panasonic.com/content/data/MT/PDF/manual/en/acs/minas-a5-2_manu_e.pdf
- Phothongkum, K. (2015). *PID+Fuzzy Control of the obstacle avoidance system for indoor mobile robots*. (Unpublished master thesis). Rajamangala University of Technology Thanyaburi, Thailand.
- Ratanaworahirunkun, R., Srikukaa, J., Supannarach, S., & Kudjomsri, P. (2013). Optimal PID controller design for automatic voltage regulator systems. *Journal of Information Science and Technology*, 4(1), 21-26.
- Ruangurai, P., Ekpanyapong, M., Pruetong, C., & Watewai, T. (2015). Automated three-wheel rice seeding robot operating in dry paddy fields. *Maejo International Journal of Science and Technology*, 9(03), 403-412.
- Su, X., Wang, C., Su, W., & Ding, Y. (2016). Control of balancing mobile robot on a ball with fuzzy self-adjusting PID. In *Proceedings of 2016 28th Chinese Control and Decision Conference (CCDC)* (pp. 5258-5262). Yinchuan, China.
- Upaphai, W., Bunyawanchakul, P., & Janthong, M. (2017). Trajectory tracking control design for an autonomous tractor using fuzzy PID controller. *International Journal of Agricultural Technology*, 13(4), 501-519.
- Zaber, N. M., Ishak, A. J., Soh, A. C., Hassan, M. K., & Abidin, Z. Z. (2015). Designing PID controller for position control with disturbance. In *Proceedings of 2015 International Conference on Computer, Communications, and Control Technology (I4CT)* (pp. 404-407). Kuching, Malaysia.

Review Article

A Review: Methodologies Review of Magnetic Water Treatment As Green Approach of Water Pipeline System

Athirah Othman*, Johan Sohaili and Nur Sumaiyyah Supian

*Department of Environmental Engineering, Faculty of Civil Engineering,
Universiti Teknologi Malaysia, 81310 UTM, Skudai, Johor, Malaysia*

ABSTRACT

This review is aimed to present an in-depth review of several methodologies on magnetic water treatment (MWT) that are employed as scale treatment in water pipeline and to critically discuss each method in order to determine the best outcome of MWT. The magnetically assisted water in pipeline in various applications are presented, argued and best variables are listed according to the performance of each MWT. The advantages and limitations of MWT are discussed and the main outcome from the review summarize the best method in MWT, especially in effectiveness of treating scale in terms of sustained environment benefits. Magnetic field application in water treatment has the potential to improve the water pipeline performance and lifetime. The application is also significant in controlling the growth of scale in upcoming system. Both of these benefits lead to healthier water treatment, increasing and maintaining the lifetime and performance of water system.

Keywords: Magnetic water treatment, permanent magnet, pipe, scale, water

ARTICLE INFO

Article history:

Received: 29 March 2018

Accepted: 12 September 2018

Published: 24 January 2019

E-mail addresses:

dr.athirah.o@gmail.com (Athirah Othman)

johansohaili@utm.my (Johan Sohaili)

maya_viaxzey89@yahoo.com (Nur Sumaiyyah Supian)

* Corresponding author

INTRODUCTION

MWT is an interesting research field because the treatment is consuming zero energy (Esmailnezhad et al., 2017) and has high potential as physical water treatment, which is more environmentally friendly compared to chemical water treatment, which is not desirable (Simonik & Urbancl, 2017). Even now, in 2018, there is still ongoing

researches that relate to magnetic water treatment, proving that this topic is still eagerly explored by researchers worldwide. It is demanded because recent incentives to 'go green' treatment (Harfst, 2010) require less budget (Mysliwiec et al., 2016) and produce less harmful effects (Alimi et al., 2007). For a long term of MWT implementation, especially in pipeline system, it will improve its life-span as the pipeline with magnetic devices were less affected by scale formation. This free-scale of pipeline is definitely having less possibility to get damaged, corrosion and leakage and it fulfils the concept of environmentally friendly. Hence, pipeline with magnetic devices are facing less problems, and its life-time period will be increased (Gholizadeh et al., 2005; Mosin & Ignatov, 2015).

The magnetization principles or hypotheses of MWT can vary depending on the objective chosen such as Lorentz Force (Chang & Thai, 2010), magnetic memory (Esmailnezhad et al., 2017), nucleation (Simonic & Urbanc, 2017), colloidal (Mosin & Ignatov, 2014) and Pauli exclusion principle (Madsen, 2004). The methodologies are strictly selected from previous researches which focus only on magnetic field, scale and water. These chosen methodologies will be elaborated in detail, where any advantages and disadvantages will be discussed. Thus, in particular, this paper reiterates conclusions of prior studies regarding the best methodology in MWT to maximize treating scale in water pipeline.

Scale is generally an assemblage of calcium carbonate, magnesium hydroxide and calcium sulfate (Sohaili et al., 2016) which is normally hard, insulator layer off-white in color. The water flowing continuously inside the water pipeline continues to be heated and cooled with additive substances that might accelerate the scale formation growth. Scale creates a cake perforation, which in turn clogs the media, decreasing internal diameter of pipe and disturbing the fluid flow in the media. The main catalyst of scale formation is water hardness which contains large quantities of dissolved compounds of calcium and magnesium.

The formation is boosted with increasing temperature, and existence of metallic elements normally coming from the pipe. The major sources of drinking water are ground water, rivers, lakes, rain water, seawater, among others. All these sources are natural water which usually contains high level of hardness. Scale in water pipeline causes many problems either in daily life or industrial activities. In daily life, scale leads to clog water instruments such as faucet, shower head and tends to affect health (Larson & Skold, 1957).

For industrial activities, the problems result in increased maintenance and operating cost (Banejad & Abdosalehi, 2009), reducing equipment performance (Quinn et al., 1997) because the scale is reducing the diameter of pipe, thus lowering the flow rate of fluid and increasing the energy consumption of the pumps (Spiegler & Laird, 1980). Previously, most scale problems were treated by chemical water treatment such as water softening (Harfst, 2010) or directly by using hydrochloric acid. This chemical water treatment cannot

overcome the problem of scale where the procedure must be conducted consistently, which becomes a very costly and harmful procedure. Physical water treatment is strongly recommended where it is implemented by applying methods or technologies without using any substances as prevention of scale problem.

MWT has been employed for almost a century (Harfst, 2010). The first research regarding this topic was in 1890 (Raisen, 1984) and first commercial device was patented in 1945 in Belgium (Vermeiran, 1958). For Malaysia, by considering all types of water distribution either in domestic or industrial purposes, the state of Johor had consumed at least 155.3 million Ringgit Malaysia for the replacement of a total of 222,741 meters of water pipes between 2003 and 2005 (Ranhill Utilities Berhad, 2006). Britain spends around £600 million each year to clean or repair pipes and boilers damaged by scale (Donaldson & Grimes, 1988). There are disagreements and debate exists on MWT due the efficacy of this treatment. However, this review paper offers unbiased information and a discussion of the claims made by various researches on MWT based on their methodology and findings. The goal of this literature review is to summarize the results of previous researches that are relevant to the MWT on treating the scale and to recommend the best MWT methodology.

The Principles of MWT

The principle of MWT is referring to various aspects. According to Busch et al. (1996), MWT principle is associated with Faraday's Law, which considers the changes in voltage and current of conducting solutions that pass through magnetic field (Salman et al., 2015). Faraday's Law formula is $E = v \times B$, where E is electric field vector, v is fluid linear velocity and B is magnetic induction vector. The magnetic application is also related to the physics of interaction between a magnetic field and a moving electric charge ion, which can be known as the theory of Lorentz's force, where Lorentz force is $F_L = q |B \times v|$, where q is quantity of charged ion, B is magnetic induction and v is flow velocity. In support of this principle, Chang & Tai (2010), Gabrielli et al. (2001), Lipus et al. (2011), Madsen (1995) and Parsons et al. (1997) demonstrated that the maximum effect of magnetic field would occur when B and v were perpendicular to each other. In regard to the contact frequency between ions and magnetic field, Gholizadeh et al. (2005) found that the magnetic field caused the ion particles to collide with each other, and the redirection of the particles tended to increase the frequency of ions with opposite charge to collide and combined to form a mineral precipitate or insoluble compound. This process has generated the formation of suspended solids contains of mineral of scale and the amount is enhanced by implementation of magnetic field (Alimi et al., 2009). Another principle of MWT is magnetic memory, which is defined as the ability of particles to sustain their magnetization properties for a period of time after being exposed to magnetic field or a transformation towards metastable state (Esmaeilnezhad et al., 2017). Zaidi et al. (2014) had supported this and found that the

high strength of permanent magnets would contribute to the higher potential of the water sample to gain higher magnetic memory.

Besides having reaction with water particles, magnetic field also shows effect on metallic, non-metallic ions and suspended solids but varies in their rate of effectiveness. Although magnet is known as a device that attract to metals, it also can attract non-metals (Alimi et al., 2009), as long as the material has a large number of electrons with parallel spins occurring within a crystal. In terms of magnetism, the materials can be classified into three, which is ferromagnetic, paramagnetic and diamagnetic. Ferromagnetic is the materials that have strongest attraction to magnetic field (cobalt, nickel, iron) even in very low intensity of magnet. These materials were able to point all of the electron spins into same direction over macroscopic length scales even without an applied magnetic field. Paramagnetic is the materials that require magnetic field to order and rearrange the spins randomly. Lastly, diamagnetic is the materials that obviously are not attracted to magnetic field even in very high intensity of magnet.

Methods of Magnetic Device Set-up for Scale Treatment

The optimum effectiveness of MWT can be achieved by proper and correct methodology. The experiment has sometimes given insufficient results due to improper set-up. The chosen methods from previous researches have been selected based on the similar concepts which are mainly related to scale that forms in pipeline due to the existence of water and treatment by permanent magnets. The existing scale in pipeline is either removed or decreased and growth of scale has been delayed.

The most basic factor having a significant influence on MWT effectiveness is the necessity of the water to perpendicularly pass through magnetic field where permanent magnets were attached to the side of water pipeline and all water flowing passes through this magnetic field (Meyer et al., 2000) as illustrated in Figure 1. The position of the permanent magnets must be oriented 90° relative to the flow of water (Gholizadeh et al., 2005). Generally, the arrangement of permanent magnets plays a more important role in efficiency of MWT than other factors such as magnetic strength, water flow rates and temperature. The set-up may differ based on the purpose i.e. either for scale removal or scale formation. In terms of removing scale in water pipeline, MWT functions by either mounting permanent magnets inside pipe sections and reaction chambers or clamped to the outside of pipe in order to cause the water to flow through magnetic field (Harfst, 2010; Faunce & Cabell, 1890; Orb, 2007).

The effect of magnetic field on water hardness reduction is focusing on the results of particle type and particle size of calcium carbonates from water sample (Banejad & Abdosalehi, 2009). The MWT has been done by using seven U-shape magnets equivalent to 25 cm in length of North Pole and South Pole. The magnet is formed from central nucleus

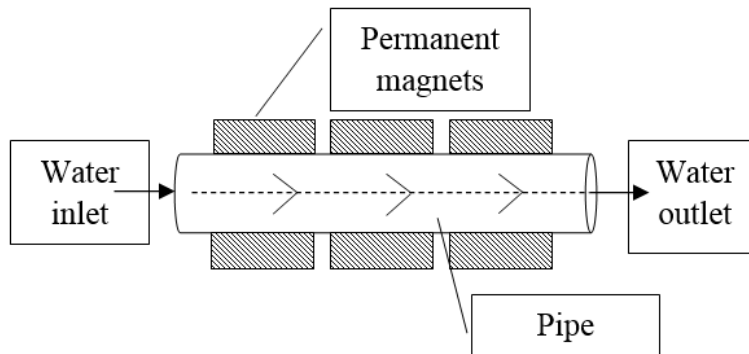


Figure 1. Schematic of the permanent magnets orientation with water pipe

that consists of 300 grams of twisted copper wire for each magnet. This experiment was accomplished by four levels of magnetic field intensity (0 T, 0.05 T, 0.075 T and 1.0 T) and two levels of water flow rate (4 l/h and 30 l/h). U-shape magnet was used as this type of magnet has strong magnetic field due to both North and South poles were facing the same direction, thereby creating a high peak of magnetic peak. The strongest magnetic flux was from magnet pole as it creates the atomic currents per unit volume that give the magnetization (Tanel & Erol, 2008). Since U-shape magnet had both poles in same direction, it was able to double the strength of magnets, especially in legs of U as the homogeneous magnetic field occurred approximately there as illustrated in Figure 2. However, there is limitation in using U-shape magnet in MWT as it only fits into certain diameter of pipes.

Note that the details of procedure, sample test and MWT set-up are not discussed in this paper. This MWT used U-shape permanent magnets in 7 units with 4 different strengths,

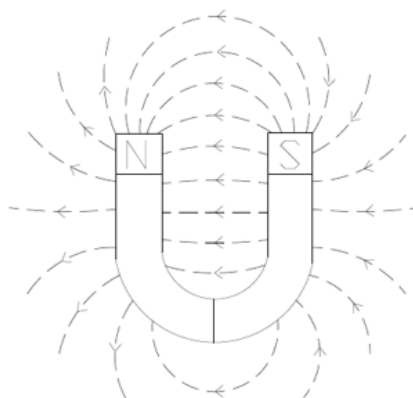


Figure 2. Magnetic flux of U-shape magnet

supported with copper wire and undergoing 2 flow rates. The higher the quantity and strength of permanent magnets used, the higher the removal rates of scale treated. Only two flow rates were used, and they were significantly different.

The study of MWT performed in the industrial boilers have investigated the effect of magnetic field on scale formation in pipeline system and to the boilers (Gholizadeh et al., 2005). A static magnetic field, with about 6000 G was installed in pipeline system right after water pump to ensure magnetized water went into boiler. Magnetic device was used to focus on the effectiveness of magnetic field without any contributions from external factors such as types of water internal flow. Thus, the results obtained were caused only by the magnetic field itself.

The duration of the treatment was started 24 hours after the installation, where the flow rate, pipeline condition and chemical of water properties were recorded. The pipeline conditions were observed every three months and the final observation will be recorded one year after installation. The observations were made in order to study the internal conditions of pipeline, boilers and water chemical properties. The ready-made magnet was used with strength of 6000 Gauss, equivalent to 0.6 Tesla. This study focused only on effectiveness of magnet without involving any other factors that might accelerate the removal rate.

Next is the study of the application of MWT on ordinary and heavy water (Madsen, 2004). The study has created artificial CaCO_3 solution where the ordinary water has been demineralized first by activated carbon and ion exchange method. Electromagnet treatment was also performed by setting a thermostat chamber with temperature of 25°C , small size of permanent block magnets of 40×25 mm with 0.25 T of strength, while mix solution had been prepared by equal volume of 2.5 cm^3 for each 0.1M CaCl_2 with 0.1M NaHCO_3 and 0.006M CaCl_2 with 0.006M Na_2HCO_3 . The samples were taken after 1 hour mixing for microscopy and crystal size distribution was determined visually with Zeiss Jenapol polarizing microscope. For electromagnetic, the duration of treatment was about 30 minutes before the samples were taken. This study used medium magnetic strength, supported by thermostat and two types of sample in order to find the variation of MWT.

MWT implementation in investigating few type of scale which is calcium carbonate (CaCO_3), calcium sulphate (CaSO_4) and barium sulphate (BaSO_4) in two configurations, closed and open loop, with different techniques at ambient temperature of 22°C (Salman et al., 2015). The experiment consisted of tank attached by three pairs of rectangular permanent magnets with north and south poles facing each other with strength of 0.16 T. The saturated solutions of CaCO_3 , CaSO_4 and BaSO_4 were prepared and magnetized for 24 hours before testing. The samples were drawn from the sample tank for every one minute at stagnant condition in order to analyse the selected parameters (turbidity and scale concentration). For the closed loop configuration, the magnetized solution in the sample tank flowed continuously throughout the system. In this configuration, moving solution helps the scale

treatment by measuring turbidity and scale concentration of these saturated solution. The samples were drawn from the sample at one minute interval at stagnant condition in order to analyse the selected parameters (turbidity and scale concentration).

This research has found that the moving solution gives better results of MWT compared with stagnant solution. Thus, this experimental set-up can be further improved. This research is much improved where it varies the type of scale, the loop and conditions of the treatment process while maintaining the basic factors such as quantity and strength of magnet used. The type of various scale, for example magnesium carbonate (Esmailnezhad et al., 2017), magnesium hydroxide and calcium sulphate (Sohaili et al., 2016) that exists inside the water pipeline is different due to different situation and place.

The study of MWT by different conditions of new pilot scale and old existing water system had created a pilot scale water distribution system built in laboratory with eight parallel lines of two materials of looping pipes, where four of them were copper pipes (upper part) and rest were high density cross-linked polyethylene (PEX) pipes (Latva et al., 2016). Water was supplied by 60 litre stainless steel storage tank to this system with the help of water pump and exposure of 26mT maximum of magnetic field. The sample were taken once in a month and sampled from nine different of sampling point through a tap which started before the system and followed by another eight taps at each lines of pipes. The pipe lines were detached from the pilot system after nine months of use and the sample of calcium content that attached onto inner surface was measured by draining 0.1M hydrochloric acid for an hour, while turning it upside-down every 15 minutes. Then, the lines were continuously rinsed with 10 mL acid to ensure complete solubility of calcium. This study considered MWT in experiment and real water system with 2 different materials of pipeline. However, the magnet strength used was very low and not supported by other variables.

FINDINGS OF THE MWT

Experimental results of Banejad and Abdosalehi (2009) indicated that magnetic field controlled with magnetic strength and water flow rate had reduced water hardness by 99%. The efficiency of MWT increased with the increment of magnetic field strength and water flow rate as the magnetic strength increase from 0 Tesla till 0.1 Tesla, the rate of efficiency was also increased. As the water flow rate was changed from 4lit/h into higher speed, 30lit/h, the rate of efficiency were getting even more higher which the increment is about 6.6 to 8.8%. As the experiment was performed under U-Shape magnet, it can be clearly seen from the figure that the higher the intensity of magnetic field, the higher the rate of magnetic treatment efficiency were recorded. Compared to the water influent, the results were only slightly higher with higher flow rate. In the perspective of another shape of permanent magnet, Gabrielli et al. (2001) was using block-shape permanent in performing

MWT resulting up to 30% reduction of calcium concentration. By comparing both cases, it was clearly shown that U-Shape gave higher rate of MWT effectiveness but most of the recent researches preferred block-shape magnet in their research work because block-shape magnet was able to be customized into many concepts, ideas and configurations. It helps the researchers to inspire more ideas in future.

The result on particles of CaCO_3 under U-Shape magnet on MWT had changed calcite to aragonite by at least 70% due to chemical analysis by X-ray and supports the findings of higher intensity of magnetic field gives higher efficiency rate of MWT. Calcite is much stronger layer than aragonite, non-soluble and adheres to the wall surfaces. When the amount of aragonite is much greater than calcite, the process of water treatment will be much easier (Orb, 2007; Simonic & Urbancl, 2017; Sohaili, et al., 2016).

Regarding the result of experiment tested using industrial boilers (Gholizadeh et al., 2005), the new pipeline was well protected from scale formation and internal corrosion, while the boilers and pipelines system were automatically cleared, the solid material became loose and fell off. As for chemical properties, there was a difference in the amount of two crystallographic forms of CaCO_3 as demonstrated by X-ray analysis. The changes of crystal forms of CaCO_3 without magnetic field and with magnetic field were (Calcite = 65%, Aragonite = 35%), (Calcite = 27%, Aragonite = 73%), respectively. Normally, calcite is a very strong layer formed in the pipe's wall and is hard to dissolve. Aragonite is a more soluble layer and normally strongly adheres to pipe walls. It is a good indicator if the content of aragonite is higher than calcite. It has been concluded that MWT required continuous and fast water flow. As for permanent magnet criteria needed, it has to be sufficient in strength and must be oriented 90° in respect of water flow direction.

The study conducted comparing ordinary and heavy water had proven that there is an effect on the crystallization of calcium carbonate in ordinary water due to the existence of magnetic field (Madsen, 2004). It found out that the median of crystal size changed against magnetic field strength. They had an inverse relationship as the median crystal size was decreasing by the increment of magnetic field strength. The smaller the size of crystal indicates the existence of aragonite which is easily removed in this treatment. It demonstrates an acceleration of nucleation of CaCO_3 . But it differs based on the field strengths applied. The relation of crystal size and the strength of magnetic field is inversely proportional as crystal size is decreasing with increasing of magnetic field strength.

According to study by Salman et al. (2015), saturated solution of scaling compounds (CaCO_3 , CaSO_4 and BaSO_4) was created, each having different method. 0.5 M of calcium chloride and 0.5 M of sodium carbonate are required in order to prepare CaCO_3 solution, 0.5 M NaSO_4 and 0.5 M CaCl_2 in preparing CaSO_4 solution and BaSO_4 was prepared by mixing barium chloride and NaSO_4 . It had been proven that moving solution helps the scale in artificial solution to accumulated together, hence the solution turbidity and concentration

was decreasing and cause the precipitation of scale. By comparison with stagnant solution, the parameters tested were only marginally different. The moving solution had enhanced the scale to precipitate and caused reduction in turbidity and concentration of the solution. According to Alimi et al. (2009), MWT helps to increase total precipitation of CaCO_3 by influencing the crystallization process. This is how magnetic field enhances the formation of suspended scale instead of incrustation on the pipe's wall. MWT has effective result in controlling scale but the performance is greater on treating CaCO_3 than CaSO_4 and BaSO_4 .

A comparison study between new and old drinking water system (Latva et al., 2016) has decided on one copper line as well as one PEX line in order to compare efficiency of magnetic water treatment in pipes made from two different materials. Other lines acted as reference lines. The parameters measured were listed in Table 1 below. The calcium content that had been taken from inner pipe surfaces was analysed with ICP-OES according to standard SYP600/SFS-EN ISO11885 and the morphologies were evaluated using field emission scanning electron microscope. For identifying electrical conductivity, a thin carbon layer was coated before the sample was analysed.

Table 1

The methods used according to the suitable parameters

Parameter	Method
Temperature, pH, dissolved oxygen, redox, electrical conductivity.	YSI professional plus meter
Free chlorine, total chlorine, sulphate, chloride, microbial nutrients ammonium, phosphate, nitrite, nitrate.	Hach Lange DR 2800 Spectrophotometer
Alkalinity.	SFS 3005
Total hardness.	SFS 3003
Copper, iron contents.	SFS-EN ISO 11885:2009

The results were plotted using the average value and standard deviations for all samples of pipes. After MWT, the value of all parameters shows that they were only slightly different (approximately to 0% of rate difference) except for alkalinity (1.60%), hardness (1.91%) and pH (2.73%). Based on the impact of MWT on pipe materials, copper pipes were more pronounced compared to PEX pipes but the percentage of calcium precipitated onto the pipe walls with MWT in both pipe materials was almost 15%. These results are in agreement with Alimi et al. (2009) that the total precipitation of scale was due to the amount of contaminants present in water, and not the pipe material. This is answering the question of two different materials of pipe that have almost the same percentage of scale

precipitate. This signifies that MWT reduced the amount of CaCO_3 either present in the bulk solution or attached onto pipe surfaces (Alimi et al., 2009; Gholizadeh et al., 2005; Salman et al., 2015).

This study also found that the calcium content from copper pipes was higher than PEX pipes which was about 63% increment. Eventhough few parameters react with positive results to the MWT such as water hardness, pH, alkalinity, crystal size and amount of CaCO_3 in the water, but there is also other parameters such as water quality parameters (temperature, ammonium, nitrite, nitrate, chloride) which do not contribute much and can be neglected due to the slight difference in value before and after MWT implementation. MWT has very little effect on water quality parameters.

Magnetic water treatment has different effectiveness on metallic and non-metallic pipes. Alimi et al. (2009) showed that non-metallic material of pipe had the most efficient results in magnetic water treatment. However, it was due to the presence of the contaminants in water while passing the magnetic field. The material of non-metallic pipe made of Tygon have tendency to create contaminant when in contact with water. Since this pipe creates substance in the water, the flux of magnetic field exerted the force to the substances ions and tends to deposit them. Referring to Chawla et al. (2012), the magnetic treatment has been performed on cast iron pipe and their scale composition was indicating the highest element was iron ($\text{Fe}= 60.52\%$), followed by oxygen ($\text{O}=34.11\%$) and the lowest is aluminium ($\text{Al}=0.15\%$). Iron and aluminium are metal ions, but the results show an opposite percentage. This findings were explained and support that the effectiveness of MWT did not rely on metallic or non-metallic properties, but most important was that the magnetism was influencing the constituents in the water that passed through magnetic field. Magnetic field created effect and exerted forces on the particles present in water and was not attracted to the metal materials of the pipe.

A summary regarding the best operational set-up for MWT based on the chosen previous researches can be easily recognised as shown in Table 2 below. As for the permanent magnet itself, the higher strength is recommended and it must attach to the pipeline 90° relative to the water flow. The water sample is perpendicular to the magnetic field in order to enhance the magnet memory and boost the scale removal ability. Many types of pipeline material such as steel, copper and PEX can be affected by MWT, but the most efficient MWT is towards the material with metal properties. The water sample can be any type of water depending on the objectives of the study, but the purer the water, the less the effectiveness of magnetic field (Barret & Parsons, 1998).

It is proven that high strength of permanent magnet, high flow rate of water, moving

Table 2

Summary of contrasting results from previous researches

Author(s)/Date	Research Title	Findings
Raisen (1984)	The control of scale and corrosion in water systems using magnetic fields.	With magnetic field, scale forms were a soft sludge that can be removed easily by blowdown. Without magnetic, scale forms was hard and only be removed by chemical treatment.
Donaldson and Grimes (1988)	Lifting the scales from our pipes.	Magnetic unit was removing existing calcite scale and that further hard scale was not forming.
Barret and Parsons (1997)	The influence of magnetic fields on calcium carbonate precipitation.	Magnetic effect maintains for at least 60 hours after exposure.
Coey and Cass (2000)	Magnetic water treatment.	Magnetic field promotes nucleation of aragonite and the magnetic memory stable for hundreds of hours.
Meyer et al. (2000)	Scale prevention in a hot-water storage tank with a magnetic physical water treatment device.	Magnetic device reduce the scale formation by 34% and have made the storage tank shinier and cleaner from the scale deposits.
Gabrielli et al. (2001)	Magnetic water treatment for scale prevention.	Magnetic decreasing the ionic calcium content of the solution even for a single-pass.
Madsen (2004)	Crystallization of calcium carbonate in magnetic field ordinary and heavy water.	Magnetic field affects the crystallization of CaCO ₃ by reducing the crystal size .
Gholizadeh et al. (2005)	The effect of magnetic field on scale prevention in the industrial boilers.	Magnetic device gives protection to the new pipeline from scale and corrosion. Magnetic field reduces the amount of calcite and enhances the amount of aragonite by 38%

Table 2 (Continue)

Author(s)/Date	Research Title	Findings
Orb (2007)	Reducing formation of scale with magnetic descaler.	Magnetic descalers; maintenance free, operate interminably, maintaining their magnetic properties, do not consume additional resources.
Banejad and Abdosatehi (2009)	The effect of magnetic field on water hardness reducing.	Magnetic field cause depletion of water hardness by 99%.
Chawla et al. (2012)	Corrosion of water pipes: a comprehensive study of deposits.	There are different type of primary constituents of brown deposits due to different pipe diameters and surrounding environment.
Mosin and Ignatov (2015)	Practical implementation of magnetic water treatment to eliminate scaling salts.	Magnetic affects both an influence on the water, mechanical impurities and scaling-form salts and ions. Magnetic changes the hydration of ions, salts solubility, pH value.
Salman et al. (2015)	The effect of magnetic treatment on retarding scaling deposition.	MWT has stronger effect on treating CaCO_3 than CaSO_4 and BaSO_4 .
Latva et al. (2016)	Studies on the magnetic water treatment in new pilot scale drinking water system and in old existing real-life water system.	MWT has minor effect on alkalinity, hardness and pH compared to other parameters such as chlorine, nitrate, nitrite, sulfate and chloride.

and continuous flow of water passing perpendicular passing through the magnetic field will increase the effectiveness of MWT towards scale removal and formation. The capability of MWT, especially in controlling scale growth in water pipeline, can be improved by ensuring these factors are implemented as many as possible in order to get the best result. Nowadays, there is MWT devices has been commercialized in various purposes, where the magnetic devices were designed as non-chemical technology for scale or hardness control. It can be found in online purchase but there is not official research or report to justify deeply in their magnetic device concept. The functions can be found in many scope such as for agriculture, vehicles and pipes.

For an example, MWT devices for water distribution system for residential purpose, are said to be made by strongest permanent magnet with high magnetic intensity and powerful combination of materials. Advantages of this is, it designed to suits the four climate countries by considering hot and cold situations with variety designs and size to suits few conditions in residential purposes, poses powerful magnetic flux to maximise the magnetic device effectiveness and it said to be forever lasting due to its magnet plating to avoid abrasion and corrosion. It comes with a fix size, thus it cannot be modified or reused to different size of pipe. It will be the best if the MWT devices can be design and commercialized in customization concept, where the holder of the permanent magnet can be adjusted in order to fit into varies diameter of pipe by keep maximising the exposure of magnetic flux towards pipe.

CONCLUSION

MWT has several types of operational system due to the different cases such as water sample, material of water pipeline, operational system and ambient surrounding. The effectiveness of the MWT implementation can be improved based on the summarisation made in this paper. Implementation of magnetic devices into water treatment with correct orientation, high strength of permanent magnet, high water flow rate and ensuring the water is not in stagnant condition must be considered as basic factors in applying MWT. The installation and maintenance procedure is relatively easy and very seldom where it prolong the life-span of pipeline, thereby minimizing operational and maintenance cost compared to other water treatment.

ACKNOWLEDGEMENT

The authors would like to appreciate the financial assistance received through the research project titled: REMOVAL OF SCALE IN WATER PIPELINE WITH MAGNETIC FIELD, under the Research University Grant (RUG of UTM) with Ref. Number: Q.J130000.2522.18H24, funded by the Ministry of Higher Education, Malaysia and Universiti Teknologi Malaysia.

REFERENCES

- Alimi, F., Tlili, M., Amor, M. B., Gabrielli, C., & Maurin, G. (2007). Influence of magnetic field on calcium carbonate precipitation. *Desalination*, 206(1-3), 163-168. doi: 10.1016/j.desal.2006.02.064.
- Alimi, F., Tlili, M. M., Amor, M. B., Maurin, G., & Gabrielli, C. (2009). Effect of magnetic water treatment on calcium carbonate precipitation: Influence of the pipe material. *Chemical Engineering and Processing: Process Intensification*, 48(8), 1327-1332. doi: 10.1016/j.cep.2009.06.008.
- Banejad, H. & Abdosalehi, E. (2009). The effect of magnetic field on water hardness reducing. In *Thirteenth International Water Technology Conference (IWTC 13)* (pp. 117-128). Hurgada, Egypt.
- Barrett, R. A., & Parsons, S. A. (1998). The influence of magnetic fields on calcium carbonate precipitation. *Water Research*, 32(3), 609-612. doi: 10.1016/S0043-1354(97)00277-7.
- Busch, K. W., Gopalakrishnan, S., Busch, M. A., & Tombácz, E. (1996). Magnetohydrodynamic aggregation of cholesterol and polystyrene latex suspensions. *Journal of Colloid and Interface Science*, 183(2), 528-538. doi: 10.1006/jcis.1996.0576.
- Chang, M. C., & Tai, C. Y. (2010). Effect of the magnetic field on the growth rate of aragonite and the precipitation of CaCO₃. *Chemical Engineering Journal*, 164(1), 1-9. doi.org/10.1016/j.cej.2010.07.018.
- Chawla, V., Gurbuxani, P. G., & Bhagure, G. R. (2012). Corrosion of water pipes: A comprehensive study of deposits. *Journal of Minerals and Materials Characterization and Engineering*, 11(5), 479-492. doi: 10.4236/jmmce.2012.115034.
- Coe, J. M. D., & Cass, S. (2000). Magnetic water treatment. *Journal of Magnetism and Magnetic materials*, 209(1-3), 71-74. doi.org/10.1016/S0304-8853(99)00648-4.
- Donaldson, J., & Grimes, S. (1988). Lifting the scales from our pipes. *New Scientist*, 117(18), 43-46.
- Esmailnezhad, E., Choi, H. J., Schaffie, M., Gholizadeh, M., & Ranjbar, M. (2017). Characteristics and applications of magnetized water as a green technology. *Journal of Cleaner Production*, 161, 908-921. doi: 10.1016/j.jclepro.2017.05.166.
- Faunce, A. B., & Cabell, S. G. (1890). United States Patent No. US438579A. United States Patent Office.
- Gabrielli, C., Jaouhari, R., Maurin, G., & Keddou, M. (2001). Magnetic water treatment for scale prevention. *Water Research*, 35(13), 3249-3259. doi.org/10.1016/S0043-1354(01)00010-0.
- Gholizadeh, M., Arabshahi, H., & Benam, M.R. (2005). The effect of magnetic field on scale prevention in the industrial boilers. *International Journal of Applied Chemistry*, 1(1), 84-89.
- Harfst, W. F. (2010). Non-Chemical Water Treatment. *Chemical Engineering*, 117(4), 66-69.
- Larson, T. E., & Skold, R. V. (1957). Corrosion and tuberculation of cast iron. *Journal American Water Works Association*, 49(10), 1294-1302.
- Latva, M., Inkinen, J., Ramo, J., Kaunisto, T., Makinen, R., Ahonen, M., ... & Pehkonen, S. (2016). Studies on the magnetic water treatment in new pilot scale drinking water system and in old existing real-life water system. *Journal of Water Process Engineering*, 9, 215-224. doi: 10.1016/j.jwpe.2016.01.009.

- Lipus, L. C., Ačko, B., & Hamler, A. (2011). Electromagnets for high-flow water processing. *Chemical Engineering and Processing: Process Intensification*, 50(9), 952-958. doi.org/10.1016/j.cep.2011.07.004.
- Madsen, H. L. (1995). Influence of magnetic field on the precipitation of some inorganic salts. *Journal of Crystal Growth*, 152(1-2), 94-100. doi.org/10.1016/0022-0248(95)00103-4.
- Madsen, H. E. L. (2004). Crystallization of calcium carbonate in magnetic field ordinary and heavy water. *Journal of Crystal Growth*, 267(1), 251-255. doi: 10.1016/j.jcrysgro.2004.03.051.
- Meyer, J. P., Smith, C., & Coetzee, P. P. (2000). Scale prevention in a hot-water storage tank with a magnetic physical water treatment device. In *Proceedings of the ASME-ZSITS International Thermal Science Seminar* (pp. 295-299). Bled, Slovenia.
- Mosin, O., & Ignatov, I. (2014). Basic concepts of magnetic water treatment. *Nanotechnology Research and Practice*, 4(4), 187-200, doi: 10.13187/ejnr.2014.4.187.
- Mosin, O., & Ignatov, I. (2015). Practical implementation of magnetic water treatment to eliminate scaling salts. *Journal of Health, Medicine and Nursing*, 10, 111-126.
- Mysliwiec, D., Szczes, A. & Chibowski, S. (2016). Influence of static magnetic field on the kinetics of calcium carbonate formation. *Journal of Industrial and Engineering Chemistry*, 35, 400-407. doi: 10.1016/j.jiec.2016.01.026.
- Orb, M. (2007). Reducing Formation of Scale with Magnetic Descaler. *Republic of Estonia Jõgeva Co-Educational Gymnasium*, P-20.
- Parsons, S. A., Judd, S. J., Stephenson, T., Udol, S., & Wang, B. L. (1997). Magnetically augmented water treatment. *Institution of Chemical Engineers*, 75(2), 98-104. doi.org/10.1205/095758297528869.
- Quinn, C. J., Molden, T. C., & Sanderson, C. H. (1997). Magnetic treatment of water prevents mineral build-up. *Iron and Steel Engineer*, 74(7), 47-53.
- Raisen, E. (1984). The control of scale and corrosion in water systems using magnetic fields. In *The International Corrosion Forum: The Protection and Performance of Materials* (pp. 1-12). Orleans, Louisiana.
- Ranhill Utilities Berhad. (2006). *Privatisation of the water supply service in the state of Johor Darul Ta'zim Malaysia*. Johor Water Project. Retrieved March 14, 2018, from http://disclosure.bursamalaysia.com/FileAccess/apbursaweb/download/?name=EA_GA_Attachments&id=11345
- Salman, M. A., Safar, M., & Al-Nuwaibit, G. (2015). The effect of magnetic treatment on retarding scaling deposition. *The Online Journal of Science and Technology*, 5(3), 62-77.
- Simonic, M., & Urbancl, D. (2017). Alternating magnetic field influence on scaling in pump diffusers. *Journal of Cleaner Production*, 156, 445-450. doi: 10.1016/j.jclepro.2017.04.080
- Sohaili, J., Shi, H. S., Baloo, L., Zardari, N. H., Ahmad, N., & Muniyandi, S. K. (2016). Removal of scale deposition on pipe walls by using magnetic field treatment and the effects of magnetic strength. *Journal of Cleaner Production*, 139, 1393-1399. doi: 10.1016/j.jclepro.2016.09.028.
- Spiegler, K. S., & Laird, A. D. K. (1980). Scale formation and prevention. In J. Glater, J. L. York & K. S. Campbell (Eds.), *Principles of Desalination* (pp. 627-678). Cambridge: Academic Press. doi: 10.1016/B978-0-12-658702-9.50009-8.

- Tanel, Z., & Erol, M. (2008). Students' difficulties in understanding the concepts of magnetic field strength, magnetic flux density and magnetization. *Latin-American Journal of Physics Education*, 2(3), 184-191.
- Vermeiren, T. (1958). Magnetic treatment of liquids for scale and corrosion prevention. *Anti-Corrosion Methods and Materials*, 5(7), 215-219.
- Zaidi, N. S., Sohaili, J., Muda, K., & Sillanpää, M. (2014). Magnetic field application and its potential in water and wastewater treatment systems. *Separation and Purification Reviews*, 43(3), 206-240. doi.org/10.1080/15422119.2013.79414

Kenaf Fibre and Its Bio-Based Composites: A Conspectus

Adole Michael Adole*, Jamaludin Mohamad Yatim, Suhaimi Abubakar Ramli, Athirah Othman and Norazura Azzmi Mizal

*Department of Structures and Materials, Faculty of Civil Engineering,
University Teknologi Malaysia, 81310 UTM, Skudai, Malaysia*

ABSTRACT

Kenaf fibre is a good reinforcement in fibre polymer composites due to its high strength and elastic modulus, high stiffness, low density, low cost and eco-efficient, less health hazards, renewability, good mechanical and thermal properties, and biodegradability. It is traditionally used for rope, twine, fish net and sacking materials. Recently, it was observed that kenaf fibre had huge potentials to replacing synthetic fibre in composites due to the rising environmental and ecological issues, thus this awareness has motivated efforts for the advancement of new innovative bio-based composites incorporating kenaf fibre for various end-use structural applications. This paper presents an overview of the development made so far in the area of kenaf fibre and its composites in terms of chemical and micro-structural properties, mechanical properties, dimensional stability, thermal stability, product development and application. Some fundamental issues and suggestions for further research in this area are also discussed.

Keywords: Kenaf fibre, mechanical properties, natural fibre, polymer composite, surface treatment, thermal properties

ARTICLE INFO

Article history:

Received: 10 February 2018

Accepted: 27 September 2018

Published: 24 January 2019

E-mail addresses:

adolemike122@gmail.com (Adole Michael Adole)

jamaludin@utm.my (Jamaludin Mohamad Yatim)

suhaimibakar@utm.my (Suhaimi Abubakar Ramli)

dr.athirah.o@gmail.com (Athirah Othman)

azuramazalzzmi@gmail.com (Norazura Azzmi Mizal)

* Corresponding author

INTRODUCTION

Kenaf fibres embedded in polymer matrices bring great benefits to diverse industries, natural environment, advanced technological sectors and end-users alike because of the depletion of petroleum resources (Nashino et al., 2003; Ochi, 2008; Wambua et al., 2003). The shift to more sustainable constructions for civil

infrastructure is not only an initiative towards a more viable environment and cost efficiency but also a demand from the world environmental and ecological regulatory bodies. To this end, the engineers and scientists have presented green composites made from renewable agricultural materials as suitable alternative to synthetic fibre reinforced composites (Fiore et al., 2015).

In addition to the environmental and economic issues poised with the used of synthetic fibres in polymeric composites, natural fibre composites have several other advantages as substitute to synthetic fibre in composites such as recyclability, renewability, biodegradability, abundant, resistance to corrosion, non-toxicity, high flexibility, competitive mechanical properties, low density, less energy consumption, minimum abrasive resistance to processing equipment and waste disposal problems (Ander et al., 2016; Hassan et al., 2017; Reza et al., 2014a; Zamri et al., 2016). The major drawback in the utilization of natural fibres in polymeric composites is that natural fibres usually contain huge amounts of the hydroxyl group which makes them polar in nature. The addition of hydrophilic natural fibres to hydrophobic polymer which is non-polar material will result to a poor mechanical and durability properties due to non-uniformity of the fibre dispersion within the polymer and poor compatibility between the fibre and the matrix, however, this issue can be addressed by chemical treatments (maleic anhydride, isocyanates, organosilanes, permanganate peroxide, sodium hydroxide) and physical treatments (corona treatment and cold plasma treatment) as reported by Wambua et al. (2003).

Among the several types of natural fibres, kenaf fibre has gained considerable attention and been largely utilized over the last two decades (Huda et al., 2008; Liu et al., 2007; Nashino et al., 2003; Vijayakumar et al., 2014). The rationale behind this acceptance is mainly due to the rapid growing abilities of kenaf plant which enables it to produce a great volume of raw materials in a short period of time and consequent low price (Abdul Hamid et al., 2009; Hossain et al., 2011; Seller & Reichert, 1999). Natural fibres such as kenaf fibres are far cheaper when compared with carbon fibre and glass fibre. The price of kenaf fibre per kg is 0.53 US\$ as against glass fibre and carbon fibre which is 3.25 US\$ and 500 US\$ per kg respectively (Li et al., 2000; Mohanty et al., 2000). In addition, Principia partners (2003) observed that natural fibre sources were cost-effective alternatives comparatively speaking. In the USA price for instance, Free on Board (FOB) were mentioned in mid-2003, ranges between 0.23 US\$ and 0.47 US\$ per pound and 500 US\$ and 1036 US\$ per metric ton for kenaf, hemb, sisal and flax fibres of numerous grades. Nashion (2004) carried out a research and stated that it took more energy to produce glass fibre than what it took to produce kenaf fibre and it was put at 54 moles per joule to produce 1kg of glass fibre while kenaf fibre took only 15 moles per joule to produce the same quantity. Figure 1 shows cost comparison between some natural fibres and E-glass as presented by Thakur et al. (2014).

Wambua et al. (2003) had demonstrated that natural fibre polymer composites including kenaf fibre polymeric composites had been linked with mechanical properties that could measure up to or even better than glass fibre reinforced composites. Also, worthy of note is the weight reduction ability of kenaf fibre as alternative to synthetic fibres in composites as well as low impact on the environment. Kenaf also maintains a competitive price as against synthetic fibres which required a large amount of energy to produce.

Kenaf Plant

Kenaf according to Vision paper (2003) has been in existence for over 4,000 years with origin traced to ancient Africa. The kenaf plant belongs to the hibiscus family (*Hibiscus cannabinus* L.) which is closely related to the family of jute, cotton and okra, which is grown in India, Bangladesh, Malaysia, United State of America, Indonesia, Vietnam, Thailand, South Africa and other parts of Africa, and some specific parts of south-east Europe. In the United State of America, kenaf grows rapidly to a height of about 3.5 – 4.5m in a short period of time while in Malaysia, this plant grows to 1.5 – 3.5m tall within short period of time. Lately in Malaysia, for example kenaf was recognised as an important natural raw fibre capable of replacing tobacco in the manufacturing of many products in construction, automotive, textile and other technological sectors (Anuar & Zuraida, 2011; Raji, 2007; Srayya & Kumar, 2015; Vision paper, 2003; Webber et al., 2002a).

Rouison et al. (2004) elucidated that kenaf had been cultivated in recent years because of some reasons. Firstly, kenaf absorbs both phosphorus and nitrogen that are found in the soil. These minerals also aid the increase of cumulative weed weight, stem diameter, fibre yield and crop height (Kuchinda et al., 2001). It was further reviewed by Kuchinda et al. (2001) that nitrogen addition at 90kgN/ha had important effect for the growing of the plant. Finally, kenaf converts carbon-dioxide to oxygen at a notably higher rate. Furthermore, Nashino et al. (2003) affirmed that the photosynthesis of kenaf was higher than other conventional trees. Kenaf's photosynthesis rate is 23.4mg CO₂/dm²/h when likened to other conventional trees of 8.7mg CO₂/dm²/h under 1000μmol/cm²/s (Lam & Liyam, 2000). This means that the kenaf plant is environmentally friendly not only in terms of its biodegradability but also produces good amount of oxygen and likewise reducing carbon-dioxide.

Morphology of Kenaf Plant

Kenaf is an herbaceous plant with strong fibrous stalk, which is not vulnerable to insect attack and requires moderately less or no pesticides for its growth (Elsaid et al., 2011). According to Akil et al. (2011), the kenaf stalk comprises two main components; the bast fibres and the core fibres. The bast fibres account for about 30-40% weight of the dry plant

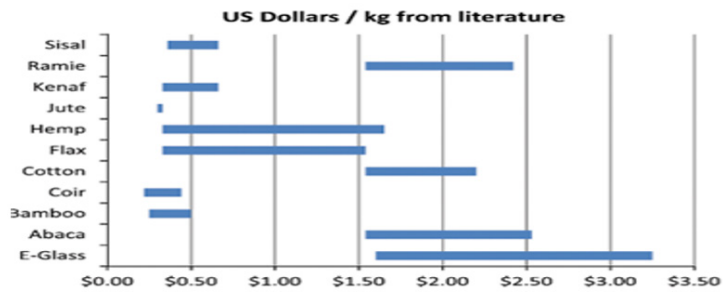


Figure 1. Cost comparison between natural fibres and E-glass (Thakur et al., 2014)

and form the outer-layer of the stalk. The bast fibre is made up of cellulose, hemicellulose and lignin with the value of (56-60%), (21-35%) and (8-15%) by weight respectively (Davoodi et al., 2010; Mazuki et al., 2011). The main attraction of the kenaf plant is the bast fibres because of their specific high strength to low density. The pectin, a natural binder found in the kenaf plant performs the function of holding the fibres to each other. Though the core fibres are not as strong as the bast fibres, but they provide the stack the necessary rigidity in bending. In a similar vein, Ashori et al. (2006) carried out a research on both the bast fibre and core fibre and concluded that fibres morphology showed that the kenaf bast fibres were slender and longer, though the core fibres were much wider and shorter. The morphology and chemical properties showed that the bast and core fibres were significantly different. Figure 2 shows the photo of kenaf plant, components of a typical stalk in cross-section showing the bast and core, kenaf bast fibre, and kenaf core fibre. Table 1 shows the chemical properties and compositions of a typical kenaf.



Figure 2. Kenaf plant, kenaf stalk and bast, and core fibres

Table 1

Chemical Properties and Compositions Kenaf in percentages (Ashori et al., 2006)

	Holo-cellulose	Cellulose	Hemi-cellulose	Lignin	Pentosan	E.B. Extract.	1% NaoH Extract.	Hot water	Ash
Bast	82.6	56.4	26.2	14.7	13.5	2.7	14.5	3.4	2.2
Whole	77.2	48.7	28.1	19.9	19	2.3	17.3	3.6	1.8
Core	75.8	46.1	29.7	22.1	20.7	2.2	20.6	3.9	1.6

Surface Modification of Kenaf fibre

The surface property is one main properties of natural fibres in the sense that it affects the interfacial bonding between the resin and the fibres surface and subsequently affects properties of the natural fibre composite in terms of physical and mechanical. All vegetable plant-derived from cellulose fibres including kenaf fibre are polar in nature, primarily due to their molecular and chemical structure (Ashori et al., 2006). Natural fibres comprise of non-cellulosic components like hemicelluloses, lignin and pectin, which hemicelluloses and pectin are hydrophilic. Hemicelluloses and pectin contain primarily functional group of hydroxyl and carboxylic structures which are vulnerable to water absorption. The cellulose constituent also contains reasonable hydroxyl groups, because minimal water may be accumulated within the extremely ordered and thoroughly crystalline microfibrils (Wambua et al., 2003). However, natural fibre pre-treatment will chemically clean up the surface, halt the absorption of moisture and increases the roughness on fibre surface. The fibre surface is usually influenced by the morphology of polymer, extractive chemical and processing condition. The degree of the interface of the matrix is paramount for applying plant fibres as reinforcement in polymer resin (Dissanayake et al., 2010; Sreekala et al., 2000). The two methods used to optimize plant fibres surface are discussed below.

Physical Modification of Kenaf Fibre. Reinforcing natural fibre can be changed by physical methods and techniques, for example, thermo-treatment, calendaring, stretching, and generation of quality hybrid yarns. These techniques don't change the chemical composition of the filaments yet anyway they change the structural and surface properties of the fibre. Physical treatments alter the morphological properties of natural vegetable fibres without the utilization of chemical agents, thus increasing the mechanical adhesion of fibres and polymer. Corona, cold plasma and heat treatments are other forms of physical treatments. Physical treatments are used to modify either the fibre or polymer matrix. (Dissanayake et al. 2010; Sreekala et al., 2000).

Corona technique exploits the corona effect which involves the fibrillation of the fibre/filler surface through the development of high electromagnetic fields energy near to charged tiny lines or points thus ensuing ionization in within the closeness, at atmospheric pressure and comparatively moderate temperature. In the ionized area, thrilled species (ions and radicals) are found to be present, subsequently become active during the surface treatment, through the introduction of functional groups containing oxygen. In addition, prolong time for treatment may give rise to fibre with noticeable rough surface (Garbassi et al., 1994). Corona treatment is a most standout amongst the most intriguing methods for fibre surface oxidation enactment. This technique modifies the surface vitality of the natural fibres, it boosts the volume of aldehyde groups. It also changes the surface energy of the cellulosic fibres, which in turn affects the melt viscosity of composites (Belgacem et al., 1994). Corona treatment has been successfully used in the modification of natural fibres such as jute, kenaf and flax fibres (Belgacem et al., 1994; Gassan & Gutowski, 2000; Salem et al., 2017).

Plasma treatment is another form of physical treatment similar to corona treatment which makes use of plasma property to modify the fibre surface. At the course of the treatment, an ionized region is formed with its composition depending on the gas fed, including high energy electrons, photons and radicals (Garbassi et al., 1994). Kalia et al. (2009) similarly reasoned that Plasma was generated by high voltage to modify the surface of cellulosic fibre for the purpose of increasing the surface energy or polarity, thus increasing the compatibility with polymer matrix. Electrical discharge is the easiest and commonest means to sustain a plasma for a long time. Plasma is believed to bring a physical change on the surface through roughening of the fibre by the sputtering effect, creating an enlargement of contact area that upsurges the friction between the fibre and polymer. In cold plasma, the electron temperature is 10-100 times higher than the low gas temperature (d'Agostina, 1990). However, due to low density and the low heat capacity of the electrons, the high temperature of electrons does not suggest that the plasma is hot. This is why cold plasma can be used in fibres surface treatment. The high electron temperature gives room to a sputtering effect on the fibres surface. The low gas temperature, being as low as room temperature in most cases permit fibres to experience such plasma surface modification without losing their mechanical properties (Xiao, 1997). Plasma treatment has been used for the treatment of coil fibre, jute fibre and many other natural fibres with satisfactory performance (Fariasa et al., 2017; Morshed et al., 2012).

Heat treatment encompasses heating the fibres to produce composites at a high temperature near to which the constituents of lignocellulose fibres start to degrade. When cellulose is subjected to elevated temperature, it experiences both chemical and physical changes. Physical properties that are likely affected for example weight, colour, strength, enthalpy and crystallinity. Chemical changes include creation of free radicals, reduction of

the degree of polymerization by bond scission, formation of carbonyl and peroxide groups (Shafizadeh, 1985). Chang et al. (2018) ascertained the mechanical and wear properties of heat treated pultruded kenaf fibre-reinforced polyester composites. The heat treatment temperatures were varied from 120°C, 140°C and 170°C. The results showed that the heat-treated pultruded kenaf fibre composites with 140°C heat treatment exhibited better wear performance than the untreated kenaf fibre composites and kenaf fibre composites treated with 120°C and 170°C heat temperatures. The flexural strength and modulus for all treated pultruded kenaf fibre composites increased after heat treatment. Ariawan et al. (2014) studied the effect of heating time during heat treatment on the mechanical and physical properties of kenaf fibre and its composites. Kenaf bast fibres were modified by constant heat temperature at 140°C for 2.5, 5, 7.5, 10, and 12.5 hours. The researchers confirmed through XRD observation that the increase of cellulose content in kenaf fibres explained the increase of crystallinity index of kenaf fibre with heat treatment. The single fibre optimum strength and modulus was obtained when the kenaf fibre was heated for 10 hours. SEM images as showed in Figure 3 explains the decreasing numbers of impurities on the fibres surface with fibre treatment compared to the untreated kenaf fibres. Also, flexural properties of the composites showed a similar behaviour to the fibre strength.

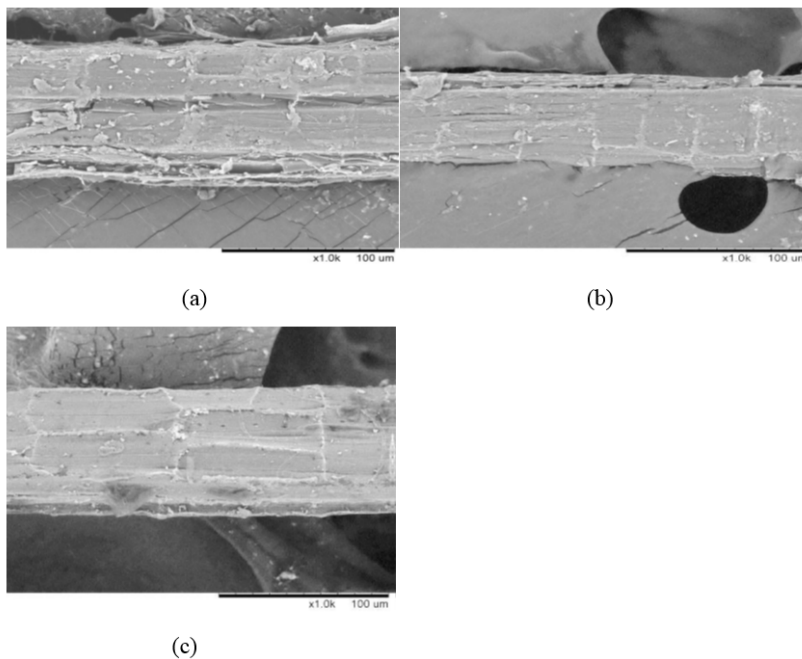


Figure 3. SEM images of heat treated kenaf fibre surface at (a) 0 hour, (b) 7.5 hours and (c) 12.5 hours of heating (Ariawan et al., 2014)

Chemical Modification of Kenaf Fibre. Chemical treatment uses chemical agents to alter the morphology of natural vegetable fibre. This is done through structural modification of the natural fibres or introducing new hydrophobic functional groups into the fibres surface to decrease the hydrophobicity of fibres. Several chemical treatments of natural fibres are being employed by numerous researchers to enhance the mechanical and durability properties of natural vegetable fibres including mercerization, oxidation, crosslinking, graft copolymerization, isocyanate treatment, acrylation, acetylation, permanganate peroxide treatment and silane coupling agent treatment (Dai & Fan, 2014; de Albuquerque et al., 2000; George et al., 2001; Kalia et al., 2009 Mehta et al., Mwaikambo & Ansell, 2002; 2006; Ray et al., 2002a).

Mergerization of kenaf fibre. Mercerization also known as alkaline treatment is the commonest method used for the treatment of natural fibres which leads to good quality fibres. Alkaline solution prompts fibrillation which leads to fibres bundle breakdown into smaller units. Li et al. (2007) affirmed that this treatment removed hemicellulose, lignin, oil and wax covering the fibre surface. Mercerization decreases the fibre diameter, thus increases the feature which prompts the advancement of rough surface structure which gives better interfacial bonding between the fibre and matrix and further gives rise to superior mechanical and durability behaviour (Ray et al., 2002a). According to Joseph et al. (2000), alkaline treatment rises the number of likely reactive sites which allows better wetting. Alkaline treatment is among the most effective methods and at the same time cost-effective method for modification of natural vegetable fibre surfaces. The chemical reaction between NaOH and natural vegetable fibre (cell-OH) assumed to take place as presented in Equation 1:



Mergerization of natural fibres. Meon et al. (2012) indicated that 6% of sodium hydroxide concentration delivered the best results on tensile properties of kenaf fibre. Kenaf fibres were soaked in 3%, 6% and 9% of sodium hydroxide concentration for one day and subsequently dried at 80°C for the period of 24 hours. Similarly, Reza et al. (2014a) conducted a research on the mechanical behaviour of kenaf yarn fibre under several conditions of fibre modifications. The kenaf fibre used for the research were both treated and non-treated. The kenaf fibres were treated in 5%, 7%, 10% and 15% concentration of alkaline solution. It was reported that 5% of alkaline concentration gave the best result for the fibre treatment as a result of the minimal tension on the fibre surface and structure. Higher alkaline concentration at 10% and 15% was discouraged because according to the authors impaired the texture of fibres as treated fibres were seen most turned, more finer and so fragile as compared to the non-treated fibres and those treated with lower concentration of alkaline solution. Figure 4 showed the physical appearance of kenaf fibre after treatment.

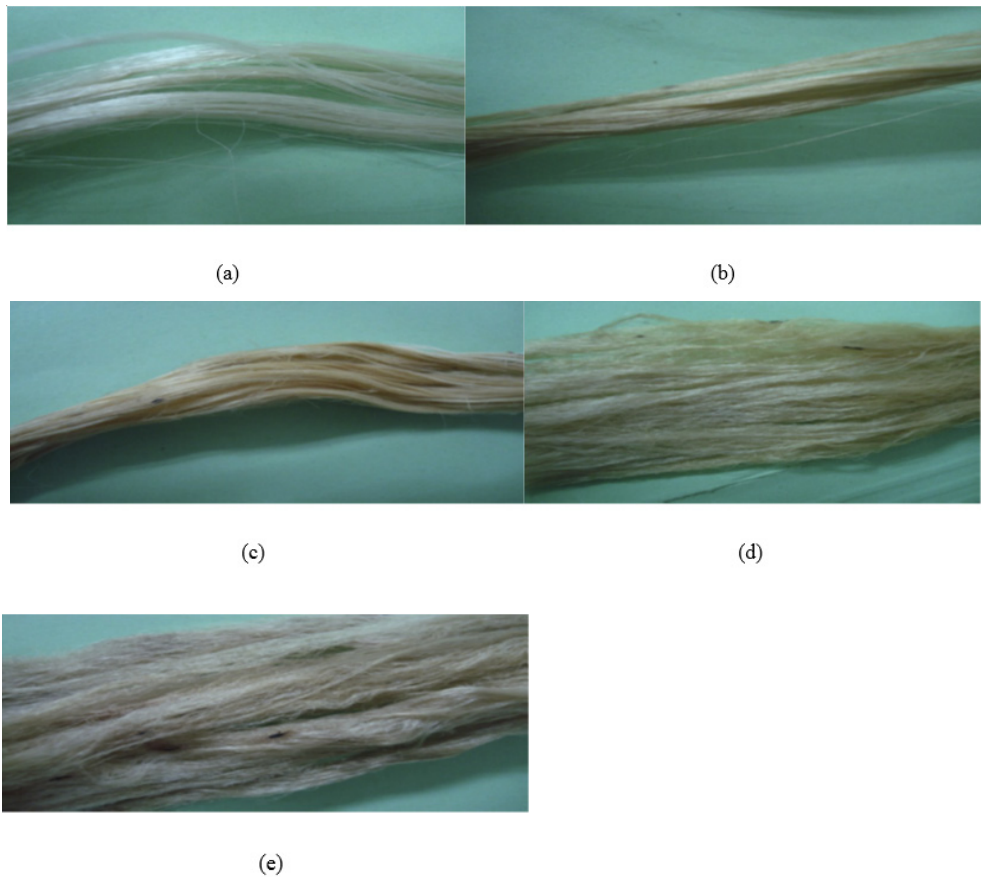


Figure 4. The physical appearance of kenaf fibre of untreated and after treatment (Reza et al. 2014a) (a) 3 hours immersion in 5% alkaline solution (b) 3 hours immersion in 10% alkaline solution (c) 3 hours immersion in 7% alkaline solution (d) 3 hours immersion in 15% alkaline solution

Several other scholars reported enhancement in mechanical behaviour of kenaf fibre when alkalinized with different concentrations of sodium hydroxide. Aziz and Ansell (2004) carried out a research on the alkalinization effects to the properties of hemp and kenaf bast fibres polymeric composites using 6% alkaline concentration for treating kenaf fibre and hemp fibre surfaces. It was found that the density of kenaf fibre and hemp fibre did not show a significant change after treatment with 6% alkaline concentration. However, the flexural strength of the polymer composites with the treated fibres has superior results in comparison with untreated composites. Dynamic mechanical analysis reviewed that the composites from treated fibres gave higher E^I values conforming to superior flexural moduli. Razak et al. (2014) conducted a research to enhance the interfacial adhesion and electronic behaviour of kenaf fibre/polyaniline bio-fibres. 6% weight of sodium hydroxide solution was used in treating the kenaf fibre and reported that the solution of sodium

hydroxide enhances the unit break of the tensile properties of the kenaf fibre owing to the elimination of impurities at the fibre surface which neutralises the hydroxyl group. It was concluded that all the treated kenaf fibres revealed higher mechanical strength than the untreated fibres. Edeerozey, Akil et al. (2007) studied the effect of chemical treatment on kenaf fibre using 3%, 6% and 9% sodium hydroxide solution. Series of fibre tests were done to assess the outcome of the treated fibre on the mechanical properties. The breaking strength was computed from the stress-strain curve and the unit break (UB) using equation 2 (Wang et al., 2003):

$$UB = F/d \quad [2]$$

Where

F = Maximum breaking load (N)

d = Cross-sectional area of fibre (mm²)

It was found that surface treatment of kenaf fibre through alkalization had enhanced the mechanical properties significantly when compared with untreated fibre. The authors stated that 6% sodium hydroxide solution gave the optimum performance for treatment of kenaf fibre (Edeerozey et al., 2007). Farahani, Ahmad and Mosadeghza (2012) carried out a research on alkaline treatment and its effect on the mechanical properties, densities and water absorption of kenaf fibre/polyester composites using 10% concentration of sodium hydroxide concentration for 3hours at ambient temperature. It was reported that alkaline treatment led to improved interfacial strength between fibre and the resin which enhanced all the properties of the polyester composites. The researchers reasoned that surface treatment lowered the absorption of water on the composites. Asumani, Reid and Paskaramoorthy (2012) demonstrated the effects of alkali-saline treatment on kenaf reinforced polypropylene composites. The kenaf bast fibre was grouped into three forms; treated with sodium hydroxide, untreated and treated with Sodium hydroxide and silane. Mechanical tests shown that alkali treatment took after by silane treatment essentially enhances the tensile property and flexural property of the composites. Furthermore, Mohd Yuhazri, Phongsakorn, Haeryip and Kannan (2012) carried out a study to ascertain the effects of alkaline treatment on the mechanical behaviour of kenaf/polyester composites using varying concentration of alkaline solution ranging from 3% to 9% as shown in (Figure 5). Figure 5(a) shows the SEM image of the untreated kenaf fibre. Impurities were visibly noticed on the untreated fibre surface. Figure 5(b) shows the image of the surface of kenaf fibre treated with 3% sodium hydroxide solution for 12hours from SEM. It was observed that the fibre was cleaner than the untreated fibre. Figure 5(d) shows the image of treated kenaf fibre using 6% of sodium hydroxide solution for 12 hours from SEM. It was noticed that most of the impurities were cleaned off from the fibre surface. The increasing immersion time as in the cases of Figure 5(c) and Figure 5(e) led to damage of the fibre surface as shown in the images from SEM. Figure 5(f) presents the image from SEM of

9% sodium hydroxide solution for 12 hours and have the cleanest the fibre surface. The research was concluded that alkaline treatment of kenaf fibre improved interfacial adhesion between the polyester resin and fibre which gave rise to superior mechanical properties.

Silane treatment of kenaf fibre. Silane is one of the essential components of the reactive species used for natural fibre treatment. The key group of coupling agents with

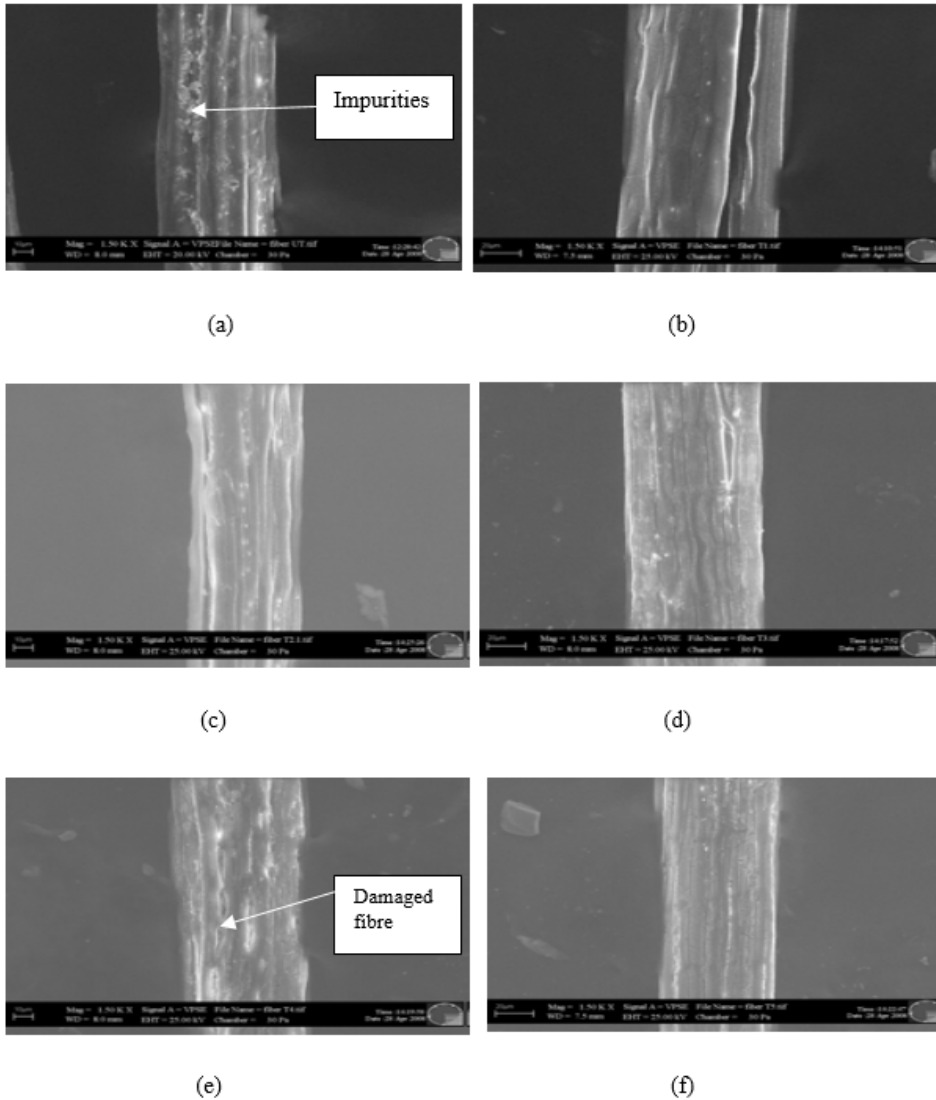


Figure 5. SEM images of untreated and treated kenaf fibre (Mohd Yuhazri et al., 2012) (a) Untreated kenaf fibre (b) 12hours immersion in 3% alkaline solution (c) 24hours immersion in 3% alkaline solution (d) 12hours immersion in 6% alkaline solution (e) 24hours immersion in 6% alkaline solution (f) 12hours immersion in 9% alkaline solution

this treatment is the organosilanes which developed to bond mineral fibres to polymer. The organo-functional group in the coupling agent trigger the reaction with the polymer, either by copolymerization and/or creation of an interpenetrating network (IPN) (Plueddemann, 1991). Weyenberg et al. (2003) investigated the effect of chemical treatment on flax fibres composites and stated the the curing reaction of silane treated natural fibre enhances the wetting of the resin. Lee et al. (2009a) used 3-Glycidoxypropyl trimethoxy silane (GPS) as coupling agent and hot pressing in PLA/Kenaf fibre composites to improve the interfacial adhesion in the carding process and reported that the effects of silane coupling agent on composite properties was highly beneficial leading to increase moduli and heat deflection temperature as well as reduced water swelling. In a similar vein, Huda et al. (2008) had attempted to use 3-aminopropyltriethoxysilane (ASP) coupling agent in kenaf fibre treatment and reported improved compatibility between the kenaf fibre and PLA resin. The surface treated kenaf-PLA composites possessed superior mechanical properties when compared to the composites made from the untreated fibres (Huda et al., 2008). Xu et al. (2009) carried out a research on the thermomechanical properties of the silanized-kenaf/polystyrene composites. The authors used synthesized polymeric coupling agent to modify the kenaf fibre. It was reported that polymeric coupling agent treatment of kenaf fibre has increased the fibre-matrix interaction through condensation reaction between alkoxy silane and hydroxyl groups of kenaf cellulose. Dynamic Mechanical Analysis (DMA) results revealed that treated kenaf fibre composites had higher E' and lower $\tan \delta$ signifying a greater interfacial bond strength and adhesion between the fibre and the matrix resin. The SEM images of the untreated kenaf fibre and treated kenaf fibre with tetrahydrofuran-polymeric coupling agent are shown in (Figures 6a and 6b). Figure 6 (a) shows the presence of wax, oil and surface impurities. The existence of these materials will affect the mechanical behaviour of the fibre composites. Also shown in Figure 6(b) is the surface of the treated kenaf fibres. It was observed by the researchers that the impurities had been cleaned without roughing the fibre surface.

Graft copolymerization of kenaf fibre. Graft copolymerization of natural fibres is an effective technique of surface treatment of natural fibres. This method involves initiation by free radicals on the vinylic monomers onto the cellulose. These free radicals are formed as an outcome of a reaction of the cellulosic chain in a redox system. The oxidation of the anhydroglucose units in the reaction occurs along the cellulosic chain and macro cellulosic radicals are created on the fibre surface (Misra et al., 2002; Valadez et al., 1999). Mohamed et al. (2013a) investigated the effect of partial delignification of kenaf bast fibre for radiation graft copolymerization. It was found that delignification condition at 80°C for 6 hours with 0.5% NaCl₂ gave 91% of lignin removal from the kenaf bast fibres. In a similar manner, Mohamed et al. (2013b) carried out a research on graft polymerization of micelle size 3% 4-chloromethyl styrene (CMS) emulsion on kenaf fibre. The influence of micelle size over

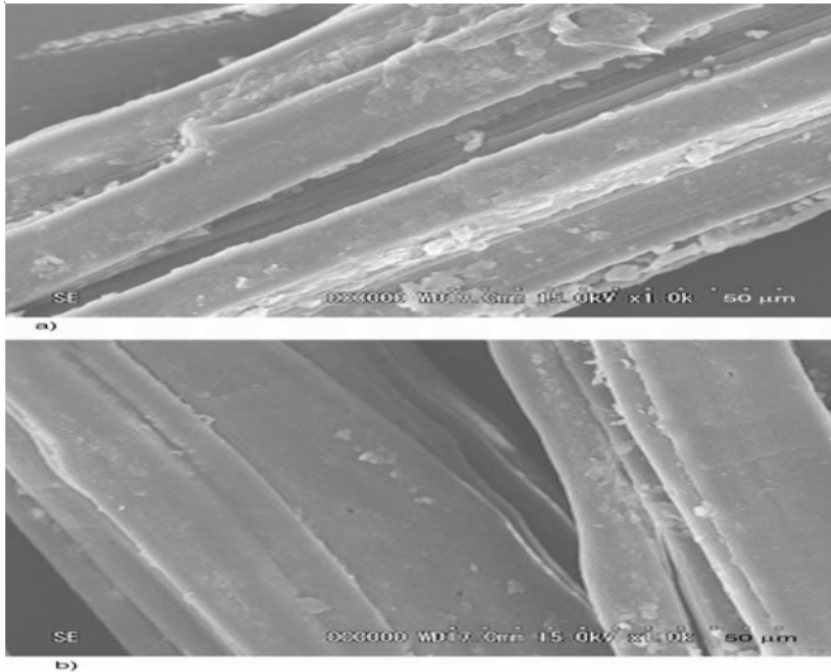


Figure 6. SEM images of longitudinal views of (a) untreated kenaf fibre and (b) treated kenaf fibre with tetrahydrofuran-polymeric coupling agent (Xu et al., 2009)

time was explored by adjusting the ratio of CMS to Tween 20 (10:1,10:2,10:4) at CMS concentration 0.2-5% in emulsion with 350 micelles at various CMS concentrations at a dose of 150K Gy. It was found by the authors that the degree of grafting (Dg) was strongly dependent on the monomer concentration and time. However, the increase in micelles diameter from 250nm to 500nm results in the increased in Dg from 3% to 153%. It was concluded that the enhancement of grafting yield is governed by emulsion break-down mechanisms through radical effect during radiation which induced graft polymerization. Graft copolymerization of glycidyl methacrylate onto delignified kenaf fibres have been investigated by Sharif et al. (2013). The kenaf fibres was prepared via pre-irradiation grafting method. Fibres were first treated with sodium chlorite solution before been used as trunk polymer. Treated kenaf fibres were irradiated by electron beam followed by grafting reaction in glycidyl methacrylate/water emulsion system. The degree of grafting was determined as a function of absorbed dose, reaction time, reaction temperature and concentration of monomer. The research results showed that the lignin content of kenaf fibre was decreased from 14.3% to as low as 3.3% with the increased sodium chlorite concentration. This was evident according to the authors by SEM images presented in Figure 7 which shows treated kenaf fibre surface cleaner and smoother when compared with the untreated kenaf fibre surface.

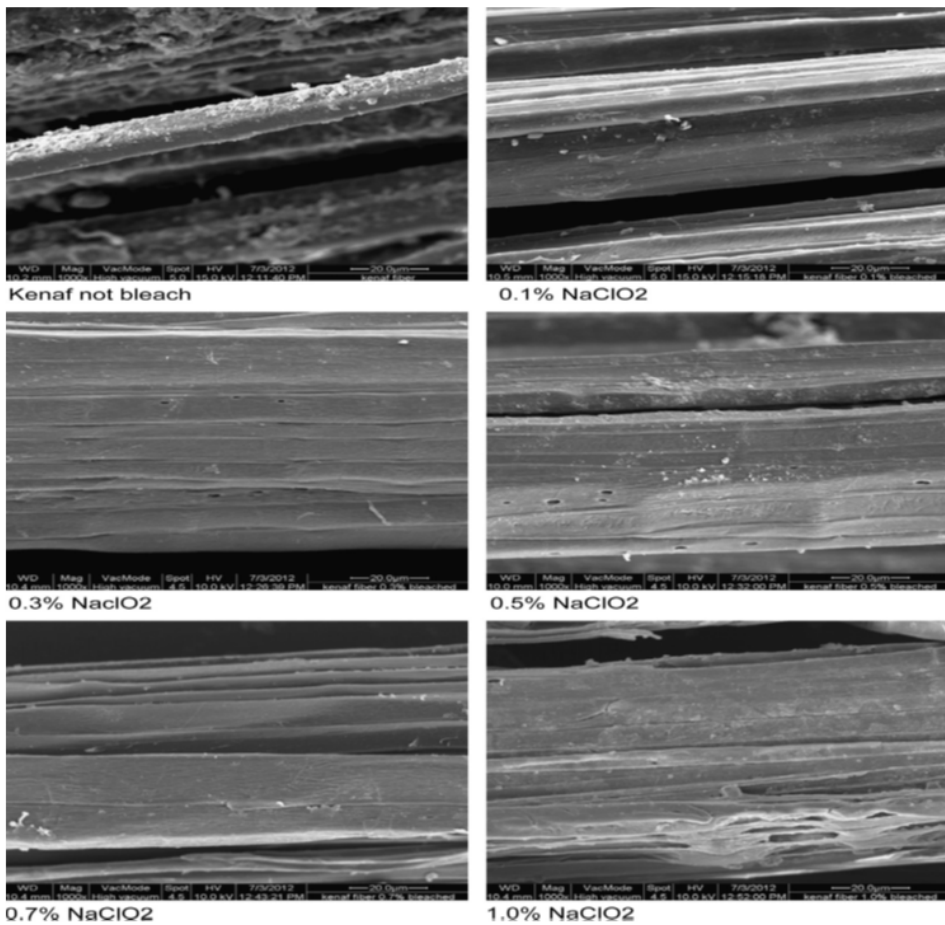


Figure 7. SEM images of kenaf fibre before and after treated with sodium chlorite (Sharif et al. 2013)

Properties of Kenaf Fibre

Researchers in the past have carried out numerous studies to determine kenaf fibre properties and the processing methods associated with the optimal properties. It was noticed from the results presented by researchers, not identical, this may be as a result of variation in categories of kenaf fibres been utilised such as the source of kenaf fibre, retting process, age, body of the plant from which the fibre is extracted, environmental conditions of the site etc. It is additionally fascinating to note that natural fibre for instance, kenaf fibre have unpredictable cross-sectional region that changes along the length of the fibre which influence the mechanical properties of the fibre. Ochi (2008) investigated the effect of environmental temperature on the growth of the kenaf plant and on the tensile and elastic

properties of the kenaf fibres and kenaf/PLA resin composites. The study showed the temperatures and heights of grown kenaf plant under two different conditions. It was established that the kenaf plant which matured at a mean temperature of 22°C had a height of 2000 mm from the ground while the one that matured at a mean temperature of 30°C had a height of 3650 mm from the ground after 168 days. The researcher stated that the production of good strength kenaf fibre reinforced plastic essentially need fibres that were gotten from the area of the plants nearest to the ground. The tensile strength and elastic modulus of kenaf fibres grown in different temperatures are shown in Figure 8. The study concluded that the tensile strength and elastic modulus of kenaf grown under an average temperature of 30°C were greater than those grown under average temperature of 22°C.

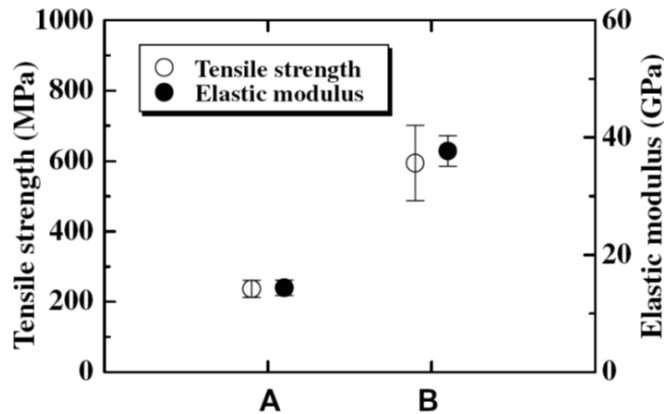


Figure 8. Tensile strength and elastic modulus of kenaf fibre, (A=22°C, B=30°C) (Ochi, 2008)

Kenaf fibres properties presented by several authors are shown in Table 2. A comparison of literature data concerning mechanical properties of kenaf fibres versus E-glass presented by several authors (Mohanty et al., 2000; Mohanty et al., 2005; Parikh et al., 2002) in Table 3, indicates that kenaf fibre could be a decent contender for reinforcement of great performance bio-based polymeric composites.

PROPERTIES OF KENAF REINFORCED COMPOSITES

Jush et al. (2016) illustrated that kenaf was found to be comparatively much available and relatively inexpensive in required form when compared with other kinds of natural fibre reinforced materials. The authors stated that kenaf was tagged as commercial kenaf owing to its potentials as raw materials for variety of products in the industrial and manufacturing sectors. Furthermore, kenaf like most other natural vegetable fibres exhibit high specific mechanical properties, easily recyclable, low density and maintain a competitive price (Mitchell, 1986; Nashino et al., 2003).

Table 2
Properties of kenaf fibres reported by different researchers

Diameter (µm)	Density (g/cm ³)	Tensile Strength (MPa)	Tensile Modulus (GPa)	Elongation at break (%)	Reference(s)
55-60	1.2	350-600	40	2.5-3.5	Fiore et al. (2015)
-	1.45	930	53	1.6	(Akil et al., 2011; Mohanty et al., 2000; Reza et al., 2014a)
-	1.5	350-600	40	2.5-3.5	(KENAF ECO-fibres, 2005; Rassmann et al., 2011)
-	1.4	284-800	21-60	1.6	(Holbery & Houston, 2006; Sivakumari et al., 2017)
140	-	223	14	-	Shinchi et al. (2005)
81	-	250	50	-	Lee et al. (2009b)
-	-	295-1191	2.86	3.5	(Cheung, Ho, Lau, Cardona, & Hui, 2009)
-	0.749	223-624	11-14.5	2.7-5.7	(Graupner et al., 2009; Malkapuram et al., 2008)
-	1.2	295	-	3-10	Jawaid and Khalil (2011)
-	1.26	393-773	26.5	1.5-1.8	Zamri et al. (2016)
14	-	223	15	-	Ozturk (2010)
68.5	1.31	476	25.1	-	Munawar et al. (2007)
61	1.386	110-358	17-25	-	Osman et al. (2013)
78	1.04	448	24.6	-	Cao et al. (2007)
24	-	135-232	15-24	-	Harun et al. (2009)

Table 3
Kenaf fibres and E-glass fibres properties

Fibre	Density (g/cm ³)	Tensile strength (MPa)	Elastic modulus (GPa)	Elongation break (%)	Reference(s)
Kenaf fibres	1.45	284-800	21-60	1.6	(Mohanty et al., 2000; Parikh et al., 2002)
E-glass fibres	2.55	2000-3000	70	2.5	Mohanty et al. (2005)

Mechanical Properties

The performance and behaviour of any structural constituents according to Akil et al. (2011), is usually attributed to their mechanical qualities, for example, compressive strength, tensile strength, flexural strength, impact resistance properties and wear properties. The authors further stated that these characteristics/qualities are relevant parameters used to fathom the material capacity, particularly under critical and severe loading arrangements which

are directly linked to engineering performance. Several research works have been carried out on kenaf fibre polymer composites to characterize fully its mechanical behaviour and properties (Anur & Zuraida, 2011; Fiore et al., 2015; Reza et al., 2014b; Yousif et al., 2012). Basically, the tensile strength and flexural strength of kenaf fibre reinforced composites differ which is dependent on the categories of fibre, fibre orientation (unidirectional or random), form and content (fabric or fibre), and the type of matrix used. Table 4 shows the mechanical properties of kenaf fibre reinforced composites presented by different researchers.

Thermal Properties

Thermal properties are vital characteristic of kenaf fibre reinforced composites which requires evaluation to understand fully the thermal behaviour of kenaf composites. The thermal decomposition of natural vegetable fibres including kenaf fibre is usually initiated with low temperature of hemicelluloses deterioration and subsequently with sharp drop of weight associated with cellulosic pyrolysis. Several methods are currently being employed to determine the thermal property of composites: Dynamic Mechanical Analysis (DMA), Thermal Gravimetric Analysis (TGA) and Differential Scanning Calorimetry (DSC). TGA allows the determination of the mass of composites sample lost due to temperature, while the DSC scan could estimate the various vital parameters for example, the melting temperature (T_m), glass transition temperature (T_g), level of crystalline and oxidation (Hassan et al., 2011; Julkapli & Akil, 2010). Hassan et al. (2011) investigated the thermal characteristic on kenaf fibre filled by chitosan bio-based composites. The two methods considered were the DSC and TGA. At the course of DSC testing, heating scan analysis was carried out twice and it was discovered that most specimens showed a wide endothermic peak throughout the scan that is related to the hydration process. For the subsequent heating scan, it was noticed by the authors that the inclusion of kenaf particles to the chitosan led to decrease of the endothermic temperature. Nevertheless, no significant differences in enthalpy data was noticed with the different fibre volume fraction used. The TGA results from the same research indicated that the incorporation of kenaf particles to the chitosan have not no significant effect on the thermal performance of the chitosan film. DMA on the other hand is an essential tool used to determine the visco-elastic behaviour of polymer plastic and composite materials. The measurement involves the monitoring of the time condition of the alteration performance of a specimen under periodic, extremely sinusoidal deformation energy with small amplitudes. El-shekeil et al. (2012) investigated the influence of volume fraction of fibre on the thermal (i.e. TGA) properties of kenaf fibre/thermos-plastic polyurethane polymeric composites. Different fibre loading of 20%, 30%, 40% and 50% by weight was used and it was observed that fibre loading decreased the

Table 4
Mechanical properties of kenaf fibre reinforced composites from previous researchers

Matrix	Fibre content (M%)	Tensile strength (MPa)	Young modulus (GPa)	Flexural Strength (MPa)	Flexural modulus (GPa)	Impact strength (Kj/m ²)	Processing	Treatment	Reference (s)
PLA	40	82(52)	8(3.4)	126(96)	7(3.2)	14(17)	CSM	-	Graupner and Mussii (2011)
PHB	40	70(22)	6.1(22)	126(43)	7(1.6)	10(5)	CSM	-	Graupner and Mussii, (2011)
Epoxy	30	124	14.4	-	-	-	UD	NaOH (5%)	Reza et al. (2014b)
Epoxy	40	164	18.15	-	-	-	UD	NaOH (5%)	Reza et al. (2014b)
PP	40	-	-	27	2	-	Random mat.	-	Wambua et al. (2003)
Polyester	64	-	-	123	13	-	UD	NaOH (6%)	Aziz and Ansell (2004)

Table 4 (Continue)

Matrix	Fibre content (M%)	Tensile strength (MPa)	Young modulus (GPa)	Flexural Strength (MPa)	Flexural modulus (GPa)	Impact strength (Kj/m ²)	Processing	Treatment	Reference (s)
PLA	35	131(33)	15(3.8)	160(72)	11.5(4.9)	-	UD		Ochi (2008)
Epoxy	30	64	4.5	90	4.9	-	CSM	-	Rassmann et al. (2011)
Polyester	30	52	6.7	98	5.2	-	CSM	-	Rassmann et al. (2011)
Vinyl ester	30	57	5.6	84	4.7	-	CSM	-	Rassmann et al. (2011)
PP	30	40	1.7	43	-	-	CSM	NaOH (5%)	Asumani et al. (2012)
PP	30	58	2.8	59	-	-	CSM	NaOH (5%)- Silane (5%)	Asumani et al. (2012)

thermal performance of composites and it was stated that the increase weight loss with fibre loading agrees with the research works conducted by (Bijwe et al., 2002; Harsha & Tewari, 2003). However, the thermal constancy of composites remained superior to the kenaf fibre. Figure 9 shows the effect of fibre loading on the TGA of thermos-plastic polyurethane /kenaf fibre composites.

Water Absorption Properties

The main issue with the utilization of natural fibre composites is connected to the its deterioration at high moist environments and absence of adhesion between the fibre-matrix interface if the fibres are not modified properly. Moisture ingress into composites, reduces fibre-matrix interfacial adhesion, drops the glass transition temperature, hydrolyses and occasionally introduced micro-cracks in the matrix (Grant & Bradley, 1995). Water can be present in polymer in numerous ways: in form of bound water, as characterised by robust interaction with the molecule of matrix and free water, existing in vessels and micro voids

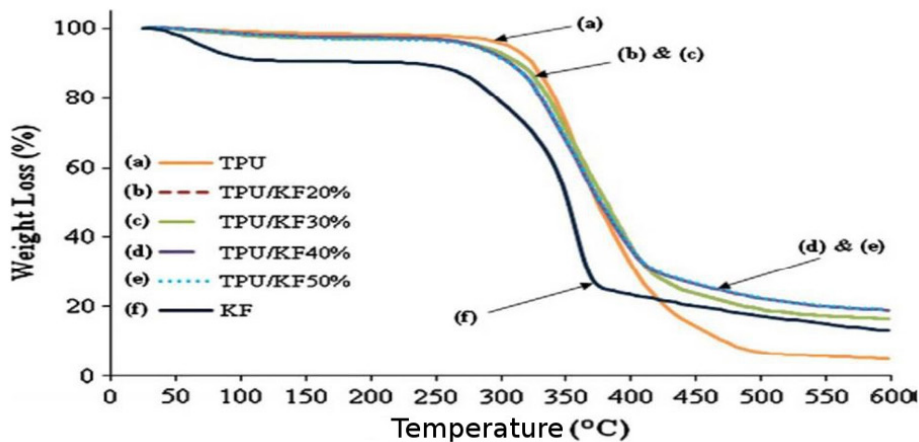


Figure 9. Effect of fibre weight fraction on the DTA of thermos-plastic polyurethane/kenaf fibre composites (El-shekeil et al., 2012)

in the polymer (Fraga et al., 2007). Several researchers have shown certain responsiveness of the mechanical and the thermal properties to moisture uptake on the utilization of natural vegetable fibre polymer composites and recommended that it could be lowered through fibre surface modification and as well as the use of coupling agents (Rashdi et al., 2009; Wambua et al., 2003). Generally, moisture ingress into composite relies upon variables, for example, weight portion of fibre, void volume, thickness of framework, fibre treatment, dampness and temperature (Najafi et al., 2008). Similarly, Nosbi et al. (2010) stated that water uptake behaviour of polymer composite was of great worries in fibre composites structure,

particularly for lignocellulosic fibre polymer composites. The researchers opined that for any composite system, the water uptake characteristics was determined by the quality of fibre, orientation of fibre, porosity of the fibres, area of unprotected surface, temperature, void content and sorption behaviour of the individual component. The percentage of weight gain is usually determined by the weight difference between specimens immersed in water and dry specimens using equation 3 (Akil et al., 2010):

$$M\% = \frac{M_1 - M_0}{M_0} \times 100 \quad [3]$$

Where M (%) is the moisture content in percentage, M_1 (g) is the weight of the wet sample at a given time and M_0 (g) is the initial weight of the sample. Rassmann et al. (2010) carried out a research on the effect of fabrication methods on the properties of kenaf fibre composite laminates and reported that water absorption was not appreciably changed by any preparing condition aside from by pressurization at low fibre weight division, water assimilation increments with fibre weight portion, and last however not the slightest, water retention makes all dimensions of composite to expand. However, the expansion of the length and of the width is very minimal when compared to the expansion in thickness. Mazuki et al. (2011) reported water absorption effect on the dynamic mechanical analysis of pultruded kenaf fibre reinforced polymer composites. The period of immersion of samples was for 24 weeks and it was reported that the thermal properties was extremely affected by the presence of absorbed water in the specimen. It also reviewed that the fibre is highly exposed to solution after 24 weeks of immersion from the morphological study. The effect of different conditions such as sea water, rain water and tap water on the mechanical properties of kenaf composites and kenaf hybrid (fibreglass) composite was investigated by Salleh et al. (2014). Specimens were immersed up to 60 days and the authors reported that both kenaf polyester and kenaf hybrid polyester composites show reduction on mechanical properties after immersion in the solutions. It was concluded that kenaf polyester and kenaf hybrid polyester followed the fickian behaviour after 40 days of immersion, where it reached equilibrium at a certain specific immersion time. Figure 10 shows the behaviour of water absorption of both kenaf polyester and kenaf hybrid polyester composites.

KENAF FIBRE IN HYBRID COMPOSITES

The incorporation of different types of fibres into a single matrix has led to the development of hybrid bio composites. A current study had shown that the hybridisation of vegetable fibre with limited quantity of synthetic fibre makes the composite less susceptible to moisture uptake as well as enhances its tensile properties. When diverse types of fibres are introduced in a composite, the benefit of one kind of fibre could make up for the shortcoming of the

other fibre. Along these lines, an adjust in cost and execution qualities, for example, light weight, high strength and stiffness can be accomplished (Karahan & Karahan, 2015). Sharba et al. (2016) did an investigation on the impact of kenaf fibre orientation on mechanical properties and exhaustion life of a polyester based glass/kenaf hybrid composite They found that the monotonic and weariness properties of the hybrid composite relied upon fibre orientation, which fundamentally influenced the mechanical strength, and the hybridisation

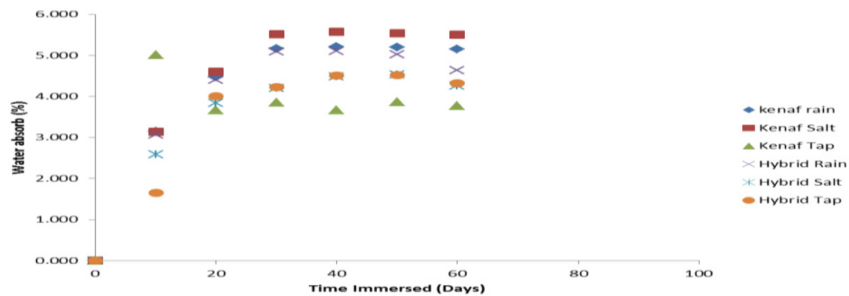


Figure 10. Water absorption of kenaf polyester and kenaf hybrid (fibreglass) polyester composites (Salleh et al., 2014)

of kenaf and glass enhanced the exhaustion debasement coefficient of the composite. Yahaya et al. (2016) demonstrated the effect of fibre orientations on the mechanical properties of kenaf-aramid hybrid composites and reported the tensile strength of kenaf woven hybrid composite was 20.78% and 43.55% more than the unidirectional samples and the mat samples. The Charpy impact test was also compared and the same trend was observed. The authors concluded that woven kenaf fibre could be a good candidate material for the production of hybrid composite with good tensile properties and impact resistance. Alavudeen et al. (2015) investigated the mechanical properties of woven banana fibre, kenaf fibre and banana/kenaf hybrid fibres composites. It was reported that the mechanical strength of woven banana/kenaf fibre hybrid composites increased due to the hybridization of kenaf with banana fibres. The tensile strength, flexural strength and impact strength of woven hybrid composites of banana/kenaf fibres are superior to those of the individual fibre composites. Hybrid bio-composites in unidirectional arrangement using kenaf fibre, bamboo fibre and coir fibre to reinforced polylactic acid resin (PLA) was studied by Yusoff et al. (2016). Three types of composites made up of kenaf fibre-coir/polylactic acid, bamboo-coir/polylactic acid and kenaf-bamboo-coir/polylactic acid composites were tested to failure in tension and flexure. It was recorded that the tensile strength of kenaf-bamboo-coir/polylactic acid composites have a value of 187MPa, roughly 20% and 78% more than bamboo-coir/polylactic acid composites and kenaf-coir/polylactic acid. Young moduli

value ranges from 6.0GPa to 7.5GPa for the three composites. The kenaf-bamboo-coir/polylactic composites have flexural strength values 199MPa and bamboo-coir/polylactic acid composites have 206MPa, which is roughly 16% and 20% more than kenaf-coir/polylactic acid composites. The authors went further to state that the kenaf-coir/polylactic acid composites gave the highest flexural modulus and it was put at approximately 70% more than the two other combinations. The entire research was concluded by saying that the hybridization of high stiffness and strong kenaf fibre and bamboo, and good ductility of the coir fibre improved tensile strength and flexural strength of composites as compared to the single fibre composites.

KENAF FIBRE-REINFORCED COMPOSITES APPLICATIONS

Natural fibre-based composite materials including kenaf fibre reinforced composite have recently been seen as a competitor for metallic fibres and synthetic fibres. Many scientists and researchers are now trying to produce structural elements, electrical components, automotive components, aircraft parts and other products by using natural vegetable fibre as reinforcements. Hafizah et al. (2014) had successfully used kenaf fibre reinforced polymer laminates to strengthen reinforced concrete beams. The researchers reported increased in the mechanical performance for all the strengthened beams and that the maximum flexural strength was increased by 40% fibre weight. Interior headliner model for an automotive have be produced using PLA/kenaf fibre content at 50% fibre weight and it was confirmed that the mechanical properties are satisfactory. Also, Davoodi et al. (2010) had used kenaf/glass hybrid epoxy composite for bumper beam of passenger car. Some conceivable utilizations of kenaf fibres and its bio-based composites are itemized below:

- Kenaf fibres is currently been viewed as a standard and commonplace raw material in the creation of particleboards, feeds for animal, paper, textiles materials and fuel (Alexopoulou, 2013; Juliana et al., 2012; Loynd, 2010).
- Kenaf fibres are been utilized as a part of assortment of utilizations, for example, burlap packs, twine, sacks, ropes, canvas, cordage, floor coverings, mechanical and business textures and bio-plastic composites (Cheng et al., 2004).
- Kenaf's internal woody main elements had high sponginess and numerous scientists have explored its uses in various field, for example, seats for car industry, sewage slop, treating the soil as a building operator, particleboard in dashboards (Webber, 1994).
- Kenaf has been utilized as dynamic retentive, creature bedding and poultry litter, gardening soil revision, adequately utilized for dangerous disposed of waste water expulsion as oil slicks on water, squander tidy up and evacuation of synthetically debased soil's organization (Tilmo et al., 1988; Webber et al., 1999; Webber et al., 2002b).

- Automotive inside coating, outside car parts, for example, front and back guards, wallboards, roof and furniture (Khan, 2011; Pang et al., 2015).
- Genetic engineering practices towards resolving problems associated with the repair and rebuilding of harmed or non-utilitarian tissues (Cheung et al., 2009).
- Bio-medical practices for example gene/drug delivery, orthopaedic and cosmetic dentistry, implantable prosthesis, soft and hard tissues application including external fixation, hip arthroplasty, and deck screw and pins (Namvar et al., 2014).

CONCLUSION

This study reviews that kenaf fibre shows a bright future when compared with other fibres. Kenaf fibre polymeric composite has good potential to substitute glass fibre reinforced composite and other petroleum based composites because it has commensurable physical and mechanical properties to the latter. Most importantly, kenaf fibre reinforced polymer composite has lower density, eco-efficient and cost effective when compared to petroleum-based composite. Interestingly, kenaf fibre reinforced polymer composite utilises various manufacturing processes such as pultrusion and filament winding that have never been used with other lignocellulosic fibres before. Interfacial bonding between kenaf fibres and matrix is still the key issue in terms of the overall performance, since it dictates the final properties of the composite, but many studies have proved that proper surface treatment or surface modification can overcome this deficiency since kenaf fibre is hydrophilic in nature. The future of kenaf fibre as stated earlier seems to be bright but there is need for relentless research and development as well as organized and commercialized policy. It is also important for kenaf fibre to be delivered in direct roving arrangements, which make it easier for the fibre to be utilized as material in reinforced composite manufacturing because, it will produce fibre-reinforced polymer composite with fibre in constant and continuous cross-section.

ACKNOWLEDGEMENT

The authors would like to appreciate the financial assistance received through the research project titled: Experimental Study on Kenaf Fibre Reinforced Concrete under Dynamic Loadings. Under the University Research Grant with Ref. NO: BT09J1300000072017011934, funded by the Ministry of Higher Education, Malaysia (MOHE). Also appreciated is the support from the Management of Tertiary Education Trust Fund (TETFUND), Nigeria.

REFERENCES

- Abdul Hamid, H., Yusoff, M. H., Shukor, N. A., Zaniel, B., & Musa, M. H. (2009). Effect of different fertilizer application level on growth and physiology of hibiscus cannabinus L. (kenaf) planted of BRIS soil. *Journal of Agricultural Science*, 1(1), 121-131.
- Akil, H. M. D., Cheng, L. W., Affzan, M. H., & Abubakar, A. (2010). Water absorption study on pultruded E-glass fibre reinforcement unsaturated polyester composites. *Advanced Composites Letters*, 19(3), 67-73.
- Akil, H. M., Omar, M. F., Mazuki, A. A. M., Safiee, S., Ishak, Z. A. M., & Abubakar, A. (2011). Kenaf fibre reinforced composites: A review. *Materials and Design*, 32(8-9), 4107- 4121.
- Alavudeen, A., Ragin, N., Karthikeyan, S., Thiruchitrambalam, M., & Venkateshwaren, N. (2015). Mechanical properties of banana/kenaf fibre-reinforced hybrid polyester composites: Effect of woven fabric and random orientation. *Materials and Design*, 66, 246-257.
- Alexopoulou, E. (2013). Kenaf (*Hibiscus Cannabinus L.*) agronomy and crop management's. Retrieved September 30, 2017, from <http://www.fibrafp7.net/portals/o/05-Alexopoulou.pdf>
- Ander, N. G., Ariawan, D., & Ishak, Z. A. M. (2016). Mechanical properties and micromechanical analysis of nonwoven kenaf fibre/epoxy composites produced by resin transfer moulding. *Journal of Composite Materials*, 0(0), 1-11.
- Anuar, H., & Zuraida, A. (2011). Improvement in mechanical properties of reinforced thermos- plastic elastomer composite with kenaf bast fibre. *Composites Part B*, 42(3), 462-465.
- Ariawan, D., Ishak, Z. A. M., Taib, R. M., Ahmad, T. M. Z. & Phua, Y. J. (2014). Effect of heat treatment on properties of kenaf fibre mat/unsaturated polyester composite produced by resin transfer molding. *Applied Mechanics and Materials*, 699, 118-123.
- Ashori, A., Harun, J., Raverty, W. D., & Yusoff, M. N. D. (2006). Chemical and morphological characteristics of Malaysia cultivated kenaf (*Hibiscus cannabinus L.*) fibre. *Polymer Plastics Technology and Engineering*, 45(1), 131-134.
- Asumani, O. M. L., Reid, R. G., & Paskaramoorthy, R. (2012). The effects of alkali-silane treatment on the tensile and flexural properties of short fibre nonwoven kenaf reinforced polypropylene composites. *Composites Part A*, 43(9), 1431-1440.
- Aziz, S. H., & Ansell, M. P. (2004). The effect of alkalization and fibre alignment on the mechanical and thermal properties of kenaf and hemp bast fibre composites: Part 1- polyester resin matrix. *Composites Science and Technology*, 64(9), 1219-1230.
- Belgacem, M. N., Bataille, P. & Sapieha, S. (1994). Effect of corona modification on the mechanical properties of polypropylene/cellulose composites. *Journal of Applied Polymer Science*, 53(4), 379-385.
- Bijwe, J., Indumathi, J., & Ghosh, A. K. (2002). On the abrasive wear behaviour of fabricated reinforced polyetherimide composites. *Wear*, 253(7-8), 768-777.
- Cao Y., Goda, K., & Chen, H. (2007). Research and development of green composites. *Journal of Materials Research*, 21, 119-125.

- Chang, B. P., Chan, W. H., Zamri, M. J., Akil, H. M. D. & Chuah, H. G. (2018). Investigating the effects of operational factors on wear properties of heat-treated pultruded kenaf fibre-reinforced polyester composites using taguchi method. *Journal of Natural fibres*, 15(4), 474-482.
- Cheng, Z., LuBao, R., Sameshima, K., Fu, D. X., & Chen, J. K. (2004). Identification and genetic relationship of kenaf (*Hibiscus Cannabinus* L) germplasm revealed by AFLP analysis. *Genetic Resources Crop Evolution*, 51(4), 393-401.
- Cheung, H. Y., Ho, M. P., Lau, K. T., Cardona, F., & Hui, D. (2009). Natural fibre reinforced composites for bio-engineering and environmental engineering applications. *Composites Part B*, 40(7), 655-663.
- d'Agostino, R. (1990). *Plasma Deposition, Treatment, and Etching of Polymers*. San Diego: Academic Press.
- Dai, D., & Fan, M. (2014). Wood fibres as reinforcements in natural fibre composites: Structure, properties, processing and application. In H. Alma & S. Robert (Eds.), *Natural fibre composites: materials, processes and properties* (pp. 3-65). Oxford: Woodhead Publishing.
- Davoodi, M. M., Sapuan, S. M., Ahmed, D., Ali, A., Khalina, A., & Jonobi, M. (2010). Mechanical properties of hybrid kenaf/glass reinforced composite for passenger car bumper beam. *Materials and Design*, 31(10), 4927-4932.
- de Albuquerque, A. C., Joseph, K., Hecter de Carvalho, L., & de Almeida, J. R. M. (2000). Effect of wettability and ageing conditions on the physical and mechanical properties of uniaxially oriented jute -roving-reinforced polyester composites. *Composites Science and Technology*, 60(6), 833-844.
- Dissanayake, N., Virk, A., & Hall, W. A. (2010). A review of bast fibres and their composites. *Composites Part B*, 41, 1336-1344.
- Edeerozey, A. M. M., Akil, H. M., Azhar, A. B., & Ariffin, M. I. Z. (2007). Chemical modification of kenaf fibres. *Materials Letters*, 61(10), 2023-2025.
- Elsaid, A., Dawood, M., Seracino, R., & Bobko, C. (2011). Mechanical properties of kenaf fibre reinforced concrete. *Construction and Building Materials*, 25(4), 1991-2001.
- El-shekeil, Y. A., Sapuan, S. M., Abdan, K., & Zainudin, E. S. (2012). Influence of fibre content on the mechanical and thermal properties of kenaf fibre reinforced thermoplastic polyurethane composites. *Materials and Design*, 40, 299-303.
- Farahani, G. N., Ahmad, I., & Mosadeghza, Z. (2012). Effect of fibre content, fibre length and alkali treatment on the properties of kenaf fibre/UPR composites based on recycled PET waste. *Polymer Plastic Technology and Engineering*, 51, 634-639.
- Fariasa, J. G. G., Cavalcantea, R. C., Canabarroa, B. R., Vianab, H. M., Scholzc, S., & Simão, R. A. (2017). Surface lignin removal on coir fibers by plasma treatment for improved adhesion in thermoplastic starch composites. *Carbohydrate Polymers*, 165, 429-436.
- Fiore, V., Di Bella, G., & Valenza, A. (2015). The effect of alkaline treatment on mechanical properties of kenaf fibres and their epoxy composites. *Composite Part B*, 68, 14- 21.
- Fraga, A. N., Frulloni, E., Dela Osa, O., Kenny, J. M., & Zquez, A. V. (2007). Relationship between water absorption and dielectric behaviour of glass fibre reinforced unsaturated polyester resin. *Journal of Composite Materials*, 41(4), 393-402.

- Garbassi, F., Morra, M., & Ochiello, E. (1994). Polymer Surfaces: from Physics to Technology. *Polymer International*, 36(3), 300-306.
- Gassan, J., & Gutowski, S. (2000). Effects of Corona Discharge and UV Treatment on the Properties of Jute-Fiber Epoxy Composites. *Composites Science and Technology*, 60(15), 2857–2863.
- George, J., Sreekala, M. S., & Thomas, S. (2001). A review on the interface modification and characterization of natural fibre reinforced plastic composites. *Polymer Engineering and Science*, 41(9), 1471-1485.
- Goforth, C. E. (1994). The evaluation of kenaf as oil absorbent. In C. E. Goforth, M. J. Fuller (Eds.), *A Summary of Kenaf Production and Product Development Research 1989-1993* (Vol. 1011, pp. 1-33). Mississippi: Mississippi State University.
- Grant, S. T., & Bradley, L. W. (1995). In-situ observation in SEM of degradation of graphite/epoxy composite material due to sea water immersion. *Journal of Composite Materials*, 29(7), 853-867.
- Graupner, N., Herrman, A., & Mussig, J. (2009). Natural and man-made cellulose fibre reinforced poly (lactic acid) (PLA) composites: An overview about mechanical characteristics and application areas. *Composites Part A*, 40(6-7), 810-821.
- Graupner, N., & Mussig, J. A. (2011). Comparison of the mechanical characteristics of kenaf and lyocell fibre reinforced poly (lactic acid) (PLA) and poly(3-hydroxybutyrate) (HB) composites. *Composites Part A*, 42(12), 2010-2019.
- Hafizah, N. A. K., Bhutta, M. A. R., Jamaludin, M. Y., Warid, M. H., Ismail, M., Rahman, M. ... & Azman, M. (2014). Kenaf fibre reinforced polymer composites for strengthening RC beams. *Journal of Advance Concrete Technology*, 12(6), 167-177.
- Harsha, A. P., & Tewari, U. S. (2003). Two-body and three-body abrasive behaviour of poly-aryethetketone composites. *Polymer Testing*, 22, 403-418.
- Harun, J., Paridah, M. T., Nor Aina, A. S., & Khalina, A. (2009, February). Kenaf-its establishment and journey towards energizing the wood-based and bio-composites industry in Malaysia. In *International Conference on Prospect of Jute and Kenaf As Natural Fibres*. Dakar, Bangladeshi.
- Hassan, A., Rahman, N. A., & Yahya, R. (2011). Extrusion and injection moulding of glass fibre/MAPP/polypropylene: Effect of coupling agent on DSC, DMA and mechanical properties. *Journal of Reinforcement Plastic and Composites*, 30(14), 1223- 1232.
- Hassan, F., Zulkifli, R., Ghazali, M. J., & Azhari, C. H. (2017). Kenaf fibre composite in automotive industry: An overview. *International Journal of Advanced Engineering and Information Technology*, 7(1), 2088-5334.
- Holbery, J., & Houston, D. (2006). National fibre reinforced polymer composites in automotive applications. *Miner Metals Materials Society*, 58(11), 80-86.
- Hossain, M. D., Hanafi, M. M., Jol, H., & Hazandy, A. H. (2011). Growth, yield and fibre morphology of kenaf (*Hibiscus Cannabinus* L.) grown on sandy BRIS soil as influenced by different levels of carbon. *Africa Journal of Biotechnology*, 10(50), 10087-10095.
- Huda, M. S., Drzal, L. T., Mohanty, A. K., & Misra, M. (2008). Effect of fibre surface treatments on the properties of laminated bio-composites from poly (lactic acid) (PLA) and kenaf fibres. *Composites Science and Technology*, 68(2), 424-432.

- Jawaid, M., & Khalil, H. P. S. A. (2011). Cellulose/synthetic fibre reinforced polymer hybrid composites. An overview. *Carbohydrate Polymer*, 86(1), 1-18.
- Joseph, K., Mattoso, L. H. C., Toledo, R. D., Thomas, S., de Carvalho, L. H., Pothen, L., Kala, S., & James, B. (2000). Natural fibre reinforced thermoplastic composites. In E. Frollini, A. L. Lea'o & L. H. C. Mattoso (Eds.), *Natural Polymer and Agro-fibres Composites* (p. 156). San carlos, Brazil.
- Juliana, A. H., Paridah, M. T., Rahim, S., Nor Azowa, I., & Anwar, U. M. K. (2012). Properties of particleboard made from kenaf (*Hibiscus Cannabinus L.*) as function of particle geometry. *Materials and Design*, 34, 406-411.
- Julkapli, N. M., & Akil, H. M. (2010). Thermal properties of kenaf filled chitosan bio-composites. *Polymer Plastics Technology*, 49(2), 147-153.
- Jusoh, A. H., Rejab, M. R. M., Sirgar, J. P., & Bactiar, D. (2016). Natural fibre reinforced composites: A review on potential for corrugated core of sandwich structures. In *MATEC Web of Conference* (Vol. 74, pp. 1-5). Les Ulis: EDP Sciences.
- Kalia, S., Kaith, B. S., & Kaur, I. (2009). Pre-treatments of natural fibres composites: A review. *Polymer Engineering and Science*, 49(7), 1253-1272.
- Karahan, M., & Karahan, N. (2015). Investigation of the tensile properties of natural and natural/synthetic hybrid fibre woven fabric composites. *Journal of Reinforced Plastics and Composites*, 34(10), 96-806.
- KENAF ECO-fibres. (2005). Italia S.P.A., N.f.a.k.f.t.i., acoustic insulation. Green Automotive Industry. Retrieved September 30, 2017, from <http://www.kenaffibre.com/en/infotec-abella10.asp>
- Khan, A. R. (2011). *Kenaf, a fibre for future: the Harusmas experience*. Retrieved September 27, 2017, from <http://www.jeccomposites.com/news/composites-new/kenaf-future-harusmas- experience>.
- Kuchinda, N. C., Ndahi, W. B., Lagoke, S. T. O., & Ahmed, M. K. (2001). The effects of nitrogen and period of weed interference on the fibre yield of kenaf (*Hibiscus cannabinus L.*) in the northern Guinea savanna of Nigeria. *Crop Protection*, 20(3), 229-235.
- Lam, T. B. T., & Liyam, K. (2000). Structural details of kenaf cell walls and fixation of carbon dioxide. In *Proceeding of the Abstract of the International Kenaf Symposium* (Vol. 14, pp. 81-91). Hiroshima, Japan.
- Lee, B. H., Kim, H. S., Lee, S., Kim, H. J. & Dorgan, J. R. (2009a). Bio-composites of kenaf fibres in polylactide: Role of improved interfacial adhesion in the carding process. *Composites Science and Technology*, 69, 2573-2579.
- Lee, B. H., Kim, H. J., & Yui, W. R. (2009b). Fabrication of long and discontinuous natural fibre reinforced polypropylene bio-composites and their properties. *Fibres and Polymers*, 10(1), 83-90.
- Li, Y., Mai, Y. W., & Ye, L. (2000). Sisal fibre and its composites: A review of recent developments. *Composites Science and Technology*, 60(11), 2037-2055.
- Li, X., Tabil, L. G., & Panigrahi, S. (2007). Chemical treatments of natural fibre for use in natural fibre reinforced composites: A review. *Journal of Polymer Environment*, 15(1), 25-33.
- Liu, W., Drzal, L. T., Mohanty, A. K., & Misra, M. (2007). Influence of processing methods and fibre length on physical properties of reinforced soy-based bio-composites. *Composite Part B*, 38(3), 352-359.

- Loynd, K. (2010). *Kenaf: The clear-cut alternative- a polishing stone*. Retrieved September 29, 2017, from <http://www.polishingstone.org/articles/kenaf-kylie.html>
- Malkapuram, R., Kumar, V., & Yuvraj, S. N. (2008). Recent development in natural fibre reinforced polypropylene composites. *Journal of Reinforced Plastics and Composites*, 28(10), 1169-1189.
- Mazuki, A. A. M., Akil, H. M., Safiee, S., Ishak, Z. A. M., & Abubakar, A. (2011). Degradation of dynamic mechanical properties of pultruded kenaf fibre reinforced composites after immersion in various solution. *Composites Part B*, 42(1), 71-76.
- Mehta, G., Drzal, L. T., Mohanty, A. K., & Misra, M. (2006). Effect of fibre surface treatment on the properties of bio-composites from nonwoven industrial hemp fibre mats and unsaturated polyester resin. *Journal of Applied Polymer Science*, 99(3), 1055-1068.
- Meon, M. S., Othman, M. F., Husain, H., Remeli, M. F., Syawal, M. S. (2012). Improving tensile properties of kenaf fibres treated with sodium hydroxide. *Procedia Engineering*, 41, 1587-1592.
- Misra, S., Misra, M., Tripathy, S. S., Nayak, S. K. & Mohanty, A. K. (2002). The influence of chemical surface modification on the performance of sisal-polyester biocomposites. *Polymer Composites*, 23(2), 164-170.
- Mitchelle, A. J. (1986). Composites of commercial wood pulp fibres and cement. *Appita*, 33(6), 461-463.
- Mohamed, N. H., Tamada, M., Ueki, Y. & Seko, N. (2013a). Effect of partial delignification of kenaf bast fibres for radiation graft copolymerization. *Journal of Applied Polymer Science*, 127(4), 2891-2895.
- Mohamed, N. H., Tamada, M., Ueki, Y. & Seko, N. (2013b). Emulsion graft polymerization of 4-chloromethylstyrene on kenaf fibre by pre-irradiation method. *Radiation Physics and Chemistry*, 82, 63-68.
- Mohanty, A. K., Misra, M., & Hinrichsen, G. (2000). Biofibres, biodegradable polymers and bio-composites: An overview. *Macromol. Materials Engineering*, 276/277, 1-24.
- Mohanty, A. K., Misra, M., & Drzal, L. T. (2005). *Natural fibres, biopolymers and bio-composites*. Boca Raton: Taylor and Francis group.
- Mohd Yuhazri, Y., Phongsakorn, P. T., Haeryip, A. M., & Kannan, R. (2012). Mechanical properties of kenaf/polyester composites. *International Journal of Engineering and Technology*, 11, 127-131.
- Morshed, M. M., Alam, M. M. & Daniels, S. M. (2012). Moisture removal from jute fibre by plasma drying process. *Plasma Chemistry and plasma Processing*, 32(2), 249-258.
- Munawar, S. S., Umemura, K., & Kawai, S. (2007). Characterization of morphological, physical and mechanical properties of seven non-wood plant fibre bundles. *Journal of Wood Science*, 53(2), 108-113.
- Mwaikambo, L. Y. & Ansell, M. P. (2002). Chemical modification of hemp, sisal, jute and kapok fibres by alkalization. *Journal of Applied Polymer Science*, 84(12), 2222-2234.
- Najafi, S., Sharifnia, H., & Tajvidei, M. (2008). Effect of water absorption on creep behaviour of wood plastic composites. *Journal of Composite Materials*, 42(10), 933-1002.
- Namvar, F., Jawaid, M., Paridah, M. D. T., Rosfarizan, M., Azizi, S., Khodavandi, A., ... & Majid, D. N. (2014). Potential use of plant fibres and their composites for biomedical applications. *Bioresources*, 9(3), 5688-5706.

- Nashino, T., Hireo, K., Kotera, M., Nakamae, K., & Inagaki, K. (2003). Kenaf reinforced biodegradable composite. *Composites Science and Technology*, 63(9), 1281- 1286.
- Nashino, T. (2004). Green composites. United Kingdom: Polymer Composites and Environment.
- Nosbi, N., Akil, H. M. D., Ishak, Z. A. M., & Abubakar, A. (2010). Degradation of compressive properties of pultruded kenaf fibre reinforced composites after immersion in various solutions. *Materials and Design*, 31(10), 4960-4964.
- Ochi, S. (2008). Mechanical properties of kenaf fibres and kenaf/PLA composites. *Mechanics of Materials*, 40(4-5), 446-452.
- Osman, E., Vakhguett, A., Sbarski, I., & Mutasher, S. (2011). Mechanical properties of kenaf – unsaturated polyester composites: Effect of fibre treatment and fibre length. *Advanced Materials Research*, 311-313, 260-271.
- Osman, E., Vakhguett, A., Mustasher, S., & Sbarski, I. (2013). Effect of water absorption on tensile properties of kenaf fibre unsaturated polyester composites. *Suranaree Journal of Science and Technology*, 20(3), 183-195.
- Ozturk, S. (2010). Effect of fibre loading on the mechanical properties of kenaf and fibrefrax fibre reinforced phenol-formaldehyde composite. *Journal of Composite Materials*, 44(19), 1-24.
- Pang, C., Shanks, R.A., & Daver, F. (2015). Characterization of kenaf fibre composites prepared with tributyl citrate plasticized cellulose acetate. *Composites Part A*, 70, 52-58.
- Parikh, D. V., Calamari, T. A., Sawhney, A. S. P., Blanchard, E. J., & Screen, F. J. (2002). Improved chemical retting of kenaf fibres. *Textile Research Journal*, 72(7), 618- 624.
- Plueddemann, E. (1991). Silane Coupling Agents. In K. L. Mittal, (Ed.), *Silanes and other coupling agents* (pp. 31-54). The Netherlands: Plenum Press.
- Principia partners. (2003). Wood flour prices rise, natural fibre prices holding steady. *National Wood Fibre Composites*, 2(7), 4-5.
- Raji, J. A. (2007). Intercropping kenaf and cowpea. *African Journal of Biotechnology*, 6(24),2807-2809.
- Rashdi, A. A. A., Sapuan, S. M., Ahmad, M. M. H. M., & Khalina, A. (2009). Water absorption and tensile properties of soil buried kenaf fibre reinforced unsaturated polyester composites (KFRUPC). *Journal of Agricultural Environment*, 17, 909-911.
- Rassmann, S., Reid, R. G., & Paskaramoorthy, R. (2010). Effects of processing conditions on the mechanical and water absorption properties of resin transfer moulded kenaf fibre reinforced polyester composite laminates. *Composites Part A*, 41(11),1612- 1619.
- Rassmann, S., Paskaramoorthy, R., & Reid, R.G. (2011). Effect of resin system on the mechanical properties and water absorption of kenaf fibre reinforced laminates. *Materials and Design*, 32(3), 1399-1406.
- Ray, D., Sarkar, B. K., & Bose, N. R. (2002a). Impact fatigue behaviour of vinyl ester resin matrix composites reinforced with alkaline treated jute fibres. *Composites Part B*, 33(2), 233-241.

- Ray, D., Sarkar, B. K., Das, S., & Rana, A. K. (2002b). Dynamic mechanical and thermal analysis of vinyl ester resin matrix composites reinforced with untreated and alkali treated jute fibres. *Composites Science and Technology*, 62(7-8), 911-917.
- Razak, S. I. A., Abdul Rahman, W., Hashim, S., & Yahya, M. Y. (2014). Enhanced interfacial interaction and electronic properties of novel conducting kenaf/polyaniline bio- fibres. *Polymer Plastics Technology and Engineering*, 52(1), 51-71.
- Reza, M., Jamaludin, M. Y., Abdul Rahman, M. S., & Sayed, H. H. (2014a). Tensile properties of kenaf fibre due to various conditions of chemical fibre surface modifications. *Construction and Building Materials*, 55, 103-113.
- Reza, M., Jamaludin, M. Y., Abdul Rahman, M. S., & Mehdi, R. (2014b). Characteristics of continuous unidirectional kenaf fibre reinforced epoxy composites. *Materials and Design*, 64, 640-649.
- Rouison, D., Sain, M., & Couturier, M. (2004). Resin transfer moulding of natural fibre reinforced composites: cure simulation. *Composites Science and Technology*, 64(5), 629-644.
- Salem, I. A. S., Rozyanty, A. R., Betar, B. O., Adam, T., Mohammed, M., & Mohammed, A. M. (2017). Study of the effect of surface treatment of kenaf fibre on mechanical properties of kenaf filled unsaturated polyester composite. *Journal of Physics: Conference Series*, 908(1), 012002.
- Salleh, Z., Hyie, M. H., Berhan, M. N., Taib, Y. M., Roseley, N. R. N., Razib, A. R. M. (2014). Effect of water absorption on mechanical properties of kenaf and kenaf hybrid polyester. *Applied Mechanics and Materials*, 465-466, 967-972.
- Seller, J. T., & Reichert, N. A. (1999). Editors. Kenaf properties, processing and products. Mississippi: Mississippi State University.
- Shafizadeh, F. (1985). Cellulose Chemistry and its Applications. *Journal of Polymer Science Part C: Polymer Letters banner*, 25(2), 87-88.
- Sharba, M. J., Leman, Z., Sultan, M. T. N., Ishak, M. R., & Hanim, M. A. A. (2016). Effect of kenaf fibre orientation on mechanical properties and fatigue life of glass/kenaf hybrid composites. *Bio-resources*, 11(1), 1448-1465.
- Sharif, J., Mohamad, S. F., Othman, N. A. F., Bakaruddin, N. A., Osman, H. N. & Guven. O. (2013). Graft copolymerization of glycidyl methacrylate onto delignified kenaf fibres through pre-irradiation technique. *Radiation Physics and Chemistry*, 91, 125-131.
- Shinchi, S., Cao, Y., & Fukumoto, I. (2005). Press forming of short natural fibre-reinforced biodegradable resin: Effects of fibre volume and length on flexural properties. *Polymer Testing*, 24(8), 1005-1011.
- Sivakumari, D., Ngi, F. E., Lau, S. M., & Lim, K. T. (2017). Fatigue life behaviour of glass/kenaf woven-ply polymer hybrid bio-composites. *Journal of Polymer Environment*, 26(2), 1-9.
- Srayya, S., & Kumar, B. S. (2015). Evaluation on the mechanical properties of hybrid composites (kenaf, E-glass, jute). *International Journal of Latest Trend in Engineering and Technology*, 5, 164-170.

- Sreekala, M. S., Kumarah, M. G., Joseph, S., Jacob. M., & Thomas, S. (2000). Oil palm fibres reinforced phenol formaldehyde composites: Influence of fibre surface modifications on the mechanical performance. *Applied Composite Materials*, 7(5-6), 295-329.
- Tilmon, H. D., Taylor, R., & Malone, G. (1988). Kenaf as an alternative crop for Delaware. In J. Janick & J. E. Simon (Eds.), *Advances in new crops* (pp. 301-302). Delaware: Delaware Cooperative Extension.
- Thakur, V. K., Thakur, M. K., & Gupta, R. K. (2014). Review: Raw natural fibre-based polymer composites. *International Journal of Polymer Analysis and Characteristics*, 19(3), 256-271.
- Valadez, G. A., Cervantes, U. J. M., Olayo, R., & Herrera, F. P. J. (1999). Effect of fibre surface treatment on the fibre-matrix bond strength of natural fibre reinforced composites. *Composites: Part B*, 30, 309-320.
- Vijayakumar, S., Nilavarasan, T., Usharani, R., & Karunamoorthy, L. (2014). Mechanical and microstructure characterisation of coconut spathe fibres and kenaf bast fibres reinforced epoxy polymer matrix composites. *Procedia Material Science*, 5, 2330- 2337.
- Vision paper (2003). About the kenaf fibre plant. Retrieved September 25, 2017, from <http://www.visionpaper.com/kenaf2.html>.
- Wambua, P., Ivens, J., & Verpoest, I. (2003). Natural fibres: Can they replace glass in fibre reinforced plastics? *Composites Science and Technology*, 63(9), 1259-1264.
- Wang, B., Panigrahi, S., Tabil, L., & Crerar, W. (2003). Modification of flax fibres by chemical Treatment (pp. 3-337). Paper presented at the *CSAE/SCGR Meeting Montreal*. Quebec, July 6-9 2003.
- Webber, C. L. (1994). Kenaf (*Hibiscus cannabinus* L.) yield components as affected by sewage sludge applications. Non-wood Plant Fibres. *Programme Presentation*, 21, 9-24.
- Webber, C. L., Whitworth, J., & Dole, J. (1999). Kenaf (*Hibiscus cannabinus* L.) core as a containerized growth medium component. *Journal of Crops Production*, 10(2), 97- 105.
- Webber, C. L., Bledsoe, V. K., & Bledsoe, R. E. (2002a). Kenaf harvesting and processing. In J. Janick & A. Whipkey (Eds.), *Trends in New Crops and New Uses* (Vol. 9, pp. 340-347). Alexandria: ASHS press.
- Webber, C. L., Bhardwaj, H. L., & Bledsoe, V. K. (2002b). Kenaf production: fibre, feed and seed. In J. Janick & A. Whipkey (Eds.), *Trends in New Crops and New Uses* (pp. 327- 339). Alexandria: ASHS press.
- Weyenberg, I., Ivens, J., de Coster, A., Kino, B., Baetens, E., & Verpoest, I. (2003). Influence of processing and chemical treatment of flax fibres on their composites. *Composites Science and Technology*, 63, 1241-1246.
- Xiao, G.Z. (1997). Effects of Solvents on the Surface Properties of Oxygen Plasma Treated Polypropylene Films. *Journal of Adhesion Science and Technology*, 11(5), 655-663.
- Xu, Y., Kawata, S., Hosoi, K. & Kuroda, S. (2009). Thermomechanical properties of the silanized-kenaf/polystyrene composites. *EXPRESS Polymer Letters*, 3(10), 657-664.
- Yahaya, R., Sapuan, S. M., Jawaid, M., Leman, Z., & Zainudin, E. S. (2016). Effect of fibre orientations on the mechanical properties of kenaf-aramid hybrid composites for spall-liner application. *Defence Technology*, 12(1), 52-58.
- Yousif, B. F., Shalwan, A., Chin, C.W., & Ming, K. C. (2012). Flexural properties of treated and untreated kenaf/epoxy composites. *Materials and Design*, 40, 378-385.

- Yusoff, R. B., Takagi, H., & Nakagaito, A. N. (2016). Tensile and flexural properties of polylactic acid-based hybrid green composites reinforced by kenaf, bamboo and coir fibres. *Industrial Crops and Products*, 94, 562-573.
- Zamri, M. H., Osman, M. R., Akil, H. M., Sanidan, M. H. A., & Ishak, Z. A. M. (2016). Development of green pultruded composites using kenaf fibre: Influence of linear mass density on weathering performance. *Journal of Cleaner Production*, 125, 320- 330.



The Physicochemical Properties of Cocoa Butter Equivalent Produced From Lipase-Catalyzed Palm Oil and Hydrogenated Palm Oil via Physical Fractionation

Siti Maslina Mohamad Alwi^{1,2*} and Lai Oi Ming³

¹Institute of Bioscience, Universiti Putra Malaysia, 43400 UPM, Serdang, Selangor, Malaysia

²FGV Innovation Centre, Bandar Enstek, 71760 Nilai, Negeri Sembilan, Malaysia

³Faculty of Biotechnology and Biomolecular Sciences, Universiti Putra Malaysia, 43400 UPM, Serdang, Selangor, Malaysia

ABSTRACT

Palm oil (PO) and fully hydrogenated palm oil (FHPO) were subjected to enzymatic interesterification using 9.5% of TLIM Lipozyme. The optimum condition for this process occurred at 62.75°C, with reaction time 172.50 minutes with the ratio of 1:1 for palm oil to hydrogenated palm oil respectively. The Palmitoyl-Oleoyl-Stereoyl (POS) yield obtained was approximately 15%. Product was subsequently subjected to a fractionation process at various cooling temperatures and reaction time. At 34°C, POS achieved was at the highest level which was approximately 31% after 12 hours cooling process. The study of physicochemical properties of the Cocoa butter Equivalent (CBE) fat was determined for the purpose of characterization identification. The properties identified were solid fat content, slip melting point (SMP) and iodine value (IV). The IV and SMP values obtained were 44.30 and 29°C respectively. However, CBE produced almost 0% of Solid Fat Content (SFC) at 30°C. Apart from the high yield of POS, the physicochemical characteristics showed significant compatibility with that of CB. In addition, the crystal polymorph of CBE 34 physicochemical characteristics of CBE34 (β' + β) was similar to CBE. Hence, from this study, CBE 34 is recommended for utilization in the confectionery industry as CBE.

Keyword: Lipase-catalyzed cocoa butter equivalent, fractionation, physicochemical properties

ARTICLE INFO

Article history:

Received: 03 April 2018

Accepted: 27 September 2018

Published: 24 January 2019

E-mail addresses:

nina.alwi@gmail.com (Siti Maslina Mohamad Alwi)

omlai.biotech@gmail.com (Lai Oi Ming)

* Corresponding author

INTRODUCTION

Modification of fats and oil is extensively applied to attain products with appropriate properties for their specific use. Since most natural oils and fats have limited application due to their inherent chemical composition,

modification through hydrogenation, interesterification and fractionation processes is required. Modifications were implemented generally to increase oxidative stability, enhance textural characteristics and to alter fatty acid composition (Rasor & Duncan, 2014). These modification processes can change the physicochemical properties of oils and fats by reducing the degree of unsaturation of the acyl groups, either by hydrogenation or interesterification; which the fatty acids chains are redistributed. Another process that can also affect the physicochemical properties of oils and fats is physical separation of the triacylglycerols through selective crystallization and filtration (Hassim & Dian, 2017).

Fractionation process enables industry to obtain several fractions of different melting points, hardness and solid fat content from solid or semisolid oils and fats, making it possible to extend the application of edible oils and fats in the related food products. Palm oil is rich in Palmitoyl-Oleoyl-Palmitoyl (POP), which is a very suitable source of CBE especially after concentrating it by modifying the fat. Since palm oil is undoubtedly the most versatile oil to be used in food products, fractions of distinct different physical characteristics can be produced, by applying multiple stage dry fractionations (Desmet Ballestra, 2015).

Palm oil can be applied in many diverse areas, both edible and non-edible usages by various modification processes such as blending, hydrogenation, fractionation crystallisation and interesterification. Fractionation process plays a big part in cocoa butter industry. Fractionation is used to isolate desirable triacylglycerols. Palmitoyl-Oleoyl-Stereoyl (POS), Palmitoyl-Oleoyl-Palmitoyl (POP) and Stereoyl-Oleoyl-Stereoyl (SOS) are important triacylglycerols in cocoa butter that are responsible to give required attributes of a good chocolate (Oracz et al., 2015). However, this research study only focused on POS yield.

Fractionation refers to the mechanical separation of the liquid from the solid of the oils and fats components. Fractionation has two stages. The first stage involves the formation of stable, larger and uniform crystals partial produced under the controlled gradual cooling to the desired temperatures in the crystallizer. Subsequently, filtration method is used to separate the solid and liquid fractions (Normah et al., 2012).

Dry fractionation is qualified as a natural and green technology because it produces less loss, and effluent and use less chemicals (Kellen et al., 2007). This method can be used especially when fats such palm oil is used in the formulation. Palm oil and palm kernel oil comprises a mixture of high and low melting triacylglycerols making it easier to separate by a simple dry fractionation process (Norizzah et al., 2014). This process consists of crystallization stage where solid crystals are produced in a liquid matrix where liquid is separated from the crystals at the separation stage. This process separated palm oil into two parts, namely liquid (olein) and numerous grades of palm stearin (Zaliha et al., 2004). It is commonly used because it is cost effective and produces considerably good yield. It is also known to improve product and nutrition functionality, improve oxidative stability and increase cold stability via winterization process. Organoleptic properties in terms of taste and flavor can be retained as well (Deffense, 2008).

Physicochemical properties of oils and fats in this case include melting point, solid fat content and iodine value. Melting point increases when fatty acids length increases. It is also influenced by the complexity of TAG components, saturation degree and *trans* fatty acids content. Solid fat content is an important indicator of melting and crystallization behaviors. It therefore determines the choice of fats to be used to achieve specific product functionality. Iodine value (IV) measures the degree of unsaturation of fat and a predictor of its oxidative stability. Physicochemical properties are vital in defining the fats produced according to specification of desired functionality (Rasor & Ducan, 2014). Fats possess the ability to crystallize in multiple forms and this influenced the consistency of the fats. The α form is the least stable and tends to impart a waxy texture. β' crystals are fine needle-like form which is less stable, but gives a smooth structure. While, β crystals are large, have grainy texture. It is the most stable crystal form. So, crystallization in β form is preferred for chocolate products due to desired gloss and snapping attributes (Rasor & Ducan, 2014). CBE and CB have the same crystals form, therefore, both need to be tempered (Lawler & Dimick, 2008). The physicochemical characteristics of CBE are close to CB in terms of crystallization, texture and melting properties due to the similar Triacylglycerol (TAG) composition which makes them compatible when mixed partially or replaced completely (Gunstone, 2011).

POS is the highest TAG percentage in CB. Many studies have concentrated on producing CBE with high SOS and POP. Thus, this study focused on producing high POS CBE instead. In this study, the enzymatically interesterified fat was subjected to dry fractionation process at various cooling temperatures and reaction time to see the effects of these parameters on the properties and yield of the solid portions of CBE fat. Based on the results obtained, cooling temperature can be defined so that optimum POS yield can be achieved.

MATERIALS AND METHOD

Materials

CBE fat was produced from refined palm oil (RBDPO) provided by Sime Darby Jomalina Food Industries Sdn. Bhd. (Telok Panglima Garang, Selangor, Malaysia) and fully hydrogenated palm oil (FHPO) from Unimills, Netherlands, via enzymatic interesterification using TLIM (Novozyme, Denmark). All chemicals used were of analytical grade except for GC and HPLC purposes, the solvents used were HPLC grade.

Methods

Fractional Crystallization. The interesterified fats (500 g) were subjected to dry fractionation using a jacketed vessel reactor. The oil was first heated in the reactor for 20 min at 70°C with stirring at 100 rpm to eliminate all crystals. The oil was then agitated and cooled at

controlled condition to the desired end-temperature. The oil was held in the crystallizer for stabilization followed by separation of the semi-slurry into olein and stearin using hydraulic filter press. The slurry was first fed into the filter press with a minimum pressure 2.0 bar/min. The filling period was 10 min with a maximum pressure 6.0 bar/min. The olein and stearin fractions were weighed and analyzed, respectively.

Analysis of Triacylglycerol (TAG) Species. This method is determined by AOCS Official Method Ce 5b-89 for the separation and quantitative determination of the triacylglycerols in oil samples in terms of their molecular weight and degree of unsaturation as a function of their equivalent carbon number (ECN) which is sometimes referred to as partition number, using high-performance liquid chromatography. The triacylglycerol profile was analyzed using Waters High Performance Liquid Chromatography (HPLC) e2695 (Milford Massachusetts, USA) separation module with Evaporative Light Scattering Detector (ELSD). The mobile phases used are Acetonitrile and Acetone (40:60). Column of stainless steel tube 250 mm in length and 4.6mm i.d. packed with 5- μ m diameter particles for silica Supercosil LC-18 (Sigma-Aldrich, USA) is used and the temperature is at 40.0°C. Gas pressure (O_2 FN) fixed at 25.0 (psi). Pump mode was Isocratic and flow rate set at 1.0ml. Injections of samples are 5 μ l. Standards used for determination of triacylglycerol species were bought from Sigma Aldrich Inc (Sigma Chemical Co., USA). Triglyceride peaks were identified and recorded.

Solid Fat Content (SFC). SFC was measured according to Malaysian Palm Oil Board (MPOB) Test Method p4.8 (2004) using pulsed nuclear magnetic resonance (NMR) spectrometry (Bruker NMS 120 minispec). The SFC of PDAG fat, olein and stearin fractions was measured at each separation temperature. The sample in the NMR tube was first melted at 70°C for 30 minutes, followed by chilling at 0°C for 90 minutes prior to measurement. Melting, chilling and holding of sample were carried out in pre-equilibrated thermostat water bath. The SFC temperature was set to 10, 20, 25, 30, 35, and 40°C. The percentage of SFC was based on three measurements.

Iodine Value (IV). Approximately, 0.130 g of all the blended oil was weighed into 500 ml conical flask with glass stopper. A blank flask which contains no oil was prepared. About 15 ml of cyclohexane and acetic acid solution were mixed in a 1:1 ratio, and then added into the sample flask and blank flask. Then, 25 ml of Wij's solution was added to both flasks and they were closed with glass stopper and properly shaken. The flasks were left in the dark for 1 hour. After that, 20 ml of potassium iodide and 150 ml of distilled water were added to release the iodine from non-reacted iodine monochloride. Finally, the mixtures were all titrated with sodium thiosulphate solution until yellow colour nearly disappeared before

1-2 ml of starch solution was added as indicator and titration continued. This process ended when blue color of starch solution totally disappeared (AOCS method Cd 1d-92, 1993b).

Slip Melting Point (SMP). SMP was measured according to AOCS Method Cc.3.25 (1993). Capillary tubes were filled with a 1 cm high column of melted fat. The capillary tubes were then rolled against a piece of ice before being chilled in a refrigerator at 10°C for 16 h to solidify the fat. The tubes were subsequently attached with a rubber band to a thermometer and suspended in a 600-mL beaker of boiled distilled water. The bath temperature was adjusted to 8-10°C below the SMP of the sample, and heat was applied using a heating coil element to increase the bath temperature at a rate of 1 C/min. The temperature at which the fat column rises was reported as the SMP.

XRD Analysis. The polymorphic forms of fat crystals were determined with an FR592 Enraf-Nonius Diffractis X-ray generator (Delft, The Netherlands) and an Enraf-Nonius model FR 552 Guinier camera equipped with a customized single-compartment cell with the temperature controlled by an external-circulating thermostatic bath. The melted sample at 60°C was placed in the cell, which was set at the crystallization temperature. Sample was held isothermally until all the polymorphic phases were fully observed.

RESULTS AND DISCUSSIONS

Triacylglycerols (TAGs)

The initial POS level was obtained at 15% after enzymatic interesterification process whereby the conditions were determined to be optimum at 9.5% TLIM enzyme with the temperature of 62.75°C and reaction time of 172.50 minutes. The ratio of palm oil to hydrogenated palm oil used is 1:1. The interesterified fats were then subjected to fractionation process to further purify the CBE.

Table 1 illustrates the yield of POS produced using different temperatures and retention times. It is observed that the yield of POS from fractionation done at 12 hours showed insignificant difference compared to 36 hours of process. The highest TAGs obtained were CBE 32 and CBE 34, with approximately the same percentage of POS yield, of 31.46±0.20% and 31.23±0.70% respectively. The crystal formation temperature during crystallization increases the melting point, which meant that POS increases when temperature decreases (Rodriguez, 2002). As shown in the result obtained, lower crystallization temperature produced higher POS yield. Since POS is dominant in these CBEs, hence they are compatible with CB. Similarly, Mutia et al., 2015 reported that by interesterifying palm mid fraction with stearic acids, the yield of POS increased from 8.59% to 20.54%. The mixture of palm mid-fraction and fully hydrogenated soybean oil produces CBE that has TAG composition of 37.7% of POS as stated by Soekopitojo et al.,

2009. CBE produced from enzymatic transesterification of palm olein and saturated fatty acid distillate produced as high as 42% of POS level (Zainal-Abideen et al., 2012). Many more recent studies showed that palm oil and its derivatives were good materials to produce CBE. Reducing the temperature, residence time, and substrate molar ratio is necessary to develop an industrially applicable and cost-effective process for producing CBE.

Table 1
Yield percentage of POS produced using different temperature and retention time

Sample	Temp (°C)	Time (hours)	Yield (%) %POS
CBE 32	32	12	31.46±0.20
	32	24	31.18±0.35
	32	36	30.83±0.15
CBE 34	34	12	31.23±0.70
	34	24	30.91±0.21
	34	36	31.90±0.94
CBE 36	36	12	22.96±0.22
	36	24	29.55±0.06
	36	36	29.47±0.40
CBE 38	38	12	27.38±0.09
	38	24	29.03±0.62
	38	36	28.54±0.03
CBE 40	40	12	12.34±0.30
	40	24	15.84±0.21
	40	36	16.27±0.03
CBE 45	45	12	23.29±0.46
	45	24	27.19±0.23
	45	36	21.97±0.25

Solid Fat Content (SFC)

SFC is another method to evaluate softness and snapping of fat. It is generally performed using pulse nuclear magnetic resonance (pulse NMR) (Hitachi High-Tech, 2008). The hardness of the fat is reflected at 25°C of solid fat content. The higher the value of solid fat content at this temperature, the harder the fat is (Quast et al, 2011). SFC between 25 and 30°C indicates heat resistance, whereas SFC at 35°C or more denotes waxiness, to which fat remains without quickly melting in the mouth (Kim et al., 2012). Figure 1 shows the SFC of CB and CBEs produced. At 25°C, CBE 32 shows the lowest percentage of solid fat content which is approximately 11%, demonstrating that this fat melts more easily than the others. CBE 45 has the highest solid fat content which is about 50%, has waxiness attribute when made into chocolate. CBE 34, 36, 38 and CB have comparable values, around 29-33°C, indicating that their hardness are nearly the same. Between 25°C-30°C, sample

CBE 40, 38, 36, 34 and 32 shared the same steepness profile and sharp melting behaviour as CB. Figure 1 indicates that at 35°C, sample CBE32, CBE34 and CBE36 presented SFC values which are very close to zero. This corresponds to another important attribute of chocolate in CB or Cocoa Butter Alternatives should have no solid left at 35°C. However, only CBE 45 is observed to have high solid content even after 35°C, which is not favoured in chocolate industry. This is because, the presence of solid fats at temperature higher than 35°C, known as the “fatty residue”, is easily detected during the sensory evaluation (Quast et al., 2011). Furthermore, of late, there is a trend toward producing chocolate which is soft rather than hard and quickly melts in the mouth without leaving an aftertaste. The soft CBE has a low SFC overall in a temperature range of 20°C to 35°C, and thus it can provide soft-texture chocolate, but does not form solid crystals at room temperature, which may cause a blooming phenomenon (Kim et al., 2012).

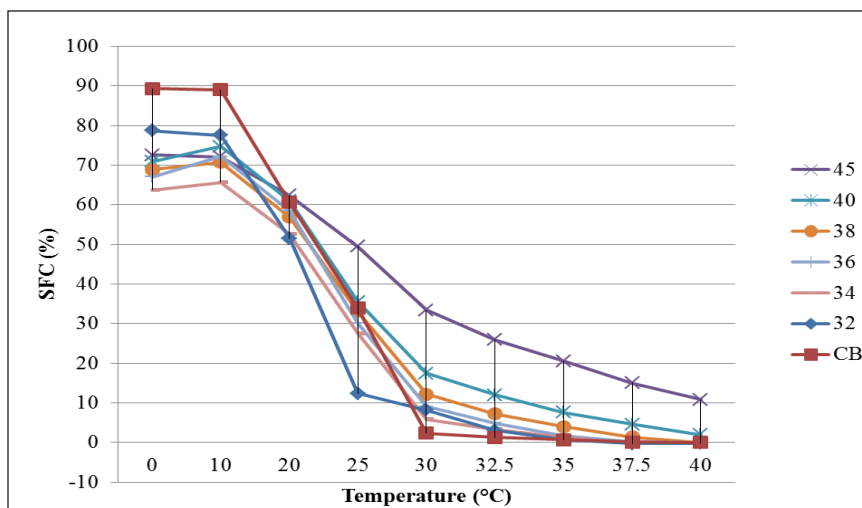


Figure 1. Solid fat content of CB and CBEs after fractional crystallization

Iodine Value (IV)

One of the important quality measurements of CBE is IV. It is to determine the unsaturation levels in oils and fats. Table 2 shows the IVs of CBE fats produced after fractional crystallization. The higher the unsaturation level (double bond) in the fatty acid chain, the more iodine is being absorbed. Thus the degree of unsaturation in the oil or fat is higher.

The IV values of all samples are higher than CB which is 32.1 indicating that the CBE fats produced are softer. This might be due to the level of oleic in the enzymatically interesterified CBEs, since palm oil is rich in oleic acids. The CBE32 had the lowest level of unsaturation level that was 39.10, while the highest was CBE36 (48.32). CBE from exotic fats such as illepe butter, kokum butter and sal fats IV ranges from 33 to 45. Whereas shea

butter is very soft, which IV is between 52-66 (Gunstone, 2011). IV correlates directly to SMP; when IV of oils or fats is higher, the SMP is lower and vice versa. In other words, the unsaturation levels in oils or fats determine their SMP.

Table 2

The iodine value of CBE32, CBE 34, CBE 36, CBE 38, CBE 40 CBE 45 and CB

CBE	IV
32	39.10 ±0.678
34	43.80 ±0.55
36	48.32 ±2.49
38	42.46 ±0.270
40	42.30 ±0.110
45	41.60 ±3.25
CB	32.10 ±0.14

Slip Melting Point (SMP)

Slip Melting Point (SMP) is where a temperature of fat starts to melt depending on the type of polymorph. This analysis is significant in determining the quality of oils and fats. Stabilization of fat prior to measurement of the slip melting point is extremely important for fats with pronounced polymorphic behaviour, such as cocoa butter (Ranken, 2012). During the changes of fats from solid to liquid phase, the fat crystals network weakens when temperature rises and starts to melt when the SMP of a product is achieved. Table 3 illustrates the SMP of CBEs and CB. It is observed that CBE 45 has the highest SMP, whereas CBE34 has the lowest values, which are 38.96 and 29.05 respectively. The SMP for CBE 32, 34 and 36 are 29.14, 29.05 and 31.30, respectively, which fall in the range as of cocoa butter (29 to 33). The presence of TAG saturated-saturated-saturated (StStSt), saturated-unsaturated-saturated (StUSt), saturated-unsaturated-unsaturated (StUU) and unsaturated-unsaturated-unsaturated (UUU) content in fat and oil affects the value of SMP (Brapson-Danthine & Gibon, 2007). Thus, oleic acids mostly, in the form of POO (palmitoyl-oleoyl-oleoyl) and OOO (oleoyl-oleoyl-oleoyl) present in these samples cause the SMPs to be lower than CB. Consequently, CBE 40 and 45 require higher temperature to melt because they contain higher StUSt and StStSt. Cocoa butter has a sharp melting point which is approximately 31-35 °C and melts completely in the mouth. Its texture is brittle and it fractures readily and does not appear oily (Gunstone, 2011). The SMP of CBEs in Table 4 varies from 28°C to 36°C which are below 37°C except for CBE45. It is essential for CBE to melt in the mouth below body temperature. In many researches done, SMP was recorded approximately from 29.9°C-34.5°C, which consisting of more percentage POS, whereas CBE with higher percentage of SOS triacylglycerols have SMPs at 39°C (Ciftci et al., 2009; Soekopitojo et al., 2009).

Table 3
The SMP of CBE32, CBE 34, CBE 36, CBE 38, CBE 40, CBE 45 and CB

CBE	SMP (°C)
32	29.14 ±0.650
34	29.05±0.870
36	31.30 ±1.03
38	35.98 ±2.50
40	36.45 ±0.289
45	38.96 ±0.990
CB	33.01 ±0

Subcell Packing and Polymorphs

CB can exist in different crystal forms, each with different thermodynamic stability. The main three polymorphic forms are α (alpha), β (beta) and β' (beta prime) (Rousseau, 2016). β -crystals have the highest melting point and have a more compact crystal structures than β' -form (Rousseau, 2007). CBE fats exhibit polymorphism similar to that of CB and they CBE should have a similar melting and crystallization behaviour. Thus, the fatty acids and triacylglycerol composition do not affect eutectic formation with CB (Rousseau, 2016). The subcell packing and polymorphs of CBEs (CBE45, CBE40, CBE38, CBE36, CBE34 and CBE32) and CB are shown in Table 4. CBE fats display polymorphism similar to cocoa butter which consist mostly β -form. Hence, it must be tempered as such. Since CBE crystallizes like cocoa butter, therefore, the physical properties of the chocolate like the sharp melting, gloss, shrinkage on solidifying and snap upon breaking are hardly affected (Akoh & Min, 2008). X-ray diffraction, used to identify crystal polymorphs by determining the long and short spacing of crystal (Rousseau, 2016). According to Table 4, only CBE45 has β form, whereas the rest have the same polymorphs as CB. The most preferred polymorph for chocolate products is for β form due to desired gloss and snapping attributes (Rasor & Ducan, 2014). This is because only β crystals contribute to a high melting point (Naik & Kumar, 2014). A study by Solís-Fuentes and Duran-de-Bazua, 2003, confirmed that β is a stable form of mango seed almond fat as CBE is compatible to CB.

Table 4
Subcell packing and polymorphs of CBE (CBE45, CBE40, CBE38 and CBE36) and CB

CBE	Subcell packing	Polymorphic form
CBE32	O [^] + T//	β' + β
CBE34	O [^] + T//	β' + β
CBE36	O [^] + T//	β' + β
CBE38	O [^] + T//	β +
CBE40	O [^] + T//	β' + β
CBE45	O [^] + T//	β'
CB	O [^] + T//	β' + β

CONCLUSION

Similar physiochemical characteristics of CBE34 fat to that of CB indicate that it could be utilized in confectionery industry as CBE. The CBE produced is slightly softer compared to CB which fulfils the ever-growing trend of softer chocolates that quickly melts in the mouth (Kim et al., 2012). The traits of the CBE produced, having high yield of POS contributed to its high the compatibility with CB. Since according to EU regulations, only 5% of CBE can be used in chocolate formulations, CBE34 can be easily blended with CB. The crystallization profile for CBE34 fits cocoa butter profile ($\beta'+\beta$), suggesting CBE34 the best suited product in this study. Nonetheless, more trials can be done to determine the fractionation yield percentage.

ACKNOWLEDGEMENT

The authors would like to thank Pertanika UPM for the opportunity to publish this paper.

REFERENCE

- Akoh, C. C., & Min, D. B. (2008). *Food Lipids: Chemistry, Nutrition and Biotechnology*. New York: CRC Press.
- AOCS Official Method Cd 1d-92. (1993b). Iodine Value of Fats and Oils, Cyclohexane-Acetic Method. The American Oil Chemists' Society.
- AOCS Official Method Cd 3-25. (1993). Slip Melting point, AOCS Standard open Tube Melting Point. The American Oil Chemists' Society.
- Braipson-Danthine, S., & Gibon, V. (2007). Comparative analysis of triacylglycerol composition, melting properties and polymorphic behavior of palm oil and fractions. *European Journal of Lipid Science and Technology*, 109(4), 359-372.
- Chiel Jedang Corp. (2012). Fat and Oil Composition for Chocolate and Confectionery. EP 2 508 077 A1. European Patent Application. Munich, Germany: European Patent Office.
- Çiftçi, O. N., Fadiloğlu, S., & Göğüş, F. (2009). Conversion of olive pomace oil to cocoa butter-like fat in a packed-bed enzyme reactor. *Bioresource Technology*, 100(1), 324-329. doi: 10.1016/j.biortech.2008.05.035.
- Deffense, E. (2008). Dry Fractionation A Booming Technology. Crystallization and Degumming. Retrieved January 15, 2018, from <https://webcache.googleusercontent.com/search?q=cache:113BM8XjNloJ:https://www.soci.org/-/media/Files/Conference-Downloads/2008/OFI-Abu-Dhabi-Apr-08/Defennse.ashx%3F1a%3Den+&cd=1&hl=en&ct=clnk&gl=my>
- Desmet Ballestra. (2015). Specialty fats fractionation: new possibilities Statoliser® Technologies. Desmet Ballestra Fractionation with Statoliser® Technology.
- Gunstone, F. D. (2011). *Vegetable Oils in Food Technology: Composition, Properties and Uses*. Chichester: John Wiley & Sons.

- Hassim, N. A. M., & Dian, N. L. H. M. (2017). Usage of Palm oil, palm kernel oil and their fractions as confectionary fats. *Journal of Oil Palm Research*, 29(3), 301–310. <https://doi.org/10.21894/jopr.2017.2903.01>
- Hitachi Hi-Tech. (2008). Estimating the Solid Fat Content of Chocolate and Butter Products using DSC to Investigate the Taste of Edible Fats. Hitachi High Tech Corporation. Retrieved January 15, 2018, from https://www.hitachi-hightech.com/file/global/pdf/products/science/appli/ana/thermal/application_TA_085e.pdf
- Kellens, M., Gibon, V., Hendrix, M., & De Greyt, W. (2007). Palm oil fractionation. *European Journal of Lipid Science and Technology*, 109(4), 336-349.
- Kim, M. J., Lee, S. B., Lee Y. J., Park, S. W., & Lee K. P. (2012). Fat and Oil Composition for Chocolate and Confectionery. European Patent No. EP 2508077A1. Munich, Germany: European Patent Office.
- Lawler, P. J., & Dimick, P. S. (2008). Crystallization and Polymorphism of Fats. In C. C. Akoh & D. B. Min (Eds.), *Food Lipids: Chemistry, Nutrition, and Biotechnology* (pp. 293-318). New York: CRC Press.
- MPOB Test Method. (2004). P4.8. Ministry of Plantation Industries and Commodities Malaysia. Kuala Lumpur: Malaysian Palm Oil Board.
- Mutia, R., Zaidel, D. N. A., & Muhamad, I. I. (2015). Synthesis of Cocoa Butter Equivalent from Formulated Hard Palm Oil Mid-Fraction and Canola Oil Blends. *Advanced Materials Research*, 1113, 453-458.
- Naik, B., & Kumar, V. (2014). Cocoa butter and its alternatives: A review. *Journal of Bioresources Engineering and Technology*, 2(1), 1-11.
- Norizzah, A. R., Norsyamimi, M., Zaliha, O., Azimah, N., & Hazirah, S. (2014). Physicochemical properties of palm oil and palm kernel oil blend fractions after interesterification. *International Food Research Journal*, 22(4), 1390–1395. <http://www.ifrj.upm.edu.my>
- Normah, I., Cheow, C. S., & Chong, C. L. (2012). Crystal habit during crystallization of palm oil: Effect of time and temperature. *International Food Research Journal*, 20(1), 417–422.
- Oracz, J., Zyzlewicz, D., Budyryn, G., Nebesny. (2015). Cocoa Butter Alternative Fats. *Plant Lipids Science, Technology, Nutritional Value and Benefit to Human Health*, 2015, 87-106.
- Quast, L. B., Luccas, V., & Kieckbusch, T. G. (2011). Physical properties of pre-crystallized mixtures of cocoa butter and cupuassu fat. *Grasas Y Aceites*, 62(1), 62-67.
- Ranken, M. D. (Ed.). (2012). *Food industries manual*. New York: Springer Science & Business Media.
- Rasor, A. S., & Duncan, S. E. (2014). Fats and Oils – Plant Based. In S. Clark, S. Jung & B. Lamsal (Eds.), *Food Processing: Principles and Applications*, (pp. 457-480). Chichester: John Wiley & Sons.
- Rodriguez, A. R. (2002). Literature Review. *American Journal of Medical Quality*, 17(3), 118–123. <https://doi.org/10.1177/106286060201700307>
- Rousseau, D. (2007). The microstructure of chocolate. In D. J. McClements (Ed.), *Understanding and controlling the microstructure of complex foods* (pp. 648-690). Cambridge: Woodhead Publishing Limited.

- Rousseau, D. (2016). Microstructural Imaging of Chocolate Confectionery. In N. Sozer (Ed.), *Imaging Technologies and Data Processing for Food Engineers* (pp. 311-333). Heidelberg: Springer.
- Soekopitojo, S., Hariyadi, P., Muchtadi, T. R., & Andarwulan, N. (2009). Enzymatic interesterification of palm oil midfraction blends for the production of cocoa butter equivalents. *Asian Journal of Food and Agro-Industry*, 2(4), 807-816.
- Solís-Fuentes, J. A., & Durán-de-Bazúa, M. C. (2004). Mango seed uses: thermal behaviour of mango seed almond fat and its mixtures with cocoa butter. *Bioresource Technology*, 92(1), 71-78.
- Zainal-Abideen, M., Aris, A., Yusof, F., Abdul-Majid, Z., Selamat, A., & Omar, S. I. (2012). Optimizing the coagulation process in a drinking water treatment plant—comparison between traditional and statistical experimental design jar tests. *Water science and Technology*, 65(3), 496-503.
- Zaliha, O., Chong, C. L., Cheow, C. S., Norizzah, A. R., & Kellens, M. J. (2004). Crystallization properties of palm oil by dry fractionation. *Food Chemistry*, 86(2), 245-250.

Extraction of Subtractive Features of Prismatic Parts from STEP File for CAD/CAM Integration

Sattanathan Sivakumar^{1*}, Venkadasamy Dhanalakshmi² and Ravichandran Vishnuvardha¹

¹Department of Mechanical Engineering, Hindustan Institute of Technology and Science, Chennai, India

²Department of Mechanical Engineering, Thiagarajar College of Engineering, Madurai, India.

ABSTRACT

Automation plays an important role in the manufacturing systems to increase the productivity with high flexibility in the production process. This may leads to the requirement of an information model to control the industrial machinery and processes. The information model contains the common product data. Hence, the data extraction is mandatory to extract the product data from the product model. This paper explains the extraction of product data through feature extraction process. A simplified system is developed to extract the data from the STEP file of a product model for subtractive features of prismatic parts. Using extracted data, the controller dependent NC codes were developed. The extracted data is also useful as reference data for checking the quality of manufactured parts by comparing with the data measured by coordinate measuring machine (CMM). In this paper, the integration concept is explained with the experiments conducted to produce the prismatic parts using the generated codes.

Keywords: CAD/CAM, STEP, CMM, Feature Extraction

INTRODUCTION

The manufacturers are trying to produce products with high quality within compete price.

ARTICLE INFO

Article history:

Received: 16 February 2018

Accepted: 12 September 2018

Published: 24 January 2019

E-mail addresses:

sivakumar71078@gmail.com (Sattanathan Sivakumar)

vdmech@tce.edu (Venkadasamy Dhanalakshmi)

rvishnuv@hindustanuniv.ac.in (Ravichandran Vishnuvardhan)

* Corresponding author

In addition, the changes of customer needs should also to be satisfied. To achieve this, computer aided systems are used to support the entire manufacturing process easier and flexible (Abouel Nasr & Kamarani, 2006, p. 390). Further the computer aided systems like CAD, CAM and CAI should work

together to fulfill the industrial needs (Babic et al., 2008). Each computer aided system requires the product data which may be commonly kept as information model. Hence, the product data extraction plays an important role to develop an information model for the integrated manufacturing environment (Berbinschi et al., 2014).

The CAD model contains product description data which can be used for various downstream applications such as process planning, NC code generation, assembly planning, inspection and so on (Besant, 1986; Bitla, 2017). An automatic interpretation is required to extract the data from CAD model based on features (Chang et al., 2002) Feature has different meaning at different contexts and its classifications are based on various factors (Gao et al., 2004; Ismail & Tan, 2002).

Many researchers proposed various approaches for automatic feature extraction process. These feature extraction processes are based on the internal representation of a particular CAD system and which cannot be applicable for other CAD systems (Li et al., 2010; Mamadou & Christian, 2011; Marri et al., 2017). To overcome this drawback some of the researchers convert the CAD model into standard neutral file format and extract the data from the same neutral file (Omid & Mahmoud, 2010; Sivakumar & Dhanalakshmi, 2013). This technique has the advantages of generalization and easy extraction of features since the neutral files such as STEP contains coordinate data in the form of text file. Based on the literature, it is observed that few complex systems have been developed for specific applications to address the issue of extracting the data from a CAD model (Sivakumar & Dhanalakshmi, 2013; Thivakar et al., 2016). The present work aims to eliminate the above and proposes a general and simplified approach for the feature extraction process.

In this paper, a generalized methodology is proposed to extract the product data from STEP file of a CAD model and to transfer the information to various downstream applications.

Integrated Manufacturing System

In this work, the main objective is to develop a feature extraction system to integrate the three stages of product lifecycle namely computer aided design (CAD), computer aided manufacturing (CAM) and computer aided inspection (CAI). The feature extraction method should be generalized and simplified method that is compatible with any standard CAD softwares which makes the integrated system to be as simple as possible (Wang et al., 2012). The methodology shown in figure 1 explains overall view of an integrated system which includes the generation of CAD model, Extraction of data from STEP file, Manufacturing of parts using NC code generated from the extracted data and Inspection of parts using machine vision.

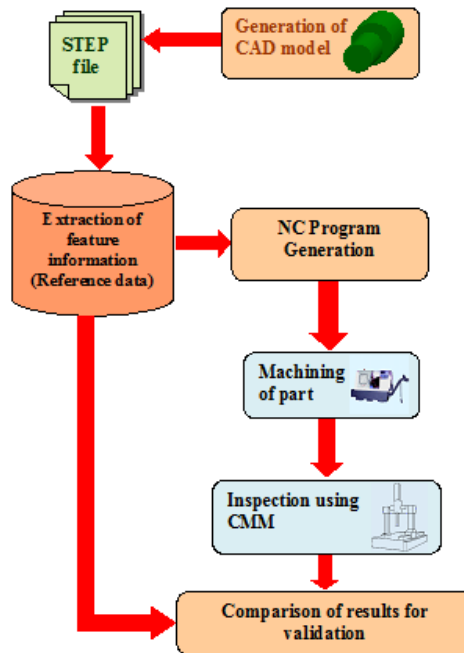


Figure 1. Proposed Methodology for integrated System

Generation of CAD model

In this work, a prismatic part is chosen as a part model. The part model is created using CAD software and it is shown in Figure 2. This part model contains three features namely slot, step and hole. The part model is converted into STEP AP203 file.

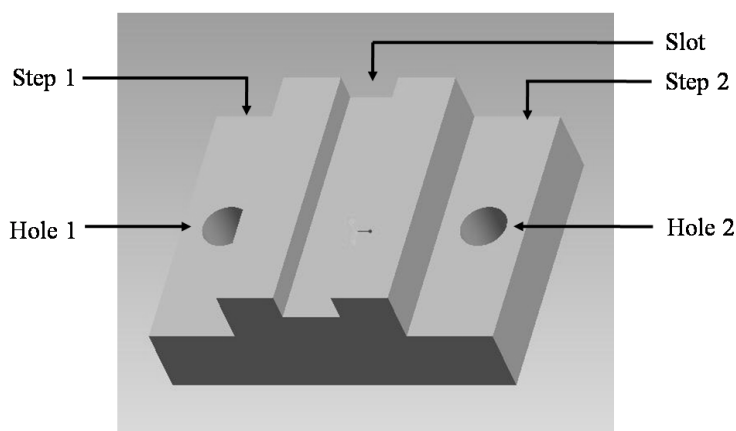


Figure 2. Part model of the sample prismatic part

Identification of Features from STEP-File

The part model is based on geometric entities such as line, circle, arc and so on. However, the information required for other computer aided systems is based on manufacturing features such as groove, chamfer and so on. Hence, it is required to convert the part information from design features to manufacturing features which is one of the major challenges in the integration process. This requires a feature extraction system for identification of features.

A feature contains the information about geometry and properties of product which includes the geometrical data and properties. In this paper, some of the subtractive features are considered and the detailed method of identification of the features is given in Table 1.

Table 1
Identification of subtractive features from STEP file

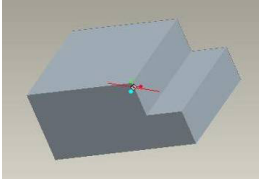
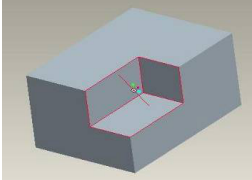
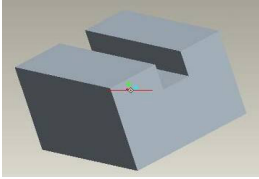
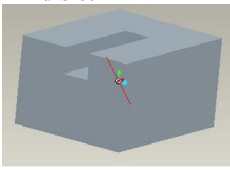
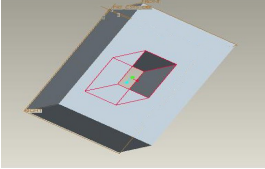
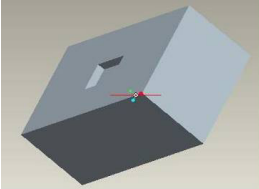
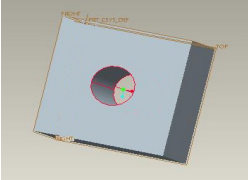
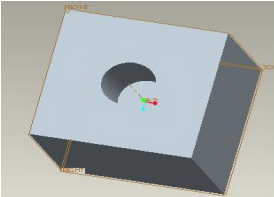
Type of feature	STEP format	Identification of feature
Step 	<pre>#1=DIRECTION("(0.E0,1.E0,0.E0)); #5=DIRECTION("(-1.E0,0.E0,0.E0)); #9=DIRECTION("(0.E0,1.E0,0.E0)); #13=DIRECTION("(-1.E0,0.E0,0.E0));</pre>	If the STEP data contains the directional sequence 'y, -x, y, -x' then the feature is identified as step. In addition, the length of the step is equal to the base cube length then the feature is called step.
Blind Step 	<pre>#1=DIRECTION("(0.E0,1.E0,0.E0)); #5=DIRECTION("(-1.E0,0.E0,0.E0)); #9=DIRECTION("(0.E0,1.E0,0.E0)); #13=DIRECTION("(-1.E0,0.E0,0.E0));</pre>	If the STEP data contains the directional sequence 'y, -x, y, -x' then the feature is identified as step. In addition, the length of the step is less than the base cube length then the feature is called blind step.
Slot 	<pre>#5=DIRECTION("(-1.E0,0.E0,0.E0)); #9=DIRECTION("(0.E0,-1.E0,0.E0)); #13=DIRECTION("(-1.E0,0.E0,0.E0)); #17=DIRECTION("(0.E0,1.E0,0.E0)); #21=DIRECTION("(-1.E0,0.E0,0.E0));</pre>	If the STEP data contains the directional sequence '-x, -y, -x, y, -x' then the feature is identified as slot. In addition, the length of the slot is equal to the base cube length then the feature is called slot.
Blind Slot 	<pre>#5=DIRECTION("(-1.E0,0.E0,0.E0)); #9=DIRECTION("(0.E0,-1.E0,0.E0)); #13=DIRECTION("(-1.E0,0.E0,0.E0)); #17=DIRECTION("(0.E0,1.E0,0.E0)); #21=DIRECTION("(-1.E0,0.E0,0.E0));</pre>	If the STEP data contains the directional sequence '-x, -y, -x, y, -x' then the feature is identified as slot. In addition, the length of the slot is less than the base cube length then the feature is called blind slot.

Table 1 (Continue)

Type of feature	STEP format	Identification of feature
Pocket 	<pre>#21=DIRECTION(",(0.E0,0.E0,1.E0)); #25=DIRECTION(",-1.E0,0.E0,0.E0)); #29=DIRECTION(",(0.E0,0.E0,-1.E0)); #33=DIRECTION(",(1.E0,0.E0,0.E0));</pre>	<p>If the STEP data contains the directional sequence 'z, -x, -z, x' then the feature is identified as pocket. In addition, the pocket height is equal to the base cube height then the feature is called pocket.</p>
Blind Pocket 	<pre>#21=DIRECTION(",(0.E0,0.E0,1.E0)); #25=DIRECTION(",-1.E0,0.E0,0.E0)); #29=DIRECTION(",(0.E0,0.E0,-1.E0)); #33=DIRECTION(",(1.E0,0.E0,0.E0));</pre>	<p>If the STEP data contains the directional sequence 'z, -x, -z, x' then the feature is identified as pocket. In addition, the pocket height is less than the base cube height then the feature is called blind pocket.</p>
Hole 	<pre>#136=FACE_BOUND("#135,.F.); #135=EDGE_LOOP(",(#132,#134)); #132=ORIENTED_EDGE("*,*,#131,.F.); #131=EDGE_CURVE("#95,#96,#25,.T.); #25=CIRCLE("#24,1.E2);</pre>	<p>If the STEP data contains FACE_BOUND with CIRCLE then the feature is identified as hole. In addition, the hole height is equal to the base cube height then the feature is called hole.</p>
Blind Hole 	<pre>#164=FACE_BOUND("#163,.F.); #163=EDGE_LOOP(",(#160,#162)); #160=ORIENTED_EDGE("*,*,#159,.T.); #159=EDGE_CURVE("#99,#100,#33,.T.); #33=CIRCLE("#32,1.E2);</pre>	<p>If the STEP data contains FACE_BOUND with CIRCLE then the feature is identified as hole. In addition, the hole height is less than the base cube height then the feature is called blind hole.</p>

Extraction of Data from STEP File

The geometrical information of the part features and their positions are extracted from the STEP file using feature extraction process. The feature data are extracted by a generalized program developed in C++ language. The extracted data are stored in a text file for further use. Algorithms are developed based on the identification procedure mentioned in Table 1 and the flowchart for extraction of subtractive features of prismatic part is shown in Figure 3. These extracted data can be used for all downstream activities.

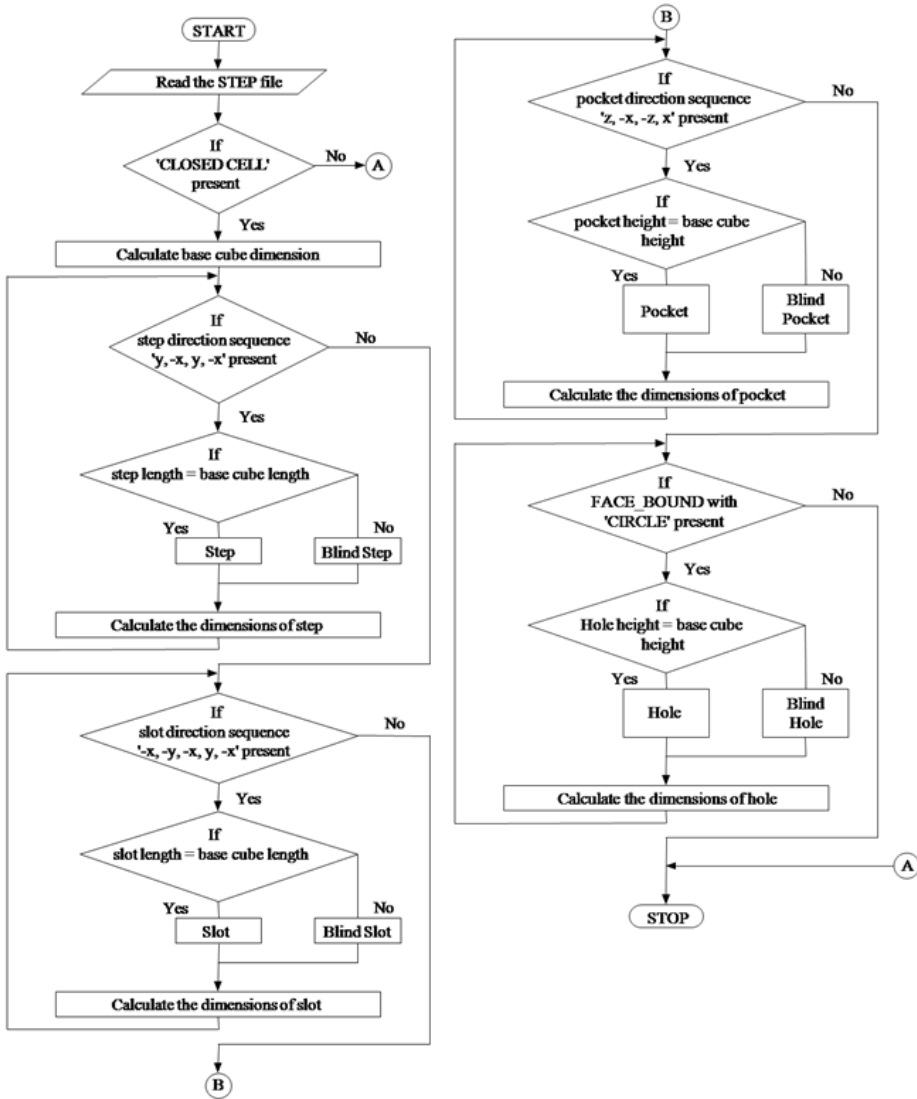


Figure 3. Flow chart for feature extraction of prismatic subtractive features

The extracted data from STEP file is shown in Table 2. In this work, the features are considered from the left end of the part, since machining is carried out from the left end of the part.

Table 2

Extracted data from STEP file of the sample part

Step1			Step2			Slot			Hole 1	Hole 2
Length (mm)	Width (mm)	Height (mm)	Length (mm)	Width (mm)	Height (mm)	Length (mm)	Width (mm)	Height (mm)	Diameter (mm)	Diameter (mm)
45	15	10	45	15	10	45	10	5	5	5

Machining of Parts in CNC Machine

The above extracted data can be used for other manufacturing activities. For example, in the computer aided manufacturing systems, the above feature data can be directly used to machine the parts. Here, a software program is developed to generate the NC code from the extracted feature data. For the machining process, some additional information is required. These additional information are given as input to the program which includes raw material, raw material size and machining parameters like depth of cut, speed and feed. The dimensional information of features is taken from the feature data text file. The NC codes were generated to machine the features individually from left end of the prismatic part. Figure 4 shows the flowchart for the procedure of NC codes generation.

The generated NC codes are to be feed into the CNC machines to produce the parts. In this work, ISEL CNC vertical milling machine is taken for machining process. The milling machine has three linear and one rotary axes movement that can be automatically controlled. For checking the consistency of the overall system, three similar parts are machined using the same NC codes. The machined part is shown in Figure 5.

Validation using CMM

Normally the parts produced in CNC machines are accurate and having good surface finish. To validate the accuracy of machining process, the machined parts are to be inspected using standard metrological equipment. In this work, the machined parts are inspected using coordinate measuring machine. The measurement results are tabulated in Table 3.

In addition, the quality related decisions may be taken according to the constraints based on the tolerance requirements of the parts. To do this, a system is developed to compare the CMM measured data and the extracted feature data (reference data). The flow diagram of the quality control system to accept or reject the part is shown in Figure 6.

RESULTS AND DISCUSSION

In this work, samples of three similar prismatic parts were machined using the generated NC program. All the dimensions of the parts were measured using CMM. The measurement data obtained from the CMM was having appreciable deviations from the reference data

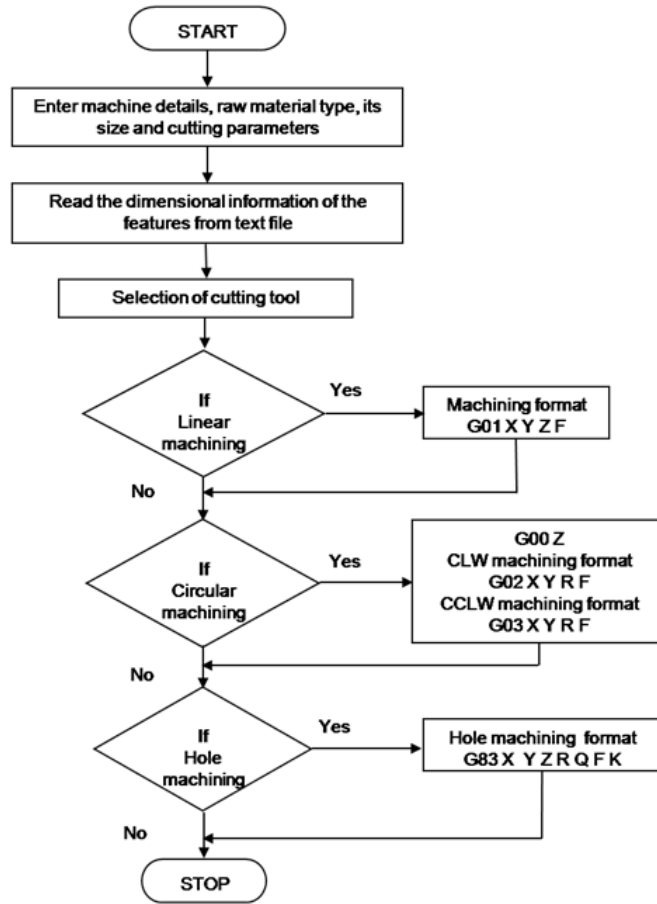


Figure 4. Flowchart for NC codes generation

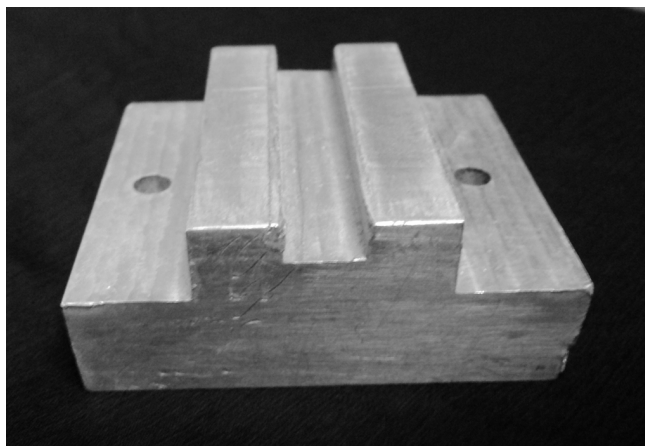


Figure 5. Image of the machined prismatic part

Table 3
Measurement details of prismatic parts using CMM

S. No.	Feature	Parameter	Measurements obtained from CMM (mm)			Percentage of deviation (CMM with Reference Data)		
			Part 1	Part 2	Part 3	Part 1	Part 2	Part 3
1.	Step 1	Length	44.93	44.86	44.89	0.156	0.311	0.244
		Width	14.87	15.12	15.08	0.867	-0.800	-0.533
		Height	9.86	9.94	9.89	1.400	0.600	1.100
2.	Step 2	Length	44.88	44.87	45.05	0.267	0.289	-0.111
		Width	15.16	15.08	15.12	-1.067	-0.533	-0.800
		Height	9.88	10.05	9.93	1.200	-0.500	0.700
3.	Slot	Length	44.84	45.01	45.08	0.356	-0.022	-0.178
		Width	10.12	10.05	10.18	-1.200	-0.500	-1.800
		Height	4.90	4.94	4.96	2.000	1.200	0.800
4.	Hole 1	Diameter	5.06	5.10	5.13	-1.200	-2.000	-2.600
5.	Hole 2	Diameter	4.91	4.94	4.96	1.800	1.200	0.800

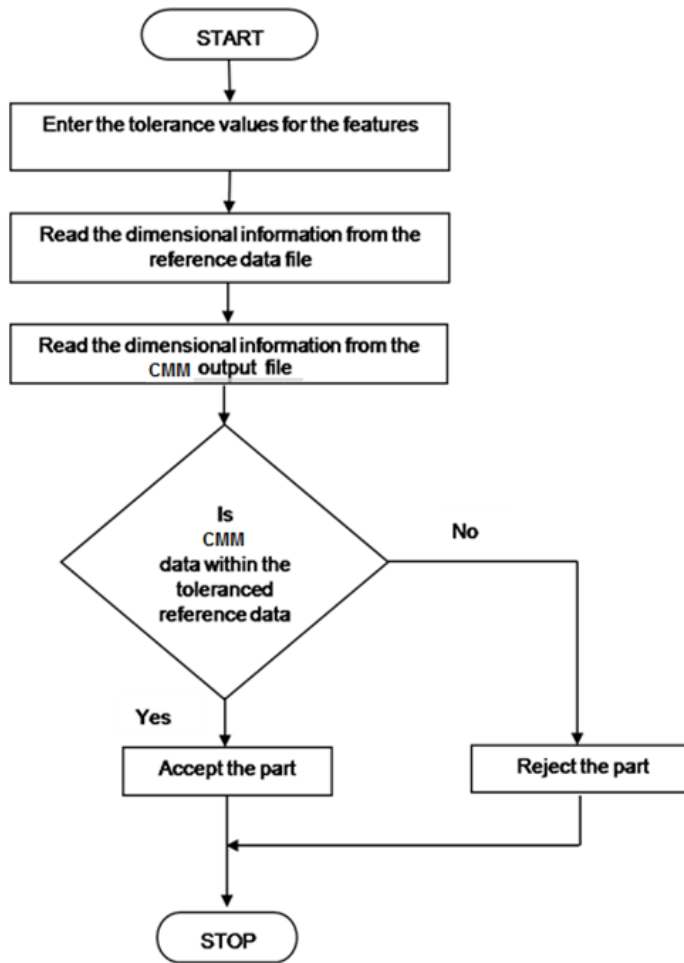


Figure 6. Flow diagram of the quality control system

extracted from the STEP file. Figures 7 shows the comparison of the CMM measurement with Reference data for various features.

The percentage of deviations are calculated and mentioned in the Table 3.

The calculation for the percentage of deviation is as follows:

Consider the diameter of hole 1 for part 3

Measurement obtained from CMM : 5.13 mm

Reference Data from STEP file : 5.00 mm

$$\text{Percentage of deviation} = \frac{(\text{Actual value} - \text{Observed value}) \times 100}{\text{Actual value}}$$

Since reference data is the standard required value, the reference data is taken as actual value and measurement obtained from CMM is taken as observed value.

$$\begin{aligned} \text{Percentage of deviation} &= \frac{(5.00 - 5.13) \times 100}{5.00} \\ &= -2.600\% \end{aligned}$$

Similarly, the percentage of deviation for all the dimensions is calculated and is given in Table 3.

From the Table 3, it is observed that the percentage of deviation falls between -2.600% to +2.000%. The maximum deviation occurs, while measuring smaller dimensions. In this work, while measuring the diameter of hole, the maximum deviations occur.

The data from the table clearly shows that the CMM measurement has a minimum error of -0.022% and maximum error of -2.600% from the reference data. The deviation occurs in both positive and negative direction. This deviation may be due to errors in the machining process and can be reduced by proper selection of machine tool and cutting conditions.

In this work, the CAD is integrated with the CAM through the generation of NC codes from the product data extracted from the STEP file of the CAD model. In similar way, CMM measured data is compared with product data extracted from STEP file of CAD model for taking quality related decisions. Thus, this work may provide a generalized and simplified method for the integration of CAD, CAM and CAI.

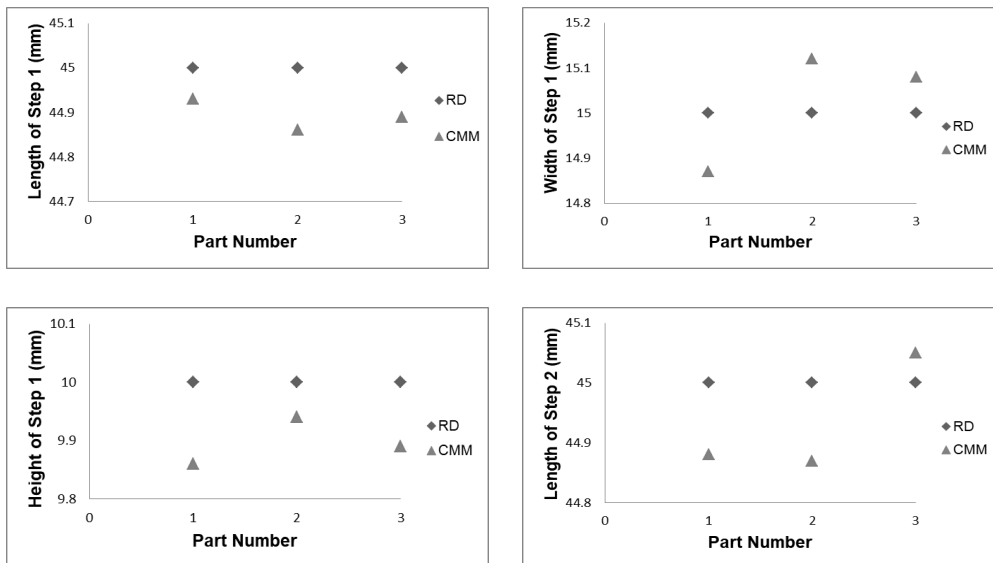


Figure 7. Comparison of measurement of different parameters of sample parts

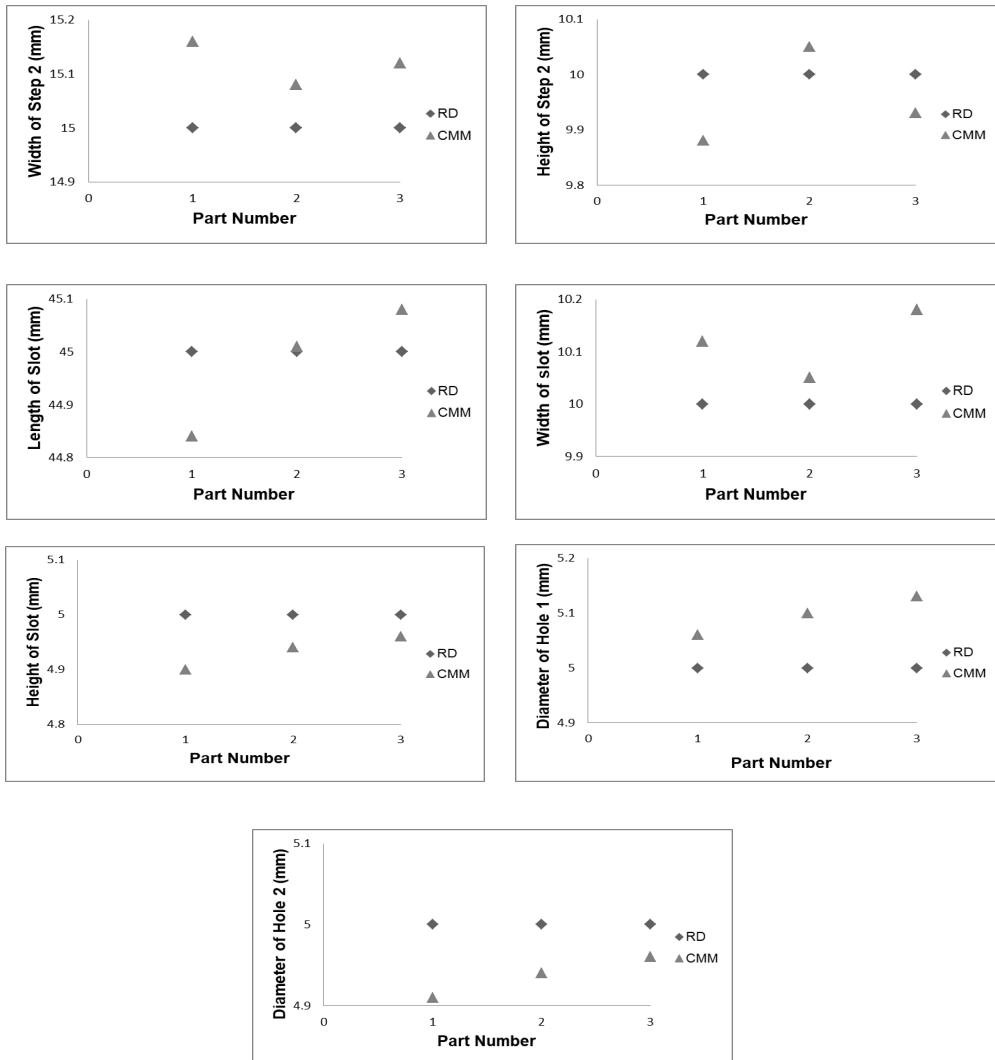


Figure 7. Continue

CONCLUSION

This work mainly concentrates on the integration of CAD and CAM systems, based on the extracted machining features from STEP AP203 file. A prototype system was developed in conjunction with a standard CAD and CAM system, to demonstrate the integration of CAD and CAM for prismatic parts. In the developed system, once the subtractive features are recognized from the STEP file of the CAD model, created using standard modeling package, the NC program can be automatically generated which minimize the necessity of user interventions. In this work, only simple features are considered and the generated codes were controller dependent unlike STEP NC. This work may be considered as a

basis for achieving fully integrated manufacturing system. In addition, the work may be extended to integrate the other stages of product lifecycle such as inspection, assembly, packing and so on.

REFERENCES

- Nasr, E. S. A., & Kamrani, A. K. (2006). A new methodology for extracting manufacturing features from CAD system. *Computers and Industrial Engineering*, 51(3), 389-415. doi:10.1016/j.cie.2006.08.004
- Babic, B., Nestic, N., & Miljkovic, Z. (2008). A review of automated feature recognition with rule-based pattern recognition. *Computers in Industry*, 59(4), 321-337. <https://doi.org/10.1016/j.compind.2007.09.001>
- Berbinschi, S., Baroiu, N., Teodor, V., & Oancea, N. (2014). End mill tool profiling by CAD method. *Indian Journal of Engineering and Material Sciences*, 21(3), 296-302.
- Besant, C. B. (1986). *Computer Aided Design and Manufacture*. Chichester: Ellis Horwood Ltd.
- Bitla, V., & Venkateswara, R. K. (2017). STEP-based feature recognition from solid models having non-planar surfaces. *International Journal of Computer Integrated Manufacturing*, 30(10), 1011-1028. <https://doi.org/10.1080/0951192X.2016.1268719>
- Chang, H. C., Lu, W. F., & Liu, F. X. (2002). Machining process planning of prismatic parts using case based reasoning and past process knowledge. *Applied Artificial Intelligence*, 16(4), 303-331. <https://doi.org/10.1080/08839510252906471>
- Gao, J., Zheng, D. T., & Gindy, N. (2004). Extraction of machining features for CAD/CAM integration. *International Journal of Advanced Manufacturing Technology*, 24(7-8), 573-581. doi: 10.1007/s00170-003-1882-9
- Ismail, N., & Tan, C. F. (2002). Ruled-based feature extraction and recognition from STEP file. In *Proceedings of student conference on research and development* (pp. 90-93). Shah Alam, Malaysia.
- Li, P., Gao, T., Wang, J., & Liu, H. (2010). Open architecture of CNC system research based on CAD graph-driven technology. *Robotics and Computer-Integrated Manufacturing*, 26(6), 720-724. <https://doi.org/10.1016/j.rcim.2010.04.004>
- Mamadou, S., & Christian, M. (2011). Product design analysis based on life cycle features. *Journal of Engineering Design*, 22(6), 387-406. <https://doi.org/10.1080/09544820903409899>
- Marri, H. B., Gunasekaran, A., Gopang, M. A., Nebhwani, M., & Soomro, A. S. (2017). Assessment of CIM implementation in SMEs: A multiple case study approach. *International Journal of Advanced Manufacturing Technology*, 90(5-8), 2193–2206. doi: 10.1007/s00170-016-9543-y
- Omid, F. V., & Mahmoud, H. (2010). INFELT STEP: an integrated and interoperable platform for collaborative CAD/CAPP/CAM/CNC machining systems based on STEP standard. *International Journal of Computer Integrated Manufacturing*, 23(12), 1095–1117. <https://doi.org/10.1080/0951192X.2010.527373>
- Sivakumar, S., & Dhanalakshmi, V. (2013). An approach towards the integration of CAD/CAM/CAI through STEP file using feature extraction for cylindrical parts. *International Journal of Computer Integrated Manufacturing*, 26(6), 561-570. <https://doi.org/10.1080/0951192X.2012.749527>

- Thivakar, M., Marcin, H., Alexander, M., & Peter, K. (2016). Knowledge integration in CAD-CAM process chain. *Computer-Aided Design and Applications*, 13(5), 729-736. <https://doi.org/10.1080/16864360.2016.1150720>
- Wang, K., Liu, R., Xu, X., Zhang, C., & Yang, L. (2012). A STEP-compliant computer numerical control based on real-time Ethernet for circuit board milling. *International Journal of Computer Integrated Manufacturing*, 25(12), 1151-1164. <https://doi.org/10.1080/0951192X.2012.684720>.

Review Article

A Review of the Thermal Effects During Pregnancy by Using Ultrasound: Doppler Mode

Umi Nadrah Amran¹, Farah Wahida Ahmad Zaiki^{1*} and Sulaiman Md Dom²

¹*Department of Diagnostic Imaging and Radiotherapy,
Kulliyah of Allied Health Sciences (KAHS), International Islamic University Malaysia (IIUM),
Bandar Indera Mahkota, 25200, Kuantan, Pahang, Malaysia*

²*Faculty of Health Sciences, Universiti Teknologi MARA, 42300, Bandar Puncak Alam,
Selangor, Malaysia*

ABSTRACT

Doppler ultrasound is used in obstetrics and gynecology fields to serve as the complement mode in the standard prenatal scan. It aids in investigating fetus blood flow in expectant mothers' wombs, usually those who come with pregnancy complications. In the conventional ultrasound beam, the heat produced by attenuation is distributed over the area. However, the Doppler ultrasound beam is focused at only one point. This leads the heat to accumulate at that particular area and hence there is an increase in the temperature. Heat is considered as a teratogen in pregnancy, whereby an increase in the fetal temperature can be fatal to the fetus. Studies have found that Doppler mode is associated with higher acoustic output as compared to the conventional two-dimensional (2D) ultrasound mode. Several studies done on animals have ruled out the evidence of Doppler ultrasound bioeffects. This narrative review only discusses the thermally induced effect of ultrasound by using Doppler mode. This study reviews prior studies with keywords such as Doppler ultrasound, bioeffects, heating effects, rabbit, and pregnancy. Earlier studies noted that the risk of thermal effects increased with the increase of exposure time. However, Doppler ultrasound wave inducing

fetal hyperthermia is not the main reason for causing adverse neonatal outcomes without taking into account other external factors. Therefore, it is essential for the practitioners to adopt and adapt the concept of 'as low as reasonably achievable' (ALARA) to avoid any subtle adverse effects.

ARTICLE INFO

Article history:

Received: 20 January 2018

Accepted: 12 September 2018

Published: 24 January 2019

E-mail addresses:

uminadrahamran@gmail.com (Umi Nadrah Amran)

farahzaiki@iium.edu.my (Farah Wahida Ahmad Zaiki)

sulaimanmd@salam.uitm.edu.my (Sulaiman Md Dom)

* Corresponding author

Keywords: Bioeffects, doppler, heating, newborns, *Oryctolagus Cuniculus*, prenatal, rabbits, thermal effects, ultrasound

INTRODUCTION

Doppler ultrasound is fast becoming a key instrument in the medical field, especially for prenatal care around the globe and has been used ever since it was introduced. It is known that Doppler ultrasound was used for years in the study of fetus blood flows. It has been used in combination with brightness mode (B-mode) ultrasound during pregnancy check-up, which is usually done to monitor the fetus heart rate and blood flows. Today, together with the advancement in technology, Doppler ultrasound is practiced in most obstetrics and gynecology fields, in which the data are color-coded onto the B-mode images. Despite its usefulness in detecting and monitoring fetus blood circulation in the womb, the usage of Doppler ultrasound itself has a higher thermal index as compared to B-mode ultrasound. It was reported that the use of Doppler imaging may increase the temperature of tissues, thus, when Doppler is used in combination with B-mode ultrasound, the risks of bioeffects tend to be higher. Therefore, the experts have come up with a question whether Doppler ultrasound is safe for pregnant women if used without any diagnostic purposes. The purpose of this paper is to write a review regarding several numbers of studies that revised and discussed the impact of Doppler ultrasound exposure on rabbits. It is expected that this study can give a clear depiction to the public about the potential risk of using Doppler ultrasound without any diagnostic purposes. It is also expected that this review can facilitate the establishment of guidelines on the using of Doppler ultrasound in the future.

The General Theory of Ultrasound and Doppler Mode

Ultrasound is theoretically one of the imaging modalities that uses sound waves propagating through body tissues and produce returning echoes to synthesize gray-scale images (Shung, 2006). Notable advantages of ultrasound are the ability to produce real-time images as well as no association with ionizing radiation exposure (U.S Food and Drug Administration, 2017).

Sound waves are transmitted through a transducer surface into the body tissues where they are attenuated depending on its acoustic impedance, then returning echoes are produced which are also being detected by the transducer. The piezoelectric material is a fundamental component of the transducer which functions by converting electrical energy to mechanical (sound) energy and also to convert the mechanical energy into electrical energy. While resolution and attenuation are directly proportional to the wavelength and frequency of the ultrasound beam, the depth of the beam penetration is inversely proportional. Higher frequency produces better resolution but gives superficial penetration. Conversely, lower

frequency associates with lower resolution but gives deeper beam penetration (Bushberg, Seibert, Leidholdt, & Boone, 2002).

In addition to conventional ultrasound, Doppler mode is occasionally being used during practices. It makes use of the Doppler effect which sometimes is also known as the Doppler shift. Doppler effect is defined as the alteration in frequency of sound wave due to a reflector moving towards or away from an object (Goel, 2015). Doppler ultrasound is used to facilitate monitoring and diagnosing in obstetric fields by taking into account its capability to assess blood movement in both fetal and placental circulation depending on Doppler effect (Mone, McAuliffe, & Ong, 2015).

As a matter of fact, the sound wave that propagates into the body will undergo the process of being scattered, reflected and absorbed into the body as heat (Zaiki & Dom, 2014). Besides its main advantage to provide real time images using non-ionizing radiation, the thermal effect from frequent and higher exposure of Doppler ultrasound may develop some potential risks to be concerned about.

The Thermal Effect of Ultrasound

Ultrasound is replacing the conventional radiography and serves as an essential service offered by most health institutions. While ultrasound provides diagnostic images without ionizing radiation (Ball & Price, 1995), the possibility of adverse effects by using ultrasound cannot be foreseen (Kremkau, 1994). Recently, the matter has been addressed by researchers in many fields.

The mechanism of ultrasound conversion into heat cannot be denied and today has become a part of a primary concern. Theoretically, as the ultrasound waves propagate through tissues, they attenuate and cause the temperature to rise (Kremkau, 1994) as well as cavitation to happen (Abramowicz, 2017). Both effects are termed as bioeffects of ultrasound, where they have been debated by researchers over the years. The American Institute of Ultrasound in Medicine (AIUM) has summarized the above matter in the consensus report on potential bioeffects of diagnostic ultrasound in 2008 (Fowlkes, 2008). The thermal effect occurs when the heat produced by-intense ultrasound exposure gives an undesirable effect on where the ultrasound waves travel to (Bushong, 1993).

In addition, Miller stated that biological effects can only occur if it reaches its threshold and the severity increases with increasing exposure to specific circumstances (Miller, 2008). The risk increases as the technology of ultrasound advanced through the decades. In the same vein, it has been reported that potential cavitation can happen when Doppler is used together with three-dimensional (3D) ultrasound (Pooh et al., 2016). A large and growing body of literature has emphasized that Doppler's acoustic outputs are relatively sufficient to result in apparent biological effects when maximum operating settings are used (Barnett & Maulik, 2001).

This matter leads to numerous studies that attempted to investigate the biological effects of ultrasound. Several studies were conducted to measure the thermal effects of ultrasound (Helmy, Bader, Koch, Tiringner, & Kollmann, 2015; Liang, Zhou, Wells, & Halliwell, 2009). Helmy et al. (2015) expressed their concern on the physical mechanism of Doppler ultrasound, which could harm pregnant women in the early gestational period (Helmy et al., 2015). Through an *in-vitro* study conducted, they found that the temperature of a water bath model significantly increased after being exposed to Doppler ultrasound within one minute. Thus, they concluded that the risk of thermally induced effects by using Doppler ultrasound in early pregnancy period cannot be left out.

Heat As Teratogen for Pregnancy

The fetus also generates heat through metabolism process in the womb but unlike its mother, it cannot dissipate the heat by its own. The fetus is said to have no control over its body thermoregulation. Heat or hyperthermia is known to give effects on pregnant woman. It is proven that elevation of maternal body temperature could give an adverse effect on both the mother and the fetus. In a hyperthermia analysis, a study in 2003 demonstrated that hyperthermia during pregnancy can lead to irreversible damage to the fetus, such as abortion, retardation of growth, developmental defects, and worst of all an embryonic death (Edwards, Saunders, & Shiota, 2003).

In accordance with the previous result, the present study also demonstrated that hyperthermia had affected both maternal and fetal outcomes. A study by Strand, Barnett, and Tong (2011) reviewed that most literature claimed that preterm birth, stillbirth, and low birth weight showed the highest numbers in both extreme seasons; summer and winter. From the literature reviewed by them, some of the authors have speculated that extreme seasons may be a risk factor for poor birth outcomes (Strand et al., 2011). The studies presented thus by far provided evidence in showing that ambient temperature during prenatal exposure taken in place can give an impact on birth consequences.

With respect to hyperthermia, the Intergovernmental Panel on Climate Change (IPCC), in 2007 presented an amount of evidence on how global warming and climate change can give impacts on humans (Rylander, Odland, & Sandanger, 2013). Pregnant women, unborn descendants, and youngsters are considered as high-risk groups in which climate change, especially direct heat exposure, gives severe effect on maternal health as well as the children. Moreover, it is very difficult to get away from complications during pregnancies. Pregnancies are associated with various complications, which may include spontaneous abortion, low birth weight, premature contractions, and neonatal mortality (Goldenberg, Culhane, Iams, & Romero, 2008; Randolph-habecker et al., 2017). Those complications can happen at any stage throughout the gestational periods (Liu et al., 2012).

A systematic review was done by Kuehn and McCormick (2017) on climate change in maternal health demonstrated that extreme heat exposure may affect fetal outcomes (Kuehn & McCormick, 2017). They also stated in their discussion that both extreme and moderate temperature exposures may result in an acute and adverse delayed birth consequences, respectively. Similarly, in 2011, years before the systematic review was done, Sheffield and Landrigan concluded that heat-related health effects include diminished school performance, increased rates of pregnancy complications, and renal effects (Sheffield & Landrigan, 2011). However, the severity of the consequences may vary by the geographical region and socioeconomic status, which later increase health inequalities.

There are several pieces of evidence telling that maternal pyrexia acts as the major determinant of fetal hyperthermia and is associated with the incidence of adverse neonatal outcomes (Trays & Banerjee, 2014). However, they made an argument that the neuronal injury can also be caused by many other factors rather than making hyperthermia as the only causal of event.

Doppler Ultrasound in Pregnancy

Ultrasound is long known as the safest imaging modality as it involves no ionizing radiation and is frequently used in prenatal care for decades. In clinical practices, especially in obstetrics, ultrasound has been crucially used in diagnosing, monitoring, and assessing the fetal progress in the womb and in some cases, ultrasound helps perform the therapeutic intervention in treating fetal anomalies (Schellpfeffer, 2013).

After the invention of ultrasound in the late 1950s, it continued to develop throughout the decades and was commonly applied in screening for pregnant women (Chau, 2002). Today, Doppler ultrasound is commercially applied by private companies and healthcare institutes in prenatal care. Even though traditional ultrasound can give enough information about the fetus well-being in the womb, the advancement of Doppler ultrasound technology, by making use of Doppler effect physics as the result of the motion of blood or direction of the blood flow (Kremkau, 1994), helps practitioners to identify any blood circulation abnormalities of the fetus in a better view.

Currently being practiced, only an expectant mother with high potential complication gets the privilege of using Doppler ultrasound to check on her fetus. As reported, the percentage of stillborn rate could be reduced if Doppler ultrasound is called as a standard practice, instead of the traditional prenatal ultrasound (Hill, 2016). Years before the trend set, the USA today reported that the American Institute of Ultrasound in Medicine (AIUM) notified parents about the possible harms of having an unregulated ultrasound for entertainment purposes (Anonymous, 2004).

Unregulated ultrasound takes a longer time and uses more energy even though there is no confirmed biological effect from the prenatal ultrasound scan was done. The Food

and Drug Administration (FDA) made a statement that concerns the unknown long term effects of tissue heating by frequent visits and prolonged examination time (Diana, 2015). Therefore, the experts stated that ultrasound by using Doppler should only be done on expectant mothers when there is a medical purpose to perform it. However, if it is performed on expectant mothers without any diagnostic purposes, it brings-the question whether it is safe for the fetus or not.

Doppler Ultrasound Bioeffects on Human

Doppler ultrasound is one of the most widely used ultrasound imaging modes and is extensively used for high-risk pregnancies to reduce stillbirths. Although some researches were carried out on its biological effects in humans, scientific understanding is very little. A review conducted by Alfirevic, Stampalija, and Dowswell (2017), showed the possible effects of Doppler ultrasound used in high-risk pregnancies to assess the fetal well-being (Alfirevic et al., 2017). They agreed to the use of Doppler in the obstetric field to reduce the number of fetal death but the fact of Doppler usage resulting in fewer obstetric interventions are yet to be certain.

Previous studies have indicated that routine Doppler ultrasound examination; which was conducted for unselected or low-risk pregnancies cases; gave no benefits to the mother and child. An investigation by Bricker and Neilson (2000) showed that routine Doppler ultrasound resulted neither in increased obstetrics and gynecology interventions nor detectable in both short and long term consequences, such as perinatal mortality and defect neurodevelopment, respectively (Bricker & Neilson, 2000).

Forward et al. (2014) analyzed the data of 20 years follow-up of the randomized controlled trial on multiple prenatal ultrasound scans and ocular development (Forward et al., 2014). The study aimed to determine the effect of frequent exposure to several ultrasound modes of ultrasound on ocular development by using previous 20 years cohort study data. They found that frequent exposures to the ultrasound had no significant influence on the ocular development, regardless B-mode or spectral Doppler used. On the other hand, Sheiner et al., (2007) found distinct differences between Doppler and B-mode ultrasound. In her study, she identified that TI reading for Pulsed wave Doppler mode is at the highest followed by color flow Doppler and B-mode. Table 1 below shows the acoustic output during the ultrasound studies adapted from Sheiner et al., (2007).

Then, recent evidence suggested that the use of Doppler ultrasound has given no impact to the fetal outcome. Alfirevic, Stampalija, and Medley (2015) found that there were no group differences seen for the analysis primary outcomes of prenatal death and neonatal morbidity (Alfirevic et al., 2015). Even though there was evidence found for group differences in prenatal death between a single Doppler assessment versus no Doppler, such exposition was unsatisfactory because the outcomes were only based on a single trial.

Table 1

Acoustic Output during the Ultrasound Studies

Mode of ultrasound	Mechanical index (MI)		Thermal index (TI)	
	Mean \pm SD	Range	Mean \pm SD	Range
Pulsed-wave (n = 118)	0.9 \pm 0.2	0.2 – 1.2	1.5 \pm 0.5	0.9 – 2.8
Color Doppler (n = 31)	1.0 \pm 0.1	0.8 – 1.2	0.8 \pm 0.1	0.6 – 1.2
B-mode (n = 190)	1.1 \pm 0.1	0.2 – 1.3	0.3 \pm 0.1	0.1 – 0.7

*Standard deviation (SD)

Note. Adapted from Sheiner et al. (2007)

Therefore, in general, it seems that researchers concluded that the use of Doppler Ultrasound did not give any benefits to both the mother and fetus as the evidence found was not conclusive enough. Even though the bioeffects of Doppler ultrasound were not conclusive enough on humans, some significant can be seen in animal studies.

Animal Studies Conducted on Assessing Doppler Bioeffects

The present studies make several noteworthy contributions towards further investigation on Doppler bioeffects by using an animal model. For a long exposure duration, which is longer than 5 minutes or exceeds 4°C, the threshold temperature elevation for hyperthermia-induced teratogenic effects in trial mammals was estimated to be approximately 1.5°C above core standards (Miller, Nyborg, & Dewey, 2002). However, the finding is yet to be tested on humans, thus the generalizability of the research on this issue seems to be problematic.

So far, the studies of Doppler ultrasound bioeffects being done on humans have shown us a negative conclusion. However, there are significant differences found throughout the animal studies. In 2005, the immediate and long-term effects of color Doppler ultrasound on myocardial cell apoptosis of fetal rate were investigated. Exposures were given in-vivo and the effects were studied for both neonatal and fetal group. They found that there were higher significant differences in the fetal insonification group than in the neonatal insonification group and myocardial apoptosis also showed higher significant differences in the fetal insonification group than I the fetal control group as expected. However, there

were no significant differences found in myocardial apoptosis between the same neonatal insonification group (Jia et al., 2005).

Then, Schneider-Kolsky et al. (2009) had undergone an experiment to assess how ultrasound exposure can affect the learning and memory of chicks (Schneider-Kolsky et al., 2009). B-mode and Doppler ultrasound were exposed to the fetal chicks' brains for several minutes on day 19 of the incubation period. After day 2 post-hatched, they found that significant memory impairment occurred following 4 and 5 minutes of Doppler exposure while no memory impairment was detected for those chicks exposed to B-mode. These findings showed that the prolonged exposure to Doppler ultrasound gave impairment to mammal's cognitive function.

Later in 2011, a study on the effect of pulsed Doppler examination on ductus venosus in rat fetuses had shown positive result where there was a linear correlation between exposure index and apoptotic activities of exposed liver tissues (Pellicer et al., 2011). They found that the longer the pulsed Doppler exposure was given at a time, the higher was the apoptotic index. However, they also found that hours after post-exposure, the cellular damage done was due to the exposure to Doppler disappeared. No significant liver damaged was found despite how long the fetal liver had been exposed.

On the other hand, in spite of much new knowledge about the Doppler effects, several other studies have also been done to investigate the heating effects of prenatal ultrasound without using the Doppler mode. In 2013, a study of fluctuations in hematological analysis and fetal weight were statistically found to be different in the newborn of *Oryctolagus cuniculus* after being exposed to traditional prenatal ultrasound (Ahmad Zaiki, Md Dom, Abdul Razak, & Hassan, 2013; Zaiki & Dom, 2014). In 2016, Zaiki and Dom later also found in their study that the heating effect during prenatal scanning interfered with the fetal neuro-development (Zaiki & Dom, 2016).

DISCUSSION

As some practitioners agreed that the development of ultrasound over the years did give benefits to humans, especially in the obstetrics and gynecology, the drawbacks of having ultrasound unnecessarily still existed. In reviewing the literature, most researchers concluded that there are long term effects that might affect the well-being of fetus, specifically. It is hypothesized that the longer ultrasound exposure time is given, the risks of having adverse effects also increase significantly. Regardless of which mode of ultrasound used, the risk of bioeffects still increases with the increase of the exposure period. It is possible, therefore, that the safety of using Doppler ultrasound without any prior concern during pregnancy may come into question.

Another important finding is that some authors have speculated that the acoustic energy produced by particular ultrasound mode is also one the potential causes of ultrasound

bioeffects. 3D ultrasound is said to be as safe as B-mode because it scans the whole volume without repeatedly being exposed on the fetal point, while four dimensional (4D) ultrasound will have the same effect as both if the exposure to 4D ultrasound is limited within 30 minutes (Pooh et al., 2016). Doppler ultrasound, which is mainly used to evaluate blood flow of the fetus in the womb of the mother can generate acoustic energy higher than other modes. This result may be explained by the fact that Doppler ultrasound uses pulse wave to generate images. Unlike conventional 2D mode ultrasound, the transducer or probe is kept stationary at a specific point. The ultrasound beam is focused on that specific region only, thus, it eventually alters the fetal exposure in terms of dwelling times as the beam is not scanned (Miller, 2008).

We can see that as we compare between modes, the spatial peak temporal average intensity (I_{SPTA}) for B-mode, motion (M) mode and Doppler are significantly increased where temporal averaged intensity can reach maximum $10\text{W}/\text{cm}^2$ (Abramowicz, 2017). The FDA put the exposure limit to $720\text{ m W}/\text{cm}^2$ for all applications, except for eye scanning after the former regulation was revised in 1992. The exposure towards ultrasound energy beyond the threshold limit might not be considered as safe anymore. Besides that, the development of scanners and transducers after 1993 may increase the possibility of tissues being exposed to higher intensities, thus, increases the risk of higher bioeffects occurrences (Deane & Lees, 2000). The practitioners need to observe the exposure of ultrasound so that it does not exceed the threshold limit.

As FDA has highlighted the threshold value of ultrasound exposure, here is where the output display standard (ODS) takes its role. Thermal index (TI) and mechanical index (MI) are two main components displayed on the screen. TI is essential in estimating the maximum tissue temperature rise for a given exposure, while MI is known as an indicator for the non-thermal phenomenon to occur. Even though TI cannot measure the actual temperature in the tissue (Abramowicz, 2017), it is important for the practitioners to follow the guidelines given as higher TI can be associated with a higher temperature rise. Miller mentioned in his paper that a slight elevation of temperature of less than $(1 - 1.5)^\circ\text{C}$ above normal body temperature is not expected to give any harm because the elevation is still within the normal variation of body temperature (Miller, 2008). It must be made clear that TI only represents a ratio of instantaneous power to the theoretical power needed to raise the tissue temperature by 1°C . However, when Doppler is in use, the temperature might increase more than when conventional ultrasound was used.

Potential bioeffects of ultrasound are crucial in pregnancy. As discussed earlier in this part, the acoustic energy is greater when Doppler mode is in used compared to other ultrasound modes. It is agreed that the thermally induced effect is more obvious by using Doppler (Barnett & Maulik, 2001). In pregnancy, the first 12 weeks of gestation period is the most crucial period because the growing fetus is very sensitive to any external

influences. Medications, exposure to X-ray, infectious diseases, and hyperthermia are categorized as teratogenic agents that can harm the fetus (Abramowicz, 2010). The heat produced by ultrasound wave is also considered as a teratogen in pregnancy. Most animal studies done had concluded that heat produced by ultrasound; mainly Doppler ultrasound, gave substantial effects to the growing fetus.

The second and third trimesters of pregnancy also cannot be left out from having potential thermally induced effects from ultrasound waves. Theoretically, in the mechanism of heat absorption, the bone absorbs heat better than tissue. This is because the bone has higher attenuation coefficient as compared to other tissues, thus greater absorption occurs. As noted by Barnett and Maulik (2001), the risk of inducing thermal effects is higher in the last two trimesters; second and third trimesters (Barnett & Maulik, 2001). This is because during these periods, bones are already formed and thus, interception of fetal bone and ultrasound beam can lead to a temperature increase in the fetal brain. This view is supported by Maeda and Kurjak, (2012) who wrote that different tissues absorbed, attenuated, and perfused differently.

Decreased birth weight, neurological impairment as well as decreased cognitive functions and altered cellular proliferation are the examples of the consequences of exposure towards both conventional and Doppler ultrasounds for a given time. Contrary to the expectations, studies did not find a significant difference between Doppler ultrasound and its bioeffects on humans. This matter opens abundant rooms for further progress in determining Doppler ultrasound bioeffects on humans. Although the current study is based on animal studies and has yet to find evidence on humans, the findings can serve as the evidence that there are roughly bioeffects of Doppler ultrasound.

However, the generalizability of these results is subjected to certain limitations. The whole-body temperature of an expectant mother (animal study) can also be elevated, not only because of the acoustic energy heat-generated but also due to other hyperthermia-induced external factors. Generally, developmental impairment in animal models is seen when the maternal core temperature increases above normal of approximately 2 °C for an extended period of time, (2-2.5)°C for 0.5-1 hour or $\geq 4^{\circ}\text{C}$ for 15 minutes (Ziskin & Morrissey, 2011). An increase in the mother's core body temperature can increase the fetal temperature. Apart from that, the inability of a fetus to remove its own heat can also lead to an increased fetal temperature in the womb. Therefore, it is void to conclude that the heat produced by ultrasound is the main reason for fetal hyperthermia without taking into account other external factors. These findings also open a new door for researchers to dig out more unknown risk associates with ultrasound.

CONCLUSION AND RECOMMENDATION

The study of bioeffects of ultrasound is still limited only on animal studies and the significance of the result is yet to be implemented. This is mainly caused by the differences between animals and human features, either physiology or anatomy. For example, even though the mammals such as rabbits, rat, and sometimes monkeys are the nearest animals mimicking humans, there are still existing gaps that need to be filled.

Therefore, in general, it seems that the heat produced by the acoustic energy from Doppler ultrasound wave can induce thermal bioeffects. Thermally induced effects can be fatal for the fetus, especially in the first trimester of pregnancy. Intense Doppler exposure throughout pregnancy period should also be avoided by all means. Since the application of ALARA principle can be found in radiology with respect to reducing radiation risk, this concept can also be directed towards reducing heat effects in ultrasound. AIUM has released their official statement in which the ALARA principle should observe the controls adjustment and transducer dwell periods which could affect the ultrasound acoustic output (American Institute for Ultrasound in Medicine, 2014). Therefore, health practitioners should always practice 'as low as reasonably achievable' (ALARA) concept and minimize the use of Doppler ultrasound in pregnancy while maintaining the diagnostic quality. This view has been also recommended by FDA (U.S Food and Drug Administration, 2017).

This review has thrown up many questions in need of further investigation. As was mentioned in the literature, the lack of evidence on the Doppler bioeffects on humans clearly showed that further research and investigation are needed. This is due to the fact that a significant difference is found in many animal studies. Even though it is known to be challenging to implement the results of animal studies onto humans, the bioeffects of Doppler ultrasound cannot be taken for granted. If the debate of ultrasound safety is to be moved forward, a better understanding of Doppler ultrasound bioeffects needs to be developed.

ACKNOWLEDGEMENT

The authors are grateful to the staff of International Islamic University Malaysia, supervisor, lecturers, peers, and everyone involved in this review paper. This review paper is funded by IIUM Research Initiative Grant (RIGS), no.: RIGS 16-300-0464.

REFERENCES

- Abramowicz, J. S. (2010). Fetal Doppler: How to keep it safe? *Clinical Obstetrics and Gynecology*, 53(4), 842–850. <https://doi.org/10.1097/GRF.0b013e3181fbae34>
- Abramowicz, J. S. (2017). Ultrasound in Assisted Reproductive Technologies and the First Trimester : Is There a Risk ? *Clinical Obstetrics and Gynecology*, 60(1), 121–132. <https://doi.org/10.1097/GRF.0000000000000256>

- Alfirevic, Z., Stampalija, T., & Dowswell, T. (2017). Fetal and umbilical Doppler ultrasound in high-risk pregnancies (review). *Cochrane Database of Systematic Reviews*, (6), 1-163. <https://doi.org/10.1002/14651858.CD007529.pub4>. Copyright
- Alfirevic, Z., Stampalija, T., & Medley, N. (2015). Fetal and umbilical Doppler ultrasound in normal pregnancy. *The Cochrane Database of Systematic Reviews*, 4(4), CD001450. <https://doi.org/10.1002/14651858.CD001450.pub4>
- American Institute for Ultrasound in Medicine. (2014). *As Low As Reasonably Achievable (ALARA) Principle*. Retrieved January 13, 2018, from <http://www.aium.org/officialStatements/39>
- USA Today. (2004, March 27). Parents ignoring FDA warning against prenatal portraits. *USA Today*. Retrieved January 13, 2018, from http://usatoday30.usatoday.com/news/health/2004-03-27-prenatal-portraits_x.htm
- Ball, J., & Price, T. (1995). *Chesney's Radiographic Imaging* (6th Ed.). Massachusetts: Wiley-Blackwell.
- Barnett, S. B., & Maulik, D. (2001). Guidelines and recommendations for safe use of Doppler ultrasound in perinatal applications. *The Journal of Maternal-Fetal Medicine*, 10(March), 75–84. <https://doi.org/10.1080/714904312>
- Bricker, L., & Neilson, J. P. (2000). Routine doppler ultrasound in pregnancy. *Cochrane Database of Systematic Reviews*, (2), CD001450. Retrieved January 13, 2018, from <https://doi.org/10.1002/14651858.CD001450>
- Bushberg, J. T., Seibert, A. J., Leidholdt, E. M., & Boone, J. M. (2002). *The Essential Physics of Medical Imaging*. Philadelphia: Lippincott Williams and Wilkins.
- Bushong, S. (1993). *Radiologic Science for Technologists: Physics, Biology, and Protection* (5th Ed.). St. Louis: Mosby-Year Book.
- Chau, M. T. (2002). Safety of Diagnostic Ultrasound. *Medical Section. Queen Mary Hospital*, 7, 3-4.
- Deane, C., & Lees, C. (2000). Doppler obstetric ultrasound: A graphical display of temporal changes in safety indices. *Ultrasound in Obstetrics and Gynecology*, 15(5), 418–423. <https://doi.org/10.1046/j.1469-0705.2000.00111.x>
- Diana, E. (2015). FDA warns against “ keepsake “ ultrasounds. *CBS News*. Retrieved January 13, 2018, from <http://www.cbsnews.com/news/3?d?ultrasounds?cause?concern?for?obgyn?doctors?and?fda/>
- Edwards, M. J., Saunders, R. D., & Shiota, K. (2003). Effects of heat on embryos and fetuses. *International Journal of Hyperthermia : The Official Journal of European Society for Hyperthermic Oncology, North American Hyperthermia Group*, 19(3), 295–324. <https://doi.org/10.1080/0265673021000039628>
- Forward, H., Yazar, S., Hewitt, A. W., Khan, J., Mountain, J. A., Pesudovs, K., ... & Newnham, J. P. (2014). Multiple prenatal ultrasound scans and ocular development: 20-year follow-up of a randomized controlled trial. *Ultrasound in Obstetrics and Gynecology*, 44(2), 166–170. <https://doi.org/10.1002/uog.13399>
- Fowlkes, J. B. (2008). American Institute of Ultrasound in Medicine consensus report on potential bioeffects of diagnostic ultrasound: executive summary. *Journal of Ultrasound in Medicine : Official Journal of the American Institute of Ultrasound in Medicine*, 27(4), 503–515. <https://doi.org/10.1177/8756479310394986>

- Bell, D. J., & Goel, A. (2015). Doppler shift. *Radiopedia*. Retrieved January 13, 2018, from <https://radiopaedia.org/articles/doppler-shift>
- Goldenberg, R. L., Culhane, J. F., Iams, J. D., & Romero, R. (2008). Epidemiology and causes of preterm birth. *The Lancet*, *371*(9606), 75-84. [https://doi.org/10.1016/S0140-6736\(08\)60074-4](https://doi.org/10.1016/S0140-6736(08)60074-4)
- Helmy, S., Bader, Y., Koch, M., Tiringier, D., & Kollmann, C. (2015). Measurement of thermal effects of doppler ultrasound: An in vitro study. *PLoS ONE*, *10*(8), 1–6. <https://doi.org/10.1371/journal.pone.0135717>
- Hill, A. (2016). News life sport. *Newsletter*, 1–5.
- Jia, H., Duan, Y., Cao, T., Zhao, B., Lv, F., & Yuan, L. (2005). Immediate and long-term effects of color Doppler ultrasound on myocardial cell apoptosis of fetal rats. *Echocardiography (Mount Kisco, N.Y.)*, *22*(5), 415–420. <https://doi.org/10.1111/j.1540-8175.2005.04035.x>
- Kremkau, F. W. (1994). Diagnostic ultrasound: principles and instruments. *Ultrasound Quarterly*, *12*(1), 65-66.
- Kuehn, L., & McCormick, S. (2017). Heat exposure and maternal health in the face of climate change. *International Journal of Environmental Research and Public Health*, *14*(8), 853-865. <https://doi.org/10.3390/ijerph14080853>
- Liang, H. D., Zhou, L. X., Wells, P. N. T., & Halliwell, M. (2009). Temperature measurement by thermal strain imaging with diagnostic power ultrasound, with potential for thermal index determination. *Ultrasound in Medicine and Biology*, *35*(5), 773–780. <https://doi.org/10.1016/j.ultrasmedbio.2008.10.017>
- Liu, L., Johnson, H. L., Cousens, S., Perin, J., Scott, S., Lawn, J. E., ... & Black, R. E. (2012). Global, regional, and national causes of child mortality: An updated systematic analysis for 2010 with time trends since 2000. *The Lancet*, *379*(9832), 2151–2161. [https://doi.org/10.1016/S0140-6736\(12\)60560-1](https://doi.org/10.1016/S0140-6736(12)60560-1)
- Maeda, K., & Kurjak, A. (2012). The safe use of diagnostic ultrasound in obstetrics and gynecology. *Donald School Journal of Ultrasound in Obstetrics and Gynecology*, *6*(3), 313–317.
- Miller, D. L. (2008). Safety assurance in obstetrical ultrasound. *Seminars in Ultrasound, CT and MRI*, *29*(2), 156–164. <https://doi.org/10.1053/j.sult.2007.12.003>
- Miller, M. W., Nyborg, W. L., & Dewey, W. C. (2002). Hyperthermic teratogenicity, thermal dose and diagnostic ultrasound during pregnancy : implications of new standards on tissue heating. *International Journal of Hyperthermia*, *18*(5), 361–384. <https://doi.org/10.1080/0265673021014689>
- Mone, F., McAuliffe, F. M., & Ong, S. (2015). The clinical application of Doppler ultrasound in obstetrics. *The Obstetrician and Gynaecologist*, *17*(1), 13–19. <https://doi.org/10.1111/tog.12152>
- Pellicer, B., Herraiz, S., Táboas, E., Felipo, V., Simon, C., & Pellicer, A. (2011). Ultrasound bioeffects in rats: Quantification of cellular damage in the fetal liver after pulsed Doppler imaging. *Ultrasound in Obstetrics and Gynecology*, *37*(6), 643–648. <https://doi.org/10.1002/uog.8842>
- Pooh, R. K., Maeda, K., Kurjak, A., Sen, C., Ebrashy, A., Adra, A., ... & Stanojevic, M. (2016). 3D/4D sonography - Any safety problem. *Journal of Perinatal Medicine*, *44*(2), 125–129. <https://doi.org/10.1515/jpm-2015-0225>

- Randolph-habecker, C. J., Palmer, A. K., Kiernan, J., & Ritman, E. L. (2017). Studies in Obstetric Sonography. *Ultrasound in Obstetrics and Gynecology*, 10(1), 1–5. <https://doi.org/10.1097/AOG.0b013e3181834608>
- Rylander, C., Odland, J. O., & Sandanger, T. M. (2013). Climate change and the potential effects on maternal and pregnancy outcomes: An assessment of the most vulnerable - the mother, fetus, and newborn child. *Global Health Action*, 6(1), 0–9. <https://doi.org/10.3402/gha.v6i0.19538>
- Schellpfeffer, M. A. (2013). Ultrasound imaging in research and clinical medicine. *Birth Defects Research Part C - Embryo Today: Reviews*, 99(2), 83–92. <https://doi.org/10.1002/bdrc.21032>
- Schneider-Kolsky, M. E., Ayobi, Z., Lombardo, P., Brown, D., Kedang, B., & Gibbs, M. E. (2009). Ultrasound exposure of the foetal chick brain: Effects on learning and memory. *International Journal of Developmental Neuroscience : The Official Journal of the International Society for Developmental Neuroscience*, 27(7), 677–83. <https://doi.org/10.1016/j.ijdevneu.2009.07.007>
- Sheffield, P., & Landrigan, P. (2011). Global climate change and children's health: Threats and strategies for prevention. *Environ Health Perspect*, 119(3), 291–8. <https://doi.org/10.1289/rhp.1002233>
- Sheiner, E., Shoham-Vardi, I., Pombar, X., Hussey, M. J., Strassner, H. T., & Abramowicz, J. (2007). An increased thermal index can be achieved when performing Doppler studies in obstetric sonography. *Journal of Ultrasound in Medicine*, 26(1), 71–76. <https://doi.org/10.1016/j.jum.2006.11.011> [pii]
- Shung, K. K. (2006). *Diagnostic ultrasound: Imaging and blood flow measurements*. Boca Raton, FL: Taylor & Francis.
- Strand, L. B., Barnett, A. G., & Tong, S. (2011). The influence of season and ambient temperature on birth outcomes: A review of the epidemiological literature. *Environmental Research*, 111(3), 451–462. <https://doi.org/10.1016/j.envres.2011.01.023>
- Trays, G., & Banerjee, S. (2014). Fetal and neonatal hyperthermia. *Paediatrics and Child Health (United Kingdom)*, 24(9), 419–423. <https://doi.org/10.1016/j.paed.2014.01.005>
- U.S. Food and Drug Administration. (2017). *Radiation-emitting products*. Retrieved January 13, 2018, from <https://www.fda.gov/Radiation-EmittingProducts/RadiationEmittingProductsandProcedures/MedicalImaging/ucm115357.htm>
- Zaiki, F. W. A., Dom, S. M., Razak, H. R. A., & Hassan, H. F. (2013). Prenatal ultrasound heating impacts on fluctuations in haematological analysis of *Oryctolagus cuniculus*. *Quantitative Imaging in Medicine and Surgery*, 3(5), 262–8. <https://doi.org/10.3978/j.issn.2223-4292.2013.10.05>
- Zaiki, F. W. A., & Dom, S. M. (2014). The effect of prenatal ultrasound heating throughout gestation on rabbit fetal weight. *International Journal of Bio-Science and Bio-Technology*, 6(3), 71–79. <https://doi.org/10.14257/ijbsbt.2014.6.3.09>
- Zaiki, F. W. A., & Dom, S. M. (2016). Morphometric Brain Measurement of Prenatal Ultrasound-Induced Rabbit Fetus Using Micro-Computed Tomography (Micro-CT). *Jurnal Teknologi*, 7, 1–3.
- Ziskin, M. C., & Morrissey, J. (2011). Thermal thresholds for teratogenicity, reproduction, and development. *International Journal of Hyperthermia : The Official Journal of European Society for Hyperthermic Oncology, North American Hyperthermia Group*, 27(4), 374–87. <https://doi.org/10.3109/02656736.2011.553769>

Simultaneous Estimation by RP-HPLC Method for the Immunosuppressant Drug Combination: Mycophenolate Mofetil, Tacrolimus with Prednisolone

Pardeep Kr. Sharma¹, Vijay Mishra¹, Surajpal Verma^{1*} and Amit Bhatia²

¹ School of Pharmaceutical Sciences, Lovely Professional University, Phagwara 144411, Punjab, India

² Department of Pharmaceutical Sciences and Technology,

Maharaja Ranjit Singh Punjab Technical University, Bathinda 151001, Punjab, India.

ABSTRACT

In current scenario, treatment of any disease depends upon two major factors i.e. patient compliance and effective dosage regimen. The effective dose delivered by a dosage form to a patient depends on various parameters, which can be assessed by an effective and economic analytical method. In the present study a precise analytical method for estimating the combination of immunosuppressant drugs mycophenolate mofetil (MMF), tacrolimus (TAC) and prednisolone through RP-HPLC was developed. The mobile phase contained a mixture of acetonitrile and 0.35% triethylamine (pH 4.2) with orthophosphoric acid (70:30). As per ICH guidelines the optimized RP-HPLC method was validated with respect to linearity, limit of detection (LOD), limit of quantitation (LOQ), accuracy, precision, repeatability, robustness, ruggedness. The accuracy of the method was determined in terms of % recovery of the standard. The obtained test results were compared with that of the standard drug. The results of the recovery study were found to be within the acceptance criteria (96.93- 103.99%), which indicated a good degree of sensitivity of the developed method in detection of analytes in a sample.

Keywords: Dosage regimen, mycophenolate mofetil, prednisolone, RP-HPLC, ICH, tacrolimus

ARTICLE INFO

Article history:

Received: 25 February 2018

Accepted: 30 August 2018

Published: 24 January 2019

E-mail addresses:

parryds2@gmail.com (Pardeep Kr. Sharma)

vijaymishra2@gmail.com (Vijay Mishra)

surajpal.15834a@gmail.com (Surajpal Verma)

drbhatiaamit@gmail.com (Amit Bhatia)

* Corresponding author

INTRODUCTION

Immunosuppression causes decrease in the immunity of the body and its ability to fight with various infections. Immunosuppressant drugs generally weaken the immune system so that it cannot differentiate the transplanted organ from the rest of the body, resulting

in a decrease in the rejection rate. Some of these drugs are used to treat autoimmune disorders. In current scenario, under the combination therapy patient receives more than one therapy during the treatment. Several individual pills, which may contain a particular drug or the multiple drugs, are given to the patient during the treatment. The multiple drugs incorporated in a single dosage form generally improve patient compliance, which involves how correctly a patient follows dosage regimen. In industrial point of view, it is easy to formulate and analyze the single drug formulation. But, as the number of drugs increases, the complexity of the formulation increases. It generates the necessity of the development of reliable and rapid analytical method for routine analysis of the drugs in combination.

Mycophenolate Mofetil (MMF) (Figure 1), chemically 2-morpholinoethyl (E)-6-(1,3-dihydro-4-hydroxy-6-methoxy-7-methyl-3-oxo-5-isobenzofuranyl)-4-methyl-4-hexenoate is a potent, non-competitive, specific and reversible inhibitor of inosine monophosphate dehydrogenase (IMPDH) (Tripodi et al., 2001). IMPDH is an important enzyme in B- and T-cells for the synthesis of guanosine nucleotides. MMF is an ester prodrug of mycophenolic acid (MPA) and is converted to MPA by hepatic esterase (Fujiyama et al., 2010). MPA shows five-fold potency as an inhibitor of type II isoform of IMPDH, resulting in more strong inhibition of cell growth and multiplication of lymphocytes (Allison & Eugui, 2000). MMF inhibits the production of antibodies and the proliferation of lymphocytes (Birnbaum et al., 2009; Häntzschel et al., 2008; Iaccarino et al., 2007). MMF generally blocks the early events of proliferation and DNA synthesis. But, it does not inhibit the initial events like the production of interleukins (IL-1 and IL-2) during the activation of human peripheral blood mononuclear cells (HPBMC) (Sepe et al., 2008; Tjeertes et al., 2007). Since MMF is an ester prodrug of MPA, hence MPA may be present as a synthetic impurity in MMF (Tang et al., 2005). On 3rd May 1995, United States Food and Drug Administration (USFDA) approved MMF as an immunosuppressant used in kidney transplantation in combination with corticosteroids (Kim, Rostas, & Gabardi, 2013).

Tacrolimus (TAC) (Figure 2), an immunomodulator (FK506), was isolated from the fungus *Streptomyces tsukubaensis* in 1984. TAC, chemically (1R, 9S, 12S, 13R, 14S, 17R, 18E, 21S, 23S, 24R, 25S, 27R)-1, 14-dihydroxy-12-[(E)-2[(1R,3R,4R)-4-hydroxy-3-methoxycyclohexyl]-1-methylethenyl]-23,25-dimethoxy 13, 19, 21, 27-tetramethyl-17-prop-2-en-1-yl-11, 28-dioxo-4-azatricyclo [22.3.1.0^{4,9}] octacos-18-ene-2, 3, 10, 16-tetrone, is T-lymphocyte-specific macrolide calcineurin inhibitor, which inhibits the transcription of IL-2 and other cytokines (Homey et al., 1998) via T-cell activation through tumor necrosis factor- α (TNF- α), IL-1 β and IL-6 (Kawai & Yamamoto, 2005; Kondo et al., 2004). In late 80's TAC is used to prevent the rejection of solid organ post transplantation (Starzl et al., 1989). But after USFDA approval in year 2000, TAC ointment was used for many skin diseases like lupus dermatopathy (Lampropoulos et al., 2004), atopic dermatitis psoriasis (Yamamoto & Nishioka, 2003), localized scleroderma (Mancuso & Berdondini,

2003), chronic actinic dermatitis (Evans, Palmer, & Hawk, 2004), pyoderma gangrenosum (Petering et al., 2001), Behçet's disease (Sakane et al., 1995), lichen planus (Lener et al., 2001), rheumatoid ulcers (Schuppe et al., 2000) and steroid rosacea (Goldman, 2001). The efficacy of TAC was found to be much better as compared to the corticosteroids due to less or no dermal side effects and systemic absorption (Jan, 2003). Some common adverse effects during the treatment of skin diseases are itching or erythema, burning sensations, which diminish as treatment progress (Soter et al., 2001).

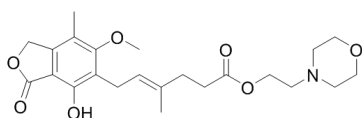


Figure 1. Chemical structure of MMF

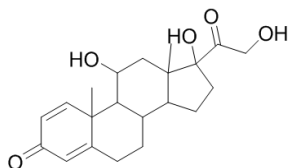


Figure 3. Chemical structure of prednisolone

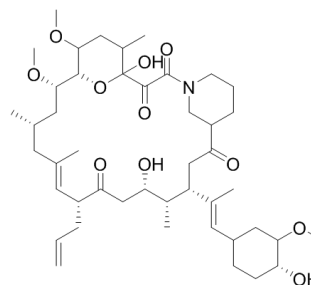


Figure 2. Chemical structure of TAC

Prednisolone (PRED) (Figure 3), chemically 11,17-dihydroxy-17-(2-hydroxyacetyl)-10,13-dimethyl-6,7,8,9,10,11,12,13,14,15,16,17-dodecahydrocyclopenta[a]phenanthren-3-one is a synthetic corticosteroid, and always remains at the forefront of anti-inflammatory and immunosuppressive therapies (Ashok et al., 2011; Morrison, 2013). The exact mechanism of immunosuppressant activity of PRED is not known, however in vitro experiments demonstrated that PRED inhibited platelet aggregation by repressing the cellular adhesion molecule (CAM1) (Hirsch et al., 2012; Liverani et al., 2012; Wehling-Henricks, Lee, & Tidball, 2004).

Various analytical techniques like spectrophotometry (Singh & Nath, 2011), spectroscopy (such as NMR) (Touzani, 2011), chromatography (such as TLC or preparative TLC, HPTLC, gas chromatography, HPLC and HPLC coupled with other techniques like MS/MS-MS) (Danafar & Hamidi, 2015; Difrancesco et al., 2007; Kawanishi et al., 2015; Douma et al., 2016; Rissling et al., 2016; Sobiak et al., 2016; Tron et al., 2016; Wang et al., 2017) are available for the detection and quantification of drugs/compounds present in a sample. No official RP-HPLC method is available for the assay of MMF, TAC and prednisolone in single formulation (Benech et al., 2007; Chozas et al., 2012; Gonzalez-Ramirez et al., 2014; Kirresh et al., 2017; Parant et al., 2017; Rivera et al., 2017; Tölgyesi et al., 2017; Tummala et al., 2013; Vosough & Tehrani, 2018; Wiesen et al., 2012). So, there

is a need for method development for the assay of MMF, TAC, and PRED in combination (Snyder, Kirkland, & Glajch, 2012).

MATERIALS AND METHODS

In present work, several attempts have been made for the simultaneous estimation of MMF, TAC and PRED and its pharmaceutical dosage forms. A number of trials have been made concerning the mobile phase, and in addition UV detector's wavelength to develop an appropriate and quick technique for the study of all the three drugs, at the same time.

Materials, Reagents, and Chemicals

Drugs Mycophenolate Mofetil, Tacrolimus and Prednisolone were received as gift samples from Biocon Ltd., Bangalore, India and Jackson Laboratories Pvt Ltd., Amritsar, Punjab, India, respectively. Acetonitrile and other HPLC grade solvents and chemicals were purchased from Thermo Fisher Scientific, Vadodara, Gujarat, India. Orthophosphoric acid and Triethylamine of analytical grade were obtained from Merck, Mumbai, India. For the entire HPLC method, in-house produced double-distilled water was used.

The HPLC (Shimadzu, Kyoto, Japan) instrument equipped with two LC-10 ATVP pumps, SPD-10AVP UV-vis detector, injector with a 20 μ L loop and Kinetex Polar, C18, 5 μ m, 4.6 \times 250 mm column was used for the experimental analysis. The results were acquired and processed using Shimadzu LC-solution version 6.42 software. A mixture of acetonitrile and 0.35% Triethylamine pH 4.2 with orthophosphoric acid (70:30) was used as mobile phase. Injection volume (20 μ L) was injected into the column using a syringe and the linear gradient flow rate was set at 1.2 mL/min. The drugs were detected at 254 nm for Prednisolone and Mycophenolate and 210 nm for Tacrolimus.

Preparation of Standard Stock Solution

10 mg of each drug was accurately weighed and transferred into 10 mL volumetric flask containing 5 mL of acetonitrile and sonicated for 10 min then the volume was made up to 10 mL with acetonitrile.

Preparation of Sample Solution

Sample solutions of different concentrations ranging from 10-100 μ g/mL were prepared from stock solution by diluting with acetonitrile.

Method Validation

As per ICH guidelines the optimized RP-HPLC method was validated with respect to Linearity, Limit of Detection (LOD), Limit of Quantitation (LOQ), Accuracy, Precision, Repeatability, Robustness, and Ruggedness.

RESULTS AND DISCUSSION

HPLC Chromatogram of Individual Drug and Mixture Sample

On HPLC analysis, chromatograms of individual drugs and in combination were optimized in terms of their retention time as shown in Figure 4.

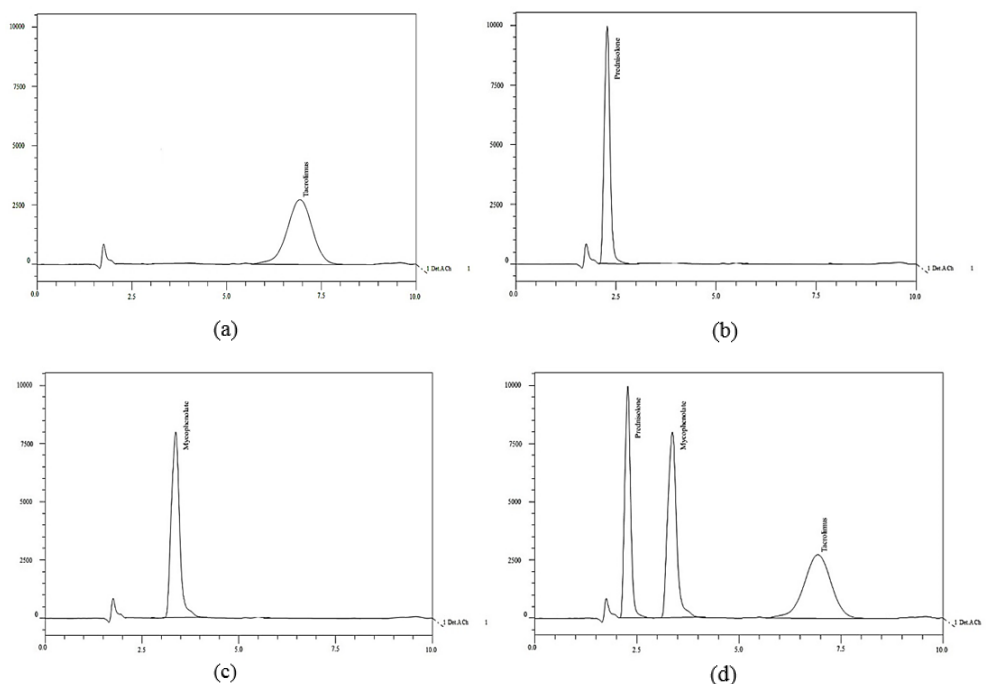


Figure 4. HPLC chromatogram of individual drugs (a) TAC, (b) PRED, (c) MMF and (d) drugs in combination

Linearity

For linearity, different concentrations ranging from 10-100 $\mu\text{g/mL}$ of MMF, TAC and PRED were prepared. All the dilutions were filtered through 0.22 μm nylon filter and injected. Each concentration was used in triplicate. A calibration curve was plotted and r^2 was determined (Figure 5). All the drugs shows the linearity in the concentration ranging from 10-100 $\mu\text{g/mL}$ (Table 1).

Accuracy and Precision

The accuracy of the method was determined in terms of percent recuperation of standard. Recuperation studies were carried out by extending the standard drug solution at the level of lower, medium and higher concentration of each drug in the pre-analyzed sample (Table 2). Results were found to be within the acceptance criteria (96.93-103.99%) representing

Table 1

Linearity observation of Prednisolone, Mycophenolate, and Tacrolimus (n=3)

Concentration (µg/mL)	PRED		MMF		TAC	
	Area	SD	Area	SD	Area	SD
10	305579.3	4048.347	192027.3	2066.726	112687.3	407.6547
20	634971	6180.709	370155.7	7401.618	239156.3	535.3264
30	1003729	2957.649	612807.7	10224.46	421809.3	4883.271
40	1329168	21710.31	768419.7	9407.889	524716	5618.779
50	1626347	16692.96	942059.7	4499.839	654758	10412.89
60	1976215	30299.37	1134766	14594.69	795546.7	2262.619
70	2321734	8966.311	1290143	11643.82	921787	1761.694
80	2651374	17168.08	1497025	20125.89	1042911	2222.671
90	2943142	366.5601	1668172	15772.36	1170387	4833.766
100	3224405	510.6959	1844333	2933.77	1286536	3677.219

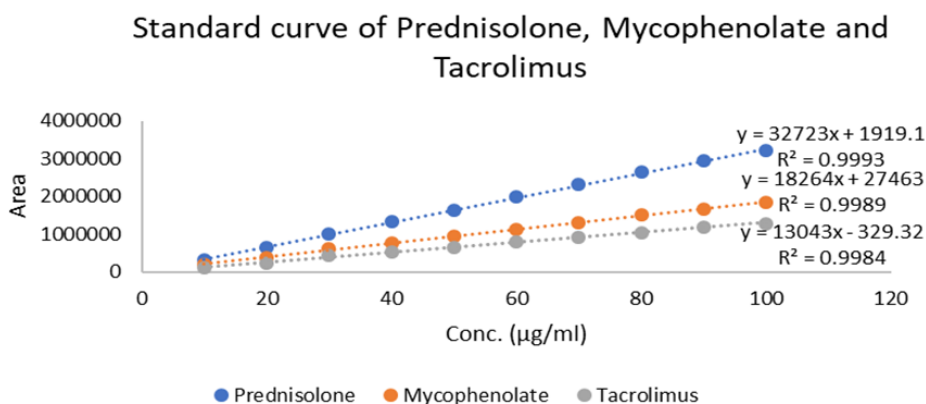


Figure 5. A standard curve of Prednisolone, Mycophenolate and Tacrolimus by RP-HPLC

a good degree of sensitivity of the method towards detection of analytes in a sample.

The intra-day and inter-day variation for determination of all the three drugs were carried out with 3 concentrations levels (i.e. low, medium and high) in the same day and 3 consecutive days where repeatability was determined with a lower concentration and injected six times and relative standard deviation (%RSD) was calculated.

Repeatability

The repeatability is established only when an observer is carrying the same experiment multiple times over a short period of time at the same place, on the same instrument, under

Table 2

Data Accuracy

conc. ($\mu\text{g}/\text{mL}$)	Intraday precision			Inter-day-1 precision			Inter-day-2 precision		
	PRED	MMF	TAC	PRED	MMF	TAC	PRED	MMF	TAC
50	1593277	814082	644690	1612348	783409	654833	1631418	746736	664976
50	1591086	814278	646370	1590942	778282	647281	1590797	740286	648192
50	1591739	811789	647013	1591951	779398	649052	1590162	737007	651091
50	1590479	809657	642863	1590849	779049	644703	1591218	736441	646543
50	1590472	807816	647326	1599090	769750	650780	1607707	731683	654234
50	1590916	805905	644609	1590694	776861	645968	1590472	747816	647326
Mean	1591328	810588	645479	1595979	777792	648769	1600296	739995	652060
SD	970.341	3102.36	1569.57	7889.46	4112.8	3353.88	15249.9	5735.01	6328.48
%RSD	0.06098	0.38273	0.24316	0.49433	0.52878	0.51696	0.95294	0.77501	0.97054

same conditions. The repeatability for the determination of MMF and TAC was estimated three times around the same day and for three continuous days. The percent RSD was calculated for each situation for all three drugs (Table 3). Repeatability was analyzed in six replicates for lowest concentration level. Intraday and inter-day studies were made in triplicate for each concentration level. In all the cases the %RSD was less than 2.

Table 3

Precision results showing repeatability

conc. ($\mu\text{g}/\text{mL}$)	Intraday precision			Inter-day-1 precision			Inter-day-2 precision		
	PRED	MMF	TAC	PRED	MMF	TAC	PRED	MMF	TAC
50	1593277	814082	644690	1612348	783409	654833	1631418	746736	664976
50	1591086	814278	646370	1590942	778282	647281	1590797	740286	648192
50	1591739	811789	647013	1591951	779398	649052	1590162	737007	651091
50	1590479	809657	642863	1590849	779049	644703	1591218	736441	646543
50	1590472	807816	647326	1599090	769750	650780	1607707	731683	654234
50	1590916	805905	644609	1590694	776861	645968	1590472	747816	647326
Mean	1591328	810588	645479	1595979	777792	648769	1600296	739995	652060
SD	970.341	3102.36	1569.57	7889.46	4112.8	3353.88	15249.9	5735.01	6328.48
%RSD	0.06098	0.38273	0.24316	0.49433	0.52878	0.51696	0.95294	0.77501	0.97054

Limit of Detection (LOD) and Limit of Quantification (LOQ)

The LOD and LOQ of developed method were accomplished according to ICH guidelines. A few methodologies for deciding the LOD and LOQ are conceivable, contingent upon the strategy i.e. a non-instrumental or instrumental. Among them, the following method was employed-

$$\text{LOD} = 3.3\sigma/S \text{ and } \text{LOQ} = 10\sigma/S$$

where, σ = the standard error of response and S = the slope of the calibration curve.

Results are represented in Table 4.

Table 4

LOD and LOQ

Sr. No.	Sample	LOD ($\mu\text{g/mL}$)	LOQ ($\mu\text{g/mL}$)
1.	Mycophenolate	0.210193	0.636949
2.	Prednisolone	0.442067	1.339597
3.	Tacrolimus	0.038667	0.117171

The LOD and LOQ were calculated on the basis of standard deviation of the response and the slope (s) of the calibration curve at approximate levels of LOD and LOQ. The obtained results were found to be within the limit.

Robustness and Ruggedness

These terms refer to the capability of an analytical method to remain unchanged by deliberately changing the method parameters like change in flow rate, and change in wavelength. The concept of remaining unchanged by deliberately varying the method parameters has two possible elucidations such as- (a) no change of the identified measure of the analyte in a specific test disregarding the variation in the method parameter or (b) no change is observed in the critical performance characteristics disregarding the variation in the method parameter.

For the calculation of robustness, the sample with lowest concentration was analyzed by deliberately changing the flow rate about $\pm 15\%$, i.e. 1 and 1.4 mL/min and changing the wavelength by ± 5 nm, i.e. 245 and 255 nm.

The robustness was studied by analyzing the sample containing lower concentration with deliberate variation in the method parameters. Robustness of the method was studied by a change in wavelength or change in flow rate. The change in the responses of drugs was noted in terms of %RSD (Table 5 and Table 6).

The ruggedness was studied by analyzing the same samples of three drugs by changing the analyst. The change in the responses of drugs was noted in terms of %RSD. Results are represented in Table 7.

Table 5

Change in wavelength

Concentration (µg/mL)	249 nm and 205 nm			254 nm and 210 nm			259 nm and 215 nm		
	Area			Area			Area		
	PRED	MMF	TAC	PRED	MMF	TAC	PRED	MMF	TAC
50	1776659	907237	933558	1573979	712879	679282	1371098	518520	425005
50	1775023	904786	935429	1571931	712900	679780	1369639	517013	424131
50	1774938	902279	935611	1572804	709292	682122	1370269	516305	426633
mean	1775540	904767	934866	1572905	711690	680395	1370335	517279	425256
SD	970.014	2479.05	1136.41	839.117	1695.9	1238.21	731.758	1131.26	1269.79
%RSD	0.05463	0.274	0.12156	0.05335	0.23829	0.18198	0.0534	0.21869	0.2986

The %RSD should not be more than 2. The %RSD obtained for a change of flow rate and wavelength was found to be below 2, which was within the acceptance criteria and indicated that the method was robust.

Table 6

Change in flow rate

Concentration (µg/mL)	1.0 mL/min			1.2 mL/min			1.4 mL/min		
	Area			Area			Area		
	PRED	MMF	TAC	PRED	MMF	TAC	PRED	MMF	TAC
50	1602980	796699	646079	1590471	788571	651924	1577962	779842	643768
50	1603518	796200	648935	1591569	788276	645042	1579619	778152	641149
50	1604539	793512	651320	1591989	785249	643826	1579439	776986	635332
mean	1603679	795470	648778	1591343	787365	646931	1579007	778327	640083
SD	791.872	1714.22	2624.02	639.994	1501.31	3565.55	909.173	1435.99	4317.85
%RSD	0.04938	0.2155	0.40446	0.04022	0.19068	0.55115	0.05758	0.1845	0.67458

Table 7

Ruggedness data

Concentration (µg/mL)	Analyst 1			Analyst 2		
	Area			Area		
	PRED	MMF	TAC	PRED	MMF	TAC
50	1593277	814082	644690	1590797	740286	648192
50	1591086	814278	646370	1593832	739687	640289
50	1591739	811789	647013	1592418	738565	638463
50	1590479	809657	642863	1595121	738156	642563

Table 7 (Continue)

Concentration ($\mu\text{g/mL}$)	Analyst 1			Analyst 2		
	Area			Area		
	PRED	MMF	TAC	PRED	MMF	TAC
50	1590472	807816	647326	1592162	737007	651091
50	1590916	805905	644609	1591218	736441	646543
Mean	1591328	810588	645479	1592591	738357	644524
SD	970.341	3102.36	1569.57	1486.52	1358.13	4456.69
%RSD	0.06098	0.38273	0.24316	0.09334	0.18394	0.69147

The %RSD obtained was found to be below 2, which was within the acceptance criteria. So, the method was found to be rugged.

Specificity

Specificity of the HPLC method was demonstrated by the separation of the analytes from other potential components such as impurities, degradants or excipients. A volume of 20 μL of individual ingredients and excipients solution was injected and the chromatograms were recorded.

The test results obtained were compared with the results of those obtained for the standard drug. It was shown that potential components except drug were not interfering with the developed method. Results are represented in Table 8.

Table 8

Specificity data

Concentration ($\mu\text{g/mL}$)	Area		
	PRED	MMF	TAC
50	1536476	726475	622028
50	1536951	726409	621097
50	1534978	726462	611111
50	1539824	726385	621563
50	1533361	725767	618875
50	1538822	725034	621366
Mean	1536735.333	726088.6667	619340
SD	2178.766904	531.4836676	3814.259736
%RSD	0.141778929	0.073198177	0.615858775

CONCLUSION

The analytical strategy depicted in the present study has great precision, accuracy, linearity and is found appropriate for the simultaneous estimation of immunosuppressant drugs like MMF and TAC. As the technique was effectively validated as per ICH guidelines, it can be promptly utilized as a part of value control laboratories for the standard pharmaceutical investigation. Additionally, this straightforward and quick technique can streamline execution in developing new formulations containing immunosuppressant drugs like MMF, TAC and PRED.

REFERENCES

- Allison, A. C., & Eugui, E. M. (2000). Mycophenolate mofetil and its mechanisms of action. *Immunopharmacology*, 47(2-3), 85-118.
- Ashok, R., Prakash, P., & Tamil Selvan, R. (2011). Development and validation of analytical method for estimation of prednisolone in bulk and tablets using UV-Visible spectroscopy. *International Journal of Pharmacy and Pharmaceutical Sciences*, 3(4), 184-186.
- Benech, H., Hascoet, S., Furlan, V., Pruvost, A., & Durrbach, A. (2007). Development and validation of an LC/MS/MS assay for mycophenolic acid in human peripheral blood mononuclear cells. *Journal of Chromatography B*, 853(1-2), 168-174. doi:10.1016/j.jchromb.2007.03.008
- Birbaum, F., Mayweg, S., Reis, A., Bohringer, D., Seitz, B., Engelmann, K., . . . & Reinhard, T. (2009). Mycophenolate mofetil (MMF) following penetrating high-risk keratoplasty: long-term results of a prospective, randomised, multicentre study. *Eye (Lond)*, 23(11), 2063-2070. doi:10.1038/eye.2008.402
- Chozas, J. V., Godino, A. S.-B., García, N. Z., Pinteño, S. G., Joumady, I., García, C. C., & Gil, F. V. (2012). Analytical validation of a homogeneous immunoassay for determination of mycophenolic acid in human plasma. *Transplantation proceedings*, 44(9), 2669-2672.
- Danafar, H., & Hamidi, M. (2015). Simple and Sensitive High-Performance Liquid Chromatography (HPLC) Method with UV Detection for Mycophenolic Acid Assay in Human Plasma. Application to a Bioequivalence Study. *Advanced pharmaceutical bulletin*, 5(4), 563-568. doi:10.15171/apb.2015.076
- Difrancesco, R., Frerichs, V., Donnelly, J., Hagler, C., Hochreiter, J., & Tornatore, K. M. (2007). Simultaneous determination of cortisol, dexamethasone, methylprednisolone, prednisone, prednisolone, mycophenolic acid and mycophenolic acid glucuronide in human plasma utilizing liquid chromatography-tandem mass spectrometry. *Journal of Chromatography B*, 859(1), 42-51. doi:10.1016/j.jchromb.2007.09.003
- Douma, M., Sabour, B., Manaut, N., Hassouani, M., Schamel, A., Oudra, B., & Loudiki, M. (2016). Cyanotoxins: Detection methods and control measures – A mini-review. *Journal of Materials and Environmental Science*, 7(11), 4079-4086.
- Evans, A. V., Palmer, R. A., & Hawk, J. L. (2004). Erythrodermic chronic actinic dermatitis responding only to topical tacrolimus. *Photodermatology, photoimmunology & photomedicine*, 20(1), 59-61.

- Fujiyama, N., Miura, M., Kato, S., Sone, T., Isobe, M., & Satoh, S. (2010). Involvement of carboxylesterase 1 and 2 in the hydrolysis of mycophenolate mofetil. *Drug Metabolism and Disposition*, 38(12), 2210-2217. doi:10.1124/dmd.110.034249
- Goldman, D. (2001). Tacrolimus ointment for the treatment of steroid-induced rosacea: A preliminary report. *Journal of the American Academy of Dermatology*, 44(6), 995-998. doi:10.1067/mjd.2001.114739
- Gonzalez-Ramirez, R., Gonzalez-Banuelos, J., Villa Mde, L., Jimenez, B., Garcia-Roca, P., Cruz-Antonio, L., ... & Medeiros, M. (2014). Bioavailability of a generic of the immunosuppressive agent mycophenolate mofetil in pediatric patients. *Pediatric Transplantation*, 18(6), 568-574. doi:10.1111/ptr.12311
- Häntzschel, I., Freiberg-Richter, J., Platzbecker, U., Kiani, A., Schetelig, J., Illmer, T., ... & Bornhäuser, M. (2008). Targeting mycophenolate mofetil for graft-versus-host disease prophylaxis after allogeneic blood stem cell transplantation. *Bone Marrow Transplantation*, 42(2), 113-120.
- Hirsch, G., Lavoie-Lamoureux, A., Beauchamp, G., & Lavoie, J. P. (2012). Neutrophils are not less sensitive than other blood leukocytes to the genomic effects of glucocorticoids. *PLoS One*, 7(9), e44606.
- Homey, B., Assmann, T., Vohr, H.-W., Ulrich, P., Lauerma, A. I., Ruzicka, T., . . . & Schuppe, H. C. (1998). Topical FK506 suppresses cytokine and costimulatory molecule expression in epidermal and local draining lymph node cells during primary skin immune responses. *The Journal of Immunology*, 160(11), 5331-5340.
- Iaccarino, L., Rampudda, M., Canova, M., Della Libera, S., Sarzi-Puttinic, P., & Doria, A. (2007). Mycophenolate mofetil: what is its place in the treatment of autoimmune rheumatic diseases? *Autoimmunity reviews*, 6(3), 190-195.
- Jan, D. (2003). Non-steroidal topical immunomodulators provide skin-selective, self-limiting treatment in atopic dermatitis. *European Journal of Dermatology*, 13(5), 455-461.
- Kawai, S., & Yamamoto, K. (2005). Safety of tacrolimus, an immunosuppressive agent, in the treatment of rheumatoid arthritis in elderly patients. *Rheumatology*, 45(4), 441-444.
- Kawanishi, M., Yano, I., Yoshimura, K., Yamamoto, T., Hashi, S., Masuda, S., ... & Matsubara, K. (2015). Sensitive and validated LC-MS/MS methods to evaluate mycophenolic acid pharmacokinetics and pharmacodynamics in hematopoietic stem cell transplant patients. *Biomedical Chromatography*, 29(9), 1309-1316. doi:10.1002/bmc.3423
- Kim, M., Rostas, S., & Gabardi, S. (2013). Mycophenolate fetal toxicity and risk evaluation and mitigation strategies. *American Journal of Transplantation*, 13(6), 1383-1389. doi:10.1111/ajt.12238
- Kirresh, T., Tuteja, S., Russo, D., Brophy, P. D., & Murry, D. J. (2017). Development and validation of a liquid chromatography-mass spectrometric assay for simultaneous determination of tacrolimus and 13-O-desmethyl tacrolimus in rat kidney tissue. *Journal of Pharmaceutical and Biomedical Analysis*, 136, 32-37. doi:10.1016/j.jpba.2016.12.034
- Kondo, H., Abe, T., Hashimoto, H., Uchida, S., Irimajiri, S., Hara, M., & Sugawara, S. (2004). Efficacy and safety of tacrolimus (FK506) in treatment of rheumatoid arthritis: a randomized, double blind, placebo controlled dose-finding study. *The Journal of Rheumatology*, 31(2), 243-251.

- Lampropoulos, C., Sangle, S., Harrison, P., Hughes, G., & D'cruz, D. (2004). Topical tacrolimus therapy of resistant cutaneous lesions in lupus erythematosus: a possible alternative. *Rheumatology*, *43*(11), 1383-1385.
- Lener, E. V., Brieva, J., Schachter, M., West, L. E., West, D. P., & el-Azhary, R. A. (2001). Successful treatment of erosive lichen planus with topical tacrolimus. *Archives of Dermatology*, *137*(4), 419-422.
- Liverani, E., Banerjee, S., Roberts, W., Naseem, K. M., & Perretti, M. (2012). Prednisolone exerts exquisite inhibitory properties on platelet functions. *Biochemical Pharmacology*, *83*(10), 1364-1373. doi:10.1016/j.bcp.2012.02.006
- Mancuso, G., & Berdondini, R. M. (2003). Topical tacrolimus in the treatment of localized scleroderma. *European Journal of Dermatology*, *13*(6), 590-592.
- Morrison, N. A. (2013). RU486 Reversal of Cortisol Repression of 1, 25-Dihydroxyvitamin D3 Induction of the Human Osteocalcin Promoter. *Open Journal of Endocrine and Metabolic Diseases*, *3*(01), 55.
- Parant, F., Ranchin, B., & Gagnieu, M.-C. (2017). The Roche Total Mycophenolic Acid® assay: An application protocol for the ABX Pentra 400 analyzer and comparison with LC-MS in children with idiopathic nephrotic syndrome. *Practical Laboratory Medicine*, *7*, 19-26.
- Petering, H., Kiehl, P., Breuer, C., Kapp, A., & Werfel, T. (2001). Pyoderma gangrenosum: successful topical therapy with tacrolimus (FK506). *Der Hautarzt; Zeitschrift fur Dermatologie, Venerologie, und verwandte Gebiete*, *52*(1), 47-50.
- Rissling, O., Bauer, S., Shipkova, M., Glander, P., Mai, M., Hambach, P., & Budde, K. (2016). Simultaneous determination of mycophenolate and its metabolite mycophenolate-7-o-glucuronide with an isocratic HPLC-UV-based method in human plasma and stability evaluation. *Scandinavian Journal of Clinical and Laboratory Investigation*, *76*(8), 612-619. doi:10.1080/00365513.2016.1230775
- Rivera, S. M., Hwang, J. K., Slovak, J. E., Court, M. H., & Villarino, N. F. (2017). Simultaneous determination of mycophenolic acid and its glucuronide and glycoside derivatives in canine and feline plasma by UHPLC-UV. *Biomedical Chromatography*, *31*(8), e3942. doi:10.1002/bmc.3942
- Sakane, T., Mochizuki, M., Inaba, G., & Masuda, K. (1995). A phase II study of FK506 (tacrolimus) on refractory uveitis associated with Behcet's disease and allied conditions. *Ryumachi*, *35*(5), 802-813.
- Schuppe, H., Richter-Hintz, D., Stierle, H. E., Homey, B., Ruzicka, T., & Lehmann, P. (2000). Topical tacrolimus for recalcitrant leg ulcer in rheumatoid arthritis. *Rheumatology (Oxford)*, *39*(1), 105-106.
- Sepe, V., Libetta, C., Giuliano, M. G., Adamo, G., & Dal Canton, A. (2008). Mycophenolate mofetil in primary glomerulopathies. *Kidney International*, *73*(2), 154-162. doi:10.1038/sj.ki.5002653
- Singh, A. V., & Nath, L. K. (2011). Evaluation of compatibility of lamivudine with tablet excipients and a novel synthesized polymer. *Journal of Materials and Environmental Science*, *2*(3), 243-250.
- Snyder, L. R., Kirkland, J. J., & Glajch, J. L. (2012). *Practical HPLC method development*. Hoboken: John Wiley & Sons.

- Sobiak, J., Resztak, M., Glyda, M., Szczepaniak, P., & Chrzanowska, M. (2016). Pharmacokinetics of mycophenolate sodium co-administered with tacrolimus in the first year after renal transplantation. *European Journal of Drug Metabolism and Pharmacokinetics*, 41(4), 331-338. doi:10.1007/s13318-015-0262-9
- Soter, N. A., Fleischer, A. B., Jr., Webster, G. F., Monroe, E., & Lawrence, I. (2001). Tacrolimus ointment for the treatment of atopic dermatitis in adult patients: part II, safety. *Journal of the American Academy of Dermatology*, 44(1), S39-46.
- Starzl, T. E., Todo, S., Fung, J., Demetris, A. J., Venkataramman, R., & Jain, A. (1989). FK 506 for liver, kidney, and pancreas transplantation. *Lancet*, 2(8670), 1000-1004.
- Tang, S., Leung, J. C., Chan, L. Y., Lui, Y. H., Tang, C. S., Kan, C. H., . . . & Lai, K. N. (2005). Mycophenolate mofetil alleviates persistent proteinuria in IgA nephropathy. *Kidney International*, 68(2), 802-812. doi:10.1111/j.1523-1755.2005.00460.x
- Tjeertes, I., Bastiaans, D., Van Ganzewinkel, C., & Zegers, S. (2007). Neonatal anemia and hydrops fetalis after maternal mycophenolate mofetil use. *Journal of Perinatology*, 27(1), 62-64.
- Tölgyesi, Á., Barta, E., Simon, A., McDonald, T. J., & Sharma, V. K. (2017). Screening and confirmation of steroids and nitroimidazoles in urine, blood, and food matrices: Sample preparation methods and liquid chromatography tandem mass spectrometric separations. *Journal of Pharmaceutical and Biomedical Analysis*, 145, 805-813. doi:10.1016/j.jpba.2017.08.005
- Touzani, R. (2011). Dendrons, dendrimers new materials for environmental and science applications. *Journal of Materials and Environmental Science*, 2(3), 2028-2508.
- Tripodi, V., Lucangioli, S., Barbara, C., Rodriguez, V., & Carducci, C. (2001). Analysis of immunosuppressive drugs and their pharmaceuticals by micellar electrokinetic chromatography. *Chromatographia*, 54(1-2), 93-98.
- Tron, C., Rayar, M., Petitcollin, A., Beaurepaire, J. M., Cusumano, C., Verdier, M. C., . . . Lemaitre, F. (2016). A high performance liquid chromatography tandem mass spectrometry for the quantification of tacrolimus in human bile in liver transplant recipients. *Journal of Chromatography A*, 1475, 55-63. doi:10.1016/j.chroma.2016.10.075
- Tummala, V. B. R., Nallagari, S. R., Golkonda, R., Sure, V. V., & Chintala, R. (2013). Development of stability indicating liquid chromatography-mass tandem spectrometric method for the estimation of mycophenolate mofetil in bulk and pharmaceutical formulations. *Journal of Pharmacy Research*, 7(7), 640-646.
- Vosough, M., & Tehrani, S. M. (2018). Development of a fast HPLC-DAD method for simultaneous quantitation of three immunosuppressant drugs in whole blood samples using intelligent chemometrics resolving of coeluting peaks in the presence of blood interferences. *Journal of Chromatography B*, 1073, 69-79.
- Wang, L., Qiang, W., Li, Y., Cheng, Z., & Xie, M. (2017). A novel freeze-dried storage and preparation method for the determination of mycophenolic acid in plasma by high-performance liquid chromatography. *Biomedical Chromatography*, 31(9), e3958. doi:10.1002/bmc.3958
- Wehling-Henricks, M., Lee, J. J., & Tidball, J. G. (2004). Prednisolone decreases cellular adhesion molecules required for inflammatory cell infiltration in dystrophin-deficient skeletal muscle. *Neuromuscular Disorders*, 14(8-9), 483-490. doi:10.1016/j.nmd.2004.04.008

- Wiesen, M. H., Farowski, F., Feldkötter, M., Hoppe, B., & Müller, C. (2012). Liquid chromatography–tandem mass spectrometry method for the quantification of mycophenolic acid and its phenolic glucuronide in saliva and plasma using a standardized saliva collection device. *Journal of Chromatography A*, 1241, 52-59.
- Yamamoto, T., & Nishioka, K. (2003). Topical tacrolimus: An effective therapy for facial psoriasis. *European Journal of Dermatology*, 13(5), 471-473.



Effects of Various Drying Methods on the Vitamin C level of Papaya Locally Grown in Brunei Darussalam

Nur Amirah Hair Mustapa and Siti Rohaiza Ahmad*

PAPRSB Institute of Health Sciences, Universiti Brunei Darussalam,
Gadong BE1410, Brunei Darussalam

ABSTRACT

Papaya (*Carica papaya* L.) belongs to the *Caricaceae* family. They are grown in almost all tropical and subtropical regions in the world. In Brunei Darussalam, papaya is a non-seasonal fruit that is locally grown. It is also common to dry papaya. Drying is the process of removing water or moisture from a product with the benefit of improving shelf-life by impeding food spoilage by microorganisms. In this research, freshly ripened papaya was subjected to various drying methods and its effect on the vitamin C levels was investigated. The drying methods include sun drying (SD), oven drying (OD), freeze-drying (FD) and deep freezing (DF). Fresh samples were also investigated and acted as the control. The determination of vitamin C levels was carried out using an accredited Association of Official Agricultural Chemists (AOAC) indophenol titrimetric method. The result showed that FD samples had the highest vitamin C levels (5.84 ± 0.83 mg/100g) while SD has the least value of vitamin C (2.96 ± 0.47 mg/100g). In conclusion, the FD method resulted in highest vitamin C levels. Therefore, the FD method serves as the best industrial application with good vitamin C retention in papaya.

Keywords: Deep freezing, freeze-drying, oven drying, papaya, sun drying, vitamin C

ARTICLE INFO

Article history:

Received: 1 March 2018

Accepted: 12 September 2018

Published: 24 January 2019

E-mail addresses:

mirahhair@gmail.com (Nur Amirah Hair Mustapa)

rohaiza.ahmad@ubd.edu.bn (Siti Rohaiza Ahmad)

* Corresponding author

INTRODUCTION

Papaya is a non-seasonal fruit in Brunei Darussalam. Papaya or its botanical name *Carica papaya* Linn is commonly called pawpaw and belongs to the *Caricaceae* family (Yogiraj et al., 2014). Papaya is usually about 15 - 50 cm long, 10 - 20 cm in diameter, and weighing up to 9 kg (Ojike

et al., 2011). It is rich in orange pulp and often has orange-red, yellow-green and yellow-orange hues (Aravind et al., 2013). It has numerous seeds, small, black and covered with gelatinous aril. Papaya trees yield fruits within 5 months and can live up to 4-5 years (Orwa et al., 2009).

Drying is among the oldest methods of food preservation (Lau & Taip, 2011). The function of drying is to remove water from solids such as fruit and vegetables by evaporation or sublimation (Kurozawa et al., 2014). Drying can discharge approximately 80 - 90% of water from the fresh product and preserve large amounts of the nutrients (Kaleem et al., 2016). Drying causes reduction in water activity to lower the moisture content of foods. It also prevents the growth of microorganisms and hence reduces the rate of chemical reaction that causes spoilage (Lau & Taip, 2011). In food industries, advances in drying methods and dehydration techniques enable the preparation of a wide range of dried products and foods from fruits and vegetables.

Vitamin C is mostly found in natural products such as fruits and vegetables. Vitamin C is also known as ascorbic acid (AA) (Fatariah et al., 2015; Offor et al., 2015). Citrus fruits such as papaya are good sources of vitamin C. The edible portion of one papaya contains about 60 to 84 mg/100 g of vitamin C (Wall, 2006). In the human body, vitamin C acts as an electron donor and to stabilise tissues. It can also be oxidised to the more unstable dehydroascorbic acid and easily converted back to vitamin C through several enzyme systems such as reduced nicotinamide adenine dinucleotide phosphate (NADPH)-dependent systems. It also functions as an enzyme cofactor that maintains the iron ion in the reduced ferrous (Fe^{2+}) state required for enzyme activity (Schlueter, & Johnston, 2016). However, vitamin C can be degraded depending on variables such as temperature, pH, light, storage, exposure to oxygen, contact with minerals (iron and copper), and alkali. Thus, if vitamin C is well maintained during the food drying process, other nutrients are probably also preserved (Marques et al, 2006).

The objective of this study is to compare the impact of various drying processes which includes sun drying (SD), oven drying (OD), freeze-drying (FD) and deep freezing (DF) on the levels of vitamin C. The results offer insights into effective approaches to papaya fruit nutritive value preservation which could benefit the food manufacturing industry.

MATERIAL AND METHODS

Papaya was washed, peeled and sliced longitudinally into four pieces (5 ± 1 mm thickness) with a stainless-steel knife. The seeds were removed. A home blender was used sparingly to cut the papaya into small pieces, and a cotton cloth was used to squeeze the juice. Papaya juices were weighed, and approximately 300 g were subjected to the different drying methods (SD, OD, DF and FD). Fresh papaya fruit was also analysed and served as the control. All of the extraction was carried out in triplicate. Several precautions were taken

in order to perform the operations such as minimal light due to the instability of vitamin C. Firstly, 10 grams of fresh papaya was transferred into a 50-ml falcon tube, and its vitamin C was analysed on the same day of preparation.

For the SD method, approximately 40 grams of fresh papaya juice was weighed and spread over a metal tray, then placed on the concrete floor under the sun. Samples were subjected to SD from 08:00 to 16:00 hours (at least 8 hours). A minimum temperature of 30 - 35 °C is required with humidity below 60% (Ahmed et al., 2013). For the FD method, freeze dryer (LABCONCO) was set to dry papaya juices with total pressure and the temperature inside the vacuum chamber of -0.102 mbar and -53 °C, respectively. The FD process was carried out by placing the extracted papaya juices into a 50ml falcon tube, which were prefrozen in a -70 °C freezer overnight. The prefrozen samples were then placed inside the FD until pure crystalline ice formed and turned into a powder-like product (Ahmed et al., 2013). For FD, 10g of the extracted papaya juices was placed in each falcon tube and processed for 3 days.

For the OD method, fresh papaya juices were spread evenly on aluminium foil and placed in a conventional laboratory oven at a constant temperature of 60 °C. The drying time lasted for 24 hours to reach 10% moisture content (Workneh et al, 2012). The initial weight of the aluminium foil with papaya was noted before drying. For the DF method, 10 grams of papaya juice was added to a 50ml falcon tube and stored in a deep freezer at -70 and 80 °C for 24 hours (Alhamdan et al, 2018; Favell, 1998).

Reagents used in the study include L-Ascorbic acid (reagent grade, Sigma Aldrich), 2, 6-Dichloroindophenol (DCIP) sodium salt hydrate (BioReagent, Sigma Aldrich) and Trichloroacetic acid (CCl₃COOH) (Merck). L-Ascorbic acid (AA) is a white, odourless crystalline acidic substance with a molecular weight of 176.06 and is very soluble in water. Trichloroacetic acid is a colourless crystalline solid. Both act as a reagent in extraction and titration method. 2, 6-Dichloroindophenol (DCIP) is a dye used for analysis of vitamin C in this project (Sigma Aldrich).

For the analysis of vitamin C, a stock solution of 10% of Trichloroacetic acid (TCA) was prepared by dissolving 16.8g in a 1000ml bottle. A volume of 10ml of 10% TCA was then added to the tube containing the juice. The tubes must remain covered with aluminium foil. The solution was mixed by placing the tube on a shaker for 10 minutes. Then, the solution was homogenised using centrifugation at 4700 rpm (494 x g) for 10 minutes at 4 °C. Lastly, the supernatant was transferred to a clean 15ml Falcon tube. The supernatant was used to determine the vitamin level using the indophenol titration method. The titrimetric method used was employed in AOAC Official methods 967.21 (Kim, 2011; Vasanth Kumar et al, 2013). Titrimetric method is used due to its simplicity to determine vitamin C in fruit juices. In addition, the reaction of indophenol dye with ascorbic acid is very fast. Since papaya have orangish colour, the end-point of the titration can be easily

detected when an excess of the unreduced dye gives a rose pink color in an acid solution (Fatin Najwa & Azrina, 2017).

Recovery assay is used to confirm the accuracy of the method used. The protocol of this assay was adopted from Thermo Fisher Scientific (Thermo Scientific, 2007). In this assay, the samples were tested in three different batches. The first batch was the unspiked samples. Samples in the second batch were spiked with an ascorbic acid solution with a concentration of 6 mg/100g, and the samples in the third batch were spiked with 10 mg/100g of ascorbic acid. Each was done in triplicate.

Spiking of the sample was done by adding 1ml of ascorbic acid solution into 10g of the sample (extracted fruit juice) and then mixed. The spiked samples were then tested for vitamin C following the procedure described above. Additionally, a diluent made up of 10% TCA was spiked with a specified concentration of ascorbic acid in the second and third batches. It was further tested for vitamin C along with the other samples. The recovery percentage was calculated using the formula below:

$$\% \text{ Recovery} = \frac{\text{observed value} \left(\frac{\text{mg}}{100\text{g}} \right)}{\text{expected value} \left(\frac{\text{mg}}{100\text{g}} \right)} \times 100$$

Where,

Observed = spiked sample value

Expected = Amount spiked into sample (calculated based on assigned concentration of spiking stock and volume spiked into sample).

The results were analysed by an analysis of variance (ANOVA). One-way ANOVA was used to determine significance difference of mean value of vitamin C content ($p < 0.05$) among the samples for each method. In addition, error bars based on standard deviation is used to determine the variation of the data and not the error of the measurement (Najwa & Azrina, 2017).

RESULTS

The vitamin C content of the papaya juices was recorded in mg/ 100g of fresh weight. Figure 1 shows the bar graph presentation of the results. The result shows that a fresh sample had 5.84 mg/100g of vitamin C level. The vitamin C level in the FD samples was 8.80 mg/100g, which was significantly higher than the other drying methods, including the fresh samples. The vitamin C level in SD was 2.96 mg/100g, which was significantly lower than OD (3.44 mg/ 100g). The vitamin C levels of DF were found to be the second highest (4.56 mg/100g). These results simply mean that there was an impact on the level of vitamin C as a result of the drying. However, in this study, the vitamin C level found in papaya is lower than those previously described in the literature. The processes detailed in

this research were repeated three times and similar trends were observed. In conclusion, the levels of vitamin C were significantly different among the drying methods ($P < 0.05$) and the standard deviation error bars do not overlap.

The recovery assay measured the accuracy of the spiked sample (known amount) by comparison to the sample matrix and standard diluent techniques. The mean recovery value for the spiked sample of 6 mg/100g AA with TCA extraction method was $95 \pm 0.7\%$ (Table 1). On the other hand, the mean recovery for the spiked sample of 10 mg/100g AA was $99 \pm 1.2\%$. In summary, the TCA extraction method gave a satisfactory quantitative analysis of AA in papaya and across the range of tested concentration. It can be concluded that drying is a valid method to determine vitamin C levels.

Table 1

Recovery Assay of Papaya Vitamin C Levels

Spike level (mg/100g)	Expected (mg/100g)	Observed (mg/100g)	Recovery %
Unspiked	0.0	5.84	N.A
Low (6.0 mg/100g)	6.0	5.7	95
High (10.0 mg/100g)	10.0	9.9	99

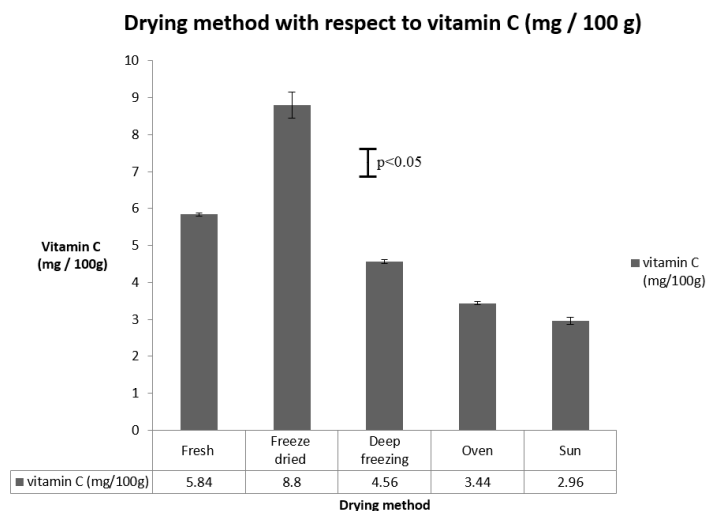


Figure 1. Level of vitamin C in mg/100g of fresh papaya and papaya that has been subjected to the various drying methods.

DISCUSSION

Several factors explain the differences in vitamin C level. It could be due to the differences in maturity stage and regional varieties of fruits (Wall, 2006). For example, male or female papaya can produce different levels of vitamin C. Differences in vitamin C levels could also be due to differences in the growing condition of the fruit (Rigi et al., 2014). For example, temperature and amount of fertiliser used in growing the plant and climatic conditions such as light can affect the vitamin C level (Tadese et al., 2014). In addition, different techniques of measuring, blending, and drying could affect the vitamin C levels of papaya (Garcia et al., 2014).

The study shows fresh papaya sample had lower vitamin C levels compared to FD papaya which could be due to the presence of moisture. Fresh papaya fruit contains about 87.67% moisture. According to the literature, the moisture content decreases with drying time (Garcia et al., 2014). Therefore, in a fresh sample, the moisture is still present, and as a result, other substance including AA is present and cause less reduction of indophenol dye. In fact, AA is the only substance in the biological material which reduces the dye (Mapson, 1942).

The FD method is recommended for drying of materials containing heat-sensitive antioxidant components such as ascorbic acid. This is because it has been found that FD products have similar characteristics to fresh products (Shofian et al., 2011). Moreover, the FD sample can preserve the nutritive value of processed products. Also, the advantage of the FD method is that it only requires low-temperature control to undergo the process (Marques et al., 2006). However, the disadvantage is its operational costs as it consumes a lot of energy and incurs costs for maintenance (Nireesha et al., 2013). Despite freeze drying retained the highest vitamin C level, freeze drying process is still expensive and limits the wide-scale application in the food industry (Ciużyńska & Lenart, 2011).

Several factors explain why the FD sample has higher vitamin C retention compared to the other methods. Previous studies have found that overnight drying preserves a larger quantity of vitamin C than day drying (Garcia et al., 2014). Secondly, high vitamin C levels were found in the dehydrated samples due to the loss of water during drying. As a result, the high vitamin C content found in the papaya slices after drying was attributed to both the evaporation of water and the reduced loss of vitamin C during the drying process (Garcia et al., 2014).

The DF method has the second highest level of vitamin C compared to the others. This shows that vitamin C is less sensitive at refrigerated storage condition (Tirkey et al., 2014). Papaya juice stored in very cold temperatures does not lose much vitamin C compared to when stored at higher temperatures. This is because vitamin C is more sensitive to hot temperature and can easily oxidise (Tadese et al., 2014). The function of freezing is to decrease the water activity and reduce enzymatic activity resulting in extending the shelf-

life of the product. During the freezing process, ice crystal is formed and cause enzymatic oxidation. The oxidation occurs due to the destruction of the cells and tissues of the product and therefore increase the contact between phenolic, oxygen and enzymes (Alhamdan et al., 2018). It can be inferred from the results of DF and FD sample that, the lower the temperature, the higher the availability of vitamin C in fruit juice. It is hence better to maintain or store vitamin C in a place below the room temperature.

For the SD method, the level of vitamin C was remarkably low compared to the other method. Papaya juices were sun-dried under varying temperatures of 24 °C – 30 °C in a day. Papaya juice was spread on a metal steel tray covered with aluminium foil and treated in open air. This could explain the low levels of vitamin C which is prone to oxidative destruction in the presence of heat, light and oxygen (Yusof et al., 2015). In addition, high temperature or exposure time of the samples during sunlight drying results in greater loss of vitamin C (Lau & Taip, 2011). This result suggests that the effect of exposure time to the air during drying was more damaging than the drying temperature itself. Thus, the low value of SD samples indicates that the vitamin C in papaya is highly sensitive to sunlight and drying.

The disadvantage of the SD method is that it is significantly slower if the air is humid. According to the finding of Santos and Silva (2008), SD is a common drying method for fruits, leaves and vegetables all over the world. One reason is that of cost. However, SD may result in poor nutrient preservation, especially for fruits having high concentrations of vitamin C (Yusof et al., 2015).

A recovery study has been conducted to confirm the validity of the method used. A standard solution of low spiked and high spiked was added to three different pre-analysed sample solutions, and the recovery of the compound was calculated. The recovery assays show that vitamin C of papaya spiked with 6 mg and 10 mg of 0.1% ascorbic acid and distilled water was successfully recovered at 95% and 99% respectively.

CONCLUSION

In this study, papaya juices were analysed for the effects of various drying methods on vitamin C levels of papaya via the AOAC indophenol method. The result showed that drying processes did have an impact on the vitamin C retention. The study also found that the most favourable drying method was FD which preserves the highest level of vitamin C. Therefore, among the various methods of drying, FD was preferred because it could be used to preserve fruits, was lightweight and increased the shelf-life of the product. The SD method is the least favourable approach as it retains the lowest amount of vitamin C.

There are some limitations to this study. The weather conditions, i.e. rain can affect the SD method. Due to rain, the papaya sample had to be discarded and the result deemed invalid causing the experiment to be repeated. Also, a portable thermohygrometer may

be useful to monitor the temperature and humidity changes. Next, according to plan, the papaya sample only needed to be squeezed using a cotton cloth. However, due to difficulty during the FD procedures, the papaya had to be blend to prevent it from producing a pungent smell during the FD processes. Lastly, to obtain more specific vitamin C measurement, high-performance liquid chromatography (HPLC) could be used to eliminate the non-polar compound such as the sugars, salt, amino acid and others. From this research, further study would be to compare the vitamin C level using titration and high performance liquid chromatography (HPLC) method.

ACKNOWLEDGEMENT

We would like to thank Universiti Brunei Darussalam for providing infrastructural and academic support to run the project.

REFERENCES

- Ahmed, N., Singh, J., Chauhan, H., Gupta, P., & Anjum, A. (2013). Different drying methods. *Their Applications and Recent Advances*, 4(1), 34–42.
- Alhamdan, A., Hassan, B., Alkahtani, H., Abdelkarim, D., & Younis, M. (2018). Cryogenic freezing of fresh date fruits for quality preservation during frozen storage. *Journal of the Saudi Society of Agricultural Sciences*, 17(1), 9-16. <https://doi.org/10.1016/j.jssas.2015.12.001>
- Aravind, G., Bhowmik, D., Duraivel, S., & Harish, G. (2013). Traditional and medicinal uses of carica papaya. *Journal of Medicinal Plants Studies*, 1(1), 7–15.
- Ciurzyńska, A., & Lenart, A. (2011). Freeze-drying - application in food processing and biotechnology - a review. *Polish Journal of Food and Nutrition Sciences*, 61(3), 165–171. <https://doi.org/10.2478/v10222-011-0017-5>
- Fatariah, Z., Tengku Zulkhairuzha, T. Y., & Wan Rosli, W. I. (2015). Ascorbic acid quantification in Benincasa hispida fruit extracted using different solvents. *International Food Research Journal*, 22(1), 208–212.
- Favell, D. J. (1998). A comparison of the vitamin C content of fresh and frozen vegetables. *Food Chemistry*, 62(1), 59–64. [https://doi.org/10.1016/S0308-8146\(97\)00165-9](https://doi.org/10.1016/S0308-8146(97)00165-9)
- Fatin Najwa, R., & Azrina, A. (2017). Comparison of vitamin C content in citrus fruits by titration and high performance liquid chromatography (HPLC) methods. *International Food Research Journal*, 24(2), 726–733.
- Garcia, C. C., Caetano, L. C., de Souza Silva, K., & Mauro, M. A. (2014). Influence of edible coating on the drying and quality of papaya (*Carica papaya*). *Food and Bioprocess Technology*, 7(10), 2828–2839. <https://doi.org/10.1007/s11947-014-1350-6>
- Kaleem, A., Nazir, H., Pervaiz, S., Iqtedar, M., Abdullah, R., Aftab, M., & Naz, S. (2016). Investigation of the effect of temperature on vitamin C in fresh and packed fruit juices. *FUUAST Journal of Biology*, 6(1), 117-120.

- Kim, Y. N. (2011). Chapter 10. Vitamins. In L. M. Nollet, & F. Toldra (Eds.), *Handbook Of Analysis of Edible Animal By-Products* (pp. 175-177). Boca Raton: CRC Press Taylor & Francis Group.
- Kurozawa, L. E., Terng, I., Hubinger, M. D., & Park, K. J. (2014). Ascorbic acid degradation of papaya during drying: Effect of process conditions and glass transition phenomenon. *Journal of Food Engineering*, 123(July), 157–164. <https://doi.org/10.1016/j.jfoodeng.2013.08.039>
- Lau, F. F., & Taip, F. S. (2011). Effects of different operating parameters in papaya halwa drying. *Pertanika Journal of Science and Technology*, 19(2), 389-396.
- Mapson, L. W. (1942). Vitamin methods. 5. A note on the determination of ascorbic acid in fruits and vegetables in the presence of SO₂. *Biochemistry Journal*, 36(1-2), 196–202.
- Marques, L. G., Prado, M. M., & Freire, J. T. (2006, May). Vitamin C content of freeze-dried tropical fruits. In *International congress on engineering and Food* (pp. 22-26). Athens, Greece.
- Nireesha, G., Divya, L., Sowmya, C., Venkateshan, N., Niranjana Babu, M., & Lavakumar, V. (2013). Lyophilization/freeze drying-an review. *International Journal of Novel Trends in Pharmaceutical Sciences*, 3(4), 87–98.
- Offor, C. E., Okechukwu, P. C. U., & Esther, U. A. (2015). Determination of ascorbic acid contents of fruits and vegetables. *International Journal of Pharmacy and Medical Sciences*, 5(1), 1–3. <https://doi.org/10.5829/idosi.ijpms.2015.5.1.1105>
- Ojike, O., Nwoke, O. O., & Okonkwo, W. I. (2011). The influence of different solar drying systems on the vitamin content of Pawpaw (*Carica papaya*). *Australian Journal of Agricultural Engineering*, 2(1), 8–11.
- Orwa, C., Mutua, A., Kindt, R., Jamnadass, R., & Anthony, S. (2009). *Carica papaya L. Agroforestry Database: a Tree Reference and Selection Guide Version 4.0*. Retrieved February 26, 2018, from http://www.worldagroforestry.org/treedb/AFTPDFS/Carica_papaya.PDF
- Rigi, S., Kamani, M. H., & Atash, M. M. S. (2014). Effect Of Temperature On Drying Kinetics, Antioxidant Capacity and Vitamin C Content Of Papaya (*Carica Papaya* Linn.). *International Journal of of Plant, Animal and Environmental Sciences*, 4(3), 413–417.
- Schlueter, A. K., & Johnston, C. S. (2016). Vitamin C : Overview and Update. *Journal of Evidence-Based Complementary and Alternative Medicine*, 16(1), 49–57. <https://doi.org/10.1177/15332101160392951>
- Shofian, N. M., Hamid, A. A., Osman, A., Saari, N., Anwar, F., Dek, M. S. P., & Hairuddin, M. R. (2011). Effect of freeze-drying on the antioxidant compounds and antioxidant activity of selected tropical fruits. *International Journal of Molecular Sciences*, 12(7), 4678–4692. <https://doi.org/10.3390/ijms12074678>
- Tadese, A., Subramanian, P. A., Woldu, A., & Pal, R. (2014). Electrochemical determination and comparison of ascorbic acid in freshly prepared and bottled fruit juices: A cyclic voltammetric study. *Journal of Chemical and Pharmaceutical Research*, 6(5), 880-888.
- Thermo Scientific. (2007). Spike-and-recovery and linearity-of-dilution assessment. *Thermo Scientific Tech Tip*, 747(815), 1–3. Retrieved February 26, 2018, from <http://scholar.google.com/scholar?hl=en&btnG=Search&q=intitle:Spike-and-recovery+and+linearity-of-dilution+assessment#0>

- Tirkey, B., Pal, U. S., Bal, L. M., Sahoo, N. R., Bakhara, C. K., & Panda, M. K. (2014). Evaluation of physico-chemical changes of fresh-cut unripe papaya during storage. *Food Packaging and Shelf Life*, *1*(2), 190–197. <https://doi.org/10.1016/j.fpsl.2014.02.002>
- Vasanth Kumar, G., Kumar, A., Patel, R., & Manjappa, S. (2013). Determination of vitamin C in some fruits and vegetables in Davanagere city, (Karanataka) -India. *International Journal of Pharmacy & Life Sciences*, *4*(3), 2489–2491.
- Wall, M. M. (2006). Ascorbic acid, vitamin A, and mineral composition of banana (*Musa sp.*) and papaya (*Carica papaya*) cultivars grown in Hawaii. *Journal of Food Composition and Analysis*, *19*(5), 434–445. <https://doi.org/10.1016/j.jfca.2006.01.002>
- Workneh, T. S., Zinash, A., & Woldetsadik, K. (2012). Blanching, salting and sun drying of different pumpkin fruit slices. *Journal of Food Science and Technology*, *51*(11), 3114–3123. <https://doi.org/10.1007/s13197-012-0835-4>
- Yogiraj, V., Goyal, P. K., Chauhan, C. S., Goyal, A., & Vyas, B. (2014). *Carica papaya* Linn: An overview. *International Journal of Herbal Medicine*, *2*(5 Part A), 1–8.
- Yusof, Y. A., Ali, M. A., Chin, N. L., & Ibrahim, M. N. (2015). Effect of different drying treatments on colour quality and ascorbic acid concentration of guava fruit. *International Food Research Journal*, *23*(December), 1–7.

Experimental Study of Hydraulic Jumps in an Inclined Rectangular Flume

Dillip K. Ghose*, Priya Mandal and Sandeep Samantaray

Department of Civil Engineering, National Institute of Technology, Silchar 788010, Assam, India

ABSTRACT

Hydraulic jumps on an inclined rectangular channel are the subject matter of this paper. The hydraulic jump is the sudden transition from a high velocity super critical flow to a subcritical flow regime in an open channel flow. The flow properties were solved using continuity and momentum principles. Laboratory experiments of hydraulic jumps in an inclined flume were conducted to verify the theoretical sequent-depth ratio, roller length and jump length. Measurements of velocities were made with an acoustic Doppler velocity meter for various Froude numbers flows. In the experiment, the bed slopes of 0.038, 0.094, 0.151, 0.210, 0.270, and 0.333 were used for measuring various flow parameters along the contour of the hydraulic jump. Results have shown that the sequent depth ratio increases with increasing the positive slope. Based on the present investigation the dimensionless length of the jump is significantly dependent on the bed.

Keywords: Bed slope, energy loss, hydraulic jump, inclined rectangular flume, sequent depth ratio

INTRODUCTION

An abrupt change from supercritical to subcritical flow is defined as a hydraulic jump. During the conversion energy is dissipated. With high turbulence, the potential break correlated with the jump has been acknowledged as the efficient method for indulgence

of energy at the downstream of hydraulic structures. Hydraulic structures need active characteristics of hydraulic jump, equivalent to specific energies. The efficiency of the jump depends upon discharge Q and energy loss E_L of the jump. An assortment of methods and empirical equations are used to validate the characteristics of flow within the specified range. Barrage/weir is

ARTICLE INFO

Article history:

Received: 16 March 2018

Accepted: 19 June 2018

Published: 24 January 2019

E-mail addresses:

dillipghose2002@gmail.com (Dillip K. Ghose)

priya3now@gmail.com (Priya Mandal)

samantaraysandeep963@yahoo.com (Sandeep Samantaray)

* Corresponding author

designed with the help of analytical equations which are valid for all probable values of discharge and energy dissipation of the jump. Tail water depth and conjugate depth vary at different discharges.

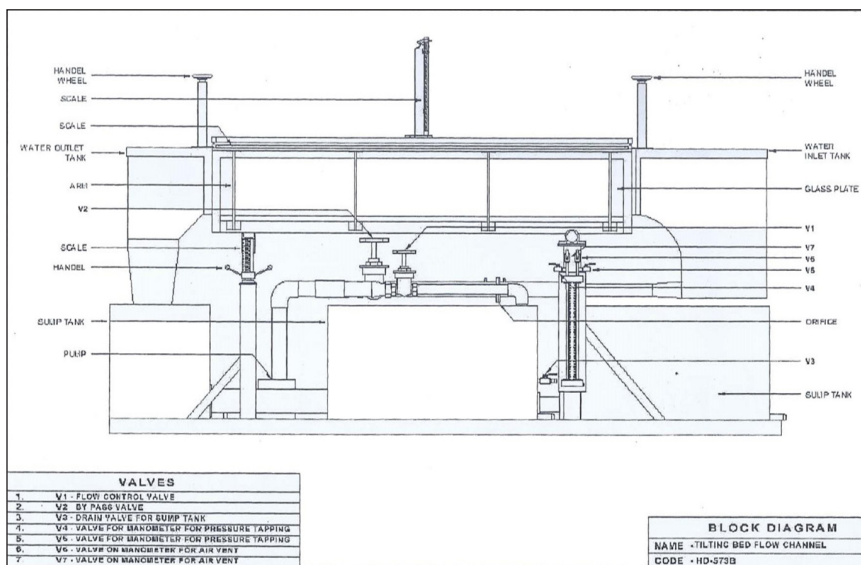
The earliest experiments on the hydraulic jump, made by Bidone, were actually done in a sloping channel (Rajaratnam, 1967). Bazin in 1865 and Beebe and Reigel in 1917 also experimented on sloping channel jumps (Rajaratnam, 1967), and in 1927 Ellms attempted a theoretical and experimental study of this problem (Rajaratnam, 1967). In 1934, Yarnell started an extensive research program with slopes of 1 in 6, 1 in 3 and 1 in 1, which was unfortunately interrupted by his death in 1937 (Rajaratnam, 1967). In 1935 Rindlaub conducted an experimental study of slopes at 8.20, 12.50, 24.20 and 300 (with the horizontal). Hager and Bremen (1990) had analysed the consequences of wall abrasion linking to sequent depth ratio. Ohtsu and Yasuda (1991) had resolved the issues related to D-jump and B-jump. Adam et al. (1993) had introduced new expressions for B-jump with Froude numbers of 2.4 to 7.4. Gunal and Narayanan (1996) had determined the variations of the mean stream flow with hydraulic jump in sloping channels. Ead and Rajaratnam (2002) had observed the range of Froude numbers from 4 to 10. Ohtsu et al (2003) had investigated undular jumps for completely built up inflow condition. Beirami and Chamani (2006) reported negative bed slope of the flow bed reduced the sequent depth ratio, and positive bed slope increased the sequent depth ratio. Carollo et al. (2007) studied effect of bed roughness on the sequent depth ratio and the roller length. Chanson (2009) had developed the recent advances in turbulent hydraulic jumps. Afzal et al., (2011) had investigated the stream flow of a turbulent hydraulic jump in a rough rectangular channel bed. Carollo et al. (2012) had studied the characteristics of classical jump and B-jumps on smooth beds. Wang and Chanson (2015) had conducted the experiments to study the fluctuation of Froude numbers ($3.8 < F_1 < 8.5$) and Reynold's number ($2.1 \times 10^4 < R < 1.6 \times 10^5$). The main objective of this study is to present an advanced assessment of the comparative studies of hydraulic properties in terms of jump parameters with variation of bed slopes, and to compare the measured versus calculated parameters associated with hydraulic jump.

METHOD

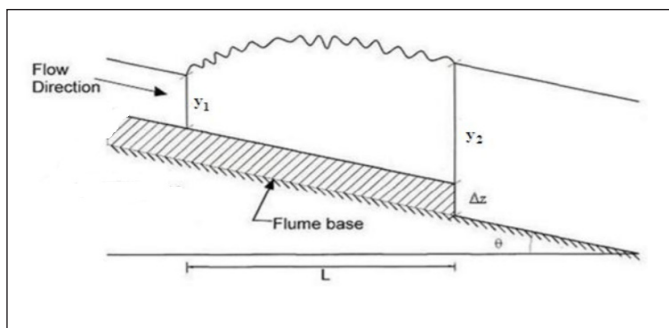
The experiment was conducted on a tilting rectangular flume of 4.90 m long, 0.308 m width and 0.50 m deep, made of stainless steel frame with smooth bed. Side walls were transparent glass sheet for visualisation of flow represented in Figures 1 and 2.



Figure 1. Photograph of Experimental setup



(a)



(b)

Figure 2. (a) Cross sectional view of experimental Tilting Flume; and (b) Schematic view of hydraulic jump (E-jump)

Experimental Procedure

The water was supplied from an inlet constant head tank through a sluice gate and discharges into water outlet tank. By controlling the tail water depth with adjustable downstream gate, the hydraulic jump was to be formed. A screw jack was located at 0.36 m distance from the downstream gate to obtain the slope of the channel. Six different bed angles 2.22°, 5.41°, 8.62°, 11.86°, 15.13°, and 18.46° respectively, were used for the laboratory experiments. Entry of water into the flume is measured with manometer. Constant head tank is used to measure the capacity of discharge. Discharge (Q), the upstream flow depth (Y_1), the downstream conjugate depth (Y_2), roller length (L_r), the horizontal distance between two section of the jump (L_j) were measured for each Hydraulic jump.

The following assumptions are considered for developing the relation between sequent depth ratio, upstream Froude number, and slope of the channel. The assumptions are: The channel is sloping, rectangular and straight. The pressure distribution is hydrostatic at both ends of the flume. Effect of turbulence is not considered during the study. The frictional resistance of sidewalls and bed of the flume are neglected.

Sequent Depth Ratio

Initial depth Y_1 is before the jump and the sequent depth Y_2 is after the jump. The sequent-depth ratio for a horizontal rectangular channel is given by the Belenger equation-

$$\frac{Y_1}{Y_2} = \frac{1}{2}(\sqrt{1 + 8F_2^2} - 1) \quad (1)$$

In an inclined channel the analysis of a hydraulic jump is done by considering the weight of water in the jump. For E-Jump the sequent depth ratio is calculated with modified Froude number by G replacing the Froude number F_1 as

$$G = \frac{F_1}{\sqrt{\cos \theta - KL_r \tan \theta / (Y_2 - Y_1)}} \quad (2)$$

L_r = roller length of the jump and; K = correction factor for the volume of the jump, and K value is calculated from equation 2.a.

$$K(\theta, F_1) = \bar{K}(\theta) - 0.05(F_1 - 3.5) \quad (2.a)$$

$\bar{K}(\theta)$ value is taken as 0.97 which is calculated from equation (Jan-Chang, 2009).

K and $L_r / (Y_2 - Y_1)$ vary through F_1 and G depends on F_1 and θ . Hence the modified sequent depth ratio is given by

$$\frac{Y_1}{Y_2} = \frac{1}{2}(\sqrt{1 + 8G^2} - 1) \quad (3)$$

Length of the Jump

To estimate the length of the jump analysis of energy dissipation is required for which length of the apron is to be measured. Length of the jump, L_j is the horizontal distance around the roller of jump or from the toe of jump to the section where the water surface becomes levelled after reaching the utmost depth. Hydraulic jump involves its length of jump L_j as the distance between two cross sections of the sequent depths Y_1 and Y_2 . No bed protection is necessary for jump length beyond the downstream side of the hydraulic jump. The jump length is difficult to analyse during experiment because of hydraulic jump formation and fluctuation of surface waves merged with turbulence.

Roller Length

The roller length (L_r) is the horizontal distance between the toes of the jump to the section where the flow depth reached a value of 98% of the tail water depth. This length is determined by visualization and with a float to localize the stagnation point.

The relationship between the roller length and sequent depth ratio is given as

$$\frac{L_r}{Y_1} = \frac{L_r}{Y_2 - Y_1} \left(\frac{Y_2}{Y_1} - 1 \right) \quad (4)$$

Dimensionless Length

Dimensionless length of the jump is defined by ratio of length to the difference between the sequent depths. Dimensionless length is denoted as L_d .

$$L_d = 6.9(\eta - 1)\exp(-3.7 \tan \theta) \quad (5)$$

Where η is the sequent depth ratio.

RESULTS AND DISCUSSION

Experimental investigations were conducted with different flow conditions ranging as follows. For Froude number ranging from 1.01 to 3.75, six slopes of the channel (2.22°, 5.41°, 8.62°, 11.86°, 15.31°, and 18.64°) were used. The discharges were varied accordingly with different slopes and gate openings to achieve the required range of inflow Froude number. Initial depth, sequent depth, discharge, average velocity and jump length were measured for the analysis.

The Important macroscopic parameters are initial depth (Y_1), sequent depth (Y_2), Initial mean velocity (V_1), mean velocity at the Table 1 presents the experimental investigation of hydraulic jump of previous researchers. In this study it is found that Froude number varies from 1.01 to 3.75 with the channel width 0.308 m, whereas the longitudinal distance of the toe jump from the upstream gate is 1.97 m to 4.07 m and the upstream flow depth ranges from 0.015 m to 0.303 m.

Table 1
Details of previous and present study experimental investigation of hydraulic jumps

<i>Previous work</i>	<i>Width of channel(m)</i>	<i>Longitudinal distance of the jump toe from the upstream gate(m)</i>	<i>Upstream flow depth(m)</i>	<i>Froude number</i>
Resh et al. (1974)	0.39	0.39-7.8	0.012-0.039	3.0-8.0
Babb & Aus (1981)	0.465	-	0.035	6.0
Long et al. (1991)	0.47	0.04-0.08	0.025	4-9
Liu et al. (2004)	0.46	0.1	0.041-0.071	2.0-3.3
Lennon & Hill (2006)	0.30	-	0.02-0.031	1.4-3.0
Valle & Pasternack (2006)	2	-	0.22	2.8
Chanson (2007)	0.25 and 0.50	0.50 and 1	0.013-0.029	5.1-8.6
Murzyn et al. (2007)	0.30	0.18-0.43	0.021-0.059	1.9-4.8
Wang & Chanson (2015)	0.50	0.80-1.87	0.012-0.047	3.8-8.5
Present study	0.308	1.97-4.07	0.015-0.030	1.01-3.75

Analysis of the Sequent Depth Ratio

Experimental runs were carried out to study the relationship among hydraulic jump, sequent depth ratio (η) and bed slope (S). Also the relationship between sequent depth ratio and Froude number were evaluated. The calculated and measured values for sequent depth ratio are plotted in Figures 3 and 4 against upstream Froude number (F_1).

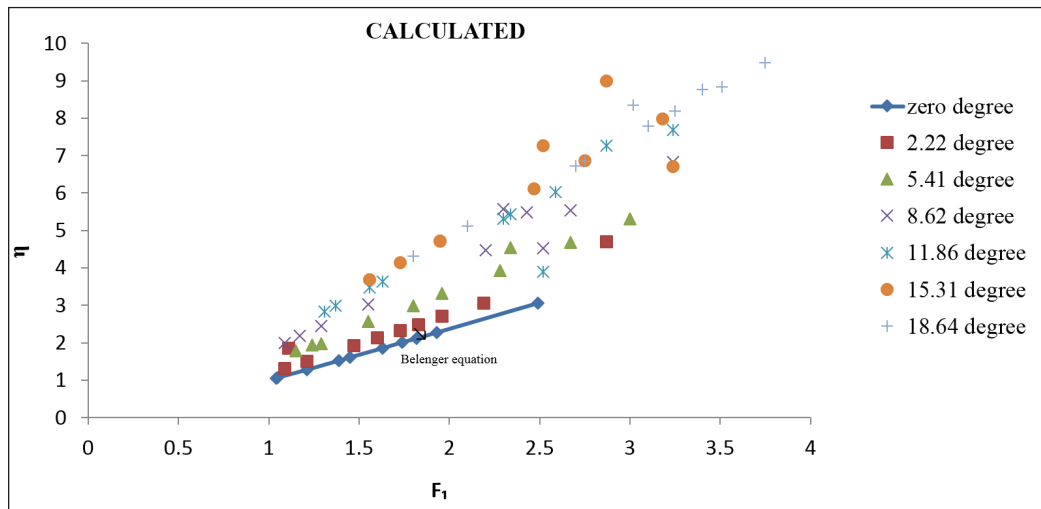


Figure 3. Comparison of variation of the calculated sequent depth ratio with upstream Froude number at different tilting angle

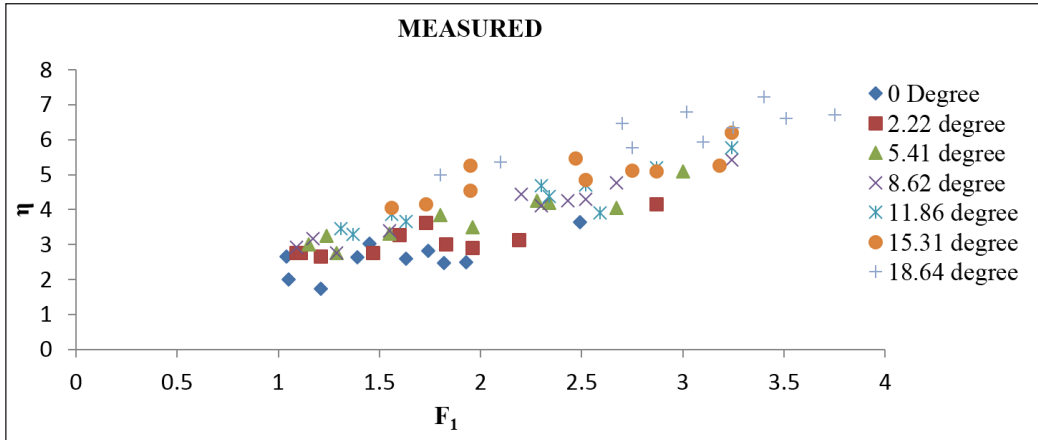


Figure 4. Comparison of variation of the calculated sequent depth ratio with Upstream Froude number at different tilting angle

Analysis of Hydraulic Jump Length

It is necessary to estimate the length of the jump through length of apron for energy dissipation. The length of the jump is the horizontal distance just about the roller of jump or from the toe of jump to a section where the water surface levels after reaching the maximum depth. The experimental runs were carried out to investigate the variation of the hydraulic jump with bed slope in present and past study made by Jan-Chang (2009) drawn in Figure 5. The present experimental data for ratio of roller length jump to pre hydraulic jump depth (L_r/Y_1) against sequent depth ratio (η), are plotted in Figure 6. The average values of L_d is evaluated as 2.50, 3.93, 4.86, 5.97 and 6.90 respectively and are presented in Table 3.

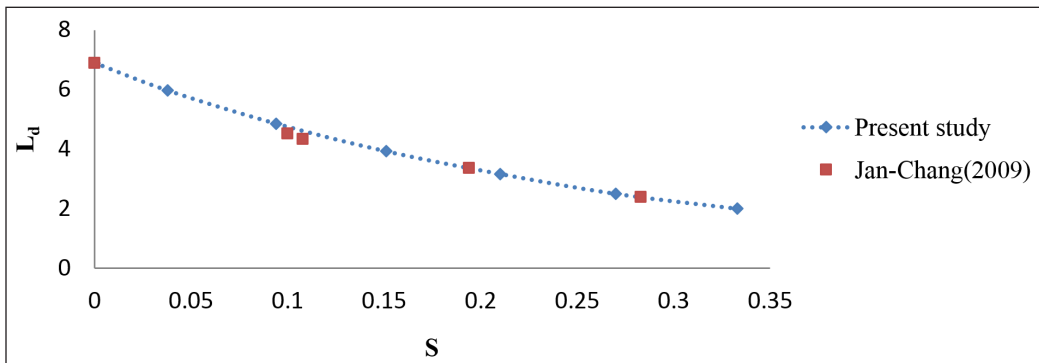


Figure 5. Comparison of relationship between dimensionless length of the Hydraulic Jump and flume bed slope

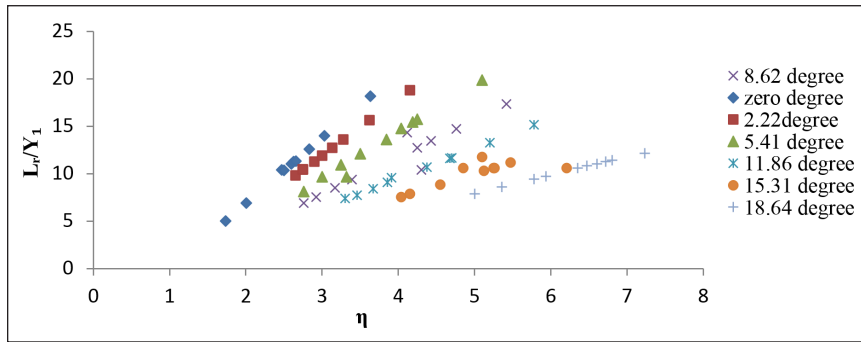


Figure 6. Comparison of ratio of Roller Length to pre hydraulic jump depth with Sequent Depth Ratio

Table 2

Experimental Results for Flows and computed hydraulic jump characteristics in the horizontal channel bed at different angles

Sl. No	Tilting angle	Mean measured roller length, L_r (m)	Mean Jump length, L_j (m)	Mean up-stream Froude number (F_1)	Mean calculated sequent depth ratio (η)	Mean calculated roller length, L_r (m)
1.	0°	0.2764	0.7728	1.575	1.783	0.3012
2.	2.22°	0.2996	1.1385	1.706	2.241	0.3231
3.	5.41°	0.3114	1.0238	1.928	3.304	0.3053
4.	8.62°	0.2591	0.261	0.9756	2.046	4.204
5.	11.86°	0.2284	0.2271	0.9605	2.173	4.854
6.	15.13°	0.2017	0.2012	1.2869	2.422	6.115
7.	18.46°	0.1937	0.1937	2.938	7.443	0.1835

Table 3

Calculation of dimensionless length of jump

Sl. no	Angle of flume bed (Degree)	Slope of channel Bed (S)	Dimensionless length of hydraulic Jump (L_d)
1.	0°	0.000	6.90
2.	2.22°	0.038	5.97
3.	5.41°	0.094	4.86
4.	8.62°	0.151	3.93
5.	11.86°	0.210	3.17
6.	15.31°	0.270	2.50
7.	18.46°	0.333	2.00

Dimensionless length of the jump is computed as ratio of hydraulic jump length to the difference between the sequent depths. From Figure 6, it is observed that as the bed slope increases the dimensionless length decreases and hence the height of jump (difference between post jump depth and pre-jump depth) decreases. The dimensionless length is highest with 6.9 at horizontal bed of the channel. As the bed slope increases and reaches

at 0.05, the L_d become 6 and decreases gradually up to bed slope 0.35. The value of L_d of tilting flume is lowest at slope 18.46° and highest in horizontal bed of the flume at slope 0° . Based on the experimental result it is found that, the value of L_d is considerable and dependent on tilting angle θ . The jump in a tilting flume of higher slope has little effect on length of jump.

Figure 7 represents the comparison of dimensionless jump length with Froude number at various tilting angle. The theoretical values of jump height for tilting angle ranging from 2.22° , 5.41° , 8.62° , 11.86° , 15.13° , and 18.46° are 5.97, 4.86, 3.93, 3.17, 2.5 and 1.98 respectively. The dimensionless jump length varies with variation of bed angles significantly and it is observed that 2.22° maximum variations occur and Froude number varies abruptly.

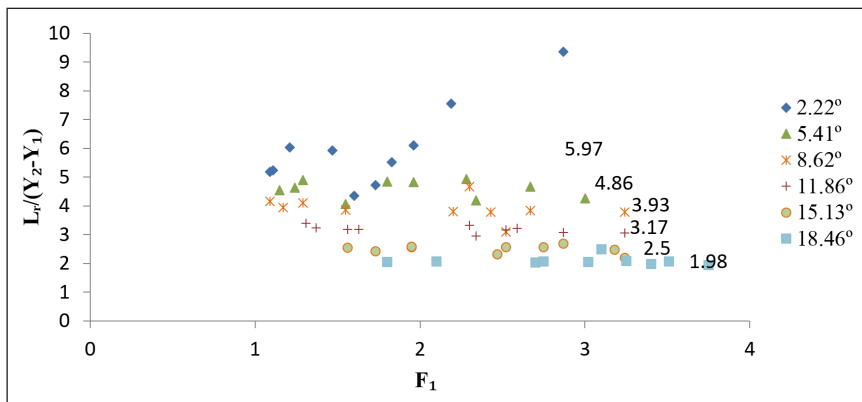


Figure 7. Dimensionless jump lengths versus approach Froude number at various flume bed angles

In this study the length of the jump means roller length of jump. In some instances of visual observation the jump was stabilized at upstream of the end sill. With a change in the Froude number, the roller length of the jump was also varied. This experimental runs were carried out to investigate the variation of the hydraulic jump length with the initial Froude's number as represented in figures. Froude number has linear relationship with L_r/Y_1 . The variation of jump length in different bed slopes with Froude number at various tilting angle are presented in Figure 8.

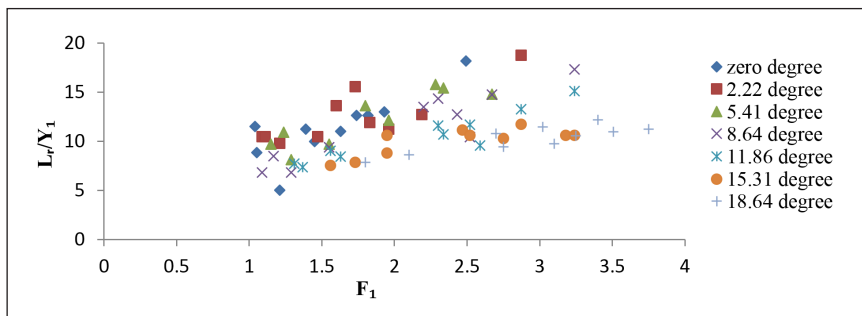


Figure 8. Comparison of variation of jump length in different bed slopes with Froude number

CONCLUSION

Design of hydraulic jump in stilling basins depends on combination of practical experience, theoretical analysis, and model studies. Laboratory tests are conducted here, to study the characteristics of hydraulic jump of a tilting flume of 4.90 meter long and 0.308 m breadth with Froude number ranges from 1.01 to 3.75. Experiments conducted in this study are to verify the theoretical equation for sequent depth ratio, roller length of the jump, and effective jump length. It is found that the values of the sequent depth ratio increases as the slope increases. At bed slope 18.64°, the sequent depth ratio is highest. The values of sequent depth ratio (η) for 2.22°, 5.41°, 8.62°, 11.86°, 15.13° and 18.46° are found to be limited within a range of 3.27% to 28.17%, 8.90% to 52%, 27.6% to 55%, 28.8% to 61.9%, and 44% to 70.6% respectively. Comparisons of the variation of Froude Numbers (calculated sequent depth ratio) and Froude Numbers (observed sequent depth ratio) with bed slope were made. The experimental measurement shows that as the bed slope increases, the Froude's number also increases with incremental variation of sequent depth ratios. The significance of result improves the design of hydraulic structures at laboratory condition to field condition. Variation characteristics of hydraulic jump will enable the designer to predict the required tail-water depth when the sequent depth ratio is known. Increasing the tail-water depth to the sequent depth will increase the stability of the jump. At bed slope 0°, 2.22°, 15.31°, the coefficient of determination and correlation coefficient differs much between calculated sequent depth ratio and measured sequent depth ratio. At bed slope 8.62° the calculated and measured value agrees closely and represents the best scenario for representing the perfect characteristics of hydraulic jump. The mean error for slope is 13.63% and the highest error is obtained for the slope of 2.22° in tilting flume. As the bed slope increases, the dimensionless length decreases and hence the height of jump decreases.

REFERENCES

- Afzal, N., Bushra, A., & Seena, A. (2011). Analysis of turbulent hydraulic jump over a transitional rough bed of a rectangular channel: Universal relations. *Journal of Engineering Mechanics*, 137(12), 835-845.
- Ahmed, M. A., Ruff, J. F., Ghassan, A. Q., & Steven, R. A. (1993). Characteristics of B-jump with different toe locations. *Journal of Hydraulic Engineering*, 119(8), 938-948. doi: 10.1061/(ASCE)0733-9429(1993)119:8(938)
- Babb, A. F., & Aus, H. C. (1981). Measurement of air in flowing water. *Journal of the Hydraulics Division*, 107(12), 1615-1630.
- Bakhmeteff, B. A. (1932). *Hydraulics of open channels*. New York: McGraw-Hill.
- Beirami, M. K., & Chamani, M. R. (2006). Hydraulic jumps in sloping channels: Sequent depth ratio. *Journal of Hydraulic Engineering*, 132(10), 1061–1068. doi: 10.1061/(ASCE)HY.1943-7900.0000100

- Carollo, F. G., Ferro, V., & Pampalone, V. (2007). Hydraulic jumps on rough beds. *Journal of Hydraulic Engineering*, 133(9), 989–999. doi: 10.1061/(ASCE)HY.1943-7900.0000036
- Carollo, F. G., Ferro, V., & Pampalone, V. (2012). New expression of the hydraulic jump roller length. *Journal of Hydraulic Engineering*, 138(11), 995-999. doi: 10.1061/(ASCE)HY.1943-7900. 0000634
- Chanson, H. (2007). Bubbly flow structure in hydraulic jump. *European Journal of Mechanics B, Fluids*, 26(3), 367-384.
- Chanson, H. (2009). Current knowledge in hydraulic jumps and related phenomena: A survey of experimental results. *European Journal of Mechanics B/Fluids*, 28(2), 191–210.
- Chow, V. T. (1959). *Open channel hydraulics*. New York: McGraw-Hill.
- Ead, S. A., & Rajaratnam, N. (2002). Hydraulic jumps on corrugated beds. *Journal of Hydraulic Engineering*, 128(7), 656–663. doi:10.1061/ (ASCE) 0733-9429(2002)128:7(656)
- Gunal, M., & Narayanan, R. (1996). Hydraulic jump in sloping channels. *Journal of Hydraulic Engineering*, 122(8), 436–442.
- Hager, W. H., & Bremen, R. (1989). Classical hydraulic jump: Sequent depths. *Journal of Hydraulic Research*, 27(5), 565–585. doi: 10.1061/(ASCE)HY.1943-7900.0000036
- Lennon, J. M., & Hill, D. (2006). Particle image velocity measurements of undular and hydraulic jumps. *Journal of Hydraulic Engineering*, 132(12), 1283-1294.
- Liu, M., Rajaratnam, N., & Zhu, D. Z. (2004). Turbulence structure of hydraulic jumps of low Froude numbers. *Journal of Hydraulic Engineering*, 130(6), 511-520.
- Long, D., Rajaratnam, N., Steffler, P. M., & Smy, P. R. (1991). Structure of flow in hydraulic jumps. *Journal of Hydraulic Research*, 29(2), 207-218. doi: 10.1080/00221689109499004
- Murzyn, F., Mouaze, D., & Chaplin, J. R. (2007). Air–water interface dynamic and free surface features in hydraulic jumps. *Journal of Hydraulic Research*, 45(5), 679-685.
- Ohtsu, I., & Yasuda, Y. (1991). Hydraulic jump in sloping channels. *Journal of Hydraulic Engineering*, 117(7), 905–921. doi: 10.1061/(ASCE)HY.1943-7900.0000533
- Ohtsu, I., Yasuda, Y., & Gotoh, H. (2003). Flow conditions of undular hydraulic jumps in horizontal rectangular channels. *Journal of Hydraulic Engineering*, 129(12), 948-955. doi:10.1061/ASCE)HY.1943-7900.0000374
- Rajaratnam, N. (1967). Hydraulic Jumps. In V. T. Chow (Ed.), *Advances in Hydro Science* (Vol. 4, pp. 197-280). New York: Academic Press. doi:10.1139/111-072
- Resch, F. J., Leutheusser, H. J., & Alemu, S. (1974). Bubbly Two-Phase Flow in Hydraulic Jump. *Journal of the Hydraulics Division*, 100(HY1), 137–149.
- Vallé, B. L., & Pasternack, G. B. (2006). Submerged and unsubmerged natural hydraulic jumps in a bedrock step-pool mountain channel. *Geomorphology*, 82(1-2), 146-159.

Wang, H., & Chanson, H. (2015). Experimental study of turbulent fluctuations in hydraulic jumps. *Journal of Hydraulic Engineering*, 141(7), 04015010.

Wang, H., & Chanson, H. (2015). Experimental study of turbulent fluctuations in hydraulic jumps. *Journal of Hydraulic Engineering*, 141(7), 04015010. doi: 10.1061/(ASCE)HY.1943-7900.0001010

Yarnell, D. L. (1934). *Bridge piers as channel obstructions* (No. 442). US Dept. of Agriculture. Retrieved October 23, 2017, from www.sciencedirect.com/science/article/pii/S016756480870443X.

Flow Measurement in Huma Tail distributary of Hirakud Command Area, India using Chiu's Equation

Ashutosh Rath¹, Sandeep Samantaray^{2*} and Prakash Chandra Swain¹

¹Department of Civil Engineering, VSS University of Technology, Burla 768018, Odisha, India

²Department of Civil Engineering, NIT, Silchar 788010, Assam, India

ABSTRACT

The present work provides a new methodology for the flow measurement in a lined canal Huma tail distributary of Hirakud canal system, Odisha, India. The acoustic Doppler velocity meter was used for the direct measurement of velocity over full area and the length of canal. The entropy based Chiu's equation is used in the present work to find out a constant ratio between the average and the peak velocity of the channel. The location for maximum value is found from the velocity profile. Applying the constant ratio, the mean velocity can be obtained at various sections. With the measured cross sectional area and the mean velocity the discharge can be found. The maximum velocity is a technically important parameter always consists of a single value regardless of the flow conditions, and a cross-sectional shape. Thus the maximum velocity can be applied to estimate the mean velocity. In this work a formula based on the entropy concept has been used to find out the maximum velocity. The accuracy was verified using 13 sets measured with the help of ADV flow tracker. A comparison of the velocity estimated with the value actually measured showed very high accuracy

Keywords: ADV flow tracker, Chiu's equation, discharge, entropy, natural stream

INTRODUCTION

The major challenges ahead of the Irrigation Associations, which are responsible for proper distribution of water, are to meet the farmers' demand as per their needs. The discharge measurements are considered seriously to ensure the availability of water for its proper distribution. Decisions are frequently made with less than adequate information. The water resource systems is

ARTICLE INFO

Article history:

Received: 04 April 2018

Accepted: 02 November 2018

Published: 24 January 2019

E-mail addresses:

samantaraysandeep963@gmail.com (Sandeep Samantaray)

erashutoshrath@gmail.com (Ashutosh Rath)

pswain.vssut@hotmail.com (Prakash Chandra Swain)

* Corresponding author

full of uncertainty so many times it is based on experience, judgment of the professional people, hit and trial methods and probabilistic methods. To describe the random behavior of water resource systems, in most cases, sufficient data are not available. To eliminate such problem and to find the least-biased probability distributions with inadequate data, the entropy theory can be applied effectively. The concept of entropy is highly acceptable in developing countries. In near past the entropy theory had been implemented to deal with various problems related to the water resources.

Chiu and Lin (1983) studied methods to compute the flow in three dimensional. Singh and Rajagopal (1987) made a study on application of the Principle of Maximum Entropy (POME) to obtain the derivation of some frequency distributions. Chiu and Chiou (1988) proposed the methodology to apply the entropy and probability concepts in hydraulic systems. Chiu (1989) research are based on finding the velocity distribution in various open-channel flow. Barbe et al. (1991) formulated the solution to find velocity distribution using entropy. Chiu and Murray (1992) made a study based on velocity distribution for a non-uniform open-channel flow. Chiu and Said (1995) studied methods to determine the peak and average velocities for a channel flow and to find the entropy in that flow. Moramarco et al. (2004) made a study on procedures to estimate the average velocities in natural streams basing on Chiu's entropy theory. Chiu and Hsu (2006) discussed about probabilistic approach for the modeling of velocity distributions in fluid flows. Marini et al. (2011) discussed the entropy approach for 2D velocity distribution in open-channel flow. Singh et al. (2013) made a study on 2D power-law velocity distribution with entropy. This study determined the discharge using the entropy based theory and comparison with the data measured using ADV. The Huma tail distributary of Hirakud canal system has been selected for the study. The canal system plays an important role for the supply of water in irrigation. Proper crop planning can be made by knowing the exact amount of flow available in canal during various seasons. Since the direct measurement of discharge in a canal is time consuming, the Chiu's equation can be applied with accuracy to find out the discharge in the canal. The people in the study area are mostly tribal and they depend on agriculture. The productivity rate of fields under consideration has decreased due to the rise in the ground water table caused by the flooding method of irrigation at the head reach of canal. Another problem is coming into consideration that people adopted a particular crop in a particular field. They were not adopting the crop rotation due to which the quality of soil decreased and thus crop losses faced by the farmers. Water is available but due to lack of irrigation management people were facing crop losses and leading to less efficiency in water use. Thus there is a scope of management of irrigation and getting of maximum yield from a particular field. This type of study will assist them for the proper crop planning and crop rotation.

MATERIALS AND METHODS

The velocity distribution as suggested by Chiu is based on Principle of Maximum Entropy (POME) to maximize the Shannon entropy. Chiu proposed another system ξ - η based on the velocity isovels against the Cartesian coordinates y - z to develop the entropy-based velocity distribution. Once the equation of ξ , which is a function of y and z is determined, the equation of η can be derived. The equation to determine the value of ξ value in the y -axis is given by

$$\xi = \frac{y}{D-h} \exp \left(1 - \frac{y}{D-h} \right) \tag{1}$$

The value of the y represents the vertical distance from the channel bed; D stands for the water depth along the y -axis; and h indicates the location of maximum velocity. The variations in velocity of flow with depth and width indicates the time-averaged and, therefore, time invariant velocity on an isovel, which is assigned a value ξ . The value of u is almost zero at ξ which corresponds to the channel boundary and u reaches u_{max} at ξ_{max} which may occur at or below the water surface. The value of u increases from ξ_0 to ξ_{max} monotonically. At any value of the spatial coordinate having value less than ξ , the velocity is less than u , which can be presented in the cumulative distribution function as

$$F(u) = \frac{\xi - \xi_0}{\xi_{max} - \xi_0} \tag{2}$$

The Shannon entropy of velocity distribution can be written as:

$$H = - \int_0^{u_{max}} P(u) \log P(u) du \tag{3}$$

Where u = value of velocity at a specified point, and u_{max} = the maximum velocity of the cross section. Chiu's velocity distribution is presented as

$$u = \frac{u_{max}}{M} \ln(1 + (\exp(M) - 1)F(u)) = \frac{u_{max}}{M} \ln(1 + (\exp(M) - 1) \frac{\xi - \xi_0}{\xi_{max} - \xi_0}) \tag{4}$$

u_{max} indicates the maximum velocity at, or below the water surface. The dimensionless parameter M is used as an index for characterization and comparison of various patterns of velocity distribution and state of flow systems. M is given as:

$$M = \ln \frac{P(u_{max})}{P(0)} \tag{5}$$

M can be used as a measurement of uniformity of probability and velocity distributions. The value of M can be determined by the mean and maximum velocity values derived from the following equation:

$$\frac{\bar{u}}{u_{\max}} = e^M (e^M - 1)^{-1} - \frac{1}{M} \tag{6}$$

With known value of M for a certain cross-section, the mean velocity can be estimated from the equation. It is natural that u_{\max} , the location for the occurrence is usually at the center of the cross section. In the present study the shape of irrigation canals is rectangular and symmetrical. So it is easy to establish the location of the y-axis in an irrigation canal is taken as with the help of constructing a set of isovels. Further in this study the discharge measurement is done with the help of ADV. Thus the maximum velocity and the mean velocity are determined using eq (6). The cross-sectional area of the channel can be estimated as:

$$A_{\text{est}} = WD \tag{7}$$

W, D represent the width and depth of the canal
 The discharge for the canal can be estimated as:

$$Q_{\text{est}} = u_{\max} WD \left[e^M (e^M - 1)^{-1} - \frac{1}{M} \right] \tag{8}$$

$$q_i = \left(\frac{v_i + v_{i+1}}{2} \right) a_i, \text{ where } a_i = d_i \times b_i \tag{9}$$

a_i is the cross sectional area of the segment i; the depth of water given by d_i where b_i is the distance from the reference point to the observed verticals i; q_i ; and v_i represent the discharge and the mean velocity at the observed vertical i.

$$A_{\text{obs}} = \sum_0^n a_i \text{ and } Q_{\text{obs}} = \sum_0^n q_n \tag{10}$$

The mean velocity on the vertical is:

$$\bar{v}_i = \frac{u_{\max}}{M} \int \ln \left[1 + (e^M - 1) \frac{\xi}{\xi_{\max}} \right] d\xi \tag{11}$$

Flow Tracker

Acoustic Doppler Velocimetry (Flow Tracker), SonTek/YSI (Figure 1) is the instrument used to measure the surface freshwater discharge in open channels. The principle on which the instrument works is it measures stream velocity by sensing the phase change caused by the doppler shift in acoustic frequency that occurs when a transmitted acoustic signal reflects off by the sediment particles in the flow. Measurements were performed by measuring the velocity of particles in a remote sampling volume based upon the Doppler shift effect. The ADV instrument consists of receivers to record the velocity components, strength of signals.

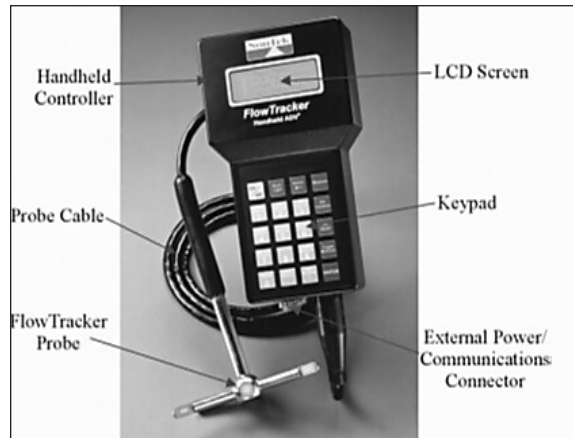


Figure 1. Various components of Flow Tracker with 2D Probe (Source: Google)

The ADV is a single point biostatic Doppler current meter. It provides 3-D velocity measurements in a remotely sampled volume. The ADV transmitter generates sound and the receivers are most sensitive to sound coming from a slightly broader angular range. The transducers are mounted such that their beams intersect over a sampling volume located some distance away. The size of the ADV sampling volume is mainly determined by two factors: the length of the transmitted pulse and receiving window. Both are controlled by the ADV software (within the limits of the transducer bandwidth). There are three types of ADV mainly 16-MHz Micro ADV, 10 MHz ADV, 5 MHz ADV. The standardized height of the sampling volume for the 16-MHz Micro ADV is 4.5 mm, for the 10 MHz ADV is 7.2 mm and for the 5 MHz ADV ocean probe is 14.4 mm.

The amplitude of received signal is also important for accurate velocity measurements although velocity measured by ADV is derived from phase. The strength of the signal return depends on the amount and type of particulate matter in water inside the sampling volume. If the water is too clear, the returned signal may not be stronger than the ambient electronics noise level thus reducing the accuracy of the velocity measurements. The discharge calculation have been done at 13 different sections of Huma tail distributary. The canal has rectangular cross section with partially lined. The velocity of flow is measured at different locations such as 0.2B, 0.4B, 0.6B and 0.8B from left side of the bank. The SENSOR was placed at different depth such as 0.2D, 0.4D and 0.8D. Total 12 readings in a cross section were taken in the channel. The average width of the canal varies from 1.5 to 1.65 meter and the depth of flow varies from 0.8 to 1.32 m.

Signal-to-Noise Ratio (SNR) are important for an accurate measurement of the flow velocity. SNR measures the intensity of the reflected acoustic with respect to the noise level of the instrument. It reflects the concentration of the water and size of sediment particles that reflect the acoustic signal. SNR was recorded for each beam with each 1s sample.

According to the manufacturer, the Flow Tracker can be applied to measure the velocity in a shallow water depth of about 3 cm with a velocity ranging from 0.001 to 4.50 m/ s with almost full accuracy.

Study Area

Hirakud Dam is built across river Mahanadi at about 15 km. upstream of Sambalpur town in State of Odisha. The project provides 155,635 hectares of Kharif and 108,385 hectares of Rabi irrigation of Sambalpur, Bargarh, Bolangir, and Subarnpur. The water released through power house irrigates further 436,000 hectares areas of Cultural command area (CCA) in Mahanadi delta. Installed capacity for power generation in 307.5 MW through its two power houses at Burla, at the right bank to and Chiplima at 22 km downstream of dam. Besides, the project provides flood protection to 9500 sqkm of delta area in district of Cuttack and Puri. Hirakud dam receives water from 83,400 sq. km of Mahanadi catchment. The reservoir has storage of 5818 million cubic meter with gross capacity of 8136 million cubic meter. In this study the command area of Huma tail distributary of Hirakud Irrigation system is selected for experimentation. The average annual rainfall of the command area is found to be approximately 1100 mm, out of which approximately 90% is received during monsoon season (mid-June to mid-October). The major crops are paddy, wheat, pulses like arhar, green gram and black gram, oilseeds like groundnuts, til and mustard, and sugarcane. Paddy is the most dominant crop. The study area is depicted in Figure 2.

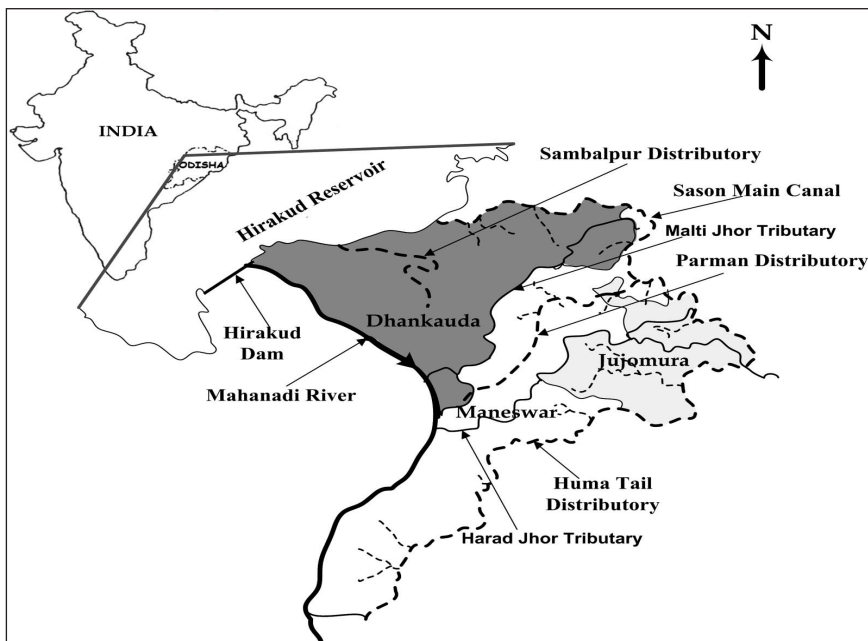


Figure 2. Ayacut Map of the Huma tail distributary system

RESULTS AND DISCUSSION

The accuracy of the entropy-based discharge estimation was established in this work by conducting various experimental and field data. Velocity data from various sections of Huma tail distributary were collected by flow tracker as depicted in Table 1. These data were used to build the velocity distribution curves as shown in Figure 3 and velocity isovels shown in Figure 4 at the measured sections.

Table 1
Discharge data at different stations as obtained from ADV flow tracker

Distance from start of canal distributary (m)	Discharge (m ³ /sec)	Distance from start of canal distributary (m)	Discharge (m ³ /sec)	Distance from start of canal distributary (m)	Discharge (m ³ /sec)
START	0.838	4850	0.618	9800	0.1792
700	0.807	5700	0.609	13500	0.1576
1500	0.799	6450	0.551	16000	0.0894
3000	0.728	7500	0.497	17000	0.0472
4300	0.687	7950	0.428		

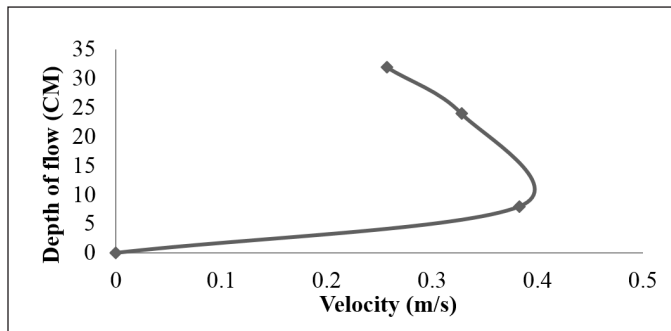


Figure 3. Velocity distribution of a section of canal along the depth of canal at R.D(0.560 Km from the start of canal)

The discharge calculations have been done at 13 different sections of the distributary. The canal has rectangular cross section with is partially lined with proper gradient. The velocity of flow was measured at different locations such as 0.2B, 0.4B, 0.6B and 0.8B from left side of the bank. The SENSOR was placed at different depth such as 0.2D, 0.4D and 0.8D. The average width of the channel is 3.2 m and the average depth is 0.9 m. Since it is a lined channel the contribution of sediments particle is not significant. From the velocity profiles plot at Figures 3 and 4, plotted with the help of MATLAB software. It is observed that maximum velocity occurs at depth of 0.2d to 0.4d. At depth near the surface (0.8d) velocity is minimum and near the bed (1.0d) it is zero. This is acceptable, since

the near bed region is more affected by the shear stress than the higher region. Generally, maximum velocity occurs at a certain distance below the water surface. This decrease in maximum velocity where surface velocities are less than the maximum velocity is due to secondary currents and is a function of the aspect ratio (ratio of depth to width) of the channel. Thus for a deep narrow channel, the location of the maximum velocity point will be much lower from the water surface than for a wider channel of same depth. This location of the maximum velocity point below the surface has nothing to do with the wind shear on the free surface.

Figure 4 shows the plot of velocity in the Huma tail distributary. It is clear that the maximum velocity occur at mid of the section.

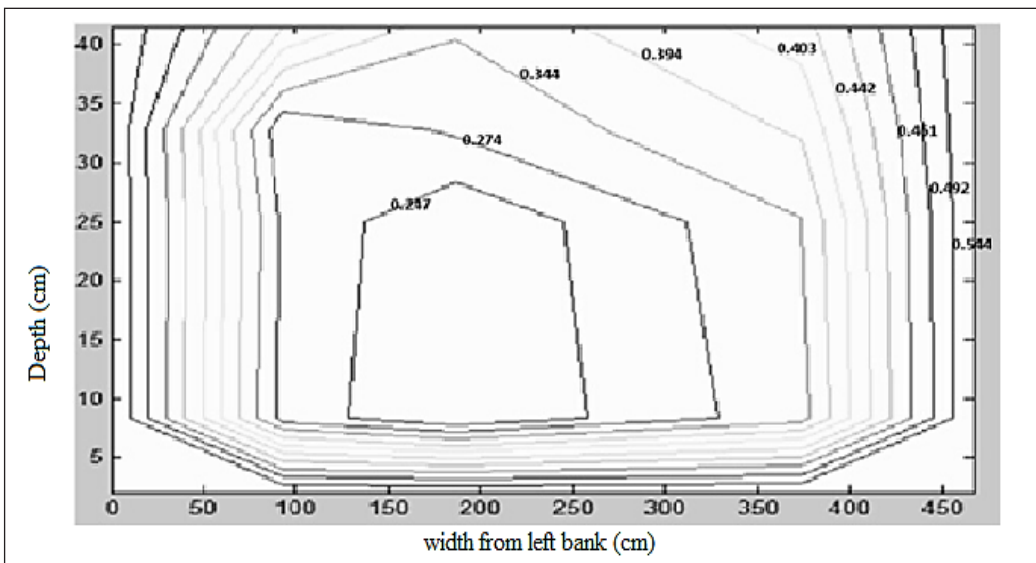


Figure 4. Isovels of the section of Huma tail distributary at RD. 0.560

Computation of Mean Velocity using Chiu’s Equation

Using data collected for each channel section the cross sectional mean velocity is calculated. The parameter of probability distribution M is calculated from the following equation. From the observed mean and maximum velocity the constant ratio Φ is first calculated and parameter M is calculated from the constant ratio.

$$\frac{\bar{u}}{u_{\max}} = e^M (e^M - 1)^{-1} \cdot \frac{1}{M} = \Phi \tag{12}$$

The variable ξ can be calculated from the eq. (1). The comparison between the maximum observed velocity and mean velocity obtained from the entropy theory are described in the Table 2.

Table 2
 Comparison of maximum observed velocity and mean estimated velocity in Huma tail distributary

Mean velocity of flow (u_{mean})	Maximum velocity of flow (u_{max})	Ratio between observed u_{mean} and u_{max} (Φ)	Parameter of probability distribution (M)	Variable's depends on depth (ξ)	ξ_{max}	u_{est}	$u_{\text{mean est.}}$
0.6751	0.7022	0.965	0.3532	0.971 0.8440 0.2921	0.9701	0.7020 0.6231 0.2390	0.5211
0.366	0.61	0.6	0.22	0.97 0.8 0.292	0.97	0.61 0.51 0.198	0.439
0.754	0.812	0.92	0.338	0.97 0.844 0.292	0.97	0.812 0.72 0.275	0.602
0.639	0.713	0.89	0.301	0.973 0.844 0.292	0.973	0.713 0.629 0.237	0.526
0.433	0.526	0.823	0.303	0.973 0.844 0.292	0.973	0.526 0.464 0.175	0.388
0.549	0.556	0.98	0.36	0.973 0.844 0.292	0.973	0.557 0.494 0.189	0.413
0.492	0.523	0.94	0.3	0.973 0.844 0.292	0.973	0.523 0.462 0.174	0.386
0.449	0.551	0.814	0.299	0.973 0.844 0.292	0.973	0.551 0.486 0.183	0.406

Figure 5 shows the plot between the maximum and mean velocity of cross sections of Huma tail distributary canal. From the graph it can be observed that a linear relationship occur between the mean and the maximum velocities with a constant ratio Φ . The result confirmed with the Chiu's theory as a constant ratio Φ , between the mean and maximum velocities are maintained throughout the section. The slope of the graph as indicated in Figure 5 is 1:1, with a very small variation, indicates the accuracy of the method. The velocity at the bottom of the channel is zero but it increases gradually again decreases at the top due to the effect of surface tension.

Figure 6 shows the plot between the mean velocity at various cross sections (at various depths and widths) of Huma tail distributary and the mean velocity computed by Chiu's equation. The slope of the line obtained from the graph between u_{obs} and u_{est} is found to be 1:1, with a very small error, that indicates the validity of the method in velocity calculation.

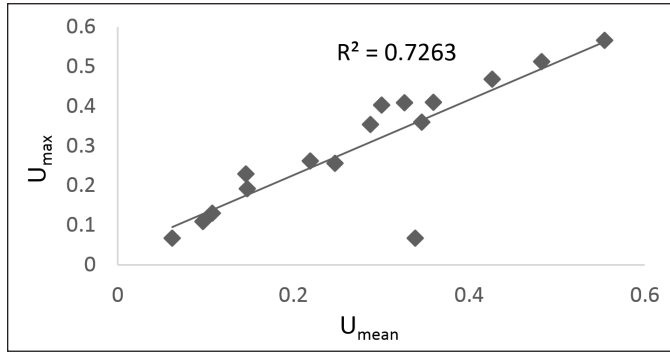


Figure 5. Graph between maximum and mean velocity estimated

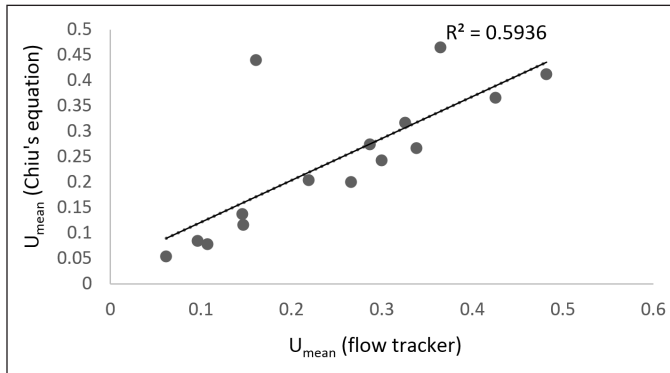


Figure 6. Graph between u_{max} calculated by Chiu's equation and u_{max} measured by flow tracker

The error in measurement is maximum at the near 0.2 and 0.4 from Chiu's equation due to not full coverage of the cross section and capturing boundaries of the channel is necessary to maximize the accuracy of discharge measurement.

Table 3
Data between the Discharge estimated and observed

Q_{obs} (m ³ /sec)	Q_{est} (m ³ /sec)	Error in %	Q_{obs} (m ³ /sec)	Q_{est} (m ³ /sec)	Error in %
0.5251	0.516	1.73	0.077	0.07	9.09
0.57398	0.5556	3.20	0.013	0.012	7.69
0.8071	0.773	4.23	0.301	0.285	5.32
0.0131	0.0122	6.87	0.008	0.006	25.00
0.751	0.737	1.86	0.172	0.164	4.65
0.039	0.036	7.69	0.14	0.132	5.71
0.13	0.124	4.62	0.091	0.079	13.19
0.023	0.02	13.04			

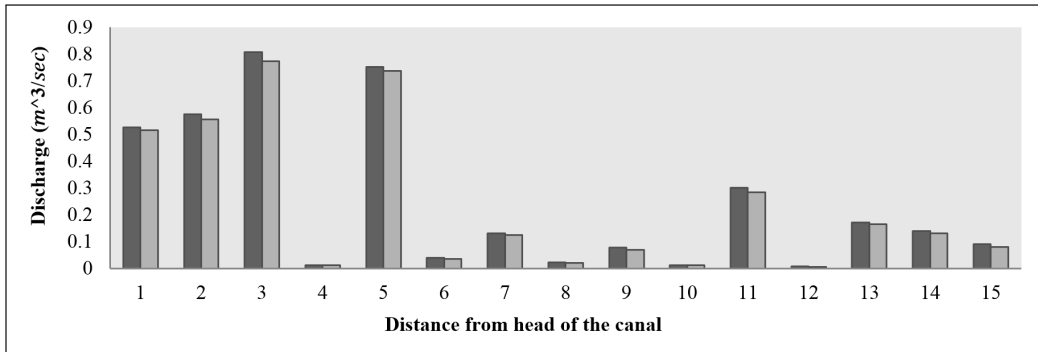


Figure 7. Plot between estimated discharge and observed discharge

The Figure 7 plot between estimated discharges and observed discharge, the discharge measurements made by the ADV. The average error as obtained from the Table 3 and Figure 7 is found to be 7.69 %. So it indicates the reliability and the accuracy of the Chiu's equation for the discharge measurement.

CONCLUSION

In this work an attempt has been made to develop a 2D velocity distribution by applying the Chiu's equation based on entropy theory at Huma tail distributary of Hirakud Irrigation system. The velocity was determined experimentally with the help of ADV flow tracker and the velocity that computed from the 2D distribution data is quite close. The mean velocity of flow is influenced by various parameters but the maximum flow velocity, remain constant at any cross section, irrespective of types of flow and the cross-sectional shape. So, it is a convenient to estimate the mean velocity by utilizing the maximum flow velocity without going for the direct measurements for the estimations of the mean velocity. In this work, a formula to determine the maximum velocity was applied. To establish the accuracy of the maximum flow velocity formula, the actual measurement data for the flow at 13 different cross sections were found out with the help of ADV Flow tracker. The results were compared with the maximum flow velocity estimated through the proposed formula. The results showed very high accuracy as the results obtained from the Chiu's equation, when compared with the value obtained from direct measurement, the error is found to be 7.69%. This methodology can also be applied to estimate the flow rate even in flood season.

ACKNOWLEDGEMENTS

The authors thank the District Civil Supplies Officer, Sambalpur, Deputy Director of Agriculture, Sambalpur, for providing Block-wise details of Sambalpur District, Odisha State and Hirakud Dam authority for their kind support to carry out the work

REFERENCES

- Barbe, D. E., Cruise, J. F., & Singh, V. P. (1991). Solution of 3-constraint entropy-based velocity distribution. *Journal of Hydraulic Engineering*, 117(10), 1389-1396.
- Chiu, C. L. (1989). Velocity distribution in open-channel flow. *Journal of Hydraulic Engineering*, 115, 576–594.
- Chiu, C. L., & Chiou, J. D. (1988). Entropy and 2-D velocity distribution in open-channels. *Journal of Hydraulic Engineering*, 114, 738–756.
- Chiu, C. L., & Hsu, S. M. (2006). Probabilistic approach to modeling of velocity distributions in fluid flows. *Journal of Hydrology*, 316(1-4), 28-42.
- Chiu, C. L., & Lin, G. F. (1983). Computation of 3-D flow and shear in open channels. *Journal of Hydraulic Engineering*, 112(11), 1424-1440.
- Chiu, C. L., & Murray, D. W. (1992). Variation of velocity distribution along nonuniform open-channel flow. *Journal of Hydraulic Engineering*, 118(7), 989-1001.
- Chiu, C. L., & Said, C. A. A. (1995). Maximum and mean velocities and entropy in Open-channel flow. *Journal of Hydraulic Engineering*, 121(1), 26-35.
- Marini, G., De Martino, G., Fontana, N., Fiorentino, M., & Singh, V. P. (2011). Entropy approach for 2D velocity distribution in open-channel flow. *Journal of Hydraulic Research*, 49(6), 784-790.
- Moramarco, T., Saltalippi, C., & Singh, V. P. (2004). Estimation of mean velocity in natural channels based on Chiu's velocity distribution equation. *Journal of Hydraulic Engineering*, 9, 42–50.
- Singh, V. P., & Rajagopal, A. K. (1987). Some recent advances in the application of the principle of maximum entropy (POME) in hydrology. In *Proceedings of the Water for the Future: Hydrology in perspective* (pp. 353-364). Rome, Italy.
- Singh, V. P., Moramarco, T., Corato, G., & Melone, F. (2013). An entropy-based method for determining the flow depth distribution in natural channels. *Journal of Hydrology*, 497, 176–188.

Modelling of Pilot-Scale Anaerobic Food Wastes Composting Process with Dry Leaves or Cow Manure

Wei Jie Lim¹, Nyuk Ling Chin^{1*}, Yus Aniza Yusof¹, Azmi Yahya² and Tuan Poy Tee³

¹Department of Process and Food Engineering, Faculty of Engineering, Universiti Putra Malaysia, 43400 UPM Serdang, Selangor, Malaysia

²Department of Biological and Agricultural Engineering, Faculty of Engineering, Universiti Putra Malaysia, 43400 UPM Serdang, Selangor, Malaysia

³Department of Animal Science, Faculty of Agriculture, Universiti Putra Malaysia, 43400 UPM Serdang, Selangor, Malaysia

ABSTRACT

Anaerobic composting is a promising method to fully transform food wastes into useful materials such as biofertilizer and biogas. In this study, the optimum proportions of food wastes containing vegetable, fruit and meat wastes with dry leaves or cow manure for composting were determined using the simplex centroid design and response optimizer. The effectiveness of the pilot-scale composting process was evaluated based on the targeted compost quality of C/N ratio at 21, pH value at 8 and electrical conductivity of 1 dS/m. Food wastes composting formulation with dry leaves suggested high percentage of dry leaves, 86.9% with low food wastes composition of 13.1% constituted by vegetable waste (1.1%), fruit waste (4.9%) and meat waste (7.1%). With cow manure formulation, only 6% of cow manure was recommended with another 94.0% of food wastes contributed by a fair mix of vegetable waste (23.2%), fruit waste (34.3%) and meat waste (36.5%). The developed regression models were experimentally validated with predicted responses obtained in acceptable ranges for C/N ratio (21.2 - 21.8), pH (7.92 - 7.99) and electrical conductivity (0.97 - 1.03 dS/m).

Keywords: Biofertilizer, biogas, mixture design, response surface optimization, simplex centroid design

ARTICLE INFO

Article history:

Received: 10 February 2018

Accepted: 12 September 2018

Published: 24 January 2019

E-mail addresses:

tortoise810@gmail.com (Wei Jie Lim)

chinnl@upm.edu.my (Nyuk Ling Chin)

yus.aniza@upm.edu.my (Yus Aniza Yusof)

azmiy@upm.edu.my (Azmi Yahya)

tttoy@upm.edu.my (Tuan Poy Tee)

* Corresponding author

INTRODUCTION

Anaerobic composting consists of four main stages, namely hydrolysis, acidogenesis, acetogenesis and methanogenesis in the absence of oxygen (Zhang et al., 2014). In the hydrolysis process, complex organic molecules are broken down into simple sugars, amino acids, and fatty acids. During the acidogenesis process, further breakdown of the remaining organic components by fermentative bacteria takes place producing short-chain fatty acids, carbon dioxide and hydrogen. Further digestion of simple molecules happens during the acetogenesis process where acetic acid, carbon dioxide and hydrogen are produced. The last stage, the methanogenesis is a biological process where intermediate products of the preceding processes are converted into methane, carbon dioxide and water, making the major components of biogas emitted from the system (Poulsen, 2013). The overall process can be described by the chemical reaction where organic material, e.g. glucose is biochemically digested into carbon dioxide (CO₂) and methane (CH₄) by anaerobic microorganisms.

Anaerobic composting of food waste is a biological process involving biodegradation of putrescible food waste into biofertilizer and by-product of biogas. It can be explained as a two-step process similar to the Bokashi composting (Power Knot, 2012). First, the beneficial microbes break down all food waste material including non-plant based through a fermentation process which creates an acidic environment that kills harmful pathogens in within and outside the system. The soil microbes then finish the decomposition. Unlike the aerobic composting which requires the help of heat for the soil microbes to break down plant materials at starting temperature of about 45°C and later the thermophilic phase at 50-70°C (Abdullah et al., 2013), the anaerobic composting happens at moderate temperatures below 45°C (mesophilic phase) and can degrade meat materials. The high biodegradability and moisture content of food waste are good characteristics for production of biofertilizer that can be used as nutrient source and soil conditioner (Giroto et al., 2015). In food waste handling, the anaerobic composting method is advantageous compared to the incineration method, owing to the high moisture content in food waste which often hinders the incineration process. Chen and colleagues (2008) found that food waste used in anaerobic composting has more potential for the biogas production than the municipal solid waste because food waste contains more than 80% organic content.

Food waste is discarded on daily basis due to routine activities of human living from domestic to agricultural and industrial. The composition of food waste is usually heterogeneous depending on the consumption habits of human, thus may affect the composting process. In optimizing the composting process, the proportion of composting materials need to be balanced or sometimes, other essential organic materials are added for functionality. In obtaining an optimized formulation, a systematic approach through statistical modelling via various design of experiment (DoE) is used to predict response

variables and optimized factor variables of the processes. The DoE is relatively more efficient and cost-effective in developing and improving process models compared to the traditional trial and error method (Rao & Baral, 2011). As the inconsistency of food waste composition affects the quality of compost produced, this work aimed to find food waste formulation in terms of the vegetable, fruit and meat wastes proportions for an optimized anaerobic composting under the mesophilic phase at moderate temperatures. The dry leaves or cow manure were added into the anaerobic composting to improve the quality of compost.

The aim of using the pilot scale composter is that the composting process can be made in-situ, it saves transporting cost of waste to landfill or open space for aerobic composting, preserves the appearance of the compost area, prevents bad odours and pests problems from open piles of aerobic composting area. The labour required to operate the composting process is also minimal as no turning pile or aeration mechanism is needed. It is also suitable for food waste which include meat waste to undergo anaerobic composting as meat is strictly forbidden for aerobic composting. Despite its installation cost, the production of biogas can be a source of renewable energy. The anaerobic composting can be a mature and effective technology for food waste management system with low operating costs and high feasibility (Chang & Hsu, 2008; Girotto et al., 2015; Zhang et al., 2015). Recently, anaerobic food digestion approach and technology are getting more attention as recent researches have evaluated the feasibility of this system as an option for organic municipal waste management in populated urban areas like city Wildemanbuurt in Amsterdam (Goossensen, 2017) and city of Milan in Italy (Grosso et al., 2012).

MATERIALS AND METHODS

Substrates Preparation

This study consisted of two experimental parts for optimization of food wastes composting. The first experiment involved composting of food wastes and dry leaves, while the second experiment used food wastes and cow manure. The food wastes consisting vegetable, fruit and meat wastes were collected from Pasar Borong Selangor, Seri Kembangan. The dry leaves and cow manure were obtained from the Animal and Agricultural Unit of Universiti Putra Malaysia. These materials acted as bulking agents to improve the quality of compost by adjusting the moisture content and providing carbon and nitrogen sources for the compost produced.

Prior to anaerobic composting, foreign materials such as rubber band and plastic bags were discarded from the collected food wastes as they can impair microbial activities during composting process. All substrates were then shredded into fine substances with diameter less than 0.001 m using a food waste grinder (FWD 600 HS, Ecofast, Milano, Italy) before loading into the composter.

Pilot-scale Anaerobic Composter

The substrates were composted in a pilot-scale anaerobic composter (Cowtech CTM-100, CH Green Sdn. Bhd., Kuala Lumpur, Malaysia) located at Ladang 2, Universiti Putra Malaysia. Figure 1 shows the schematic diagram of the composter with dimensions of 1.8 m (height) × 1 m (width) × 4.5 m (length).

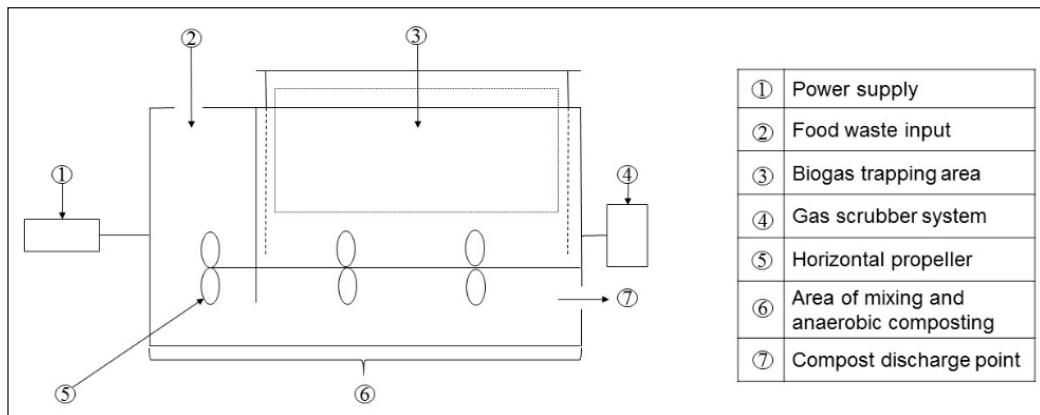


Figure 1. Schematic diagram of pilot-scale anaerobic composter

It is a hi-dry solid batch continuous composting system equipped with a power supply unit, feeding hopper, mixing and composting tank with 3000 kg volume, horizontal propeller, gas scrubber unit and discharge pump. The production capacity of biogas is approximately 2.76 - 5.52 kg/day. The start-up of the composting process was monitored for 30 days at 30 – 35°C with the first fill of 40 kg of effective microbe powder mixture in 40 kg of water. The effective microbe powder consists of microbes suitable for anaerobic composting, function well at lower temperature and acidic environment which included mainly yeasts, photosynthetic bacteria and lactic acid bacteria. They are meant to break down the food waste through fermentation process first and then the acidic environment created kills harmful pathogens, and lastly the soil microbes finish the decomposition. The temperature throughout the composting process was dependent on the surrounding environmental temperature. The maximum substrates input of the composter was 100 kg/day but a daily input of 40 kg substrates was used in this study. The liquid compost was removed from the composter through a discharge pump and stored inside a pail. The amount of biogas produced was recorded daily before burning using a gas stove.

Mixture Experimental Design

Two types of mixtures, food wastes with dry leaves and food wastes with cow manure were used to evaluate the effects of substrates on the compost quality in terms of carbon to nitrogen (C/N) ratio, pH and electrical conductivity. These are the general physicochemical

parameters widely used to examine the quality of compost produced (Bernal et al., 2009). The C/N ratio and moisture content of each substrate were determined to verify their capabilities as carbon source, nitrogen source and bulking agent.

The proportions for each substrate were generated following the simplex centroid design using Minitab 16 Statistical Software (Minitab Incorporation, Pennsylvania, USA). The simplex centroid design is capable in solving more complex experimental model as it contains higher order terms such as quadratic, full cubic, special cubic and special quartic models (Rao & Baral, 2011). This design is appropriate for the experimental design of this study with all components having the same range from 0 to 100 (Abdullah & Chin, 2010). A total of 23 runs were generated for food wastes with dry leaves experiment, and food wastes with cow manure experiment. The experiments were performed in random order to avoid bias sampling. The compost produced was collected after a minimum composting period of 30 days and analysed for physicochemical properties. The response parameters investigated were C/N ratio, pH and electrical conductivity.

Determination of Physicochemical Properties

The substrates and compost were analysed for various physicochemical properties including volatile solid content, total carbon content, total nitrogen content, C/N ratio, pH, electrical conductivity and moisture content. The volatile solid content and total carbon content were determined based on ash content (Larney et al., 2003). The ash content was assessed following Abdullah and Chin (2010), and Mohee and co-workers (2008). About 2.5 g of sample was placed in clean crucible in a muffle furnace at 550°C for 2 hours. The ash content is defined by the difference of sample weight before and after placing in the furnace. The percentage of ash content was calculated using Eq. 1.

$$\% \text{ Ash} = \frac{\text{Weight}_{\text{Before}} - \text{Weight}_{\text{After}}}{\text{Weight}_{\text{Before}}} \times 100\% \quad (1)$$

The volatile solid of sample was then calculated using Eq. 2 (Abdullah & Chin, 2010), followed by total carbon content using Eq. 3 (Larney et al., 2003).

$$\% \text{ Volatile solid} = 100\% - \% \text{ Ash} \quad (2)$$

$$\% \text{ Total organic carbon} = \frac{\% \text{ Volatile solid}}{1.8} \quad (3)$$

The nitrogen content was determined by Kjeldahl method (Unmar & Mohee, 2008). The sample of 0.15 g was inserted into a boiling tube with 0.8 g of mixed catalyst and 2.5 mL of concentrated sulphuric acid were added. The boiling tube was heated slowly on a heating coil to break all the bonds in the sample. The digestion process was completed when the solution became clear greenish blue. After cooling, the sample was added with

10 mL of distilled water and transferred into distillation tube. Prior to distillation process, 10 mL of 45% sodium hydroxide solution was slowly added to separate the solution into two layers. A conical flask containing 10 mL of 2% boric acid and three drops of indicator was used to collect the distillate. After distillation process of 120 seconds, the conical flask with distillate and boric acid was titrated using 0.05 N of sulphuric acid until light pink persist. A similar procedure was performed for the blank sample. The percentage of nitrogen content was calculated following Eq. 4 (Codell & Verderame, 1954).

$$\% \text{ Total nitrogen} = \frac{(R-S) \times 1.4007 \times N}{W} \times 100\% \quad (4)$$

where R is volume of sulphuric acid to titrate boric acid (mL), S is volume of sulphuric acid to titrate blank (mL), N is normality of sulphuric acid of 0.05 N, and W is sample weight (g).

The C/N ratio refers to total organic carbon content to total nitrogen content of the sample as shown in Eq. 5.

$$\text{C/N ratio} = \frac{\text{Total organic carbon}}{\text{Total nitrogen}} \times 100\% \quad (5)$$

The pH value was measured using a handheld pH meter (Mi806, Milwaukee Instruments Inc., North Carolina, USA) (Kumar et al., 2010). The sample was diluted with deionized water in a weight ratio of 1:10, and stirred for 1 hour at 150 rpm in a shaking water bath (BS-21, Jeio Tech Co. Ltd., Korea). The mixture was left standing to reach dormant state followed by measuring the pH of the top layer or supernatant.

The electrical conductivity was determined following Lin (2008) and Chen et al. (2008). The sample of 5 g was diluted with 25 mL of deionized water and mixed for 30 minutes at room temperature until a homogenous state is reached prior to filtration using Whatman No.1 filter paper. The electrical conductivity of the filtrate was measured using a portable electrical conductivity meter (Mi806, Milwaukee Instruments Inc., North Carolina, USA).

The moisture content was determined by conventional oven method as described by Kumar et al. (2010). About 200 g of sample was dried in an oven at 105°C for 24 hours until constant weight is obtained. The moisture content is defined as the weight loss of sample. The percentage of moisture content was calculated following Eq. 6 (Schwab et al., 1994).

$$\% \text{ Moisture} = \frac{M_W - M_S}{M_W} \times 100\% \quad (6)$$

where M_W is weight of food wastes compost (kg) and M_S is the weight of dry solids of food wastes compost (kg). The response variables values are reported as the average of triplicate measurements to ensure its repeatability.

RESULTS AND DISCUSSION

Characteristics of Substrates for Anaerobic Composting

The substrates used for anaerobic composting in this study were characterised for carbon content, nitrogen content, C/N ratio, pH and moisture content as summarised in Table 1. The meat waste and cow manure contained relatively high nitrogen contents of 5.87% and 3.96%, respectively implying that both meat waste and cow manure could be good nitrogen sources. The meat waste showed the lowest C/N ratio while dry leaves had the highest C/N ratio. The moisture level in fruit waste is the highest (81.34%) followed by meat waste, vegetable waste, cow manure and dry leaves has the least (3.48%). These indicate that dry leaves possess good absorption capacity and is suitable as bulking agent for adjusting the moisture of food wastes in order to achieve better composting process.

Table 1
Physicochemical properties of substrates used

Properties	Vegetable waste	Fruit waste	Meat waste	Dry leaves	Cow manure
Carbon content (%)	38.79 ± 2.13	42.29 ± 1.14	39.87 ± 1.14	46.4 ± 2.27	34.88 ± 1.91
Nitrogen content (%)	2.45 ± 0.04	1.21 ± 0.06	5.87 ± 0.06	0.24 ± 0.04	3.96 ± 0.10
C/N ratio	16.86	39.90	6.79	193.33	8.81
pH	6.35 ± 0.01	5.50 ± 0.01	5.78 ± 0.01	6.61 ± 0.02	9.21 ± 0.01
Moisture content (%)	74.78 ± 0.93	81.34 ± 0.93	75.19 ± 1.36	3.48 ± 0.50	72.23 ± 2.80

Food Wastes with Dry Leaves Composting

Modelling of Composting Process. Table 2 presents the effects of food wastes with dry leaves composting on the quality of compost such as C/N ratio, pH and electrical conductivity including the biogas amount. Several regression models were fitted into the data obtained including linear, quadratic, special cubic, full cubic, and special quartic models.

The criteria in selecting the best fitted model to the data are low standard deviation, low predicted sum of squares (PRESS), and high predicted R -squared (R^2_{pred}) (Cornell, 2002). Based on the selection criteria for best model, it was found that special cubic model, linear model, and quadratic model were the best fitted models for C/N ratio ($R^2_{\text{pred}} = 0.873$), pH value ($R^2_{\text{pred}} = 0.772$) and electrical conductivity ($R^2_{\text{pred}} = 0.798$), respectively (Table 3).

The regression coefficients of the three responses of food wastes with dry leaves composting are shown in Table 4.

All of the models fitted the experimental data well as indicated by the high coefficients of determination ranging from 0.835 to 0.997. The best fitted mathematical models for C/N ratio, pH, and electrical conductivity are given in Eq. 7 - Eq. 9.

Table 2
Mixture experimental design of food wastes with dry leaves composting

Run	Independent variables				Response variables				Biogas amount (m ³)
	Vegetable waste, x ₁ (%)	Fruit waste, x ₂ (%)	Meat waste, x ₃ (%)	Dry leaves, x ₄ (%)	C/N ratio, Y _{CN}	pH, Y _{pH}	Electrical conductivity, Y _{EC}		
1	25	25	25	25	36.32	7.81	0.915	3.60	
2	50	50	0	0	49.92	7.77	0.679	3.45	
3	62.50	12.50	12.50	12.50	30.76	7.85	0.836	3.75	
4	0	50	0	50	37.25	7.88	0.913	3.75	
5	33.33	0.00	33.33	33.33	27.86	7.90	0.937	3.50	
6	33.33	33.33	0.00	33.33	32.78	7.82	0.857	3.45	
7	50	0	50	0	26.73	8.04	0.756	3.75	
8	33.33	33.33	33.33	0	21.25	7.85	0.808	3.70	
9	12.50	12.50	12.50	62.50	23.34	7.95	1.005	3.60	
10	0	0	100	0	46.60	8.24	1.216	3.85	
11	50	0	0	50	24.11	7.97	0.944	3.65	
12	0	0	50	50	29.92	8.01	0.953	3.75	
13	0	33.33	33.33	33.33	31.72	7.90	0.867	0.95	
14	0	100	0	0	182.00	7.77	0.581	0.80	
15	12.50	12.50	62.50	12.50	29.19	7.98	0.979	1.10	
16	100	0	0	0	43.12	7.65	0.706	1.20	
17	12.50	62.50	12.50	12.50	63.73	7.85	0.644	0.75	
18	0	0	0	100	24.27	8.01	1.065	0.95	
19	0	50	50	0	33.20	8.06	0.765	0.70	
20	100	0	0	0	42.73	7.72	0.713	0.85	
21	0	100	0	0	186.40	7.81	0.586	0.90	
22	0	0	100	0	43.67	8.23	1.254	1.00	
23	0	0	0	100	26.85	8.05	1.076	2.70	

Table 3
 Model summary statistics for response variables of food wastes with dry leaves composting

Source	Standard deviation	Regression, R^2 (%)	Predicted regression, R^2_{pred} (%)	Adjusted regression, R^2_{adj} (%)	Predicted sum of square, PRESS
C/N ratio					
Linear	28.34	64.63	41.33	59.04	25308
Quadratic	6.56	98.70	92.92	97.81	30555
Special cubic	3.56	99.73	87.31	99.35	5475
Full cubic	3.22	99.86	42.25	99.47	24914
Special quartic	4.62	99.70	43.09	98.91	24552
pH					
Linear	0.065	83.48	77.18	80.87	0.110
Quadratic	0.051	92.97	56.85	88.10	0.208
Special cubic	0.034	97.82	50.72	94.66	0.237
Full cubic	0.033	98.67	47.16	95.14	0.255
Special quartic	0.033	98.66	0.00	95.07	3.384
Electrical conductivity					
Linear	0.077	84.56	77.19	82.13	0.167
Quadratic	0.048	95.85	79.80	92.98	0.148
Special cubic	0.038	98.25	25.21	95.72	0.547
Full cubic	0.015	99.81	60.79	99.30	0.287
Special quartic	0.020	99.68	0.00	98.84	0.943

Table 4
 Regression coefficients for response variables of food wastes with dry leaves composting

Term	C/N ratio	pH	Electrical conductivity
b_1	43.3	7.72	0.707
b_2	183.5	7.78	0.567
b_3	45.5	8.19	1.230
b_4	25.6	7.99	1.070
b_{12}	-258.1*	-	0.246
b_{13}	-69.9*	-	-0.560
b_{14}	-42.2*	-	0.361
b_{23}	-329.5*	-	-0.432*
b_{24}	-275.1*	-	0.329
b_{34}	-23.5*	-	-0.625*
b_{123}	146.5*	-	-
b_{124}	375.3	-	-
b_{134}	210.9	-	-
b_{234}	483.8	-	-
R^2	0.997	0.835	0.959

Note. Subscripts: 1 = vegetable waste; 2 = fruit waste; 3 = meat waste; 4 = dry leaves.
 * indicates significant effect at $P < 0.05$.

$$Y_{\text{CN}} = 43.3x_1 + 183.5x_2 + 45.5x_3 + 25.6x_4 - 258.1x_1x_2 - 69.9x_1x_3 - 42.2x_1x_4 - 329.5x_2x_3 - 275.1x_2x_4 - 23.5x_3x_4 + 146.5x_1x_2x_3 + 375.3x_1x_2x_4 + 210.9x_1x_3x_4 + 483.8x_2x_3x_4 \quad (7)$$

$$Y_{\text{pH}} = 7.72x_1 + 7.78x_2 + 8.19x_3 + 7.99x_4 \quad (8)$$

$$Y_{\text{EC}} = 0.707x_1 + 0.567x_2 + 1.230x_3 + 1.070x_4 + 0.246x_1x_2 - 0.560x_1x_3 + 0.361x_1x_4 - 0.432x_2x_3 + 0.329x_2x_4 - 0.625x_3x_4 \quad (9)$$

A positive interaction coefficient indicates a synergistic effect while a negative term denotes an antagonistic effect of the parameters on the response value (Abdullah & Chin, 2010). The linear coefficients of b_1 , b_2 , b_3 and b_4 denote that vegetable waste, fruit waste, meat waste, and dry leaves have synergistic effects on C/N ratio (Table 4). For the quadratic interaction coefficients, all of the substrates have significant antagonistic effects ($P < 0.05$) for the reduction of C/N ratio which is desirable. Moreover, the coefficients b_{23} and b_{34} imply that reduction of fruit waste and meat waste, and meat waste and dry leaves significantly ($P < 0.05$) increased the electrical conductivity of the compost. These results recommend the blending of two substrates in producing the best quality compost for food wastes with dry leaves anaerobic composting.

Contour Plots and Response Surface Plots. Figures 2(a) - (c) illustrate the contour plots and 3D surface plots of the three responses, C/N ratio, pH and electrical conductivity of food wastes with dry leaves composting. Figure 2(a) shows that increasing dry leaves reduced the C/N ratio and produced a better quality of compost. The compost with good C/N ratio ranging from 10 to 25 (Aparma et al., 2008) can be met when the mixture contained moderate amount of vegetable and meat wastes as well as minute amount of fruit waste with abundance of dry leaves. The level of pH increased with meat waste and dry leaves but decreased with vegetable and fruit wastes as shown in Figure 2(b). The pH of each substrate is affected by its individual physicochemical properties (Table 1) and also its percentage used in the mixture experimental design. Figure 2(c) shows that almost all combination of food wastes with dry leaves composting produced electrical conductivity of less than 1.0. This reveals that compost generated from food wastes with dry leaves could be used to a certain extent as the direct substitution for soil (US Composting Council, 1990). Higher electrical conductivity can be achieved using larger amount of meat waste and dry leaves.

The overlaid contour plots of all responses, C/N ratio, pH and electrical conductivity for food wastes with dry leaves composting are shown in Figure 3. It is observed that good quality organic compost can be achieved using any combination of vegetable, fruit and meat wastes with dry leaves that fall within the white zone, also known as the feasible region.

These results suggest using a combination of higher amount of dry leaves, lesser fruit and meat wastes, and little vegetable waste to obtain good quality of compost.

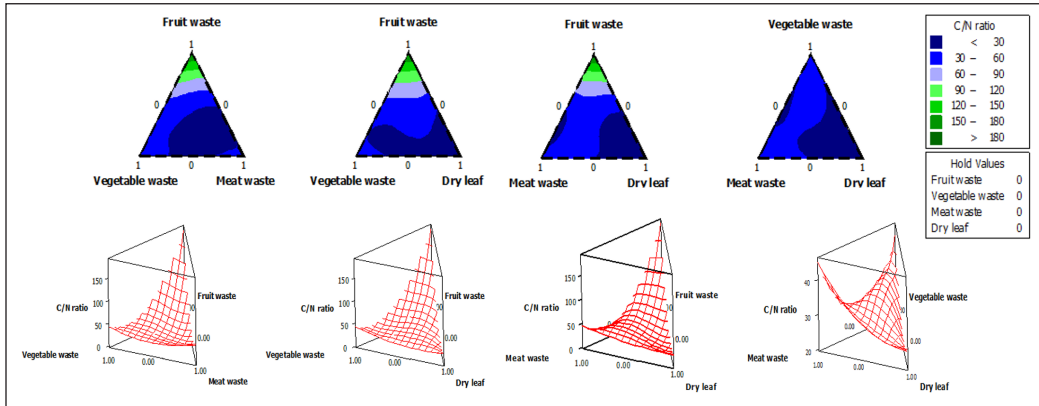


Figure 2(a). Mixture contour plots and 3D surface plots of C/N ratio of food wastes with dry leaves composting

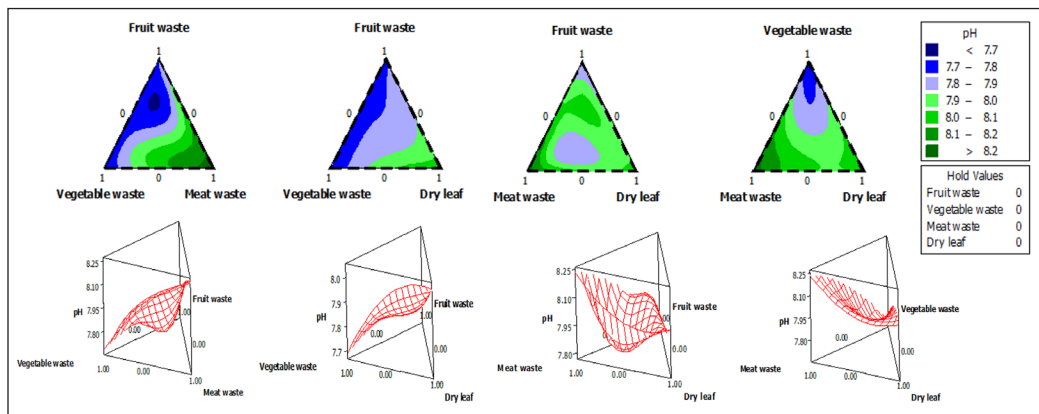


Figure 2(b). Mixture contour plots and 3D surface plots of pH of food wastes with dry leaves composting

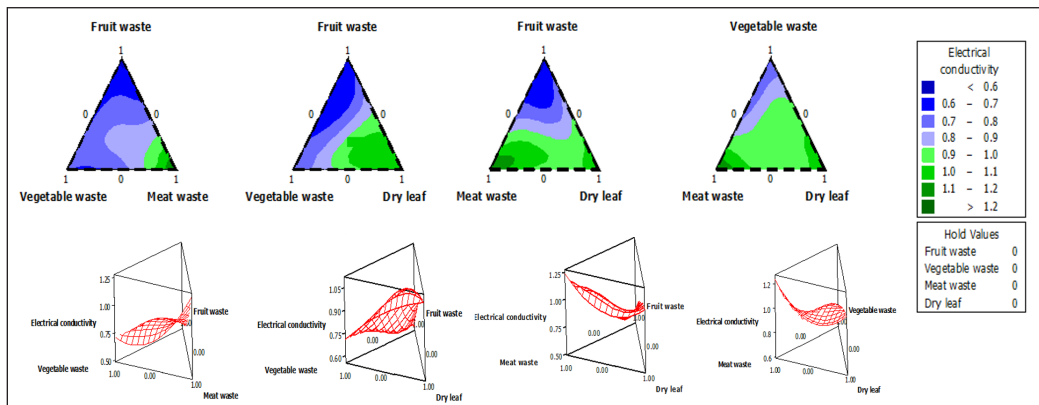


Figure 2(c). Mixture contour plots and 3D surface plots of electrical conductivity of food wastes with dry leaves composting

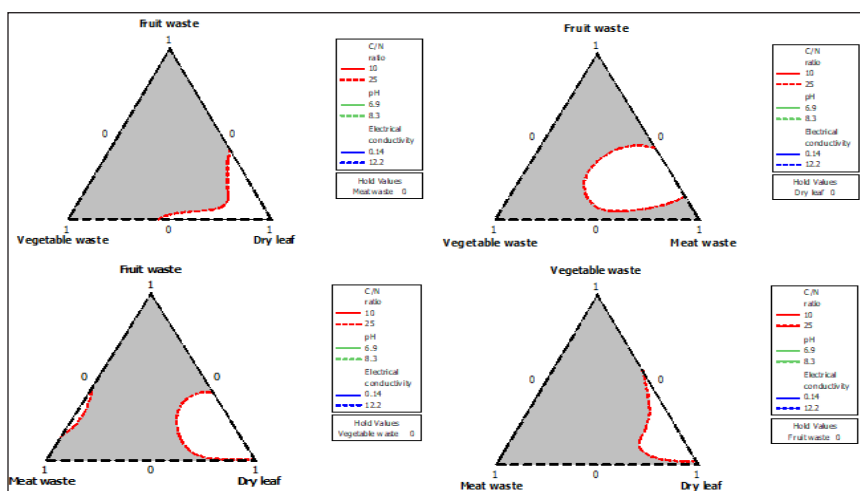


Figure 3. Overlaid contour plots of C/N ratio, pH and electrical conductivity of food wastes with dry leaves composting

Response Optimization and Model Validation. Response optimization allows simultaneous identification of variable settings that jointly optimize a set of responses and illustrates in optimization plot. The joint optimization must fulfil the requirements of all responses and measured by the composite desirability. Figure 4 shows the optimization plot of food wastes with dry leaves composting. The optimum proportion for food wastes with dry leaves composting was 1.16% vegetable waste, 4.89% fruit waste, 7.07% meat waste, and 86.88% dry leaves with the composite desirability of 0.998. These imply that the all the target values for responses were achieved. The range of individual desirability (0.997 - 0.998) reveals that the model developed is equally effective at minimising C/N ratio, maximising pH value, and maximising electrical conductivity. The desirable responses attained are 20.98 for C/N ratio, 7.99 for pH, and 1.02 dS/m for electrical conductivity.

An increase in vegetable and fruit wastes increases the C/N ratio and reduces the electrical conductivity and pH value which is not favourable for the compost quality (Figure 4). The goal is to minimise C/N ratio, maximise pH value, and maximise electrical conductivity. Therefore, the optimal settings of both vegetable and fruit wastes are at the minimum levels in the experiment. An increase in meat waste and dry leaves increases the three responses as the electrical conductivity and pH were greater than the C/N ratio. In order to compromise between the contradictory goals, the optimal settings of vegetable, fruit and meat wastes with dry leaves are in the intermediate range of 1.16%, 4.89%, 7.07% and 86.88%, respectively. The possible usage of high percentage of dry leaves at 86.88% could be related to its antagonistic effects of higher pH values 6.61 to raise the alkalinity of food waste pH averaging at 5.88 and relatively lower moisture content of 3.48% to balance the electrical conductivity to 1 dS/m.

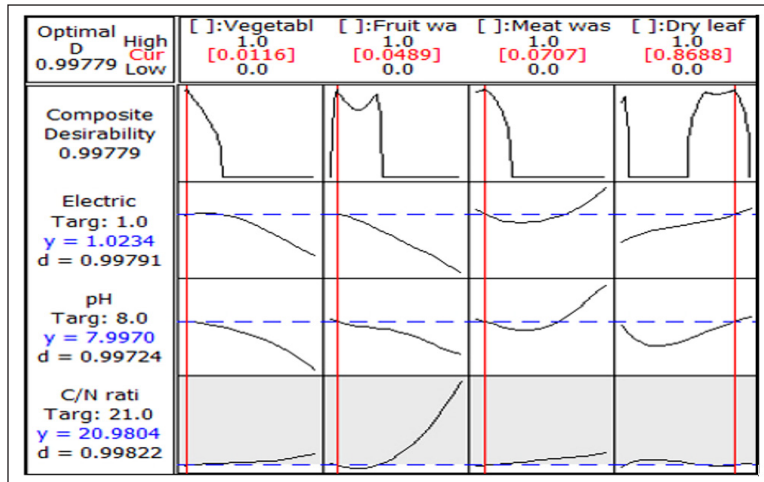


Figure 4. Optimization plot of food wastes with dry leaves composting

The optimum proportion of food wastes with dry leaves obtained was used for validating the models. The predicted responses obtained were C/N ratio of 21.83, pH value of 7.99, and electrical conductivity of 1.03 dS/m, which are very close to the target values from the responses of 21.0, 8.0 and 1.0, respectively. These results are in agreement with Aparma et al. (2008) who reported the C/N ratio of compost ranging from 10 to 25, Shyamala and Belagali (2012) on pH range between 6.9 and 8.3, and US Composting Council (1990) on electrical conductivity of 0.14 - 12.2 dS/m.

Food Wastes with Cow Manure Composting

Modelling of Composting Process. The effects of food wastes with cow manure composting on the compost quality based on C/N ratio, pH, electrical conductivity, and the biogas content are shown in Table 5.

The responses data were fitted into several regression models such as linear, quadratic, special cubic, full cubic and special quartic. Following the model selection criteria of low standard deviation, low R^2_{pred} and high PRESS, it is observed that special quartic model best fitted to C/N ratio with $R^2_{pred} = 0.933$, quadratic model to pH value with $R^2_{pred} = 0.623$, and full cubic model to electrical conductivity with $R^2_{pred} = 0.820$ (Table 6).

Generally, a model is considered a valid model by having the R^2 value greater than 0.6 (Gong et al., 2007). Table 7 presents the regression coefficients for the three responses of food wastes with cow manure composting.

The high coefficients of determination ranging between 0.876 and 0.998 indicate that all of the models fit the experimental data well. The best fitted regression models for C/N ratio, pH, and electrical conductivity are presented in Eq. 10 - Eq. 12.

Table 5
Mixture experimental design of food wastes with cow manure composting

Run	Independent variables				Response variables				Biogas amount (m ³)
	Vegetable waste, x_1 (%)	Fruit waste, x_2 (%)	Meat waste, x_3 (%)	Cow manure, x_4 (%)	C/N ratio, Y_{CN}	pH, Y_{pH}	Electrical conductivity, Y_{EC}		
1	50	0	50	0	25.67	8.02	0.812	4.10	
2	33.33	33.33	0.00	33.33	37.68	7.78	1.271	3.75	
3	0	0	50	50	30.45	7.94	1.284	3.85	
4	0	0	0	100	28.73	8.09	1.313	3.75	
5	62.50	12.50	12.50	12.50	32.14	7.95	1.178	3.80	
6	0	100	0	0	185.00	7.75	0.584	3.90	
7	12.50	62.50	12.50	12.50	63.96	7.91	0.957	3.80	
8	33.33	0.00	33.33	33.33	33.33	7.88	1.357	3.40	
9	50	0	0	50	41.42	7.85	1.379	3.90	
10	12.50	12.50	62.50	12.50	33.72	7.97	1.256	3.65	
11	100	0	0	0	43.00	7.67	0.704	3.94	
12	0	50	50	0	32.89	8.03	0.767	3.60	
13	0	50	0	50	34.18	7.92	1.149	0.80	
14	33.33	33.33	33.33	0.00	22.45	7.87	0.802	1.00	
15	25	25	25	25	34.71	7.84	1.280	1.00	
16	50	50	0	0	49.98	7.77	0.651	1.10	
17	0	0	100	0	45.78	8.21	1.212	0.90	
18	0.00	33.33	33.33	33.33	30.80	7.83	1.190	0.85	
19	12.50	12.50	12.50	62.50	31.08	8.02	1.292	0.75	
20	100	0	0	0	40.73	7.81	0.578	0.85	
21	0	100	0	0	184.40	7.74	0.721	0.94	
22	0	0	100	0	44.53	8.24	1.253	0.98	
23	0	0	0	100	25.85	8.04	1.470	2.80	

Table 6
 Model summary statistics for three responses of food wastes with cow manure composting

Source	Standard deviation	Regression, R^2 (%)	Predicted regression, R^2_{pred} (%)	Adjusted regression, R^2_{adj} (%)	Predicted sum of square, PRESS
<i>C/N ratio</i>					
Linear	28.92	62.19	38.11	56.22	26001
Quadratic	6.12	98.84	93.13	98.04	2888
Special cubic	3.46	99.74	89.62	99.37	4361
Full cubic	2.20	99.94	92.70	99.79	3068
Special quartic	3.33	99.84	93.26	99.42	2833
<i>pH</i>					
Linear	0.080	73.03	61.73	68.77	0.175
Quadratic	0.066	87.63	62.26	79.06	0.171
Special cubic	0.072	89.66	0.00	74.72	0.984
Full cubic	0.074	92.78	0.00	73.52	1.770
Special quartic	0.073	93.00	0.00	74.34	25.384
<i>Electrical conductivity</i>					
Linear	0.163	72.58	60.48	68.56	0.731
Quadratic	0.112	91.22	54.71	85.16	0.837
Special cubic	0.098	95.31	0.00	88.54	2.506
Full cubic	0.076	98.11	81.99	93.08	0.333
Special quartic	0.084	97.72	0.00	91.63	3.730

$$\begin{aligned}
 Y_{CN} = & 42x_1 + 185x_2 + 45x_3 + 27x_4 - 253x_1x_2 - 71x_1x_3 + 27x_1x_4 - 328x_2x_3 - \\
 & 287x_2x_4 - 23x_3x_4 + 2550x_1^2x_2x_3 - 413x_1^2x_2x_4 - 1605x_1^2x_3x_4 + 1506x_2^2x_3x_4 - \\
 & 1986x_1x_2^2x_3 + 2027x_1x_3^2x_4 + 1437x_1x_2x_4^2 \quad (10)
 \end{aligned}$$

$$\begin{aligned}
 Y_{pH} = & 7.75x_1 + 7.75x_2 + 8.22x_3 + 8.08x_4 + 0.12x_1x_2 + 0.06x_1x_3 - 0.120x_1x_4 - \\
 & 0.04x_2x_3 + 0.02x_2x_4 - 0.96x_3x_4 \quad (11)
 \end{aligned}$$

$$\begin{aligned}
 Y_{EC} = & 0.643x_1 + 0.655x_2 + 1.235x_3 + 1.394x_4 + 0.013x_1x_2 - 0.503x_1x_3 + \\
 & 1.447x_1x_4 - 0.706x_2x_3 + 0.504x_2x_4 - 0.116x_3x_4 + 2.981x_1x_2x_3 + 4.733x_1x_2x_4 + \\
 & 5.243x_1x_3x_4 + 4.068x_2x_3x_4 \quad (12)
 \end{aligned}$$

Table 7 shows positive magnitudes in all of the linear coefficients (b_1 , b_2 , b_3 and b_4) implying that vegetable waste, fruit waste, meat waste and cow manure have synergistic effect on C/N ratio. In quadratic terms, vegetable waste with fruit waste (b_{12}) or meat waste (b_{13}), and fruit waste with meat waste (b_{23}) or cow manure (b_{24}) show significant antagonistic effect ($P < 0.05$) on the C/N ratio of compost. In addition, the coefficient b_{34} denotes that

Table 7
Regression coefficients for response variables of food wastes with cow manure composting

Term	C/N ratio	pH	Electrical conductivity
b_1	42	7.75	0.643
b_2	185	7.75	0.655
b_3	45	8.22	1.235
b_4	27	8.08	1.394
b_{12}	-253*	0.12	0.013
b_{13}	-71*	0.06	-0.503
b_{14}	27	-0.12	1.447*
b_{23}	-328*	-0.04	-0.706
b_{24}	-287*	0.02	0.504
b_{34}	-23	-0.96*	-0.116
b_{123}	-	-	2.981
b_{124}	-	-	4.733
b_{134}	-	-	5.243
b_{234}	-	-	4.068
b_{1123}	2550*	-	-
b_{1124}	-413	-	-
b_{1134}	-1605	-	-
b_{2234}	1506*	-	-
b_{1223}	-1986*	-	-
b_{1334}	2027*	-	-
b_{1244}	1437	-	-
R^2	0.998	0.876	0.981

Note. Subscripts: 1 = vegetable waste; 2 = fruit waste; 3 = meat waste; 4 = cow manure.

* indicates significant effect at $P < 0.05$.

the two-blend mixture of meat waste and cow manure significantly ($P < 0.05$) contributes to the reduction of pH value. The significant coefficient of b_{14} indicates that vegetable waste and cow manure have a significant effect on electrical conductivity of compost. It is suggested that by using two-blend mixture of vegetable waste and cow manure would produce a better quality of compost in terms of electrical conductivity.

Contour Plots and Response Surface Plot. The contour plots and 3D surface plots of all the responses, C/N ratio, pH and electrical conductivity of food wastes with cow manure composting are shown in Figure 5(a) - (c). Figure 5(a) illustrates that higher amount of cow manure produced compost with lower C/N ratio which is of better quality. It can be deduced that the mixture consisting moderate amount of vegetable and meat wastes, and little fruit waste with larger amount of cow manure for composting is suitable to generate good quality compost having the desired C/N ratio. The pH level increased with meat waste

and cow manure but decreased with vegetable and fruit wastes as shown in Figure 5(b). An excessive amount of cow manure in composting contributes to a very high pH value of compost which is unfavourable for the use of plantation. Figure 5(c) illustrates that the increase in vegetable and fruit wastes reduces the electrical conductivity of compost to less than 1 dS/m. It is suggested that the compost produced from mixture of large vegetable and fruit wastes with little cow manure could be used for soil substitution (US Composting Council, 1990). An increase in cow manure also increases the electrical conductivity of the compost generated which is highly desirable.

Figure 6 presents the overlaid contour plots of the three responses including C/N ratio, pH, and electrical conductivity for food wastes with cow manure composting. Any combination of vegetable, fruit, and meat wastes with cow manure that falls into the white zone also known as feasible region, is consider suitable for composting in producing good quality compost. The suggested combination of substrates for food wastes with cow manure composting is moderate amount of vegetable, fruit, and meat wastes with little cow manure.

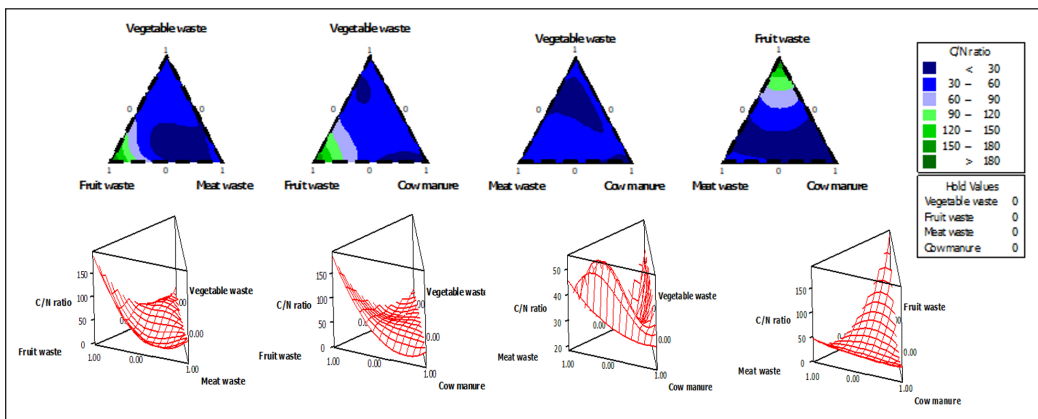


Figure 5(a). Mixture contour plots and 3D surface plots of C/N ratio of food wastes with cow manure composting

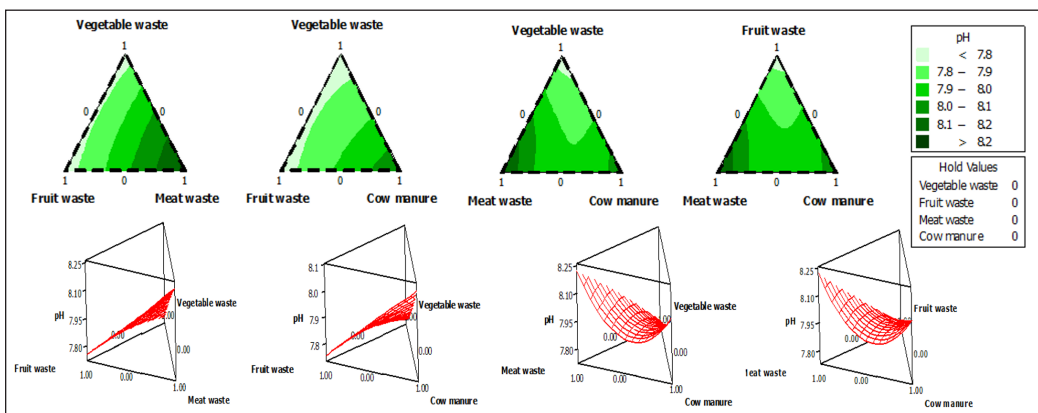


Figure 5(b). Mixture contour plots and 3D surface plots of pH of food wastes with cow manure composting

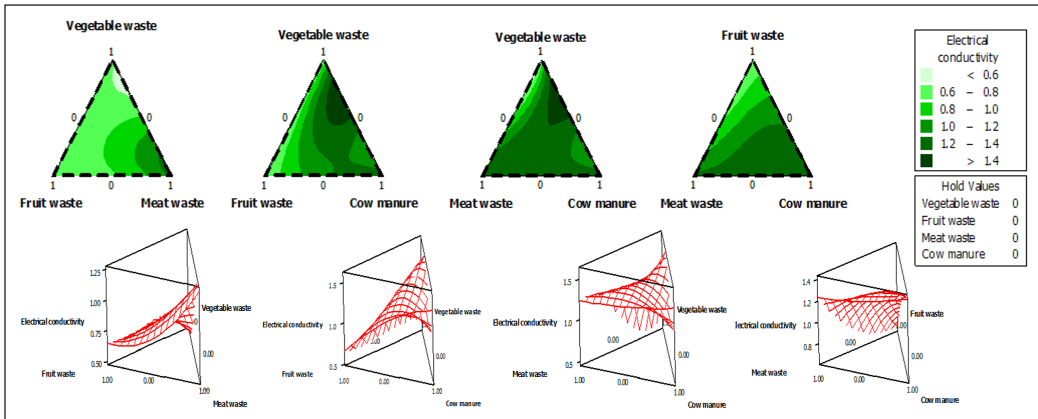


Figure 5(c). Mixture contour plots and 3D surface plots of electrical conductivity of food wastes with cow manure composting

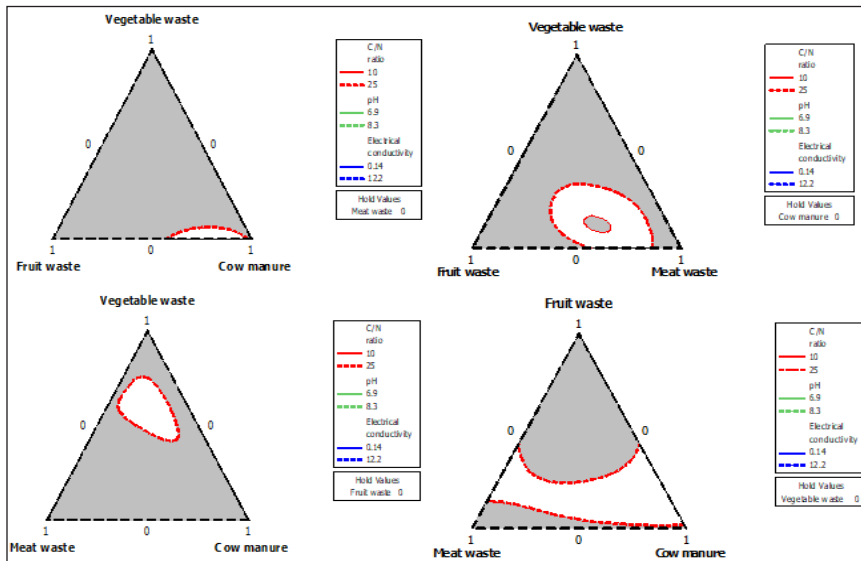


Figure 6. Overlaid contour plots of C/N ratio, pH and electrical conductivity of food wastes with cow manure composting

Response Optimization and Model Validation. The optimization plot of food wastes with cow manure composting is illustrated in Figure 7. The optimum settings for food wastes with dry leaves composting were 23.18% vegetable waste, 34.34% fruit waste, 36.46% meat waste, and 6.01% cow manure, with composite desirability of 0.977. The composite desirability is close to unity, indicating that the settings have achieved favourable results for all responses. The individual desirability shows that the settings are effective at maximising electrical conductivity (0.999) followed by minimising C/N ratio (0.997) and

maximising pH value (0.937). The favourable responses obtained for C/N ratio, pH and electrical conductivity were 21.01, 7.93, and 1.0 dS/m, respectively. The recommended percentage of cow manure at 6.01% is relatively lower than the earlier section using dry leaves at 86.88% because of its antagonistic effect. Cow manure has high pH values of 8.81 and high moisture content of 72.23% which are not required for targeted pH=8 and electrical conductivity of 1.0 dS/m. The suggested usage percentage of dry leaves or cow manure is based on the balancing of the pH and electrical conductivity for a conducive environment for microbial activity with main substrates composition comprising of vegetable, fruit and meat wastes.

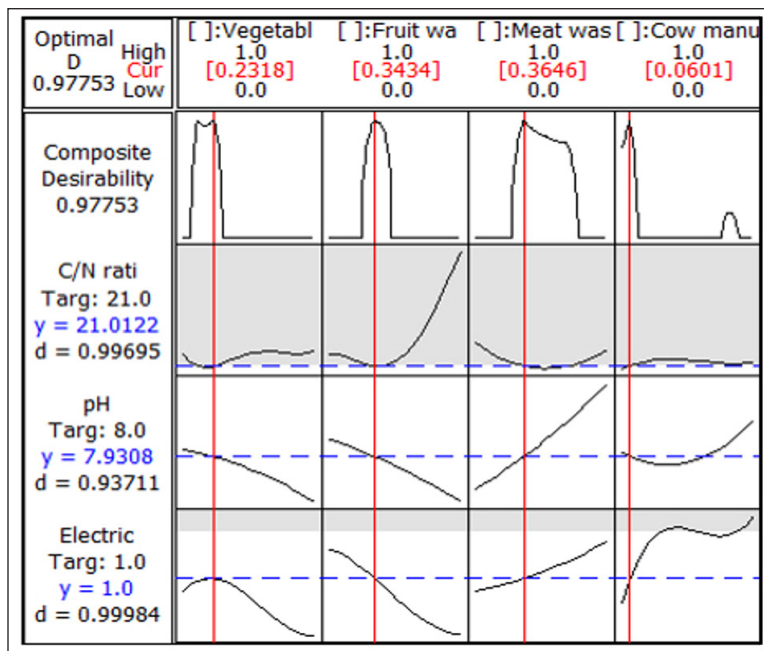


Figure 7. Optimization plot of food wastes with cow manure composting

Figure 7 shows that an increase in vegetable and fruit wastes will cause higher C/N ratio and reduces both, the pH value and electrical conductivity; hence, reduces the compost quality. This ultimate aim is to minimise C/N ratio, maximise pH value, and maximise electrical conductivity. In order to compromise between the conflicting goals, the optimal settings of both vegetable and fruit wastes are in the middle intervals between 23.18% and 34.34% in the experiment, respectively. An increase in meat waste and cow manure drastically increases the pH value and electrical conductivity which exhibits minimal effect on the C/N ratio. Thus, the optimal setting of meat waste is at 36.46% and cow manure is at 6.01% in the experiment.

The optimum proportion of food wastes with cow manure obtained from the optimization plot was employed to validate the models developed for the responses. The predicted response for C/N ratio is 21.19, pH value is 7.92, and electrical conductivity is 0.97 dS/m which are close to the targeted responses of C/N ratio (21.0), pH (8.0), and electrical conductivity (1.0 dS/m), respectively.

CONCLUSION

Each food waste substrate, *e.g.* the vegetable, fruit and meat wastes, and its bulking agent of dry leaves or cow manure exhibited different effects on the C/N ratio, pH and electrical conductivity of the compost produced. The vegetable and fruit wastes contributed to drastic reduction in pH value and electrical conductivity. The C/N ratio increased significantly with fruit waste. Contrarily, meat waste gave significant increase in pH level and electrical conductivity which are desirable for producing good quality compost. In general, addition of dry leaves or cow manure in food wastes composting has reduced the C/N ratio and increased both the pH value and electrical conductivity of the compost produced and this is helpful in building the characteristics of organic soil substitutes or biofertilizer. The pilot scale anaerobic digester can be used to produce consistent compost from food waste.

ACKNOWLEDGMENTS

This research work was funded by Universiti Putra Malaysia through the UPM Putra Grant Scheme (GP-IPS/2016/9475300). We thank Dr Meei Chien Quek for help in analysis and proofreading of this manuscript.

REFERENCES

- Abdullah, N., Chin, N. L., Mokhtar, M. N., & Taip, F. S. (2013). Effects of bulking agents, load size or starter cultures in kitchen-waste composting. *International Journal of Recycling of Organic Waste in Agriculture*, 2(1), 3-12
- Abdullah, N., & Chin, N. L. (2010). Simplex-centroid mixture formulation for optimized composting of kitchen waste. *Bioresource Technology*, 101(21), 8205-8210.
- Aparna, C., Saritha, P., Himabindu, V., & Anjaneyulu, Y. (2008). Techniques for the evaluation of maturity for composts of industrially contaminated lake sediments. *Waste Management*, 28(10), 1773-1784.
- Bernal, M. P., Albuquerque, J. A., & Moral, R. (2009). Composting of animal manures and chemical criteria for compost maturity assessment. A review. *Bioresource Technology*, 100(22), 5444-5453.
- Chang, J. I., & Hsu, T. E. (2008). Effects of compositions on food waste composting. *Bioresource Technology*, 99(17), 8068-8074.
- Chen, W. C., Chen, W. C., & Geng, D. S. (2008). The strategy and bioenergy potential for kitchen waste recycling in Taiwan. *Journal Environmental Engineering Management*, 18(4), 281-287.

- Codell, M., & Verderame, F. D. (1954). The determination of nitrogen in copper-titanium alloys. *Analytica Chimica Acta*, 11, 40-47.
- Cornell, J. A. (2002). *Experiment with Mixtures: Designs, Models, and the Analysis of Mixture Data* (3rd Ed.). New York, USA: John Wiley and Sons, Incorporation.
- Giroto, F., Alibardi, L., & Cossu, R. (2015). Food waste generation and industrial uses: a review. *Waste Management*, 45, 32-41.
- Gong, W. J., Zhang, Y. P., Zhang, Y. J., Xu, G. R., Wei, X. J., & Lee, K. P. (2007). Optimization strategies for separation of sulfadiazines using Box-Behnken design by liquid chromatography and capillary electrophoresis. *Journal of Central South University Technology*, 14(2), 196-201.
- Goossensen, M. (2017). *Anaerobic digestion of municipal organic waste in Amsterdam* (MSc Thesis). Wageningen University and Research, Wageningen, Netherlands.
- Grosso, M., Nava, C., Testori, R., Rigamonti, L., & Viganò, F. (2012). The implementation of anaerobic digestion of food waste in a highly populated urban area: an LCA evaluation. *Waste Management & Research*, 30(9), Supplement 78-87.
- Kumar, M., Ou, Y. L., & Lin, J. G. (2010). Co-composting of green waste and food waste at low C/N ratio. *Waste Management*, 30(4), 602-609.
- Larney, F. J., Yanke, L. J., Miller, J. J., & McAllister, T. A. (2003). Fate of coliform bacteria in composted bacteria in composted beef cattle feedlot manure. *Journal Environmental Quality*, 32(4), 1508-1515.
- Lin, C. (2008). A negative-pressure aeration system for composting food wastes. *Bioresource Technology*, 99(16), 7651-7656.
- Mohee, R., Driver, M. F., & Sobratee, N. (2008). Transformation of spent broiler litter form exogenous matter to compost in a sub-tropical context. *Bioresource Technology*, 99(1), 128-136.
- Poulsen, T. G. (2013). Chapter 5. Anaerobic digestion. In T. G. Poulsen (Ed.), *Solid Waste Management* (pp. 93-115). Aalborg University, Aalborg, Denmark. Retrieved January 23, 2018, from http://www.compost.org/CCC_Science_Web_Site/pdf/Digestate/Facts%20and%20Outputs.pdf
- Power Knot. (2012). Aerobic Composting vs. Anaerobic Composting. Retrieved January 23, 2018, from <http://www.powerknot.com/2012/07/23/aerobic-composting-vs-anaerobic-composting/>
- Rao, P. V., & Baral, S. S. (2011). Experimental design of mixture for the anaerobic co-digestion of sewage sludge. *Chemical Engineering Journal*, 172(2-3), 977-986.
- Schwab, B. S., Ritchie, C. J., Kain, D. J., Dobrin, G. C., King, L. W., & Palmisano, A. C. (1994). Characterization of compost form a pilot plant scale composter utilizing simulated solid waste. *Waste Management Resource*, 12(4), 289-303.
- Shyamala, D. C., & Belagali, S. L. (2012) Studies on variations in physico-chemical and biological characteristics at different maturity stages of municipal solid waste compost. *International Journal of Environmental Sciences*, 28(10), 1984-1997.
- Unmar, G., & Mohee, R. (2008). Assessing the effect of biodegradable and degradable plastics on the composting of green wastes and compost quality. *Bioresource Technology*, 99(15), 6738-6744.

- US Composting Council. (1990). *Test methods for the examination of composting and compost*. Retrieved January 23, 2018, from <http://compostingcouncil.org/wp/wp-content/plugins/wp-pdfupload/pdf/34/TMECC%20Purpose,%20Composting%20Process.pdf>
- Zhang, C., Su, H., Baeyens, J., & Tan, T. (2014). Reviewing the anaerobic digestion of food waste for biogas production. *Renewable and Sustainable Energy Reviews*, 38, 383-392.
- Zhang, W., Zhang, L., & Li, A. (2015). Anaerobic co-digestion of food waste with MSW incineration plant fresh leachate: process performance and synergistic effects. *Chemical Engineering Journal*, 259, 795-805.

Response of Cadmium Accumulation in Rice (*Oryza sativa* L. cv. SPR1) Grown with Different Organic Soil Amendments

Chitsanuphong Pratum

Faculty of Environment and Resource Studies, Mahidol University, Nakhon Pathom 73170, Thailand

ABSTRACT

Rice (*Oryza sativa* L.) is one of the food crops, which is found to have the great capacity of cadmium (Cd) accumulation. This research was done to investigate the response to Cd accumulation in rice grown with different organic soil amendments (OA), namely soil supplemented with swine manure (SM), cow manure (CM), mixed chicken manure and rice husk (CR), vermicompost (VC), and greensward compost (GC), respectively. Each OA (4% w/w basis) was applied in each treatment with 3 Cd levels at 20, 40, and 60 mg/kg, respectively. The results showed that rice plants were not able to grow in 4% w/w of SM and CM, respectively and wither following 70 d of planting. It was found in the other treatment results that CR, VC, and GC increased harvest index (HI) as well as soil pH while decreasing soil Eh and Cd-HI, compared with the control treatment. All the Cd concentrations did not affect the height, but the wet weight of plants, decreased with increase in Cd concentrations. Regarding the Cd accumulation, it was found that CR is most effective in absorbing Cd in the paddy soils. In terms of Cd uptake, it was found that GC was the only OA that could reduce the Cd uptake in the rice plant parts. The result is consistent with reduction observed in the accumulation of cadmium in stems, leaves, and especially rice grain. Therefore, based on the current finding, both CR and GC soil amendments can be considered for immobilizing Cd in the contaminated fields.

Keywords: Cadmium accumulation, organic soil amendments, paddy soil, rice plants

ARTICLE INFO

Article history:

Received: 30 March 2018

Accepted: 27 June 2018

Published: 24 January 2019

E-mail address:

chitsanuphong.pra@mahidol.ac.th, enchitsanu@gmail.com

INTRODUCTION

Heavy metal soil contamination is a serious and globally widespread problem that limits crop yields. Heavy metal pollutants do not easily biodegrade and remain almost indefinitely in the environment. When

it comes to heavy metal types, cadmium (Cd) is one of the highly toxic heavy metals which has a negative impact on the living cell at a very low concentration. From a health perspective, WHO (2003) agreed to maintain the Provisional Tolerable Weekly Intake of Cd at 7 µg/kg of body weight. Nowadays, the main sources of Cd entry into the environment come from anthropogenic sources. The most significant anthropogenic sources are fuel combustion, base-metal mining, sludge from paint and plastic stabilizer industries, and phosphate fertilizers as well as bio-solids in agriculture.

Rice (*Oryza sativa* L.) is one of the staple foodstuffs for many countries in Asia, especially Thailand, where contamination with Cd has been detected (Liu et al., 2007; Tang et al., 2016). The range of Cd concentration from 7.15 to 14.24 mg/kg was found in the rice grains from Mae Tao floodplains of Tak Province, Thailand (Pluemphuak et al., 2014). Meanwhile, CAC (2006) proposed a draft provisional maximum level for Cd content in polished rice of 0.4 mg/kg, used for the safety of both consumption and international trade. Simmons et al. (2003) revealed that rice grains accumulate higher Cd than stems and leaves, which significantly increases the risks to human health. Hence, the accumulation of Cd in the rice plants, especially rice grains, has been a major concern.

Therefore, reducing Cd bioavailability would be an urgent demand for safe rice production. A large number of methods have been employed to reduce Cd mobility such as a control in pH and increase in additional binding sites in the paddy soil (Zhou et al., 2014). Li et al. (2008) showed that the several soil amendments (namely; calcium magnesium phosphate, calcium silicate, pig manure, and peat) were able to increase the rice yield by 0.3-15.3 fold, and effectively decreased the Cu and Cd concentrations in rice grain by 23.0%-50.4%. This research demonstrated the effectiveness of organic soil amendments (OA) to reduce Cd bioavailability in a paddy soil and reduce Cd uptake by rice plants under continuous flooding conditions.

MATERIALS AND METHODS

Paddy Soil and Organic Wastes Characterization

A clean soil sample was collected from a paddy field in the topsoil layer at a depth of 0 to 20 cm in Nakhon Pathom Province, Thailand. Then, plant detritus and adulterated things were removed. Meanwhile, five OA: swine manure (SM), cow manure (CM), mixed chicken manure and rice husk (CR), vermicompost (VC), and greensward compost (GC) were prepared in the same way as the paddy soil samples. The selected physicochemical properties of paddy soil and OAs were listed in Table 1.

Cd-contaminated Soil Preparation

The preparation of Cd-contaminated soil consisted of 3 Cd levels; 20, 40, and 60 mg/kg, respectively. The Cd stock solution needed for mixing into the paddy soil sample

was prepared using cadmium chloride pentahydrate, $\text{CdCl}_2 \cdot 2.5\text{H}_2\text{O}$, dissolved in 500 ml distilled water (Liu et al., 2003). The Cd solution was slowly poured into and thoroughly mixed with the paddy soil sample. The initial concentrations of Cd in the spiked soil were 19.60 ± 0.20 , 40.22 ± 0.62 , and 62.87 ± 0.37 mg/kg, respectively. The soil was air dried and stored at room temperature.

Table 1

Selected physicochemical properties of paddy soil and organic soil amendments

Characterization	Paddy soil	Organic soil amendments				
		SM	CM	CR	VC	GC
pH	6.9	7.4	8.1	7.5	6.7	7.2
Electric Conductivity (dS/m)	0.1	4.6	9.1	8.8	2.6	1.5
Organic Matter (%)	1.1	48.8	61.8	46.4	28.2	28.9
Available Phosphorus (mg/kg)	6.0	2,055.0	282.0	2,574.0	173.0	157.0
Available Potassium (mg/kg)	186.0	7,419.0	22,853.0	13,206.0	2,454.0	1,634.0
Total Nitrogen (%)	0.1	3.1	1.5	1.8	1.4	1.5
Total Organic Carbon (mg/kg)	8.6	127.4	67.4	125.2	112	112.3
Cadmium (mg/kg)	nd	nd	nd	nd	nd	nd
Cation Exchange Capacity (cmol/kg)	62.6	1,110.0	1,450.0	98.0	39.0	65.0
C/N ratio	-	15.7	41.2	25.8	20.1	19.3
Particle size distribution (%)						
Sand	28	-	-	-	-	-
Silt	31	-	-	-	-	-
Clay	41	-	-	-	-	-

Note: nd = not detected

Rice Variety

The breeder seed, Suphan Buri 1 (SPR1) rice, was obtained from the Thai Rice Science Institution (TESI), Suphan Buri Province, Thailand. For the preparation of seedlings, rice seeds were soaked in tap water without chlorine for about 2 day (d) at room temperature and the germinated seeds were grown in the Cd-contaminated soil sample. After 30 d, the seedlings with 2 - 3 tillers or height of tillers about 10 cm were transplanted into plastic pots (Liu et al., 2007).

Experimental Design

A completely randomized experimental design was used and, in addition, greenhouse

experiments were also carried out at the Faculty of Environment and Resource Studies, Mahidol University, Thailand. Each 4% w/w basis of OAs was thoroughly mixed with Cd-contaminated soil and then, stored in the plastic pot (10-L cylindrical plastic container). Furthermore, the pot experiments were submerged with 2 - 3 cm tap water without chlorine above the soil surface for 14 d before transplanting rice (Liu et al., 2005). The pot treatment was arranged in the six treatments according to the addition of OA: control treatment without any OA (T1), added SM (T2), added CM (T3), added CR (T4), added VC (T5), and added GC (T6), respectively. All the pot treatments received macronutrient (N-P-K) thrice; i.e. the 3rd day before the seedling transplant, the 20th day after the transplant, and the 5th day before the panicles heading, respectively. One gram of urea and 1 g of $K_2HPO_4 \cdot 3H_2O$ were applied to each pot experiment on each occasion (Liu et al., 2007; Liu et al., 2003). The total growth periods in the pot experiments were maintained under the flooded conditions. The experiments were carried out in triplicates.

Analytical Methods

Rice Plant Growth. The rice plants from each pot were harvested at 45, 90, and 120 d after planting for the rice plant growth analysis. The wet weights of the shoots and roots of the rice plant samples were measured. The stem height was measured from the aboveground portion to the top of the stem. Any symptoms of Cd-induced toxicity exhibited by rice plant samples were visually noted throughout the experimental period. In addition, the harvest index (HI) was also measured by the total weight of harvested rice plants at the final of the experimental period (120 d) in each pot. Then, HI was calculated according to Eqn. 1 (Liu et al., 2005).

$$\text{Harvest index} = \frac{W_{\text{grains}}}{W_{\text{grains}} + W_{\text{shoots}}} \quad [\text{Eqn.1}]$$

where W_{grains} and W_{shoots} represent the dry weight content in rice grains and shoots, respectively.

Selected Soil Chemical Properties. The selected soil chemical properties were divided into 2 parameters namely, soil pH and soil redox potential (Eh). The electrode was placed 5 cm below the submerged paddy soil in each pot for measurements, which were repeated at intervals of 7 d (Pluemphuak et al., 2014).

Cd Concentration in Rice Plants and Paddy Soils. The rice plants from each pot were harvested 120 d after planting for Cd accumulation analysis. After harvesting, the rice plants were washed thoroughly 3 times with tap water and 3 times with distilled water (Liu et al., 2003), and then separated into rice grains (pedicel, husk, bran, and polished rice), leaves, stems, and roots and finally oven-dried at 60 – 65 °C until constant weight was obtained.

The dried rice plants were ground into powder and sieved through 2-mm mesh sieve. Then, the rice plants (1.0 g) were digested in concentrated HNO₃ and 30% H₂O₂, 4:1 (v/v). In the case of paddy soil, plant detritus and any visible fragments were separated and the soil air-dried at room temperature till constant weight. The dried paddy soils were ground into powder and sieved through 2-mm mesh sieve. Further, the soils (0.5 g) were digested in 37% HCl and concentrated HNO₃, 3:1 (v/v). The total Cd in these solutions was determined with Atomic Absorption Spectrophotometer (Hseu, 2004; Siswanto et al., 2013).

Cd Accumulation Potential in Rice Plants. The Cd accumulation potential in rice plants was divided into 2 parameters namely, the Cd-harvest index (Cd-HI) and the correlation coefficient of Cd in paddy soil and rice plant parts. The Cd-HI was estimated using Eqn. 2 (adapted from ur Rehman et al., 2017).

$$\text{Cd -Harvest index} = \frac{Cd_{grains} + Cd_{straw}}{Cd_{grains} + Cd_{straw} + Cd_{soil}} \quad [\text{Eqn.2}]$$

where Cd_{grains} , Cd_{straw} , and Cd_{soil} represent the Cd content in rice grains, straw, and paddy soil, respectively.

In addition, the rice plant parts (namely; rice grains, shoots, and roots) were used for the correlations coefficient of Cd. The linear correlation coefficient studies were made to evaluate the relationships among Cd concentrations in the paddy soil and the Cd concentrations and accumulation in various parts of rice plants.

Statistical Analysis

All data were analyzed by the SPSS Program for Windows. One-way ANOVA at confidence intervals of 95% ($P < 0.05$) was used for statistical analysis. Where significant, the multiple comparisons of means were made using Duncan's new multiple range tests (DMR test). In addition, Pearson's correlation coefficient (r) was used for a statistical measure of the strength of a linear relationship between paired data: Cd concentrations in the paddy soil and the Cd concentrations and accumulation in various parts of rice plants at confidence intervals of 95% ($P < 0.05$) and 99% ($P < 0.01$).

RESULTS AND DISCUSSION

Rice Plant Growth

The rice plants in T2 and T3 were not able to grow at 70 d after planting. The rice roots showed symptoms of black root rotting with a characteristic rotten egg odor, stunted growth, lack of tillering, yellowish rice foliage, and wilting. Therefore, T2 and T3 rice plant growth cannot be measured. This might be due to hydrogen sulfide (H₂S) toxicity in rice roots as shown in Figure 1. One of the main gases related to pig manure and cow manure is H₂S, which oxidizes rapidly to sulfuric acid (H₂SO₄) in the presence of water (Koelsch et al.,

2004; Ni et al., 2000). The formation of H₂S often results from the microbial breakdown of organic matter in anaerobic digestion (Joshi et al., 1975). As H₂S toxicity progresses, rice plants suffer reductions in the absorption of nutrients and its metabolic system (Lamers et al., 2013).

In other treatments, the study of the rice plants height revealed that all Cd level (20, 40, and 60 mg/kg) did not affect the rice plants height and neither did it show any abnormalities in stems and leaves of rice plant. However, Cd level at 100 mg/kg was found to directly affect and reduce the height of the rice plants (Herath et al., 2014). On the part of the rice plants wet weight, all Cd level did affect the rice plants wet weight. Wet weight was found to decrease as the Cd concentrations increased. The reduction of wet weight might be due to inhibition of Cd on the physiological processes, namely, photosynthesis, cell division, plant metabolism and cellular respiration. (Li et al., 2017).

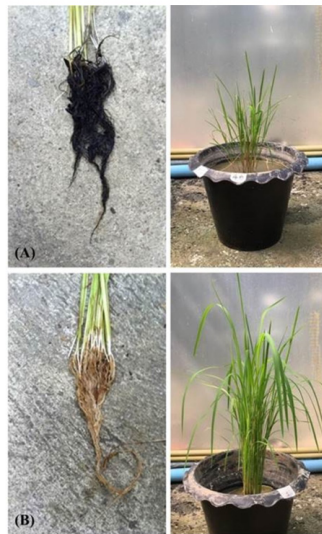


Figure 1. Symptoms of hydrogen sulfide toxicity on rice roots; (A) the black root rotting in T2 and T3 and (B) the normal root in T1 (control treatment)

Harvest Index (HI)

The HI was used as an indicator of plant efficiency in dry weight accumulation. In general, the harvest index of rice is 0.17 - 0.56 (Ju et al., 2009). As shown in Table 2, Cd level at 20 and 40 mg/kg did not affect the HI, which was not significantly different ($P > 0.05$). In addition, Cd level at 60 mg/kg has the highest HI with significant differences ($P < 0.05$) at T6. The low Cd concentration (at 20 and 40 mg/kg) did not affect the harvest index of SPR1 rice. This might be attributed to its tolerance mechanism to Cd toxicity (Juang et al., 2012; Tang et al., 2016). The glutathione (GSH) of rice plants played an important role in keeping the cellular redox balance under Cd stress (Sebastian & Prasad, 2014). In

Table 2

HI of rice plants grown in Cd-contaminated soil at different Cd levels

Treatment	Cd levels (mg/kg)		
	20	40	60
T4	0.36±0.06 ^{a, A}	0.31±0.04 ^{a, A}	0.28±0.01 ^{ab, A}
T5	0.34±0.02 ^{a, A}	0.32±0.05 ^{a, A}	0.31±0.02 ^{ab, A}
T6	0.41±0.09 ^{a, A}	0.40±0.04 ^{a, A}	0.35±0.09 ^{b, A}
T1 (control treatment)	0.43±0.05 ^{a, C}	0.34±0.05 ^{a, B}	0.23±0.09 ^{a, A}

Note: Data with the small letters (a, b) showed differences between Cd contents (rows) and the capital letters (A, B, C) showed differences between treatment (columns) at $P < 0.05$ according to the DMR test

addition, phytochelatin is also produced to enhance the tolerance of rice plants to Cd stress (Tiryakioglu et al., 2006) The Cd is trapped in the vacuole of the roots and leaves in rice plants (Li et al., 2017). A decrease of HI was observed with increase in Cd concentrations. Khampuang et al. (2016) reported a similar observation.

Selected Soil Chemical Properties

Soil pH. Results regarding average soil pH (throughout planting at 120 d) are presented in Figure 2. Cd level 20 at mg/kg, the soil pH increased due to the OAs in the following order: T5 > T6 > T4 > T1 (control treatment). Cd level at 40 and 60 mg/kg, the soil pH increased due to the OAs in the following order T6 > T4 > T5 > T1 (control treatment). The soil pH was significantly ($P < 0.05$) increased, which may be due to alkaline properties of the OAs. The soil pH has been shown to be one of the key factors which govern the availability of heavy metals in acidic soil (Hooda & Alloway, 1998). Lower pH levels in soil have resulted in rice plants absorbing high amounts of Cd and accumulations in various parts, especially the rice grains. Therefore, increasing the pH of the soil can reduce the Cd absorption by rice, which can be used both in highland and lowland areas (Kikuchi et al., 2008).

Soil Eh. The Eh, an index to relatively quantify the oxidizing and reducing substances, is also an important factor that can control the Cd bioavailability. In paddy soil, continuous flooding, and the OAs had impacts on soil Eh. Cd level at 20 and 40 mg/kg, soil Eh was decreased by the OAs in the following order: T4 > T5 > T6 > T1 (control treatment). While for the Cd level at 60 mg/kg, soil Eh was decreased by the OAs in the following order: T4 > T6 > T5 > T1 (control treatment). The results showed that the OAs could significantly ($P < 0.05$) decrease Eh, which are presented in Figure 3. The soil Eh decreased after applying the OAs probably from increasing the amount of reducing matters (e.g., ferrous ion (Fe^{2+}), humic acids, and fulvic acids) in paddy soil during the interaction between the OAs and paddy soil components (Ji et al., 2007; Liu et al., 2010). Therefrom, Cd in paddy soil was in the form of insoluble compounds, combined with the reducing matters. In addition, root

exudates include both organic ligands and inorganic ligands (e.g., Cl^- , SO_4^{2-} , NH_4^+ , CO_3^{2-} , PO_4^{3-} , etc.). These substances function not only as the energy source of microorganisms but also as ligands to chelate with Cd^{2+} and then influence the pH and Eh conditions as well as chemical characteristics in the rhizosphere (Dong et al., 2007).

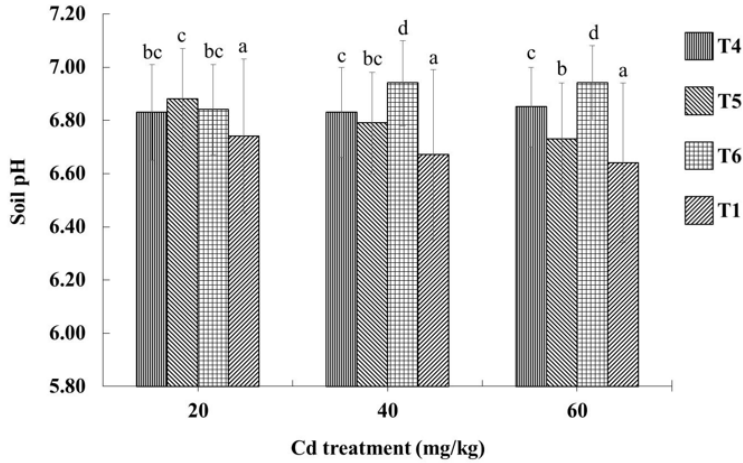


Figure 2. Average soil pH (throughout planting at 120 d) in Cd-contaminated soil and the small letters (a, b,.. d) showed differences each bar diagram at $P < 0.05$ according to the DMR test

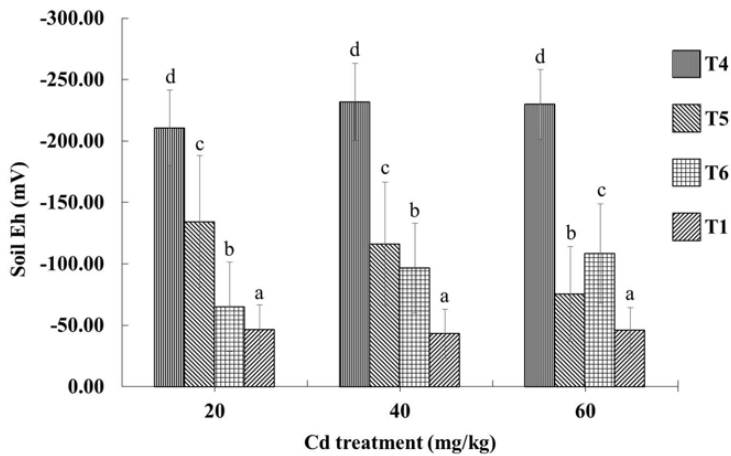


Figure 3. Average soil Eh (throughout planting at 120 d) in Cd-contaminated soil and the small letters (a, b,.. d) showed differences each bar diagram at $P < 0.05$ according to the DMR test

Table 3
Cd accumulation in rice plants and paddy soils at different Cd levels

Cd levels (mg/kg)	Treatment	Cd concentration (mg/kg)										¹ Capacity to adsorb Cd (%)			
		Paddy soil	Roots	Stems			Leaves			Shoots					
				Polished rice	Bran	Husk	Rice grain	Husk	Pedicle	Polished rice	Bran		Husk		
20	T4	17.63±0.31 ^a	1.06±0.06 ^a	0.07±0.01 ^a	0.36±0.04 ^a	0.19±0.01 ^b	0.02±0.00 ^a	0.12±0.03 ^a	0.12±0.00 ^a	0.02±0.00 ^a	0.05±0.01 ^a	0.11±0.02 ^a	0.19±0.01 ^b	0.00±0.00 ^b	13.70±4.65 ^c
	T5	14.39±1.37 ^a	4.20±0.15 ^c	0.09±0.01 ^a	0.43±0.06 ^a	0.05±0.01 ^a	0.05±0.01 ^a	0.05±0.01 ^a	0.11±0.02 ^a	0.05±0.01 ^a	0.09±0.03 ^b	0.21±0.01 ^b	0.19±0.01 ^b	0.00±0.00 ^a	0.00±0.00 ^a
	T6	12.60±1.09 ^a	4.95±0.02 ^d	0.15±0.02 ^b	0.90±0.05 ^c	0.33±0.00 ^c	0.09±0.03 ^b	0.21±0.01 ^b	0.19±0.01 ^b	0.09±0.03 ^b	0.09±0.03 ^b	0.21±0.01 ^b	0.19±0.01 ^b	0.00±0.00 ^a	0.00±0.00 ^a
	T1	14.89±1.24 ^a	3.35±0.05 ^b	0.22±0.01 ^c	0.71±0.02 ^b	0.18±0.04 ^b	0.05±0.01 ^{ab}	0.13±0.02 ^a	0.11±0.00 ^a	0.05±0.01 ^{ab}	0.18±0.04 ^b	0.13±0.02 ^a	0.11±0.00 ^a	0.00±0.00 ^b	0.00±0.00 ^b
40	T4	35.67±1.22 ^b	2.42±0.04 ^a	0.18±0.01 ^a	1.18±0.02 ^a	0.29±0.04 ^a	0.04±0.00 ^a	0.04±0.02 ^a	0.20±0.00 ^a	0.04±0.00 ^a	0.04±0.00 ^a	0.04±0.02 ^a	0.20±0.00 ^a	0.00±0.00 ^a	27.83±7.80 ^c
	T5	29.85±1.78 ^a	8.11±0.07 ^b	0.17±0.00 ^a	1.21±0.13 ^a	0.25±0.03 ^a	0.13±0.03 ^a	0.21±0.00 ^b	0.27±0.01 ^b	0.13±0.03 ^a	0.25±0.03 ^a	0.21±0.00 ^b	0.27±0.01 ^b	0.00±0.00 ^a	13.28±6.40 ^b
	T6	27.53±1.85 ^a	10.76±0.41 ^c	0.27±0.02 ^b	1.01±0.02 ^b	0.31±0.07 ^a	0.09±0.02 ^b	0.19±0.01 ^b	0.21±0.00 ^b	0.09±0.02 ^b	0.31±0.07 ^a	0.19±0.01 ^b	0.21±0.00 ^a	0.00±0.00 ^a	7.48±6.22 ^{ab}
	T1	24.54±4.34 ^a	9.85±0.09 ^b	1.06±0.02 ^c	3.01±0.02 ^c	0.49±0.04 ^b	0.26±0.02 ^d	0.44±0.01 ^c	0.36±0.01 ^c	0.49±0.04 ^b	0.49±0.04 ^b	0.44±0.01 ^c	0.36±0.01 ^c	0.00±0.00 ^a	0.00±0.00 ^a
60	T4	54.50±3.55 ^c	5.92±0.07 ^a	0.13±0.01 ^a	1.12±0.05 ^b	0.17±0.00 ^a	0.08±0.01 ^a	0.27±0.02 ^b	0.27±0.00 ^b	0.17±0.00 ^a	0.08±0.01 ^a	0.27±0.02 ^b	0.27±0.00 ^b	0.00±0.00 ^a	16.75±0.62 ^d
	T5	51.06±2.39 ^{bc}	8.76±0.10 ^c	0.37±0.03 ^c	1.23±0.03 ^c	0.33±0.01 ^b	0.16±0.04 ^b	0.32±0.00 ^c	0.34±0.00 ^c	0.33±0.01 ^b	0.16±0.04 ^b	0.32±0.00 ^c	0.34±0.00 ^c	0.00±0.00 ^a	11.02±2.55 ^c
	T6	47.56±6.45 ^{ab}	13.22±0.34 ^d	0.23±0.01 ^b	0.83±0.04 ^a	0.19±0.04 ^a	0.07±0.01 ^a	0.18±0.02 ^a	0.19±0.01 ^a	0.19±0.04 ^a	0.19±0.04 ^a	0.18±0.02 ^a	0.19±0.01 ^a	0.00±0.00 ^a	5.18±4.22 ^b
	T1	44.45±3.92 ^a	8.54±0.07 ^b	1.31±0.04 ^d	3.98±0.04 ^d	1.30±0.05 ^c	0.37±0.03 ^c	0.81±0.02 ^d	0.48±0.00 ^d	1.30±0.05 ^c	1.30±0.05 ^c	0.81±0.02 ^d	0.48±0.00 ^d	0.00±0.00 ^a	0.00±0.00 ^a

Note: Data with the small letters (a, b, ...d) showed differences between columns at $P < 0.05$ according to the DMR test.

¹ the capacity to adsorb Cd of T4, T5, and T6 when compared with T1 (control treatment)

Table 4

Cd-HI of rice plants grown in Cd-contaminated soil

Treatment	Cd levels (mg kg ⁻¹)		
	20	40	60
T4	0.48±0.08 ^{b,A}	0.51±0.02 ^{b,A}	0.36±0.03 ^{a,A}
T5	0.57±0.11 ^{ab,A}	0.70±0.03 ^{b,A}	0.51±0.03 ^{a,B}
T6	1.30±0.10 ^{c,C}	0.70±0.03 ^{b,A}	0.35±0.04 ^{a,A}
T1 (control treatment)	0.86±0.07 ^{a,B}	1.89±0.26 ^{b,B}	1.57±0.11 ^{b,C}

Note: Data with the small letters (a, b,c) showed differences between Cd contents (rows) and the capital letters (A, B, C) showed differences between treatment (columns) at P<0.05 according to the DMR test

Table 5

Pearson's correlation coefficient between Cd in paddy soil, rice grains, shoots, and roots

		Paddy soil	Rice grains	Shoots	Roots
T4	Paddy soil	-	0.877**	0.728*	0.964**
	Rice grains	-	-	0.341	0.965**
	Shoots	-	-	-	0.561
	Roots	-	-	-	-
T5	Paddy soil	-	0.961**	0.914**	0.879**
	Rice grains	-	-	0.978**	0.955**
	Shoots	-	-	-	0.990**
	Roots	-	-	-	-
T6	Paddy soil	-	-0.598	-0.406	0.920**
	Rice grains	-	-	0.572	-0.504
	Shoots	-	-	-	-0.132
	Roots	-	-	-	-
T1	Paddy soil	-	0.934**	0.916**	0.595
	Rice grains	-	-	0.997**	0.805**
	Shoots	-	-	-	0.844**
	Roots	-	-	-	-

Note: *, ** Correlation is significant at P<0.05 and P<0.01, respectively.

Cd Concentration in Rice Plants and Paddy Soils

As shown in Table 3, an increase of Cd was observed in both rice plants and paddy soils of all treatments when Cd concentration was increased in soils. Meanwhile, the polished rice Cd concentration in T4, T5, T6, and T1 (control treatment) increased when Cd concentration in soil increased and reached a maximum value of 0.48 mg/kg cadmium in T1 (Cd level at 60 mg/kg). The influence of the OAs on Cd adsorption in the paddy soils revealed that CR (at 4% w/w basis) was most effective for Cd adsorption. On the average, the capacity to adsorb Cd when compared with T1 was $13.70 \pm 4.65\%$, $27.83 \pm 7.80\%$, and $16.75 \pm 0.62\%$ with 20, 40, and 60 mg/kg applied paddy soil, respectively. These results agree with those of Shokalu et al. (2017), in which a high capacity adsorb Cd of 99.7% was observed when poultry manure was applied at 4% w/w basis. In addition, the results also reported that the addition of poultry manure (4% w/w) caused the significant reduction in the bioavailable Cd concentration.

The analysis of the efficiency of the OAs to increase Cd accumulation in the rice plants revealed that the GC (at 4% w/w basis) was most effective in stimulating Cd accumulation, especially the roots. As a result, the Cd accumulation in roots increased, while Cd in polished rice significantly decreased ($P < 0.05$). This reduces the accumulation of cadmium in stems, leaves, and especially rice grain. In addition, the accumulation of cadmium in various parts of the rice plants found that the Cd accumulation is greater than stems followed by leaves and then rice grain, respectively. The paddy soil properties can be improved by the binding between organic matter in the GC and clay particles via cation bridges because it increases soil porosity and stimulates root growth (Gao et al., 2010; Leroy et al., 2008). Organic matter can also indirectly improve soil structure by increasing microbial activity and thus the production of microbial slimes, fungal hyphae and/or roots to bind aggregates together (Tisdall & Oades, 1982). In addition, the chemical fertility (e.g., soil pH electric conductivity (EC) and CEC), was also increased by compost application (Bulluck et al., 2002; Ouédraogo et al., 2011). On the average, Cd concentration (mg/kg) in polished rice was 0.19 ± 0.01 , 0.21 ± 0.00 and 0.19 ± 0.01 with 20, 40 and 60 mg/kg applied paddy soil, respectively. The Cd content was lower than 0.4 mg/kg, which is the highest acceptable Cd concentration in polished rice (CAC, 2006). Hence, applying the OAs to paddy soil can reduce Cd accumulation in rice plants (Wang et al., 2012).

Cd-harvest Index (Cd-HI)

The Cd-HI calculation is a proximal approach (Qayyum et al., 2017). It has been described for the Cd absorption from soil by the use of plants such as rice plants in the present study. For Cd level at 20 mg/kg, the T6 showed that the Cd-HI significantly increased ($P > 0.05$). For Cd level at 40 and 60 mg/kg, the T1 showed that the Cd-HI significantly increased ($P > 0.05$). The higher Cd-HI in T6 might be due to the GC stimulating root growth, resulting

in an increase in the Cd absorption. Plant root growth can increase greatly when using organic compost (Gao et al., 2010). Whereas, all types of the OAs (CR, VC, and GC) were effective in decreasing the Cd absorption from paddy soil by rice plants. However, the decreasing Cd-HI in each treatment might be due to a decrease in available Cd concentration in the soil with the application of the OAs, as shown in Table 4.

The Trend of Cd Uptake

Pearson's correlation coefficient was used to study the trend of Cd uptake of rice plants. As shown in Table 5, the increase of Cd concentration in the paddy soils has an influence on the increase of Cd accumulation in the rice parts, especially rice grains, at T4, T5, and T1 (control treatment). It has increased significantly ($P < 0.01$). These results agree with those of Tang et al. (2016), Sebastian and Prasad (2014), Hanč et al. (2008), and Rizk et al. (2014) found that Cd accumulation in rice plant parts increased when Cd concentration in the paddy soil increased. In Cd translocation, the xylem is the major physiological process determining the Cd accumulation level in shoots and rice grains of rice plants (Uraguchi et al., 2009).

At T6, the Cd concentration in paddy soil was negatively correlated with the Cd concentrations in rice grains and shoots. This showed that the increase in Cd concentration in paddy soil did not increase the Cd concentrations in rice grains and shoots. However, the Cd concentrations in paddy soil were positively correlated with the Cd concentrations in roots. This showed that the increase in Cd concentration in paddy soil increased the Cd concentrations in roots. This result showed that Cd accumulation decreased in rice plant parts with the GC applied compared with other OAs. The Cd in paddy soil did not tend to accumulate in rice plants because it was mostly absorbed by the roots (see data section; Cd concentration in rice plants and paddy soils). Abe et al. (1995) also reported GC stimulated root growth (particularly nodal roots), which helped in absorbing nutrients or heavy metals. In addition, the application of the GC combined with the chemical fertilizer can increase the length and weight of roots from 30 to 40 % (Rizk et al., 2014; Yang et al., 2004).

CONCLUSIONS

In this research, OAs had a positive effect on reducing Cd uptake by rice. All OAs increased HI and soil pH while decreasing soil Eh and Cd-HI, compared with the control treatment. Among the OAs, CR was highly effective in absorbing and retaining Cd in the paddy soil. Whereas, GC was the only OA that could reduce the Cd uptake into the rice plant parts, especially polished rice. The studied indicated that Cd in paddy soil do not tend to accumulate in rice plants because it is mostly absorbed by the rice roots. Therefore, it can be suggested that both CR and GC might be used to immobilize Cd in the Cd-contaminated

fields. Future work should evaluate on the combination of CR and GC organic soil amendments and its application to immobilize Cd.

ACKNOWLEDGMENT

The financial support (No. 004/2016) from Asia Research Center, Chulalongkorn University, Thailand, is gratefully acknowledged.

REFERENCES

- Abe, J., Songmuang, P., & Harada, J. (1995). Root growth of paddy rice with application of organic materials as fertilizers in Thailand. *Japan Agricultural Research Quarterly*, 29(2), 77–82.
- Bulluck, L. R., Brosius, M., Evanylo, G. K., & Ristaino, J. B. (2002). Organic and synthetic fertility amendments influence soil microbial, physical and chemical properties on organic and conventional farms. *Applied Soil Ecology*, 19(2), 147–160.
- CAC. (2006). *Report of the Thirty-eighth Session of the Codex Committee on Food Additives and Contaminants* (ALINORM 06/29/12). Hague: Codex Alimentarius Commission.
- Dong, J., Mao, W. H., Zhang, G. P., Wu, F. B., & Cai, Y. (2007). Root excretion and plant tolerance to cadmium toxicity – A review. *Plant Soil Environment*, 53(5), 193–200.
- Gao, M., Liang, F., Yu, A., Li, B., & Yang, L. (2010). Evaluation of stability and maturity during forced-aeration composting of chicken manure and sawdust at different C/N ratios. *Chemosphere*, 78, 614–619.
- Hanč, A., Tlustoš, P., Száková, J., Habart, J., & Gondek, K. (2008). Direct and subsequent effect of compost and poultry manure on the bioavailability of cadmium and copper and their uptake by oat biomass. *Plant Soil Environment*, 54(7), 271–278.
- Herath, H. M. D. A. K., Bandara, D. C., Weerasinghe, P. A., Iqbal, M. C. M., & Wijayawardhana, H. C. D. (2014). Effect of Cadmium on Growth Parameters and Plant Accumulation in Different Rice (*Oryza sativa* L.) Varieties in Sri Lanka. *Tropical Agricultural Research*, 25(4), 532–542.
- Hooda, P. S., & Alloway, B. J. (1998). Cadmium and Lead sorption behavior of selected English and Indian soils. *Geoderma*, 84, 121–134.
- Hseu, Z. Y. (2004). Evaluating heavy metal contents in nine composts using four digestion methods. *Bioresource technology*, 95(1), 53–59.
- Ji, X. H., Liang, Y. C., Lu, Y. H., Liao, Y. L., Nie, J., Zheng, S. X., & Li, Z. J. (2007). The effect of water management on the mechanism and rate of uptake and accumulation of cadmium by rice growing in polluted paddy soil. *Acta Ecologica Sinica*, 27(3), 393–3,939.
- Joshi, M. M., Ibrahim, I. K. A., & Hollis, J. P. (1975). Hydrogen sulfide: Effects on the physiology of rice plants and relation to straighthead disease. *Phytopathology*, 65(10), 1165–1170.
- Ju, J., Yamamoto, Y., Wang, Y. L., Shan, Y. H., Dong, G. C., Miyazaki, A., & Yoshida, T. (2009). Genotypic differences in dry matter accumulation, nitrogen use efficiency and harvest index in recombinant inbred lines of rice under hydroponic culture. *Plant Production Science*, 12, 208–216.

- Juang, K. W., Ho, P. C., & Yu, C. H. (2012). Short-term effects of compost amendment on the fractionation of cadmium in soil and cadmium accumulation in rice plants. *Environmental Science and Pollution Research*, 19(5), 1696–1708.
- Khampuang, K., Sooksamiti, P., Lapanantnoppakun, S., Yodthongdee, Y., & Prom-u-thai, C. T. (2016). Response of grain yield among 3 rice varieties grown at different soil Cd concentrations. *Khon Kaen Agricultural Journal*, 44(3), 409–416.
- Kikuchi, T., Okazaki, M., Kimura, S. D., Motobayashi, T., Baasansuren, J., Hattori, T., & Abe, T. (2008). Suppressive effects of magnesium oxide materials on cadmium uptake and accumulation into rice grains: II: Suppression of cadmium uptake and accumulation into rice grains due to application of magnesium oxide materials. *Journal of hazardous materials*, 154(1), 294–299.
- Koelsch, R. K., Woodbury, B. L., Stenberg, D. E., Miller, D. N., & Schulte, D. D. (2004). Total reduced sulfur concentrations in the vicinity of beef cattle feedlots. *Applied Engineering in Agriculture*, 20(1), 77–85.
- Lamers, L. P. M., Govers, L. L., Janssen, I. C. J. M., Geurts, J. J. M., Van der Welle, M. E. W., Van Katwijk, M. M., ... & Smolders, A. J. (2013). Sulfide as a soil phytotoxin—a review. *Frontiers in Plant Science*, 268(4), 1–14.
- Leroy, B. L. M., Herath, H. M. S. K., Sleutel, S., de Neve, S., Gabriels, D., Reheul, D., & Moens, M. (2008). The quality of exogenous organic matter: short-term effects on soil physical properties and soil organic matter fractions. *Soil Use and Management*, 24(2), 139–147.
- Li, H., Luo, N., Li, Y. W., Cai, Q. Y., Li, H. Y., Mo, C. H., & Wong, M. H. (2017). Cadmium in rice: Transport mechanisms, influencing factors, and minimizing measures. *Environmental Pollution*, 224, 622–630.
- Liu, J., Li, K., Xu, J., Liang, J., Lu, X., Yang, J., & Zhu, J. (2003). Interaction of Cd and five mineral nutrients for uptake and accumulation in different rice cultivars and genotypes. *Field Crops Research*, 83, 271–281.
- Liu, J., Qian, M., Cai, G., Yang, J., & Zhu, Q. (2007). Uptake and translocation of Cd in different rice cultivars and the relation with Cd accumulation in rice grain. *Journal of Hazardous Materials*, 143, 443–447.
- Liu, J., Zhu, Q., Zhang, Z., Xu, J., Yang, J., & Wong, H. M. (2005). Variations in Cadmium accumulation among rice cultivars and types and the selection of cultivars for reducing cadmium in the diet. *Journal of the Science of Food and Agriculture*, 85, 147–153.
- Liu, J. G., Cao, C. X., & Wong, M. H. (2010). Variations between rice cultivars in iron and manganese plaque on roots and the relation with plant cadmium uptake. *Journal of Environmental Sciences*, 22, 1067–1072.
- Li, P., Wang, X., Zhang, T., Zhou, D., & He, Y. (2008). Effects of several amendments on rice growth and uptake of copper and cadmium from a contaminated soil. *Journal of Environmental Sciences*, 20(4), 449–455.
- Ni, J. Q., Heber, A. J., Diehl, C. A., & Lim, T. T. (2000). Ammonia, Hydrogen Sulphide and Carbon Dioxide Release from Pig Manure in Under-floor Deep Pits. *Journal of Agricultural Engineering Research*, 77(1), 53–66.
- Ouédraogo, E., Mando, A., & Zombré, N. P. (2001). Use of compost to improve soil properties and crop productivity under low input agricultural system in West Africa. *Agriculture, Ecosystems and Environment*, 84(3), 259–266.

- Pluemphuak, T., Mala, T., & Kumlung, A. (2014). Cadmium contents in rice grown in Cd contaminated paddy fields in Mae Tao floodplains Tak Province Thailand. *Journal of Science and Technology*, 3(2), 26–38.
- Qayyum, M. F., ur Rehman, M. Z., Ali, S., Rizwan, M., Naeem, A., Maqsood, M. A., ... & Ok, Y. S. (2017). Residual effects of monoammonium phosphate, gypsum and elemental sulfur on cadmium phytoavailability and translocation from soil to wheat in an effluent irrigated field. *Chemosphere*, 174, 515–523.
- Rizk, A. H., Zaazaa, E. I. & Shower, S. S. (2014). Effect of Cadmium on Yield, Nutrient Contents and Toxicity Tolerance of Some Rice Varieties. *Middle East Journal of Applied Sciences*, 4(4), 1110–1117.
- Sebastian, A., & Prasad, M. N. V. (2014). Photosynthesis mediated decrease in cadmium translocation protect shoot growth of *Oryza sativa* seedlings up on ammonium phosphate–sulfur fertilization. *Environmental Science and Pollution Research*, 21(2), 986–997.
- Shokalu, A. O., Adetunji, M. T., Bodunde, J. G., Akintoye, H. A., & Azeez, J. O. (2017). Cadmium adsorption as influenced by poultry manure addition in soils of South-Western Nigeria. *Archives of Agronomy and Soil Science*, 63(8), 1070–1081.
- Simmons, R. W., Pongsakul, P., Chaney, R. L., Saiyasitpanich, D., Klinphoklap, S., & Nobuntou W. (2003). The relative exclusion of zinc and iron from rice grain in relation to rice grain cadmium as compared to soybean: Implications for human health. *Plant Soil*, 257(1), 163–170.
- Siswanto, D., Suksabye, P., & Thiravetyan, P. (2013). Reduction of cadmium uptake of rice plants using soil amendments in high cadmium contaminated soil: a pot experiment. *The Journal of Tropical Life Science*, 3(2), 132–137.
- Tang, H., Li, T., Yu1, H., & Zhang, X. (2016). Cadmium accumulation characteristics and removal potentials of high cadmium accumulating rice line grown in cadmium-contaminated soils. *Environmental Science and Pollution Research*, 23(15), 15351–15357.
- Tiryakioglu, M., Eker, M., Ozkutlu, F., Husted, S., & Cakmak, I. (2006). Antioxidant defense system and cadmium uptake in barley genotypes differing in cadmium tolerance. *Journal of Trace Elements in Medicine and Biology*, 20, 181–189.
- Tisdall, J. M., & Oades, J. M. (1982). Organic matter and water stable aggregates in soils. *Journal of Soil Science*, 33, 141–163.
- ur Rehman, M. Z., Khalid, H., Akmal, F., Ali, S., Rizwan, M., Qayyum, M. F., ... & Azhar, M. (2017). Effect of limestone, lignite and biochar applied alone and combined on cadmium uptake in wheat and rice under rotation in an effluent irrigated field. *Environmental Pollution*, 227, 560–568.
- Uraguchi, S., Mori, S., Kuramata, M., Kawasaki, A., Arao, T., & Ishikawa, S. (2009). Root-to-shoot Cd translocation via the xylem is the major process determining shoot and grain cadmium accumulation in rice. *Journal of Experimental Botany*, 60(9), 2,677–2,688.
- Wang, L., Xu, Y. M., Liang, X. F., Sun, G. H., Sun, Y. B., & Lin, D.S. (2012). Remediation of contaminated paddy soil by immobilization of pollutants in the Diaojiang Catchment, Guangxi Province. *Journal of Ecology and Rural Environment*, 28, 563–568.

- WHO. (2003). *WHO technical report series; 922 on Evaluation of certain food additives and contaminants: sixty-first report of the Joint FAO/WHO Expert Committee on Food Additives*. Rome: World Health Organization.
- Yang, C., Yang, L., Yang, Y., & Ouyang, Z. (2004). Rice root growth and nutrient uptake as influenced by organic manure in continuously and alternately flooded paddy soils. *Agricultural Water Management*, 70(1), 67–81.
- Zhou, H., Zhou, X., Zeng, M., Liao, B. H., Liu, L., Yang, W. T., ... & Wang, Y. J. (2014). Effects of combined amendments on heavy metal accumulation in rice (*Oryza sativa* L.) planted on contaminated paddy soil. *Ecotoxicology and Environmental Safety*, 101, 226–232.

Review article

Titanium and Titanium Based Alloys as Metallic Biomaterials in Medical Applications – Spine Implant Case Study

Nur Azida Che Lah and Muhamad Hellmy Hussin*

Fabrication and Joining Section, Universiti Kuala Lumpur Malaysia France Institute, 43650 Bandar Baru Bangi, Selangor, Malaysia

ABSTRACT

Titanium (Ti) and Ti-based alloys presence the most widely applied as advanced biomaterials in biomedical implant applications. Moreover, these alloys are known to be the most valuable metallic materials including spinal cord surgical treatment. It becomes an interest due to its advantages compared to others, including its bio compatibility and corrosion resistant. However, an issue arises when it comes for permanent implant application as the alloy has a possible toxic effect produced from chemical reaction between body fluid environments with alloys chemical compositions. It also relies on the performance of neighbouring bone tissue to integrate with the implant surface. Abnormalities usually happen when surrounding tissue shows poor responses and rejection of implants that would leads to body inflammation. These cause an increase in foreign body reaction leading to severe body tissue response and thus, loosening of the implant. Corrosion effects and biocompatibility behaviour of implantation usage also become one of the reasons of implant damage. Here, this paper reviews the importance of using Ti and Ti-based alloys in biomedical implantation, especially in orthopaedic spinal cord injury. It also reviews the basic aspects of corrosion effects that lead to implant mechanical damage, poor response of body rejection and biocompatibility behaviour of implantation usage.

Keywords: Bacterial infection, corrosion, mechanical damage, metal discolouration, metal hypersensitivity

ARTICLE INFO

Article history:

Received: 05 April 2018

Accepted: 11 June 2018

Published: 24 January 2019

E-mail addresses:

nurazida@unikl.edu.my (Nur Azida Che Lah)

hellmy@unikl.edu.my (Muhamad Hellmy Hussin)

* Corresponding author

INTRODUCTION

Several of materials including metals which have appropriate physical properties and biocompatibility are selected for biomaterials fabrication. Common metallic materials used in medical applications such as cobalt based alloys, austenitic stainless

steel, titanium and titanium based alloys and magnesium based alloys (Adzali et al., 2012). Titanium (Ti) and Ti-based alloys act as the newest metallic biomaterials that widely used in medical and dental territories. These alloys have displayed successful achievements as biomedical instruments (Elias et al., 2008). In medicine, widely applications were found for implant instrumentation which can substitute failed hard tissue for example, artificial hip and knee joints, fracture fixation screws, bone plates and artificial hearts. Moreover, in dentistry metallic materials are widely used as implants in oral surgery to replace single or an array of teeth or in dental prosthesis (Mary & Rajendran, 2012).

In medical applications, Ti and Ti-based alloys are intended to be the most excellence biocompatible metallic materials since its surface properties result in the spontaneous build-up oxide layer which protects the metal's surface. It is said as biocompatible materials because of its physical properties such as low level of electronic conductivity, good corrosion resistance, thermodynamic state at physiological pH values, and also because of low-ion-formation tendency in aqueous environment (Elias et al., 2008). Hence, these alloys are used for reconstructive bone and teeth.

However, in spite of its advantages, the development of human implants with respect to corrosion resistance becomes vital in medical applications. As well known, human body environment presents a corrosive medium for various implant materials which include a highly oxygenated saline electrolyte at a pH of around 7.4, body temperature of 37°C, containing water, dissolved oxygen, sodium, chloride, bicarbonate, calcium, potassium, magnesium, phosphate, saliva, and various organic compounds. Moreover, bacteria exist in the human body also influence the corrosion behavior of implant materials. When it is infected, it can create an imbalance in the electrochemical equilibrium.

Here, this review focuses on electrochemical corrosion phenomena in alloys used for orthopaedic implants and also the importance of using Ti and Ti-based alloys in biomedical implantation, especially in orthopaedic spinal cord injury. It also reviews the basic aspects of corrosion effects that lead to implant mechanical damage, poor response of body rejection and biocompatibility behaviour of implantation usage of one real case study. Hence, in future this study will become a basic directions focusing on biomaterials research and development with regard to corrosion processes that need to be considered to answer the possible corrosion mechanism concern.

TI AND TI-BASED ALLOYS IMPLANT PROPERTIES

In medical application, pure Ti and low interstitial Ti-6Al-4V are commercially used as accepted Ti-base implant biomaterials (Findik, 2017). These alloys are categorized as biologically inert biomaterials. In addition, these materials presents good reactions with human body and was found tolerated well with human tissues. Instead of that its physical

properties such as high biocompatibility, specific strength, high corrosion resistance, long fatigue life, nontoxic and allergy-free elements make them suitable for implantation used materials (Niinomi & Nakai, 2011). Ti alloys are known as stable beta alloys. This type of alloy shows no second phase precipitation formation during long-time thermal exposure. The microstructures were controlled to optimize its mechanical properties essentially as ductility, strength, fatigue resistance and fracture toughness (Bhola et al., 2011).

Elemental composition of Ti and Ti-based alloys acts as a valuable role in deciding the biomaterials physical properties. One of the essential element is Vanadium which presence as an important element, on the other hand it is categorized in the toxic group. Instead of that, titanium, zirconium, niobium and tantalum present superior biocompatibility properties and was found to be in the loose connective vascularized group such as in tissue reaction (Okazaki & Gotoh, 2002). Patrascu et al., (2014) reported that titanium did not react with organic-metallic compound, it was toxic, or if they were produced, the organic-metallic were doubtful and unstable.

Ti and Ti-based alloys is said to be biocompatible to human body is mainly for the sake of the oxide film formation such as TiO_2 over its outer surface. The development of this oxide performs a strong and stable layer which spontaneously grows when it is in contact with air. The layer avoids the diffusion of the oxygen from the environment which contribute to the corrosion degradation (de Viteri & Fuentes, 2013). Instead of its superficial properties, Ti-based alloys for example, Ti6Al4V also have some disadvantages such as low elastic modulus, and has low wear resistance and it shows to have problem in articulations surfaces. It was found that Vanadium shows potential cytotoxicity and adverse tissue reactions. On the other hand, Al was found to cause long-term Alzheimer diseases (Oldani & Dominguez, 2012). When Ti implant that contains vanadium shows critical response, the releasing of vanadium ions in the body would lead to severe damages especially to the respiratory system and the blood plaquettes producing systems. By replacing V with Nb, the harmful effects to the human body can be tolerated (Nouri et al, 2010).

As investigated by Maehara et al., (2002) two types of vanadium-free Ti alloy were used to develop an artificial hip joints which are Ti-15Mo-5Zr-3Al and Ti-6Al-2Nb-1Ta-0.8Mo alloys. Both alloys were chosen because of its high fatigue strength and its low elastic modulus.

BIOCOMPATIBILITY BEHAVIOR

Biocompatibility is an important concept and vital characteristic of material to which related with living organism compatibility in implantation process. It must be accepted by body without causing any critical response including unwanted effects and also damages including chemically nor mechanically (Patrascu et al., 2014).

It is also substantial to note that mechanical properties such as the Young's modulus, tensile strength, ductility, fatigue life, fretting fatigue life, wear properties, and functionalities show significant effects to the implant performance. It should be tolerated and keep the level under controlled so that their levels are acceptable for structural biomaterials used in hard tissue implantation (Niinomi, 2003). These mechanical biocompatibility properties were found to be an essential factor for long term usage of implantation. It must also be safe, reliable, economic and physiologically acceptable to human body.

Kirmanidou et al. (2016) investigated that, the percentage of survival rates of dental and orthopaedic implants was found at satisfactory level. In dentistry, medical implants the range is from 90 to 96.5%. Meanwhile, in orthopaedic implants it shows 80-94% at 15 years for total hip arthroplasty, and the range of 98.4 – 98.7% was found at 10 years specifically in total knee prosthesis implantation. Moreover, the range of 91% was found at 10 years for shoulder arthroplasty, and 53% and 90% at 5 years for total elbow arthroplasty for patients with posttraumatic arthritis or fractures and having inflammatory arthritis. It is not biocompatible to human body if the implants are infected, fractured, and having wear of the articulating surfaces. Instead of that, patients may also diagnose with implant loosening. Commonly, this implant failure consistently relates with stress-shielding effect, septic or aseptic inflammation, fatigue and excessive activity by patient's movement which include de-bonding at the tissue-implant interface (Kirmanidou et al., 2016). It was found by Maehara et al. (2002) that both Ti-15Mo-5Zr-3Al and Ti-6Al-2Nb-1Ta-0.8Mo alloys, which are vanadium-free alloys are clear from toxicity test.

Thus, it is necessary to categorize whether the implant usage biocompatible or not when it interacts which enable them to function inside the human body. As studied previously by Patrascu et al. (2014), Kirmanidou et al. (2016), Maehara et al. (2002), Niinomi (2003), Niinomi and Nakai (2011), and Akahori et al. (2004), they presented and stressed out the importance of biocompatibility behaviour of implant usage which determine whether the material suitable for biomedical implant applications that include bio-adhesion, bio-functionality and corrosion resistance. Although the review has been limited to the study of titanium and its alloys because this metal whose widespread use has been limited by its high cost. Furthermore, Ti and Ti-alloys is considered to be biocompatible because it has low electrical conductivity which contributes to the electrochemical oxidation of Ti leading to the formation of a thin passive layer (Sidambe, 2014).

In order to that, Ti and Ti-alloy is an ideal implant material that is said to be compatible with human body if no adverse tissue response recorded. Still, it is difficult to combine all these properties if body rejection occurred because each human bodies show different rejection and responses. Some metal can be tolerated and some metals can only be tolerated in small amounts even as metallic ions. The consequences of this issue focused on corrosion of the implant material which will weaken the implant and harmful to the surrounding

tissues and organs of human body. Thus, due to complex human body surroundings, it can be said that different body responses show different compatibility behaviour of implant material.

CORROSION ACCELERATED MECHANICAL DAMAGE AND BACTERIAL INFECTION

One of the failure causes of metallic biomaterials is corrosion. This destructive attack mostly occurred on metal surface by chemical or electrochemical reaction with its surroundings (Souza et al., 2015). In this scope, implants are exposed to the corrosive environment and it is focusing on human body fluid environment. Most of the implants are permanent and thus it is exposed to human body environment for a certain or long period of time. Human body fluids are liquids that originating from inside the living humans including fluids that are excreted or secreted from the body. In other words, it consist of human blood, body fluids and other body tissues which identified as vehicles for human disease transmission of transportation (Mary & Rajendran, 2012). Moreover, human body's tissue fluid comprised of water, dissolved oxygen, proteins and various ions for example, chloride and hydroxide. In other words, human body is very aggressive environment for metal used for implantation and it is an important aspects of its biocompatibility reasons (Muslim & Abbas, 2015). Hence, it is a complex environment that is different from one human body to another.

Mary and Rajendran (2012) reported that Ti and its alloys had significant properties that were caused by passive films. The films were rapidly formed in the body fluid environment. They also stated that the corrosion of Ti was suppressed in solutions containing fluoride and eugenol. Well established surface oxide film formed on Ti protects the surface from degradation. When the surface oxide film is disorganized, the corrosion would continue and metal ions are released progressively unless the film is regenerated. The time taken for repassivation which is also termed as regeneration time is different for various materials used. It was studied that regeneration time for Ti-6Al-4V is shorter compared to stainless steel. Moreover, the repassivation rate of Ti in Hank's solution is found to be slower than that in saline and remains uninfluenced by the pH of the solution (Geetha et al., 2009). Maehara et al. (2002) found that the corrosion resistance of vanadium-free alloys which were Ti-15Mo-5Zr-3Al and Ti-6Al-2Nb-1Ta-0.8Mo alloys was as high as commercial pure Ti and Ti-6Al-4V. In addition, they found that these alloys were stable in the living human body. Prominently, an implant failure in the form of aseptic loosening may result forming metal ions in the form of wear debris or electrochemical products generated during corrosion such as Ti^{4+} , Co^{2+} and Al^{3+} . These metal ions have been reported to decrease DNA synthesis, mitochondrial dehydrogenase activity, mineralization and mRNA expression of alkaline phosphatase and osteocalcin in ROS 17/2.5 cells (Gitten et al., 2011).

As reported by Findik (2017), the discharge of non-compatible metal ions from implants bio materials into the body was mainly because of the low corrosion and wear resistance in human body fluid. It caused allergic and toxic response where it is crucial to human structure. An interaction between the implant material and chemical compound induced by electrochemical reaction may leads to mechanical and biological complications. Mechanical complication accelerated by corrosion usually results in fatigue fracture. Meanwhile, biological complications related to corrosion could cause toxicity, carcinogenicity and hypersensitivity (Kirmanidou et al., 2016). As aforementioned, highly loaded applications on bone implantation might leads to fatigue failure. Ryan et al., (2006) reported that both Co-Cr alloys and Ti-6Al-4V alloys experienced drastic reductions in fatigue strengths when fabricated as porous coatings on solid core structures. They stated that stress intensification due to localized notch acted as stress concentration that affected implant strength in the region of the porous coating.

On the other hand, bacterial infection also distinguished in destruction of implant. This could accelerate the mechanical damage of spine implant and it is reported that bacterial adhesion is the first and most important step in implant infection (Ribeiro et al., 2012). Bacterial adhesion is a complex process and it is influenced by environmental factors, bacterial properties, material surface properties and by the presence of serum or tissue proteins. It is mainly related to the implant surface material properties. When bacterial adhesion occurs, surface colonization for certain bacterial species that capable of forming protective biofilm layer cannot be prevented. Therefore, it is essential to prevent implant-associated infection in order to inhibit bacterial adhesion. Moreover, this biofilm layer is extremely resistant to both immune system and antibiotics (Ribeiro et al., 2012).

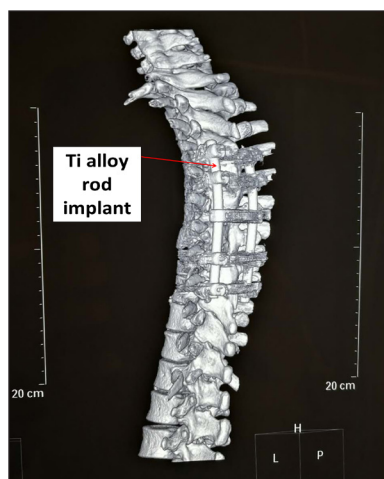


Figure 1. MRI image of spine implant taken from female patient's spinal cord having major surgical operation due to accident, (with 4.5 mm spinal locking plate and 5.5 mm Ti locking screws, Kuala Lumpur General Hospital, Malaysia)

SURGICAL SPINE IMPLANT CASE STUDY

A 44-year-old female involved in a motor vehicle collision presented with fractured spinal cord. Six years after her surgery, she developed increasing back pain with small wound. She returned with hardware infection and underwent extensive debridement of the infection site and removal of spine implant. Figure 1 shows an image of Ti-alloy spine implant taken from female patient's spinal cord before underwent major surgical operation of implant removal. Complete implant removal was suggested by the surgeon and it was considered essential to treat patient's infection. The patient is now over three months out from her final operation without any recurrences of infection and with great improvement in her pain.

Spinal infections from implants represent a difficult challenge in medical surgery. The situation when dealing with spine infection is more difficult and high risk challenge to the spinal surgeon and physician due to the requirement for stability and to protect neurological function (Quaile, 2012). Other than that, spinal infections can also be of acute onset and delayed appearance. As reported by Jung-Tung et al., (2015) postoperative surgical site infection (SSIs) is one of the most common complications after spinal surgery and the incidence of spinal SSIs in the literature is around 0.7 - 16.0%. From medical approach, these spinal infections often require extended antibiotic therapy, repeated surgery for wound debridement, hardware removal, and prolonged hospitalization (Crawford et al., 2015; Jung-Tung et al., 2015). Furthermore, as reported in previous literature, the spinal surgeries carry a higher risk of infection compared with other orthopaedic procedures.

In clinical and medical review, for an infection to occur at the surgical site, bacteria must be present at the operative or procedural site in substantial quantity which is $>10^5$ organism. As discussed by (Chaudhary et al., 2007), three possible sources of bacteria are direct inoculation at the time of surgery, soiling of the incision in the fresh postoperative phase, or through hematogenous seeding. They concluded that most post procedural infections were a consequence of direct inoculation. Instead of that, several patient-related factors play an important role in the pathogenesis of infection which includes modifiable and non-modifiable factors. Some non-modifiable factors are spinal trauma, diabetes, advanced age and development delay. Meanwhile, obesity, smoking, malnutrition and extended hospitalization are modifiable risk factors (Chaudhary et al., 2007; Quaile, 2012). Hoelzer et al. (2017) reported that retrospective review was conducted on 2737 unique implants or revisions of SCS (spinal cord stimulation) systems. It showed that patient demographics, risk factors including diabetes, tobacco use, and obesity did not independently increase the rate of infection.

Basically, in this case study only failure analysis work was carried out. This methodology often regarded as a diagnostic post-mortem activity and in this work, it focused on Ti-alloy spine implant taken from female patient's spinal cord after underwent major surgical operation of implant removal. The outcomes of this observation can benefits

others as a learning process which sometimes are ignored or neglected. The failed of implants part had been initially observed only using visual observation technique and as for continuation, the experimental work on this parts will be carried out in our next article.

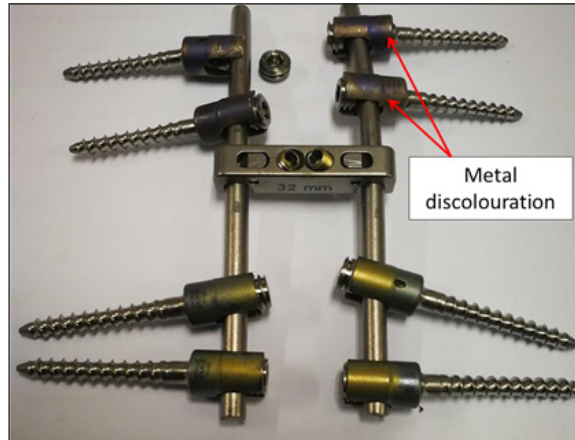


Figure 2. Photograph of the screws, rods and plate after implant removal

Apparently, it can be found that some location on the failed implants showed some colour changes as shown in Figures 1 and 2. The changes could be attributed by metal hypersensitivity. Metal hypersensitivity involves a metal exposure to degradation product such as wear particles of metal on metal bearing surfaces. It was found that it is in agreement with Sakellariou et al. (2011) that mostly the spinal implants are static load-bearing devices subjected to micro-motion. It is possible to indicate that the 6 years of implant usage might leads to spinal implant deformity which involve several couplings of screws, rods and interconnecting devices. It can be said that, all of the observation could be related to fretting corrosion.

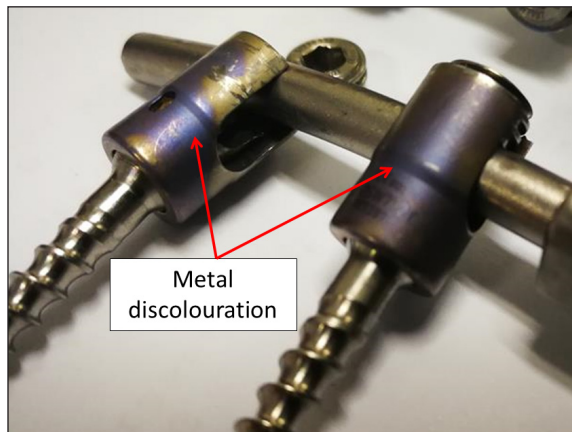


Figure 3. Enlargement and closed-up view in Figure 2 showing and effect of metal discoloration

In the presence of fretting, the condition may change because the passivating oxide layer may be abraded away, thus, expose the bare metal to the electrolyte solution (Jacobs et al., 1998). As shown in Figure 2, the Ti-alloy metal plate shows effects of discoloration which might related with the effects of corrosion degradation. As well discussed in previous study, metallic discoloration is uncommon disorder defined by the accumulation of metallic particles in the skin through the blood stream or surface application (Park et al., 2013).

In order to evaluate the relation of between corrosion and implant-related hypersensitivity reaction in patients, the presence of corrosion products can view significantly as shown in Figures 2 and 3. Several spots on Ti-implant location show some stain of metal discoloration related with corrosion effects and all of these can impair their function. As indicated, Ti or Ti alloy will initially discolour as it is oxidizes producing a colour changes on the surface of the metal. As reported by Takahashi et al. (2014) the discoloured location on Ti alloy surface was found to be thicker and it was presumed to be the result of the interference colour because of the thickness difference of the oxide film due to film growth. Moreover, corrosion which related with implant can result in a shortened instrument life which additionally could results in increased cost.

As well known, the surface of Ti and Ti alloys consist of a thin oxide layer which ranges from 2 to 6 nm. This protective oxide layer usually acts to protect the metal surface from further degradation. Moreover, this oxide layer is amorphous or poorly crystalline and is composed of a slightly oxygen-deficient titanium oxide (Takahashi et al., 2014). The oxide layer will be produced spontaneously to protect the metal surface. However, when the Ti is brought into contact with body fluid environment for long duration of exposure, a complex phenomenon will take place at the metal interface. Thus, the formation of oxide film is far thicker than the one obtained if it is exposed to simple immersion exposure. Furthermore, when the discoloured locations are subjected to simple motion for long periods of duration, this would lead to mechanical implant failure such as fretting corrosion.

In this case, it is possible to note that the metal discoloration on spinal instrumentation also can possibly cause metal ions release from fretting corrosion into patient's body fluids. Thus, causing back pain and the small wound that appeared at the surgical site as experienced by the 44-year old female patient as described earlier. As explained in Figure 4, the metal particles that are leached from the metal implant substrate as an output of fretting corrosion process under the influence of mild body tissue response. The releases of metal ions show effects of localized discoloration and metal hypersensitivity. These effects would lead to body inflammation, forming an infection from a small wound. These cause an increase in foreign body reaction leading to severe body tissue response and thus, loosening of the implant.

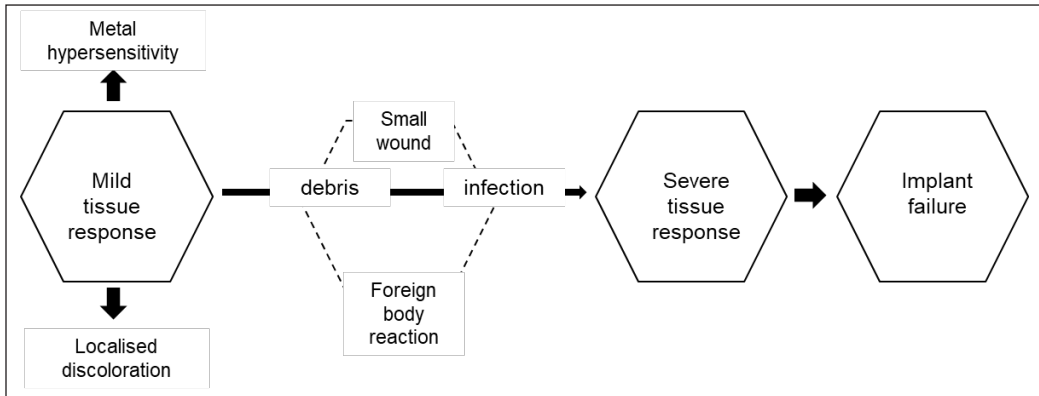


Figure 4. Body response to an implant failure

This finding is also in agreement with Singh et al. (2012), Simon and Fabry (1991), Niinomi and Nakai (2011) and Kirkpatrick et al. (2005). They reported that, instead of corrosion damage which involved spinal implants, mechanical failure such as fatigue was also observed in previous study. Singh et al., (2012) found that posterior spinal fusion implants subjected to micro-motion under physiological loading conditions inducing a potential for fretting corrosion which referred to the damage of contact surfaces. In Posterior Spinal Fusion (PSF) surgery, to stabilize the spine it involves an incision in the midline of the back (posterior) and in some patient metal screws and rods that are placed in the spine to hold the bones while the fusion heals. In this case when rubbing action between metal and tissue interface increase, the release of metal particulate wear debris shown to increase metal ion level which is dangerous to human body (Simon & Fabry, 1991). Niinomi and Nakai (2011) stated that, there was possibility of fretting fatigue condition especially in the contact area of two bodies such as between bone plate and screws. Kirkpatrick et al. (2005) also stated that Ti alloy implants showed no significant corrosion but had three constructs with fatigue failure of anchoring screws. They found to take preventive methods in minimizing the effects of localized changes over time especially on the implants surface finishes between rods and connectors which were the most susceptible to corrosion.

The other factor that might to take into consideration is the presence of bacteria inside the living human bodies which cause an infection to the implants. It is known as microbial induced corrosion (MIC). As investigated by Ayer et al., (2017) the nature of bacteria on the skin and deep dermal layers might lead to an infection which can occur when implanted metallic materials is utilized especially in spine and orthopedic procedures. Instead of that, the level of bacterial contamination also varies in relation to the grade of open fractures. It is also reported that even in clean surgical procedures, the low level of bacterial contamination must be assumed (Arens et al., 1996).

In this case, spine implant instrumentations can be affected also by corrosion. It may cause local and systemic complications. Although the diagnosis of corrosion is difficult several test were conducted by previous literature to detect the metal degradation. del Rio et al. (2007) conducted a study to determine and measure the metal levels on patients with posterior instrumented spinal fusion. They revealed that the patients with spinal implants without radiological signs of corrosion had increased levels of Cr in serum and urine compared to volunteers without implants. It can be said that, corrosion significantly raised the metal levels, including Ni and Cr in serum and urine when compared to patients without metallic implants. Beguiristain et al. (2006) reported that a after 14 years, a female patient with a 316L SS instrumentation presented progressive paraparesis during last 2 months. Plain radiography, computed tomography scan and computed tomography-scan-guided needle biopsy revealed that a metallotic mass penetrated into the spinal canal causing compression of the spinal cord implant at the T5-T6 level (Beguiristain et al., 2006). The results show that the patient's symptoms were related to the corrosion of the implant and it was found that the infection by *Propionibacterium acnes*. In this case, MIC is a concept to be taken into account and it is possible to conclude that the bacteria may modify the rate of metal corrosion (Beguiristain et al., 2006; Farnsworth et al., 2014).

It is well discussed in previous literature, pertaining to the corrosion of spine biomedical alloys which currently focused on galvanic, pitting, crevice and fretting corrosion. The real concern is on galvanic corrosion specifically when involved Ti-6Al-4V and CoCrMoC where these two alloys are in intimate contact. It is also observed in spine instrumentation where the mixing of these alloys is applied such as Ti-6Al-4V pedicle screw with CoCrMoC tulip and an interlocking Ti-6Al-4V or CoCrMoC spine rod (Ayer et al., 2017). It can be said that due to complex environment of human body, most likely for the corrosion of alloys in spine is fretting wear and microbial induced corrosion. It also depends on human body response and it is reasonable to note that living human body could provide nutrients for bacterial growth. As reviewed by Gitten et al., (2011) spine implant constructs consisting of pedicle screws, connectors, and rods that have mixed components made of stainless steel (SS) and Ti shows signs of galvanic corrosion under cyclic loads. The results showed an evidence of minor signs of corrosion at the interfaces between SS-Ti, Ti-Ti, and SS-SS. In this case, the surrounding tissue could serve as a medium for electrical flow between metallic implants (Gittens et al., 2011). Sakellariou et al. (2011) reported a case study on a 14 year-old girl with a history of extended posterior spinal fusion due to idiopathic scoliosis. They identified two potential contributing factors for the development of a secondary systematic reaction which were late infection which was not unusual and metal allergy to Ti or Ti-alloy components that was relatively rare to be found.

CONCLUSION

In this study, the importance of using Ti and Ti-based alloys in biomedical implantation, especially in orthopaedic spinal cord injury was successfully reviewed. From the case study, it is possible to propose that the possibility of metal particles that are leached from the metal implant substrate as an output of fretting corrosion process under the influence of mild body tissue response. The releases of metal ions show effects of localized discoloration and metal hypersensitivity on implant instrumentation. These caused body inflammation, forming an infection from a small wound of the human's body. Thus, increase in foreign body reaction leads to severe body tissue response and finally, loosening of the implant. Based on our comprehensive review of the literature and randomized studies with a focus on the failed part of implant usage, it shows that scientific evidence for in-depth analysis of the failed part are lacking especially in a real case study since the sampling method is limited. Further, well-designed studies are necessary to better understand the possible corrosion mechanism concern.

REFERENCES

- Adzali, N. M. S., Jamaludin, S. B., & Derman, M. N. (2012). Mechanical properties, corrosion behavior, and bioactivity of composite metal alloys added with ceramic for biomedical applications. *Reviews on Advanced Materials Science*, 30, 262-266.
- Akahori, T., Niinomi, M., Fukui, H., & Suzuki, A. (2004). Fatigue, fretting fatigue and corrosion characteristics of biocompatible beta type Titanium alloy conducted with various thermo-mechanical treatments. *Materials Transaction*, 45(5), 1540-1548.
- Arens, S., Schlegel, U., Printzen, G., Ziegler, W. J., Perren, S. M., & Hansis, M. (1996). Influence of materials for fixation implants on local infection. An experimental study of steel versus Titanium DCP in Rabbits. *Journal of Bone and Joint Surgery*, 78-B, 647-651.
- Ayer, R., Kleck, C., Miller, M., & Burger, E. (2017). Bacterial infection of spine instrumentation and microbial induced corrosion (MIC): Chicken or Egg. *Biomedical Journal of Scientific & Technical Research*, 1(6), 1-2.
- Beguiristain, J., Del Rio, J., Duart, J., Barroso, J., Silva, A., & Villas, C. (2006). Corrosion and late infection causing delayed paraparesis after spinal instrumentation. *Journal of Pediatric and Orthopaedic B*, 15(5), 320-323.
- Bhola, R., Bhola, S. M., Mishra, B., & Olson, D. L. (2011). Corrosion in Titanium dental implants / prostheses - A review. *Trends in Biomaterials & Artificial Organs*, 25(1), 34-46.
- Chaudhary, S. B., Vives, M. J., Basra, S. K., & Reiter, M. F. (2007). Postoperative spinal wound infections and postprocedural diskitis. *The Journal of Spinal Cord Medicine*, 30(5), 441-451.
- Crawford, B., Lenarz, C., Tracy Watson, J., & Alander, D. (2015). Case Report Complication with removal of a lumbar spinal locking plate. *Hindawi*, 2015, 1-4.

- de Viteri, V. S., & Fuentes, E. (2013). Titanium and Titanium alloys as biomaterials. In J. Gegner (Ed.), *Tribology-Fundamental and Advancements* (pp. 155-181). London: InTechOpen.
- del Rio, J., Beguiristain, J., & Duart, J. (2007). Metal levels in corrosion of spine implants. *European Spine Journals*, 16(7), 1055-1061.
- Elias, C. N., Lima, J. H. C., Valiev, R., & Meyers, M. A. (2008). Biomedical applications of Titanium and its alloys. *Journal of The Minerals, Metals and Materials Society*, 60(3), 46-49.
- Farnsworth, C. L., Newton, P. O., Breisch, E., Rohmiller, M. T., Jung Ryul, K., & Akbarnia, B. A. (2014). The biological effects of combining metals in a posterior spinal implant: In vivo model development report of the first two cases. *Advances in Orthopedic Surgery*, 2014, 1-9.
- Findik, F. (2017). Titanium based biomaterials. *Current Trends in Biomedical Engineering and Biosciences*, 7(3), 001-003.
- Geetha, M., Singh, A. K., Asokamani, R., & Gogia, A. K. (2009). Ti based biomaterials, the ultimate choice for orthopedic implants - A review. *Progress in Materials Science*, 54, 397-425.
- Gittens, R. A., Olivares-Navarrete, R., Tannenbaum, R., Boyan, B. D., & Schwartz, Z. (2011). Electrical implications of corrosion for Osseointegration of Titanium implants. *Journal of Dental Research*, 90(12), 1389-1397.
- Hoelzer, B. C., Bendel, M. A., Deer, T. R., Eldrige, J. S., Walega, D. R., Wang, Z., ... & Choi, D. Y. (2017). Spinal cord stimulator implant infection rates and risk factors: A multicenter retrospective study. *Neuromodulation*, 20(6), 558-562.
- Jacobs, J. J., Gilbert, J. L., & Urban, R. M. (1998). Current concepts review - Corrosion of metal orthopaedic implants. *The Journal of Bone and Joint Surgery*, 80-A(2), 269-282.
- Jung-Tung, L., Wen-Jui, L., Cheng-Siu, C., & Yung-Hsiang, C. (2015). Management of deep infection after instrumentation on lumbar spinal surgery in a single institution. *BioMed Research International*, 2015, 1-5.
- Kirkpatrick, J. S., Venugopalan, R., Beck, P., & Lemons, J. (2005). Corrosion on spinal implants. *Journal of Spinal Disorders and Techniques*, 18(3), 247-251.
- Kirmanidou, Y., Sidira, M., Drosou, M.E., Bennani, V., Bakopoulou, A., Tsouknidas, A., ... & Michalakis, K. (2016). New Ti-Alloys and surface modifications to improve the mechanical properties and the biological response to orthopedic and dental implants: A review. *BioMed Research International*, 2016, 1-21.
- Maehara, K., Doi, K., Matsushita, T., & Sasaki, Y. (2002). Application of Vanadium-free Titanium alloys to artificial hip joints. *Materials Transactions*, 43(12), 2936-2942.
- Mary, S. J., & Rajendran, S. (2012). Corrosion behavior of metals in artificial body fluid overview. *Zastita Materijala*, 53, 181-189.
- Muslim, Z. R., & Abbas, A. A. (2015). The effect of pH and temperature on corrosion rate stainless steel 316L used as biomaterials. *International Journal of Basic and Applied Sciences*, 4(2), 17-20.
- Niinomi, M. (2003). Recent research and development in titanium alloys for biomedical applications and healthcare goods. *Science and Technology of Advanced Materials*, 4, 445-454.

- Niinomi, M., & Nakai, M. (2011). Titanium-based biomaterials for preventing stress shielding between implant devices and bone. *International Journal of Biomaterials*, 2011, 1-10.
- Nouri, A., Hodgson, P. D., & Wen, C. (2010). Biomimetic porous Titanium scaffolds for orthopedic and dental applications. In H. Le, C. A. Wang, & Y. Huang (Eds.), *Biomimetics, Learning from Nature* (pp. 415-450). Croatia: InTech.
- Okazaki, Y., & Gotoh, E. (2002). Implant applications of highly corrosion-resistant Ti-15Zr-4Nb-4Ta alloy. *Materials Transactions*, 43(12), 2943-2948.
- Oldani, C., & Dominguez, A. (2012). Titanium as a biomaterial for implants. In S. Fokter (Ed.), *Recent Advances in Arthroplasty* (pp. 149-162). Croatia: Intech
- Park, J. Y., Shin, D. H., Choi, J. S., & Kim, K. H. (2013). Metallic discoloration on the right shim caused by titanium alloy prostheses in a patient with right total knee replacement. *Annals of Dermatology*, 25(3), 356-359.
- Patrascu, I., Vasilescu, E., Gatin, E., & Cara-Ilici, R. R. (2014). Corrosion of biomaterials used in dental reconstruction dentistry. In M. Aliofkhaezraei (Ed.), *Development in Corrosion Protection* (pp. 633-658). London: InTechOpen.
- Quaile, A. (2012). Infections associated with spinal implants. *International Orthopaedics*, 36(2), 451-456.
- Ribeiro, M., Monteiro, F. J., & Ferraz, M. P. (2012). Infection of orthopedic implants with emphasis on bacterial adhesion process and techniques used in studying bacterial-material interactions. *Biomatter*, 2(4), 176-194.
- Ryan, G., Pandit, A., & Apatsidis, D. P. (2006). Fabrication methods of porous metals for use in orthopaedic applications. *Biomaterials*, 27, 2651-2670.
- Sakellariou, V., Atsali, E., Strantzis, K., Batistaki, C., Brozou, T., Pantos, P., ... & Soultanis, K. (2011). Postoperative spinal infection mimicking systemic vasculitis with titanium-spinal implants. *Scoliosis*, 6(1), 20-25.
- Sidambe, A. T. (2014). Biocompatibility of advanced manufactured titanium implants - A review. *Materials (Basel)*, 7(12), 8168-8188.
- Simon, J. P., & Fabry, G. (1991). An overview of implant materials. *Acta Orthopædica Belgica*, 57(1), 1-5.
- Singh, V., Shorez, J. P., Sitton, K., Gilbert, J. L., & Hllab, N. J. (2012). Long term corrosion potential of three posterior spinal implant materials. In *Annual Meeting of Orthopaedic Research Society* (p. 1). San Francisco, California.
- Souza, J. C. M., Henriques, M., Teughels, W., Ponthiaux, P., Celis, J., & Rocha, L.A. (2015). Wear and corrosion interactions on Titanium in oral environment: Literature review. *Journal of Bio- and Tribo-Corrosion*, 1(13), 1-13.
- Takahashi, K., Hayashi, T., Tokuno, K., Muto, I., Kaneko, M., Tamenari, J., & Kimura, K. (2014). Development of titanium sheets with superior discoloration resistance for architectural applications. *Nippon Steel and Sumitomo Metal Technical Report*, 106, 28-33.

Physico-Mechanical Properties and Formaldehyde Emission of Rubberwood Particleboard Made With UF Resin Admixed With Ammonium and Aluminium-Based Hardeners

Abd Ghani Aizat¹, Bawon Paiman^{1*}, Seng Hua Lee² and Ashaari Zaidon^{1,2}

¹Department of Forest Production, Faculty of Forestry, Universiti Putra Malaysia, 43400 UPM, Serdang, Selangor, Malaysia

²Institute of Tropical Forestry and Forest Products, Universiti Putra Malaysia, 43400 UPM, Serdang, Selangor, Malaysia

ABSTRACT

In this study, the effects of addition of ammonium and aluminium-based hardeners into urea formaldehyde resin (UF) on the physico-mechanical properties and formaldehyde emission of the rubberwood particleboard were investigated. Four types of hardeners, namely ammonium chloride (AC), ammonium sulphate (AS), aluminium chloride (AIC) and aluminium sulphate (AIS), were added into UF resin. The acidity, gelation time, viscosity and free formaldehyde content of the UF/hardener mixtures were determined. Particleboard made with the UF/hardener mixtures were tested for physico-mechanical properties and formaldehyde emission. The pH values of the resin after addition of aluminium-based hardeners were higher and resulted in higher viscosity and shorter gelation time. Consequently, despite lower formaldehyde emission was recorded, the physico-mechanical properties of the resulted particleboard were inferior compared to that of ammonium-based hardeners. The best quality particleboard in terms of mechanical, physical and formaldehyde emission were obtained from the particleboard made with AS, followed by AC.

Keywords: Ammonium, aluminium, hardener, formaldehyde emission, particleboard

ARTICLE INFO

Article history:

Received: 9 January 2018

Accepted: 2 November 2018

Published: 24 January 2019

E-mail addresses:

aizatabdghani@gmail.com (Abd Ghani Aizat)

paiman@upm.edu.my (Bawon Paiman)

leesenghua@hotmail.com (Seng Hua Lee)

zaidon@upm.edu.my (Ashaari Zaidon)

* Corresponding author

INTRODUCTION

A great variety of aminoplastic resins are in use in present-day wood-based panels industry. Among the aminoplastic resins,

urea formaldehyde (UF) resin is the most prevalently used binding agent in wood based panels industry, particularly in particleboard manufacturing, owing to its low cost and high reactivity (Moslemi, 1974). Nevertheless, aminomethylene linkages in UF resin are unstable and susceptible to hydrolysis in high relative humidity state, which generate a permanently release of formaldehyde (Dunky, 1998). Formaldehyde is classified as carcinogen to human by The International Agency for Research on Cancer (IARC) and therefore the emittance of formaldehyde has caused concern among the users and manufacturers.

In order to tackle the aforementioned issue, efforts have been taken over the past decades in reducing the level of formaldehyde emission (Younesi-Kordkheili et al., 2016). The most economic and direct ways of reducing formaldehyde emission is through lowering the formaldehyde to urea (F/U) molar ratio in UF resin. Unfortunately, lowering F/U molar ratio inevitably gives adverse effect on the properties of the produced particleboard. In addition, Maminski et al. (2008) reported that the possibilities by lowering F/U ratio had been exhausted with the ratio reduced to 0.85. The results revealed that the formaldehyde emission did not reduce significantly but the strength of joints produced from the mentioned resin was around 20% lower compared to that of the resin with F/U ratio of 1.1.

On account to that, addition of formaldehyde scavenger, or formaldehyde catcher into the resin is the most convenient and effective method to reduce the emittance of formaldehyde from wood or wood-based products (Aizat et al., 2017; Lum et al., 2014; Zaidon et al., 2016). One of the methods to reduce formaldehyde emission is to modify the chemistry of urea formaldehyde resins by using other ammonium salts as cure catalysts or hardener instead of latent ammonium chloride. Curing agents, also called hardener or catalyst are chemical substances added to the UF resin to speed up polymerization. UF resins are acid catalyzed resin and therefore acidic environment is needed for it to cure. These chemicals are either acidic substance by themselves or can liberate acids when mixed with the adhesives. These hardeners are normally used for UF-resin curing, however, in excess, they can act as formaldehyde scavengers which react with free formaldehyde to form hexamine (Moslemi, 1974). The most widely used hardeners are ammonium salts of strong acids which usually include the salts of chloride, sulphate, phosphate, nitrate, fluoride and borate. Non-ammoniacal salts such as aluminium and magnesium salts was also reported as potential hardener as well as formaldehyde scavengers for UF resin (Atar et al., 2014). Dunky (1998) reported that direct addition of acids such as maleic acid, formic acid, and phosphoric acid or acid compounds which dissociated in water such as aluminium sulphate were also one common practice in facilitate the curing speed of the resin.

The function of hardener is to react with the free formaldehyde or any uncombined free formaldehyde that presents in the UF resins where the reaction releases acid, hexamine as a by-product and water. The amount and type of hardener used in the resin formulation were found have a significant influence on the formaldehyde release from the resin and the UF-

bonded particleboard (Atar et al., 2014). Saffari (2011) identified that particleboard made with magnesium chloride released higher formaldehyde emission than those particleboards made with ammonium chloride and ammonium sulphate, respectively. On the other hand, Aras, Kalaycioglu et al. (2015) compared the effects of ammonium chloride and ammonium nitrate and found that the latter improved the physical properties and reduced the formaldehyde emission of the particleboard produced.

Therefore, it is important to study the effect of hardener used in UF-bonded particleboard production in order to obtain the lowest formaldehyde emission from the particleboard produced with most optimum quality of particleboard. The objective of this study was to evaluate the effects of ammonium- and aluminium-based hardeners addition to the UF resin properties and its effects on the particleboard fabricated from the resin. Properties such as thickness swelling, bending strength, internal bonding strength and formaldehyde emission of the particleboard were determined.

MATERIALS AND METHOD

Materials Preparation

Urea formaldehyde (UF) resin typed E1 was provided by Aica Chemical Sdn. Bhd and the resin specifications are listed in Table 1. Four types of hardeners, namely ammonium chloride (AC), ammonium sulphate (AS), aluminium chloride (AIC) and aluminium sulphate (AIS) were purchased from Evergreen Engineering & Resources. Rubberwood particles with 3% moisture content were obtained from a local particleboard manufacturing plant, Heveaboard Berhad which located in Gemas, Negeri Sembilan.

Table 1

Specifications of the urea formaldehyde resin used in this study provided by the supplier

Properties	Results	Specifications
Viscosity at 30°C (cps)	215	200-270
% N.V.C 3hrs at 105°C	66.9	66.0-68.0
pH at 30°C	8.62	8.5-10.0
Density at 30°C	1.282	1.280-1.290
Gel time at 100°C (Sec)	75	55-75

Evaluation of Properties of Admixture of Urea Formaldehyde (UF) Resin and Hardeners

Approximately 50g of UF resin was weighed to serve as a control. 1% of each type of hardener (based on the solid content of the UF resin) was weighed and added to UF resin,

respectively. The acidity, viscosity, gelation time and free formaldehyde content of the resin/hardener mixtures were determined.

Acidity (pH). Mi105 pH/temperature professional portable meter was calibrated with buffer 4.0 and 10.0 and the resin/hardener mixtures were cooled to 30°C. Next, the pH meter electrode was immersed into the mixtures and the pH reading was recorded.

Viscosity. Viscosity of the UF/hardener mixtures were measured with an AMETEK Brookfield rotational viscometer & rheometer at 20 °C with a spinning rate of 1 rpm according to the procedures stated in Ghani et al. (2018). 75ml of UF resin was poured into a 100ml beaker. Then, the spindle was lowered into the resin until the notch was just touched the liquid surface. Next, the reading from the viscometer was recorded.

Gelation time. Gelation time of the UF/hardener mixtures were determined according to the Ghani et al. (2018). Mixtures of UF resin and hardeners were poured into a beaker and stirred well. After that, 6.5g of the mixture was poured into a test tube which was then immersed (below water line) in 100 °C water bath. Immediately, the content was continuously stirred and the time (in seconds) needed for the resin mixtures to cure was recorded.

Free formaldehyde content. UF resin (10g) and 50ml of dimethyl sulphoxide solution were weighed and poured into a 250ml Erlenmyer flask. HCl (0.1M, 30ml) and Na₂SO₃ (0.1M, 30 ml) was added immediately to the mixture and stirred well. The mixture solution was cooled in an ice bath for 3 minutes to ensure complete reaction of the formaldehyde with sulphite. After 3 minutes, 1 ml 0.1% tymlolphtalein solution was added and the excessive acid was titrated with 0.1M NaOH solution to blue color. Volume of the 0.1M NaOH used was recorded as V₁. The blank test without addition of UF resin was carried out under the same condition and the volume of 0.1M NaOH used was recorded as V₂. The experiment was repeated using 1% of each hardener added to the UF resin. The free formaldehyde content was then calculated using the equation 1 as below:

$$\% \text{ free formaldehyde} = [(V_2 - V_1) \times M \times 3.002] / W \quad [1]$$

where;

V₁ = Volume in ml of 0.1M NaOH solution for resin

V₂ = volume in ml of 0.1M NaOH solution for blank test

M = molarity of NaOH solution

W = weight in grams for resin

Fourier Transform Infra-Red (FTIR) Spectroscopy

Perkin-Elmer FT-IR Spectroscopy (model spectrum 100 series, USA) was used to determine any differences occurring to the functional group on UF resin sample and after the UF resin

was mixed with different hardeners. FT-IR spectra tests were run at ambient temperature using cured samples within the wave number range of 4000 to 500 cm^{-1} and at a resolution of 4 cm^{-1} .

Particleboard Production

Particleboards with dimensions of 340 mm width x 340 mm length x 12 mm thickness were fabricated from the rubberwood particles resinated with the UF resin admixed with four respective type of hardeners. The target density for the boards produced was 650 kg/m^3 . 8% of UF resin (based on the oven-dried particles weight) was mixed with 0.5% wax (based on oven-dried particles weight) and 1% proposed hardener (based on resin solid content) and sprayed onto the rubberwood particles during blending process. After the particles were blended with resin, the resinated rubberwood particles were manually distributed into a wooden mold having dimensional of 340 mm length x 340 mm width to form a mat. The formed mats were then hot-pressed in a hot press at 180 °C for 270 s under pressure of 4 MPa. The produced particleboards were kept in a conditioning room at relative humidity of $65 \pm 5\%$ and temperature of 23 ± 3 °C until constant weight was reached. After conditioned, the samples were cut according to the relevant standard for properties evaluation.

Properties Evaluation

Samples for properties evaluation were prepared in accordance with JIS A 5908: 2003. Properties such as density, moisture content, thickness swelling, water absorption, modulus of rupture, modulus of elasticity and internal bonding strength were conducted according to the procedure specified in JIS A 5908: 2003. On the other hand, formaldehyde emission from the particleboards was determined in accordance with JIS A 1406: 2001.

Statistical Analysis

The data were analyzed statistically to verify the significance of the variable studied. The data were analyzed using Statistical Package for the Social Science (SPSS) procedure for the analysis of variance (ANOVA) at 95% confidence level ($P \leq 0.05$). Tukey's HSD (Honestly significance difference) test was performed to further determine the significance level of the test properties.

RESULTS AND DISCUSSION

Properties of the UF resin and UF/hardener Mixtures

Acidity, gelation time, viscosity and free formaldehyde content of the UF resin before and after addition of different hardeners, namely ammonium chloride (AC), ammonium sulphate

(AS), aluminium chloride (AIC) and aluminium sulphate (AIS) are listed in Table 2. The initial pH value and gelation time of the UF resin without addition of hardener was 7.4 and 75 s, respectively, with the viscosity of 186 cp and free formaldehyde content of 0.25%. After the addition of hardeners, the selected properties of the UF resin varied accordingly to the type of hardener used.

Generally, after the addition of hardener, the mixtures of UF and hardener displayed lower pH values, shorter gelation time, higher viscosity and lower free formaldehyde content. The lowest pH value was recorded when UF were mixed with AIC and AIS, which was 3.2 and 3.0, respectively. The findings were in line with Bektha et al. (2016) who reported that the pH values of the UF resin admixed with aluminium sulphate for birch plywood production were ranged from 2.7-2.8. Correspondingly, these mixtures had the shortest gelation time of 28 and 31 s, respectively, and the highest viscosity. In comparison, higher pH value of 5.7 and 5.5 were observed when UF were mixed with ammonium-based hardener, AC and AS, as well as longer gelation time and lower viscosity.

UF resin is well known as an acid catalyzed curing resin. Reducing pH value values from alkaline to acidic condition indicating that the addition of hardener has increased the acidity of the UF resin and such acidity is necessary as it acted as an acid catalyst to facilitate the curing of the UF resin (Atar et al., 2014). The ammonium and aluminium based hardeners, also called as curing agents, are chemical substances added to the UF resin to speed up the polymerization, where these substances can liberate acids when mixed with the UF adhesive by reacting with any uncombined formaldehyde shown in the following equations. The reaction of ammonium chloride hardener with formaldehyde will form hexamethylenetetramine, hydrochloric acid and water as shown in equation 2.



On the other hand, reaction of ammonium sulphate with formaldehyde will form hexamethylenetetramine, sulphuric acid and water as shown in equation 3.



As for aluminium chloride, the hardener will react with free formaldehyde in the UF adhesive, then it will liberate aluminium formate and hydrochloric acid.



By using the aluminium sulphate as the hardener, the reaction will produce aluminium formate, sulphuric acid and hydrogen ion.



According to Atar et al. (2014), the free formaldehyde in the UF adhesives resin reacts with the hardener to generate acid. The liberation of acid in this reaction results in immediate decreases of pH value. The hardener acts as an acid catalyst for the curing

reaction of the UF resin and subsequently shortens the gel time and leads to increasing of the viscosity of the resin.

The addition of hardener also affects the free formaldehyde content in the UF resin. When 1% hardener were incorporated into the UF resin, a slight reduction in free formaldehyde content was observed in comparison to UF resin alone (0.25%). Based on the result, the free formaldehyde content after the addition of aluminium-based hardener into the UF resin was reduced to 0.20%-0.21% compared to 0.22%-0.24% after the addition of ammonium-based hardener. Aluminium-based hardener portrayed a relatively lower free formaldehyde content as the hardener increased the depth of hardening of urea formaldehyde oligomers. Additionally, in the case of using aluminium-based hardener, a quite low pH obtained due to the formation of acetal linkage and resulted in additional formaldehyde binding (Bekhata et al., 2016).

Table 2

Acidity, gelation time and viscosity of the UF resin admixed with different hardeners

Type	pH of resin	Gelation time (s)	Viscosity (cp)	Free formaldehyde content (%)
UF	7.4	75	186	0.25
UF + AC	5.7	66	201	0.24
UF + AS	5.5	65	217	0.22
UF + AIC	3.2	28	277	0.20
UF + AIS	3	31	283	0.21

Characterization of UF resin and UF/hardener Mixtures Using FT-IR Spectroscopy

The effects addition of different type of hardeners on the chemical structure of the urea formaldehyde resins were analyzed by FT-IR spectroscopy and the results are illustrated in Figure 1. The assignments of the characteristic IR absorption peaks are summarised in Table 3.

From the FTIR spectra shown in Figure 1, basic structures of UF resin ($\text{CO}(\text{NH}_2)_2$) are shown where strong absorptions were detected at 1637 cm^{-1} and 1554 cm^{-1} which is assigned to amide I (C=O stretching) and amide II (N-H bending and C-N stretching), respectively, as well as CH_2OH , CH_3 and CN at the regions around $1400\text{--}1360\text{ cm}^{-1}$ (Zorba et al., 2008). The broad bands at $3000\text{ to }3700\text{ cm}^{-1}$ has been identified as hydroxyl (-OH) stretching of the methylol group (Jada 1988). From the figure, it can be seen that

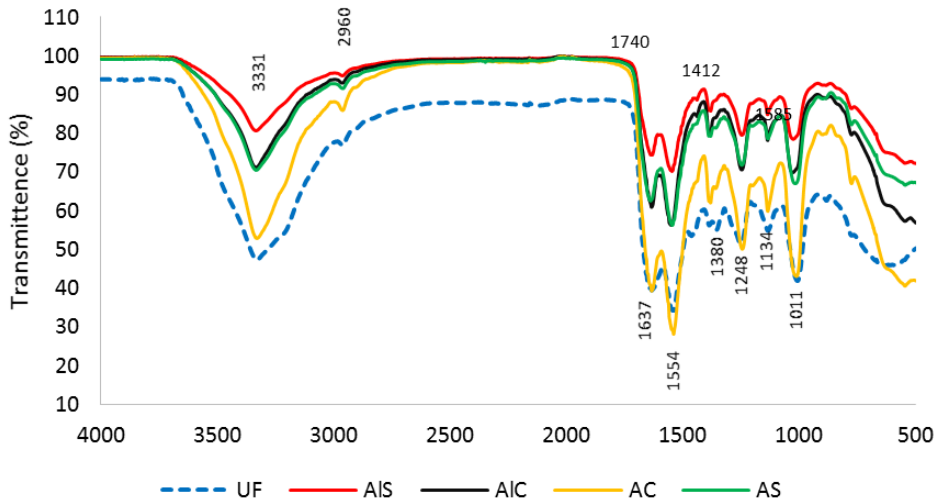


Figure 1. FT-IR spectra of urea formaldehyde (UF) and UF mixed with ammonium and aluminium based hardener

Table 3

Absorption band assignment of FT-IR spectra of UF resin (Jada 1988, Myers 1981)

Absorption (cm ⁻¹)	Observed Band (cm ⁻¹)	UF functional group
3500-3100	3331	N-H stretching mode
2960-2970	2960	CH mode of CH ₂ , CH ₂ OH and N-CH ₂
1740-1720	1740	C=O stretch aliphatic aldehyde (formaldehyde)
1680-1630	1637	Amide I, mainly due to C=O stretching
1600-1550	1554	Amide II, mixture of C-N and N-H deformation
1400-1360	1380	C-H stretching of the CH ₂ OH group
1300-1260	1260	-OH, deformation of CH ₂ OH
1150-1130	1134	Asymmetric stretching of >N-CH ₂ <N
1060-970	1011	C-O stretch in methylol

the addition of hardeners had reduced the intensity of the absorption in comparison to the pure UF resin. The finding was in agreement with Puttasukkha et al. (2015) who observed a decrement in these OH groups when formaldehyde scavenger was added into the UF resin. Another weak yet distinct absorption band appears around 2960 cm^{-1} is assigned to the asymmetric -CH stretching of the $-\text{CH}_2\text{OH}$. As can be seen from the figure, frequency of this peak for ammonium- and aluminium-based hardener become less intense compared to the urea formaldehyde peak and it is probably due to the high conversion of the $-\text{CH}_2\text{OH}$ in the polymer (Jada, 1988). According to Poljansek et al. (2006), the peaks at 1720 cm^{-1} to 1740 cm^{-1} are correspondent to the -CO stretching of the formaldehyde. Clearly from the band, the peak for formaldehyde was decreased after the addition of the ammonium and aluminium-hardeners. The absorption band at around 1585 cm^{-1} might be attributed to the formic acid salts (HCOO^-) while the band near 1248 and 1011 cm^{-1} might be attributed to hexamethylenetetramine (Vinogradoff et al., 2011).

The absorption bands at $1443 - 1487\text{ cm}^{-1}$ and $1097 - 1145\text{ cm}^{-1}$ has been identified as methylene ($-\text{CH}_2-$) bridge and methylene-ether ($-\text{CH}_2\text{OCH}_2-$) bridge, respectively, by Jada (1988). The intensity of the methylene bridge at around $1443 - 1487\text{ cm}^{-1}$ increased when the hardeners were added into the UF resin. Acid released by the hardeners accelerated the curing process of the UF resin and subsequently affected the change of methylene-ether bridges to the methylene bridges (Puttasukkha et al., 2015). On the contrary, the absorption intensity at 1101 cm^{-1} , which represents methylene ether bridges, decreased after the addition of hardeners (Wu et al., 2016). According to Dunky (1998), hydrolysis of these methylene ether bridges contributed to the increment in emittable formaldehyde from wood-based products. Garnier et al. (2002) stated that the methylene ether bridges are relatively instable and tend to rearrange themselves to methylene bridges by splitting off formaldehyde. Therefore, reduction in methylene ether bridges resulted in lesser emittance of formaldehyde. The lowest content of methylene ether bridges was recorded when aluminium sulphate was added into UF resin and had the lowest free formaldehyde correspondingly.

Physico-mechanical Properties of Particleboard

Physico-mechanical properties of particleboard fabricated from the rubberwood particles resinated with four different resin/hardener mixtures were evaluated. All of the particleboards produced in this study achieved the targeted density (650 kg/m^3) with average density ranged from 660 to 685 kg/m^3 . However, a great variation of densities of $599\text{ kg/m}^3 - 778\text{ kg/m}^3$ were recorded in the individual particleboard samples after cutting. Owing to this, all the properties tested in this study were adjusted by performing and analysis of covariance (ANOCOV) where the density and moisture content are selected as concomitant variables. Table 4 listed the mean values density and moisture content of particleboard.

The adjusted thickness swelling (TS) and water absorption (WA) values of the particleboard made with UF admixed with different types of hardener after 24-h soaking are tabulated in Table 5. TS values of 28.01% to 36.79% were recorded in all the produced panels while WA values ranged from 46.07% to 54.08% were obtained. Generally, the particleboard made with aluminium-based hardener had higher TS and WA compared to that of the particleboard made with ammonium-based hardener. The lowest thickness swelling value of 28.01% was recorded in the samples made with AS while the highest TS value of 36.79% was observed in the sample made with AIC. The pattern of the WA mirrored that of the TS as the highest WA was recorded in the particleboard made of AIC (54.08%) and the lowest WA was recorded in the AS samples (46.07%). It was found that all the panels produced did not meet the requirement of TS ($\leq 12\%$) as stated in standard JIS A 5908. However, the requirement is not easy to achieve as the water soaking method is more severe than the actual outdoor environment. This finding was in agreement with Ashori and Nourbaksh (2008) who reported that the thickness swelling of particleboard made with different species of wood exceeded 12% even only immersed for 2 hours.

As can be seen from the Table 5, the aluminium-based hardener shows a relatively higher value for both TS and WA value compare to particleboard made from ammonium-based hardener. A possible explanation for these results might be due to the acidity of the UF/hardener mixtures. For good adhesion between the particles, the pH should be between 4 to 5 to results better adhesive performance among the particles (Akyuz et al. 2010). The acidity test showed that aluminium-based hardener (3.0-3.2 pH) have a lower pH than ammonium-based hardener (5.5-5.7 pH) and therefore the particleboard made from it displayed inferior TS and WA. Table 6 provides the adjusted mean value for internal bonding (IB), modulus of rupture (MOR) and modulus of elasticity (MOE) for UF-bonded particleboard made with different type of hardeners. The modulus of rupture (MOR) and modulus of elasticity (MOE) of all types of particleboard produced was ranging from 11.26 to 16.05 N/mm² and 1498 to 1982 N/mm², respectively. The hardener type significantly affected the MOR and MOE. From the results obtained, only particleboards made with ammonium-based hardener met the minimum requirement (13 N/mm²) for MOR as specified in JIS 5908:2003. The highest MOE value was recorded in the particleboard panels made with AC, followed by AS, AIS and the lowest MOE were from particleboard made with AIC.

As for internal bonding strength, the panels made with ammonium-based hardeners displayed higher internal bonding strength compared to that of panels made with aluminium-based hardeners. However, all of the particleboard produced have fulfilled the minimum requirement of IB values of 0.2 N/mm² according to JIS A 5908:2003. Properties of the UF resin after the addition of the hardener played an important role in influence the physical and mechanical properties of the particleboards produced. Since the UF resin admixed

with aluminium-based hardener had a shorter gelation time, it hardened very fast during pressing and consequently inhibited an even spread of resin that help promoting good particle-particle bonding. Consequently, particleboard produced from UF resin admixed with aluminium-based hardeners exhibited inferior properties. Akyuz et al. (2010) stated that the low pH (< 4) of the admixture of UF resin and hardener caused precuring of the resin before hot pressing and consequently weakened the adhesive bond. In addition, acidic condition might degrade the cured UF resin and subsequently led to reduction in strength (Uner & Olgun, 2010).

Table 4

Mean density and moisture content (MC) values of the particleboard made with different type of hardener

Type of hardener	Density (kg/m ³)	Moisture content (%)
AC	684 (60.97)	6.01 (0.31)
AS	685 (7.97)	6.08 (0.18)
AIC	660 (48.05)	5.50 (0.08)
AIS	666 (40.62)	5.96 (0.14)

Note. AC: ammonium chloride; AS: ammonium sulphate; AIC: aluminium chloride; AIS: aluminium sulphate. Numbers in the parenthesis are standard deviation.

Table 5

Adjusted thickness swelling and water absorption of the particleboard made with different type of hardener

Type of hardener	Thickness swelling (%)	Water absorption (%)
AC	28.49 ^a (2.6)	46.74 ^a (2.1)
AS	28.01 ^a (2.9)	46.07 ^a (1.5)
AIC	36.79 ^c (2.5)	54.08 ^{bc} (1.1)
AIS	29.75 ^b (0.9)	50.29 ^b (2.6)

Note. AC: ammonium chloride; AS: ammonium sulphate; AIC: aluminium chloride; AIS: aluminium sulphate. Numbers in the parenthesis are standard deviation. Means in a column followed by the same letter is not significantly different at $p \leq 0.05$

Formaldehyde Emission

The average formaldehyde emission (FE) from the particleboard made with different hardeners are shown in Table 7. As shown in the table, the formaldehyde emission amount released from the particleboards produced with different types of hardener ranged from 0.45 mg/L to 1.14 mg/L. Since the particleboards produced with UF type E1, all the panels were emitting formaldehyde below 1.5 mg/L and met the requirement of F** class according to JIS A 1460: 2001. Based on the findings obtained, it can be said that the FE of the particleboard were significantly affected by hardener type. The lowest formaldehyde emission was measured from the particleboard manufactured with AIS (0.45 mg/L) while the highest formaldehyde emission was observed in particleboard made with AC (1.14 mg/L). Generally, particleboard made with aluminium-based hardener emitted a relatively lower FE (0.45 mg/L to 0.55 mg/L) than ammonium-based hardener (0.7 mg/L to 1.14 mg/L). The results correlate well with the FTIR spectra as exhibited in Figure 1. This may be explained by aluminium-based hardener holds more free formaldehyde than ammonium-based hardener.

Figure 2 displays the correlation between the formaldehyde emission from the particleboard and the free formaldehyde content of the UF resin used in the fabrication of those particleboard. As shown in the figure, a strong positive correlation ($R= 0.92$) between formaldehyde emission and free formaldehyde content was observed, suggested that the formaldehyde emission increased along with increasing free formaldehyde content. Although aluminium-based hardener particleboard emitted a relatively lower formaldehyde

Table 6

Adjusted bending strength and internal bonding values of the particleboard made with different type of hardener

Type of hardener	Modulus of rupture (N/mm ²)	Modulus of elasticity (N/mm ²)	Internal bonding (N/mm ²)
AC	16.05 ^a (1.1)	1982 ^a (431)	1.28 ^a (0.5)
AS	15.13 ^{ab} (1.9)	1772 ^{ab} (231)	1.40 ^a (0.31)
AIC	11.26 ^c (2.2)	1498 ^d (311)	0.95 ^a (0.23)
AIS	12.74 ^{cd} (3.7)	1644 ^c (204)	0.87 ^a (0.26)

Note. AC: ammonium chloride; AS: ammonium sulphate; AIC: aluminium chloride; AIS: aluminium sulphate. Numbers in the parenthesis are standard deviation. Means in a column followed by the same letter is not significantly different at $p \leq 0.05$

Table 7

Formaldehyde emission of the particleboard made with different type of hardener

Hardener	Formaldehyde emission (mg/L)
Ammonium chloride	1.14 ^a (0.02)
Ammonium sulphate	0.70 ^b (0.03)
Aluminium chloride	0.55 ^c (0.07)
Aluminium sulphate	0.45 ^d (0.13)

Note. Numbers in the parenthesis are standard deviation. Means in a column followed by the same letter is not significantly different at $p \leq 0.05$

compared to ammonium-based hardener, AS is commonly used as the hardener for particleboard manufacturing (Stefka & Dunky, 2006; Xing et al., 2007). According to Markessini (1994), in most central and northern Europe countries, AS has replaced AC as hardener as AC imposed some environmental issues. As mentioned by Roffael (1993), the burning residue of UF-bonded particleboard containing AC may form dioxins compounds which is a group of polyhalogenated organic compounds that are significant environmental pollutants. On the other hand, there is no dioxins on burning residues found on UF-bonded particleboard hardened with AS. In addition, the physico-mechanical properties of the particleboard made with aluminium-based hardeners exhibited inferior properties in comparison to the ammonium-based hardeners. Therefore, AS is the most suitable hardener for the production of particleboard in this study.

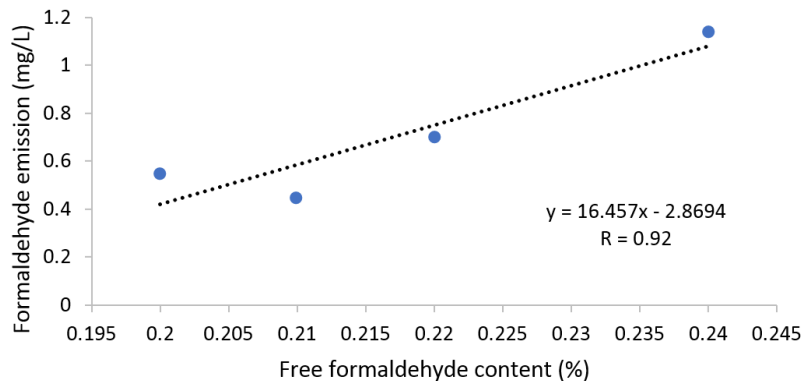


Figure 2. Correlation between formaldehyde emission and free formaldehyde content

CONCLUSION

In this study, the effects of addition of various hardeners on the viscosity, gelation time, acidity and free formaldehyde content of UF resin were evaluated. Physico-mechanical properties and formaldehyde emission level of the particleboard made from the UF/hardener mixtures were also assessed. The results revealed that both properties of UF resin and particleboard were significantly affected by the type of hardener used. Generally, aluminium-based hardeners (AIS and AIC) displayed higher efficiency in the reduction of formaldehyde emission from the particleboard. Nevertheless, physico-mechanical of the particleboard made with these hardeners were adversely affected to a greater extent in comparison to the ammonium-based hardeners. The particleboard made with aluminium-based hardeners failed to meet the minimum requirement of bending strength as stated in JIS A 5908. The reason for such phenomenon was closely related to the relatively higher viscosity, shorter gelation time and higher acidity of the UF resin after mixing that inhibit the formation of stronger bond between particles and adhesives. Based on the results obtained from the present study, it can be concluded that, among the hardeners used in this study, AS is the most suitable hardener for particleboard production. Among the two ammonium-based hardeners, AS exhibited better physical properties, internal bonding strength and lower formaldehyde emission compared to that of AC.

ACKNOWLEDGEMENT

This study was financially supported by Geran Universiti Putra Malaysia under the project number GP-IPM/2014/9444600 and Higher Institution Centres of Excellence (HiCoE).

REFERENCES

- Aizat, G., Bawon, P., Ashaari, Z., Wahab, M. W., Lee, S. H., & Lum, W. C. (2017). Addition of propylamine as formaldehyde scavenger for urea formaldehyde-bonded particleboard. *Wood Research*, 62(2), 329-334.
- Akyuz, K. C., Nemli, G., Baharoglu, M., & Zekovic, E. (2010). Effects of acidity of the particles and amount of hardener on the physical and mechanical properties of particleboard composite bonded with urea formaldehyde. *International Journal of Adhesion and Adhesives*, 30(3), 166-169. <https://doi.org/10.1016/j.ijadhadh.2009.12.006>
- Aras, U., Kalaycioglu, H., Yel, H., & Bitek, G. (2015). Effects of ammonium nitrate on physico-mechanical properties and formaldehyde contents of particleboard. *Procedia - Social and Behavioral Sciences*, 195, 2130-2134. <https://doi.org/10.1016/j.sbspro.2015.06.270>
- Ashori, A., & Nourbakhsh, A. (2008). Effect of press cycle time and resin content on physical and mechanical properties of particleboard panels made from underutilized low-quality raw materials. *Industrial Crops and Products*, 28(2), 225-230. <https://doi.org/10.1016/j.indcrop.2008.02.015>

- Atar, I., Nemli, G., Ayrilmis, N., Baharoglu, M., Sari, B., & Bardak, S. (2014). Effects of hardener type, urea usage and conditioning period on the quality properties of particleboard. *Materials and Design*, *56*, 91–96. <https://doi.org/10.1016/j.matdes.2013.10.078>
- Bekhta, P., Sedliacik, J., Saldan, R., & Novak, I. (2016). Effect of different hardeners for urea-formaldehyde resin on properties of birch plywood. *Acta Facultatis Xylogiae Zvolen*, *58*(2), 65-72. doi: 10.17423/afx.2016.58.2.07
- Dunky, M. (1998). Urea formaldehyde (UF) adhesive resins for wood. *International Journal of Adhesion and Adhesives*, *18*(2), 95-107. [https://doi.org/10.1016/S0143-7496\(97\)00054-7](https://doi.org/10.1016/S0143-7496(97)00054-7)
- Garnier, S., Pizzi, A., Vorster, O. C., & Halasz, L. (2002). Rheology of polyflavonoid tannin–Formaldehyde reactions before and after gelling. I. Methods. *Journal of Applied Polymer Science*, *86*(4), 852-863. doi: 10.1002/app.10991
- Ghani, A., Ashaari, Z., Bawon, P., & Lee, S. H. (2018). Reducing formaldehyde emission of urea formaldehyde-bonded particleboard by addition of amines as formaldehyde scavenger. *Building and Environment*, *142*, 188-194. doi: <https://doi.org/10.1016/j.buildenv.2018.06.020>
- Jada, S. S. (1988). The structure of urea-formaldehyde resins. *Journal of Applied Polymer Science*, *35*(6), 1573–1592. doi: 10.1002/app.1988.070350614
- Lum, W. C., Lee, S. H., & H'ng, P. S. (2014). Effects of formaldehyde catcher on some properties of particleboard with different ratio of surface to core layer. *Asian Journal of Applied Sciences*, *7*(1), 22-29. doi: 10.3923/ajaps.2014.22.29
- Maminski, M., Borysiuk, P., & Boruszewski, P. (2008). An attempt of improvement of a low-formaldehyde UF resin performance by glyoxal addition. *Annals of Warsaw University of Life Sciences – SGGW, Forestry and Wood Technology*, *64*, 44-46.
- Markessini, E. (1994). Formaldehyde emissions from wood-based panels and ways to reduce them. *Monument and Environment*, *2*, 57-64.
- Moslemi, A. A. (1974). *Particleboard volume 1: Materials*. Amsterdam: Southern Illinois University Press.
- Myers, G. E. (1981). Investigation of urea-formaldehyde polymer cure by infrared. *Journal of Applied Polymer Science*, *26*(3), 747-764. doi: 10.1002/app.1981.070260301
- Poljansek, I., Urska, S., & Krajnc, M. (2006). Characterization of phenol–urea–formaldehyde resin by inline FTIR spectroscopy. *Journal of Applied Polymer Science*, *99*(5), 2016–2028. doi: 10.1002/app.22161
- Puttasukha, J., Khongtong, S., & Chaowana, P. (2015). Curing behavior and bonding performance of urea formaldehyde resin admixed with formaldehyde scavenger. *Wood Research*, *60*(4), 645-654.
- Roffael, E. (1993). *Formaldehyde release from particleboard and other wood based panels*. Kuala Lumpur: Forest Research Institute Malaysia.
- Saffari, M. (2011). Effects of hardener type and particles size on formaldehyde emission pollution. In *International Proceedings of Chemical, Biological and Environmental Engineering* (Vol. 8, pp. 242-244). Singapore.

- Stefke, B., & Dunky, M. (2006). Catalytic influence of wood on the hardening behavior of formaldehyde-based resin adhesives used for wood-based panels. *Journal of Adhesion Science and Technology*, 20(8), 761-785. <https://doi.org/10.1163/156856106777638752>
- Uner, B., & Olgun, C. (2017). The effect of hardener on adhesive and fiberboard properties. *Wood Research*, 62(1), 27-36.
- Vinogradoff, V., Duvernay, F., Danger, G., Theulé, P., & Chiavassa, T. (2011) New insight into the formation of hexamethylenetetramine (HMT) in interstellar and cometary ice analogs. *Astronomy and Astrophysics*, A128, 1-7. doi :10.1051/0004-6361/201116688
- Wu, Z., Lei, H., Du, G., Cao, M., Xi, X., & Liang, J. (2016). Urea-formaldehyde resin prepared with concentrated formaldehyde. *Journal of Adhesion Science and Technology*, 30(24), 2655-2666. <https://doi.org/10.1080/01694243.2016.1193963>
- Xing, C., Zhang, S. Y., Deng, J., & Wang, S. (2007). Urea-formaldehyde-resin gel time as affected by the pH value, solid content, and catalyst. *Journal of Applied Polymer Science*, 103(3), 1566-1569. doi: 10.1002/app.25343
- Younesi-Kordkheili, H., Pizzi, A., & Niyatzade, G. (2016). Reduction of formaldehyde emission from particleboard by phenolated kraft lignin. *The Journal of Adhesion*, 92(6), 485-497. <https://doi.org/10.1080/00218464.2015.1046596>
- Zaidon, A., Lee, S. H., Abdul Aziz, M. H., & Nordin, M. N. (2016). Addition of ammonium hydroxide as formaldehyde scavenger for sesenduk (*Endospermum diadenum*) wood compregnated using phenolic resins. *European Journal of Wood and Wood Products*, 74(2), 277-280. <https://doi.org/10.1007/s00107-015-0995-9>
- Zorba, T., Papadopoulou, E., Hatjiissaak, A., Paraskevopoulos, K. M., & Chrissafis, K. (2008). Urea-formaldehyde resins characterized by thermal analysis and FTIR method. *Journal of Thermal Analysis and Calorimetry*, 92(1), 29-33. <https://doi.org/10.1007/s10973-007-8731-2>

Preparation and Swelling Study of CMC Hydrogel as Potential Superabsorbent

Nur Fitrah Che Nan, Norhazlin Zainuddin* and Mansor Ahmad

Department of Chemistry, Faculty of Science, Universiti Putra Malaysia, 43400 UPM, Serdang, Selangor, Malaysia

ABSTRACT

Carboxymethylcellulose (CMC) is a water-soluble polymer, which is widely used in various fields such as food additives, textiles, pharmaceuticals and cosmetics. In this study, hydrogel was prepared from CMC by using calcium chloride as a crosslinking agent. Optimization of the reaction was done through investigation of four different parameters which had different percentage of CMC (w/v), percentage of calcium chloride (w/v), reaction time and temperature. The gel content and swelling properties of the CMC hydrogel were studied. The highest gel content was 85.33% at 7% of CMC (w/v) with 2% of calcium chloride (w/v) in 24 hours reaction time at room temperature. The gel content increased with the increasing concentration of CMC and CaCl₂. This was due to the higher number of functional groups of COO⁻ that were available in more concentrated CMC which could crosslink with CaCl₂ to give higher gel content. Increasing the percentage of CaCl₂ will increase the electrostatic attraction between anionic charges of polymer chains and multivalent cation (Ca²⁺) that leads to increase in ionic crosslinking of CMC. The swelling properties of CMC hydrogel showed that the optimum degree of swelling was 45.33 (g/g). The swelling capacity of the hydrogel in water decreased with the increase of the gel content of CMC hydrogel. This could be due to the increase in the degree of crosslinking of the CMC hydrogel.

Keywords: Calcium chloride, carboxymethylcellulose, hydrogel, polymer, superabsorbent

ARTICLE INFO

Article history:

Received: 13 November 2017

Accepted: 28 August 2018

Published: 24 January 2019

E-mail addresses:

norhazlin@upm.edu.my (Norhazlin Zainuddin)

nurfitrahchenan@yahoo.com (Nur Fitrah Che Nan)

mansorahmad@upm.edu.my (Mansor Ahmad)

* Corresponding author

INTRODUCTION

Polysaccharides play crucial roles in life processes of all plants. Furthermore, polysaccharides can form glycoconjugates with proteins and lipids resulting in biological macromolecules in the cell wall and cell wall membranes, which play important roles in many physiological

and biochemical processes. The main polysaccharides of primary walls are cellulose, hemicellulose, and pectin.

Cellulose is the most inexhaustible natural polymer on earth and rich with hydroxyl groups which can easily form hydrogen bonding. It is characterized by its hydrophilicity, chirality, and biodegradability which is formed from repeated connection of *D*-glucose building blocks (Klemm, et al., 2005). Cellulose is suitable in the making of cellulose-based hydrogel and can be applied in various fields such as food additives, agriculture, civil engineering, cosmetic and pharmaceuticals. Cellulose is biorenewable material that represents one of the largest and renewable sources of environmentally friendly raw materials (Thakur & Thakur, 2014). Cellulose is the main component that provides the strength in plants. Other than cellulose, starches and chitin are also part of natural polymers that can be obtained from plants and animals. Both of cellulose and starches are made from sugars and are known as polysaccharides.

Cellulose derivatives such as hydroxypropyl cellulose (HPC), methyl cellulose, and carboxymethylcellulose (CMC) have been used to make cellulose based hydrogel (Shen, Shamshina, Berton, & Rogers, 2016). It can be made through physical, chemical and radical crosslinking (Pourjavadi and Hosseinzadeh, 2010). In this study, we concentrated on carboxymethylcellulose (CMC) since it has great properties that can be applied in various applications especially in hydrogel form.

Carboxymethylcellulose (CMC) known as a polyelectrolyte cellulose derivative that contains carboxyl and hydroxyl groups (Benhalima, Ferfera-Harrar, & Lerari, 2017). This polymer chain is composed of anhydroglucopyranose units joined together by 1,4-glycosidic bonds. Moreover, CMC is regarded as anionic carboxymethyl ether which is prepared by reacting alkali cellulose with sodium monochloroacetate. The polar carboxyl group makes CMC chemically reactive, tasteless, nontoxic, and have water soluble characteristics (Wang et al., 2013). CMC is an important material in industries especially as stabilizing and bonding agent.

Hydrogels which are physically or chemically crosslinked with hydrophilic polymer networks are capable of absorbing large amount of water and retain significant amount of water in their structures. Hydrogels do not dissolve and can swell in the water. The rate of absorption of hydrogels in the water is influenced by the presence of functional groups such as alcohols, carboxyls, sulphonic acid on the polymer backbone (Dafader et al., 2011). Many physical forms of formulating hydrogel can be obtained due to the ability of the semi-flexible polymer. For example slabs, membranes, beads, microgels (microspheres), and nanogels (nanoparticles). Other than that, once the hydrogels had been dried using freeze-dried or supercritically dried, hydrogels will become aerogels or cryogels respectively (Shen et al., 2016).

By definition, superabsorbent can be considered as a three-dimensional network structure that can absorb a large amount of water without dissolving it in the water due to particular amounts of hydrophilic groups (Wang et al., 2013). Superabsorbent mostly

comes from polymer that are highly crosslinked and able to swell when they are immersed in aqueous solutions. In terms of the crosslinking, either through chemical or physical crosslinking, solubilization can be avoided as water can invade without breaking the vigorous interaction that binds the polymer chains.

In this study, calcium chloride was used as a crosslinker via ionic crosslinking. Many researchers investigated the potential of CMC in various applications especially in the making of CMC hydrogel that acts as superabsorbent. However, the making of superabsorbent from CMC using divalent salts as crosslinker has not been studied widely. It has been reported previously that cellulose hydrogel is capable in response to external stimuli such as solvents, temperature, pH, ionic force, electric field, light irradiation, and salt concentration (Sanna, 2013). In this study, optimization and swelling studies of CMC hydrogel were investigated and the reaction of four different parameters with different percentage of CMC (w/v), percentage of calcium chloride (w/v), reaction time and temperature were studied as it can be used as potential superabsorbent in the future.

MATERIALS AND METHODS

Carboxymethylcellulose sodium salt (CMC) and calcium chloride were purchased from R&M Chemical. All the other chemicals used were of analytical grade. Distilled and deionized water were used throughout the experiment.

Preparation of CMC Hydrogel

The preparation of CMC hydrogel in calcium chloride solution which acts as a crosslinker was carried out according to the method published by (Chia et al., 2015). (1-7%) of CMC (w/v) was dissolved in (1-6%) of calcium chloride (w/v). The paste-like solution of CMC-CaCl₂ was then transferred into petri dish and it was expected to crosslink for 24h reaction time at room temperature. The optimization of CMC hydrogel was determined by percentage of gel content and degree of swelling.

Determination of Gel Content

The CMC hydrogel was immersed in deionized water for 72 hours at room temperature. After 72 hours, the hydrogel was dried in an oven at 60°C until constant weight was obtained. The percentage of gel content was calculated using the following formula:

$$\text{Percentage of gel content (\%)} = \frac{(W_i - W_o)}{W_i} \times 100 \quad (1)$$

where W_i = initial weight of the sample, and W_o = weight of the sample after immersion and drying process.

Determination of Degree of Swelling

The degree of swelling of CMC hydrogel was calculated after removal of the surface water until equilibrium swelling value was obtained. The degree of swelling was determined by following equation:

$$\text{Degree of swelling} = \frac{(W_t - W_o)}{W_i} \times 100 \quad (2)$$

where W_t and W_o are the weight of the swollen hydrogel at time t and the weight of dry samples. All experiments were carried out in triplicate or quadruplicate. Where appropriate, data were presented as means \pm standard deviation.

RESULTS AND DISCUSSION

Effect of Concentration of CMC on CMC Hydrogel

Figure 1(a) shows the gel content of CMC hydrogels. To isolate the effect of percentage of CMC, all other parameters were fixed. Percentage of calcium chloride was kept at 1% (w/v), and the experiment was conducted for 24 hours of reaction time at room temperature. In this study, the percentage of CMC was varied from 1 to 9% (w/v). The gel content increased from 4% to 7%. At higher concentration of CMC, the distance between CMC molecules became closer and consequently allowed the Ca^{2+} ions to crosslink the CMC molecules. However, the gel content started to decrease at 8% of CMC concentration. This may be due to incomplete dissolution of CMC powder in the salt solution. Interactions between $-\text{OH}$ groups of the polymer (CMC) and the metal ions (Ca^{2+}) contributed to the stability and the water insolubility of these polymer aggregated (Patil et al., 2010). CMC was found to be at the optimum condition at 7% w/v with 50.83% gel content.

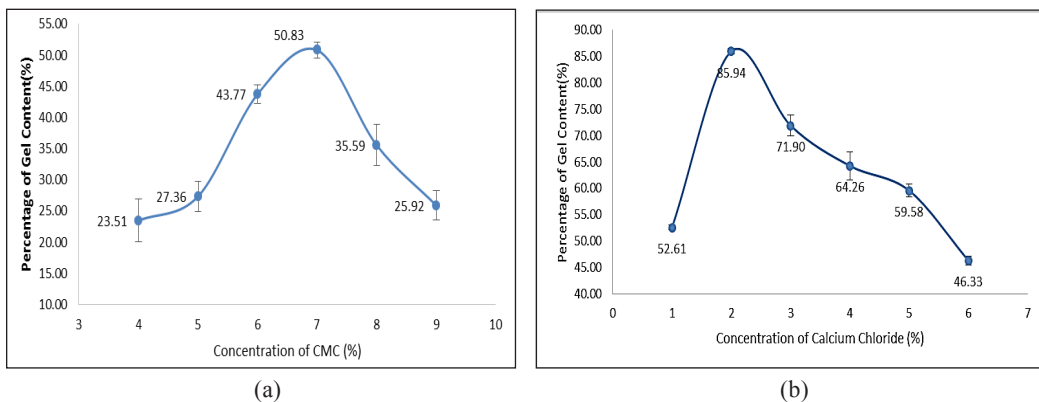


Figure 1. Percentage of gel content: (a) Effect of concentration of CMC; and (b) Effect of concentration of calcium chloride

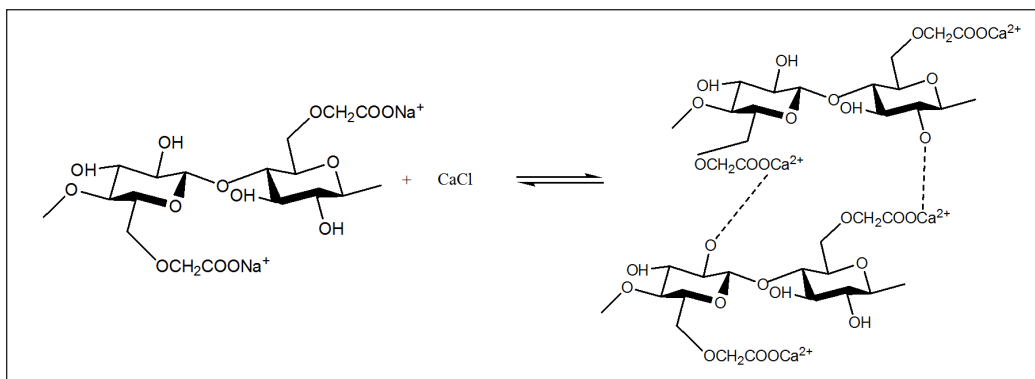
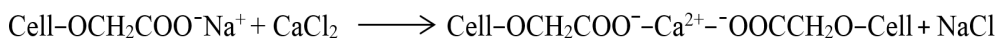


Figure 2. Reaction between carboxymethylcellulose and calcium chloride

Effect of Percentage of Calcium Chloride on CMC Hydrogel

Figure 1(b) shows that the percentage of gel content rapidly increased when less than 2% of CaCl_2 were used and gradually decreased when more than 2% were used. The reduction was slightly rapid when the concentration of CaCl_2 was between 2%-3% where the percentage dropped from 85.94% to 71.90%. Increasing the electrostatic attraction between anionic charges of polymer chains and multivalent cation (Ca^{2+}) lead to the increase of ionic crosslinking of polymer (Sultana et al., 2012). Figure 2 shows the reaction between carboxymethylcellulose and calcium chloride. Ionic strength of salt had a remarkable effect on the cross-linking of CMC but at 3% CaCl_2 , ionic strength showed a reversible result. At high concentrations of salt, the CMC chains lose their flexibility. Thus, the hydrodynamic size of the molecule diminished, producing an agglomeration of polymer chains. The presence of high concentration of calcium ion prevented the full hydration of the CMC in water, thus, reducing the dissolution of CMC in the water. (Khaled & Abdelbaki, 2012). Equation 1.1 shows the reaction between CMC and CaCl_2 to form CMC hydrogel.



Equation 1.1

Effect of Reaction Time on CMC Hydrogel

In this investigation, the reaction time of cross-linking was varied from 12 hours to 96 hours. 7% CMC (w/v) was dissolved in 2% of CaCl_2 (w/v) at different reaction time. It was found that, 24 hours was the optimum condition for the highest gel content. Figure 3(a) shows that after 24 hours, the gel content reduced and reached to half of its optimum value at 96 hours reaction time. There was a weak electrostatic attraction between CMC molecule and Ca^{2+} ion. The longer the CMC was in contact with calcium chloride solution, the stronger the physical appearance of the gel formed, as more crosslinks were formed (Patil et al.,

2010). However, after 24 hours, the reduction of the gel content of CMC hydrogel was observed. This could be due to the presence of NaCl in the hydrogel. As the Ca^{2+} ions attached to the polymer chains and formed crosslinkages, the Na^+ ion from $-\text{CH}_2\text{COONa}$ combined with Cl^- ions to form NaCl. The presence of NaCl will weaken the electrostatic attraction between the charges on the polymer chains. Therefore, the longer reaction time may trigger reversible reaction in CMC hydrogel (Qiao et al., 2012).

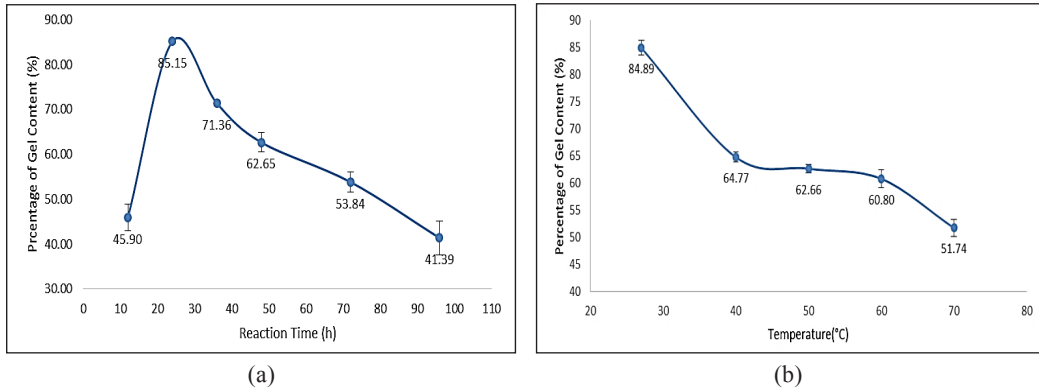


Figure 3. Percentage of gel content at different: (a) reaction time; and (b) reaction temperature

Effect of Temperature on CMC Hydrogel

Figure 3(a) shows the percentage of gel contents of CMC hydrogel formed at room temperature to 70°C. The trend of the graph depicts that, the higher the reaction temperature, the lower the gel content. The highest percentage of gel content obtained was at room temperature with 84.89% gel content. The gel content reduced to 64.77% when the temperature increased to 40°C. As ionic interaction is a physical crosslinking then it could be a reversible reaction. At high temperature with low concentration of calcium chloride it triggered the reversible reaction thus lowering the gel content. Similar finding was reported by Nie et al. (2004) where they stated that hydrogel structure formed through salt crosslinking with CMC was stable at low temperature and easily decomposed at high temperature.

Degree of Swelling

The swelling capacity of the hydrogel is inversely proportional to gel content for all parameters studied using deionized water (Figure 4). The swelling emulated the degree of crosslinking of CMC hydrogel. The swelling behavior is influenced by hydrophilicity of the carboxylic group in the structure of the hydrogels (Jamingan et al., 2015). As cross-linked density of CMC hydrogel increased, the swelling capacity of CMC hydrogel was reduced as a result of the limited space available for the free water to enter into the

hydrogel network. Therefore, the lowest degree of swelling was found in all parameters at the highest gel content of CMC hydrogel which due to the limited space available for the water. Furthermore, swelling process can occur in three particular steps: (a) diffusion of water molecules through the matrix, (b) relaxation of polymer chains via hydration, and (c) expansion of polymer network upon relaxation. This process occurred when CMC hydrogel was immersed in deionized water, the hydrophilic polymeric chains created an osmotic pressure within the hydrogel leading to the swelling of the hydrogel matrix (Abd El-salam Deghiedy, 2004).

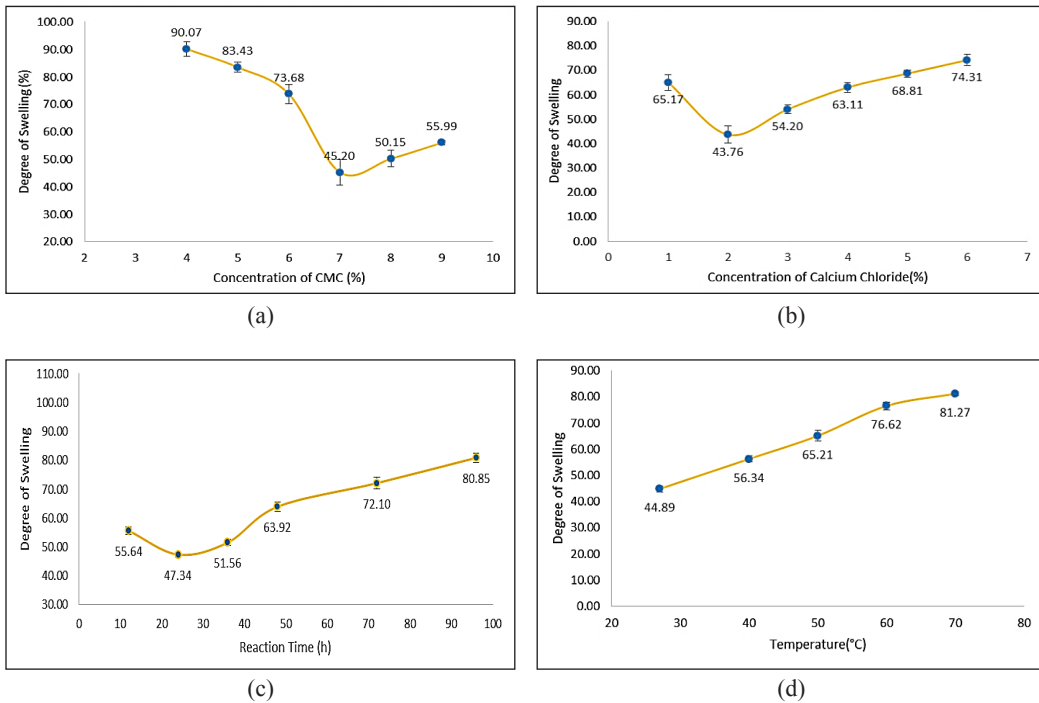


Figure 4. Degree of swelling of CMC hydrogel at different parameters: (a) concentration of CMC; (b) concentration of calcium chloride; (c) reaction time; and (d) temperature

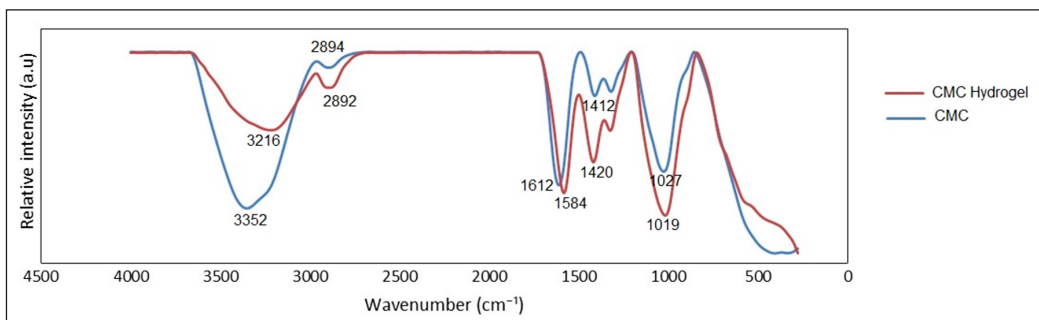


Figure 5. IR spectra for a) CMC and b) CMC hydrogel

Figure 5 shows the IR spectra for CMC and CMC hydrogel. In comparison to CMC, the absorbance region of O-H bonds for CMC hydrogel shifted to lower wavenumber. The difference occurs due to the engagement of hydroxyl and carboxylate groups of CMC to calcium ion forming chelating structure and subsequent decrease in hydrogen bonding between hydroxyl functional groups that promote shifting to lower wavenumber. In addition, the asymmetric stretching vibration of carboxylate ion at 1612 cm^{-1} deviates to lower wavenumber at 1584 cm^{-1} . This could be due to substitution of calcium ion for sodium ion in CMC to form CMC hydrogel. The replacement of sodium ion contribute to the change of charge density, the radius and the atomic weight (Daemi & Barikani, 2012). Hence, the absorbance was expected to shift to lower wavenumber. The formation of COO^- group will give resonance effect between two C-O bond that caused the carbonyl absorbance to vanish and replaced by two bands between $1610\text{-}1550\text{ cm}^{-1}$ and $1400\text{-}300\text{ cm}^{-1}$ due to anti-symmetrical and symmetrical vibration of -COO^- structure.

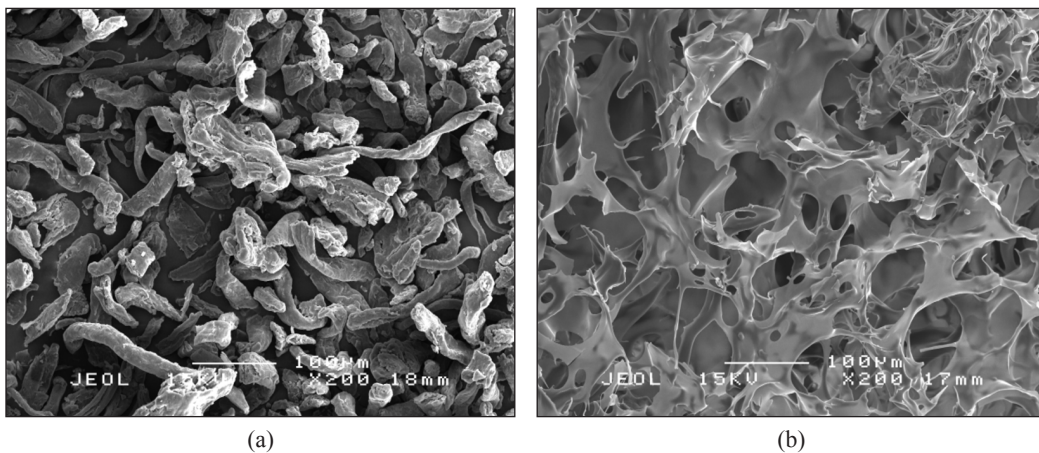


Figure 6. SEM micrograph of: (a) CMC and (b) CMC hydrogel at $200\times$

Figure 6 shows a $200\times$ magnification morphology of CMC and CMC hydrogels, respectively. CMC exhibited irregular granular surfaces and long 'thread' in structure while CMC hydrogel confirmed the macroporous structure of the crosslinked hydrogels which has three dimensional networks with empty pores. The presence of these pores in CMC hydrogel proved that a better matrix-water interaction and easier water absorption can be achieved through large surface area of the pore.

CONCLUSION

Several natural polymers have been effectively utilized as potential superabsorbent hydrogel based on natural resources. These polymers can replace and avoid excessive use of petroleum based polymer. In this study, we investigated the potential of CMC hydrogel as superabsorbent. The highest percentage of gel content obtained was 85.33% and the degree of swelling was 45.29 g/g. Overall, CMC hydrogel was obtained by ionic crosslinking and addition of calcium chloride has a significant effect on crosslinking of CMC. Optimum conditions of formation of CMC hydrogel obtained were 7% (w/v) of CMC, 2% (w/v) CaCl₂, 24h reaction time at room temperature. High percentage of gel content gives low degree of swelling due to less spaces available for the free water to enter the hydrogel network.

ACKNOWLEDGEMENT

The authors gratefully acknowledged the assistance from Universiti Putra Malaysia and the financial support provided by Trans-disciplinary grant scheme TRGS/2/2014/STG/UPM vot no:5535401 Ministry of Higher Education (MOHE).

REFERENCES

- Abd El-salam Deghiedy, N. M. (2004). *Synthesis and characterization of superabsorbent hydrogels based on natural polymers using ionizing radiations*. (Master Thesis). Al-Azhar University, Cairo, Egypt.
- Benhalima, T., Ferfera-Harrar, H., & Lerari, D. (2017). Optimization of carboxymethyl cellulose hydrogels beads generated by an anionic surfactant micelle templating for cationic dye uptake: Swelling, sorption and reusability studies. *International Journal of Biological Macromolecules*, 105, 1025–1042.
- Chia, P. X., Tan, L. J., May, C., Huang, Y., Wei, E., & Chan, C. (2015). Hydrogel beads from sugar cane bagasse and palm kernel cake, and the viability of encapsulated *Lactobacillus acidophilus*. *e-Polymers*, 15(6), 411–418.
- Daemi, H., & Barikani, M. (2012). Synthesis and characterization of Calcium Alginate nanoparticles, Sodium Homopolymannuronate Salt and its Calcium Nanoparticles. *Scientia Iranica*, 19(6), 2023–2028.
- Dafader, N. C., Adnan, M. N., Haque, M. E., Huq, D., & Akhtar, F. (2011). Study on the properties of copolymer hydrogel obtained from Acrylamide/2-Hydroxyethyl Methacrylate (HEMA) by the application of gamma radiation. *African Journal of Pure and Applied Chemistry*, 5(5), 111–118.
- Jamingan, Z., Ahmad, M. B., Hashim, K., & Zainuddin, N. (2015). Sago starch based hydrogel prepared using electron beam irradiation technique for controlled release application. *Malaysian Journal of Analytical Sciences*, 19(3), 503–512.
- Khaled, B., & Abdelbaki, B. (2012). Rheological and electrokinetic properties of carboxymethylcellulose-water dispersions in the presence of salts. *International Journal of Physical Sciences*, 7(11), 1790–1798.

- Klemm, D., Heublein, B., Fink, H. P., & Bohn, A. (2005). Cellulose: Fascinating biopolymer and sustainable raw material. *Angewandte Chemie International Edition*, 44, 3358–3393.
- Nie, H., Liu, M., Zhan, F., & Guo, M. (2004). Factors on the preparation of carboxymethylcellulose hydrogel and its degradation behavior in soil. *Carbohydrate Polymers*, 58(2), 185–189.
- Patil, J. S., Kamalapur, M. V., Marapur, S. C., & Kadam, D. V. (2010). Ionotropic gelation and polyelectrolyte complexation: The novel techniques to design hydrogel particulate sustained, modulated drug delivery system: A review. *Digest Journal of Nanomaterials and Biostructures*, 5(1), 241–248.
- Pourjavadi, A., & Hosseinzadeh, H. (2010). Synthesis and properties of partially hydrolyzed acrylonitrile-co-acrylamide superabsorbent hydrogel. *Bulletin of the Korean Chemical Society*, 31(11), 3163–3172.
- Qiao, C., Cao, X., & Wang, F. (2012). Swelling behavior study of physically cross linked gelatin hydrogels. *Polymers and Polymer Composites*, 20, 53-58.
- Sanna, S. R. (2013). *Synthesis and Characterization of New Polymeric Materials for Advanced Applications*. (Doctoral dissertation). University of Sassari, Sassari, Italy.
- Shen, X., Shamshina, J. L., Berton, P., & Rogers, R. D. (2016). Hydrogels based on cellulose and chitin: fabrication, properties, and applications. *Green Chemistry*, 18(1), 53–75.
- Sultana, S., Islam, M. R., Dafader, N. C., Haque, M. E., Nagasawa, N., & Tamada, M. (2012). Effect of mono- and divalent salts on the properties of carboxymethyl cellulose hydrogel under irradiation technique. *International Journal of Chemical Sciences*, 10(2), 627–634.
- Thakur, V. K., & Thakur, M. K. (2014). processing and characterization of natural cellulose fibers/thermoset polymer composites. *Carbohydrate Polymers*, 109, 102–117.
- Wang, Y., Shi, X., Wang, W., & Wang, A. (2013). Synthesis, characterization, and swelling behaviors of a pH-responsive CMC-g-poly(AA-co-AMPS) superabsorbent hydrogel. *Turkish Journal of Chemistry*, 37(1), 149–159.

Review article

A Review of the Mechanism and Role of Wax Inhibitors in the Wax Deposition and Precipitation

Lim Zhen Hao^{1*}, Hikmat Said Al-Salim¹ and Norida Ridzuan²

¹*Department of Chemical and Petroleum Engineering, UCSI University, 56000 Cheras, Kuala Lumpur, Malaysia*

²*Faculty of Chemical and Natural Resources Engineering, Universiti Malaysia Pahang, 26300 UMP, Gambang, Kuantan, Malaysia*

ABSTRACT

The continuous depletion of global oil reserves with the propensity for light distillates propels the oil and gas industry to explore heavier fractions of crude oils with significant amount of paraffin waxes. However, the precipitation and deposition of waxes during the transportation of these waxy crude oils in the pipelines contribute to several issues, such as the flowability reduction, excessive pumping cost, and wax gel formation, that adversely affect the supposedly steady offshore oil production. As a result, substantial resources are expended to resolve these flow assurance problems. The wax inhibitors and pour point depressants are developed and modified to meet the wax remediation criteria. Essentially, the wax crystals are formed through the nucleation, growth, and agglomeration processes, while the deposition of these waxes occurs via molecular diffusion and shear dispersion. The wax inhibitors are able to control the growth of wax crystals through nucleation, co-crystallization, adsorption, and dispersion interactions. This paper particularly assessed the following compounds: (1) polymeric wax inhibitors, (2) nano-hybrid pour point depressants, (3) organic solvents, and (4) surfactants. Given the significance of these compounds in the deposition and precipitation of waxes, it is imperative to comprehensively explore the types and nature of these compounds and their recent applications as well as to critically assess their strengths and drawbacks, which were addressed in this paper. Furthermore, the challenges of using these compounds and

ARTICLE INFO

Article history:

Received: 07 February 2018

Accepted: 12 September 2018

Published: 24 January 2019

E-mail addresses:

billylim0610@gmail.com (Lim Zhen Hao)

hikmatsaid@ucsiuniversity.edu.my (Hikmat Said Al-Salim)

norida@ump.edu.my (Norida Ridzuan)

* Corresponding author

the factors that govern their efficiencies were also discussed. Accordingly, the carbon length and the molecular weight of both paraffin waxes and wax inhibitors are among the most influential factors.

Keywords: Paraffin wax, pour point depressant, wax appearance temperature, wax inhibition, waxy crude oil

INTRODUCTION

Following the continuous depletion of conventional oil reserves, the production of unconventional oils, such as waxy crude oils and heavy crude oils, increases (Li et al., 2015). In fact, approximately 20% of the global oil reserves are of waxy crude oils, while heavy crude oils constitute about half of the recoverable oil reserves (Ghannam et al., 2012; Kumar et al., 2015). These oil reserves are often produced in the deepwater region with the ambient seawater of extremely low temperature (Shafquet et al., 2015). However, the presence of paraffin waxes in a substantial amount significantly impedes the exploration and production of these unconventional oils, which lead to the gelation of waxy crude oils and eventually, the shutdown of these production pipelines (Lira-Galeana & Hammami, 2000). As the temperature of bulk oil hits below its wax appearance temperature (WAT), the wax molecules precipitate and subsequently transform into wax gel with high yield strength, which surrounds the cross-sectional area of the production pipelines (if there are no remediation steps taken) (Chala et al., 2014). The continuous deposition of the precipitated waxes on the surface of these pipelines subsequently lead to gelation, wherein at this point, the liquid waxy crude oil undergoes three stages of phase transformation (Chala et al., 2018). Firstly, the wax particles aggregate in the oil clusters with the changing temperature and pressure and then precipitate when these oil clusters become large enough. Following that, the gelation of wax layer (wax molecules form a net-like or cage-like structure) takes shape, which is the main cause to the poor fluidity of waxy crude oils (Na et al., 2017). The gel-like wax structure continuously deposits layer-wise, resulting in clogged gel. At this point, the production pipelines have to be brought to a halt. In brief, the oil and gas industry experiences significant challenge in dealing with the deposition and precipitation of these waxes.

Considering that the paraffin wax is the primary cause to the poor flowability of waxy crude oils at low temperature, it is pivotal to consider the nature of hydrocarbons to effectively remediate this issue. Essentially, the paraffin wax consists of long, saturated hydrocarbon chains, with at least 15 or more carbon atoms per molecule (Yang et al., 2013; Ganeeva et al., 2016). The paraffin waxes are generally divided into (1) macrocrystalline wax and (2) microcrystalline wax, which are naturally found in unconventional oils (Japper-Jaafar et al., 2016; Mohamed et al., 2017). The macrocrystalline wax is characterized by low molecular weight and straight chain paraffin (n-alkanes) with varying carbon chain length (between C₁₆ and C₄₀). It predominantly crystallizes in the shape of either a platelet-like or

a needle-like. Meanwhile, the microcrystalline wax, which is also known as “amorphous” wax, contains high percentage of isoparaffinic hydrocarbons and naphthenic rings with carbon chain length of between C_{30} and C_{60} . Both types of paraffin wax precipitate and deposit in the production pipelines when the temperature drops below their WAT (Paso et al., 2009; Yang et al., 2015).

Various methods to address the deposition and precipitation of waxes are theoretically proposed and applied in practice with the purpose of improving the flowability of waxy crude oils. After all, the prevention methods are undoubtedly more economical compared to what the remediation methods offer. Fundamentally, these prevention methods are broadly categorized as (1) thermal, (2) mechanical, and (3) chemical (Al-Yaari, 2011). A blend of chemicals or a combination of methods is typically applied to attain the optimum effectiveness in improving the flowability of these waxy crude oils. Some of the most widely used conventional thermal methods to enhance the fluidity are the dilution with light ends method and heating method, but they come with an economic drawback (considering the long-term operation costs these methods require). Apart from these methods, the mechanical pigging method, is also widely recognized to remove paraffin waxes, but it requires periodic production shutdowns; thus, resulting in substantial economic predicament. Therefore, the pigging frequency must be greatly reduced in order to attain higher economic returns. Consequently, the chemical methods, such as wax inhibitors (WIs) and pour point depressants (PPDs), are preferred (Wei, 2015).

The significance of WIs and PPDs have gained growing interest among academicians and industrial practitioners over the past decades. These chemical methods serve as a preventive measure, which forms a “kinetic barrier” and subsequently delays the precipitation of these waxes and the formation of hardened wax. These methods also aid in the removal of deposited wax. With that, the chemical methods are considered as significant practical applications to improve the flowability of waxy crude oils; thus, reducing the maintenance cost of these pipeline facilities. These widely used chemicals include ethylene vinyl acetate (EVA) copolymers, comb-type copolymers, nano-hybrid compounds, organic solvents, and surfactants, which were particularly explored in this paper. Accordingly, this paper explored several categories of WIs and PPDs as well as their purpose to prevent the formation of wax crystals and high pour point (PP). In addition, the mechanisms of WIs and PPDs in waxy crude oils, the factors that govern their efficiencies, and the summary of recent applications and challenges of using these compounds were also critically assessed.

THEORY OF WAX FORMATION

Principally, the wax formation is conceptually similar to the crystallization process. Considering that the wax crystals are exothermic in nature, they emit small amount of heat. Likewise, these crystals require certain amount of heat to dissolve (endothermic process)

(Bhat & Mehrotra, 2004). The crystallization process involves the production of solid ordinate structure from a disordered phase, which typically occurs in thermodynamically unstable solutions. The concentration of solute (or strictly, its chemical potential) in excess of its equilibrium or saturation value serves as the driving force for the formation of these wax particles (Lashkarbolooki et al., 2011).

Firstly, the formation of tiny solid aggregates initiates the nucleation process. Basically, these atoms in the liquid state are prompted to bond and form solids. The subsequent stage is the growth of crystals, which mass transports the solute in the nuclei direction that is formed in the nucleation process. These crystals increase in size with the progressive addition of atoms. The final stage involves the agglomeration process, wherein the size of crystals increases in conjunction with the growing crystals. The cooling surface may experience extremely high supersaturation, which leads to the extensive formation of small crystals by nucleation. When these crystals are not dragged by the system agitation and turbulent flow, they stick to one another as well as to the cooling surface; thus, causing deposition. As a result, the deposition on the surface then behaves as thermal insulation for the flow system (dos Santos et al., 2004).

The deposition of wax occurs via two primary mechanisms (Kelland, 2014). If the pipe wall has lower temperature than the WAT, the wax forms and deposits on the surface of the pipe wall. This scenario is possible even if the temperature of the bulk fluid is above the WAT. In this case, the mechanism is known as molecular diffusion (Yang et al., 2018). Secondly, the shear dispersion potentially shifts the molecules of precipitated wax (that are near to the surface of the pipe wall) and deposits the wax at the lower velocity region in the production pipeline.

MECHANISMS OF WAX INHIBITORS

The mechanisms of WIs and the influence of WIs on the morphology of wax crystals using actual crude oils were extensively explored in various studies. In fact, the inclusion of WIs is widely recognized for delaying the agglomeration of wax crystals by modifying their shape and size (Li et al., 2010). Despite being extensively studied, the mechanisms of WIs are not adequately grasped and can be rather controversial to a certain degree. The present section briefly describes the core theories and mechanisms of WIs. Table 1 summarizes the mechanisms of different WIs and PPDs.

The molecules of both wax and WI undergo the nucleation process. The wax molecules precipitate out from the oil phase of below WAT, which form crystalline nucleus (of a critical size); thus, prompting the formation of a larger compound, specifically the wax crystal. Meanwhile, the high molecular weight of WI propels the crystalline nucleus to self-assemble into a micelle-like aggregate. This eventually forms more subcritical nuclei, which reduce supersaturation and prompt the formation of smaller wax crystals (Yang et

Table 1
Summary of wax inhibitors and pour point depressants and their corresponding mechanisms

Crude oil	WI/PPD	Mechanism	References
Iranian	Ethylene Vinyl Acetate copolymers	Co-crystallization Nucleation Adsorption	Taraneh et al. (2008)
Brazilian	Ethylene Vinyl Acetate copolymers	Co-crystallization	Machado et al. (2001)
Egyptian	Octadecyl Maleate-Vinyl Acetate copolymers	Co-crystallization Wax dispersion	Atta et al. (2015)
Indian	Non-ionic Phenyl-Polyethylene Glycol surfactant	Emulsification	Kumar & Mahto (2017)
Malaysian	Ethylene Vinyl Acetate co-Diethanolamine	Co-crystallization	Anisuzzaman et al. (2017)
China	Polyhedral Oligomeric Silsesquioxane nanocomposites	Co-crystallization Aggregation	Yao et al. (2017)
Indian	Polyhexyl Oleate-co-Hexadecyl Maleimide-co-Alkyl Oleate	Co-crystallization	Patel et al. (2017)
China	Polyoctadecyl Acrylate nanocomposites	Co-crystallization	Yao et al. (2016)
Nigerian	Trichloroethylene-Xylene	Dilution Wax dispersion	Bello et al. (2005)
Model sample	Polyethylene-butene	Co-crystallization	Ashbaugh et al. (2002)
China	Cetyl Trimethyl Ammonium Chloride	Co-crystallization	Gu et al. (2018)
Malaysian	3-2-Methoxyethoxy Propyl-Methyl-bis Trimethylsilyloxy Silane nanohybrid	Wax dispersion Adsorption	Lim et al. (2018)
Indian	Tri-Triethanolamine Monosunflower Ester	Emulsification	Kumar & Mahto (2017)
Egyptian	Ethoxylated fatty alcohols	Wax dispersion Co-crystallization	Khidr & Mahmoud (2007)

al., 2015). As a result, these smaller wax crystals remain stable in the oil phase, which suggests improved flowability (Marie et al., 2005; Naiya et al., 2015).

Another mechanism involves the co-crystallization process when the WI molecules disrupt the crystallization process and modify the growth of wax crystals (Jin et al., 2014). The paraffin wax molecules adsorb on the surface of inhibitors with similar chemical structure, which are then bound together and subsequently form a wax crystal lattice structure (Figure 2e) in the crude oil. This alters the morphology of growing wax crystals and delays the formation of three-dimensional crystals. Tiny spherical-like crystals (altered in shape from large plate-like crystals) are expected to increase the flowability (Soni et al., 2010; Jafari Ansaroudi et al., 2013).

Meanwhile, the adsorption of wax molecules on the surface of the WI inhibits the growth of crystals and alters the formation pattern of crystals through the formation of micelle core (El Mehad, 2017). In general, the WI serves as a “wrapper” that envelopes

the wax molecules and prevents their growth with the reduced crystal-crystal adhesion (Wei, 2015). Following the co-crystallization process of the WI, tiny spherical-like crystals appear in the solubilization process, which improves the dispersion of tiny wax crystals and eventually reduces the WAT (Cao et al., 2013). Besides that, the interaction of van der Waals forces between the wax crystals and the long alkyl chain of WI also increases the solubility of wax in the crude oil (Yang et al., 2015).

TYPES OF WAX INHIBITORS AND POUR POINT DEPRESSANTS

The previous section briefly described the examples and mechanisms of WIs. The current section discusses the types and the nature of WIs and PPDs, their mechanisms, their recent applications, and the factors that govern their efficiencies. This section explores the following chemicals, which included EVA copolymers, comb-type copolymers, crystalline-amorphous polymers, nano-hybrid PPDs, organic solvents, and surfactants. Table 2 provides recent applications on the reduction of PP using different WIs and PPDs.

Table 2
Reduction of pour point using different wax inhibitors and pour point depressants

Crude oil	PP (°C)	Resulted PP (°C)	WI/PPD	References
Indian	42	1	Non-ionic Phenyl-Polyethylene Glycol surfactant	Kumar & Mahto (2016)
Nigerian	2	-8	Trichloroethylene-Xylene	Bello et al. (2005)
Russian	21	14	Alkyl Acrylates-Dodecylammonium Acrylate-Dodecylammonium Sulfate	Litvinets et al. (2016)
Egyptian	24	3	Gemini surfactant	Ahmed et al. (2017)
China	19	7	Polyoctadecyl Acrylate nanocomposites	Yao et al. (2016)
Egyptian	24	6	Polyalkyl Linoleate-co-Succinic Anhydride	Soliman et al. (2018)
Egyptian	24	-3	Styrene Maleic Anhydride copolymers-Aniline- Triethanolamine with Oleic acid blend	Al-Sabagh et al. (2017)
Egyptian	27	6	Modified Maleic Anhydride-co-Octadecane copolymers	El-Ghazawy et al. (2014)
Iranian	8	-10	Ethylene Vinyl Acetate copolymers	Taraneh et al. (2008)
Brazilian	18	-17	Ethylene Vinyl Acetate copolymers	Machado et al. (2001)
Indian	22	16	Polyhexyl Oleate-co-Hexadecyl Maleimide-co-Alkyl Oleate	Patel et al. (2017)
Malaysian	35	10	Ethylene Vinyl Acetate co-Diethanolamine	Anisuzzaman et al. (2017)
China	15	7.5	Cetyl Trimethyl Ammonium Chloride	Gu et al. (2018)

Ethylene Vinyl Acetate Copolymers

The copolymerization of ethylene and vinyl acetate (VA) forms EVA copolymer. VA, which is a polar compound, consists of methyl and methylene groups with two active oxygen atoms ($C_4H_6O_2$). The simulation of the molecular dynamics (Figure 1) displays strong van der Waals interaction that EVA copolymer exhibits via oxygen atom (in the VA functional group) and hydrogen atom (in n-octacosane wax); thus, contributing to higher probability value of inhibition. As propounded by Al-Sabagh et al. (2007) and Taiwo et al. (2012), the oxygen-containing groups in the WIs inhibit the growth of these waxes. In other words, the oxygen atoms in the EVA copolymers, which reflect intermolecular interaction, increase the solubility of wax and subsequently prevent the wax solid formation.

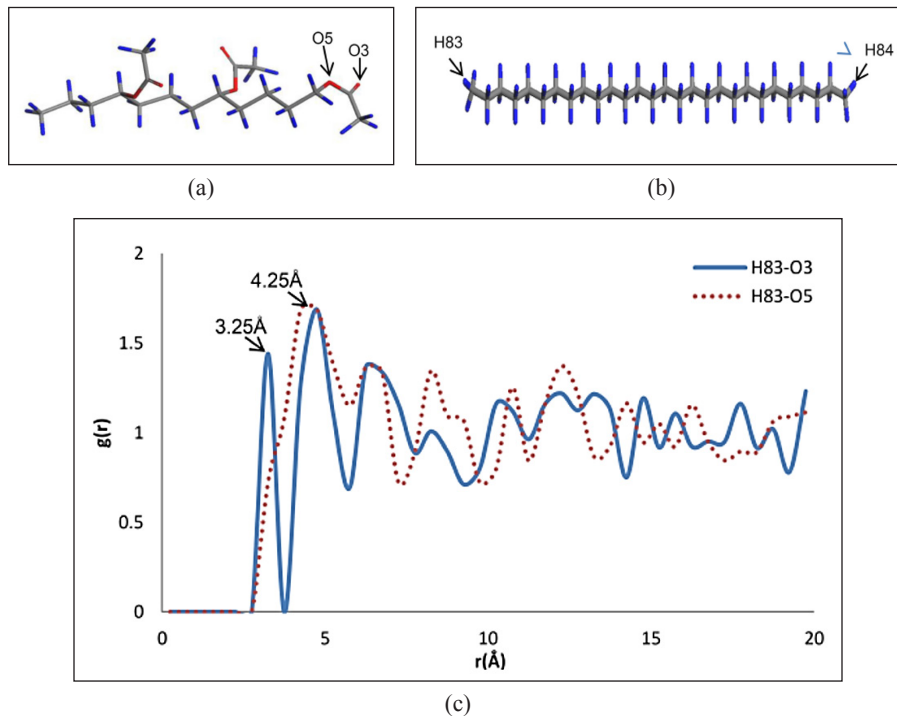


Figure 1. Structure properties defining the active atom of (a) ethylene vinyl acetate (EVA) copolymer, (b) n-octacosane, and (c) Rdf pattern H83 of n-octacosane in EVA inhibitor (Source: Ridzuan et al., 2014) Copyright 2014 by the Society of Petroleum Engineers. Reprinted with permission.

The polymeric WIs are able to optimally interact with the soluble wax in crude oil when the temperature is slightly above WAT. This is due to the interaction between the non-polar long alkyl moieties of WIs and the long-chain paraffin waxes (Yang et al., 2015). The presence of VA functional groups along with the side chains potentially impede the crystallization process of wax and reduce the PP, which eventually improve the overall

flowability (Kelland, 2014; Ridzuan et al., 2014). These side chains co-crystallize into long-chain paraffin, which leaves the polar moiety end tail and creates steric hindrance that interferes with the alignment of new incoming wax molecules. Moreover, the favorable interaction of van der Waals forces between the wax particles and the functional groups in EVA copolymer reduces the gel strength of the wax, which subsequently weakens the tendency of wax deposition. Besides that, the increase in the solubility of wax in crude oil, which is mainly caused by these van der Waals forces, contributes to the reduction of WAT (Ridzuan et al., 2015; Yang et al., 2015)

Various studies on EVA copolymer, as WI, demonstrated significant relevance in the varying VA contents (between 10 wt% and 40 wt%). The optimum VA content for the reduction of PP was reported at 30 wt% under similar conditions (Ashbaugh et al., 2005; Machado et al., 2001). Machado et al. (2001) specifically assessed the influence of EVA copolymer on the viscosity and the PP of Brazilian crude oil with varying VA contents (20 wt%, 30 wt%, 40 wt%, and 80 wt%), which reaffirmed the significant role of EVA copolymer in lowering the viscosity optimally, but only when the temperature was set higher than WAT. The study further reported that there was significant relevance between the VA content and the PP of crude oil.

Meanwhile, Jafari Ansaroudi et al. (2013) examined the influence of EVA copolymer on the viscosity of five Iranian waxy crude oils with different molecular weights. The results of viscosity reduction showed that EVA copolymer with high molecular weight (80) exhibited good influence for the crude oil with relatively low asphaltene content (0.3%), while EVA copolymer with lower molecular weight (32) demonstrated the best efficiency for the crude oil with relatively high asphaltene content (7.8%) under similar conditions. In terms of the PP, the performance of EVA copolymer with different molecular weights exhibited similar regularity.

In addition, Wu et al. (2005) and Ridzuan et al. (2014) performed the simulation of molecular dynamics on EVA copolymer to explore the interaction between EVA copolymer and wax crystals. Due to the high polarity of EVA copolymer (as compared to the wax molecules), the addition of EVA copolymer in the crude oil was found to modify the shape and growth of wax crystals on the surface in the axial direction. Moreover, the concentration of EVA copolymer was also found to govern the morphology of wax crystals to grow in different directions (x-axis, y-axis, and z-axis).

Comb-Type Copolymers

The comb-type polymer consists of polyvinyl backbone with different pendant chains. This type of polymeric WIs fulfilled the statement made by Soni & Bharambe (2008) that emphasized the significance of a good influencer to possess certain characteristics. The length of pendant chains is considered the most crucial feature, considering that the WI

and the long-chain paraffin should exhibit similar length to achieve optimum inhibition. Moreover, the polyvinyl backbone has minimal influence on the performance of WI. However, changing the regularity of this backbone, which serves as the structure for the pendant chains to suspend from, significantly influences the structure of the polymer, which reduces both PP and the degree of crystallinity. Apart from that, the comb-type polymers are widely accepted as WIs and PPDs due to the flexibility these polymers possess. The comb-type polymers are typically divided into two different polymer classes, namely (1) maleic anhydride copolymers (MACs) and (2) poly-acrylate or methacrylate (PA or PMA) ester polymers.

Xu et al. (2009) examined a series of MACs in waxy crude oil, which revealed that the MAC with the longest chain length (C_{18})—as compared to C_{12} —had the best performance in significantly reducing the size of wax crystals. Essentially, the length of alkyl side chain plays a significant role in affecting the performance of these comb-type polymers (Wang et al., 2003a; Soldi et al., 2007). In other words, the longer the length of alkyl chain, the higher the solubility of copolymer in the structure of paraffin wax. Thus, it is assumed that the increased interaction and solubility of wax impede the wax formation and contribute to the reduction of PP (Al-Sabagh et al., 2009). Moreover, the addition of the polyvinyl backbone to the alkyl side chain improves the resistance to the formation of wax crystals. Apart from the improvement of PP, the MACs were found to contribute to the reduction of both deposition rate of wax and yield stress of wax gel, which eventually ease the wax removal process due to lower gel strength (Li et al., 2012). Nonetheless, it remains a challenge to develop a specific type of WI that is universally applicable for diverse fields, which emphasizes the need to have a wide range of comb-type polymers for different compositions of crude oils.

Another important polymer class, which contains the PA and PMA, are also widely used as WIs and PPDs. As previously discussed, the compatibility between the alkyl chains and the structure of paraffin wax in crude oil influences the degree of flowability. The length on the alkyl side chain is also suggested to be longer than C_{18} to match with the long paraffin wax chain, which is usually longer than C_{15} . The discussion on the optimal alkyl side chain length ($> C_{18}$) is further strengthened by a recent study by Jafari Behbahani et al. (2017). Essentially, the specific series of comb polymers and the paraffin chain length must be compatible to hinder the formation of interlocking crystals, as demonstrated in Figure 2. The specific main criteria are aligned with those results of other comb-type polymers (Wang et al., 2003b; Soldi et al., 2007; Al-Sabagh et al., 2013). Nevertheless, the resultant outcomes are highly dependent on the composition of crude oil and the paraffin chain length in specific crude oil.

Apart from the composition of crude oil and the molecular structure of these comb-type polymers, the depressive effect on the waxy crude oil was found to rely on the average molecular weight of these polymers (Borthakur et al., 1996; Yang et al., 2009; Zhang et

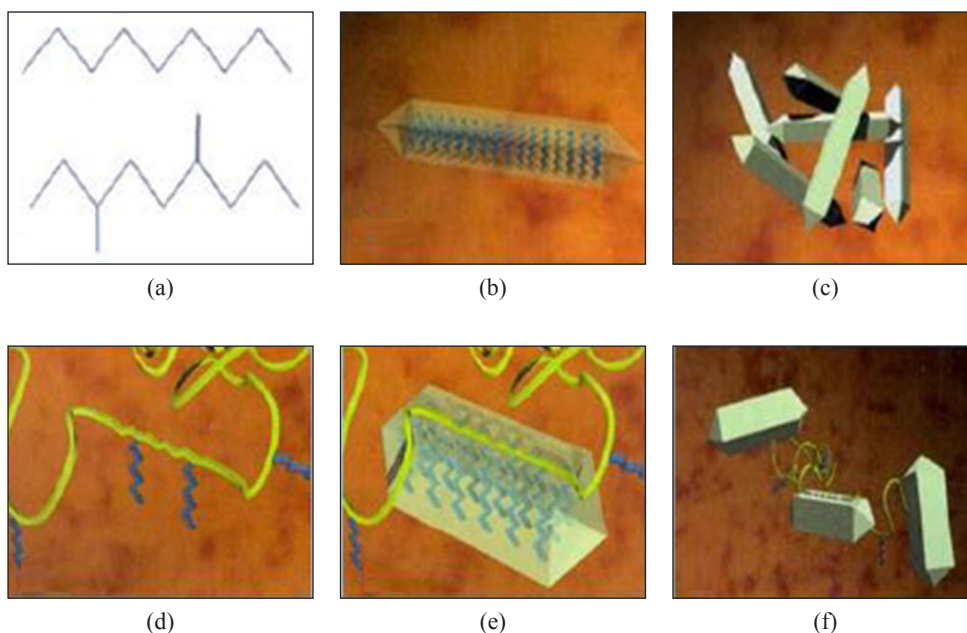


Figure 2. Modification process of the paraffin crystal with the polymeric wax inhibitor, (a) chemical structure of wax, (b) crystal shape of wax structure, (c) crystal structure of growing wax lattice, (d) polymeric wax inhibitor with wax-like components, (e) co-crystallization of wax and wax inhibitor, and (f) sterically hindered wax structure
 (Source: Al-Sabagh et al., 2016) Copyright 2016 by the American Chemical Society. Reprinted with permission.

al., 2014). This implies that the average molecular weight holds the key to influence the depressive effect of polymeric WIs (the reduction of PP). Furthermore, the influence of molecular weight on the wax inhibition is significantly related to the carbon number range of the paraffin wax in crude oil. Crude oils with wide range of normal paraffin and lower mean carbon number are recommended to be treated by high molecular weight copolymers whereas low molecular weight copolymers are recommended for crude oils with narrow range of normal paraffin and higher mean carbon number (Borthakur et al., 1996). Apart from that, El-Gamal et al. (1994) revealed that the increase in the polydispersity index (broadened distribution of the molecular weight) enhances the inhibition capability of wax; thus, indicating that the polymers with the highest polydispersity index attain the best PP depression. However, Chanda et al. (1998) and Ahmed et al. (2012) revealed contradictory findings on the molecular weight—which is possibly due to the different structure of WIs, the composition of crude oil, and the composition of asphaltene (El-Gamal et al., 1992;

Borthakur et al., 1996; Taraneh et al., 2008). Thus, it can be concluded that the average molecular weight of the comb-type polymers potentially influences the wax inhibition in waxy crude oil. Nonetheless, future studies should consider the composition of crude oil as well as the molecular weight of WIs in the selection of appropriate WI for the specific oil field.

Crystalline-amorphous Copolymers

Polyethylene-polyethylenepropylene (PE-PEP) and polyethylenebutene (PEB) are few examples of crystalline-amorphous diblock copolymers, which contain polyethylene (PE) groups (as crystalline groups) and polybutene (PB) or polyethylenepropylene (PEP) (as amorphous moieties) (Ashbaugh et al., 2002). The presence of two non-polar groups (crystalline non-polar group and amorphous non-polar group) presents an exception case to the standard structural character (Yang et al., 2015).

Previous studies demonstrated that the utilization of PE-PEP controls the size and rheological properties of wax crystals in the middle distillate fuel and crude oils (Leube et al., 2000; Monkenbusch et al., 2000; Ashbaugh et al., 2002). Figure 3 illustrates the difference in the size of these crystals. Meanwhile, Figure 4 reveals that PEP, which has the appearance of brush hairs, envelops the large surface area of PE crystalline core and is likely to self-assemble due to the presence of van der Waals force. On the other hand, the PE crystalline core in the oil phase serves as the nucleation platform for more wax fractions to nucleate at the PE surface. At this point, the PEP simultaneously maintains the micelles in the solution. These diblock copolymers are considered as appropriate wax crystal modifiers and PPDs, given their capability, even at lower concentration.

Apart from the PE-PEP, PEB is another example of diblock copolymers, which were explored in several studies (Guo et al., 2006; Radulescu et al., 2006). The ethylene side chains of PEB are able to self-assemble into the structure of a needle shape or co-crystallize with long-chain n-paraffin, which creates small, thin sheets of paraffin layer in the decane solvent (Radulescu et al., 2006). Meanwhile, Guo et al. (2006) specifically examined the model waxy crude oil with the addition of PEB (into the long-chain wax solution) in the decane solvent, which revealed heterogeneous nucleation upon cooling. Furthermore, the wax was found to crystallize into the structure of a rod shape or a shuttle shape, which demonstrated enhanced yield stress of crude oil (as compared to the structure of a plate shape without the addition of PEB). Generally, these crystalline-amorphous copolymers were shown to manipulate the morphology of wax crystals in either the model waxy crude oil or the distillate fuel; however, the applications and mechanisms of PE-PEP and PEB in actual crude oil are rarely presented over the recent years.

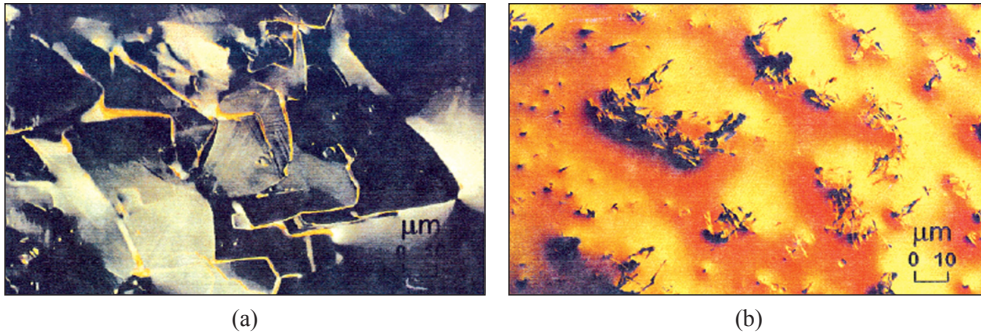


Figure 3. Micrographs of untreated polyethylene-polyethylenepropylene (PE-PEP) (left) and treated PE-PEP (right) for diesel fuel at -13°C
 (Source: Leube et al., 2000) Copyright 2000 by the American Chemical Society. Reprinted with permission.

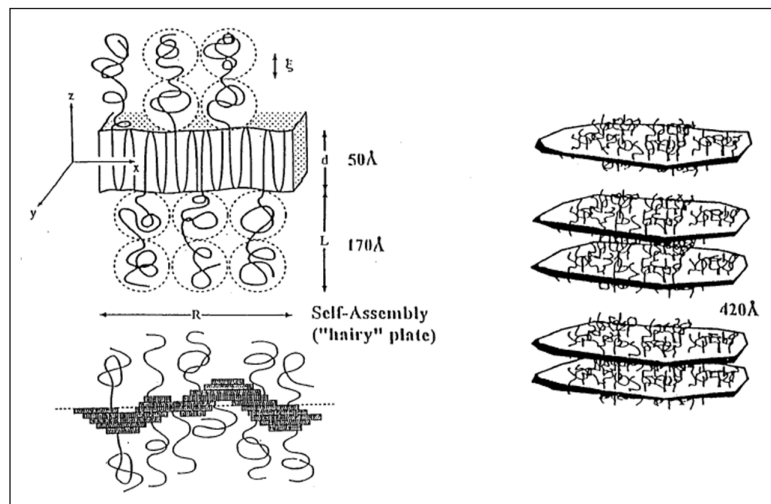


Figure 4. Generic structure of the polyethylene-polyethylenepropylene (PE-PEP) aggregates. The crystallization of polyethylene (PE) forms extended (R) platelets, while the polyethylenepropylene (PEP) hairs form brushes on both sides
 (Source: Leube et al., 2000) Copyright 2000 by the American Chemical Society. Reprinted with permission.

Nano-hybrid Pour Point Depressants

The conventional polymeric WIs or PPDs are typically applied for the transportation system of waxy crude oil, but there are certain restrictions that these WIs or PPDs cannot satisfy—certain WIs or PPDs exhibit limited depressive effect, particularly for crude oil with high wax content (Yang et al., 2015). With the recent progress in nanotechnology, there have been new developments such as the polymer/inorganic nano-composites or nano-hybrids for the industrial applications. The nanoparticles exhibit potential in modifying the polymers due to their unique size, high surface adsorption effect, and quantum size effect.

Various studies have successfully demonstrated the efficiency of nano-hybrid PPDs with the organic modification of nanomaterials by polymeric PPDs (such as polyoctadecyl acrylate, EVA copolymers, and methacrylate) (Wang et al., 2011; Yang et al., 2015; Norrman et al., 2016; Song et al., 2016; Sun et al., 2018).

Wang et al. (2011) and Song et al. (2016) modified the polymeric PPDs to enhance their performance (such as introducing the nanomaterials into the polymeric PPDs), which reaffirmed the capability of nanoparticles in altering the morphology of crystals (into spherical shape) to reduce the WAT, gelation temperature, and rheological behavior. In addition, Wang et al. (2011) recommended several possible mechanisms that may account for the enhanced performance—the changes in nucleation (the nanoparticles serve as dispersed nucleation sites), co-crystallization (the incorporation of nanoparticles into the wax crystals hinders their growth), or the adsorption of nanoparticles on the surface of wax crystals (which modulates or hinders the growth of wax crystals). Moreover, Yang et al. (2017) and Sun et al. (2018) demonstrated that the nano-hybrid PPDs did exhibit superior pour point depression than the EVA copolymers alone. In the presence of nanoparticles, the crystallized waxes were found smaller and more dispersed. Furthermore, the nanoparticles that were coated with PPDs performed more efficiently than the neat PPDs. Apart from the commonly known copolymers, the magnetic surfactant-coated nanoparticles were reportedly suspended in the carrier fluid to assist the dispersion of wax in the production tubing (Haindade et al., 2012). Table 3 summarizes the difference in pour point reduction between the pure EVA copolymers and the nano-hybrid PPDs.

Table 3
Difference in the pour point reduction between the pure ethylene vinyl acetate copolymers and nano-hybrid pour point depressants

Sample	PP (°C)
Native crude oil	30.5
EVA treated crude oil	23.0
Nano-hybrid EVA treated crude oil	16.5

Source: Wang et al., 2011

Organic Solvent

The dilution method is one of the oldest, effective methods to reduce the viscosity of oils, which improves the mobility of oils through the pipelines (Gateau et al., 2004). The classical (light ends) diluents include gas condensates, naphtha, and kerosene (Bassane et al., 2016). In the case of heavy crude oils, the organic solvents have been widely used as PPDs over the past decades prior to the emerging of polymeric WIs (Hart, 2014; Santos et al., 2018). Light ends and organic solvents are two main groups of solvent used on the

oilfields. The addition of light ends and organic solvents downhole and to the flow lines effectively remove the deposition of these waxes, which ease the transportation of crude oils to the surface. Other effective organic solvents with proven success include benzene, chlorinated hydrocarbons, and carbon disulphide, but these solvents are not environmentally friendly and pose higher risk (Woo et al., 1984).

There are several methods that enhance the performance of solvents: (1) the mixture of xylene or toluene and aliphatic solvent increases the removal of waxes (Norland, 2012); (2) the incorporation of surfactant enhances the performance of the solvent in dispersing the waxes (Sahai et al., 2018); (3) heating up the xylene and toluene solvent increases the removal efficiency of waxes (Straub et al., 1989). Despite the advantages offered by the solvent combination, the conventional organic solvent has certain limitations, such as low specific gravity, which disallows the solvent to reach downhole (to dissolve the deposited paraffin waxes). The low flash point of these solvents generally presents handling and storage problems too.

Meanwhile, Bello et al. (2005) claimed that the ability of binary PPD system of trichloroethylene and xylene to significantly depress the PP and the deposition of waxes. However, this method may not be economically feasible due to the need to utilize high dosage of chemicals. Accordingly, Santos et al. (2018) significantly reduced the PP on the heavy crude oil with high asphaltene content using gas condensates and turpentine. Moreover, the heavy crude oil was found flowing even at -36°C , which is desirable for the flow assurance in the deepwater region.

The applications of both light ends and organic solvents for heavy crude oils have revealed rather promising outcomes. Considering the cost estimation, the light ends are favored over the polymeric WIs and PPDs because they can be retrieved during the distillation of crude oils. However, the method of using organic solvents is only recommended if there are inexpensive light ends and solvents with substantial amount in the oil field.

Gemini Surfactant

Gemini surfactant (GS) is considered as the novel surfactant for wax inhibition. The surfactant can reduce the growth of wax crystals in diesel oils, but its capabilities in waxy crude oils and heavy crude oils are only recently explored (Maithufi et al., 2010; Ahmed et al., 2017; Sahai et al., 2018). GS contains more than one ionic or polar hydrophilic heads and hydrophobic hydrocarbon tails, which are chemically bonded by a spacer. With that, GS is able to perform more efficiently than the other conventional surfactants. Its enhanced surface properties (to decrease the surface tension) and lower critical micelle concentration (CMC) have gained growing interest among academicians and industrial practitioners (Kamal, 2016).

Accordingly, Ahmed et al. (2017) posited that the length of alkyl chain played a crucial factor in affecting the depression of PP. In particular, the relationships of the surface properties, especially the interfacial tension (IFT) of the GS, the side chain length, and their efficiency in the depression of PP, were evaluated. Under similar conditions, the depression of PP seemed to correlate with the value of CMC, free energy of micellization, and energy adsorption. The negative value for the energy adsorption, which denotes maximum adsorption of surfactant molecules on the surface of growing wax crystals, impedes the formation of an interlocking network of waxes in the crude oils. Similar to the polymeric WIs, the longer the gemini long-chain esters, the higher the reduction of PP and surface tension, which reaffirmed the theoretical similarity in the inhibition mechanisms of surfactants and copolymers based on the chain length. Surfactant with the longest chain ester (C_{18}) in the study adsorbed to the wax crystals and subsequently altered their morphology. Thus, tiny isotropic crystals were formed through the co-crystallization process, which subsequently improved the flowability.

Meanwhile, Sahai et al. (2018) found that the combination of GS and toluene did significantly reduce the viscosity of bituminous crude. Maithufi et al. (2010) also demonstrated that the polymeric WIs improved the performance of GS with the inhibition of wax crystallization in diesel oils. In fact, these experiments on diesel oils addressed the flowability issue of diesel in the car engine, which is particularly beneficial for those in cold countries. More specifically, the flowability is attainable through the interaction of the wax crystals with the self-assembled structures (or micelles), which leads to the growth of one-dimensional aggregates by preventing the growth of the adsorbed or co-crystallized wax crystals (Maithufi et al., 2010). If the micelles are unable to interact with the wax crystals, they are likely to agglomerate without hindrance; thus, resulting to flowability issue with the sedimentation in the storage tank or pipelines.

Conventional Surfactant

The conventional surfactant is also known as the wax dispersant, which typically includes alkyl sulfonates and fatty amine ethoxylates (Kelland, 2014). Accordingly, with the presence of water, these dispersants either function as the deposition inhibitor of waxes or the growth inhibitor of wax crystals, which water-wet and disperse these wax particles to a certain size that is small enough to be carried in the oil stream; thus, preventing these wax particles from uniting and depositing in the production lines (Figure 5) (Al-Yaari, 2011). The wax dispersant was found to successfully prevent the deposition of waxes in the New Mexico field, while other applications involving WIs and PPDs, such as EVA, were found unsuccessful (McClaffin & Whitfill, 1984). Basically, the adsorption of wax dispersant molecules to the growing wax crystals impedes the agglomeration of wax crystals. The wettability of the surface of the pipe wall is enhanced, which establishes

unfavorable circumstance for the wax crystals to deposit or adhere to (Kelland, 2014; Zhang et al., 2014; Lim et al., 2018). Apart from that, the wax dispersant prevents the deposition of wax crystals with the formation of oil-water emulsion. The deposited wax in the presence of emulsion was found softer with lower average molecular weight, compared to the untreated deposited wax. Meanwhile, the polymeric WIs were found to produce harder deposited wax with higher average molecular weight, compared to the untreated deposited wax (Kelland, 2014).

Ridzuan et al. (2016) explored diethanolamine (DEA) (water-soluble wax dispersant) as well as other wax deposition inhibitors, which revealed the ineffectiveness of a single application of DEA. Marie et al. (2004) demonstrated high efficiency of wax dispersants coupled with EVA, compared to the single application of EVA or wax dispersant. The polymeric WIs aggregate and improve the flowability of crude oils whereas the wax dispersants reduce the size of wax crystals and improve the stability of the suspended wax crystals in the bulk fluid. The EVA alone was found to reduce the size of wax crystals to 20 μm with the deposition of harder wax, but with the addition of wax dispersant, the size of wax crystals was reduced to 5 μm (El-Gamal et al., 1998). Thus, different wax dispersants are often mixed with the polymeric WIs for enhanced performance. The wax dispersants, on its own, may experience limited success in the field (Kelland, 2014).

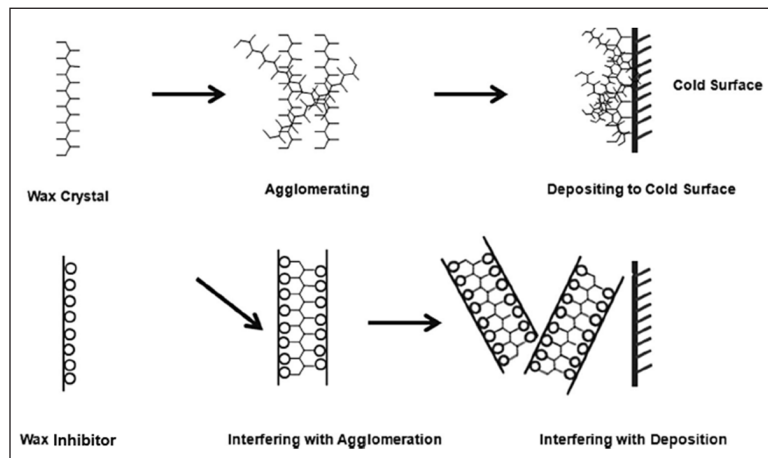


Figure 5. Schematic presentation of the influence of wax inhibitor on the wax deposition (Source: Al-Yaari, 2011) Copyright 2011 by the Society of Petroleum Engineers. Reprinted with permission.

Non-ionic Surfactant

New non-ionic surfactants are recently synthesized and considered as PPDs (Khidr et al., 2015a; 2015b). These surfactants appear in the form of viscous sticky liquid, which possesses extra surface-active properties and acts as a stronger emulsifier. Besides that,

they do not ionize in the aqueous solution due to the presence of hydrophilic groups, such as alcohol, phenol, ether, and ester. When these surfactants are in the water of higher temperature, they reveal the following characteristics: (1) they become less soluble, (2) they produce significantly lesser foam, and (3) they are environmentally friendly in removing oily and natural dirt, compared to those of anionic surfactants. The non-ionic surfactants function well in the reservoir temperature and are deemed effective in brines. Additionally, they form less viscous emulsions, which are easier to break in the refinery (Kelland, 2014). Considering all these characteristics, the non-ionic surfactants are highly considered.

Prior studies (Khidr & Mahmoud, 2007; Khidr et al., 2015b) explored several non-ionic ethoxylated surfactants, which revealed similar mechanism between surfactants and polymeric WIs of altering the morphology of wax crystals through co-crystallization that impedes the formation of tri-dimensional structure of wax. The addition of non-ionic surfactants assists in transporting the viscous crude oil in oil and water mixture of low viscosity, which is relatively stable oil in water (O/W) emulsion (Ahmed et al., 1999). Khidr et al. (2015b) selected the non-ionic ethoxylated surfactants with different chain lengths instead, which demonstrated that the increase of alkyl chain length (C_{16}) compared to C_{14} exhibited the most improved interaction between the surfactant and the paraffin fuel oil. Thus, Khidr et al. (2015b) postulated that the occurrence of co-crystallization between the surfactant and the paraffin modifies these crystals. Furthermore, the adsorption of the tested non-ionic surfactants with the increasing hydrophobic chain length (from C_{14} to C_{16}) demonstrated improved effectiveness, which is in line with the literature on GS (Ahmed et al., 2017).

Natural Surfactant

The bio-based surfactants and natural surfactants are also widely studied as PPDs in the petroleum flow assurance chemistry (Okoliegbe & Agarry, 2012). In comparison to the classical surfactants, the natural surfactants possess the following strengths: (1) lower toxicity; (2) biodegradable; (3) wide structural variety; (4) synthesized from inexpensive renewable materials; (5) stable in wide range of pH (Oguntimein et al., 1993). Kumar et al. (2017) discovered that *Sapindus mukorossi*, as a natural surfactant, significantly reduced the viscosity by 80% when it was used as PPD on the heavy crude oil. Furthermore, another type of bio-surfactant, which is generated from *Halomonas xianhensis* bacteria, was found to reduce the PP up to 24°C (El-Sheshtawy & Khidr, 2016). Besides that, the bio-based drag-reducing surfactant also successfully depressed the viscosity up to 70% (Wang et al., 2016).

In other recent studies, the synthesis of polyamine amide from canola oil, as PPD, was found useful for the depression of PP in crude oil. Specifically, the PP was reduced to 10°C with the concentration of only 0.05–0.10% (Chen et al., 2016). Meanwhile, Akinyemi et

al. (2016) explored the application of vegetable oils, such as jatropha, rubber, and castor, on the flowability of waxy crude oil, which revealed the capability of these vegetable oils to depress the PP and the viscosity of waxy crude oil appreciably within the dosage of 0.1–0.3 vol%.

In general, the surfactant can be an excellent flow improver in the crude oil due to the promising flowability improvement. The wax inhibition can be achieved by either water-wetting the surface of production facilities (which reduces the tendency of wax particles to adhere) or adding the surfactant in the crude oil (which reduces the entanglements of long-chain hydrocarbons and eventually forms a thin film over the wax particles); thus, preventing them from agglomerating to larger wax crystals (Kumar et al., 2017).

In addition, the increase in the concentration of surfactant was found to significantly reduce the IFT of crude oil (Ahn et al., 2005). The presence of surfactant in the waxy crude oil enables the formation of stable O/W micro-emulsion, which decreases the IFT and modifies these wax crystals into a needle-like structure. The pumping ability of waxy crude oil was reportedly enhanced with the formation of O/W emulsion and appreciable PP reduction (Kumar & Mahto, 2016).

CHALLENGES OF USING WAX INHIBITORS AND POUR POINT DEPRESSANTS

The applications of WIs and PPDs in waxy crude oils have received growing interest especially in those countries that encounter issues pertaining to the production of waxy oils, such as China, India, and Egypt. Table 2 summarizes the applications of WIs and PPDs for crude oils in these countries. The WIs and PPDs ultimately serve to improve the flowability by reducing the tendency of wax formation. In fact, the applications of WIs have significantly improved the economy with the flow assurance process in waxy oil fields by optimizing the performance of WIs. Nonetheless, these methods have certain economic and technical drawbacks. Even the oldest and the most preferred flow improving technique (light ends dilution) over the past few decades also has limitations despite facilitating the downstream operations (such as dehydration and desalting). Typically, these drawbacks can be observed in the case of high volume of light ends for dilution in order to attain optimum viscosity.

Most WIs and PPDs contain a non-polar moiety and a polar moiety. The non-polar moiety is also known as the long alkyl chain, which co-crystallizes with the alkane chain in paraffin wax, while the polar moiety takes charge of altering the morphology of these wax crystals. Based on the literature, higher number of carbon chain length and molecular weight of polymeric WIs are usually preferred to effectively inhibit the formation of wax

crystals due to the nature of high carbon number of alkane chain in crude oils. These advantages in wax inhibition turn into drawbacks in the downstream refinery as high molecular weight and thermos stability of WIs and PPDs, such as EVA polymers and comb-type polymers, experience difficulty to decompose in the refinery process (Gu et al., 2018). Thus, it is necessary to utilize lighter and smaller molecular compounds that exhibit similar performance to these polymeric WIs. Expectedly, inexpensive and environmental friendly WIs are preferred, which explains the recommendation of applying the bio-surfactants that are synthesized from plants. After all, these bio-surfactants are non-toxic in nature; have lower cost of extraction; are able to recover in the refining process.

Apart from the drawbacks of polymeric WIs in nature, the selection of suitable WIs for different oil fields is complex due to certain factors, such as the properties of inhibitors, the temperature and location of field, the original properties of crude oil, environmental concerns, economic feasibility, and the accuracy of lab findings. These factors govern the selection of a suitable PPD, which is strictly based on a case-by-case basis. In addition, the mechanisms of wax inhibition remain controversial due to the significant uncertainties involved in the interactions between the PPDs and these crude oils.

PARAMETERS GOVERNING THE SELECTION OF WAX INHIBITORS AND POUR POINT DEPRESSANTS

The design and the selection of suitable WI for specific crude oil are imperative to ensure long-term flow assurance. Fundamentally, heavy crude oils or waxy crude oils are complex in nature with wide range of hydrocarbons. Among these components, there are high molecular components that are primarily responsible for the poor fluidity in the production pipelines, such as saturates, asphaltenes, resins, aromatics, and paraffin waxes (de Souza Mendes & Thompson, 2012). The composition of hydrocarbons is the primary factor that governs the WAT and the PP of crude oils, subjected to the location of the oil field (El-Ghazawy et al., 2014; Ganeeva et al., 2016). Table 4 summarizes the composition of hydrocarbons of different oils. Additionally, not all WIs are suitable for all crude oils; thus, these characterizations are expected to assist researchers and industrial practitioners to grasp the nature of these crude oils and assure higher accuracy in the selection of suitable WI. Prior to the selection of WI, it is necessary to analyze the carbon length and the molecular weight of both long-chain saturated paraffin and selected WIs, considering that most polymeric WIs emphasize on their compatibility with these paraffin chain.

Table 4
Properties of different crude oils and their wax inhibitors

Crude oil	PP (°C)	Wax (wt %)	Asphaltene (wt %)	WI/PPD	References
Indian	42	11	6.50	Non-ionic Phenyl-Polyethylene Glycol surfactant	Kumar & Mahto (2016)
Malaysian	3	20	12.2	Ethylene Vinyl Acetate copolymers	Ridzuan et al. (2015)
Russian	21	19	1.28	Alkyl Acrylates-dodecylammonium Acrylate-dodecylammonium Sulfate	Litvinets et al. (2016)
Nigerian	27	35	N/A	Ethylene Vinyl Acetate copolymers	Oyekunle et al. (2017)
China	19	16	1.00	Polyoctadecyl Acrylate nanocomposites	Yao et al. (2016)
Egyptian	24	12	1.32	Polyalkyl Linoleate-co-succinic Anhydride	Soliman et al. (2018)
Egyptian	24	12	2.56	Styrene Maleic Anhydride copolymers-Aniline-Triethanolamine with Oleic acid blend	Al-Sabagh et al. (2017)
Egyptian	27	8	N/A	Modified Maleic anhydride-co-octadecane copolymers	El-Ghazawy et al. (2014)
Iranian	8	5	7.80	Ethylene Vinyl Acetate copolymers	Taraneh et al. (2008)

Note: *N/A denotes not available.

CONCLUSION

It is imperative to grasp how WIs and PPDs, even in small dosage, serve as an effective preventive measure in the transportation pipelines, considering the critical flow assurance problems that are caused by the paraffin waxes. This paper provides an overview on the major mechanisms of these WIs and PPDs in delaying the formation of wax crystals as well as their recent applications. The mechanisms of these WIs are largely similar, which are governed by various factors, such as the composition of crude oil, the structure of WIs, the length of alkyl side chains, the average molecular weight, and the carbon number of alkane chain in the crude oil. The parameters heavily depend on one another to achieve optimum co-crystallization and surface adsorption for these wax crystals. In this regard, the most

common mechanism is the co-crystallization, which highly emphasizes on the compatibility of the length of alkyl side chain to increase the interaction and solubility of WI in the structure of paraffin wax. Despite the documented effectiveness of these polymeric WIs across different oilfields at the global scale, these polymeric WIs have several significant limitations, such as their high molecular weight (that impedes the decomposition in the refinery), the deposition of harder wax in the production pipelines, and the uneconomical cost of polymeric WIs. Meanwhile, it is imperative to critically explore the selectivity of these polymers WIs that is highly dependent on the nature of crude oil. Considering that, it is recommended to seek for cleaner and universal inhibitor for waxy crude oils with small molecules. Additionally, the use of surfactants should be critically explored in the laboratory research or field application settings. These surfactants possess similar co-crystallization ability and the emulsifying ability with the presence of water to form O/W emulsion, which ease the pigging operation. Besides that, their wax dispersion ability places these surfactants as a desirable WI compared to the conventional polymeric WI. Most importantly, certain non-toxic bio-surfactants have lower cost of extraction with the ability to recover in the refining process, which leads to a greener and more economical flow assurance industry. Apart from that, it is recommended for future research to further assess the development of surfactant-polymer hybrid despite the proven results of enhanced performance in prior studies. Moreover, the surfactant nano-hybrids were found to be inadequately explored, which should be comprehensively addressed in the future research, as well.

ACKNOWLEDGEMENT

This work was supported by Universiti Malaysia Pahang through UMP Research Grant Scheme (RDU 170352 & RDU 190106). We would like to express our utmost appreciation to UCSI University and Universiti Malaysia Pahang for the completion of this review paper.

REFERENCES

- Ahmed, N. S., Nassar, A. M., Nasser, R. M., Khattab, A. F., & Abdel-Azim, A. A. A. (2012). Synthesis and evaluation of some polymers as lubricating oil additives. *Journal of Dispersion Science and Technology*, 33(5), 668–675.
- Ahmed, N. S., Nassar, A. M., Zaki, N. N., & Gharieb, H. K. H. (1999). Stability and rheology of heavy crude oil-in-water emulsion stabilized by an anionic-nonionic surfactant mixture. *Petroleum Science and Technology*, 17(5–6), 553–576.
- Ahmed, S. M., Khidr, T. T., & Ismail, D. A. (2017). Effect of gemini surfactant additives on pour point depressant of crude oil. *Journal of Dispersion Science and Technology*, 39(8), 1160-1164.
- Ahn, S., Wang, K. S., Shuler, P. J., Creek, J. L., & Tang, Y. (2005, January). Paraffin crystal and deposition control by emulsification. In *SPE International Symposium on Oilfield Chemistry*. The Woodlands, Texas.

- Akinyemi, O. P., Udonne, J. D., Efevbokhan, V. E., & Ayoola, A. A. (2016). A study on the use of plant seed oils, triethanolamine and xylene as flow improvers of Nigerian waxy crude oil. *Journal of Applied Research and Technology*, 14(3), 195–205.
- Al-Sabagh, A. M., Betiha, M. A., Osman, D. I., Hashim, A. I., El-Sukkary, M. M., & Mahmoud, T. (2016). Preparation and evaluation of poly(methyl methacrylate)-graphene oxide nanohybrid polymers as pour point depressants and flow improvers for waxy crude oil. *Energy & Fuels*, 30(9), 7610–7621.
- Al-Sabagh, A. M., El-Din, M. R. N., Morsi, R. E., & Elsabee, M. Z. (2009). Styrene-maleic anhydride copolymer esters as flow improvers of waxy crude oil. *Journal of Petroleum Science and Engineering*, 65(3–4), 139–146.
- Al-Sabagh, A. M., El-Hamouly, S. H., Khidr, T. T., El-Ghazawy, R. A., & Higazy, S. A. (2013). Preparation the esters of oleic acid-maleic anhydride copolymer and their evaluation as flow improvers for waxy crude oil. *Journal of Dispersion Science and Technology*, 34(11), 1585–1596.
- Al-Sabagh, A. M., Khidr, T. T., Moustafa, H. M., Mishrif, M. R., & Al-Damasy, M. H. (2017). Investigating the synergistic effect between oil soluble surfactants and styrene–maleic anhydride copolymers to enhance the flow properties of waxy crude oil. *Petroleum Science and Technology*, 35(13), 1381–1388.
- Al-Yaari, M. (2011, January). Paraffin wax deposition: mitigation and removal techniques. In *SPE Saudi Arabia section Young Professionals Technical Symposium*. Dhahran, Saudi Arabia.
- Al-Sabagh, A. M., El-Kafrawy, A. F., Khidr, T. T., El-Ghazawy, R. A., & Mishrif, M. R. (2007). Synthesis and evaluation of some novel polymeric surfactants based on aromatic amines used as wax dispersant for waxy gas oil. *Journal of Dispersion Science and Technology*, 28(6), 976–983.
- Anisuzzaman, S. M., Abang, S., Bono, A., Krishnaiah, D., Karali, R., & Safuan, M. K. (2017, December). Wax inhibitor based on ethylene vinyl acetate with methyl methacrylate and diethanolamine for crude oil pipeline. In *29th Symposium of Malaysian Chemical Engineers (SOMChE)* (Vol. 206, p. 12074). Sarawak, Malaysia.
- Ashbaugh, H. S., Fetters, L. J., Adamson, D. H., & Prud'homme, R. K. (2002). Flow improvement of waxy oils mediated by self-aggregating partially crystallizable diblock copolymers. *Journal of Rheology*, 46(4), 763–776.
- Ashbaugh, H. S., Guo, X., Schwahn, D., Prud'homme, R. K., Richter, D., & Fetters, L. J. (2005). Interaction of paraffin wax gels with ethylene/vinyl acetate co-polymers. *Energy and Fuels*, 19(1), 138–144.
- Ashbaugh, H. S., Radulescu, A., Prud'homme, R. K., Schwahn, D., Richter, D., & Fetters, L. J. (2002). Interaction of paraffin wax gels with random crystalline/amorphous hydrocarbon copolymers. *Macromolecules*, 35(18), 7044–7053.
- Atta, A. M., El-Ghazawy, R. A., Morsy, F. A., Hebishy, A., & Elmorsy, A. (2015). Adsorption of polymeric additives based on vinyl acetate copolymers as wax dispersant and its relevance to polymer crystallization mechanisms. *Journal of Chemistry*, 2015, 1-8.
- Bassane, J. F. P., Sad, C. M. S., Neto, D. M. C., Santos, F. D., Silva, M., Tozzi, F. C., ... & da Silva, J.O. (2016). Study of the effect of temperature and gas condensate addition on the viscosity of heavy oils. *Journal of Petroleum Science and Engineering*, 142, 163–169.

- Bello, O. O., Fasesan, S. O., Macaulay, S. R. A., & Latinwo, G. K. (2005). Study of the influence of xylene-based chemical additive on crude oil flow properties and paraffin deposition inhibition. *Engineering Journal of the University of Qatar*, 18, 15-28.
- Bhat, N. V., & Mehrotra, A. K. (2004). Measurement and prediction of the phase behavior of wax-solvent mixtures: significance of the wax disappearance temperature. *Industrial and Engineering Chemistry Research*, 43(13), 3451-3461.
- Borthakur, A., Chanda, D., Dutta Choudhury, S. R., Rao, K. V., & Subrahmanyam, B. (1996). Alkyl fumarate-vinyl acetate copolymer as flow improver for high waxy Indian crude oils. *Energy and Fuels*, 10(3), 844-848.
- Cao, K., Wei, X., Li, B., Zhang, J., & Yao, Z. (2013). Study of the influence of imidization degree of poly(styrene-co-octadecyl maleimide) as waxy crude oil flow improvers. *Energy and Fuels*, 27(2), 640-645.
- Chala, G. T., Sulaiman, S. A., & Japper-Jaafar, A. (2018). Flow start-up and transportation of waxy crude oil in pipelines-A review. *Journal of Non-Newtonian Fluid Mechanics*, 251, 69-87.
- Chala, G. T., Sulaiman, S. A., Japper-Jaafar, A., Kamil Wan Abdullah, W. A., & Mior Mokhtar, M. M. (2014). Gas void formation in statically cooled waxy crude oil. *International Journal of Thermal Sciences*, 86, 41-47.
- Chanda, D., Sarmah, A., Borthakur, A., Rao, K. V., Subrahmanyam, B., & Das, H. C. (1998). Combined effect of asphaltenes and flow improvers on the rheological behaviour of Indian waxy crude oil. *Fuel*, 77(11), 1163-1167.
- Chen, G., Bai, Y., Zhang, J., Yuan, W., Song, H., & Jeje, A. (2016). Synthesis of new flow improvers from canola oil and application to waxy crude oil. *Petroleum Science and Technology*, 34(14), 1285-1290.
- de Souza Mendes, P. R., & Thompson, R. L. (2012). A critical overview of elasto-viscoplastic thixotropic modeling. *Journal of Non-Newtonian Fluid Mechanics*, 187, 8-15.
- dos Santos, J. da S. T., Fernandes, A. C., & Giulietti, M. (2004). Study of the paraffin deposit formation using the cold finger methodology for Brazilian crude oils. *Journal of Petroleum Science and Engineering*, 45(1-2), 47-60.
- El-Gamal, I. M., Khidr, T. T., & Ghuiba, F. M. (1998). Nitrogen-based copolymers as wax dispersants for paraffinic gas oils. *Fuel*, 77(5), 375-385.
- El-Ghazawy, R. A., Atta, A. M., & Kabel, K. I. (2014). Modified maleic anhydride-co-octadecene copolymers as flow improver for waxy Egyptian crude oil. *Journal of Petroleum Science and Engineering*, 122, 411-419.
- El-Sheshtawy, H. S., & Khidr, T. T. (2016). Some biosurfactants used as pour point depressant for waxy egyptian crude oil. *Petroleum Science and Technology*, 34(16), 1475-1482.
- El-Gamal, I. M., Gad, E. A. M., Faramawi, S., & Gobieli, S. (1992). Flow improvement of waxy western desert gas oil. *Journal of Chemical Technology and Biotechnology*, 55(2), 123-130.
- El-Gamal, I. M., Ghuiba, F. M., El-Batanoney, M. H., & Gobieli, S. (1994). Synthesis and evaluation of acrylate polymers for improving flow properties of waxy crudes. *Journal of Applied Polymer Science*, 52(1), 9-19.

- El Mehad, N. (2017). Efficiency of n-decyl-n-benzyl-n-methylglycine and n-dodecyl-n-benzyl-n-methylglycine surfactants for flow improvers and pour point depressants. *Journal of Molecular Liquids*, 229, 609–613.
- Ganeeva, Y. M., Yusupova, T. N., & Romanov, G. V. (2016). Waxes in asphaltenes of crude oils and wax deposits. *Petroleum Science*, 13(4), 737–745.
- Gateau, P., Hénaut, I., Barré, L., & Argillier, J. F. (2004). Heavy oil dilution. *Oil and Gas Science and Technology*, 59(5), 503–509.
- Ghannam, M. T., Hasan, S. W., Abu-Jdayil, B., & Esmail, N. (2012). Rheological properties of heavy & light crude oil mixtures for improving flowability. *Journal of Petroleum Science and Engineering*, 81, 122–128.
- Gu, X., Zhang, F., Li, Y., Zhang, J., Chen, S., Qu, C., & Chen, G. (2018). Investigation of cationic surfactants as clean flow improvers for crude oil and a mechanism study. *Journal of Petroleum Science and Engineering*, 164, 87–90.
- Guo, X., Pethica, B. A., Huang, J. S., Adamson, D. H., & Prud'homme, R. K. (2006). Effect of cooling rate on crystallization of model waxy oils with microcrystalline poly (ethylene butene). *Energy and Fuels*, 20(1), 250–256.
- Haidade, Z. M. W., Bihani, A. D., Javeri, S. M., & Jere, C. B. (2012, June). Enhancing flow assurance using Co-Ni nanoparticles for dewaxing of production tubing. In *SPE International Oilfield Nanotechnology Conference and Exhibition*. Noordwijk, The Netherlands.
- Hart, A. (2014). A review of technologies for transporting heavy crude oil and bitumen via pipelines. *Journal of Petroleum Exploration and Production Technology*, 4(3), 327–336.
- Jafari Ansaroudi, H. R., Vafaie-Sefti, M., Masoudi, S., Behbahani, T. J., & Jafari, H. (2013). Study of the morphology of wax crystals in the presence of ethylene-co-vinyl acetate copolymer. *Petroleum Science and Technology*, 31(6), 643–651.
- Jafari Behbahani, T., Miranbeigi, A. A., & Sharifi, K. (2017). A new experimental investigation on upgrading of waxy crude oils by methacrylate polymers. *Petroleum Chemistry*, 57(10), 874–880.
- Japper-Jaafar, A., Bhaskoro, P. T., & Mior, Z. S. (2016). A new perspective on the measurements of wax appearance temperature: Comparison between DSC, thermomicroscopy and rheometry and the cooling rate effects. *Journal of Petroleum Science and Engineering*, 147, 672–681.
- Jin, W., Jing, J., Wu, H., Yang, L., Li, Y., Shu, X., & Wang, Y. (2014). Study on the inherent factors affecting the modification effect of EVA on waxy crude oils and the mechanism of pour point depression. *Journal of Dispersion Science and Technology*, 35(10), 1434–1441.
- Kamal, M. S. (2016). A review of gemini surfactants: potential application in enhanced oil recovery. *Journal of Surfactants and Detergents*, 19(2), 223–236.
- Kelland, M. A. (2014). *Production chemicals for the oil and gas industry*. Baton Rouge, Florida: CRC press.
- Khidr, T. T., Doheim, M. M., & El-Shamy, O. A. A. (2015a). Effect of ethoxylate on pour point depressant of fuel oil. *Energy Sources, Part A: Recovery, Utilization, and Environmental Effects*, 37(15), 1697–1703.
- Khidr, T. T., Doheim, M. M., & El-Shamy, O. A. A. (2015b). Pour point depressant of fuel oil using non-ionic surfactants. *Petroleum Science and Technology*, 33(17–18), 1619–1626.

- Khidr, T. T., & Mahmoud, S. A. (2007). Dispersion of waxy gas oil by some nonionic surfactants. *Journal of Dispersion Science and Technology*, 28(8), 1309–1315.
- Kumar, L., Paso, K., & Sjöblom, J. (2015). Numerical study of flow restart in the pipeline filled with weakly compressible waxy crude oil in non-isothermal condition. *Journal of Non-Newtonian Fluid Mechanics*, 223, 9–19.
- Kumar, R., Banerjee, S., Mandal, A., & Naiya, T. K. (2017). Flow improvement of heavy crude oil through pipelines using surfactant extracted from soapnuts. *Journal of Petroleum Science and Engineering*, 152, 353–360.
- Kumar, S., & Mahto, V. (2016). Emulsification of Indian heavy crude oil in water for its efficient transportation through offshore pipelines. *Chemical Engineering Research and Design*, 115, 34–43.
- Kumar, S., & Mahto, V. (2017). Emulsification of Indian heavy crude oil using a novel surfactant for pipeline transportation. *Petroleum Science*, 14(2), 372–382.
- Lashkarbolooki, M., Esmailzadeh, F., & Mowla, D. (2011). Mitigation of wax deposition by wax-crystal modifier for Kermanshah crude oil. *Journal of Dispersion Science and Technology*, 32(7), 975–985.
- Leube, W., Monkenbusch, M., Schneiders, D., Richter, D., Adamson, D., Fetters, L., Dounis, P., Lovegrove, R. (2000). Wax-crystal modification for fuel oils by self-aggregating partially crystallizable hydrocarbon block copolymers. *Energy and Fuels*, 14(2), 419–430.
- Li, H., Zhang, J., Song, C., & Sun, G. (2015). The influence of the heating temperature on the yield stress and pour point of waxy crude oils. *Journal of Petroleum Science and Engineering*, 135, 476–483.
- Li, L., Guo, X., Adamson, D. H., Pethica, B. A., Huang, J. S., & Prud'homme, R. K. (2010). Flow improvement of waxy oils by modulating long-chain paraffin crystallization with comb polymers: an observation by X-ray diffraction. *Industrial & Engineering Chemistry Research*, 50(1), 316–321.
- Li, L., Xu, J., Tinsley, J., Adamson, D. H., Pethica, B. A., Huang, J. S., Prud'homme, R. K., & Guo, X. (2012). Improvement of oil flowability by assembly of comb-type copolymers with paraffin and asphaltene. *AIChE Journal*, 58(7), 2254–2261.
- Lim, Z. H., Al Salim, H. S., Ridzuan, N., Nguete, R., & Sasaki, K. (2018). Effect of surfactants and their blend with silica nanoparticles on wax deposition in a Malaysian crude oil. *Petroleum Science*, 15(3), 577–590.
- Lira-Galeana, C., & Hammami, A. (2000). Wax precipitation from petroleum fluids: A review. In F. Y. The & G. V. Chilingarian, (Eds.), *Developments in petroleum science* (Vol. 40, pp. 557–608). New York: Elsevier.
- Litvinets, I. V., Prozorova, I. V., Yudina, N. V., Kazantsev, O. A., & Sivokhin, A. P. (2016). Effect of ammonium-containing polyalkyl acrylate on the rheological properties of crude oils with different ratio of resins and waxes. *Journal of Petroleum Science and Engineering*, 146, 96–102.
- Machado, A. L. C., Lucas, E. F., & González, G. (2001). Poly (ethylene-co-vinyl acetate)(EVA) as wax inhibitor of a Brazilian crude oil: oil viscosity, pour point and phase behavior of organic solutions. *Journal of Petroleum Science and Engineering*, 32(2–4), 159–165.
- Maithufi, M. N., Joubert, D. J., & Klumperman, B. (2010). Application of gemini surfactants as diesel fuel wax dispersants. *Energy and Fuels*, 25(1), 162–171.

- Marie, E., Chevalier, Y., Brunel, S., Eydoux, F., Germanaud, L., & Flores, P. (2004). Settling of paraffin crystals in cooled middle distillate fuels. *Journal of Colloid and Interface Science*, 269(1), 117–125.
- Marie, E., Chevalier, Y., Eydoux, F., Germanaud, L., & Flores, P. (2005). Control of n-alkanes crystallization by ethylene–vinyl acetate copolymers. *Journal of Colloid and Interface Science*, 290(2), 406–418.
- McClaffin, G. G., & Whitfill, D. L. (1984). Control of Paraffin Deposition in Production Operations. *Journal of Petroleum Technology*, 36(11), 1-965.
- Mohamed, N. H., Soliman, F. S., El Maghraby, H., & Moustfa, Y. M. (2017). Thermal conductivity enhancement of treated petroleum waxes, as phase change material, by α nano alumina: Energy storage. *Renewable and Sustainable Energy Reviews*, 70, 1052–1058.
- Monkenbusch, M., Schneiders, D., Richter, D., Willner, L., Leube, W., Fetters, L. J., Huang, J.S., & Lin, M. (2000). Aggregation behaviour of pe–pep copolymers and the winterization of diesel fuel. *Physica B: Condensed Matter*, 276, 941–943.
- Na, L., Mao, G., Shi, X., Tian, S., & Liu, Y. (2017). Advances in the research of polymeric pour point depressant for waxy crude oil. *Journal of Dispersion Science and Technology*, 39(8), 1165-1171.
- Naiya, T. K., Banerjee, S., Kumar, R., & Mandal, A. (2015, November). Heavy crude oil rheology improvement using naturally extracted surfactant. In *SPE Oil and Gas India Conference and Exhibition*. Mumbai, India.
- Norland, A. K. (2012). *Organic flow assurance, pour point depressant development through experimental design* (Master's thesis). University of Stavanger, Norway.
- Norrman, J., Solberg, A., Sjöblom, J., & Paso, K. (2016). Nanoparticles for waxy crudes: Effect of polymer coverage and the effect on wax crystallization. *Energy and Fuels*, 30(6), 5108–5114.
- Oguntimein, G. B., Erdmann, H., & Schmid, R. D. (1993). Lipase catalysed synthesis of sugar ester in organic solvents. *Biotechnology Letters*, 15(2), 175–180.
- Okoliegbe, I. N., & Agarry, O. O. (2012). Application of microbial surfactant (a review). *Scholarly Journals of Biotechnology*, 1(1), 15–23.
- Oyekunle, L. O., Adeyanju, O. A., & Phillips, T. I. (2017). Evaluations of the effect of selected wax inhibitive chemicals on wax deposition in crude oil flow in sub-sea pipe-lines. *Petroleum Science and Technology*, 35(20), 1967–1973.
- Paso, K. G., Kallevik, H., & Sjöblom, J. (2009). Measurement of wax appearance temperature using near-infrared (NIR) scattering. *Energy and Fuels*, 23(10), 4988–4994.
- Patel, M. R., Chitte, P. S., & Bharambe, D. P. (2017). Oleic acid based polymeric flow improvers for Langhnaj (North Gujarat, India) crude oil. *Egyptian Journal of Petroleum*, 26(4), 895–903.
- Radulescu, A., Schwahn, D., Stellbrink, J., Kentzinger, E., Heiderich, M., Richter, D., & Fetters, L. J. (2006). Wax crystallization from solution in hierarchical morphology templated by random poly (ethylene-co-butene) self-assemblies. *Macromolecules*, 39(18), 6142–6151.
- Ridzuan, N., Adam, F., & Yaacob, Z. (2014, December). Molecular recognition of wax inhibitor through pour point depressant type inhibitor. In *International Petroleum Technology Conference*. Kuala Lumpur, Malaysia.

- Ridzuan, N., Adam, F., & Yaacob, Z. (2015). Effects of shear rate and inhibitors on wax deposition of Malaysian crude oil. *Oriental Journal of Chemistry*, 31(4), 1999–2004.
- Ridzuan, N., Adam, F., & Yaacob, Z. (2016). Evaluation of the inhibitor selection on wax deposition for Malaysian crude oil. *Petroleum Science and Technology*, 34(4), 366–371.
- Sahai, M., Singh, R. K., Kukrety, A., Kumar, A., Ray, S. S., Chhibber, V. K., & Kumar, S. (2018). Application of triazine-based gemini surfactants as viscosity reducing agents of tar sand derived bituminous crude. *Energy and Fuels*, 32(3), 3031–3038.
- Santos, F. D., Sad, C. M. S., Bassane, J. F. P., Neto, D. M. C., Filgueiras, P. R., Silva, M., ... & Pereira, L.B. (2018). Improvement on Pour Point of Heavy Oils by Adding Organic Solvents. *Revista Virtual de Química*, 9(6), 2404-2413.
- Shafquet, A., Ismail, I., Japper-Jaafar, A., Sulaiman, S. A., & Chala, G. T. (2015). Estimation of gas void formation in statically cooled waxy crude oil using online capacitance measurement. *International Journal of Multiphase Flow*, 75, 257–266.
- Soldi, R. A., Oliveira, A. R. S., Barbosa, R. V., & César-Oliveira, M. A. F. (2007). Polymethacrylates: Pour point depressants in diesel oil. *European Polymer Journal*, 43(8), 3671–3678.
- Soliman, E. A., Elkatory, M. R., Hashem, A. I., & Ibrahim, H. S. (2018). Synthesis and performance of maleic anhydride copolymers with alkyl linoleate or tetra-esters as pour point depressants for waxy crude oil. *Fuel*, 211, 535–547.
- Song, X., Yin, H., Feng, Y., Zhang, S., & Wang, Y. (2016). Effect of SiO₂ nanoparticles on wax crystallization and flow behavior of model crude oil. *Industrial and Engineering Chemistry Research*, 55(23), 6563–6568.
- Soni, H. P., Agrawal, K. S., Nagar, A., & Bharambe, D. P. (2010). Designing maleic anhydride- α -olefin copolymeric combs as wax crystal growth nucleators. *Fuel Processing Technology*, 91(9), 997–1004.
- Soni, H. P., & Bharambe, D. P. (2008). Performance-based designing of wax crystal growth inhibitors. *Energy and Fuels*, 22(6), 3930–3938.
- Straub, T. J., Autry, S. W., & King, G. E. (1989, January). An investigation into practical removal of downhole paraffin by thermal methods and chemical solvents. In *SPE Production Operations Symposium*. Oklahoma City, Oklahoma.
- Sun, Z., Jing, G., & Tu, Z. (2018). Effect of modified nano-silica/EVA on flow behavior and wax crystallization of model oils with different wax contents. *Journal of Dispersion Science and Technology*, 39(1), 71–76.
- Taiwo, E., Otolorin, J., & Afolabi, T. (2012). Crude Oil Transportation: Nigerian Niger-Delta Waxy Crude. In M. Younes (Ed.), *Crude Oil Exploration in the World* (pp. 135-154). Rijeka: InTech.
- Taraneh, J. B., Rahmatollah, G., Hassan, A., & Alireza, D. (2008). Effect of wax inhibitors on pour point and rheological properties of Iranian waxy crude oil. *Fuel Processing Technology*, 89(10), 973–977.
- Wang, Z., Yu, X., Li, J., Wang, J., & Zhang, L. (2016). The use of biobased surfactant obtained by enzymatic syntheses for wax deposition inhibition and drag reduction in crude oil pipelines. *Catalysts*, 6(5), 61-76.
- Wang, W., Creek, J. L., Shuler, P. J., & Tang, Y. (2003a). Evaluation of effects of selected wax inhibitors on paraffin deposition. *Petroleum Science and Technology*, 21(3–4), 369–379.

- Wang, W., Creek, J. L., Shuler, P. J., & Tang, Y. (2003b). Evaluation of effects of selected wax inhibitors on wax appearance and disappearance temperatures. *Petroleum Science and Technology*, 21(3–4), 359–368.
- Wang, F., Zhang, D., Ding, Y., Zhang, L., Yang, M., Jiang, B., ... & Huo, L. (2011). The effect of nanohybrid materials on the pour-point and viscosity depressing of waxy crude oil. *Chinese Science Bulletin*, 56(1), 14–17.
- Wei, B. (2015). Recent advances on mitigating wax problem using polymeric wax crystal modifier. *Journal of Petroleum Exploration and Production Technology*, 5(4), 391–401.
- Woo, G. T., Garbis, S. J., & Gray, T. C. (1984, September). Long-term control of paraffin deposition. In *SPE Annual Technical Conference and Exhibition*. Houston, Texas.
- Wu, C., Zhang, J., Li, W., & Wu, N. (2005). Molecular dynamics simulation guiding the improvement of EVA-type pour point depressant. *Fuel*, 84(16), 2039–2047.
- Xu, J., Zhang, X., Sun, J., Li, L., & Guo, X. (2009). How comb-type poly (maleic acid alkylamide-co- α -olefin) assemble in waxy oils and improve flowing ability. *Asia-Pacific Journal of Chemical Engineering*, 4(5), 551–556.
- Yang, F., Cheng, L., Liu, H., Yao, B., Li, C., Sun, G., & Zhao, Y. (2018). Comb-like polyoctadecyl acrylate (POA) wax inhibitor triggers the formation of heterogeneous waxy oil gel deposits in a cylindrical couette device. *Energy and Fuels*, 32(1), 373–383.
- Yang, F., Li, C., Li, C., & Wang, D. (2013). Scaling of structural characteristics of gelled model waxy oils. *Energy and Fuels*, 27(7), 3718–3724.
- Yang, F., Li, C., Lin, M., Li, Z., & Yu, T. (2009). Depressive effect of polyacrylate (PA) pour point depressant on waxy crude oils. *Journal of Petrochemical Universities*, 22(2), 20–25.
- Yang, F., Paso, K., Norrman, J., Li, C., Oschmann, H., & Sjöblom, J. (2015). Hydrophilic nanoparticles facilitate wax inhibition. *Energy and Fuels*, 29(3), 1368–1374.
- Yang, F., Yao, B., Li, C., Shi, X., Sun, G., & Ma, X. (2017). Performance improvement of the ethylene-vinyl acetate copolymer (EVA) pour point depressant by small dosages of the polymethylsilsesquioxane (PMSQ) microsphere: An experimental study. *Fuel*, 207, 204–213.
- Yang, F., Zhao, Y., Sjöblom, J., Li, C., & Paso, K. G. (2015). Polymeric wax inhibitors and pour point depressants for waxy crude oils: A critical review. *Journal of Dispersion Science and Technology*, 36(2), 213–225.
- Yao, B., Li, C., Yang, F., Zhang, Y., Xiao, Z., & Sun, G. (2016). Structural properties of gelled Changqing waxy crude oil benefitted with nanocomposite pour point depressant. *Fuel*, 184, 544–554.
- Yao, B., Mu, Z., Li, C., Yang, F., & Zhang, X. (2017). Effective flow improving agents for waxy crude oil. *Petroleum Science and Technology*, 35(17), 1775–1783.
- Zhang, C., Gao, C., Gao, F., Wang, J., Zhang, D., Wang, Y., & Xu, D. (2014). Synthesis of comb bipolymers and their pour point depressing properties. *Petroleum Science*, 11(1), 155–160.
- Zhang, F., Ouyang, J., Feng, X., Zhang, H., & Xu, L. (2014). Paraffin deposition mechanism and paraffin inhibition technology for high-carbon paraffin crude oil from the kazakhstan pk oilfield. *Petroleum Science and Technology*, 32(4), 488–496.

Performance of SVM with Multiple Kernel Learning for Classification Tasks of Imbalanced Datasets

Sana Saeed^{1*} and Hong Choon Ong²

¹College of Statistical and Actuarial Sciences, University of the Punjab, 54590, Lahore, Pakistan

²School of Mathematical Sciences, Institute of Post Graduate Studies, University Sains Malaysia, 11800 USM, Gelugor, Penang, Malaysia

ABSTRACT

Support vector machine (SVM) is one of the most popular algorithms in machine learning and data mining. However, its reduced efficiency is usually observed for imbalanced datasets. To improve the performance of SVM for binary imbalanced datasets, a new scheme based on oversampling and the hybrid algorithm were introduced. Besides the use of a single kernel function, SVM was applied with multiple kernel learning (MKL). A weighted linear combination was defined based on the linear kernel function, radial basis function (RBF kernel), and sigmoid kernel function for MKL. By generating the synthetic samples in the minority class, searching the best choices of the SVM parameters and identifying the weights of MKL by minimizing the objective function, the improved performance of SVM was observed. To prove the strength of the proposed scheme, an experimental study, including noisy borderline and real imbalanced datasets was conducted. SVM was applied with linear kernel function, RBF kernel, sigmoid kernel function and MKL on all datasets. The performance of SVM with all kernel functions was evaluated by using sensitivity, G Mean, and F measure. A significantly improved performance of SVM with MKL was observed by applying the proposed scheme.

Keywords: Hybrid algorithm, imbalanced datasets, multiple kernel learning, oversampling algorithm, support vector machine

ARTICLE INFO

Article history:

Received: 21 March 2018

Accepted: 10 July 2018

Published: 24 January 2019

E-mail addresses:

sana.aqeel2010@gmail.com (Sana Saeed)

hcong@usm.my (Hong Choon Ong)

* Corresponding author

INTRODUCTION

SVM is a popular supervised machine learning algorithm, successfully handling classification tasks in many real-world applications: for example, credit scoring, text classification and bankruptcy prediction (Chaudhuri & De, 2011; Shin et al., 2005;

Sun et al., 2009; Huang et al., 2007). SVM has a strong theoretical and mathematical background and a high generalization capability of finding the global and non-linear classification solutions (Ben-Hur & Weston, 2010). However, its performance becomes limited for the classification task of imbalanced noisy and borderline datasets (Imam et al., 2006; Eitrich & Lang, 2006).

As the optimal performance of SVM is based on the decent choices of its parameters with kernel settings, the model selection problem essentially includes the search for the best values of the slack variable penalty weight (C) and kernel parameters, which are supposed to be used for the classification task. Traditionally, a grid search selection is adopted. Nevertheless, this method is time-consuming and does not produce the desired results (Hsu & Lin, 2002; Hsu et al., 2003). The present study is based on this prevailing issue of SVM. The current research work will address and discuss the issues of SVM for binary imbalanced datasets. Besides the use of a single kernel function, the current study will examine the performance of SVM with MKL. This study aims to present a new scheme for the said task.

Primary research works in MKL from the perspective of optimization techniques, can be seen from an interesting and brief research work presented by Lanckriet et al. (2004). The authors proposed an idea of using semidefinite programming (SDP) for kernel learning. Since SDP is a convex form of optimization and avoids being trapped in local optima, a transductive algorithm was offered. Furthermore, a learning method of SVM parameters was discussed. Afterward, an idea of using semi-infinite programming for the conic combination of kernels was proposed by Sonnenburg et al. (2006). The authors suggested the use of evolutionary approach, genetic algorithm (GA) in determining the weights of combined kernels of SVM. The authors gave a new direction to kernel learning by embedding the metaheuristic algorithms in it. Zhang (2006) proposed kernel optimization for SVM using the Levenberg-Marquardt (LM) algorithm instead of using the gradient descent approach to test the protein location data from yeast. Linear combinations of kernels for SVM in regards to speaker verification were used by Dehak et al. (2008). The combination weights were speaker dependent as compared to the universal weights on score level fusion. Another comprehensive study on the linear and nonlinear combinations of kernels was conducted by Cortes et al. (1995).

Cao et al. (2013) proposed an idea of optimized cost-sensitive SVM. An effective wrapper framework incorporating the area under the curve (AUC) and G Mean into the objective function of SVM was introduced to gain a better performance of SVM. A subset of feature selection, parameters, and misclassification cost were simultaneously optimized. Jiang et al. (2014) presented an idea for the optimal selection of SVM parameters by using three metrics namely AUC, accuracy and balanced accuracy using computational data. The authors engaged different levels of separability, different levels of imbalances and different levels of training sets in the study.

To enhance the performance of SVM for imbalanced datasets, different resampling approaches were also proposed by researchers. Most of them suggested the use of the oversampling technique, synthetic minority oversampling technique (SMOTE) in combination with SVM. Different kinds of sampling techniques were proposed; for example, a combined sampling approach using SMOTE and Tomek link with SVM for binary classification, a hybrid sampling approach using under and oversampling, and an ensemble method i.e. bagging of extrapolation borderline SMOTE (BEBS), which all can be studied from the available literature (Sain & Purnami, 2015; Wang, 2014; Wang et al., 2017).

Due to the emerging use of metaheuristic techniques for optimization problems, the use of these techniques for SVM can also be justified. For example, GA based feature selection and parameter optimization procedure for SVM can be found in the literature (Wang et al., 2011). GA and particle swarm optimization (PSO) for SVM and ant colony optimization (ACO) for SVM model selection can also be seen in the available studies on SVM optimization (Alwan & Ku-Mahamud, 2013; Ren & Bai, 2010; Blondin & Saad, 2010). An efficient memetic algorithm based on PSO and pattern search (PS) was proposed for SVM parameter optimization. PSO was used for the exploration purpose while PS was applied for exploitation (Bao et al., 2013). Another study proposed a combination of optimization and classification algorithms for SVM by using SMOTE and PSO (Cervantes et al., 2017). Wu et al. (2017) applied two-phase sequential minimal optimization (TSMO) and differential learning particle swarm optimization (DPSO) for SVM.

This article is organized as follows: material and methods are provided in Section 2. In Section 3, the proposed scheme is presented. Results of the experimental studies are given in Section 4. The conclusion is discussed in Section 5.

MATERIAL AND METHODS

According to Abe (2005), SVM as a nonlinear classifier can offer a better precision in many real-world applications. The process of making linear classifiers become nonlinear is to map the data from input space X to feature space F by using a nonlinear function $\varphi : X \rightarrow F$. In the feature space F , the discriminant function can be written as:

$$g(x) = \theta^T \varphi(x) + \theta_0 \quad (1)$$

where θ is known as the weight vector and θ_0 represents the bias. Kernel methods provide the best way of tackling this problem of mapping data to the high dimensional feature space instead of computing their dot products. Suppose that the weight vector may be expressed as a linear combination of training examples (T_r) as follows:

$$\theta = \sum_{i=1}^{T_r} \beta_i x_i \quad (2)$$

Therefore, in terms of a discriminant function, it can be written as:

$$g(x) = \sum_{i=1}^{T_r} \beta_i x_i^T x_i + \theta_0 \quad (3)$$

In the feature space, Equation (1) can be written as:

$$g(x) = \sum_{i=1}^{T_r} \beta_i \varphi(x_i)^T \varphi(x_i) + \theta_0 \quad (4)$$

This representation in terms of the variables β_i is called the dual representation of the decision boundary (Ben-Hur & Weston, 2010). According to Scholkopf and Smola (2001), a kernel function is a function that returns the dot product of the vectors by taking vectors as inputs in the original space. Mathematically, for data $x, x_1 \in X$, a kernel function is defined by $k(x, x_1) = \langle \varphi(x)^T, \varphi(x_1) \rangle$, where φ is a kernel function. In terms of the kernel function, Equation (4) can be rewritten as:

$$g(x) = \sum_{i=1}^{T_r} \beta_i k(x, x_i) + \theta_0 \quad (5)$$

Kernel-based methods such as SVM have been proven as an effective technique for data analysis in different fields of life. These methods employ the kernel functions that can compute the similarity between two vectors x and x_1 (Sonnenburg et al., 2006). Since different kernels correspond to different designs of similarity. Therefore, forming a combination of different kernels may lead to a better solution to the problem.

Multiple Kernel Learning

MKL is a set of machine learning strategies that use the predefined set of kernels. The predefined set of kernels may or may not be linear but its optimality is always demanding. Instead of creating a new kernel, MKL is an efficient way to combine the existing kernels. In MKL, it is assumed that for T_r training data point (x_i, y_i) , $i = 1, 2, \dots, T_r$ where $x_i \in X$ for some input space X and $y_i \in \{-1, 1\}$, there are M kernel matrices that are assumed to be symmetric and positive semi-definite (PSD). The problem is to find the best linear combination of the kernel $\sum_{l=1}^M \gamma_l k_l$ with non-negative weights i.e. $\gamma_l \geq 0$ and $\sum_{l=1}^M \gamma_l = 1$ for $l = 1, 2, \dots, M$ (Bach et al., 2004; Shawe-Taylor & Cristianini, 2004). In this study, three kernel functions are engaged: linear kernel function, RBF kernel and sigmoid kernel

function (Scholkopf & Smola, 2001). The linear kernel function is computed by using $k(x, x_1) = x'x_1$, RBF kernel can be defined by $k(x, x_1) = \exp(-\nu \|x - x_1\|^2)$ where ν is the positive parameter of RBF kernel for controlling its radius, and sigmoid kernel function can be stated as $k(x, x_1) = \tanh(\alpha_s x'x_1 + c_0)$ where $\alpha_s > 0$ is the scaling parameter and $c_0 \leq 0$ is the shifting parameter (Wang & Xu, 2017). The MKL practices different learning methods to combine kernels. The comprehensive details of these methods can be studied from Gonen and Alpaydin's (2011) work. The current study will apply an optimization approach for MKL to combine the kernel functions for the classification tasks of binary imbalanced datasets. The linear weighted combination of these three kernel functions is cast-off to learn them in terms of MKL.

$$MKL = \sum_{l=1}^3 \gamma_l k_l = \gamma_1 k_1 + \gamma_2 k_2 + \gamma_3 k_3 \quad (6)$$

where $\gamma_l \geq 0$, $\sum_{l=1}^3 \gamma_l = 1$, and k_1, k_2 , and k_3 are linear, RBF, and sigmoid kernel function respectively. γ_1, γ_2 , and γ_3 are the weights of the respective kernels.

Proposed Hybrid Algorithm

A hybrid algorithm is proposed during our research work for the optimization of continuous and nonlinear test functions. The bi-objective version of this hybrid algorithm was discussed by Saeed & Ong (2018). This hybrid algorithm grabbed the advantages of evolution strategies (ES) and swarm intelligence (SI). Covariance matrix adaptation evolution strategy (CMA-ES) and cuckoo search (CS) are combined for this task. As an application, this hybrid algorithm is engaged in this study.

Covariance Matrix Adaptation Evolution Strategy. CMA-ES is one of the most powerful evolutionary strategy proposed by Hansen et al. (1997). The key idea of CMA-ES lies in its invariance properties, which can be achieved by carefully planned variation, selection operators and efficient self-adaptation of mutation distribution (Igel et al., 2007). CMA-ES works with three operations: (1) Sampling from the multivariate normal distribution (2) Selection and recombination and (3) Adaptation of the covariance matrix.

Cuckoo Search. CS is one of the most popular nature-inspired metaheuristic algorithms proposed by Yang & Deb (2009), for the continuous nonlinear optimization problems. This algorithm is inspired by the cuckoos, the fascinating birds not only due to their sounds but also because of their hostile reproductive approach (Yang and Deb, 2009). Based on the egg-laying behavior of cuckoos, CS algorithm has the following three rules (1) each cuckoo lay one egg at a time and dumps it in a randomly chosen nest. (2) For the next generation,

the best nest with high-quality eggs are approved only. (3) The number of host nests (n) is fixed and the egg laid by a cuckoo is discovered by the host bird with a probability Pa . In this case, the host bird has two choices either to get rid of the egg or simply abandon the nest to build a completely new nest.

For the hybrid algorithm, after setting the objective function in CS, and after generating the initial solution, the best solution (X_{cs}^s) are produced at s^{th} iteration. Then with the recombination operator of CMA-ES, the weighted means m^s are produced. Before moving to the next iteration, in order to produce the new solution the best solution obtained from CS and the weighted mean from CMA-ES are plugged in into this new solution with the help of this following equation:

$$X^s = X_{cs}^s + m^s \quad (7)$$

For the next iteration ($s + 1$), X^s is used to get new solutions. Then the procedure of discovery and randomization are completed. All details are provided in the pseudocode of algorithm (see Algorithm 1).

Synthetic Minority Oversampling Technique

SMOTE is an oversampling algorithm for imbalanced datasets proposed by Chawla et al. (2002). This sampling technique uses oversampling of the minority class by creating synthetic samples. Subject to the amount of oversampling requirement, neighbors from the k nearest are selected. For example, if the amount of oversampling needed 200 percent then only two of the five nearest neighbors are selected and produce one sample in the direction of each. For synthetic samples following steps are applied:

1. Compute the difference between nearest neighbor and feature vector (sample).
2. Generate a random number between 0 and 1, multiply the difference by this random number.
3. Add it, to the feature vector under consideration. This will originate the selection of random point beside the line segment between two specific features.

The implementation of this algorithm requires five nearest neighbors (Han et al., 2005; Blagus & Lusa., 2013).

Proposed Scheme

The given classification scheme is proposed to study the performance of SVM with MKL (SVM+MKL) for binary imbalanced datasets. The proposed scheme is based on the above mentioned oversampling and hybrid algorithm. An oversampling algorithm (SMOTE) is applied to overcome the imbalance problem of the datasets. Each imbalanced dataset is partitioned into training, test, and validation sets using 60:20:20 ratios. As the performance of SVM is highly based on the appropriate choices of its parameters. Consequently, the

parameters of SVM including the parameters of the kernel functions along with the linear combination weights γ_l are optimized by using the proposed hybrid algorithm.

Algorithm 1

Hybrid Algorithm

Begin

1. Setting the initial parameters, number of nests n and number of solutions N_d .
2. Setting the objective function $f(x)$, $x = (x_1, x_2, \dots, x_d)$, adjusting the lower and upper bounds of the test function, and constraints (if any).
3. Initialize CS by generating the random initial solution of n host nests.
4. Find the best solution (X^{cs}) from CS at s^{th} iteration. Initialize CMA-ES algorithm, and generate the m^s weighted means at s^{th} iteration with the help of recombination operators.
5. Generate the new solution X^s at s^{th} iteration using Equation (7).
6. Set the number of iterations and a maximum number of iterations.
7. **While** (number of iteration < Maximum iteration) or (stop criterion).
8. Produce the new solution at $(s+1)^{th}$ iteration by levy flights.
9. Evaluate its quality or fitness.
10. Choose a nest among n say (j) randomly.
11. **If** ($f_i > f_j$) then
12. Replace j with the new solution.
- End if**
13. Abandoned the new nest using Pa and new ones are built.
14. Keep the best solution.
15. Rank the solution and find the current best.
- End while**
16. Post process results and visualization.

End

The objective function to be minimized is the misclassification error of the minority (positive). This optimization procedure is completed on the training dataset. Optimized parameters obtained from the training process are engaged with the test sets, where after completing the classification task, all standard evaluation measures are computed. Three established evaluation measures for imbalanced datasets namely, sensitivity, G Mean, and F measure are computed. G Mean is the geometric mean of the two prediction accuracies i.e. sensitivity: accuracy on the positive examples (minority class) and specificity: accuracy on the negative examples (majority class). It can be calculated with the help of the given below formula:

$$G\text{ Mean} = \sqrt{\text{Sensitivity} \times \text{Specificity}}$$

Sensitivity and specificity can be defined as:

$$\text{Sensitivity} = \frac{Tp}{Tp + Fn}$$

$$\text{Specificity} = \frac{Tn}{Tn + Fp}$$

where Tp represents true positive examples, Fp is used for false positive, Tn for true negative and Fn is used to show false negative examples. The second evaluation measure, F measure, the harmonic mean of the precision and sensitivity can be calculated with the help of the following formula:

$$F \text{ measure} = \frac{2 \times \text{Sensitivity} \times \text{Precision}}{\text{Sensitivity} + \text{Precision}}$$

and precision can be defined as:

$$\text{Precision} = \frac{Tp}{Tp + Fp}$$

The complete details of these evaluation measures can be studied from Bekkar et al. (2013). The values of G Mean and F measure varies between 0 and 1. The values near to 1 reflect the good performances by the classifiers and weak performances of the classifiers can be assessed by the low values (values near to 0). On the other hand, the high values of sensitivities reflect the good performances of the classifiers on the positive examples (minority class) only. The complete proposed scheme for the classification task is provided in a flowchart in Figure 1.

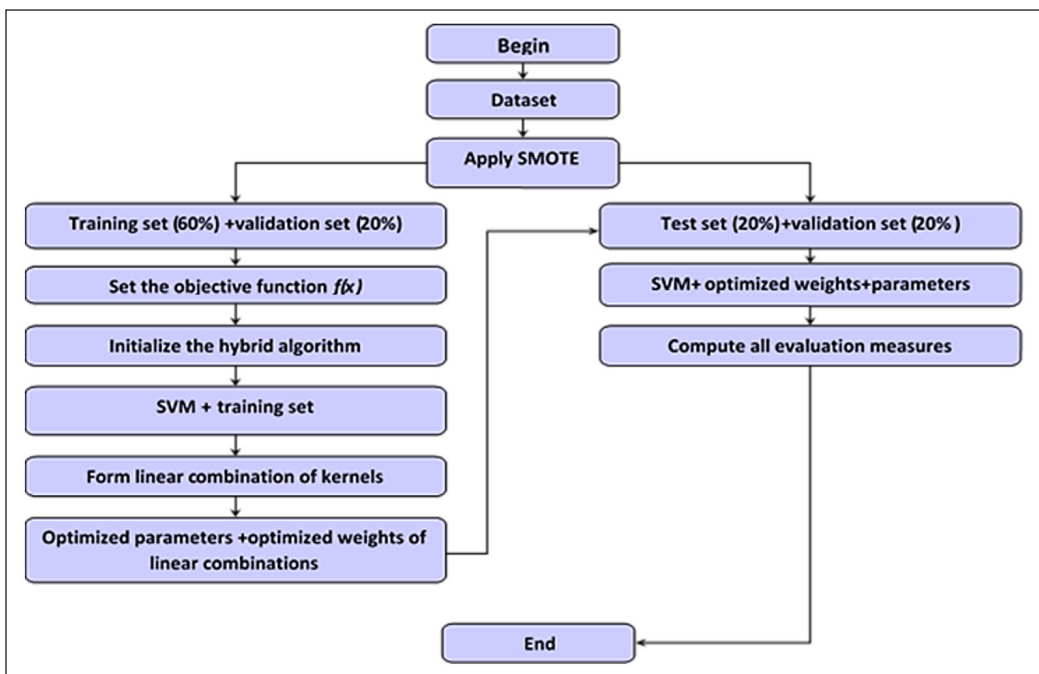


Figure 1. Flowchart of the proposed scheme for SVM+MKL

RESULTS AND DISCUSSIONS

An experimental study was conducted by engaging two types of datasets: (1) Noisy borderline imbalanced datasets and (2) Real imbalanced datasets. These datasets are taken from a well-known datasets repository KEEL (Alcala-Fdez et al., 2011). SVM is applied to each preprocessed dataset by using different kernel functions: SVM+linear, SVM+RBF, SVM+sigmoid, and SVM+MKL.

Noisy Borderline Imbalanced Datasets

Six noisy borderline imbalanced datasets namely Clove0, Clove30, Paw0, Paw30, Subclus0, and Subclus30 are engaged. Each dataset is classified by using SVM+linear, SVM+RBF, and SVM+MKL. For all noisy borderline datasets, by adding sigmoid kernel function in the linear combinations of kernels, the condition of PSD could not be satisfied. As a result, the sigmoid kernel function is excluded from the linear combinations of kernel functions. The MKL for noisy borderline imbalanced datasets is studied only by using the linear weighted combinations of the linear kernel function and RBF kernel, which can be defined as follows:

$$MKL = \gamma_1 k_1 + \gamma_2 k_2 \quad (8)$$

where k_1 represents the linear kernel function, k_2 represents the RBF kernel and γ_1, γ_2 are the weighted coefficients of these kernel function respectively. For the individual applications of the linear kernel function and RBF kernel with SVM, parameters are selected by the grid search methods. For SVM+MKL, parameters including the kernel parameter (ν) and slack variable (C) and the weights of kernel functions (γ_1 and γ_2) are optimized by using the proposed hybrid algorithm (see Table 1).

Three above mentioned evaluation measures, sensitivity represented by Sen, G Mean by G, and F measure by F are computed. The obtained results are provided in Table 2. Starting from first dataset (Clove0) to the last dataset (Subclus30), SVM+linear and

Table 1
Optimized parameters and weights of MKL for noisy borderline imbalanced datasets

Datasets	Parameters	MKL= $\gamma_1 k_1 + \gamma_2 k_2$
Clove0	$\nu = 51.950, C = 827.34$	MKL= $0.20k_1 + 0.80k_2$
Clove30	$\nu = 84.53, C = 628.62$	MKL= $0.50k_1 + 0.50k_2$
Paw0	$\nu = 49.493, C = 0.794$	MKL= $0.183k_1 + 0.817k_2$
Paw30	$\nu = 381.07, C = 436.63$	MKL= $0.2k_1 + 0.8k_2$
Subclus0	$\nu = 101.29, C = 403.58$	MKL= $0.425k_1 + 0.575k_2$
Subclus30	$\nu = 182.16, C = 219.70$	MKL= $0.42k_1 + 0.58k_2$

SVM+RBF performed well in terms of the good values of evaluation measures. However, SVM+RBF performed comparatively better than SVM+linear resulting in good values of all evaluation measures on all datasets. But SVM+RBF took longer testing time than SVM+linear. An outstanding performance of SVM+MKL is observed by using the proposed scheme. The proposed scheme based on the combined effect of oversampling and hybrid algorithm showed a very remarkable performance on noisy borderline datasets by using the linear combination of kernel functions with SVM. For all datasets, the maximum values of evaluation measures obtained by SVM+MKL are provided and highlighted in Table 2. A significant point in all experiments is the least testing time of SVM+MKL with the proposed scheme for all datasets.

Table 2
Performance of SVM using all kernel function on noisy borderline imbalanced datasets

Evaluation measures	Sen	G	F	Time (sec)	Sen	G	F	Time (sec)
Datasets	Clover0				Clover30			
SVM+linear	0.708	0.586	0.754	7.209	0.629	0.546	0.705	7.216
SVM+RBF	0.950	0.975	0.974	8.593	0.872	0.934	0.931	7.616
SVM+MKL	1.000	4.168						
	Paw0				Paw30			
SVM+linear	0.775	0.586	0.810	5.722	0.868	0.631	0.853	6.012
SVM+RBF	0.717	0.847	0.835	7.823	0.815	0.903	0.898	7.610
SVM+MKL	1.000	1.000	1.000	3.105	1.000	1.000	1.000	3.420
	Subclus0				Subclus30			
SVM+linear	0.957	0.664	0.897	6.193	0.586	0.563	0.684	5.818
SVM+RBF	0.838	0.911	0.907	8.724	0.725	0.851	0.840	7.850
SVM+MKL	1.000	1.000	1.000	3.046	1.000	1.000	1.000	3.612

Real Imbalanced Datasets

Another experimental study is conducted on six real imbalanced datasets to observe the role of MKL in the performance of SVM by applying the proposed scheme. A brief detail of these datasets is provided in Table 3. For MKL, the linear weighted combination is defined by using three kernel functions as follows:

$$MKL = \gamma_1 k_1 + \gamma_2 k_2 + \gamma_3 k_3 \quad (9)$$

where k_1 represents the linear kernel function, k_2 shows the RBF kernel and k_3 represents the sigmoid kernel function, γ_1 , γ_2 and γ_3 are the respective weights of these kernel functions. During the formation of the weighted linear combination of kernel functions for all datasets, the condition of PSD is carefully satisfied. For sigmoid kernel

function, only one parameter (α_s) is optimized whereas the other parameter is taken as fixed ($c_0 = -1$) to maintain the simplicity of the optimization process. All optimized parameters and weights of MKL are provided in Table 4.

Table 3
Datasets description

Datasets	Imbalance ratio (IR)	Total instances
Pima	1.87	768
Haberman	2.78	306
Thyroid	5.14	215
Yeast	9.08	514
Cleveland	12.62	177
Wine	29.17	1599

Table 4
Optimized parameters and weights of MKL for real imbalanced datasets

Datasets	Parameters	MKL= $\gamma_1 k_1 + \gamma_2 k_2 + \gamma_3 k_3$
Pima	$\nu = 26.902$, $C = 100.0503$, $\alpha_s = 3.2877$	MKL= $0.57519 k_1 + 0.14168 k_2 + 0.28313 k_3$
Haberman	$\nu = 69.244$, $C = 471.96$, $\alpha_s = 2.5022$	MKL= $0.22969 k_1 + 0.56385 k_2 + 0.2064 k_3$
Thyroid	$\nu = 2.4396$, $C = 6.7346$, $\alpha_s = 2.6732$	MKL= $0.10047 k_1 + 0.083496 k_2 + 0.81604 k_3$
Yeast	$\nu = 60.837$, $k_1 = 867.40$	MKL= $0.20840 k_1 + 0.79160 k_2$
Cleveland	$\nu = 50.046$, $C = 855.44$, $\alpha_s = 0.95289$	MKL= $0.200 k_1 + 0.71 k_2 + 0.09 k_3$
Wine	$\nu = 59.949$, $C = 870.621$, $\alpha_s = 0.90236$	MKL= $0.11414 k_1 + 0.76884 k_2 + 0.0.11702 k_3$

For yeast dataset, by adding the sigmoid kernel function, the condition could not be satisfied. Therefore, for this dataset, a weighted linear combination is formed by using only two kernel functions, linear kernel function, and RBF kernel. To study the performance of SVM with MKL by applying the proposed scheme, all real imbalanced datasets are classified by using SVM+linear, SVM+RBF, SVM+sigmoid, and SVM+MKL. For SVM+MKL, all parameters and their respective weights are optimized by applying the proposed hybrid algorithm.

The obtained results of all evaluation measures namely Sen, G, and F from all datasets are provided in Table 5. For the first dataset (Pima), with imbalance ratio (IR=1.87), RBF and sigmoid kernel performed very well resulting in maximum values of evaluation measures. SVM+linear also performed well. Nevertheless, its performance is not better than SVM+RBF and SVM+sigmoid. SVM+MKL showed maximum sensitivity for this dataset with minimum testing time.

For the second dataset, Haberman, again RBF and sigmoid kernels performed well but their performances on the minority class are less admirable than SVM+MKL (Sen=1.000). For the Thyroid dataset with IR=5.14, an outstanding performance is observed by SVM+linear and SVM+MKL. This time although SVM+RBF and SVM+sigmoid performed well their performances are less as compared to SVM+linear and SVM+MKL. On the other hand, the minimum testing time for SVM+MKL is observed for this dataset. For the fourth dataset (Yeast) with IR= 9.08, the average performances are observed by SVM+linear, SVM+RBF, and SVM+sigmoid. SVM+MKL remained successful in producing the maximum value of G (0.764) in minimum testing time. Approximately the same performances of RBF and sigmoid kernel functions are observed on Cleveland dataset. For Cleveland (IR=12.62) and Wine (IR=29.17), an outstanding performance of SVM+MKL can be seen resulting in maximum values of all evaluation measures. Though, for these two datasets, the testing time taken by SVM+MKL is longer than the other methods. Out of six datasets, the outstanding performance of SVM+MKL in terms of the maximum values of all evaluation measures (Sen, G, and F) is observed for three datasets (Thyroid, Cleveland, and Wine). All maximum values of evaluation measures obtained from SVM+MKL are highlighted in Table 5. The proposed scheme for SVM+MKL based on the oversampling and hybrid algorithm successfully handled imbalanced datasets.

Table 5
Performance of SVM using all kernel functions on real imbalanced datasets

Evaluation measures	Sen	G	F	Time (sec)	Sen	G	F	Time (sec)
Datasets	Pima				Haberman			
SVM+linear	0.844	0.880	0.913	6.797	0.574	0.732	0.728	6.029
SVM+RBF	1.000	1.000	1.000	7.230	0.984	0.992	0.992	5.601
SVM+sigmoid	1.000	1.000	1.000	6.854	0.991	0.995	0.995	5.095
SVM+MKL	1.000	0.727	0.678	1.745	1.000	0.845	0.879	1.861
	Thyroid				Yeast			
SVM+linear	1.000	1.000	1.000	1.947	0.676	0.737	0.780	3.375
SVM+RBF	0.813	0.901	0.897	1.825	0.407	0.638	0.579	3.492
SVM+sigmoid	0.872	0.934	0.932	1.899	0.395	0.628	0.566	3.342
SVM+MKL	1.000	1.000	1.000	1.508	0.653	0.764	0.731	2.126
	Cleveland				Wine			
SVM+linear	1.000	0.990	0.996	1.162	0.758	0.711	0.745	0.834
SVM+RBF	0.631	0.794	0.774	1.808	0.129	0.359	0.229	0.938
SVM+sigmoid	0.631	0.794	0.774	1.663	0.646	0.804	0.785	0.828
SVM+MKL	1.000	1.000	1.000	1.591	1.000	1.000	1.000	1.553

Statistical Ranks to SVM's with all Kernel Functions

Statistical ranks to SVM's with all kernel functions are assigned by using two well-known statistical non-parametric rank test: Friedman test and Quade test. These rank tests are applied to both types of datasets: noisy borderline datasets and real imbalanced datasets. The details of these tests can be found in Demsar (2006), Garcia et al. (2007), Trawinski et al. (2012) and Pohlert (2014). The null hypothesis to be tested, in both tests, is that on the average the performances of SVM's with all kernel functions are equal. Friedman's test follows an approximately Chi-square distribution for a large number of blocks (datasets) and treatments (SVM with all kernel functions). As we have a small number of treatments. Therefore, the critical values are derived from their tables. For noisy borderline imbalanced datasets, as the number of blocks is 6 and number of treatment is 3. Hence, 7.00 and 4.10 are the critical values of Friedman and Quade test respectively. All obtained results are provided in Table 6. The minimum ranks in Table 6 (bold ranks) are justifying the leading position of SVM+MKL. Graphically, these ranks are presented in Figure 2. For six real imbalanced datasets, as the number of treatments is 4 and number of blocks is also 6. Thus, the critical values for Friedman and Quade tests are 7.6 and 3.29 respectively. For these datasets, both tests showed insignificant results for most of the cases (see Table 7). On the other hand, the minimum ranks obtained by these tests justify the leading position of SVM+MKL. The obtained ranks for SVM+MKL are bold and shown in Table 7. The graphical representation of all ranks for all cases is shown in Figure 3.

Table 6

The average ranking of SVM performances by using all kernel functions on noisy borderline imbalanced datasets

Methods	With respect to sensitivity		With respect to G Mean	
	Friedman test	Quade test	Friedman test	Quade test
SVM+linear	2.5	2.7143	3	3
SVM+RBF	2.5	2.2857	2	2
SVM+MKL	1	1	1	1
Test statistics	9	9	12	21
Critical values	7	4.10	7	4.10
Decision (5%)	significant	significant	significant	significant
Methods	With respect to F measure		With respect to testing time	
	Friedman test	Quade test	Friedman test	Quade test
SVM+linear	3	3	2	2
SVM+RBF	2	2	3	3
SVM+MKL	1	1	1	1
Test statistics	12	21	12	21
Critical values	7	4.10	7	4.10
Decision (5%)	significant	significant	significant	significant

CONCLUSION

A study was conducted to observe the performance of SVM with MKL for binary imbalanced datasets including noisy borderline and real imbalanced datasets. For this given task, a new scheme based SMOTE and hybrid algorithm had proposed. An experimental study was conducted to justify the validity of the proposed scheme, by engaging the noisy borderline and real imbalanced datasets. For MKL, the weighted linear combinations of kernel functions were formed after satisfying the condition of PSD. By applying SMOTE and optimizing the parameters of SVM along with the weights of the kernel functions on the training datasets, these optimized parameters were engaged with testing datasets to fulfill the classification tasks. SVM is applied by using SVM+linear, SVM+RBF, SVM+sigmoid, and SVM+MKL to all datasets. Three evaluation measures (Sen, G, and F) were observed. An outstanding performance of the proposed scheme for SVM+MKL was observed for noisy borderline datasets. Though, an average performance was observed for real imbalanced datasets. In all, it can be said that our proposed scheme for SVM+MKL showed an enhanced performance for the classification of binary imbalanced datasets.

Table 7
The average ranking of SVM performances by using all kernel functions on real imbalanced datasets

Methods	With respect to sensitivity		With respect to G Mean	
	Friedman test	Quade test	Friedman test	Quade test
SVM+linear	2.1667	2.2381	2.5833	2.8810
SVM+RBF	3.25	3.4286	3	2.8571
SVM+sigmoid	2.9167	2.9524	2.5	2.1429
SVM+MKL	1.5	1.333	1.9167	2.1190
Test statistics	3.65	3.38	2.15	0.48
Critical values	7.6	3.29	7.6	3.29
Decision (5%)	insignificant	significant	insignificant	insignificant
Methods	With respect to F measure		With respect to testing time	
	Friedman test	Quade test	Friedman test	Quade test
SVM+linear	2.4167	2.7857	2.667	2.6667
SVM+RBF	3.00	2.8571	3.333	3.5238
SVM+sigmoid	2.50	2.1429	2.333	2.2857
SVM+MKL	2.0833	2.2143	1.6667	1.5238
Test statistics	1.55	0.36	5.20	2.52
Critical values	7.6	3.29	7.6	3.29
Decision (5%)	insignificant	insignificant	insignificant	insignificant

Performance of SVM for Imbalanced Datasets

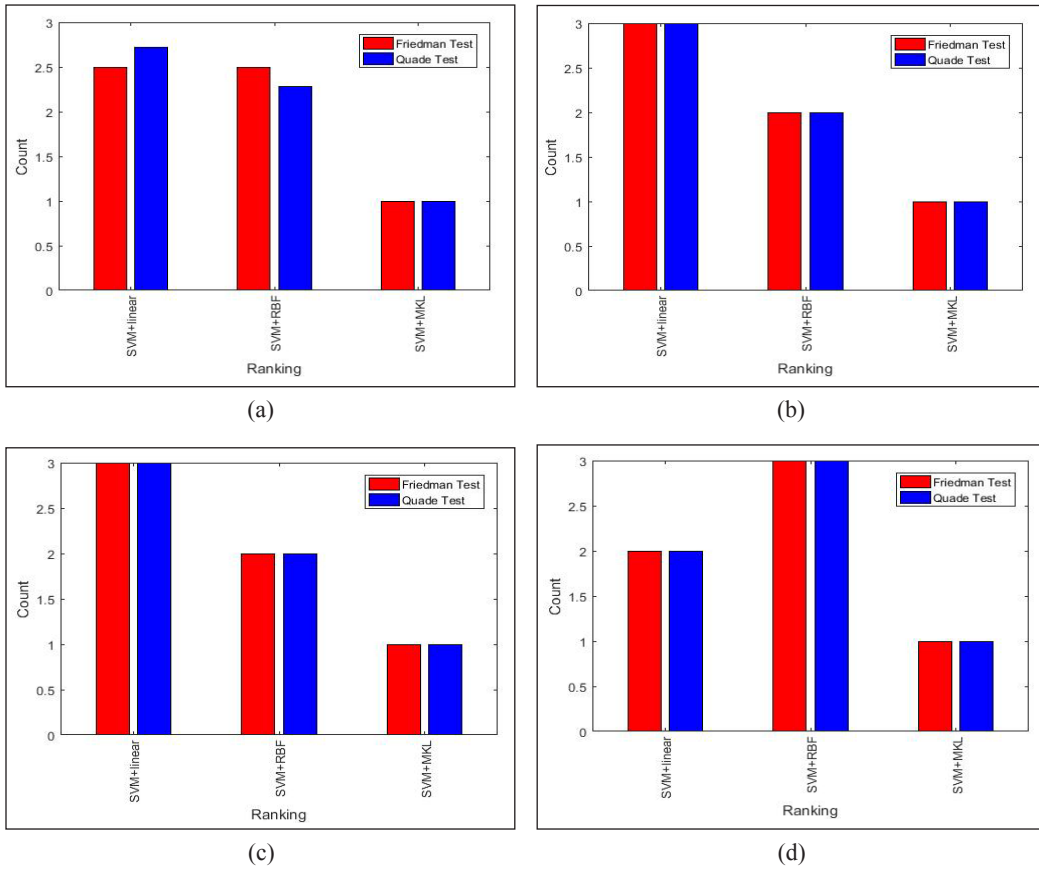


Figure 2. Average ranks of SVM's with all kernel functions on noisy borderline imbalanced datasets: (a) with respect to sensitivity; (b) with respect to G Mean; (c) with respect to F measure; and (d) with respect to testing time

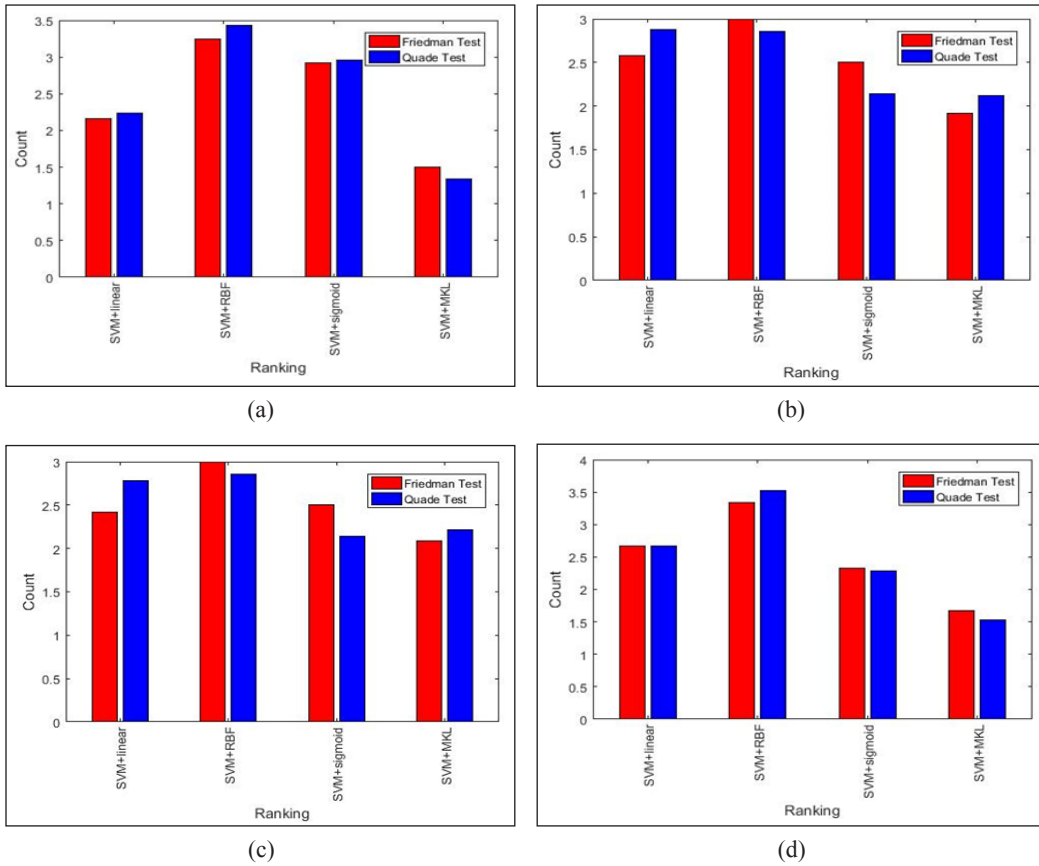


Figure 3. Average ranks of SVM's with all kernel functions on real imbalanced datasets: (a) with respect to sensitivity; (b) with respect to G Mean; (c) with respect to F measure; and (d) with respect to testing time (sec)

REFERENCES

- Abe, S. (2005). *Support vector machines for pattern classification* (2nd Ed.). London: Springer.
- Alcala-Fdez, J., Fernandez, A., Luengo, J., Derrac, J., Garcia, S., Sanchez, L., & Herrera, F. (2011). Keel data-mining software tool: data set repository, integration of algorithms and experimental analysis framework. *Journal of Multiple-Valued Logic and Soft Computing*, 17, 255-287.
- Alwan, H. B., & Ku-Mahamud, K. R. (2013). Solving svm model selection problem using acor and iacor. *WSEAS Transactions on Computers*, 12(9), 277-288.
- Bach, F. R., Lanckriet, G. R., & Jordan, M. I. (2004). Multiple kernel learning, conic duality, and the smo algorithm. In *Proceedings of the Twenty-First International Conference on Machine Learning* (p. 6). Banff, Alberta, Canada.

- Bao, Y., Hu, Z., & Xiong, T. (2013). A pso and pattern search based memetic algorithm for svms parameters optimization. *Neurocomputing*, *117*, 98-106.
- Bekkar, M., Djemaa, H. K., & Alitouche, T. A. (2013). Evaluation measure for models assessment over imbalanced data sets. *Journal of Information Engineering and Applications*, *3*(10), 27-38. Retrieved from <https://eva.fing.edu.uy/mod/resource/view.php?id=33977>
- Ben-Hur, A., & Weston, J. (2010). A user' guide to support vector machines. *Data Mining Techniques for the Life Sciences*, *609*, 223-239. doi: 10.1007/978-1-60327-24/-4_13
- Blagus, R., & Lusa, L. (2013). Smote for high-dimensional class-imbalanced data. *BMC Bioinformatics*, *14*, 106-121.
- Blondin, J., & Saad, A. (2010). Metaheuristic techniques for support vector machine model selection. In *Proceedings of the 10th International Conference on Hybrid Intelligent Systems* (pp. 197-200). Atlanta, GA, USA.
- Cao, P., Zhao, D., & Zaiane, O. (2013). An optimized cost-sensitive svm for imbalanced data learning. In *Proceedings of the 17th Pacific-Asia Conference on Advances in Knowledge Discovery and Data Mining, Pakdd* (pp. 280-292). Berlin, Heidelberg.
- Cervantes, J., Garcia, L. F., Rodriguez, L., Lopez, A., Castilla, J. R., & Trueba, A. (2017). Pso-based method for svm classification on skewed data set. *Neurocomputing*, *228*, 187-197.
- Chaudhuri, A., & De, K. (2011). Fuzzy support vector machine for bankruptcy prediction. *Applied Soft Computing*, *11*, 2472-2486.
- Chawla, N. V., Bowyer, K. W., Hall, L. O., & Kegelmeyer, W. P. (2002). Smote: synthetic minority over-sampling technique. *Journal of Artificial Intelligence Research*, *16*, 321-357.
- Cortes, C., & Vapnik, V. (1995). Support-vector network. *Machine Learning*, *20*(3), 273-297.
- Dehak, R., Dehak, N., Kenny, P., & Dumouchel, P. (2008). Kernel combination for svm speaker verification. In *Odyssey: The Speaker and Language Recognition Workshop Stellenbosch* (p. 21). South Africa.
- Demsar, J. (2006). Statistical comparisons of classifiers over multiple data sets. *Journal of Machine Learning Research*, *7*, 1-30.
- Eitrich, T., & Lang, B. (2006). Efficient optimization of support vector machine learning parameters for unbalanced data sets. *Journal of Computational and Applied Mathematics*, *196*(2), 425-436.
- Garcia, S. A., Bentez, A. D., Herrera, F., & Fernandez, A. (2007). Statistical comparisons by means of non-parametric tests: a case study on genetic based machine learning. In *Proceedings of EI Congreso Espanol de Informatica (CEDI 2007)*. Zaragoza, Spain.
- Gonen, M., & Alpaydin, E. (2011). Multiple kernel learning algorithms. *Journal of Machine Learning Research*, *12*, 2211-2268.
- Han, H., Wang, W. Y., & Mao, B. H. (2005). Borderline-smote: a new oversampling method in imbalanced data sets learning. In *International Conference on Intelligent Computing* (pp. 878-887). Berlin, Heidelberg.

- Hansen, N., & Ostermeier, A. (1997). Convergence properties of evolution strategies with derandomized covariance matrix adaptation: The $(\mathbf{u} \setminus \mathbf{u}_1, \lambda)$ cma-es. In *Proceedings of the 5th European Congress on Intelligent Techniques and Soft Computing* (pp. 650-654). Berlin, Germany. doi: 10.1.130.648
- Hsu, C. W., & Chang, C. C., & Lin, C. J. (2003). *A practical guide to support vector classification*. Department of Computer Science, National Taiwan University. Retrieved February 19, 2018, from www.csie.ntu.edu.tw/~cjlin/papers/guide/guide.pdf
- Hsu, C., & Lin, C. J. (2002). A simple decomposition method for support vector machines. *Machine Learning*, 46(1), 291-314.
- Huang, C. L., Chen, M. C., & Wang, C. J. (2007). Credit scoring with a data mining approach based on support vector machines. *Expert Systems with Applications*, 33, 847-856.
- Igel, C., Hansen, N., & Roth, S. (2007). Covariance matrix adaptation for multi-objective optimization. *Evolution Computation*, 15(1), 1-28.
- Imam, T., Ting, K. M., & Kamruzzaman, J. (2006). Z-svm: an svm for improved classification of imbalanced data. In *Proceedings of the Australian Conference on Artificial Intelligence* (pp. 264-273). Berlin, Heidelberg.
- Jiang, P., Missoum, S., & Chen, Z. (2014). Optimal svm parameter selection for non-separable and unbalanced datasets. *Structural and Multidisciplinary Optimization*, 50(4), 523-535.
- Lanckriet, G. R., Cristianini, N., Bartlett, P., Ghaoui, L. E., & Jordan, M. I. (2004). Learning the kernel matrix with semidefinite programming. *Journal of Machine Learning Research*, 5, 27-72.
- Pohlert, T. (2014). *The pairwise multiple comparison of means ranks package (pmcmmr)*. Retrieved February 19, 2018, from <http://CRAN.R-project.org/package=PMCMR>.
- Ren, Y., & Bai, G. (2010). Determination of optimal svm parameters by using ga/psa. *Journal of Computers*, 5, 1160-1168.
- Saeed, S., & Ong, H. C. (2018). A bi-objective hybrid algorithm for the classification of imbalanced noisy and borderline data sets. *Pattern Analysis and Applications*, 2018, 1-20. doi: [org/10.1007/s10044-018-0693-4](https://doi.org/10.1007/s10044-018-0693-4)
- Sain, H., & Purnami, S. W. (2015). Combine sampling support vector machine for imbalanced data classification. *Procedia Computer Science*, 72, 59-66.
- Scholkopf, B., & Smola, A. J. (2001). *Learning with kernels: support vector machines, regularization, optimization and beyond*. MA: MIT press.
- Shawe-Taylor, J., & Cristianini, N. (2004). *Kernel methods for pattern analysis*. Cambridge: Cambridge University Press.
- Shin, K. S., Lee, T. S., & Kim, H. J. (2005). An application of support vector machines in bankruptcy prediction model. *Expert Systems with Applications*, 28, 127-135.
- Sonnenburg, S., Ratsch, G., Schafer, C., & Scholkopf, B. (2006). Large Scale multiple kernel learning. *Journal of Machine Learning Research*, 7, 1531-1565.
- Sun, A., Lim, E. P., & Liu, Y. (2009). On strategies for imbalanced text classification using svm: a comparative study. *Decision Support Systems*, 48(1), 191-201.

- Trawinski, B., Smetek, M., Telec, Z., & Lasota, T. (2012). Nonparametric statistical analysis for multiple comparisons of machine learning regression algorithms. *International Journal of Applied Mathematics and Computer Science*, 22(4), 867-881.
- Wang, H., & Xu, D. (2017). Parameter selection method for support vector regression based on adaptive fusion of the mixed kernel function. *Journal of Control Science and Engineering*, 2017, 1-12. doi:10.1155/2017/3614790
- Wang, L., Xu, G., Wang, J., Yang, S., Guo, L., & Yan, W. (2011). Ga-svm based feature selection and parameters optimization for bci research. In *Proceedings of the Seventh International Conference on Natural Computation* (pp. 580-583). Shanghai, China. doi: 10.1109/ICNC.2011.6022083
- Wang, Q. (2014). A hybrid sampling svm approach to imbalanced data classification. In *Abstract and Applied Analysis* (Vol. 2014, pp. 1-7). Cairo: Hindawi Publishing Corporation. doi: 10.1155/2014/972786
- Wang, Q., Luo, Z., Huang, J., Feng, Y., & Liu, Z. (2017). A novel ensemble method for imbalanced data learning: bagging of extrapolation-smote svm. *Computational Intelligence and Neuroscience*, 2017, 1-11. doi: org/10.1155/2017/1827016
- Wu, S. J., Pham, V. H., & Nguyen, T. N. (2017). Two phase optimization for support vectors and parameter selection of support vector machines: two-class classification. *Applied Soft Computing*, 59, 129-142.
- Yang, X. S. (2010). *Nature inspired metaheuristic algorithms* (2nd Ed.). Frome: Luniver press.
- Yang, X. S., & Deb, S. (2009). Cuckoo search via levy flights. In *Proceedings of the World Congress on Nature and Biologically Inspired Computing* (pp. 210-214). Coimbatore, India. doi: 10.1109/NABIC.2009.5393690
- Zhang, B. (2006). *Svm kernel optimization: an example in yeast protein subcellular localization prediction*. Retrieved February 19, 2018, from <http://www.cs.cmu.edu/~epxing/class/10701-06f/project-reports/buck-zhang.pdf>.



**REFEREES FOR THE PERTANIKA
JOURNAL OF SCIENCE AND TECHNOLOGY**

VoL. 27 (1) Jan. 2019

The Editorial Board of the Journal of Science and Technology wishes to thank the following:

A. Saravanakumar
(GMRIT, India)

Fakhru'l-Razi Ahmadun
(UPM, Malaysia)

Md Azlin Md Said
(USM, Malaysia)

Abdul Fatah Wahab
(UMT, Malaysia)

Farah Nora Aznieta Abd Aziz
(UPM, Malaysia)

Mohamad Kamarol Mohd Jamil
(USM, Malaysia)

Achutha Kini
(MIT, India)

Ghasem Najafpour
(NIT, Iran)

Mohd Khairol Anuar Mohd
Ariffin
(UPM, Malaysia)

Agus Arsad
(UTM, Malaysia)

Girma T. Chala
(INTI, Malaysia)

Mohd Nizar Hamidon
(UPM, Malaysia)

Ahmad Baharuddin Abdullah
(USM, Malaysia)

Heng Swee Huay
(MMU, Malaysia)

Mohd Zalisham Jali
(USIM, Malaysia)

Ahmad Taufek Abdul Rahman
(UiTM, Malaysia)

Ibrahim Venkat
(USM, Malaysia)

Muhammad Ekhlasur Rahman
(Curtin University, Malaysia)

Ainul Akmar Mokhtar
(UTP, Malaysia)

Jacek Uziak
(University of Botswana, Botswana)

Muhammad Syafiq Hazwan
Ruslan
(UTP, Malaysia)

Amin Ismail
(UPM, Malaysia)

Jolius Gimibun
(UMP, Malaysia)

Napsiah Ismail
(UPM, Malaysia)

Arien Heryansyah
(UTM, Malaysia)

Kek Sie Long
(UTHM, Malaysia)

Narayanan Kumar
(Vels University, India)

Arunodaya Raj Mishra
(ITM University, India)

Koh You Beng
(UM, Malaysia)

Narongrit Sombatsompop
(KMUTT, Thailand)

Azura Che Soh
(UPM, Malaysia)

Law Ming Chiat
(Curtin University, Malaysia)

Nazmi Mat Nawi
(UPM, Malaysia)

Biswa Mohan Biswal
(USM, Malaysia)

Lee Teang Shui
(UPM, Malaysia)

Norazilawati Muhamad Sarih
(UM, Malaysia)

Che Zalina Zulkifli
(UPSI, Malaysia)

Lilly Suriani Affendey
(UPM, Malaysia)

Nurfadhlina Mohd Sharef
(UPM, Malaysia)

Cherry Bhargava
(IKGPTU, India)

Loh Su Peng
(UPM, Malaysia)

Othman A. Karim
(UKM, Malaysia)

Chua Han Bing
(Curtin University, Malaysia)

Low Siew Chun
(USM, Malaysia)

Perumal Kumar
(Curtin University, Malaysia)

Darius El Pebrian
(UiTM, Malaysia)

M. Muthu Krishnan
(KIT, India)

Poonam Jindal
(NIT Kurukshetra, India)

David B.L. Bong
(UNIMAS, Malaysia)

Masnida Hussin
(UPM, Malaysia)

Pradeep Kumar Gupta
(JUIT, India)

Riza Wirawan
(UNJ, Indonesia)

Rosni Abdullah
(USM, Malaysia)

Samsuzana Abd Aziz
(UPM, Malaysia)

Samuel Olatunbosun Sojini
(FUNAAB, Nigeria)

Sani Muhamad Isa
(BINUS, Indonesia)

Saratha Sathasivam
(USM, Malaysia)

Sathya Shankara Sharma
(MIT, India)

Sayed Inayatullah Shah
(IIUM, Malaysia)

Shaifulazuar Rozali
(UM, Malaysia)

Shruti Chopra
(Amity University, India)

Siow Chun Lim
(Taylor's University, Malaysia)

Sudeep Tanwar
(Nirma University, India)

Suppachai Howimanporn
(KMUTNB, Thailand)

Tay Chia Chay
(UiTM, Malaysia)

Thamer Ahmed Mohamed
(UPM, Malaysia)

Thongpin Chanchai
(Silpakorn University, Thailand)

Zulkifli Ahmad
(USM, Malaysia)

BINUS - Bina Nusantara University
FUNAAB - Federal University Of Agriculture, Abeokuta
GMRIT - GMR Institute of Technology
IIUM - International Islamic University Malaysia
IKGPTU - IK Gujral Punjab Technical University
INTI - INTI International University
ITM University - Institute of Technology and Management University
JUIT - Jaypee University of Information Technology
KIT - Kalaignarkaranidhi Institute of Technology
KMUTNB - King Mongkut's University of Technology North Bangkok
KMUTT - King Mongkut's University of Technology Thonburi
MIT - Manipal Institute of Technology
MMU - Multimedia University
NIT - Nashirvani University of Technology
NIT Kurukshetra - National Institute of Technology, Kurukshetra

UiTM - Universiti Teknologi MARA
UKM - Universiti Kebangsaan Malaysia
UM - Universiti Malaya
UMP - Universiti Malaysia Pahang
UMT - Universiti Malaysia Terengganu
UNIMAS - University Malaysia Sarawak
UNJ - Universitas Negeri Jakarta
UPM - Universiti Putra Malaysia
UPSI - Universiti Pendidikan Sultan Idris
USIM - Universiti Sains Islam Malaysia
USM - Universiti Sains Malaysia
UTHM - Universiti Tun Hussein Onn Malaysia
UTM - Universiti Teknologi Malaysia
UTP - Universiti Teknologi Petronas

While every effort has been made to include a complete list of referees for the period stated above, however if any name(s) have been omitted unintentionally or spelt incorrectly, please notify the Chief Executive Editor, *Pertanika* Journals at executive_editor.pertanika@upm.my

Any inclusion or exclusion of name(s) on this page does not commit the *Pertanika* Editorial Office, nor the UPM Press or the University to provide any liability for whatsoever reason.

Pertanika Journals

Our goal is to bring high quality research to the widest possible audience

INSTRUCTIONS TO AUTHORS (Manuscript Preparation & Submission Guide)

Revised: August 2018

Please read the Pertanika guidelines and follow these instructions carefully. Manuscripts not adhering to the instructions will be returned for revision without review. The Chief Executive Editor reserves the right to return manuscripts that are not prepared in accordance with these guidelines.

MANUSCRIPT PREPARATION

Manuscript Types

Pertanika accepts submission of mainly **four** types of manuscripts for peer-review.

1. REGULAR ARTICLE

Regular articles are full-length original empirical investigations, consisting of introduction, materials and methods, results and discussion, conclusions. Original work must provide references and an explanation on research findings that contain new and significant findings.

Size: Generally, these are expected to be between 8 and 12 journal pages or not exceeding 5000 words (excluding the abstract, references, tables and/or figures), a maximum of 80 references, and an abstract of 100–200 words.

2. REVIEW ARTICLE

These report critical evaluation of materials about current research that has already been published by organizing, integrating, and evaluating previously published materials. It summarizes the status of knowledge and outline future directions of research within the journal scope. Review articles should aim to provide systemic overviews, evaluations and interpretations of research in a given field. Re-analyses as meta-analysis and systemic reviews are encouraged. The manuscript title must start with "Review Article:".

Size: These articles do not have an expected page limit or maximum number of references, should include appropriate figures and/or tables, and an abstract of 100–200 words. Ideally, a review article should be of 7 to 8 printed pages.

3. SHORT COMMUNICATIONS

They are timely, peer-reviewed and brief. These are suitable for the publication of significant technical advances and may be used to:

- (a) report new developments, significant advances and novel aspects of experimental and theoretical methods and techniques which are relevant for scientific investigations within the journal scope;
- (b) report/discuss on significant matters of policy and perspective related to the science of the journal, including 'personal' commentary;
- (c) disseminate information and data on topical events of significant scientific and/or social interest within the scope of the journal.

The manuscript title must start with "*Brief Communication:*".

Size: These are usually between 2 and 4 journal pages and have a maximum of three figures and/or tables, from 8 to 20 references, and an abstract length not exceeding 100 words. Information must be in short but complete form and it is not intended to publish preliminary results or to be a reduced version of Regular or Rapid Papers.

4. OTHERS

Brief reports, case studies, comments, concept papers, Letters to the Editor, and replies on previously published articles may be considered. **PLEASE NOTE: NO EXCEPTIONS WILL BE MADE FOR PAGE LENGTH.**

Language Accuracy

Pertanika **emphasizes** on the linguistic accuracy of every manuscript published. Articles must be in **English** and they must be competently written and argued in clear and concise grammatical English. Contributors are strongly advised to have the manuscript checked by a colleague with ample experience in writing English manuscripts or a competent English language editor.

Author(s) **must provide a certificate** confirming that their manuscripts have been adequately edited. A proof from a recognised editing service should be submitted together with the cover letter at the time of submitting a manuscript to Pertanika. **All editing costs must be borne by the author(s)**. This step, taken by authors before submission, will greatly facilitate reviewing, and thus publication if the content is acceptable.

Linguistically hopeless manuscripts will be rejected straightaway (e.g., when the language is so poor that one cannot be sure of what the authors really mean). This process, taken by authors before submission, will greatly facilitate reviewing, and thus publication if the content is acceptable.

MANUSCRIPT FORMAT

The paper should be submitted in one column format with at least 4cm margins and 1.5 line spacing throughout. Authors are advised to use Times New Roman 12-point font and *MS Word* format.

1. Manuscript Structure

Manuscripts in general should be organised in the following order:

Page 1: Running title

This page should **only** contain the running title of your paper. The running title is an abbreviated title used as the running head on every page of the manuscript. The running title should not exceed 60 characters, counting letters and spaces.

Page 2: Author(s) and Corresponding author information.

This page should contain the **full title** of your paper not exceeding 25 words, with name(s) of all the authors, institutions and corresponding author's name, institution and full address (Street address, telephone number (including extension), hand phone number, and e-mail address) for editorial correspondence. First and corresponding authors must be clearly indicated.

The names of the authors may be abbreviated following the international naming convention. e.g. Salleh, A. B.¹, Tan, S. G.^{2*} and Sapuan, S. M.³

Authors' addresses. Multiple authors with different addresses must indicate their respective addresses separately by superscript numbers:

Abu Bakar Salleh¹ and Mohd Adzir Mahdi²

¹Faculty of Biotechnology and Biomolecular Sciences, Universiti Putra Malaysia, 43400 Serdang, Selangor, Malaysia

²Faculty of Engineering, Universiti Putra Malaysia, 43400 Serdang, Selangor Malaysia

A **list** of number of **black and white / colour figures and tables** should also be indicated on this page. Figures submitted in color will be printed (upon request) in colour. See "5. Figures & Photographs" for details.

Page 3: Abstract

This page should **repeat** the **full title** of your paper with only the **Abstract** (the abstract should be less than 250 words for a Regular Paper and up to 100 words for a Short Communication), and **Keywords**.

Keywords: Not more than eight keywords in alphabetical order must be provided to describe the contents of the manuscript.

Page 4: Introduction

This page should begin with the **Introduction** of your article and followed by the rest of your paper.

2. Text

Regular Papers should be prepared with the headings *Introduction, Materials and Methods, Results and Discussion, Conclusions, Acknowledgements, References, and Supplementary data* (if available) in this order.

Title	_____
Abstract	_____
Keywords	_____
(IMRAD)	
Introduction	_____
Methods	_____
Results	_____
And	_____
Discussions	_____
Conclusions	_____
Acknowledgements	_____
References	_____
Supplementary data	_____

MAKE YOUR ARTICLES AS CONCISE AS POSSIBLE

Most scientific papers are prepared according to a format called IMRAD. The term represents the first letters of the words Introduction, Materials and Methods, Results, And, Discussion. It indicates a pattern or format rather than a complete list of headings or components of research papers; the missing parts of a paper are: Title, Authors, Keywords, Abstract, Conclusions, and References. Additionally, some papers include Acknowledgments and Appendices.

The Introduction explains the scope and objective of the study in the light of current knowledge on the subject; the Materials and Methods describes how the study was conducted; the Results section reports what was found in the study; and the Discussion section explains meaning and significance of the results and provides suggestions for future directions of research. The manuscript must be prepared according to the Journal's instructions to authors.

3. Equations and Formulae

These must be set up clearly and should be typed double spaced. Numbers identifying equations should be in square brackets and placed on the right margin of the text.

4. Tables

All tables should be prepared in a form consistent with recent issues of Pertanika and should be numbered consecutively with Roman numerals. Explanatory material should be given in the table legends and footnotes. Each table should be prepared on a new page, embedded in the manuscript.

When a manuscript is submitted for publication, tables must also be submitted separately as data - .doc, .rtf, Excel or PowerPoint files- because tables submitted as image data cannot be edited for publication and are usually in low-resolution.

5. Figures & Photographs

Submit an **original** figure or photograph. Line drawings must be clear, with high black and white contrast. Each figure or photograph should be prepared on a new page, embedded in the manuscript for reviewing to keep the file of the manuscript under 5 MB. These should be numbered consecutively with Roman numerals.

Figures or photographs must also be submitted separately as TIFF, JPEG, or Excel files- because figures or photographs submitted in low-resolution embedded in the manuscript cannot be accepted for publication. For electronic figures, create your figures using applications that are capable of preparing high resolution TIFF files. In general, we require **300 dpi** or higher resolution for **coloured and half-tone artwork**, and **1200 dpi or higher** for **line drawings** are required.

Failure to comply with these specifications will require new figures and delay in publication.

NOTE: Illustrations may be produced in colour at no extra cost at the discretion of the Publisher; the author could be charged Malaysian Ringgit 50 for each colour page.

6. References

References begin on their own page and are listed in alphabetical order by the first author's last name. Only references cited within the text should be included. All references should be in 12-point font and double-spaced.

NOTE: When formatting your references, please follow the **APA reference style** (6th Edition). Ensure that the references are strictly in the journal's prescribed style, failing which your article will **not be accepted for peer-review**. You may refer to the *Publication Manual of the American Psychological Association* for further details (<http://www.apastyle.org/>).

7. General Guidelines

Abbreviations: Define alphabetically, other than abbreviations that can be used without definition. Words or phrases that are abbreviated in the introduction and following text should be written out in full the first time that they appear in the text, with each abbreviated form in parenthesis. Include the common name or scientific name, or both, of animal and plant materials.

Acknowledgements: Individuals and entities that have provided essential support such as research grants and fellowships and other sources of funding should be acknowledged. Contributions that do not involve researching (clerical assistance or personal acknowledgements) should **not** appear in acknowledgements.

Authors' Affiliation: The primary affiliation for each author should be the institution where the majority of their work was done. If an author has subsequently moved to another institution, the current address may also be stated in the footer.

Co-Authors: The commonly accepted guideline for authorship is that one must have substantially contributed to the development of the paper and share accountability for the results. Researchers should decide who will be an author and what order they will be listed depending upon their order of importance to the study. Other contributions should be cited in the manuscript's Acknowledgements.

Copyright Permissions: Authors should seek necessary permissions for quotations, artwork, boxes or tables taken from other publications or from other freely available sources on the Internet before submission to Pertanika. Acknowledgement must be given to the original source in the illustration legend, in a table footnote, or at the end of the quotation.

Footnotes: Current addresses of authors if different from heading may be inserted here.

Page Numbering: Every page of the manuscript, including the title page, references, tables, etc. should be numbered.

Spelling: The journal uses American or British spelling and authors may follow the latest edition of the Oxford Advanced Learner's Dictionary for British spellings.

SUBMISSION OF MANUSCRIPTS

Owing to the volume of manuscripts we receive, we must insist that all submissions be made electronically using the **online submission system ScholarOne™**, a web-based portal by Thomson Reuters. For more information, go to our web page and [click "Online Submission"](#).

Submission Checklist

1. **MANUSCRIPT:** Ensure your MS has followed the Pertanika style particularly the first four pages as explained earlier. The article should be written in a good academic style and provide an accurate and succinct description of the contents ensuring that grammar and spelling errors have been corrected before submission. It should also not exceed the suggested length.

COVER LETTER: All submissions must be accompanied by a cover letter detailing what you are submitting. Papers are accepted for publication in the journal on the understanding that the article is **original** and the content has **not been published** either **in English** or **any other language(s)** or **submitted for publication elsewhere**. The letter should also briefly describe the research you are reporting, why it is important, and why you think the readers of the journal would be interested in it. The cover letter must also contain an acknowledgement that all authors have contributed significantly, and that all authors have approved the paper for release and are in agreement with its content.

The cover letter of the paper should contain (i) the title; (ii) the full names of the authors; (iii) the addresses of the institutions at which the work was carried out together with (iv) the full postal and email address, plus telephone numbers and emails of all the authors. The current address of any author, if different from that where the work was carried out, should be supplied in a footnote.

The above must be stated in the cover letter. Submission of your manuscript will not be accepted until a cover letter has been received.

2. **COPYRIGHT:** Authors publishing the Journal will be asked to sign a copyright form. In signing the form, it is assumed that authors have obtained permission to use any copyrighted or previously published material. All authors must read and agree to the conditions outlined in the form, and must sign the form or agree that the corresponding author can sign on their behalf. Articles cannot be published until a signed form (*original pen-to-paper signature*) has been received.

Please do **not** submit manuscripts to the editor-in-chief or to any other office directly. Any queries must be directed to the **Chief Executive Editor's** office via email to executive_editor.pertanika@upm.my.

Visit our Journal's website for more details at <http://www.pertanika.upm.edu.my/home.php>.

HARDCOPIES OF THE JOURNALS AND OFF PRINTS

Under the Journal's open access initiative, authors can choose to download free material (via PDF link) from any of the journal issues from Pertanika's website. Under "**Browse Journals**" you will see a link, "*Current Issues*" or "*Archives*". Here you will get access to all current and back-issues from 1978 onwards. No hard copy of journals or off prints are printed.



Chemical Sciences

Preparation and Swelling Study of CMC Hydrogel as Potential Superabsorbent 489

Nur Fitrah Che Nan, Norhazlin Zainuddin and Mansor Ahmad

Engineering Sciences

Review Article 499

A Review of the Mechanism and Role of Wax Inhibitors in the Wax Deposition and Precipitation

Lim Zhen Hao, Hikmat Said Al-Salim and Norida Ridzuan

Mathematical Sciences

Performance of SVM with Multiple Kernel Learning for Classification Tasks of Imbalanced Datasets 527

Sana Saeed and Hong Choon Ong

Medical and Health Sciences

Review Article

- A Review of the Thermal Effects During Pregnancy by using Ultrasound:
Doppler Mode 357

*Umi Nadrah Amran, Farah Wahida Ahmad Zaiki and
Sulaiman Md Dom*

- Simultaneous Estimation by RP-HPLC Method for the 371
Immunosuppressant Drug Combination: Mycophenolate Mofetil,
Tacrolimus with Prednisolone

Pardeep Kr. Sharma, Vijay Mishra, Surajpal Verma and Amit Bhatia

- Effects of Various Drying Methods on the Vitamin C level of Papaya 387
Locally Grown in Brunei Darussalam

Nur Amirah Hair Mustapa and Siti Rohaiza Ahmad

Earth Sciences

- Experimental Study of Hydraulic Jumps in an Inclined Rectangular Flume 397

Dillip K. Ghose, Priya Mandal and Sandeep Samantaray

- Flow Measurement in Huma Tail distributary of Hirakud Command Area, 409
India using Chiu's Equation

Ashutosh Rath, Sandeep Samantaray and Prakash Chandra Swain

Environmental Sciences

- Modelling of Pilot-Scale Anaerobic Food Wastes Composting 421
Process with Dry Leaves or Cow Manure

*Wei Jie Lim, Nyuk Ling Chin, Yus Aniza Yusof, Azmi Yahya and
Tuan Poy Tee*

- Response of Cadmium Accumulation in Rice (*Oryza sativa* L. cv. SPR1) 443
Grown with Different Organic Soil Amendments

Chitsanuphong Pratum

Material Sciences

Review Article

- Titanium and Titanium Based Alloys as Metallic Biomaterials in Medical 459
Applications – Spine Implant Case Study

Nur Azida Che Lah and Muhamad Hellmy Hussin

- Physico-Mechanical Properties and Formaldehyde Emission of 473
Rubberwood Particleboard Made With UF Resin Admixed With
Ammonium and Aluminium-Based Hardeners

Abd Ghani Aizat, Bawon Paiman, Seng Hua Lee and Ashaari Zaidon

SPAS: An Authentication Scheme to Prevent Unauthorized Access of Information from Smart Card <i>Ajay Kumar Sahu and Ashish Kumar</i>	175
 Engineering Sciences	
Improvement in the Mechanical Strength of Compacted Urea Fertilizer Tablets through Die Wall Lubrication <i>Intan Soraya Shamsudin, Mohd Shamsul Anuar, Yus Aniza Yusof, Ahmad Husni Mohd. Hanif and Suraya Mohd Tahir</i>	193
Two-dimensional Modeling of Water Distribution under Capillary Wick Irrigation System <i>Rowshon Md Kamal, Hadi Hamaaziz Muhammed, Mohammad Abdul Mojid, Ruediger Anlauf and Mohd Amin Mohd Soom</i>	205
Reliability based Redundancy Assessment of a Cogeneration Plant <i>Meseret Nasir, Wan Mansor Wan Muhamad and Raja Aziz Raja Maarof</i>	225
Utilization of Normal and Treated Cement Kiln Dust as Cement Replacement Materials in Concrete <i>Yaser Gamil, Ismail Bakar and Lee Yee Loon</i>	247
Design of Self-tuning Fuzzy PID Controllers for Position Tracking Control of Autonomous Agricultural Tractor <i>Witcha Upaphai, Pracha Bunyawanichakul and Manusak Janthong</i>	263
 Applied Sciences and Technologies	
<i>Review Article</i>	
A Review: Methodologies Review of Magnetic Water Treatment as Green Approach of Water Pipeline System <i>Athirah Othman, Johan Sohaili and Nur Sumaiyyah Supian</i>	281
Kenaf Fibre and Its Bio-Based Composites: A Conspectus <i>Adole Michael Adole, Jamaludin Mohamad Yatim, Suhaimi Abubakar Ramli, Athirah Othman and Norazura Azzmi Mizal</i>	297
The Physicochemical Properties of Cocoa Butter Equivalent Produced from Lipase- Catalyzed Palm Oil and Hydrogenated Palm Oil via Physical Fractionation <i>Siti Maslina Mohamad Alwi and Lai Oi Ming</i>	331
Extraction of Subtractive Features of Prismatic Parts from STEP File for CAD/CAM Integration <i>Sattanathan Sivakumar, Venkadasamy Dhanalakshmi and Ravichandran Vishnuvardha</i>	343

Contents

Foreword	i
<i>Abu Bakar Salleh</i>	
Information, Computer and Communication Technologies	
<i>Review Article</i>	1
A Review: Customers Online Security on Usage of Banking Technologies in Smartphones and Computers	
<i>Natarajan Sundaram, Cherian Thomas and Loganathan Agilandeeswari</i>	
Non-Binary Serial Turbo LDPC Codes Combined with High Order Constellations	33
<i>Latifa Mostari and Abdelmalik Taleb-Ahmed</i>	
Ma-Ease: An Android-Based Technology for Corn Production and Management	49
<i>Sales Gamponia Aribé Jr., Jhon Michael H. Turtosa, Jul Maico B. Yamba and Alvin B. Jamisola</i>	
Market Matching Online to Recommend MSME Export Products Destination by Using Fuzzy Control	69
<i>Bambang Nurdewanto, Elta Sonalitha, Ratih Salnan and Nadia Rosmalita Sari</i>	
Supervised Clustering based on a Multi-objective Genetic Algorithm	81
<i>Vipa Thananant and Surapong Auwatanamongkol</i>	
Adaptive Genetic Algorithm for Feature Weighting in Multi-Criteria Recommender Systems	123
<i>Gursimarpreet Kaur and Saroj Ratnoo</i>	
Customizable Smart Food Cabinet and Refrigerator	143
<i>Chandra Manuel, Janitra Avila, Lukas Budiman, Rico Wijaya and Rinda Hedwig</i>	
SQL-Injection Vulnerabilities Resolving using Valid Security Tool in Cloud	159
<i>Niharika Singh and Ashutosh Kumar Singh</i>	



Pertanika Editorial Office, Journal Division
Office of the Deputy Vice Chancellor (R&I),
1st Floor, IDEA Tower II,
UPM-MTDC Technology Centre
Universiti Putra Malaysia
43400 UPM Serdang
Selangor Darul Ehsan
Malaysia

<http://www.pertanika.upm.edu.my/>
E-mail: executive_editor.pertanika@upm.my
Tel: +603 8947 1622/1616

PENERBIT
UPM
UNIVERSITI PUTRA MALAYSIA
PRESS

<http://penerbit.upm.edu.my>
E-mail : penerbit@upm.edu.my
Tel : +603 8946 8855/8854

